

# **OXIDATIVE STRESS MARKERS IN NEUROLOGICAL DISEASES AND DISORDERS: ELECTROCHEMICAL DETECTION OF HYDROGEN PEROXIDE AND NITRIC OXIDE**

A thesis submitted by

**Saidhbhe L. O’Riordan B.Sc. (Hons.)**

to the

**National University of Ireland, Maynooth**

For the degree of Doctor of Philosophy



**NUI MAYNOOTH**

Ollscoil na hÉireann Má Nuad

**Volume 1 of 1**

Based on the research carried out in the

Department of Chemistry, Faculty of Science and Engineering,

National University of Ireland, Maynooth

under the supervision and direction of

**Prof. John P. Lowry and Dr. Niall J. Finnerty**

**February 2013**

## 1. Introduction

---

|   |    |
|---|----|
| 1.1 Neurotransmission .....   | 1  |
| 1.2 Neurochemical analysis .....                                      | 2  |
| 1.3 Hydrogen peroxide (H <sub>2</sub> O <sub>2</sub> ) .....          | 4  |
| 1.4 Nitric oxide (NO) .....   | 6  |
| 1.5 Oxidative stress in neurodegenerative diseases/dysfunctions ..... | 8  |
| 1.6 Autism spectrum disorders (ASDs) .....                            | 9  |
| 1.7 Parkinson's disease (PD) .....                                    | 11 |
| 1.9 Mitochondrial dysfunction (MTdys) in PD and ASDs .....            | 16 |
| 1.10 Current therapeutic strategies for PD .....                      | 20 |
| 1.11 Conclusion .....   | 22 |
| References .....  | 23 |

## 2. Theory

---

|   |    |
|---|----|
| 2.1 Introduction .....  | 34 |
| 2.2 Oxidation/Reduction .....   | 35 |
| 2.3 Mass transport .....  | 38 |
| 2.3.1 Diffusion .....   | 38 |
| 2.3.2 Convection .....  | 41 |
| 2.3.3 Migration .....   | 41 |
| 2.4 Constant Potential Amperometry (CPA) .....                                | 41 |
| 2.4.1 Hydrogen peroxide (H <sub>2</sub> O <sub>2</sub> ) .....                | 42 |
| 2.4.2 Nitric oxide (NO) .....   | 43 |
| 2.4.3 Ascorbic acid (AA) .....  | 44 |
| 2.5 Electropolymerisation of <i>o</i> -Phenylenediamine ( <i>o</i> -PD) ..... | 45 |
| 2.6 Nafion <sup>®</sup> .....   | 46 |
| 2.7 Catalase .....  | 47 |
| 2.8 Paired catalase-based H <sub>2</sub> O <sub>2</sub> biosensor .....       | 48 |
| 2.9 Microdialysis .....   | 50 |
| 2.10 Oxidative and nitrosative stress .....                                   | 51 |
| 2.10.1 Antioxidants .....   | 52 |
| 2.10.2 Reactive oxygen species (ROS) .....                                    | 54 |

|   |    |
|---|----|
| 2.10.3 <i>Reactive nitrogen species (RNS)</i> ..... | 56 |
| References.....                                     | 59 |

### 3. Experimental

---

|   |    |
|---|----|
| 3.1 Introduction.....   | 64 |
| 3.2 Computer based Instrumentation .....                                      | 65 |
| 3.2.1 <i>The Computer</i> .....   | 65 |
| 3.2.2 <i>The Powerlab<sup>®</sup></i> .....                                   | 65 |
| 3.2.3 <i>The Potentiostat</i> .....   | 66 |
| 3.3 Chemicals & Solutions.....  | 66 |
| 3.3.1 <i>Chemicals</i> .....  | 66 |
| 3.3.1.1 <i>In-vitro chemicals</i> .....                                       | 67 |
| 3.3.1.2 <i>In-vivo chemicals</i> .....  | 67 |
| 3.3.2 <i>Solutions</i> .....  | 68 |
| 3.3.2.1 <i>In-vitro solutions</i> .....                                       | 68 |
| 3.3.2.2 <i>In-vivo solutions</i> .....  | 70 |
| 3.4 Working electrode preparation .....                                       | 72 |
| 3.4.2 <i>Nitric oxide sensor</i> .....  | 73 |
| 3.4.3 <i>H<sub>2</sub>O<sub>2</sub> catalase-based paired biosensor</i> ..... | 74 |
| 3.5 Electrode modifications .....   | 74 |
| 3.5.1 <i>PPD-modified electrodes</i> .....                                    | 75 |
| 3.5.2 <i>Nafion<sup>®</sup> dip-absorption modification</i> .....             | 75 |
| 3.5.3 <i>Catalase modification</i> .....                                      | 75 |
| 3.6 Electrode treatments.....   | 76 |
| 3.6.1 <i>BSA treated sensors</i> .....  | 76 |
| 3.6.2 <i>PEA treated sensors</i> .....  | 77 |
| 3.6.3 <i>BT treated sensors</i> .....   | 77 |
| 3.6.4 <i>Long-term sensor stability investigations</i> .....                  | 77 |
| 3.6.5 <i>Post-implanted sensors</i> .....                                     | 77 |
| 3.7 Electrochemical experiments .....   | 78 |
| 3.7.1 <i>Electrochemical cell set-up</i> .....                                | 78 |
| 3.7.2 <i>Experimental techniques</i> .....                                    | 79 |
| 3.7.3 <i>AA calibrations</i> .....  | 79 |
| 3.7.4 <i>NO calibrations</i> .....  | 80 |

|   |    |
|---|----|
| 3.7.5 <i>H<sub>2</sub>O<sub>2</sub> calibrations</i> .....    | 80 |
| 3.7.6 <i>Data recording and analysis</i> .....                | 81 |
| 3.8 <i>Microdialysis</i> .....                                | 81 |
| 3.9 <i>Scanning electron microscopy (SEM)</i> .....           | 82 |
| 3.10 <i>In-vivo experiments</i> .....                         | 82 |
| 3.10.1 <i>Subjects</i> .....                                  | 82 |
| 3.10.2 <i>Surgical protocol</i> .....                         | 82 |
| 3.10.3 <i>In-vivo reference and auxiliary electrode</i> ..... | 85 |
| 3.11 <i>In-vivo injections</i> .....                          | 86 |
| 3.11.1 <i>Intraperitoneal injection (i.p.)</i> .....          | 86 |
| 3.11.2 <i>Subcutaneous injection (s.c.)</i> .....             | 86 |
| 3.12 <i>NO Synthesis and UV Spectroscopy</i> .....            | 87 |
| 3.13 <i>Additional equipment</i> .....                        | 87 |
| 3.13.1 <i>Anaesthesia system</i> .....                        | 87 |
| 3.13.2 <i>Electrode wire</i> .....                            | 87 |
| 3.13.3 <i>Incubator</i> .....                                 | 87 |
| 3.13.4 <i>Microdialysis pump</i> .....                        | 87 |
| 3.13.5 <i>Microdialysis probes</i> .....                      | 87 |
| 3.13.6 <i>Microscope</i> .....                                | 87 |
| 3.13.7 <i>pH meter</i> .....                                  | 87 |
| 3.13.8 <i>Sonicator</i> .....                                 | 88 |
| 3.13.9 <i>Stereotaxic frame</i> .....                         | 88 |
| 3.13.10 <i>Vortex</i> .....                                   | 88 |
| References .....  | 89 |

#### **4. *In-vitro* characterisation of a paired catalase-based H<sub>2</sub>O<sub>2</sub> biosensor**

---

|  |    |
|--|----|
| 4.1 <i>Introduction</i> .....  | 91 |
| 4.2 <i>Experimental</i> .....  | 92 |
| 4.3 <i>Sensitivity of the H<sub>2</sub>O<sub>2</sub> sensor in-vitro</i> ..... | 93 |
| 4.3.1 <i>Pt<sub>c</sub></i> .....  | 93 |
| 4.3.2 <i>Pt<sub>c</sub>/Nafion<sup>®</sup></i> .....                           | 94 |
| 4.3.3 <i>Pt<sub>c</sub>/PPD</i> .....  | 96 |
| 4.3.4 <i>Pt<sub>c</sub>/Nafion<sup>®</sup>/PPD</i> .....                       | 98 |

|  |     |
|--|-----|
| 4.3.5 <i>Pt<sub>c</sub>/PPD/Cat-Ga</i> .....   | 100 |
| 4.3.6 <i>Pt<sub>c</sub>/Nafion<sup>®</sup>/PPD/Cat-Ga</i> .....                          | 102 |
| 4.4 <b>H<sub>2</sub>O<sub>2</sub> sensor sensitivity summary</b> .....                   | 104 |
| 4.5 <b>Selectivity of the H<sub>2</sub>O<sub>2</sub> sensor <i>in-vitro</i></b> .....    | 106 |
| 4.5.1 <i>Pt<sub>c</sub></i> .....  | 106 |
| 4.5.2 <i>Pt<sub>c</sub>/Nafion<sup>®</sup></i> .....                                     | 107 |
| 4.5.3 <i>Pt<sub>c</sub>/PPD</i> .....  | 108 |
| 4.5.4 <i>Pt<sub>c</sub>/Nafion<sup>®</sup>/PPD</i> .....                                 | 110 |
| 4.5.5 <i>Pt<sub>c</sub>/PPD/Cat-Ga</i> .....   | 111 |
| 4.5.6 <i>Pt<sub>c</sub>/Naf/PPD/Cat-Ga</i> .....   | 113 |
| 4.6. <b>H<sub>2</sub>O<sub>2</sub> sensor selectivity summary</b> .....                  | 114 |
| 4.7. <b>Paired H<sub>2</sub>O<sub>2</sub> sensor sensitivity</b> .....                   | 116 |
| 4.7.1 <i>Limit of detection</i> .....  | 118 |
| 4.7.2 <i>Response time</i> .....   | 118 |
| 4.8. <b>Paired H<sub>2</sub>O<sub>2</sub> sensor selectivity</b> .....                   | 119 |
| 4.8.1 <i>Paired H<sub>2</sub>O<sub>2</sub> sensor AA selectivity</i> .....               | 121 |
| 4.8.2 <i>H<sub>2</sub>O<sub>2</sub> sensitivity in the presence of AA</i> .....          | 122 |
| 4.8.3 <i>H<sub>2</sub>O<sub>2</sub> sensitivity in the presence of DA</i> .....          | 123 |
| 4.8.4 <i>H<sub>2</sub>O<sub>2</sub> sensitivity in aCSF</i> .....                        | 124 |
| 4.9 <b>Paired H<sub>2</sub>O<sub>2</sub> sensor stability and biocompatibility</b> ..... | 126 |
| 4.10 <i>Blank stability (long-term)</i> .....  | 127 |
| 4.11 <i>Cat stability (long-term)</i> .....  | 130 |
| 4.12 <i>Blank biocompatibility (BSA)</i> .....   | 133 |
| 4.13 <i>Cat biocompatibility (BSA)</i> .....   | 136 |
| 4.14 <i>Blank biocompatibility (PEA)</i> .....   | 141 |
| 4.15 <i>Cat biocompatibility (PEA)</i> .....   | 144 |
| 4.16 <i>Blank biocompatibility (BT)</i> .....  | 148 |
| 4.17 <i>Cat biocompatibility (BT)</i> .....  | 152 |
| 4.18 <b>Blank stability and biocompatibility summary</b> .....                           | 157 |
| 4.19 <b>Cat stability and biocompatibility summary</b> .....                             | 159 |
| 4.20 <b>Post <i>in-vivo</i> stability</b> .....  | 161 |
| 4.21 <b>Conclusion</b> .....   | 166 |
| <b>References</b> .....  | 169 |

## 5. *In-vivo* characterisation of a paired catalase-based H<sub>2</sub>O<sub>2</sub> biosensor

---

|   |     |
|---|-----|
| 5.1 Introduction.....   | 173 |
| 5.2 Experimental .....  | 174 |
| 5.3 Local and systemic control experiments (freely-moving).....   | 176 |
| 5.3.1 Local <i>a</i> CSF Administration.....  | 176 |
| 5.3.2 Systemic (s.c.) Saline Administration.....  | 179 |
| 5.4 Local H <sub>2</sub> O <sub>2</sub> Administration (freely-moving).....                                       | 181 |
| 5.4.1 25 $\mu$ M H <sub>2</sub> O <sub>2</sub> .....  | 182 |
| 5.4.2 100 $\mu$ M H <sub>2</sub> O <sub>2</sub> .....   | 184 |
| 5.4.3 200 $\mu$ M H <sub>2</sub> O <sub>2</sub> .....   | 186 |
| 5.4.4 500 $\mu$ M H <sub>2</sub> O <sub>2</sub> .....   | 188 |
| 5.4.5 1000 $\mu$ M H <sub>2</sub> O <sub>2</sub> .....  | 190 |
| 5.5 Local H <sub>2</sub> O <sub>2</sub> administration summary (freely-moving) .....                              | 193 |
| 5.5.1 Paired H <sub>2</sub> O <sub>2</sub> sensor summary (freely-moving).....                                    | 193 |
| 5.5.2 Blank sensor summary (freely-moving) .....  | 195 |
| 5.5.3 Cat sensor summary (freely-moving) .....  | 197 |
| 5.6 Local sodium azide (SA) administration.....   | 198 |
| 5.6.1 Systemic SA administration .....  | 200 |
| 5.6.2 The effect of systemic SA administration on the local administration of H <sub>2</sub> O <sub>2</sub> ..... | 201 |
| 5.7 Local mercaptosuccinate (MCS) administration .....  | 202 |
| 5.8 Local ascorbic acid (AA) administration .....   | 204 |
| 5.8.1 Systemic AA administration.....   | 206 |
| 5.9 Local H <sub>2</sub> O <sub>2</sub> administration (acute preparation).....                                   | 209 |
| 5.9.1 <i>a</i> CSF .....  | 209 |
| 5.9.2 50 $\mu$ M H <sub>2</sub> O <sub>2</sub> .....  | 213 |
| 5.9.3 100 $\mu$ M H <sub>2</sub> O <sub>2</sub> .....   | 215 |
| 5.9.4 200 $\mu$ M H <sub>2</sub> O <sub>2</sub> .....   | 218 |
| 5.9.5 500 $\mu$ M H <sub>2</sub> O <sub>2</sub> .....   | 220 |
| 5.9.6 1000 $\mu$ M H <sub>2</sub> O <sub>2</sub> .....  | 222 |
| 5.9.7 10 mM H <sub>2</sub> O <sub>2</sub> .....   | 224 |
| 5.9.8 100 mM H <sub>2</sub> O <sub>2</sub> .....  | 226 |
| 5.10 Local H <sub>2</sub> O <sub>2</sub> administration summary (acute preparation).....                          | 228 |

|  |     |
|--|-----|
| 5.10.1 Paired H <sub>2</sub> O <sub>2</sub> sensor summary ( <i>acute</i> )..... | 228 |
| 5.10.2 Blank sensor summary ( <i>acute</i> ) .....                               | 231 |
| 5.10.3 Cat sensor summary ( <i>acute</i> ) .....                                 | 232 |
| 5.11 Baseline stability ( <i>freely-moving</i> ) .....                           | 234 |
| 5.11.2 Blank sensor baseline stability ( <i>freely-moving</i> ) .....            | 236 |
| 5.11.3 Cat sensor baseline stability ( <i>freely-moving</i> ) .....              | 237 |
| 5.12 Baseline comparison ( <i>acute and freely-moving</i> ).....                 | 239 |
| 5.13 Conclusion .....  | 241 |
| References.....  | 245 |

## **6. *In-vitro* and *in-vivo* characterisation of a nitric oxide sensor**

---

|   |     |
|---|-----|
| 6.1 Introduction.....   | 249 |
| 6.2 Experimental .....  | 251 |
| 6.3 <i>In-vitro</i> characterisation of the NO sensor.....                    | 252 |
| 6.4 Sensitivity of the NO sensor <i>in-vitro</i> .....                        | 253 |
| 6.4.2 Limit of detection of the NO sensor <i>in-vitro</i> .....               | 254 |
| 6.4.3 Response time of the NO sensor <i>in-vitro</i> .....                    | 255 |
| 6.5 Selectivity of the NO sensor <i>in-vitro</i> .....                        | 256 |
| 6.5.1 AA Selectivity of the NO sensor.....                                    | 257 |
| 6.5.2 AA <i>Pt<sub>d</sub></i> .....  | 258 |
| 6.5.3 AA response comparison.....   | 259 |
| 6.6 <i>In-Vitro</i> Sensitivity and Selectivity of the NO sensor summary..... | 259 |
| 6.7 Post <i>in-vivo</i> stability .....                                       | 260 |
| 6.7.1 Post <i>in-vivo</i> NO sensitivity .....                                | 261 |
| 6.7.2 Post <i>in-vivo</i> AA selectivity .....                                | 264 |
| 6.8 <i>In-vivo</i> characterisation of the NO sensor.....                     | 265 |
| 6.8.1 Systemic administration of saline ( <i>i.p.</i> ) .....                 | 266 |
| 6.8.2 Systemic administration of L-arginine .....                             | 267 |
| 6.8.2.1 Systemic administration of L-arginine vs. saline .....                | 269 |
| 6.8.3 Systemic administration of L-NAME .....                                 | 270 |
| 6.8.3.1 Systemic administration of L-NAME vs. saline .....                    | 271 |
| 6.8.4 Systemic administration of sodium ascorbate .....                       | 272 |
| 6.8.4.1 Systemic administration of Sodium ascorbate vs. saline .....          | 273 |

|  |     |
|--|-----|
| 6.8.5 Baseline stability of the NO sensor..... | 274 |
| 6.9 Conclusion .....                           | 277 |
| References.....                                | 281 |

## **7. The detection of nitric oxide in an animal model of autism**

---

|   |     |
|---|-----|
| 7.1 Introduction.....   | 285 |
| 7.2 Experimental .....  | 288 |
| 7.3 Systemic control experiments (s.c.) .....                       | 289 |
| 7.3.1 Systemic (s.c.) saline administration (NA) .....              | 289 |
| 7.4 Propionic acid (PPA) administration dose response.....          | 291 |
| 7.5 Chronic Propionic acid (PPA) administration (NA).....           | 294 |
| 7.5.1 24 hr Control NO data (NA) .....                              | 294 |
| 7.5.2 Chronic PPA administration (NA) day 1-6 .....                 | 296 |
| 7.5.3 Chronic PPA administration (NA) day 7-12 .....                | 301 |
| 7.5.4 AUC comparison chronic PPA administration (NA) day 1-12 ..... | 306 |
| 7.6 Chronic Propionic acid (PPA) administration (DH).....           | 308 |
| 7.6.1 24 hr Control NO data (DH).....                               | 309 |
| 7.6.2 Chronic PPA administration (DH) day 1-6.....                  | 311 |
| 7.6.3 Chronic PPA administration (DH) day 7-12.....                 | 315 |
| 7.6.4 AUC comparison chronic PPA administration (DH) day 1-14 ..... | 320 |
| 7.7 Regional comparison (Chronic PPA administration) DH and NA..... | 323 |
| 7.8 Behavioural observations .....                                  | 327 |
| 7.9 Conclusion .....  | 329 |
| References.....   | 333 |

## **8. The detection of NO and H<sub>2</sub>O<sub>2</sub> in an animal model of Parkinson's disease**

---

|  |     |
|--|-----|
| 8.1 Introduction.....                              | 339 |
| 8.2 Experimental .....                             | 344 |
| 8.3 Systemic control experiments .....             | 345 |
| 8.4. Chronic Paraquat (PQ) dose response (NA)..... | 347 |

|   |     |
|---|-----|
| <b>8.4.1 Control NO data (NA)</b> .....   | 347 |
| <b>8.4.2 PQ dose response (NO)</b> .....  | 348 |
| <b>8.4.3 Preliminary PQ dose response (NO and H<sub>2</sub>O<sub>2</sub>)</b> .....         | 354 |
| <b>8.5 PQ additive dose response (NO)</b> .....   | 356 |
| <b>8.6 PQ repetitive dose response (NO)</b> .....   | 358 |
| <b>8.7 Preliminary PQ ascending dose response (NO and H<sub>2</sub>O<sub>2</sub>)</b> ..... | 362 |
| <b>8.7 Behavioural observations</b> .....   | 363 |
| <b>8.8 PQ mediated toxicity <i>in-vivo</i></b> .....  | 365 |
| <b>8.9 Conclusion</b> .....   | 368 |
| <b>References</b> .....   | 374 |

## **9. General Conclusions**

---

|   |     |
|---|-----|
| <b>References</b> .....                     | 391 |
| <b>Publications &amp; Conferences</b> ..... | 397 |

*Declaration*

This thesis has not been submitted before, in whole or in part, to this or any other University for any degree, and except where otherwise stated, is the original work of the author.

Signed: \_\_\_\_\_

Saidhbhe O’Riordan

*To Labhaoise, Aoibheann and Saoirse*

## *Acknowledgements*

Firstly I would like to thank my supervisors Prof. John Lowry and Dr. Niall Finnerty. John, thank you for the wonderful opportunity you have given me. I am very grateful for all of your patience, advice and encouragement. Niall thank you very much for all of your help and direction. Your enthusiasm for our line of work and knowledge of our research area is inspirational and your guidance and constant support has been very important to me. I have been blessed with wonderful supervision which has helped me with the whole process and I am very appreciative for this.

Thank you to my family without your love and support none of this would have been possible. Thank you dad for your 'keep going' attitude, for your belief in me and for everything you have helped me to achieve. Thank you to my sister Dee, your constant support and advice are extremely important to me. Thank you to my brother Enda for looking out for me and for your words of encouragement. Thank you big brother Niall for your genuine interest in the work and your support. Thank you to my lovely nieces Labhaoise, Aoibheann and the latest addition Saoirse (we await your return from Oz), you girls are very important to me and have been a wonderful distraction to me during this process and this thesis is dedicated to you all. Thank you to Donal and Eimear, cheers for looking after the spouses and the nieces.

Thank you very much to Grace and Aisling, for all of your support, for always being good to me and for never failing to cheer me up. Thank you Sharon and Dee, for looking after me, feeding me, for doing the washing and for the occasional trips out.

Thank you to Prof. Peter Wellstead and Dr. Mathieu Cloutier, the research surrounding Parkinson's disease has inspired me a great deal. Thank you to all the people in our research group that I have worked with over the years. Thank you to Dr. Fiachra Bolger, for your willingness to answer questions and help with the work. Thank you to Dr. John Kealy, Emma, Ken, Rachel, Keeley, Andrea and Michelle. I wish you all the very best with everything and thank you very much. Thank you for the constant brew cycle, breakfast/lunch/dinner days, jaunts around campus, general craic, ventures to the roost and for all of your support particularly during the write-up stage when it was especially needed.

Thank you to all the staff, postgrads and postdocs in the chemistry department that I have had the pleasure of working with over the years. I have been lucky to work with a wonderful group of people. There are a lot of people who have helped me and kept me going along the way and anyone who I haven't mentioned I will thank you in person.

## *Abbreviations*

|                                   |   |
|-----------------------------------|---|
| <b>AA</b>                         | Ascorbic acid                               |
| <b>aCSF</b>                       | Artificial cerebrospinal fluid              |
| <b>ASDs</b>                       | Autism spectrum disorders                   |
| <b>ATP</b>                        | Adenosine triphosphate                      |
| <b>BBB</b>                        | Blood brain barrier                         |
| <b>BSA</b>                        | Bovine serum albumin                        |
| <b>BT</b>                         | Brain tissue                                |
| <b>CNS</b>                        | Central nervous system                      |
| <b>CPA</b>                        | Constant Potential Amperometry              |
| <b>DA</b>                         | Dopamine                                    |
| <b>DH</b>                         | Dorsal hippocampus                          |
| <b>ECF</b>                        | Extracellular fluid                         |
| <b>ETC</b>                        | Electron transport chain                    |
| <b>GPx</b>                        | Glutathione peroxidase                      |
| <b>GSH</b>                        | Glutathione                                 |
| <b>H<sub>2</sub>O<sub>2</sub></b> | Hydrogen peroxide                           |
| <b>I.P.</b>                       | Intraperitoneal injection                   |
| <b>IVV</b>                        | <i>In-vivo</i> voltammetry                  |
| <b>L.I.V.E</b>                    | Long Term <i>In-Vivo</i> Electrochemistry   |
| <b>L-NAME</b>                     | N (G)-nitro-L-arginine methyl ester         |
| <b>MCS</b>                        | Mercaptosuccinate                           |
| <b>MD</b>                         | Microdialysis                               |
| <b>MTdys</b>                      | Mitochondrial dysfunction                   |
| <b>MPTP</b>                       | 1,2,3,6,-methyl-phenyl-tetrahydropyridine   |
| <b>NA</b>                         | Nucleus accumbens                           |
| <b>NADH</b>                       | Nicotinamide adenine dinucleotide           |
| <b>NADPH</b>                      | Nicotinamide adenine dinucleotide phosphate |
| <b>NMDA</b>                       | N-methyl-D-aspartate                        |
| <b>NO</b>                         | Nitric oxide                                |
| <b>NOS</b>                        | Nitric oxide synthase                       |
| <b>eNOS</b>                       | endothelial NOS                             |
| <b>iNOS</b>                       | inducible NOS                               |
| <b>LOD</b>                        | Limit of detection                          |
| <b>nNOS</b>                       | neuronal NOS                                |
| <b>NT(s)</b>                      | Neurotransmitter(s)                         |
| <b>O<sub>2</sub></b>              | Oxygen                                      |
| <b>O<sub>2</sub><sup>·-</sup></b> | Superoxide                                  |
| <b><i>o</i>-PD</b>                | <i>Ortho</i> -phenylenediamine              |
| <b>ONOO<sup>-</sup></b>           | Peroxynitrite                               |
| <b>PBS</b>                        | Phosphate buffered saline                   |
| <b>PD</b>                         | Parkinson's disease                         |
| <b>PPD</b>                        | Poly- <i>o</i> -phenylenediamine            |
| <b>PEA</b>                        | L- $\alpha$ -phosphatidylethanolamine       |
| <b>PPA</b>                        | Propionic acid                              |

|              |   |
|--------------|---|
| <b>PPD</b>   | Poly- <i>o</i> -phenylenediamine              |
| <b>PQ</b>    | Paraquat (methyl viologen dichloride hydrate) |
| <b>Pt</b>    | Platinum                                      |
| <b>RD</b>    | Retrodialysis                                 |
| <b>RNS</b>   | Reactive nitrogen species                     |
| <b>ROS</b>   | Reactive oxygen species                       |
| <b>SA</b>    | Sodium azide                                  |
| <b>S.C.</b>  | Subcutaneous injection                        |
| <b>SCE</b>   | Saturated calomel electrode                   |
| <b>SEM</b>   | Standard error mean                           |
| <b>S.E.M</b> | Scanning Electron Microscopy                  |
| <b>Snc</b>   | Substantia nigra pars compacta                |
| <b>SOD</b>   | Superoxide dismutase                          |
| <b>UV</b>    | Ultra-violet (spectroscopy)                   |
| <b>VTA</b>   | Ventral tegmental area                        |

## *Abstract*

The aim of this thesis is to further demonstrate the electrochemical detection of nitric oxide (NO) and hydrogen peroxide (H<sub>2</sub>O<sub>2</sub>) *in-vitro*, to advance the previously demonstrated detection of brain NO and to demonstrate the novel *in-vivo* detection of H<sub>2</sub>O<sub>2</sub> using a paired catalase-based biosensor.

We have recently successfully demonstrated the real-time detection of brain NO using a previously characterised Nafion<sup>®</sup>-modified platinum (Pt) electrochemical sensor. Additionally, the preliminary *in-vitro* development of a paired catalase based Pt sensor for the purpose of H<sub>2</sub>O<sub>2</sub> detection in the physiological environment has previously been reported by our research group.

A validation of the previously reported *in-vitro* characteristics of the NO sensor with the inclusion of novel post *in-vivo* stability attributes is presented in this thesis (see Chapter 6). Also, the suitable functionality of the NO sensor in the neuronal environment as has been published recently is supported in Chapter 6.

A verification of the previously reported *in-vitro* attributes of the paired catalase based H<sub>2</sub>O<sub>2</sub> sensor is shown in Chapter 4. Additionally, advancements to the initial *in-vitro* characterisation of the paired H<sub>2</sub>O<sub>2</sub> sensor are described in Chapter 4. The previously unreported real-time detection of brain H<sub>2</sub>O<sub>2</sub> in freely-moving animals is presented in Chapter 5.

The main focus of this thesis is the detection of NO and H<sub>2</sub>O<sub>2</sub> as oxidative/nitrosative stress markers in neurological disease and dysfunction. As such the role of oxidative/nitrosative stress in Parkinson's disease (PD) and autism spectrum disorders (ASDs) is investigated in this thesis. The novel detection of NO in a propionic acid (PPA) induced animal model of ASDs is presented in Chapter 7. The electrochemical detection of NO and the preliminary dual detection of NO and H<sub>2</sub>O<sub>2</sub> in a paraquat (PQ) mediated model of PD is presented in Chapter 8. The specific focus of these investigations is to elucidate the role of oxidative/nitrosative stress in the etiology and pathophysiology of PD and ASDs.

---

# **1. Introduction**

---

## 1.1 Neurotransmission

The reciprocal interplay between the external environment and the processes which determine brain function are principally governed by electrical and chemical pathways inherent to the neuronal environment. These endogenous pathways map the intricate processes which determine behaviour, emotion, memory and thought itself.

The primary cell types present in the brain are nerve cells and glial cells. The brain consists of billions of nerve cells or neurons which can interact with other neurons via thousands of connections. Neurons are essentially the basic functioning unit of the brain and glial cells provide metabolic support and insulation. Axons and dendrites extend from the neuron into projections which facilitate the transmission of signals in the brain.

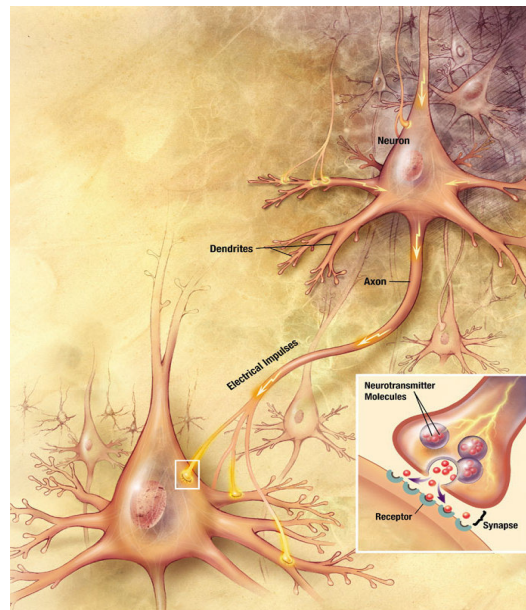


**Fig 1.1 Neuronal signal transmission.** ([https://sitn.hms.harvard.edu/sitnflash\\_wp/wp-content/uploads/2011/01/Chemical\\_synapse\\_schema.jpg](https://sitn.hms.harvard.edu/sitnflash_wp/wp-content/uploads/2011/01/Chemical_synapse_schema.jpg)).

The resting state of a neuron is maintained by a transmembrane concentration gradient of ions. Neuronal activation is triggered by a stimulus which leads to a change in resting membrane potential due to ionic influxes ( $\text{Na}^+$ ,  $\text{K}^+$ ) which results in the propagation of an electrical action potential. This action potential stimulates the release of neurotransmitters (NTs) into the synapse which is the cleft between nerve terminals and the dendrites of other neurons.

The release of NTs facilitates the communication between the pre and post synaptic cell via various receptors which leads to excitatory or inhibitory processes. NTs and their metabolites may then overflow from the synapse into the extracellular fluid (ECF). These processes may take place in the brain over sub-second time scales which leads to reflex reactions and additionally extended processes involved in the formation of memories which last decades. The concentration of NTs and their metabolites in the ECF is regulated by their release rate into the cerebrospinal fluid or transmission across the blood brain barrier (BBB).

## 1.2 Neurochemical analysis

Understanding the mechanisms underlying the function of the central nervous system (CNS) is of paramount importance in modern day science. A variety of techniques have been developed in recent years which facilitate the analysis of brain function. These include non-invasive techniques such as functional magnetic resonance imaging (fMRI) (Matthews *et al.*, 2006), positron emission tomography (PET) (Shibasaki, 2008) and electrophysiological techniques include electroencephalography (EEG) (Kenemans & Kahkonen, 2011).

Invasive techniques are also available such as microdialysis (MD) (Lonnroth *et al.*, 1987; Fillenz, 2005) and *in-vivo* voltammetry (IVV); including amperometric and voltammetric techniques (Lowry *et al.*, 2006; Borland & Michael, 2007). Together they provide improved spatial and temporal resolution and in the case of IVV the real-time detection of chemical changes in the ECF. In addition to animal studies the application of MD in the clinical environment has also been shown to enable the detection of target species in the human brain (Ungerstedt & Rostami, 2004). The detection of target intercellular chemical messengers (neuromediators) in the brain may provide an insight into the processes behind numerous neurodegenerative diseases and disorders in addition to normal cognitive function. Many neurodegenerative conditions are not fully understood and the application of these techniques may yield previously undetermined information required to develop novel therapeutic strategies.

The implantation of electrochemical sensors into the brain allows the detection of chemical changes in the ECF. Monitoring neuromediators by IVV in the ECF is complicated by the nature of endogenous factors. A variety of NTs in the ECF are not electroactive, many species oxidise at similar potentials and the brain is a complex environment which consists of lipids and proteins which may interfere with the response of the implanted sensor. Since the pioneering work conducted by Clark *et al.* (Clark *et al.*, 1958) and Adams *et al.* (Kissinger *et al.*, 1973; Adams, 1990), which led to the development of IVV; various advancements have been made to the technique to overcome these inherent technical obstacles.

Various strategies have been employed in order to improve the sensitivity, selectivity and stability of implanted electrochemical sensors. The inclusion of a biological recognition unit, typically an enzyme into the construction of the sensor facilitates the detection of non-electroactive species (Hu *et al.*, 1994; Lowry *et al.*, 1994; Garguilo & Michael, 1996; Ryan *et al.*, 1997). The application of a suitable potential and the modification of the electrode surface with various permselective membranes has also led to an improvement in the selectivity and stability of the IVV technique (McAteer & O'Neill, 1996; Lowry *et al.*, 1998a; Brown *et al.*, 2009).

As discussed by Lowry *et al.* IVV may be used in conjunction with processes that lead to a change in concentration of NTs in the ECF including depolarisation of the nerve terminal (Lowry *et al.*, 2006). This may be achieved via electrical stimulation, behavioural activation and the application of substances which are known to lead to this process such as  $K^+$  and glutamate which activate receptors linked to  $Na^+$  channels. Additionally, pharmacological manipulations may be utilised such as inhibition of neurotransmitter (NT) synthesis (e.g.  $\alpha$ -methyl-*p*-tyrosine), displacement of NT from the nerve terminal (e.g. amphetamine), inhibition of NT metabolising enzymes (e.g. pargyline) and substances which block NT uptake (e.g. cocaine). Together these processes lead to a change in NT concentration in the ECF which may be detected by the implanted electrochemical sensor (Lowry *et al.*, 2006).

The main focus of this thesis is to establish the detection of hydrogen peroxide ( $\text{H}_2\text{O}_2$ ) and nitric oxide (NO) in the *in-vitro* environment and to demonstrate the detection of these species in the ECF of the brain.

Glutamate and dopamine are amongst others, examples of the most important NTs present in the brain. Glutamate has been implicated in processes such as learning and memory (Lamprecht & LeDoux, 2004). Dopamine is responsible for vital neurological processes such as reward and motivation (Wise, 2004). Additionally a dysfunction in glutamatergic and dopaminergic pathways has been implicated in a variety of neurodegenerative diseases and disorders such as schizophrenia (Goff & Coyle, 2001) and Parkinson's disease (Lotharius & Brundin, 2002). A number of chemical messengers have been shown to modulate glutamatergic and dopaminergic pathways including NO (see Section 1.4) (Fejgin *et al.*, 2009; Palsson *et al.*, 2009) and  $\text{H}_2\text{O}_2$  (see Section 1.3) (Avshalumov *et al.*, 2003; Bao *et al.*, 2009).

### 1.3 Hydrogen peroxide ( $\text{H}_2\text{O}_2$ )

$\text{H}_2\text{O}_2$  has in recent years been indicated to act as a neuromodulator (Rice, 2011) and as a signalling molecule (Stone & Yang, 2006). Specifically the synaptic release of dopamine (DA) has been shown to be regulated by  $\text{H}_2\text{O}_2$  (Rice, 2011). The effect of exogenously applied and endogenously altered  $\text{H}_2\text{O}_2$  via various inhibitors/inducers on the evoked production of DA in *ex-vivo* brain slices has been examined (Avshalumov *et al.*, 2003; Bao *et al.*, 2009). Rice *et al.* have demonstrated that endogenous  $\text{H}_2\text{O}_2$  modulates DA release by activation of  $\text{K}^+$  sensitive adenosine triphosphate (ATP) channels in *ex-vivo* striatal and substantia nigra neurons (Rice, 2011).

$\text{H}_2\text{O}_2$  is neutral and membrane permeable and it is also a relatively stable molecule which makes it highly suitable as a diffusible signalling molecule (Maier & Chan, 2002; Rice, 2011). The primary source of  $\text{H}_2\text{O}_2$  in the brain is mitochondrial respiration.  $\text{H}_2\text{O}_2$  is produced through the catalytic action of superoxide dismutase (SOD) and additionally by the considerably slower process of spontaneous dismutation (see Section 2.10.2).  $\text{H}_2\text{O}_2$  production in the brain is a tightly regulated process as when present at high concentrations  $\text{H}_2\text{O}_2$  can initiate neurotoxic events (Barnham *et al.*, 2004). The main

source of  $\text{H}_2\text{O}_2$  regulation is enzymatic removal by catalase and glutathione peroxidase (GPx). A detailed description of the regulation of  $\text{H}_2\text{O}_2$  production in the brain is described in Section 2.10.1.  $\text{H}_2\text{O}_2$  is an electroactive species and it can be detected at +700 mV vs. SCE by oxidation at platinum (Pt) surfaces.  $\text{H}_2\text{O}_2$  is oxidised at a diffusion controlled rate which yields a current response that is linear and directly proportional to the concentration of  $\text{H}_2\text{O}_2$  (Lowry *et al.*, 1994; O'Brien *et al.*, 2007).

At present a limited amount of analytical techniques exist to enable the detection of  $\text{H}_2\text{O}_2$  in the physiological environment. To date microdialysis (MD) is the main method of  $\text{H}_2\text{O}_2$  detection *in-vivo* (Lei *et al.*, 1997, 1998; Chen *et al.*, 2012). However, MD suffers from poor temporal and spatial resolution and other significant drawbacks as discussed in Section 2.9. Electrochemical methods are highly advantageous relative to the MD technique as they provide long-term real-time measurements of neurochemical species of interest. The detection of  $\text{H}_2\text{O}_2$  has previously been reported in the anaesthetised animal (Kulagina & Michael, 2003). However, the sensor described in this publication requires a mediator and an additional method to remove interference from AA; which is not necessary with the dual  $\text{H}_2\text{O}_2$  sensor presented in this thesis.

Research previously conducted by O'Brien *et al.* has demonstrated a highly sensitive and selective dual catalase-based sensor for the detection of  $\text{H}_2\text{O}_2$  in the *in-vitro* environment (O'Brien *et al.*, 2007). The novel electrochemical detection of  $\text{H}_2\text{O}_2$  in the freely-moving animal is presented in this thesis.

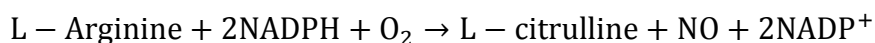
$\text{H}_2\text{O}_2$  is implicated in a variety of normal cellular functions and also in the pathophysiology of certain disease states (Andersen, 2004; Barnham *et al.*, 2004; Rhee, 2006; Rice, 2011). A dysfunction in  $\text{H}_2\text{O}_2$ /reactive oxygen species (ROS) regulation, which subsequently leads to the overproduction of  $\text{H}_2\text{O}_2$ /ROS, has been implicated in a number of neurodegenerative diseases such as Parkinson's and Alzheimer's disease (Valko *et al.*, 2007; Melo *et al.*, 2011). Enzymatically produced  $\text{H}_2\text{O}_2$  by electrochemical biosensors is used to measure non-electroactive substrates such as glucose (Lowry *et al.*, 1998b), choline (Garguilo & Michael, 1996) and glutamate (Hu *et al.*, 1994; Lowry *et al.*, 1998c) in the brain.

H<sub>2</sub>O<sub>2</sub> is implicated in a number of neurochemical processes and electrochemical detection methods, therefore the real-time detection of H<sub>2</sub>O<sub>2</sub> *in-vivo* would provide a significant contribution to the field of neurochemistry.

#### 1.4 Nitric oxide (NO)

The physiological role of nitric oxide (NO) as the endothelium derived relaxing factor (EDRF) was discovered in the late 1980's (Ignarro *et al.*, 1987). This research demonstrated the involvement of NO in the process of vasodilation and regulation of blood pressure and since then much interest has developed around the role of NO in the body.

NO is a radical species generated in the physiological environment from three main NO synthase enzymes (NOS). These consist of inducible NOS (iNOS), endothelial NOS (eNOS) and neuronal NOS (nNOS) (Kiechle & Malinski, 1993; Bruckdorfer, 2005; Guix *et al.*, 2005). The type of NO produced is dependent on the source of NOS in the body. NO is produced from its precursor L-arginine, in the presence of numerous co-factors including NOS, BH<sub>4</sub> (tetrahydrobiopterin), FMN (flavin mononucleotide), FAD (flavin adenine dinucleotide), haem iron and Ca<sup>2+</sup>/calmodulin as shown in Equation 1.1.



(1.1)

L-Arginine reacts with the co-substrates molecular oxygen (O<sub>2</sub>) and nicotinic adenine dinucleotide phosphate (NADPH); which provides the electrons necessary for the reaction to proceed. The nitrogen of NO is derived from the guanidine nitrogen atoms of L-arginine and the oxygen from O<sub>2</sub>. This reaction produces NO and L-citrulline in equimolar quantities. L-citrulline can then be converted back to L-arginine as part of the normal nitrogen metabolism of the body (Alderton *et al.*, 2001; Bruckdorfer, 2005).

NOS contains an oxygenase domain for binding of L-arginine, haem and BH<sub>4</sub> and a reductase domain facilitates FAD, FMN redox carriers and NADPH electron transfer. Both domains are linked through a binding site for calmodulin. The production of NO

from the constitutive forms of NOS (eNOS and nNOS) is  $\text{Ca}^{2+}$  dependent. The inducible form of NO produced from iNOS is released from macrophages and is produced in a  $\text{Ca}^{2+}$  independent manner. Following binding with calmodulin NO is produced from the catalytic oxidation of L-arginine to citrulline which requires  $\text{O}_2$  and NADPH as co-factors (Alderton *et al.*, 2001; Bruckdorfer, 2005).

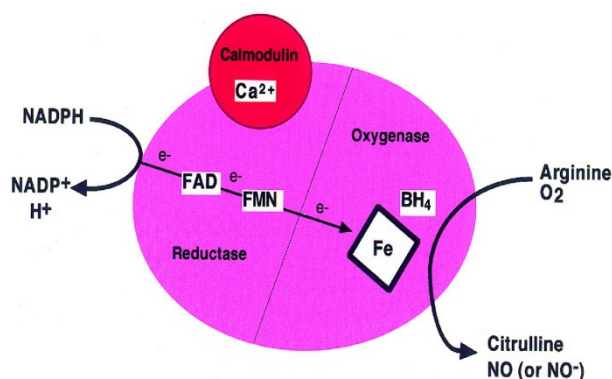


**Fig 1.1** Production of NO by NOS (<http://www.biochemj.org/bj/357/0593/bj3570593a01.jpg>).

The global function of NO in the physiological environment has been studied in diverse processes such as the immune response (Bogdan *et al.*, 2000), anti-microbial activity (Fang, 2004) and penile erection (Mas *et al.*, 2002). Of the three isoforms of NOS, nNOS is present in the most abundance in the brain. Neuronal NO has been implicated in vital neurological processes including sleep and appetite regulation (Williams *et al.*, 2002; Cavas & Navarro, 2006) synaptic plasticity, neurotransmission and learning and memory (Wass *et al.*, 2006a; Wass *et al.*, 2006b; Nugent *et al.*, 2007). Therefore the detection of NO in the CNS provides an insight into a variety of vital neurological functions.

The majority of NO analytical techniques rely on indirect detection methods, by measuring nitrite and other markers of NO production using spectroscopic methods (Hetrick & Schoenfisch, 2009). The poor sensitivity of these techniques are not suitable for the detection of NO *in-vivo*, due to the estimated short half-life (< 10s) and relatively low concentration of NO in the biological environment (Wink & Mitchell, 1998; Kelm, 1999). The selectivity of these spectroscopic methods also suffer due to interference from nitrite and nitrate from sources other than NO (Finnerty *et al.*, 2012a).

Electrochemical techniques provide the required temporal and spatial resolution which is necessary to detect NO in the physiological environment to enable long-term *in-vivo* NO recordings.

The electrochemical reduction of NO has previously been demonstrated (Meulemans, 1993; Maskus *et al.*, 1996; Liu *et al.*, 2003), as O<sub>2</sub> reduces at a similar potential to NO this technique is not suitable for *in-vivo* monitoring of NO. The electro-oxidation of NO is the most suitable monitoring technique and various modified electrode materials have been used for this purpose. They are predominantly carbon fibre (Friedemann *et al.*, 1996; Park *et al.*, 1998; Heinzen & Pollack, 2002), glassy carbon (Pallini *et al.*, 1998), and Pt electrodes (Park *et al.*, 2010; Park *et al.*, 2012).

Our research group has successfully demonstrated a highly sensitive, selective and stable NO sensor for the purpose of *in-vivo* NO monitoring (Brown & Lowry, 2003; Brown *et al.*, 2009). The previously described NO sensor exhibits the required operational characteristics i.e. a highly suitable response time and detection limit to enable the detection of NO in the physiological environment (Brown *et al.*, 2009). Furthermore the application of this NO sensor *in-vivo* for the continuous real-time detection of NO in the brain has previously been shown (Finnerty *et al.*, 2012a; Finnerty *et al.*, 2012b).

## **1.5 Oxidative stress in neurodegenerative diseases/dysfunctions**

H<sub>2</sub>O<sub>2</sub> is an example of an oxidative stress marker and the free radical species NO is an example of a nitrosative stress marker. H<sub>2</sub>O<sub>2</sub> and NO both exert beneficial and harmful effects in the neuronal environment (Calabrese *et al.*, 2007; Rice, 2011). The uncontrolled elevation of H<sub>2</sub>O<sub>2</sub> and NO levels in the brain leads to the further production of other ROS and reactive nitrogen species (RNS) and consequently the development of oxidative/nitrosative stress (see section 2.10). The level of ROS/RNS in the brain is controlled by a protective highly robust antioxidant network. The processes which lead to the production of ROS/RNS and the mechanism of action of the opposing antioxidant network which serves to maintain redox homeostasis in the brain is described in detail in Section 2.10. The role of oxidative/nitrosative stress in a range of neurodegenerative

diseases and dysfunctions such as Alzheimer's disease, amyotrophic lateral sclerosis (ALS) and Friedrich's ataxia (FD) has been extensively reviewed elsewhere (Barnham *et al.*, 2004; Melo *et al.*, 2011; Ramalingam & Kim, 2012). Section 1.6 and 1.7 will focus specifically on the role of oxidative/nitrosative stress in autism spectrum disorders (ASDs) and Parkinson's disease (PD) as studied in Chapter 7 and 8 respectively.

## **1.6 Autism spectrum disorders (ASDs)**

ASDs consist of complex related neurodevelopmental disorders which are defined by a varying degree of social impairment, difficulties with communication, repetitive behaviours and restricted interests (Rapin & Tuchman, 2008). ASDs are relatively common in that they occur in 1 in 88 children in the United States alone as determined by the U.S centre for disease control (CDC). Much focus is given to the negative aspects of ASDs as symptoms may be extremely debilitating in certain individuals depending on the severity of the condition. However, little attention is given to the positive attributes seen in certain cases of ASDs such as an enhanced memory, heightened ability in areas such as mathematics or the arts and a superior ability to concentrate (Walsh *et al.*, 2011).

Currently the relationship between the brain and the behavioural traits which are characteristic of ASDs are not fully understood. Research has indicated that ASDs have a strong genetic basis however inherited factors do not entirely explain the etiology of the condition (Folstein & Rosen-Sheidley, 2001). A variety of environmental agents have been indicated in the development of autism such as prenatal exposure to infection (Meyer *et al.*, 2011), ethanol and valproic acid (Arndt *et al.*, 2005).

A wide range of evidence has indicated that oxidative/nitrosative stress is implicated in the pathophysiology of ASDs. Increased levels of oxidative/nitrosative stress markers have been found in ASDs post mortem brain tissue preparations. Specifically the level of glutathione (GSH) one of the key antioxidant substances in the brain is reduced in ASDs individuals (Rose *et al.*, 2012). This research group indicated that the balance between GSH and its oxidised form GSSG is disrupted in ASDs individuals; which is one of the major indications of the presence of oxidative stress (see Section 2.10.1). Additionally, Rose *et al.* found an abnormally high level of 3-nitrotyrosine (3-NT) and

superoxide ( $O_2^{\cdot-}$ ) in ASDs brain tissue preparations. 3-NT is derived from NO through its production of the highly toxic secondary RNS peroxynitrite ( $ONOO^-$ ) and  $O_2^{\cdot-}$  which is the primary source of  $H_2O_2$  production in the brain (Winterbourn, 2008; Rose *et al.*, 2012). Chauhan *et al.* have also reported a decreased level of GSH in post mortem autistic brain preparations in comparison to controls (Chauhan *et al.*, 2012).

A decrease in the catalytic function of catalase one of the primary sources of  $H_2O_2$  removal in the brain and an elevated level of xanthine oxidase, which is a major source of superoxide ( $O_2^{\cdot-}$ ) production have been found in the blood of individuals with ASDs (Zoroglu *et al.*, 2004). Additionally, haematological studies conducted by Yorbik *et al.* and Sogut *et al.* have demonstrated a decreased level of antioxidant enzyme activity (Yorbik *et al.*, 2002) and an increased level of NO respectively in individuals with ASDs (Sogut *et al.*, 2003).

This combined research indicates that oxidative/nitrosative stress is highly implicated in the pathophysiology of ASDs. However, these techniques rely on the indirect detection of oxidative/nitrosative stress markers, i.e. nitrate/nitrite and the activity of ROS removal enzymes (aconitase) (Chauhan & Chauhan, 2006; Rose *et al.*, 2012). Additionally conflicting results have been reported by Yorbik *et al.* and Sogut *et al.*, between the levels of superoxide dismutase (SOD) activity in ASDs erythrocytes. Specifically Yorbik *et al.* reported a decreased level of SOD activity and Sogut *et al.* demonstrated unchanged SOD enzymatic function (Yorbik *et al.*, 2002; Sogut *et al.*, 2003). This may reflect a variation in the sensitivity of the chosen analytical technique. Also, the limited availability of post mortem ASDs brain tissue preparations restricts the application of these techniques.

The exact mechanism of possible NO production in ASDs remains to be elucidated. The role of iNOS in the expression of NO has been demonstrated in neurodegenerative disease states such as Parkinson's and Alzheimer's disease (Calabrese *et al.*, 2007). Additionally, the expression of iNOS has been implicated in the development of autism (Chauhan & Chauhan, 2006). Neuropathological investigations of post mortem autistic brain preparations have indicated the presence of activated microglia and astrocytes

(Vargas *et al.*, 2005). Cytokines produced by this process lead to an inflammatory process which is known to activate iNOS and hence elicit an increase in NO (Guix *et al.*, 2005).

The specific mechanism of oxidative/nitrosative stress development in individuals with ASDs has yet to be elucidated. It has been postulated that the development of ASDs is multifactorial and is influenced by genetic, environmental and immunological factors in addition to oxidative/nitrosative stress (Chauhan & Chauhan, 2006). The direct electrochemical detection of H<sub>2</sub>O<sub>2</sub>/NO in an animal model of ASDs would provide a major insight into the role of ROS/RNS in the etiology ASDs. The electrochemical detection of NO in an animal model of autism is demonstrated in Chapter 7 of this thesis.

Currently the core symptoms of ASDs are ameliorated with behavioural and educational interventions. The medical treatment of ASDs is directed towards cases of severe impairment by debilitating restricted and repetitive traits seen in certain ASDs cases. Risperidone and aripiprazole which are antipsychotic medications may be useful in certain cases where severe ASDs negative behavioural characteristics manifest (McPheeters *et al.*, 2011). However, these medical treatments may exhibit serious side effects which facilitate the need for novel ASDs therapeutic strategies.

## **1.7 Parkinson's disease (PD)**

Parkinson's disease (PD) is a severe progressive neurodegenerative movement disorder. PD affects approximately 1 in 100 people over the age of 65 in the USA alone. PD is clinically characterised by a resting tremor, rigidity, bradykinesia (slowness of voluntary movement), postural imbalance and gait abnormalities. Non-motor symptoms also present in PD such as neuropsychiatric symptoms and sleep abnormalities. The pathological hallmark of PD is dopamine (DA) cell degeneration in an area of the midbrain known as the substantia nigra pars compacta (SNc) leading to a loss of striatal DA. The presence of intracytoplasmic inclusions known as 'Lewy bodies' that are composed of  $\alpha$ -synuclein and parkin is characteristic of PD (Olanow & Tatton, 1999; Lotharius & Brundin, 2002; Schapira & Jenner, 2011). One hypothesised normal

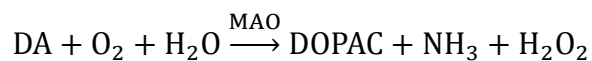
physiological role of the protein  $\alpha$ -synuclein is in the intracellular storage of DA within the presynaptic terminal (Lotharius & Brundin, 2002). Additionally,  $\alpha$ -synuclein has been postulated to play a role in synaptic plasticity (Maguire-Zeiss *et al.*, 2005).

There are various familial forms of PD which have been linked to genetic mutations in specific proteins including  $\alpha$ -synuclein and parkin (Olanow & Tatton, 1999; Lotharius & Brundin, 2002; Schapira & Jenner, 2011) which tend to affect relatively younger individuals. Parkin has been postulated to function as an intermediate in the ubiquitin pathway, controlling levels of other proteins such as  $\alpha$ -synuclein or itself by regulated degradation (Gu *et al.*). However, familial forms of PD are relatively uncommon and count for less than 10 % of all PD cases (Maguire-Zeiss *et al.*, 2005).

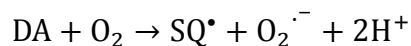
Sporadic idiopathic forms of PD which are relatively more common and have been linked to certain environmental factors including exposure to pesticides, herbicides and toxins (Olanow & Tatton, 1999; Schapira & Jenner, 2011). The toxic effect of MPTP (1,2,3,6,-methyl-phenyl-tetrahydropyridine); a by-product in the synthesis of the analog of the narcotic drug meperidine, was accidentally discovered following its distribution in 'synthetic heroin' in certain parts of California in the 1980's and following a botched meperidine analog synthesis attempt by a college student in the late 1970's (Davis *et al.*, 1979). The compound was injected intravenously by these individuals who subsequently developed severe irreversible parkinsonism (Langston *et al.*, 1983). The role of various toxins including rotenone, paraquat (PQ) and MPTP in the development of PD has previously been examined and utilised to study PD in animal models (Beal, 2001; McCormack *et al.*, 2005; McCormack *et al.*, 2006). In addition to environmental toxins other risk factors contribute to the development of PD including advancing age and head trauma (Tanner *et al.*, 2011; Wirdefeldt *et al.*, 2011).

The contribution of oxidative stress to the loss of dopaminergic neurons predominantly in the SNc which is a pathological outcome of PD is possibly as a result of DA metabolism related oxidative stress (Lotharius & Brundin, 2002; Andersen, 2004; Chinta & Andersen, 2008). Equation 1.2 to 1.6 demonstrates the enzymatic and

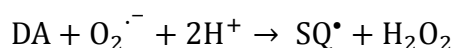
chemical metabolism of DA in the neuronal environment (Olanow & Tatton, 1999; Lotharius & Brundin, 2002).



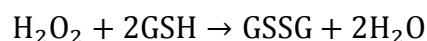
(1.2)



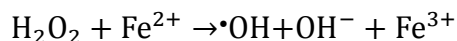
(1.3)



(1.4)



(1.5)



(1.6)

DA may be metabolised enzymatically by MAO (monoamine oxidase) into DOPAC (3, 4-dihydroxyphenylacetic acid) and may auto-oxidise to form  $\text{H}_2\text{O}_2$  as shown in Equations 1.2 to 1.4. The metabolism of DA leads to the production of other toxic species such as  $\text{O}_2^{\cdot-}$ , DA-quinone species ( $\text{SQ}^\bullet$ ) and hydroxy radicals ( $\bullet\text{OH}$ ). A deficiency in the normal enzymatic/non-enzymatic function of the antioxidant network leads to the uncontrolled production of these species which leads to oxidative/nitrosative stress (see Section 2.10).

Neuropathological investigations of post mortem PD brain preparations have indicated the presence of activated microglia (Jenner, 2003). This process is known to activate iNOS and lead to the production of NO (Guix *et al.*, 2005). In a pro-oxidant environment NO can interact directly with  $\text{O}_2^{\cdot-}$  and lead to the formation of the main secondary highly toxic RNS;  $\text{ONOO}^-$  (see Section 2.10.3).

This imbalance between ROS/RNS control and production may be accelerated due to exposure to environmental toxins, advancing age or an underlying genetic malfunction (Lotharius & Brundin, 2002; Chinta & Andersen, 2008; Wirdefeldt *et al.*, 2011). The uncontrolled production of ROS or other reactive intermediates, (e.g. RNS) leads to damage to cell structures, DNA, lipids and proteins (Valko *et al.*, 2007).

DA dependent oxidative stress has been postulated to lead to the loss of dopaminergic neurons in the SNc (Olanow & Tatton, 1999; Lotharius & Brundin, 2002). A deficiency in the catalytic function of SOD, the main source of  $O_2^{\cdot-}$  removal (see Section 2.10.1) has been demonstrated in nigral tissues of PD patients which would support this hypothesis (Chinta & Andersen, 2008).

Post mortem findings have indicated an increased level of 'free iron' (see Section 2.10.2) and a decreased level of glutathione (GSH) in PD (Olanow & Tatton, 1999; Lotharius & Brundin, 2002; Chinta & Andersen, 2008). Additionally, iron related oxidative stress has been postulated to promote  $\alpha$ -synuclein accumulation (Chinta & Andersen, 2008). These contributing factors directly demonstrate that oxidative stress is implicitly linked to the development of PD. Degeneration of dopaminergic neurons due to oxidative stress may lead to a vicious cycle of further ROS/RNS production primarily from DA oxidation and the consequential further loss of DA nerve cells.

Much contention arises around the role of oxidative stress in the process of neurodegeneration particularly in the case of PD (Jenner, 2003; Andersen, 2004; Schapira & Jenner, 2011). Much debate has arisen over whether oxidative stress is the causative factor in the development of PD or whether it is as a result of a cascade of events initiated by some other influence.

Schapira *et al.* and Jenner *et al.* amongst others have questioned the role of oxidative stress in PD due specifically to DA metabolism (Olanow & Tatton, 1999; Jenner, 2003; Schapira & Jenner, 2011). As previously stated SNc dopaminergic neurons are affected in PD whereas other DA containing neurons may be spared e.g. DA cells in the ventral tegmental area (VTA). Additionally, non dopaminergic neurons also die in PD (Schapira

& Jenner, 2011) which necessitates a discussion on the role of DA related oxidative stress in the pathology of PD.

The regional difference in neurodegeneration of dopaminergic cells in PD may be explained by a difference in the level of function of the antioxidant network. For example the normal level of activity of catalase and GPx is higher in the VTA and nucleus accumbens (NA) in comparison to the SNc (Hung & Lee, 1998). This may explain why certain dopaminergic cells are spared in the progression of PD whereas others are not.

Chen *et al.* and Rice *et al.* have demonstrated that endogenous H<sub>2</sub>O<sub>2</sub> regulates the production of somatodendritic release of DA in *ex-vivo* brain slices (Chen *et al.*, 2002; Rice, 2011). This research demonstrates that endogenous H<sub>2</sub>O<sub>2</sub> suppresses the release of DA in the SNc and striatum but has no effect on DA release in the VTA (Chen *et al.*, 2002). These findings reflect a lower production of modulatory endogenous H<sub>2</sub>O<sub>2</sub> in the VTA or stronger regulation of its production (Chen *et al.*, 2002). Therefore, impairment in the neuromodulatory role of endogenous H<sub>2</sub>O<sub>2</sub> such as that caused by DA metabolism related oxidative stress in PD, may exert a higher effect in the SNc in comparison to the VTA. This may account for the destruction of dopaminergic cells in some regions which is not as detrimental elsewhere in PD.

Neurodegeneration of non-dopaminergic cells is also a consequence of PD (Obeso *et al.*, 2010; Schapira & Jenner, 2011). Braak's staging hypothesis indicates that 'Lewy body' formation progresses once initiated in a stepwise manner throughout PD, this may explain the loss of non-dopaminergic cells in PD (Braak *et al.*, 2004). It has been postulated that oxidative stress may lead to the accumulation of  $\alpha$ -synuclein which is the main component of 'Lewy bodies' (Maguire-Zeiss *et al.*, 2005). Theoretically this suggests that oxidative stress may trigger the accumulation and regional distribution of 'Lewy body' formation in PD. However, current pathological outcomes of PD are routinely assessed by post mortem techniques. This process does not facilitate the analysis of PD progression over time, which leads to a difficulty in the assessment as to what exact mechanisms contribute to the initiation of PD and propagate the progression of the disease.

The general consensus of the etiology of PD is of a multifactorial disorder influenced by genetics, environmental factors (including various toxins), advancing age and oxidative stress (Olanow & Tatton, 1999; Lotharius & Brundin, 2002; Schapira & Jenner, 2011). Various animal models of PD exist (Beal, 2001), it may be possible to determine the role of oxidative stress as a cause or a consequence of PD through the use of electrochemical methods in conjunction with an animal model of PD. The real-time detection of NO/H<sub>2</sub>O<sub>2</sub> in an animal model of PD may facilitate a further understanding of PD progression and etiology. Therefore this strategy may facilitate new therapeutic advances. The detection of NO and the preliminary detection of H<sub>2</sub>O<sub>2</sub> in an animal model of PD is presented in Chapter 8.

### **1.9 Mitochondrial dysfunction (MTdys) in PD and ASDs**

Mitochondria are the site of many vital biochemical pathways which maintain normal cellular function (Calabrese *et al.*, 2001). Mitochondria produce energy in the form of ATP via the process of oxidative phosphorylation. Mitochondria play a central role in the process of cell survival and cell death via apoptosis and necrosis. Inherited or acquired mitochondrial DNA (mtDNA) mutations impair the function of the electron transport chain (ETC). Dysfunction of mitochondrial energy metabolism leads to reduced ATP production, disruption in Ca<sup>2+</sup> homeostasis, and generates ROS/RNS such as O<sub>2</sub><sup>-</sup>, H<sub>2</sub>O<sub>2</sub>, <sup>•</sup>OH and ONOO<sup>-</sup> (Lin & Beal, 2006).

Due to the high energy demand of the brain the impact of mitochondrial impairment is particularly significant in the neuronal environment. Mitochondrial dysfunction (MTdys) and the subsequent unregulated production of ROS/RNS has long been implicated in neurodegenerative diseases such as multiple sclerosis (MS), amyotrophic lateral sclerosis (ALS) and Alzheimer's disease (Lin & Beal, 2006). This section will focus on the role of MTdys in the pathophysiology of PD and ASDs.

The part played by mitochondria in the etiology of PD was discovered by the role of MPTP a by-product of 'synthetic heroin' synthesis, in the development of severe parkinsonism (Langston *et al.*, 1983). The metabolite of MPTP, MPP<sup>+</sup> inhibits Complex I of the mitochondrial ETC (Abou-Sleiman *et al.*, 2006; Lin & Beal, 2006). Genetic

mutations or polymorphisms in mtDNA in several genes including  $\alpha$ -synuclein and parkin have also been linked to the pathophysiology of PD (Lin & Beal, 2006). Complex I inhibition by  $MPP^+$  can directly result in increased oxidative stress particularly through the production of  $O_2^{\cdot-}$ . This process leads to the further generation of secondary RNS/ROS and subsequent deleterious processes which can damage DNA, lipids and proteins (Lin & Beal, 2006; Valko *et al.*, 2007; Melo *et al.*, 2011) (see Section 2.10.2).

The herbicide paraquat (PQ) is an environmental toxin which has previously been linked to the development PD (Tanner *et al.*, 2011). A detailed description of the properties of PQ and the mechanism of action of this herbicide in the physiological environment is provided for in Chapter 8 of this thesis.

Briefly PQ may be reduced to form a PQ monocation free radical ( $PQ^{\cdot+}$ ) in the neuronal environment by cellular diaphorases, which are enzymes that transfer electrons from NADPH to small molecules such as PQ.  $PQ^{\cdot+}$  is rapidly re-oxidised in the presence of molecular oxygen which generates  $O_2^{\cdot-}$  and initiates the processes which lead to oxidative/nitrosative stress (see Section 2.10). Under normal physiological conditions Complex I of the mitochondrial ETC accepts electrons from NADH. However when PQ is present PQ preferentially accepts these electrons and leads to Complex I inhibition and subsequently MTdys (Dinis-Oliveira *et al.*, 2006; Mohammadi-Bardbori & Ghazi-Khansari, 2008). The characteristics of PQ,  $MPP^+$  and rotenone as Complex I inhibitors and oxidative stressors have enabled the successful replication of certain aspects of the pathophysiology of PD in animal models (Beal, 2001; McCormack *et al.*, 2005; McCormack *et al.*, 2006).

MTdys leads to an insufficient supply of ATP. ATP is necessary for the normal physiological function of various cellular processes including sequestering DA into synaptic vesicles by the vesicular monoamine transporter (VMAT2) (Andersen, 2004). Therefore insufficient ATP may lead to increased cytoplasmic DA and subsequently DA metabolism related oxidative stress (Lotharius & Brundin, 2002; Andersen, 2004).

SNc DA neurons are rich in glutamate receptors, a lack of ATP due to MTdys leads to the glutamate mediated activation of N-methyl-D-aspartate (NMDA) receptors which

results in an influx of  $\text{Ca}^{2+}$  and leads to depolarisation of the cell (Olanow & Tatton, 1999). The constitutive forms of NOS (eNOS and nNOS) are activated by  $\text{Ca}^{2+}$  followed by binding with calmodulin which leads directly to the production of NO (Alderton *et al.*, 2001; Saulskaya & Fofonova, 2006).

Classical mitochondrial disease occurs in a subset of ASDs due to genetic abnormalities and a subsequent deficiency in mitochondrial respiration (Frye & Rossignol, 2011). MTdys has also been implicated in the pathophysiology of ASDs and is not directly related to mitochondrial disease. Several biochemical, pathological and neuroimaging studies have suggested that MTdys is implicated in certain cases of ASDs (Chauhan & Chauhan, 2006; Palmieri & Persico, 2010). Specifically, diminished levels of ATP have been indicated in the brain of ASDs individuals by PET and NMR imaging (Lombard, 1998). An elevated level of lactate and pyruvate has also been demonstrated in biological ASDs samples (Haas, 2010). A disruption to oxidative phosphorylation would lead to increased levels of lactate/pyruvate in the periphery and suggest that MTdys plays a role in the development of ASDs. Chauhan *et al.* have demonstrated that the protein levels of various mitochondrial ETC complexes were decreased in different brain regions of children with autism. This study was determined by western blot analysis of post mortem ASDs brain tissue samples which were compared against age matched controls (Chauhan *et al.*, 2011).

Although a variety of evidence indicates that MTdys is related to the etiology of ASDs it has been postulated by several research groups not to be a primary initiating event in the disorder (Palmieri & Persico, 2010). It has been hypothesised that MTdys seen in ASDs individuals is a secondary event due to oxidative stress possibly initiated by environmental agents (Frye & Rossignol, 2011). A variety of environmental agents may contribute to the process of MTdys in ASDs such as prenatal exposure to infection (Meyer *et al.*, 2011), ethanol and valproic acid (Arndt *et al.*, 2005).

Gastrointestinal (GI) disturbances are commonly associated with ASDs, specifically due to an abnormal composition of gut bacteria in ASDs individuals (Parracho *et al.*, 2005; de Theije *et al.*, 2011). Propionic acid (PPA) is produced by opportunistic enteric bacteria such as *clostridial* species in the gut and elevated levels of these bacteria have

been found in ASDs individuals (Finegold *et al.*, 2002). PPA may lead to MTdys by the direct inhibition of oxidative phosphorylation (MacFabe *et al.*, 2007). Additionally, MacFabe *et al.* have demonstrated that PPA may be used in rats to mimic the behavioural changes and neuroinflammatory responses which are associated with autism spectrum disorders (ASDs) (MacFabe *et al.*, 2008; Shultz *et al.*, 2009).

It is known that MTdys leads to oxidative/nitrosative stress and the consequential production of ROS and RNS which subsequently leads to a vicious cycle of further MTdys and antioxidant impairment (Lin & Beal, 2006).

Neuropathological investigations of PPA treated rat brain tissue and post mortem autistic brain preparations have indicated the presence of activated microglia and astrocytes which are indicative of an inflammatory response (Vargas *et al.*, 2005; MacFabe *et al.*, 2011). As previously stated cytokines produced by this process are known to activate iNOS and hence elicit an increase in NO (Guix *et al.*, 2005). In a pro-oxidant environment NO can interact directly with  $O_2^{\cdot-}$  and lead to the formation of the main secondary highly toxic RNS;  $ONOO^-$  (see Section 2.10.3). This process may be accelerated in response to an inflammatory insult where  $O_2^{\cdot-}$  and NO specifically produced by iNOS, are produced and lead to MTdys (Calabrese *et al.*, 2007).

The detection of oxidative/nitrosative stress markers in an animal model of ASDs may contribute to a more complete understanding of the processes which lead to the development of ASDs. This information may yield new strategies to treat and alleviate ASDs symptoms. The detection of NO in a PPA induced animal model of ASDs is presented in Chapter 7 of this thesis.

## 1.10 Current therapeutic strategies for PD

The primary treatment for the motor symptoms which are characteristic of PD is the DA replacement therapy drug Levodopa (Schapira, 2008; Lipski *et al.*, 2011). Levodopa/L-dopa is orally administered and absorbed in the intestine where it is distributed in the blood and subsequently crosses the BBB. L-dopa is metabolised in the dopaminergic cells of the SNc where it is then converted by decarboxylation to DA by aromatic L-amino acid decarboxylase (Schapira, 2008; Lipski *et al.*, 2011).

L-dopa is highly efficient in the initial treatment of PD by the direct replacement of insufficient DA. However, the long-term administration of L-dopa results in the appearance of motor complications such as dyskinesias and motor fluctuations due to the effect of the drug ‘wearing off’ (Kieburtz, 2008; Schapira, 2008; Lipski *et al.*, 2011). Additionally, serious side effects such as nausea and vomiting are associated with L-dopa treatment (Schapira, 2008). The ‘wearing off’ effect of L-dopa administration may be ameliorated by the joint or pre-administration of DA agonists which result in a more consistent release of DA or in conjunction with other methods which reduce L-dopa peripheral metabolism and improve absorption e.g. carbidopa (Schapira *et al.*, 2009).

The role of other potential therapeutic options in the treatment of PD have been suggested including antioxidants and vitamins, metal chelators and antiglutamatergic agents (Barnham *et al.*, 2004; Melo *et al.*, 2011). However, clinical trials have not supported a beneficial effect of antioxidant (Vitamin E) treatment of PD (Barnham *et al.*, 2004). The production of ROS in PD activates glutamate-mediated excitotoxicity; NMDA receptor antagonists which may prevent this process have been used in the treatment of PD and some clinical efficiency has been observed (Melo *et al.*, 2011). The potential benefit of metal chelators in the prevention of iron mediated oxidative stress in neurodegenerative disease has also been investigated (Barnham *et al.*, 2004; Melo *et al.*, 2011). However, the primary treatment of PD remains to be the ‘gold standard’ therapy of L-dopa administration (Schapira *et al.*, 2009).

Some evidence has been presented that treatment with L-dopa may have a propensity to induce DA metabolism related oxidative stress (Schapira *et al.*, 2009; Lipski *et al.*,

2011). The negative aspects of L-dopa treatment are highly dependent on the L-dopa dose concentration and length of administration. *In-vitro* studies have demonstrated that L-dopa is toxic in cell cultures via the process of oxidative stress (Lipski *et al.*, 2011). However, clinical trials in humans and studies conducted with animals, including rodents and primates, have failed to conclusively reveal a toxic effect following the administration of L-dopa (Fahn *et al.*, 2004; Schapira, 2008; Schapira *et al.*, 2009; Lipski *et al.*, 2011). The general consensus is that L-dopa is not capable of stopping the progression of dopaminergic cell loss in the SNc but can only slow the rate of PD progression (Fahn *et al.*, 2004; Lipski *et al.*, 2011). This fact necessitates the further development of novel PD therapeutic strategies.

## 1.11 Conclusion

This thesis demonstrates the further *in-vitro* development of a paired catalase-based  $\text{H}_2\text{O}_2$  sensor and the utilisation of this sensor design to detect changes in  $\text{H}_2\text{O}_2$  in the physiological environment. The verification of previous *in-vitro* and *in-vivo* characterisations of a Nafion<sup>®</sup>-modified Platinum disc ( $\text{Pt}_d$ ) (5 pre-coats, 2 applications) NO sensor is presented in this thesis. The detection of NO/ $\text{H}_2\text{O}_2$  in animal models of neurodegenerative disease and dysfunction is also presented.

The present chapter outlines the concept of neuronal transmission, details of the role of  $\text{H}_2\text{O}_2$  and NO in normal physiological function and dysfunction are also given. The theoretical aspects which form the fundamental basis of experimental studies conducted in this thesis are described in Chapter 2. The materials and methods utilised throughout the course of this body of work are described in detail in Chapter 3.

The sensitivity, selectivity and stability of the paired  $\text{H}_2\text{O}_2$  sensor in the *in-vitro* environment is demonstrated in Chapter 4. The novel *in-vivo* characterisation of the dual  $\text{H}_2\text{O}_2$  sensor in the anaesthetised animal and the previously unreported electrochemical detection of  $\text{H}_2\text{O}_2$  in the freely-moving animal is presented in Chapter 5. Verification of the detection of NO *in-vitro* and in the physiological environment and novel stability characteristics of the NO sensor are presented in Chapter 6. Details of the original electrochemical detection of NO in an animal model of autism and Parkinson's disease are presented in Chapter 7 and 8 respectively. Additionally, the preliminary detection of  $\text{H}_2\text{O}_2$  in conjunction with NO in a parkinsonian animal model is reported in Chapter 8. Finally Chapter 9 concludes the thesis and outlines the main experimental outcomes.

## References

- Abou-Sleiman PM, Muqit MMK & Wood NW. (2006). Expanding insights of mitochondrial dysfunction in Parkinson's disease. *Nature Reviews Neuroscience* **7**, 207-219.
- Adams RN. (1990). *In vivo* electrochemical measurements in the CNS. *Prog Neurobiol* **35**, 297-311.
- Alderton WK, Cooper CE & Knowles RG. (2001). Nitric oxide synthases: structure, function and inhibition. *Biochemical Journal* **357**, 593-615.
- Andersen JK. (2004). Oxidative stress in neurodegeneration: cause or consequence? *Nature Medicine* **10**, S18-S25.
- Arndt TL, Stodgell CJ & Rodier PM. (2005). The teratology of autism. *International Journal of Developmental Neuroscience* **23**, 189-199.
- Avshalumov MV, Chen BT, Marshall SP, Pena DM & Rice ME. (2003). Glutamate-dependent inhibition of dopamine release in striatum is mediated by a new diffusible messenger, H<sub>2</sub>O<sub>2</sub>. *Journal of Neuroscience* **23**, 2744-2750.
- Bao L, Avshalumov MV, Patel JC, Lee CR, Miller EW, Chang CJ & Rice ME. (2009). Mitochondria Are the Source of Hydrogen Peroxide for Dynamic Brain-Cell Signaling. *Journal of Neuroscience* **29**, 9002-9010.
- Barnham KJ, Masters CL & Bush AI. (2004). Neurodegenerative diseases and oxidative stress. *Nature Reviews Drug Discovery* **3**, 205-214.
- Beal MF. (2001). Experimental models of Parkinson's disease. *Nat Rev Neurosci* **2**, 325-334.
- Bogdan C, Rollingshoff M & Diefenbach A. (2000). Reactive oxygen and reactive nitrogen intermediates in innate and specific immunity. *Current Opinion in Immunology* **12**, 64-76.
- Borland LM & Michael AC. (2007). An Introduction to Electrochemical Methods in Neuroscience. In *Electrochemical Methods for Neuroscience*, ed. Michael ACBLM, pp. 1-15. CRC Press.
- Braak H, Ghebremedhin E, Rub U, Bratzke H & Del Tredici K. (2004). Stages in the development of Parkinson's disease-related pathology. *Cell and Tissue Research* **318**, 121-134.

- Brown FO, Finnerty NJ & Lowry JP. (2009). Nitric oxide monitoring in brain extracellular fluid: characterisation of Nafion<sup>®</sup>-modified Pt electrodes *in vitro* and *in vivo*. *Analyst* **134**, 2012-2020.
- Brown FO & Lowry JP. (2003). Microelectrochemical sensors for *in vivo* brain analysis: an investigation of procedures for modifying Pt electrodes using Nafion<sup>®</sup>. *Analyst* **128**, 700-705.
- Bruckdorfer R. (2005). The basics about nitric oxide. *Molecular Aspects of Medicine* **26**, 3-31.
- Calabrese V, Mancuso C, Calvani M, Rizzarelli E, Butterfield DA & Stella AMG. (2007). Nitric oxide in the central nervous system: neuroprotection versus neurotoxicity. *Nature Reviews Neuroscience* **8**, 766-775.
- Calabrese V, Scapagnini G, Stella AMG, Bates TE & Clark JB. (2001). Mitochondrial involvement in brain function and dysfunction: Relevance to aging, neurodegenerative disorders and longevity. *Neurochemical research* **26**, 739-764.
- Cavas M & Navarro JF. (2006). Effects of selective neuronal nitric oxide synthase inhibition on sleep and wakefulness in the rat. *Progress in Neuro-Psychopharmacology & Biological Psychiatry* **30**, 56-67.
- Chauhan A, Audhya T & Chauhan V. (2012). Brain region-specific glutathione redox imbalance in autism. *Neurochemical research* **37**, 1681-1689.
- Chauhan A & Chauhan V. (2006). Oxidative stress in autism. *Pathophysiology : the official journal of the International Society for Pathophysiology / ISP* **13**, 171-181.
- Chauhan A, Gu F, Essa MM, Wegiel J, Kaur K, Brown WT & Chauhan V. (2011). Brain region-specific deficit in mitochondrial electron transport chain complexes in children with autism. *Journal of Neurochemistry* **117**, 209-220.
- Chen BT, Avshalumov MV & Rice ME. (2002). Modulation of somatodendritic dopamine release by endogenous H<sub>2</sub>O<sub>2</sub>: Susceptibility in substantia nigra but resistance in VTA. *Journal of Neurophysiology* **87**, 1155-1158.
- Chen W, Cai S, Ren QQ, Wen W & Zhao YD. (2012). Recent advances in electrochemical sensing for hydrogen peroxide: a review. *Analyst* **137**, 49-58.
- Chinta SJ & Andersen JK. (2008). Redox imbalance in Parkinson's disease. *Biochimica Et Biophysica Acta-General Subjects* **1780**, 1362-1367.

- Clark LC, Misrahy G & Fox RP. (1958). Chronically implanted polarographic electrodes. *Journal of Applied Physiology* **13**, 85-91.
- Davis GC, Williams AC, Markey SP, Ebert MH, Caine ED, Reichert CM & Kopin IJ. (1979). Chronic parkinsonism secondary to intravenous-injection of meperidine analogs. *Psychiatry Research* **1**, 249-254.
- de Theije CGM, Wu J, da Silva SL, Kamphuis PJ, Garssen J, Korte SM & Kraneveld AD. (2011). Pathways underlying the gut-to-brain connection in autism spectrum disorders as future targets for disease management. *European Journal of Pharmacology* **668**, S70-S80.
- Dinis-Oliveira RJ, Remiao F, Carmo H, Duarte JA, Navarro AS, Bastos ML & Carvalho F. (2006). Paraquat exposure as an etiological factor of Parkinson's disease. *Neurotoxicology* **27**, 1110-1122.
- Fahn S, Shoulson I, Kieburtz K, Rudolph A, Lang A, Olanow CW, Tanner C, Marek K & Parkinson Study G. (2004). Levodopa and the progression of Parkinson's disease. *New England Journal of Medicine* **351**, 2498-2508.
- Fang FC. (2004). Antimicrobial reactive oxygen and nitrogen species: Concepts and controversies. *Nature Reviews Microbiology* **2**, 820-832.
- Fejgin K, Palsson E, Wass C, Finnerty N, Lowry J & Klamer D. (2009). Prefrontal GABA(B) receptor activation attenuates phencyclidine-induced impairments of prepulse inhibition: involvement of nitric oxide. *Neuropsychopharmacology* **34**, 1673-1684.
- Fillenz M. (2005). *In vivo* neurochemical monitoring and the study of behaviour. *Neuroscience and Biobehavioral Reviews* **29**, 949-962.
- Finegold SM, Molitoris D, Song YL, Liu CX, Vaisanen ML, Bolte E, McTeague M, Sandler R, Wexler H, Marlowe EM, Collins MD, Lawson PA, Summanen P, Baysallar M, Tomzynski TJ, Read E, Johnson E, Rolfe R, Nasir P, Shah H, Haake DA, Manning P & Kaul A. (2002). Gastrointestinal microflora studies in late-onset autism. *Clinical Infectious Diseases* **35**, S6-S16.
- Finnerty NJ, O'Riordan SL, Brown FO, Serra PA, O'Neill RD & Lowry JP. (2012a). *In vivo* characterisation of a Nafion<sup>®</sup>-modified Pt electrode for real-time nitric oxide monitoring in brain extracellular fluid. *Analytical Methods* **4**, 550-557.
- Finnerty NJ, O'Riordan SL, Palsson E & Lowry JP. (2012b). Brain nitric oxide: Regional characterisation of a real-time microelectrochemical sensor. *Journal of Neuroscience Methods* **209**, 13-21.

- Folstein SE & Rosen-Sheidley B. (2001). Genetics of autism: Complex aetiology for a heterogeneous disorder. *Nature Reviews Genetics* **2**, 943-955.
- Friedemann MN, Robinson SW & Gerhardt GA. (1996). *o*-phenylenediamine-modified carbon fiber electrodes for the detection of nitric oxide. *Analytical Chemistry* **68**, 2621-2628.
- Frye RE & Rossignol DA. (2011). Mitochondrial Dysfunction Can Connect the Diverse Medical Symptoms Associated With Autism Spectrum Disorders. *Pediatric Research* **69**, 41R-47R.
- Garguilo MG & Michael AC. (1996). Amperometric microsensors for monitoring choline in the extracellular fluid of brain. *Journal of Neuroscience Methods* **70**, 73-82.
- Goff DC & Coyle JT. (2001). The emerging role of glutamate in the pathophysiology and treatment of schizophrenia. *American Journal of Psychiatry* **158**, 1367-1377.
- Gu Z, Nakamura T, Yao D, Shi ZQ & Lipton SA. *Nitrosative and oxidative stress links dysfunctional ubiquitination to Parkinson's disease*. *Cell Death Differ.* 2005 Sep;12(9):1202-4.
- Guix FX, Uribealago I, Coma M & Munoz FJ. (2005). The physiology and pathophysiology of nitric oxide in the brain. *Progress in Neurobiology* **76**, 126-152.
- Haas RH. (2010). Autism and mitochondrial disease. *Dev Disabil Res Rev* **16**, 144-153.
- Heinzen EL & Pollack GM. (2002). Use of an electrochemical nitric oxide sensor to detect neuronal nitric oxide production in conscious, unrestrained rats. *Journal of Pharmacological and Toxicological Methods* **48**, 139-146.
- Hetrick EM & Schoenfisch MH. (2009). Analytical Chemistry of Nitric Oxide. In *Annual Review of Analytical Chemistry*, pp. 409-433.
- Hu YB, Mitchell KM, Albahadily FN, Michaelis EK & Wilson GS. (1994). Direct measurement of glutamate release in the brain using a dual enzyme-based electrochemical sensor. *Brain Research* **659**, 117-125.
- Hung HC & Lee EHY. (1998). MPTP produces differential oxidative stress and antioxidative responses in the nigrostriatal and mesolimbic dopaminergic pathways. *Free Radical Biology and Medicine* **24**, 76-84.
- Ignarro LJ, Buga GM, Wood KS, Byrns RE & Chaudhuri G. (1987). Endothelium-derived relaxing factor produced and released from artery and vein is nitric-

- oxide. *Proceedings of the National Academy of Sciences of the United States of America* **84**, 9265-9269.
- Jenner P. (2003). Oxidative stress in Parkinson's disease. *Annals of Neurology* **53**, S26-S36.
- Kelm M. (1999). Nitric oxide metabolism and breakdown. *Biochimica Et Biophysica Acta-Bioenergetics* **1411**, 273-289.
- Kenemans JL & Kahkonen S. (2011). How Human Electrophysiology Informs Psychopharmacology: from Bottom-up Driven Processing to Top-Down Control. *Neuropsychopharmacology* **36**, 26-51.
- Kieburz K. (2008). Therapeutic strategies to prevent motor complications in Parkinson's disease. *Journal of Neurology* **255**, 42-45.
- Kiechle FL & Malinski T. (1993). Nitric-oxide - biochemistry, pathophysiology, and detection. *American Journal of Clinical Pathology* **100**, 567-575.
- Kissinger PT, Hart JB & Adams RN. (1973). Voltammetry in brain tissue-a new neurophysiological measurement. *Brain Res* **55**, 209-213.
- Kulagina NV & Michael AC. (2003). Monitoring hydrogen peroxide in the extracellular space of the brain with amperometric microsensors. *Analytical Chemistry* **75**, 4875-4881.
- Lamprecht R & LeDoux J. (2004). Structural plasticity and memory. *Nat Rev Neurosci* **5**, 45-54.
- Langston JW, Ballard P, Tetrud JW & Irwin I. (1983). Chronic Parkinsonism in humans due to a product of meperidine-analog synthesis. *Science* **219**, 979-980.
- Lei BP, Adachi N & Arai T. (1997). The effect of hypothermia on H<sub>2</sub>O<sub>2</sub> production during ischemia and reperfusion: A microdialysis study in the gerbil hippocampus. *Neuroscience Letters* **222**, 91-94.
- Lei BP, Adachi N & Arai T. (1998). Measurement of the extracellular H<sub>2</sub>O<sub>2</sub> in the brain by microdialysis. *Brain Research Protocols* **3**, 33-36.
- Lin MT & Beal MF. (2006). Mitochondrial dysfunction and oxidative stress in neurodegenerative diseases. *Nature* **443**, 787-795.
- Lipski J, Nistico R, Berretta N, Guatteo E, Bernardi G & Mercuri NB. (2011). L-DOPA: A scapegoat for accelerated neurodegeneration in Parkinson's disease? *Progress in Neurobiology* **94**, 389-407.

- Liu XJ, Shang LB, Pang JT & Li GX. (2003). A reagentless nitric oxide biosensor based on haemoglobin/polyethyleneimine film. *Biotechnology and Applied Biochemistry* **38**, 119-122.
- Lombard J. (1998). Autism: a mitochondrial disorder? *Medical Hypotheses* **50**, 497-500.
- Lonroth P, Jansson PA & Smith U. (1987). A microdialysis method allowing characterization of intercellular water space in humans. *American Journal of Physiology* **253**, E228-E231.
- Lotharius J & Brundin P. (2002). Pathogenesis of Parkinson's disease: Dopamine, vesicles and alpha-synuclein. *Nature Reviews Neuroscience* **3**, 932-942.
- Lowry JP, McAteer K, Elatrash SS, Duff A & O'Neill RD. (1994). Characterisation of glucose oxidase-modified poly(phenylenediamine)-coated electrodes *in-vitro* and *in-vivo*: homogeneous interference by ascorbic acid in hydrogen-peroxide detection. *Analytical Chemistry* **66**, 1754-1761.
- Lowry JP, Miele M, O'Neill RD, Boutelle MG & Fillenz M. (1998a). An amperometric glucose-oxidase/poly(*o*-phenylenediamine) biosensor for monitoring brain extracellular glucose: *in vivo* characterisation in the striatum of freely-moving rats. *Journal of Neuroscience Methods* **79**, 65-74.
- Lowry JP, O'Neill RD & (2006). *Neuroanalytical Chemistry In Vivo Using Biosensors.*, vol. 10. American Scientific Publishers.
- Lowry JP, O'Neill RD, Boutelle MG & Fillenz M. (1998b). Continuous monitoring of extracellular glucose concentrations in the striatum of freely moving rats with an implanted glucose biosensor. *Journal of Neurochemistry* **70**, 391-396.
- Lowry JP, Ryan MR & O'Neill RD. (1998c). Behaviourally induced changes in extracellular levels of brain glutamate monitored at 1 s resolution with an implanted biosensor. *Analytical Communications* **35**, 87-89.
- MacFabe DF, Cain DP, Rodriguez-Capote K, Franklin AE, Hoffman JE, Boon F, Taylor AR, Kavaliers M & Ossenkopp K-P. (2007). Neurobiological effects of intraventricular propionic acid in rats: Possible role of short chain fatty acids on the pathogenesis and characteristics of autism spectrum disorders. *Behavioural Brain Research* **176**, 149-169.
- MacFabe DF, Cain NE, Boon F, Ossenkopp K-P & Cain DP. (2011). Effects of the enteric bacterial metabolic product propionic acid on object-directed behavior, social behavior, cognition, and neuroinflammation in adolescent rats: Relevance to autism spectrum disorder. *Behavioural Brain Research* **217**, 47-54.

- MacFabe DF, Rodríguez-Capote K, Franklin JE, Kavaliers M, Possmayer F, Ossenkopp K-P & Franklin AE. (2008). A Novel Rodent Model of Autism: Intraventricular Infusions of Propionic Acid Increase Locomotor Activity and Induce Neuroinflammation and Oxidative Stress in Discrete Regions of Adult Rat Brain. *American Journal of Biochemistry and Biotechnology* **4**, 146-166.
- Maguire-Zeiss KA, Short DW & Federoff HJ. (2005). Synuclein, dopamine and oxidative stress: co-conspirators in Parkinson's disease? *Molecular Brain Research* **134**, 18-23.
- Maier CM & Chan PH. (2002). Role of superoxide dismutases in oxidative damage and neurodegenerative disorders. *Neuroscientist* **8**, 323-334.
- Mas M, Escrig A & Gonzalez-Mora JL. (2002). *In vivo* electrochemical measurement of nitric oxide in corpus cavernosum penis. *Journal of Neuroscience Methods* **119**, 143-150.
- Maskus M, Pariente F, Wu Q, Toffanin A, Shapleigh JP & Abruna HD. (1996). Electrocatalytic reduction of nitric oxide at electrodes modified with electropolymerized films of Cr(v-tpy)(2) (3+) and their application to cellular NO determinations. *Analytical Chemistry* **68**, 3128-3134.
- Matthews PM, Honey GD & Bullmore ET. (2006). Applications of fMRI in translational medicine and clinical practice. *Nature Reviews Neuroscience* **7**, 732-744.
- McAteer K & O'Neill RD. (1996). Strategies for decreasing ascorbate interference at glucose oxidase-modified poly(*o*-phenylenediamine)-coated electrodes. *Analyst* **121**.
- McCormack AL, Atienza JG, Johnston LC, Andersen JK, Vu S & Di Monte DA. (2005). Role of oxidative stress in paraquat-induced dopaminergic cell degeneration. *Journal of Neurochemistry* **93**, 1030-1037.
- McCormack AL, Atienza JG, Langston JW & Di Monte DA. (2006). Decreased susceptibility to oxidative stress underlies the resistance of specific dopaminergic cell populations to paraquat-induced degeneration. *Neuroscience* **141**, 929-937.
- McPheeters ML, Warren Z, Sathe N, Bruzek JL, Krishnaswami S, Jerome RN & Veenstra-VanderWeele J. (2011). A Systematic Review of Medical Treatments for Children With Autism Spectrum Disorders. *Pediatrics* **127**, E1312-E1321.
- Melo A, Monteiro L, Lima RMF, Oliveira DMd, Cerqueira MDd & El-Bacha RS. (2011). Oxidative stress in neurodegenerative diseases: mechanisms and

- therapeutic perspectives. *Oxidative medicine and cellular longevity* **2011**, 467180.
- Meulemans A. (1993). Continuous monitoring of n-nitroso-l-arginine using microcarbon electrode in rat brain. *Neuroscience Letters* **157**, 7-12.
- Meyer U, Feldon J & Dammann O. (2011). Schizophrenia and Autism: Both Shared and Disorder-Specific Pathogenesis Via Perinatal Inflammation? *Pediatric Research* **69**, 26R-33R.
- Mohammadi-Bardbori A & Ghazi-Khansari M. (2008). Alternative electron acceptors: Proposed mechanism of paraquat mitochondrial toxicity. *Environmental Toxicology and Pharmacology* **26**, 1-5.
- Nugent FS, Penick EC & Kauer JA. (2007). Opioids block long-term potentiation of inhibitory synapses. *Nature* **446**, 1086-1090.
- O'Brien KB, Killoran SJ, O'Neill RD & Lowry JP. (2007). Development and characterization *in vitro* of a catalase-based biosensor for hydrogen peroxide monitoring. *Biosensors & Bioelectronics* **22**, 2994-3000.
- Obeso JA, Rodriguez-Oroz MC, Goetz CG, Marin C, Kordower JH, Rodriguez M, Hirsch EC, Farrer M, Schapira AHV & Halliday G. (2010). Missing pieces in the Parkinson's disease puzzle. *Nature Medicine* **16**, 653-661.
- Olanow CW & Tatton WG. (1999). Etiology and pathogenesis of Parkinson's disease. *Annual Review of Neuroscience* **22**, 123-144.
- Pallini M, Curulli A, Amine A & Palleschi G. (1998). Amperometric nitric oxide sensors: a comparative study. *Electroanalysis* **10**, 1010-1016.
- Palmieri L & Persico AM. (2010). Mitochondrial dysfunction in autism spectrum disorders: cause or effect? *Biochim Biophys Acta*, 9.
- Palsson E, Finnerty N, Fejgin K, Klamer D, Wass C, Svensson L & Lowry J. (2009). Increased cortical nitric oxide release after phencyclidine administration. *Synapse* **63**, 1083-1088.
- Park JK, Tran PH, Chao JKT, Ghodadra R, Rangarajan R & Thakor NV. (1998). *In vivo* nitric oxide sensor using non-conducting polymer-modified carbon fiber. *Biosensors & Bioelectronics* **13**, 1187-1195.
- Park SS, Hong M, Song C-K, Jhon G-J, Lee Y & Suh M. (2010). Real-Time *in vivo* Simultaneous Measurements of Nitric Oxide and Oxygen Using an Amperometric Dual Microsensor. *Analytical Chemistry* **82**, 7618-7624.

- Park SS, Kim J & Lee Y. (2012). Improved Electrochemical Microsensor for the Real-Time Simultaneous Analysis of Endogenous Nitric Oxide and Carbon Monoxide Generation. *Analytical Chemistry* **84**, 1792-1796.
- Parracho H, Bingham MO, Gibson GR & McCartney AL. (2005). Differences between the gut microflora of children with autistic spectrum disorders and that of healthy children. *Journal of Medical Microbiology* **54**, 987-991.
- Ramalingam M & Kim S-J. (2012). Reactive oxygen/nitrogen species and their functional correlations in neurodegenerative diseases. *Journal of Neural Transmission* **119**, 891-910.
- Rapin I & Tuchman RF. (2008). Autism: Definition, Neurobiology, Screening, Diagnosis. *Pediatric Clinics of North America* **55**, 1129-+.
- Rhee SG. (2006). H<sub>2</sub>O<sub>2</sub>, a necessary evil for cell signaling. *Science* **312**, 1882-1883.
- Rice ME. (2011). H<sub>2</sub>O<sub>2</sub>: A Dynamic Neuromodulator. *Neuroscientist* **17**, 389-406.
- Rose S, Melnyk S, Pavliv O, Bai S, Nick TG, Frye RE & James SJ. (2012). Evidence of oxidative damage and inflammation associated with low glutathione redox status in the autism brain. *Translational psychiatry* **2**, e134.
- Ryan MR, Lowry JP & Oneill RD. (1997). Biosensor for neurotransmitter L-glutamic acid designed for efficient use of L-glutamate oxidase and effective rejection of interference. *Analyst* **122**, 1419-1424.
- Saulskaya NB & Fofonova NV. (2006). Effects of N-methyl-D-aspartate on extracellular citrulline level in the rat nucleus accumbens. *Neuroscience Letters* **407**, 91-95.
- Schapira AH & Jenner P. (2011). Etiology and Pathogenesis of Parkinson's Disease. *Movement Disorders* **26**, 1049-1055.
- Schapira AHV. (2008). The clinical relevance of levodopa toxicity in the treatment of Parkinson's disease. *Movement Disorders* **23**, S515-S520.
- Schapira AHV, Emre M, Jenner P & Poewe W. (2009). Levodopa in the treatment of Parkinson's disease. *European Journal of Neurology* **16**, 982-989.
- Shibasaki H. (2008). Human brain mapping: Hemodynamic response and electrophysiology. *Clinical Neurophysiology* **119**, 731-743.
- Shultz SR, MacFabe DF, Martin S, Jackson J, Taylor R, Boon F, Ossenkopp K-P & Cain DP. (2009). Intracerebroventricular injections of the enteric bacterial metabolic product propionic acid impair cognition and sensorimotor ability in

- the Long-Evans rat: Further development of a rodent model of autism. *Behavioural Brain Research* **200**, 33-41.
- Sogut S, Zoroglu SS, Ozyurt H, Yilmaz HR, Ozugurlu F, Sivasli E, Yetkin O, Yanik M, Tutkun H, Savas HA, Tarakcioglu M & Akyol O. (2003). Changes in nitric oxide levels and antioxidant enzyme activities may have a role in the pathophysiological mechanisms involved in autism. *Clinica Chimica Acta* **331**, 111-117.
- Stone JR & Yang SP. (2006). Hydrogen peroxide: A signaling messenger. *Antioxidants & Redox Signaling* **8**, 243-270.
- Tanner CM, Kamel F, Ross GW, Hoppin JA, Goldman SM, Korell M, Marras C, Bhudhikanok GS, Kasten M, Chade AR, Comyns K, Richards MB, Meng C, Priestley B, Fernandez HH, Cambi F, Umbach DM, Blair A, Sandler DP & Langston JW. (2011). Rotenone, Paraquat, and Parkinson's Disease. *Environmental Health Perspectives* **119**, 866-872.
- Ungerstedt U & Rostami E. (2004). Microdialysis in neurointensive care. *Current Pharmaceutical Design* **10**, 2145-2152.
- Valko M, Leibfritz D, Moncol J, Cronin MTD, Mazur M & Telser J. (2007). Free radicals and antioxidants in normal physiological functions and human disease. *International Journal of Biochemistry & Cell Biology* **39**, 44-84.
- Vargas DL, Nascimbene C, Krishnan C, Zimmerman AW & Pardo CA. (2005). Neuroglial activation and neuroinflammation in the brain of patients with autism. *Annals of Neurology* **57**, 67-81.
- Walsh P, Elsabbagh M, Bolton P & Singh I. (2011). In search of biomarkers for autism: scientific, social and ethical challenges. *Nature Reviews Neuroscience* **12**, 603-612.
- Wass C, Archer T, Palsson E, Fejgin K, Alexandersson A, Klamer D, Engel JA & Svensson L. (2006a). Phencyclidine affects memory in a nitric oxide-dependent manner: Working and reference memory. *Behavioural Brain Research* **174**, 49-55.
- Wass C, Archer T, Palsson E, Fejgin K, Klamer D, Engel JA & Svensson L. (2006b). Effects of phencyclidine on spatial learning and memory: Nitric oxide-dependent mechanisms. *Behavioural Brain Research* **171**, 147-153.
- Williams IL, Wheatcroft SB, Shah AM & Kearney MT. (2002). Obesity, atherosclerosis and the vascular endothelium: mechanisms of reduced nitric oxide bioavailability in obese humans. *International Journal of Obesity* **26**, 754-764.

- Wink DA & Mitchell JB. (1998). Chemical biology of nitric oxide: Insights into regulatory, cytotoxic, and cytoprotective mechanisms of nitric oxide. *Free Radical Biology and Medicine* **25**, 434-456.
- Winterbourn CC. (2008). Reconciling the chemistry and biology of reactive oxygen species. *Nature Chemical Biology* **4**, 278-286.
- Wirdefeldt K, Adami HO, Cole P, Trichopoulos D & Mandel J. (2011). Epidemiology and etiology of Parkinson's disease: a review of the evidence. *Eur J Epidemiol* **26**, 28.
- Wise RA. (2004). Dopamine, learning and motivation. *Nat Rev Neurosci* **5**, 483-494.
- Yorbik O, Sayal A, Akay C, Akbiyik DI & Sohmen T. (2002). Investigation of antioxidant enzymes in children with autistic disorder. *Prostaglandins Leukotrienes and Essential Fatty Acids* **67**, 341-343.
- Zoroglu SS, Armutcu F, Ozen S, Gurel A, Sivasli E, Yetkin O & Meram I. (2004). Increased oxidative stress and altered activities of erythrocyte free radical scavenging enzymes in autism. *European Archives of Psychiatry and Clinical Neuroscience* **254**, 143-147.

---

## **2. Theory**

---

## 2.1 Introduction

This thesis describes the electrochemical detection of hydrogen peroxide ( $\text{H}_2\text{O}_2$ ) and nitric oxide (NO) *in-vitro* and in the brain of freely moving-animals. The main aim of this chapter is to explain the fundamental electrochemical principles and techniques utilised in this thesis in order to detect  $\text{H}_2\text{O}_2$  and NO in the *in-vitro* and *in-vivo* environment.

A description of the electrochemical cell set-up utilised for the attainment of *in-vitro* data is given in Section 3.7. Additionally the protocol for implantation of the working electrodes for the attainment of *in-vivo*  $\text{H}_2\text{O}_2$  and NO data is outlined in Section 3.10. Both strategies rely on the same basic electrochemical principles. In each case the electrochemical circuit consists of a reference electrode, an auxiliary electrode and a specified number of working electrodes.

The electrochemical changes being investigated take place at the working electrode. The reference electrode has a fixed potential against which the potential of the working electrodes in the cell can be measured. The final electrode is the auxiliary or counter which functions as a source or sink for electrons and completes the electrical circuit.

Many electroanalytical techniques are available, however Constant Potential Amperometry (CPA) was utilised without exception in this thesis (see Section 2.4). CPA provides the appropriate time resolution necessary *in-vivo* to detect species such as  $\text{H}_2\text{O}_2$  and NO which are expected to have a relatively short lifetime in tissue (Wink & Mitchell, 1998; Kelm, 1999; Maier & Chan, 2002; Rice, 2011). An extensive description of the basic electrochemical principles outlined in this chapter have previously been described by Bard and Faulkner (Bard & Faulkner, 2001).

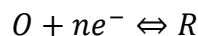
The process of oxidation and reduction at the electrode surface is described in Section 2.2. The three processes which contribute to mass transport of the analyte to the electrode surface including diffusion, convection and migration are outlined in Section 2.3. CPA is discussed in detail in Section 2.4, the oxidation mechanisms of  $\text{H}_2\text{O}_2$ , NO and ascorbic acid (AA) are also presented in Section 2.4.

The structure of the permselective membranes used in the design of the sensors described in this thesis including Nafion<sup>®</sup> and PPD are shown in Section 2.5 and 2.6 respectively.

A detailed description of the function of the catalase enzyme utilised in this research project is provided in Section 2.7. Additionally the derivation of the paired catalase-based H<sub>2</sub>O<sub>2</sub> sensor response is mathematically presented in section 2.8. An overview of the main principles of microdialysis (MD) and retrodialysis (RD) is given in Section 2.9. A detailed description of the development of oxidative and nitrosative stress is provided in Section 2.10.

## 2.2 Oxidation/Reduction

CPA involves the application of a fixed potential between the working and reference electrode which causes oxidation or reduction of the target species. The equation for oxidation/reduction of a species is given in Equation 2.1. *O* and *R* represent the oxidised and reduced forms and *n* refers to the number of electrons.



(2.1)

When a potential is applied oxidation or reduction processes occur at the active surface of an electrode and a resulting faradaic current flows. As the variation in potential gives rise to the transfer of electrons that are governed by Faraday's law (Equation 2.3) they are termed faradaic processes.

As shown in Figure 2.1 at equilibrium ( $E_{eq}$ ), i.e. no negative (-ve) or positive (+ve) potential is applied consequently no oxidation/reduction processes occur. The fermi level ( $E_f$ ) or highest energy level of the metal based working electrode is equal in energy to the highest occupied molecular orbital (HOMO) of the solution species.

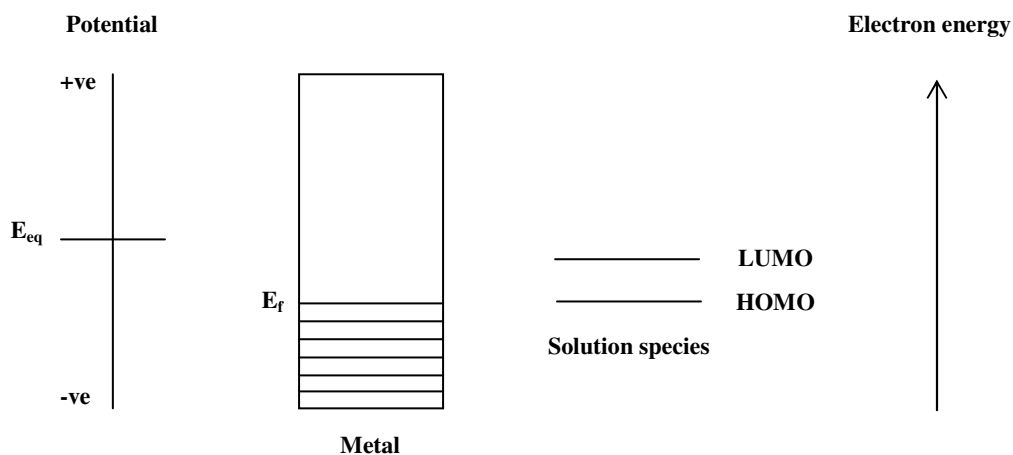


Figure 2.1 The system at equilibrium.

Upon the application of a potential ( $E_{app}$ ) which is more positive than  $E_{eq}$  the  $E_f$  of the metal decreases. It is now energetically more favourable for electrons to move from the HOMO level of the solution species to the lower lying  $E_f$  of the metal. This process results in an oxidation reaction and a corresponding oxidation current (Figure 2.2). A reduction reaction occurs where a negative potential is applied relative to  $E_{eq}$  and electrons move from the increased  $E_f$  of the metal to the LUMO level of the solution species.

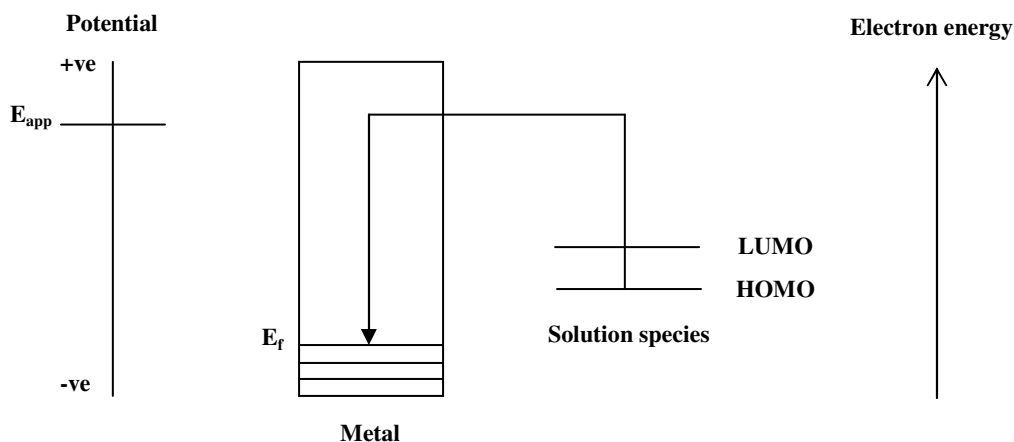


Figure 2.2 An oxidation reaction.

Additionally a capacitance current (charging/background current) arises following the application of a potential which is due to opposing charges between the electrode and target medium. However this charging current is not due to the presence of the analyte and is excluded from the experimental data presented in this thesis. The two main contributing processes to the reaction (Equation 2.1) are mass transport of the analyte to the electrode surface and electron transfer.

Long-term *in-vivo* electrochemistry (L.I.V.E) involves the chronic detection of changes in concentration of a particular analyte in the biological environment. For the evaluation of the concentration of a given analyte the Nernst equation is used (Equation 2.2). With the consideration that electron transfer is relatively fast as is the case with microelectrodes (Forster, 1994). The Nernst equation describes the variation of electrode potential for each electrochemical reaction with the concentrations of oxidised [O] and reduced species [R] under conditions of equilibrium at the electrode surface. Diffusion is an important contributing factor and is discussed in Section 2.2.1.

$$E_{eq} = E^* = \frac{RT}{nF} \ln \frac{[O]}{[R]}$$

(2.2)

Where  $E^*$  is the standard electrode potential. R is the gas constant, T is the temperature, F is the Faraday constant (96,485 C mol<sup>-1</sup>) and  $n$  is the number of electrons.

## 2.3 Mass transport

Mass transport of the analyte to the electrode surface and the rate of electron transfer determines how the reaction proceeds. The experimentally measured current ( $I$ ) is a direct indication of the rate of the electrochemical reaction and is given by Faraday's law.

$$I = nFAJ$$

(2.3)

Where ( $I$ ) indicates the current,  $n$  refers to the number of moles,  $F$  is the Faraday constant,  $A$  is the area of the electrode ( $\text{m}^2$ ) and  $J$  is the flux of ions ( $\text{mol m}^{-2} \text{s}^{-1}$ ).

Three processes control the movement of charged species to the electrode surface and these are diffusion, convection and migration.

### 2.3.1 Diffusion

Assuming that the electron transfer is very rapid as is the case with microelectrodes (Forster, 1994) the measured current is directly related to diffusion of the target species to the electrode surface. Diffusion is defined as the movement of molecules from an area of high concentration to an area of low concentration across a concentration gradient as described by Fick's first law (Equation 2.4).

$$J_b = -D_b \frac{\partial c}{\partial x}$$

(2.4)

Where  $J_b$  is the flux of species  $b$ ,  $D_b$  is the proportionality factor between flux and concentration gradient known as the diffusion coefficient and  $\frac{\partial c}{\partial x}$  is the concentration gradient in direction  $x$ . The negative sign is present as the flux of species  $b$  tends to cancel the concentration gradient. Fick's first law describes the flux ( $J_b$ ) as being directly proportional to the concentration gradient.

Concentration changes over time of the electroactive species of interest ( $b$ ) near to the electrode surface due to the movement described in Figure 2.3 may be determined using Fick's second law (Equation 2.5).

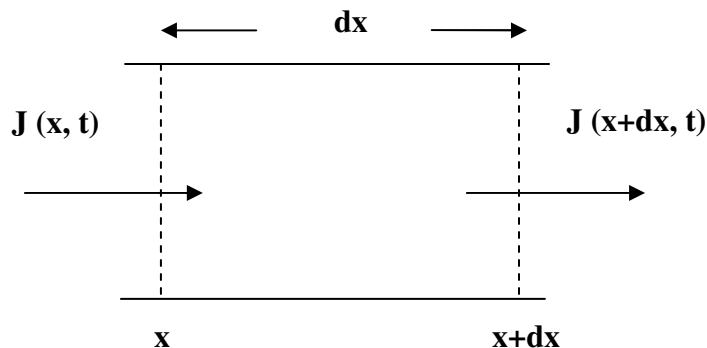


**Figure 2.3** One dimensional diffusion opposing a concentration gradient. In relation to movement of a position ( $x$ ) within an element of width ( $dx$ )

$$\frac{\partial [b]}{\partial t} = D \frac{\partial^2 c}{\partial x^2}$$

(2.5)

Assuming that the concentration gradient is constant (no change in  $[b]$  with  $t$ ), as is the case with microelectrodes due to the small dimensions of the electrode and the minimal removal of the analyte from the surrounding solution. A steady-state current response is obtained. No change in concentration is observed with respect to time according to Fick's second law due to the absence of a change in concentration gradient.

For planar electrodes where the geometry permits uniform access to the bulk solution. The variation in current with time may be calculated from Fick's second law which results in the Cottrell equation (Equation 2.6). Therefore for a disc electrode the steady-state current in the limiting region is given by Equation 2.6.

$$I = nFAJ = \frac{nFAD^{1/2}c_{\infty}}{(\pi t)^{1/2}}$$

(2.6)

( $I$ ) represents the measured current,  $n$  is the number of electrons,  $F$  is the Faraday constant,  $A$  is the surface area,  $D$  being the diffusion coefficient, where  $J$  is the flux and  $c_\infty$  represents the concentration of the electroactive species in the bulk solution.

A Laplace operator ( $\nabla$ ) is substituted into Equation 2.4 to determine the flux for any geometry of electrode. As shown in Equation 2.7.

$$J = -D\nabla^2 c$$

(2.7)

Fick's second law for any geometry is given by Equation 2.8.

$$\frac{\partial c}{\partial t} = D\nabla^2 c$$

(2.8)

The laplacian operator for cylinder electrodes is given by Equation 2.8.1

$$\frac{\partial^2}{\partial r^2} + \left(\frac{1}{r}\right)\left(\frac{\partial}{\partial r}\right)$$

(2.8.1)

If initial conditions pertaining to  $t = 0$  and two boundary conditions relating to spatial coordinates are obeyed. From Fick's first law the flux can be directly related to current density,  $\frac{i}{A}$ ; as follows.

$$-J_b(0, t) = \frac{i}{nFA} = D_b \left[ \frac{\partial c_b(x, t)}{\partial x} \right]_{x=0}$$

(2.9)

Where  $J$  relates to flux,  $i$  is the current,  $n$  is the number of transferred electrons,  $F$  is the Faraday constant and  $A$  relates to the active surface area of the electrode.

### 2.3.2 Convection

Convection relates to movement of species due to an applied external force as with the process of stirring. With *in-vitro* experiments aliquots of substrate were introduced into the electrochemical cell via brief agitation of the bulk solution with a magnetic stirrer. The contribution of convection to the process of mass transport is negated as rapidly achieved steady-state currents in the quiescent environment were utilised in the analysis of all calibration data.

### 2.3.3 Migration

Migration is the movement of charged species due to the presence of an electric field. The electric field is limited to small distances away from the electrode surface. Migration process are eliminated with microelectrodes from the process of mass transport due the large amount of an inert electrolyte utilised i.e. phosphate buffer saline (PBS) (see Section 3.3.2.1). Additionally, the background electrolyte (PBS) reduces the resistance of the solution and prevents ohmic potential drop otherwise termed IR drop as given by Ohm's law (Equation 2.10).

$$V = IR$$

(2.10)

## 2.4 Constant Potential Amperometry (CPA)

All data presented in this thesis was recorded using CPA. CPA involves the application of a fixed potential and the continuous detection of a corresponding current change. Consumption of the analyte by the microelectrode is rapid and produces a current which is limited by mass transport. With CPA diffusion to the electrode surface is assumed to be the only form of mass transport which results in a steady-state diffusion limited current( $i_{ss}$ ).

$$i_{ss} = \frac{nFACD}{r}$$

(2.11)

Where  $n$  refers to the number of electrons,  $F$  is the Faraday constant,  $A$  refers to the surface area,  $C$  relates to concentration,  $D$  is the diffusion coefficient and  $r$  is the radius. The resulting current is directly proportional to the diffusion coefficient and the concentration of the target substrate.

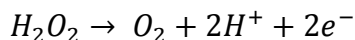
Practically the steady-state current is also dependent on aspects such as the insulation thickness of the electrode (Dayton *et al.*, 1980) and as a result a geometric factor ( $G$ ) is incorporated into Equation 2.11.

$$i_{ss} = \frac{GnFACD}{r}$$

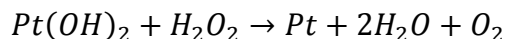
(2.12)

#### 2.4.1 Hydrogen peroxide ( $H_2O_2$ )

Platinum (Pt) electrodes are commonly used for the oxidation of  $H_2O_2$ . Pt is widely used in first generation biosensors for the detection of enzymatically produced  $H_2O_2$  (Lowry *et al.*, 2006). At +700 mV vs. SCE  $H_2O_2$  is oxidised on the surface of Pt at a diffusion controlled rate which results in a current response which is linear and directly proportional to the concentration of the target species (Lowry *et al.*, 1994; O'Brien *et al.*, 2007). The oxidation of  $H_2O_2$  is known to be a two-electron process as outlined below in Equation 2.13 This process is similar to the oxidation of  $H_2O_2$  at palladium electrodes where the formation of an oxide at the surface of the electrode is an essential step in the process of  $H_2O_2$  oxidation (Hall *et al.*, 1998) as seen in Equations 2.14 and 2.15.



(2.13)



(2.14)



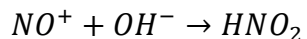
(2.15)

### 2.4.2 Nitric oxide (NO)

Nitric oxide (NO) can be electrochemically detected at the surface of Pt via a three-electron oxidation mechanism.



(2.16)



(2.17)



(2.18)

In this thesis a Nafion<sup>®</sup>-modified Pt disc electrode was constructed as previously described in detail by Brown *et al.* (Brown *et al.*, 2009) for the detection of NO. Briefly Nafion<sup>®</sup>, a negatively charged species, is thermally annealed onto the Pt surface of the electrode to facilitate interference rejection. Additionally an increase in NO sensitivity occurs following the Nafion<sup>®</sup> modification procedure (Brown *et al.*, 2009). The oxidation of NO at bare Pt surfaces involves the presence of adsorbed intermediates. As described by Brown *et al.* the presence of Nafion<sup>®</sup> in the modified NO sensor design eliminates these adsorbed species by stabilising the production of NO<sup>+</sup> (Equation 2.16) thereby preventing the processes described in Equation 2.17 and 2.18. The oxidation of NO at the Nafion<sup>®</sup> modified active surface may be described in terms of Equation 2.16.

### 2.4.3 Ascorbic acid (AA)

AA is an electroactive substance with an  $E_{1/2}$  of between -100 and +400 mV vs. SCE (Lowry *et al.*, 2006). The mechanism for oxidation of AA is represented below in Figure 2.4. AA is oxidised and in the process it loses two electrons and two hydrogen ions. The reaction is a  $2e^-$  process whereby L-dehydroascorbic acid is formed, this is then hydrated and exists in equilibrium with its hydrated form. L-dehydroascorbic is readily hydrolysed to form L-2-3-diketogulonic acid which is not electroactive.

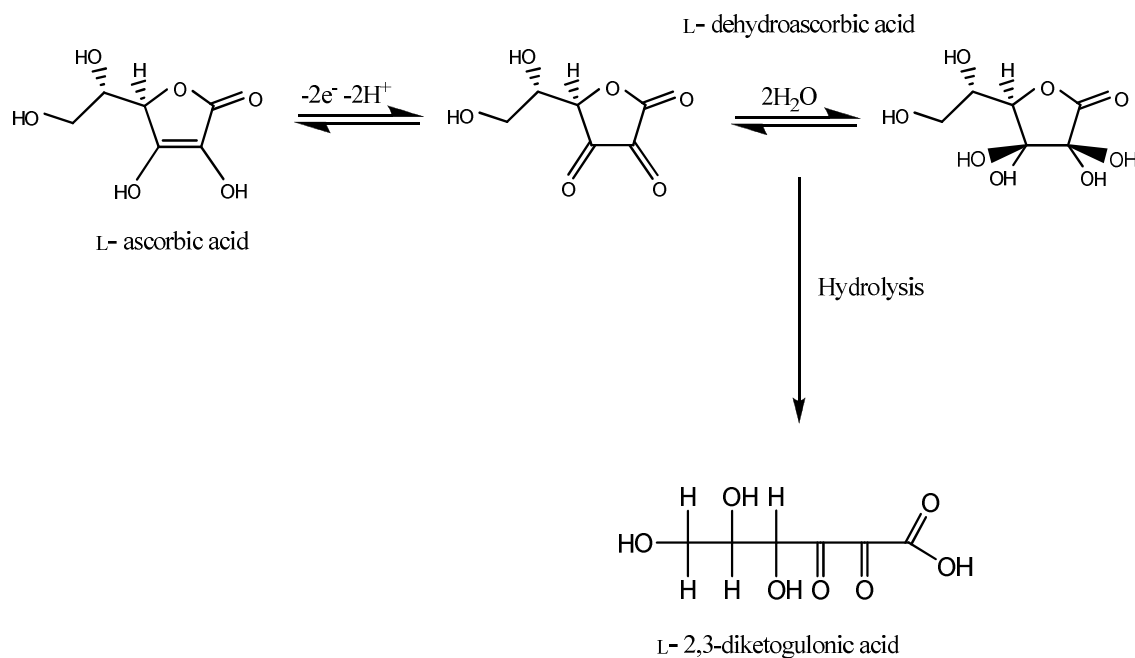


**Figure 2.4** Reaction scheme for the oxidation of ascorbic acid.

## 2.5 Electropolymerisation of *o*-Phenylenediamine (*o*-PD)

*o*-Phenylenediamine (*o*-PD) (1, 2-diaminobenzene) may be electropolymerised onto the surface of a Pt electrode to form an insulating poly-*o*-phenylenediamine (PPD) polymer. The use of PPD in sensor design has previously been demonstrated by Lowry *et al.* amongst other research groups (Sasso *et al.*, 1990; Lowry & O'Neill, 1992; Lowry *et al.*, 1994; Lowry *et al.*, 1998a; Rothwell *et al.*, 2010).

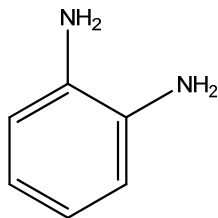


**Figure 2.4 Structure of the monomer (*o*-PD).**

The purpose of the PPD layer is to act as a permselective membrane which permits access of small molecules such as  $\text{H}_2\text{O}_2$  to the Pt surface and prevents the access of relatively larger molecules such as AA. The formation of PPD as a conducting polymer has previously been demonstrated (Malitesta *et al.*, 1990). In this thesis PPD was electropolymerised onto the surface of the Pt electrode in a neutral electrolyte (PBS) which facilitates the formation of an insulating polymer. This process results in the formation of a thin layer (10-30 nM) of PPD on the active surface of the electrode (O'Neill *et al.*, 2008). The PPD modified sensor maximises  $\text{H}_2\text{O}_2$  sensitivity and effectively eliminates the detection of AA. This aspect is important in relation to the selectivity of the catalase-based paired  $\text{H}_2\text{O}_2$  sensor design described in this thesis (see Section 4.3.3 and 4.5.3).

The exact structure of the non-conducting PPD structure has yet to be determined. As discussed by Losito *et al.* two possible structures exist (Losito *et al.*, 2001). These proposed structures consist of a 'ladder' (phenazine-like) structure presented in Figure 2.4(A) where the amino groups ( $\text{NH}_2$ ) are condensed within the benzene ring adjacent to each other along the polymer chain. The other proposed PPD formation consists of an 'open-ring' formation (1, 4 substituted benzenoid-quinoid structure) as shown in Figure 2.4(B). Losito *et al.* have shown that increased  $\text{NH}_2$  content is found when PPD is

formed at a more neutral pH (Losito *et al.*, 2003). This finding indicates that the ‘open-ring’ structure is formed under the polymerisation conditions outlined in this thesis (see Section 3.5.1).

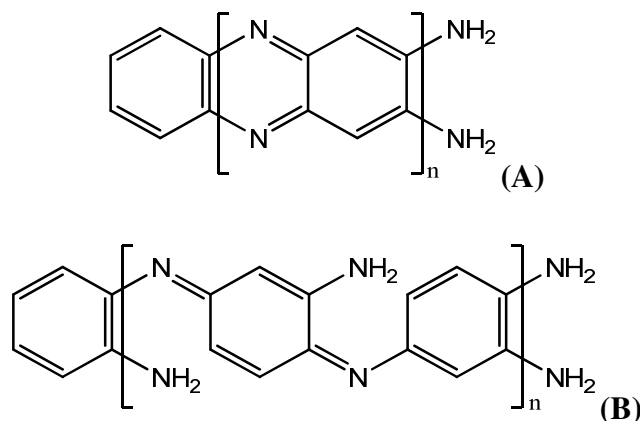


Figure 2.5 Proposed PPD polymer structures. (A) ‘ladder’ formation and (B) ‘open-ring’ structure

## 2.6 Nafion<sup>®</sup>

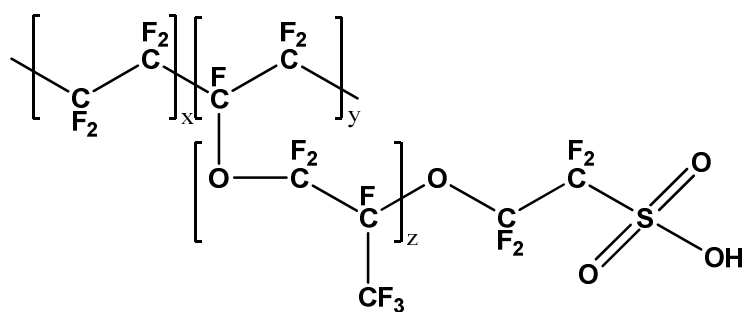


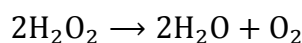
Figure 2.4 The structure of Nafion<sup>®</sup>.

Nafion<sup>®</sup> (Section 3.3.1.1) is a polyfluorinated polyacid which consists of a hydrophobic fluorocarbon scaffold permeated with clusters of hydrophilic ionic sulfonic acid groups ( $\text{SO}_3^-$ ). Nafion<sup>®</sup> is commonly used in sensor design due to the cation exchange properties of this polyacid (Mercado & Moussy, 1998; Park *et al.*, 1998; Mas *et al.*, 2002). Additionally, our research group has previously demonstrated a highly sensitive and selective NO sensor design which incorporates a Nafion<sup>®</sup> layer (Brown & Lowry, 2003; Brown *et al.*, 2009; Finnerty *et al.*, 2012a; Finnerty *et al.*, 2012b). The negatively charged Nafion<sup>®</sup> membrane repels anions such as AA and enables the stabilisation of

$\text{NO}^+$  which is formed upon the oxidation of  $\text{NO}$  as discussed in Section 2.4.2. Additionally the anionic rejection characteristics of Nafion<sup>®</sup> facilitate the selective detection of other cationic and neutral species such as  $\text{H}_2\text{O}_2$  against interference species such as AA in sensor design (O'Brien *et al.*, 2007).

## 2.7 Catalase

Catalase is one of the primary antioxidant enzymes present in the brain (Rice, 2011). The primary function of this enzyme is the catalytic removal of potentially harmful  $\text{H}_2\text{O}_2$  by the conversion of  $\text{H}_2\text{O}_2$  into inert substances i.e. water and oxygen (Equation 2.19).



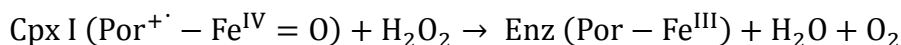
(2.19)

The catalase enzyme found in humans has a tetrameric structure with a heme group at the central active site (Kirkman & Gaetani, 2007). The catalytic dismutation of  $\text{H}_2\text{O}_2$  by the heme-containing enzyme is outlined in Equation 2.20 and 2.21. The overall process occurs by a two stage mechanism. In the initial step (Equation 2.20)  $\text{H}_2\text{O}_2$  oxidises the heme-containing enzyme to form a porphyrin (Por) cationic radical.



(2.20)

In the second step of the  $\text{H}_2\text{O}_2$  dismutation mechanism (Equation 2.21) an additional molecule of  $\text{H}_2\text{O}_2$  will reduce Complex I (CPx I) to regenerate the resting state of the catalase enzyme (Enz) and produce water and oxygen.



(2.21)

These combined processes (Equation 2.20 and 2.21) lead to the conversion of  $\text{H}_2\text{O}_2$  into water and oxygen (Equation 2.19).

## 2.8 Paired catalase-based H<sub>2</sub>O<sub>2</sub> biosensor

The paired H<sub>2</sub>O<sub>2</sub> sensor utilised in this thesis was fabricated and modified by a process previously described by O'Brien *et al.* (O'Brien *et al.*, 2007). Additionally, a detailed description of the fabrication process is given in Chapter 3 Section 3.4.3.

Briefly, the paired H<sub>2</sub>O<sub>2</sub> sensor utilised in this thesis consists of a pair of Pt cylinder electrodes both modified with the permselective membranes Nafion<sup>®</sup> (Section 2.6) and PPD (Section 2.5). One of these electrodes was further modified with catalase (Section 2.7). This process yielded two amperometric electrodes one with catalase adhered (*Cat*) and the other without (*Blank*). Two sensors are produced by this process; one capable of detecting H<sub>2</sub>O<sub>2</sub> [Pt<sub>c</sub>/Nafion<sup>®</sup>/PPD (*Blank*)] and a paired sensor capable of removing H<sub>2</sub>O<sub>2</sub> [Pt<sub>c</sub>/Nafion<sup>®</sup>/PPD/Cat-Ga (*Cat*)].

The H<sub>2</sub>O<sub>2</sub> sensitivity of the paired biosensor design was derived by subtracting the *Cat* sensor current response from that recorded at the *Blank* sensor. A detailed description of the overall subtracted response of the paired H<sub>2</sub>O<sub>2</sub> sensor has previously been described by O'Brien *et al.* (O'Brien *et al.*, 2007). For the purpose of clarity a synopsis of the previously described subtracted response of the paired H<sub>2</sub>O<sub>2</sub> sensor is given in this section.

When implanted in the physiological environment the current measured at the *Blank* sensor ( $I_{Blank}$ ) and *Cat* sensor ( $I_{Cat}$ ) will arise from interference species  $I_{INTb}$  and  $I_{INTc}$  respectively in addition to H<sub>2</sub>O<sub>2</sub> ( $I_{HP}$ ).

$$I_{Blank} = I_{INTb} + I_{HP}$$

(2.22)

$$I_{Cat} = I_{INTc} + C_{HP}I_{HP}$$

(2.23)

Equation 2.22 represents the current response of the *Blank* sensor *in-vivo*. Equation 2.23 demonstrates overall current response of the *Cat* sensor implanted in the physiological environment.  $C_{HP}$  represents the fraction of H<sub>2</sub>O<sub>2</sub> not degraded by the catalase-based

sensor (*Cat*). The value of  $C_{HP}$  is effectively eliminated from the equation as ~98 % of the  $H_2O_2$  signal is removed by the *Cat* sensor (see Section 4.7). Provided the value of  $I_{INTb}$  and  $I_{INTc}$  are essentially the same the overall response of the paired catalase-based  $H_2O_2$  sensor ( $\Delta I$ ) is determined by subtracting the current response of the *Cat* sensor from the *Blank* sensor. The matched interference rejection characteristics of the *Blank* and *Cat* sensor are demonstrated in Section 4.8. The overall  $H_2O_2$  response of the paired sensor is described as follows.

$$\Delta I = I_{Blank} - I_{Cat} = (1 - C_{HP})I_{HP} \quad (2.24)$$

As discussed the interference rejection properties of the *Cat* ( $I_{INTc}$ ) and *Blank* ( $I_{INTb}$ ) sensor are matched (see Section 4.8).

$$\text{If } I_{INTb} \neq I_{INTc} \text{ and } I_{INTc} = C_{INT}I_{INTb} \quad (2.25)$$

Where  $C_{INT}$  represents the proportionality factor between ( $I_{INTc}$ ) and ( $I_{INTb}$ ).

$$\therefore \Delta I = (1 - C_{INT})I_{INTb} + (1 - C_{HP})I_{HP} \quad (2.26)$$

The value of  $C_{INT}$  is effectively unity and also the value of  $C_{HP}$  is effectively zero.

$$\therefore \Delta I = I_{INTb} + I_{HP} \quad (2.27)$$

The value of  $I_{INTb}$  is very low as shown by the response of the *Blank* sensor to the addition of AA *in-vitro* (see Section 4.5.4). Additionally, the impact of the value of  $I_{INTb}$  diminishes relative to large response of  $I_{HP}$ . Therefore, the overall response of the paired catalase-based  $H_2O_2$  sensor *in-vivo* is simply yielded by subtraction of the *Cat* sensor response from that of the *Blank* sensor ( $I_{Blank} - I_{Cat}$ ).

## 2.9 Microdialysis

Microdialysis (MD) is a technique which may be used to sample low molecular weight substances in the physiological environment. The use of the MD sampling technique for the collection of small molecules present in the extracellular fluid (ECF) of the brain has previously been extensively reviewed (Lonroth & Smith, 1990; Peters *et al.*, 2000; Tisdall & Smith, 2006).

A small probe is implanted into the brain which consists of a hollow fibre dialysis membrane. A liquid is perfused through this probe (perfusate) and low molecular weight substances are recovered from the outlet fluid (dialysate) by the process of diffusion. The perfusate normally used is artificial cerebrospinal fluid (aCSF) (see Section 3.3.2.2).

The MD technique functions by the diffusion of a higher concentration of analyte in the surrounding tissue across a concentration gradient towards the lower concentration present within the microdialysis probe. Subsequently, the dialysate may be analysed by various methods including high performance liquid chromatography (HPLC) (Perry *et al.*, 2009). The primary disadvantage of this technique is the time lag associated with the collection of the dialysate (O'Neill & Lowry, 2000).

In this thesis the dialysate was not collected for the purpose of analysis. The paired H<sub>2</sub>O<sub>2</sub> sensor was glued to the microdialysis probe and the entire construct was implanted into the brain (see Chapter 5). In this way real-time electrochemical data from the implanted sensor was facilitated following the perfusion of substances of interest (see Chapter 5). The local administration of substances to the brain in this manner has previously been demonstrated and is termed retrodialysis (RD) (Huynh *et al.*, 2007).

Additionally, the ECF concentration of the target substrate may be estimated by the RD method. The perfusion of substrate, which has a higher concentration to that present in the surrounding tissue, will result in an increase in the recorded current at the implanted sensor. Correspondingly the perfusion of a lower substrate concentration in relation to the ECF will result in a decrease in the current recorded by the sensor. The perfusion of various concentrations of substrate will yield a calibration curve from the implanted

sensor. The basal concentration of substrate in the ECF may be determined from this calibration curve as previously shown (Miele & Fillenz, 1996; Lowry *et al.*, 1998b). This method is a modification of the zero net flux technique as previously demonstrated by Lonroth *et al.* (Lonroth *et al.*, 1987).

However, the determination of the ECF concentration of the target analyte in this manner has significant drawbacks. The implanted sensor may disturb the natural processes taking place in the surrounding brain tissue. For example the absolute basal concentration of dopamine determined by microdialysis has been much debated due to uptake mechanisms present *in-situ* and a proposed trauma layer induced by implantation of the probe itself (Bungay *et al.*, 2003).

Additionally, the delivery of the target substrate to the electrochemical sensor implanted in the brain may be restricted by recovery issues associated with the MD/RD technique. The recovery ratio of a substance using the MD technique is defined as the concentration in the dialysate expressed as a percentage of the concentration present in the interstitial fluid. Ideally the recovery ratio should be 100 % however under maximal conditions where a slow flow rate and relatively long MD membrane are utilised the recovery ratio has been estimated to be only 70 % (Ungerstedt & Rostami, 2004). Therefore with the RD technique not all of the substrate added to the perfusate will reach the tissue surrounding the implanted sensor. Thus this inherent recovery issue may result in a lower than expected recorded response by the implanted sensor.

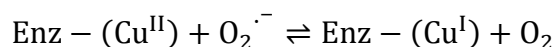
## 2.10 Oxidative and nitrosative stress

Reactive oxygen species (ROS) such as  $H_2O_2$  and reactive nitrogen species (RNS) such as NO exert both beneficial and harmful effects in the neuronal environment (Calabrese *et al.*, 2007; Rice, 2011). An extensive antioxidant network tightly regulates the production of ROS and RNS in the brain and exists to maintain normal redox homeostasis (Simonian & Coyle, 1996; Valko *et al.*, 2007). A disruption to this robust network leads to the over production of ROS (e.g.  $H_2O_2$ ) and RNS (e.g. NO) which leads to the development of oxidative/nitrosative stress and consequently a disruption to normal cell function. Oxidative/nitrosative stress has been linked to a variety of

neurodegenerative diseases and dysfunctions such as Parkinson's disease, Alzheimer's disease and more recently autism spectrum disorders (ASDs) (Barnham *et al.*, 2004; Chauhan & Chauhan, 2006). This section will outline the main antioxidant defence processes and mechanisms which lead to ROS/RNS production in the brain.

### 2.10.1 Antioxidants

As previously stated a variety of defence mechanisms exist to control the excess production of ROS/RNS and hence maintain redox homeostasis in the brain. These consist of various enzymatic and non-enzymatic sources. The primary enzymes responsible for the maintenance of redox balance are catalase (Cat) superoxide dismutase (SOD) and glutathione peroxidase (GPx). The mechanism of action of the catalase enzyme in the removal of potentially harmful H<sub>2</sub>O<sub>2</sub> is presented in Section 2.7. The metalloenzyme SOD catalyses the disproportionation of superoxide (O<sub>2</sub><sup>·-</sup>) into H<sub>2</sub>O<sub>2</sub> and O<sub>2</sub> (Liochev & Fridovich, 2000). The dismutation i.e. oxidation and reduction of O<sub>2</sub><sup>·-</sup>, due to the variable oxidation state of the metallic centre of the enzyme occurs by a two-step mechanism and is outlined below in Equation 2.28 and 2.29.

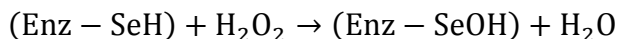


(2.28)

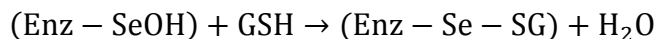


(2.29)

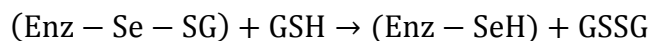
The selenoprotein i.e. selenium containing enzyme GPx is one of the primary enzymes responsible for the regulation of H<sub>2</sub>O<sub>2</sub>/ROS levels in the brain (Dringen *et al.*, 2005). The presence of glutathione (GSH) is a necessary requirement in the catalytic reduction of H<sub>2</sub>O<sub>2</sub> by GPx. The catalytic removal of H<sub>2</sub>O<sub>2</sub> by GPx occurs by a multi-step mechanism which involves the recycling of GSH from its oxidised form glutathione disulfide (GSSG) (Dringen, 2000; Prabhakar *et al.*, 2005).



(2.30)



(2.31)



(2.32)

GSSG is converted back to GSH by the glutathione reductase enzyme (GR). The GR enzyme transfers electrons from nicotinamide adenine dinucleotide phosphate (NADPH) to GSSG which produces GSH. The entire mechanism of GPx mediated  $\text{H}_2\text{O}_2$  removal results in the production of water and is dependent on the cyclic conversion between GSH and GSSG (Valko *et al.*, 2007). The contributing processes of catalytic removal of  $\text{H}_2\text{O}_2$  by Cat, SOD and GPx are summarised below in Figure 2.5.

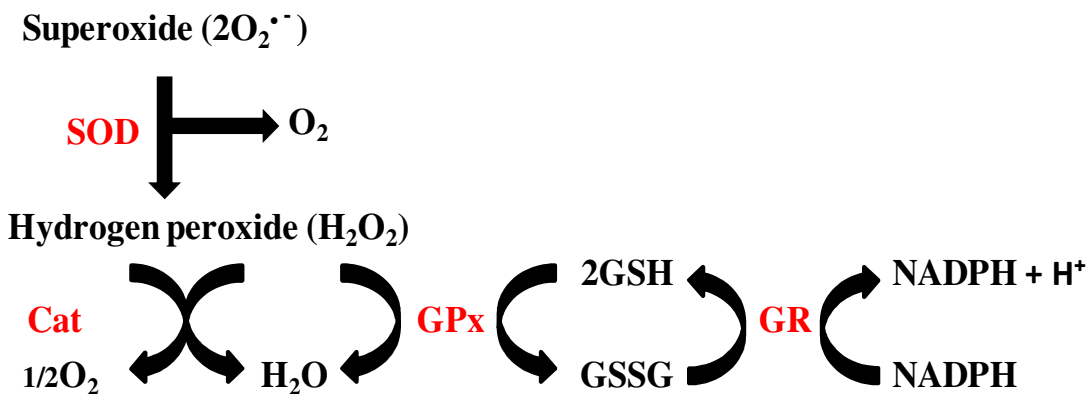


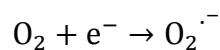
Figure 2.5 Enzymatic antioxidant processes.

A variety of non-enzymatic sources of antioxidants also exist in the neuronal environment including ascorbate (vitamin C),  $\alpha$ -tocopherol (vitamin E) and GSH which collectively contribute to maintain redox homeostasis (Rice, 2000; Valko *et al.*, 2007; Winterbourn, 2008). The basic mechanism of action of ascorbate as an antioxidant relies

on its ability to donate electrons to directly scavenge ROS/RNS such as  $O_2^{\cdot-}$  or peroxynitrite ( $ONOO^-$ ) (Rice, 2000). The oxidation of ascorbate in this manner produces dehydroascorbate (Section 2.4.3) and this radical intermediate may be reduced to reform ascorbate by GSH (Rice, 2000). Vitamin E carries out its antioxidant effects in a similar manner to vitamin C (Winterbourn, 2008). Additionally the oxidised form of Vitamin E can be reduced and replenished by Vitamin C and GSH (Valko *et al.*, 2007). A disruption to the normal physiological function of these various enzymatic and non-enzymatic antioxidant sources leads to the over production of ROS and RNS and hence the development of oxidative/nitrosative stress (Barnham *et al.*, 2004).

### 2.10.2 Reactive oxygen species (ROS)

The primary ROS;  $O_2^{\cdot-}$  is produced within the mitochondria of a cell. Molecular oxygen ( $O_2$ ) is routinely reduced to form water by the mitochondrial electron transport chain (ETC) which produces energy in the form of ATP. Molecular oxygen has a unique electronic configuration in that it consists of two unpaired electrons and exists essentially as two free radicals. The addition of one electron to  $O_2$  will result in the formation of  $O_2^{\cdot-}$ . During the mitochondrial energy transduction process a small number of electrons may 'leak' to molecular oxygen and form  $O_2^{\cdot-}$  as shown in Equation 2.33. Due to the high energy demand of the brain this process is particularly relevant in the neuronal environment. Additional sources of  $O_2^{\cdot-}$  production exist including the action of NADPH oxidases (NOXs) and xanthine oxidase (Maier & Chan, 2002).



(2.33)

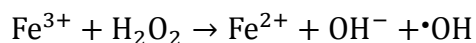
$O_2^{\cdot-}$  is readily scavenged by the antioxidant network in the physiological environment which leads to the production of secondary ROS such as  $H_2O_2$ .  $H_2O_2$  is a relatively stable ROS and is primarily produced by the action of the catalytic enzyme SOD as discussed in Section 2.10.1. Additionally,  $H_2O_2$  may form spontaneously by dismutation although this process is considerably slower (Equation 2.34). Detailed descriptions of

the various normal physiological functions of H<sub>2</sub>O<sub>2</sub> are outlined in Chapter 1. However, this section will outline the production of excess H<sub>2</sub>O<sub>2</sub> amongst other ROS in a pro-oxidant environment.

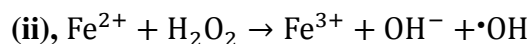
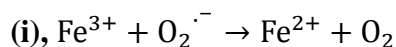


(2.34)

The highly reactive ROS hydroxyl radical ( $\cdot\text{OH}$ ) can be formed from the interaction between H<sub>2</sub>O<sub>2</sub> and transition metal ions. The process of  $\cdot\text{OH}$  formation occurs via the Fenton reaction which relies on the presence of free catalytic iron (Valko *et al.*, 2007). This process commonly occurs *in-vitro* however in the physiological environment iron is bound and sequestered as ferritin (Jomova & Valko, 2011). In a pro-oxidant neuronal environment the presence of O<sub>2</sub><sup>·-</sup> results in the release of iron from sequestered sources, thereby leading to the production of  $\cdot\text{OH}$  via the Fenton reaction (Equation 2.35) (Maier & Chan, 2002). O<sub>2</sub><sup>·-</sup> may drive the Fenton reaction in the physiological environment due to the release of free iron by the action of O<sub>2</sub><sup>·-</sup> itself through the Haber-Weiss reaction [Equation 2.36 (i) and (ii)] (Liochev & Fridovich, 1999).



(2.35)



(2.36)

A schematic representation of the main sources of primary and secondary ROS production in the physiological environment is shown in Figure 2.6.

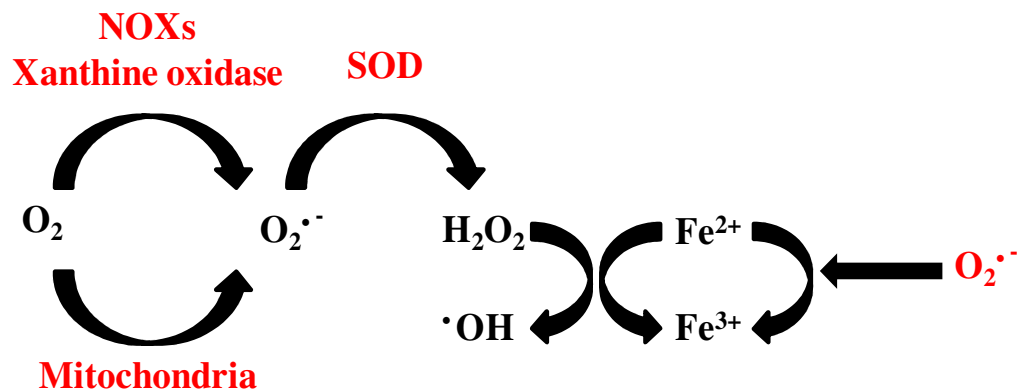


Figure 2.6 Main sources of ROS.

Collectively the uncontrolled production of ROS leads to damage to cell structures, DNA, lipids and proteins (Valko *et al.*, 2007).  $H_2O_2$  is a relatively stable ROS, it is considerably less reactive than  $O_2^{\bullet -}$  and  $\bullet OH$  (Rice, 2011). Additionally  $H_2O_2$  has a relatively longer half-life *in-vivo* (Maier & Chan, 2002). Therefore the detection of this stress marker ( $H_2O_2$ ) is a highly suitable target for the purpose of monitoring oxidative stress in the physiological environment.

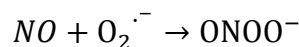
### 2.10.3 Reactive nitrogen species (RNS)

NO is a radical species generated in the physiological environment from three main NO synthase enzymes (NOS). The source of NOS determines the specific type of NO produced in the body and these consist of inducible NOS (iNOS), endothelial NOS (eNOS) and neuronal NOS (nNOS) (Bruckdorfer, 2005; Guix *et al.*, 2005). A detailed description of the biosynthesis of NO is described in Section 1.4. Briefly NO is produced from L-arginine in the presence of numerous co-factors including NOS,  $BH_4$  (tetrahydrobiopterin), FMN (flavin mononucleotide), FAD (flavin adenine dinucleotide) haem and calmodulin. The variety of neuroprotective physiological functions of NO while present at tonic levels are discussed in Section 6.1. This section primarily outlines the role of high levels of NO in a pro-oxidant environment.

All three isoforms of NOS consist of a reductase and an oxygenase domain which facilitate the interaction with the stated co-factors for the purpose of NO biosynthesis (Alderton *et al.*, 2001). A deficiency in the co-factor  $BH_4$  can lead to electron transfer

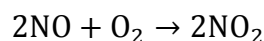
between NOS and molecular oxygen and result in the formation of the primary ROS ( $O_2^{\cdot-}$ ). This process is referred to as ‘NOS uncoupling’ and results in the preferential formation of  $O_2^{\cdot-}$  over NO by NOS (Kuzkaya *et al.*, 2003).

In a pro-oxidant environment NO can interact directly with  $O_2^{\cdot-}$  and lead to the formation of the main secondary highly toxic RNS; ONOO<sup>-</sup> (Equation 2.37). This process may be accelerated in response to an inflammatory insult where  $O_2^{\cdot-}$  and NO specifically produced by iNOS, are produced (Calabrese *et al.*, 2007). ONOO<sup>-</sup> is a powerful oxidising agent which may lead to the degradation of DNA and lipids (Ramalingam & Kim, 2012).



(2.37)

The interaction between NO and other ROS can lead to the production of other secondary RNS such as nitrogen dioxide (NO<sub>2</sub>) and dinitrogen trioxide (N<sub>2</sub>O<sub>3</sub>) which exert toxic effects in the body (Equation 2.38 and 2.39) (Wink & Mitchell, 1998).



(2.38)



(2.39)

NO can also activate the constitutive and inducible forms of cyclooxygenase which are recruited in response to an inflammatory insult (Mollace *et al.*, 2005). The consumption of cyclooxygenase leads to the release of free radicals which can lead to deleterious neuronal processes (Mancuso *et al.*, 2007). Figure 2.7 outlines the main mechanisms of RNS production in the *in-vivo* environment.

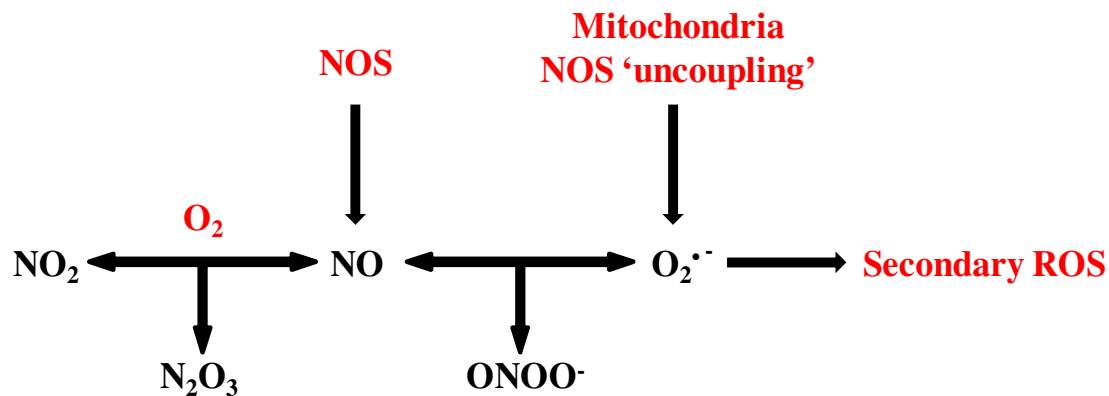


Figure 2.7 Main sources of RNS.

The real-time electrochemical detection of  $\text{NO}$  which is represented in this thesis may facilitate the analysis of nitrosative stress processes amongst other applications.

This section outlines the main processes underlying the intricate natural balance which exists between the processes of ROS/RNS production and the defence mechanism of the robust antioxidant network in the neuronal environment. A disruption to these myriad of vital neuronal processes leads to redox imbalance and consequently oxidative/nitrosative stress. A detailed description of the role of oxidative/nitrosative stress in specific neurodegenerative diseases and dysfunctions is provided in Chapter 1.

## References

- Alderton WK, Cooper CE & Knowles RG. (2001). Nitric oxide synthases: structure, function and inhibition. *Biochemical Journal* **357**, 593-615.
- Bard AJ & Faulkner LR. (2001). *Electrochemical Methods: Fundamentals and Applications, 2nd Edition*. John Wiley & Sons Inc.
- Barnham KJ, Masters CL & Bush AI. (2004). Neurodegenerative diseases and oxidative stress. *Nature Reviews Drug Discovery* **3**, 205-214.
- Brown FO, Finnerty NJ & Lowry JP. (2009). Nitric oxide monitoring in brain extracellular fluid: characterisation of Nafion<sup>®</sup>-modified Pt electrodes *in vitro* and *in vivo*. *Analyst* **134**, 2012-2020.
- Brown FO & Lowry JP. (2003). Microelectrochemical sensors for *in vivo* brain analysis: an investigation of procedures for modifying Pt electrodes using Nafion<sup>®</sup>. *Analyst* **128**, 700-705.
- Bruckdorfer R. (2005). The basics about nitric oxide. *Molecular Aspects of Medicine* **26**, 3-31.
- Bungay PM, Newton-Vinson P, Isele W, Garris PA & Justice JB. (2003). Microdialysis of dopamine interpreted with quantitative model incorporating probe implantation trauma. *Journal of Neurochemistry* **86**, 932-946.
- Calabrese V, Mancuso C, Calvani M, Rizzarelli E, Butterfield DA & Stella AMG. (2007). Nitric oxide in the central nervous system: neuroprotection versus neurotoxicity. *Nature Reviews Neuroscience* **8**, 766-775.
- Chauhan A & Chauhan V. (2006). Oxidative stress in autism. *Pathophysiology : the official journal of the International Society for Pathophysiology / ISP* **13**, 171-181.
- Dayton MA, Brown JC, Stutts KJ & Wightman RM. (1980). Faradaic electrochemistry at microvoltammetric electrodes. *Analytical Chemistry* **52**, 946-950.
- Dringen R. (2000). Metabolism and functions of glutathione in brain. *Prog Neurobiol* **62**, 649-671.
- Dringen R, Pawlowski PG & Hirrlinger J. (2005). Peroxide detoxification by brain cells. *Journal of Neuroscience Research* **79**, 157-165.
- Finnerty NJ, O'Riordan SL, Brown FO, Serra PA, O'Neill RD & Lowry JP. (2012a). *In vivo* characterisation of a Nafion<sup>®</sup>-modified Pt electrode for real-time nitric oxide monitoring in brain extracellular fluid. *Analytical Methods* **4**, 550-557.

- Finnerty NJ, O’Riordan SL, Palsson E & Lowry JP. (2012b). Brain nitric oxide: Regional characterisation of a real-time microelectrochemical sensor. *Journal of Neuroscience Methods* **209**, 13-21.
- Forster RJ. (1994). Microelectrodes: new dimensions in electrochemistry. *Chemical Society Reviews* **23**, 289-297.
- Guix FX, Uribealago I, Coma M & Munoz FJ. (2005). The physiology and pathophysiology of nitric oxide in the brain. *Progress in Neurobiology* **76**, 126-152.
- Hall SB, Khudaish EA & Hart AL. (1998). Electrochemical oxidation of hydrogen peroxide at platinum electrodes. Part 1. An adsorption-controlled mechanism. *Electrochimica Acta* **43**, 579-588.
- Huynh GH, Ozawa T, Deen DF, Tihan T & Szoka FC, Jr. (2007). Retro-convection enhanced delivery to increase blood to brain transfer of macromolecules. *Brain Research* **1128**, 181-190.
- Jomova K & Valko M. (2011). Advances in metal-induced oxidative stress and human disease. *Toxicology* **283**, 65-87.
- Kelm M. (1999). Nitric oxide metabolism and breakdown. *Biochimica Et Biophysica Acta-Bioenergetics* **1411**, 273-289.
- Kirkman HN & Gaetani GF. (2007). Mammalian catalase: a venerable enzyme with new mysteries. *Trends in Biochemical Sciences* **32**, 44-50.
- Kuzkaya N, Weissmann N, Harrison DG & Dikalov S. (2003). Interactions of peroxynitrite, tetrahydrobiopterin, ascorbic acid, and thiols - Implications for uncoupling endothelial nitric-oxide synthase. *Journal of Biological Chemistry* **278**, 22546-22554.
- Liochev SI & Fridovich I. (1999). Superoxide and iron: Partners in crime. *Iubmb Life* **48**, 157-161.
- Liochev SI & Fridovich I. (2000). Copper- and zinc-containing superoxide dismutase can act as a superoxide reductase and a superoxide oxidase. *Journal of Biological Chemistry* **275**, 38482-38485.
- Lonroth P, Jansson PA & Smith U. (1987). A microdialysis method allowing characterization of intercellular water space in humans. *American Journal of Physiology* **253**, E228-E231.

- Lonroth P & Smith U. (1990). Microdialysis - a novel technique for clinical investigations. *Journal of Internal Medicine* **227**, 295-300.
- Losito I, De Giglio E, Cioffi N & Malitesta C. (2001). Spectroscopic investigation on polymer films obtained by oxidation of *o*-phenylenediamine on platinum electrodes at different pHs. *Journal of Materials Chemistry* **11**, 1812-1817.
- Losito I, Palmisano F & Zambonin PG. (2003). *o*-Phenylenediamine Electropolymerization by Cyclic Voltammetry Combined with Electrospray Ionization-Ion Trap Mass Spectrometry. *Analytical Chemistry* **75**, 4988-4995.
- Lowry JP, McAteer K, Elatrash SS, Duff A & O'Neill RD. (1994). Characterisation of glucose oxidase-modified poly(phenylenediamine)-coated electrodes *in-vitro* and *in-vivo*: homogeneous interference by ascorbic acid in hydrogen-peroxide detection. *Analytical Chemistry* **66**, 1754-1761.
- Lowry JP, Miele M, O'Neill RD, Boutelle MG & Fillenz M. (1998a). An amperometric glucose-oxidase/poly(*o*-phenylenediamine) biosensor for monitoring brain extracellular glucose: *in vivo* characterisation in the striatum of freely-moving rats. *Journal of Neuroscience Methods* **79**, 65-74.
- Lowry JP & O'Neill RD. (1992). Homogenous mechanism of ascorbic-acid interference in hydrogen-peroxide detection at enzyme-modified electrodes. *Analytical Chemistry* **64**, 453-456.
- Lowry JP, O'Neill RD & (2006). *Neuroanalytical Chemistry In Vivo Using Biosensors.*, vol. 10. American Scientific Publishers.
- Lowry JP, O'Neill RD, Boutelle MG & Fillenz M. (1998b). Continuous monitoring of extracellular glucose concentrations in the striatum of freely moving rats with an implanted glucose biosensor. *Journal of Neurochemistry* **70**, 391-396.
- Maier CM & Chan PH. (2002). Role of superoxide dismutases in oxidative damage and neurodegenerative disorders. *Neuroscientist* **8**, 323-334.
- Malitesta C, Palmisano F, Torsi L & Zambonin PG. (1990). Glucose fast-response amperometric sensor based on glucose-oxidase immobilized in an electropolymerized poly(ortho-phenylenediamine) film. *Analytical Chemistry* **62**, 2735-2740.
- Mancuso C, Scapagnini G, Curro D, Giuffrida Stella AM, De Marco C, Butterfield DA & Calabrese V. (2007). Mitochondrial dysfunction, free radical generation and cellular stress response in neurodegenerative disorders. *Frontiers in Bioscience* **12**, 1107-1123.

- Mas M, Escrig A & Gonzalez-Mora JL. (2002). *In vivo* electrochemical measurement of nitric oxide in corpus cavernosum penis. *Journal of Neuroscience Methods* **119**, 143-150.
- Mercado RC & Moussy F. (1998). *In vitro* and *in vivo* mineralization of Nafion membrane used for implantable glucose sensors. *Biosensors & Bioelectronics* **13**, 133-145.
- Miele M & Fillenz M. (1996). *In vivo* determination of extracellular brain ascorbate. *Journal of Neuroscience Methods* **70**, 15-19.
- Mollace V, Muscoli C, Masini E, Cuzzocrea S & Salvemini D. (2005). Modulation of prostaglandin biosynthesis by nitric oxide and nitric oxide donors. *Pharmacological Reviews* **57**, 217-252.
- O'Brien KB, Killoran SJ, O'Neill RD & Lowry JP. (2007). Development and characterization *in vitro* of a catalase-based biosensor for hydrogen peroxide monitoring. *Biosensors & Bioelectronics* **22**, 2994-3000.
- O'Neill RD & Lowry JP. (2000). Voltammetry In Vivo for Chemical Analysis of the Living Brain. In *Encyclopedia of Analytical Chemistry*. John Wiley & Sons, Ltd.
- O'Neill RD, Lowry JP, Rocchitta G, McMahon CP & Serra PA. (2008). Designing sensitive and selective polymer/enzyme composite biosensors for brain monitoring *in vivo*. *Trac-Trends in Analytical Chemistry* **27**, 78-88.
- Park JK, Tran PH, Chao JKT, Ghodadra R, Rangarajan R & Thakor NV. (1998). *In vivo* nitric oxide sensor using non-conducting polymer-modified carbon fiber. *Biosensors & Bioelectronics* **13**, 1187-1195.
- Perry M, Li Q & Kennedy RT. (2009). Review of recent advances in analytical techniques for the determination of neurotransmitters. *Analytica Chimica Acta* **653**, 1-22.
- Peters JL, Yang H & Michael AC. (2000). Quantitative aspects of brain microdialysis. *Analytica Chimica Acta* **412**, 1-12.
- Prabhakar R, Vreven T, Morokuma K & Musaev DG. (2005). Elucidation of the mechanism of selenoprotein glutathione peroxidase (GPx)-catalyzed hydrogen peroxide reduction by two glutathione molecules: A density functional study. *Biochemistry* **44**, 11864-11871.
- Ramalingam M & Kim S-J. (2012). Reactive oxygen/nitrogen species and their functional correlations in neurodegenerative diseases. *Journal of Neural Transmission* **119**, 891-910.

- Rice ME. (2000). Ascorbate regulation and its neuroprotective role in the brain. *Trends in Neurosciences* **23**, 209-216.
- Rice ME. (2011). H<sub>2</sub>O<sub>2</sub>: A Dynamic Neuromodulator. *Neuroscientist* **17**, 389-406.
- Rothwell SA, Killoran SJ & O'Neill RD. (2010). Enzyme Immobilization Strategies and Electropolymerization Conditions to Control Sensitivity and Selectivity Parameters of a Polymer-Enzyme Composite Glucose Biosensor. *Sensors* **10**, 6439-6462.
- Sasso SV, Pierce RJ, Walla R & Yacynych AM. (1990). Electropolymerized 1,2-diaminobenzene as a means to prevent interferences and fouling and to stabilize immobilized enzyme in electrochemical biosensors. *Analytical Chemistry* **62**, 1111-1117.
- Simonian NA & Coyle JT. (1996). Oxidative stress in neurodegenerative diseases. *Annual Review of Pharmacology and Toxicology* **36**, 83-106.
- Tisdall MM & Smith M. (2006). Cerebral microdialysis: research technique or clinical tool. *British Journal of Anaesthesia* **97**, 18-25.
- Ungerstedt U & Rostami E. (2004). Microdialysis in neurointensive care. *Current Pharmaceutical Design* **10**, 2145-2152.
- Valko M, Leibfritz D, Moncol J, Cronin MTD, Mazur M & Telser J. (2007). Free radicals and antioxidants in normal physiological functions and human disease. *International Journal of Biochemistry & Cell Biology* **39**, 44-84.
- Wink DA & Mitchell JB. (1998). Chemical biology of nitric oxide: Insights into regulatory, cytotoxic, and cytoprotective mechanisms of nitric oxide. *Free Radical Biology and Medicine* **25**, 434-456.
- Winterbourn CC. (2008). Reconciling the chemistry and biology of reactive oxygen species. *Nature Chemical Biology* **4**, 278-286.

---

## **3. Experimental**

---

### 3.1 Introduction

This chapter details the experimental procedures involved in the *in-vitro* and *in-vivo* characterisation of a catalase-based hydrogen peroxide ( $\text{H}_2\text{O}_2$ ) biosensor pair. The excellent sensitivity and selectivity of the  $\text{H}_2\text{O}_2$  biosensor has previously been demonstrated *in-vitro* (O'Brien et al., 2007). Further investigations utilising a previously characterised nitric oxide (NO) sensor will also be discussed; the *in-vivo* application of this NO sensor enables real time detection of rapid fluctuations in brain NO (Brown *et al.*, 2009).

Section 3.2 will give an overview of the computer based instrumentation used in this research project. A detailed description of the chemicals and solutions used throughout the project will be given in Section 3.3. Section 3.4 will describe how each sensor was constructed during the course of this body of work. The modifications and treatments made to the fabricated sensors will be presented in Sections 3.5 and 3.6 respectively. A detailed description of the experiments used in the *in-vitro* characterisation of each sensor is outlined in Section 3.7.

Section 3.8 will discuss the technique of microdialysis (MD) and its application in this research project. The use of scanning electron microscopy (SEM) will be outlined in Section 3.9. The protocol followed for the application of these sensors in the *in-vivo* environment will be detailed in Section 3.10. Section 3.11 will outline the systemic administrations utilised throughout the *in-vivo* experiments.

The in-house synthesis of NO is referred to in Section 3.12 and any additional equipment used during the project will be described in Section 3.13.

## 3.2 Computer based Instrumentation

Three main components were used in the acquisition of experimental data. These three instruments consist of the computer, the Powerlab<sup>®</sup> and the potentiostat. The function of each instrument is outlined in this section. The arrangement of the *in-vitro* instrumentation is displayed in the image below.

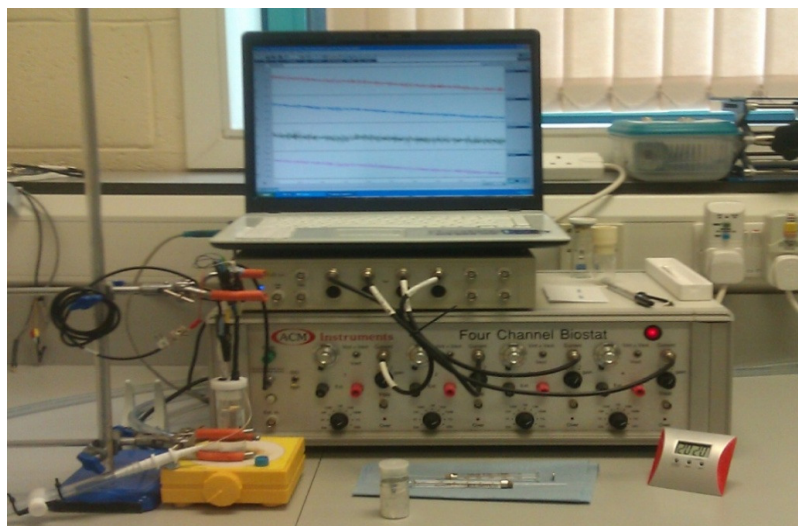


Fig 3.1: The *in-vitro* experimental set-up.

### 3.2.1 The Computer

A logiQ M76OTG notebook with an Intel dual core processor running at 1.8 GHz was used for the attainment of *in-vitro* data. *In-vivo* data was recorded using a MAC OS X with an Intel core 2 duo processor running at 2.4 GHz.

### 3.2.2 The Powerlab<sup>®</sup>

The Powerlab<sup>®</sup> is a data acquisition system comprising hardware and software to record and display experimental data. The Powerlab<sup>®</sup> is an interface between the computer and potentiostat which allows digital-analogue and analogue-digital conversion. In this research project an eight channel Powerlab<sup>®</sup> 8/30 from AD Instruments was utilised.



**Fig 3.2: PowerLab<sup>®</sup> 8/30.**

### 3.2.3 The Potentiostat

The potentiostat utilised was a four channel Biostat from ACM Instruments. The basic operating principle of the biostat is to control the potential of the working electrode at a constant level with respect to the reference electrode. This device allows the application of a fixed potential and the detection of a corresponding current change.



**Fig 3.3: ACM instruments four channel biostat.**

## 3.3 Chemicals & Solutions

### 3.3.1 Chemicals

The following is a list of all chemicals, and the relevant suppliers, used throughout this research project. For clarity the list is divided into *in-vitro* and *in-vivo* chemicals.

**3.3.1.1 In-vitro chemicals**

|   |                     |
|---|---------------------|
| L-ascorbic acid                               | Sigma Chemical Co.  |
| Bovine serum albumin (Fraction V)             | Fluka Chemical Co.  |
| Catalase                                      | Sigma Chemical Co.  |
| Glutaraldehyde ~25% in H <sub>2</sub> O       | Sigma Chemical Co.  |
| Hydrogen peroxide 30% w/w ACS reagent         | Sigma Chemical Co.  |
| Nafion <sup>®</sup> , 5% in aliphatic alcohol | Sigma Chemical Co.  |
| N-1-Naphthyl-ethylenediamine                  | Sigma Chemical Co.  |
| Nitric oxide gas                              | In-house synthesis  |
| Nitrogen gas                                  | BOC Gases           |
| <i>o</i> -Phenylenediamine                    | Sigma Chemical Co.  |
| L- $\alpha$ -Phosphatidylethanolamine         | Sigma Chemical Co.  |
| Potassium chloride                            | Sigma Chemical Co.  |
| Potassium hydroxide                           | Sigma Chemical Co.  |
| Pyrogallol                                    | Hopkin and Williams |
| Sodium chloride                               | Sigma Chemical Co.  |
| Sodium hydroxide                              | Sigma Chemical Co.  |
| Sodium nitrite                                | Sigma Chemical Co.  |
| Sodium phosphate                              | Sigma Chemical Co.  |
| Sulphanilamide                                | Sigma Chemical Co.  |
| Sulphuric acid                                | 97 %, BDH           |

**3.3.1.2 In-vivo chemicals**

|  |                     |
|--|---------------------|
| L-arginine   | Sigma Chemical Co.  |
| Buprenorphine hydrochloride (Temgesic <sup>®</sup> ) | Sigma Chemical Co.  |
| Calcium chloride                                     | Sigma Chemical Co.  |
| Dentalon <sup>®</sup>                                | Hereaus Kulzer Gmbh |
| Isoflurane   | Abbott Diagnostics  |
| Magnesium chloride                                   | Sigma Chemical Co.  |

|   |                    |
|---|--------------------|
| Mercaptosuccinate                             | Sigma Chemical Co. |
| Methyl viologen dichloride hydrate (Paraquat) | Sigma Chemical Co. |
| N (G)-nitro-L-arginine methyl ester (L-NAME)  | Sigma Chemical Co. |
| Sodium ascorbate                              | Sigma Chemical Co. |
| Sodium azide                                  | Sigma Chemical Co. |
| Sodium propionate                             | Sigma Chemical Co. |
| Videne <sup>®</sup>                           | Ecolab Ltd.        |

### 3.3.2 Solutions

All solutions required were prepared on the day of the experiment unless otherwise stated. Each solution was made by the procedure outlined below. All solutions were made using doubly distilled deionised water denoted by H<sub>2</sub>O unless mentioned otherwise. The list is divided into *in-vitro* and *in-vivo* solutions.

#### 3.3.2.1 *In-vitro* solutions

##### *Ascorbic acid (AA)*

A 0.1 M stock solution of AA was prepared in H<sub>2</sub>O and used for up to 12 hours (0.176 g/10 mL).

##### *Bovine serum albumin (BSA)*

A 10% (w/v) solution of BSA was prepared by dissolving 0.1 g in 1 mL H<sub>2</sub>O.

##### *Catalase-Glutaraldehyde (Cat-Ga<sub>(0.25%)</sub>)*

A Cat-Ga<sub>(0.25%)</sub> solution was prepared by dissolving 25 mg of catalase in 1 mL of 0.25% Glutaraldehyde.

*Glutaraldehyde (Ga<sub>(0.25%)</sub>)*

A 0.25% solution of Glutaraldehyde was made up by dissolving 0.1 mL of 25% Glutaraldehyde in 25 mL of PBS.

*H<sub>2</sub>O<sub>2</sub>*

A 0.1 M solution of H<sub>2</sub>O<sub>2</sub> was prepared by dissolving 255 μL of a 30% w/w stock solution in 25 mL H<sub>2</sub>O.

*L-α-phosphatidylethanolamine (PEA)*

A 10% (w/v) solution was prepared by dissolving 0.1 g of PEA in 1 mL H<sub>2</sub>O.

*Neutral Griess reagent*

A reagent consisting of 0.4 mM N-1-Naphthyl-ethylenediamine (NEDD) and 0.017 mM Sulfanilamide (SULF) was prepared in air saturated 100 μM PBS, pH 7.4, containing 0.293 g SULF and 0.0104 g NEDD/100 mL.

*Nitric oxide (NO)*

A stock solution of NO was prepared by bubbling NO gas into H<sub>2</sub>O and its subsequent concentration was determined using UV spectroscopy.

*o-Phenylenediamine (o-PD)*

Using nitrogen (N<sub>2</sub>) saturated PBS a 300 mM stock solution was made up using (0.341 g / 10 mL).

*Potassium hydroxide (KOH)*

A 4 N KOH stock solution was prepared in H<sub>2</sub>O (224 g/L), which was stored at room temperature.

*Phosphate buffered saline (PBS)*

PBS was prepared by dissolving 8.9 g NaCl (0.15 M), 1.76 g NaOH (0.044 M) and 6.86 g NaH<sub>2</sub>PO<sub>4</sub>·2H<sub>2</sub>O (0.044 M) in 1 L of H<sub>2</sub>O. The pH was adjusted to 7.4. The solution was then N<sub>2</sub> saturated for a minimum of one hour and stored at 4 °C.

*Pyrogallol 5% alkaline*

A 5 % stock solution was prepared in 4 N KOH (5 g / 100 mL).

*Sodium nitrite (NaNO<sub>2</sub>)*

A saturated stock solution of NaNO<sub>2</sub> was prepared in H<sub>2</sub>O.

*Sulfuric acid (H<sub>2</sub>SO<sub>4</sub>)*

A 6 M H<sub>2</sub>SO<sub>4</sub> stock solution was prepared from a 97 % H<sub>2</sub>SO<sub>4</sub> commercial solution. 329 mL of H<sub>2</sub>SO<sub>4</sub> is added carefully to H<sub>2</sub>O, made up to 1 L and stored at room temperature.

**3.3.2.2 In-vivo solutions**

*Artificial cerebrospinal fluid (aCSF)*

aCSF was prepared by dissolving 8.6 g NaCl (0.15 M), 0.298 g KCl (0.004 M), 0.176 g CaCl<sub>2</sub> (0.0016 M) and 0.204 g MgCl<sub>2</sub> (0.021 M) in 1 L of H<sub>2</sub>O.

*Buprenorphine hydrochloride (Temgesic<sup>®</sup>)*

Temgesic<sup>®</sup> is a stock solution of 0.3 mg/mL buprenorphine hydrochloride which is injected in a volume of 1 mL/kg.

*H<sub>2</sub>O<sub>2</sub>*

For local administrations various dilutions of a 0.1 M solution of H<sub>2</sub>O<sub>2</sub> made up in aCSF were prepared including 25, 50, 100, 200, 500 and 1000 μM.

*L-arginine*

For systemic administration 300 mg/kg was dissolved in normal saline and injected in a volume of 1 mL.

*L-NAME*

For systemic administration a 30 mg/kg dose was prepared and administered in a volume of 1 mL of normal saline.

*Mercaptosuccinate*

For local administration various dilutions including, 0.1 mM and 1 mM, were made up in aCSF.

*Normal saline solution*

A 0.9% solution was prepared by dissolving 0.9 g NaCl in 100 mL H<sub>2</sub>O.

*Paraquat (Methyl viologen dichloride hydrate)*

Varying systemic administrations of 5, 10, 20 and 30 mg/kg were prepared in normal saline and injected in a volume of 2 mL/kg.

*Propionic acid (PPA)*

For systemic administration a stock solution of PPA was prepared by dissolving 0.5 g of sodium propionate in 1 mL saline which was subsequently injected at 1 mL/kg.

*Sodium ascorbate*

A 2g/kg dose was prepared and injected systemically in a volume of 1 mL of normal saline. It is preferable to use sodium ascorbate as an interferent *in-vivo* as AA, even with pH adjustment, causes significant discomfort to the animal. For local administration a 1 mM solution was prepared in aCSF.

*Sodium azide*

For systemic administration 20 mg/kg was prepared in normal saline and injected in a volume of 2 mL/kg. For local administration a 10 mM solution was prepared in aCSF.

### 3.4 Working electrode preparation

#### 3.4.1 Disc and cylinder platinum electrodes

Platinum (Pt) was the material utilised in the manufacture of all working electrodes (sensors) in this body of work. Two basic electrode types were fabricated throughout the course of this study, electrodes with disc and cylinder geometries were utilised during all investigations. Approximately 4 cm of Teflon<sup>®</sup> coated Pt/Ir (90%/10%) wire (125  $\mu\text{m}$  bare diameter, 175  $\mu\text{m}$  coated diameter (5T); Advent Research Materials, Suffolk, UK) was used to construct each sensor. 2 mm of Teflon<sup>®</sup> was carefully removed from one end of the wire. The exposed section was soldered into a gold electrical contact to improve rigidity and to provide a transducer that could be attached to the potentiostat (see section 3.2.3). The opposite end of the wire was then cut transversely with a sharp scalpel blade to expose a Pt disc. A schematic of the Pt disc working electrode ( $\text{Pt}_d$ ) is shown in Figure 3.4. The exposed disc surface denoted below by (E) is the active region of the electrode where the redox reactions occur.

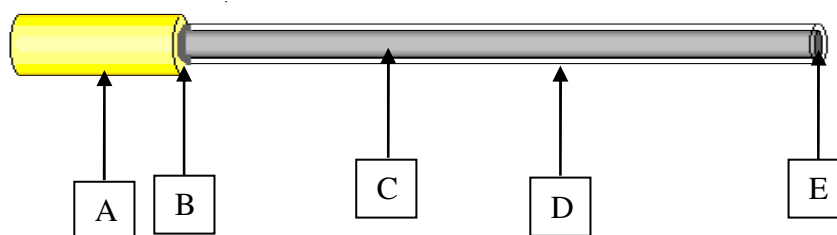


**Fig 3.4:** A schematic of a  $\text{Pt}_d$  electrode: (A) Gold clip (B); Solder (C); Pt/Ir wire (D); Teflon<sup>®</sup> (E); exposed Pt disc surface

A 1 mm cylinder Pt electrode ( $Pt_c$ ) was constructed in a similar manner to the Pt disc. Following the soldering procedure 1.5 mm of Teflon<sup>®</sup> was removed from the opposite end of the wire. The exposed length of wire was accurately cut back to 1 mm with the aid of a microscope. A schematic of a  $Pt_c$  electrode is illustrated below in Figure 3.5.



Fig 3.5: Schematic of a  $Pt_c$  electrode (A) 1mm of exposed Pt/Ir wire

### 3.4.2 Nitric oxide sensor

A Nafion<sup>®</sup>-modified  $Pt_d$  was constructed as previously described in detail by Brown *et al.* (Brown *et al.*, 2009) for the detection of NO. A schematic of the sensor is shown below in Figure 3.6. Further applications of this sensor type in novel animal models will be discussed in Chapter 7 and 8. The modified disc surface denoted below by (A) is where Nafion<sup>®</sup> has been thermally annealed onto the surface of the electrode by a pre-cast procedure as previously reported (Brown *et al.*, 2009).



Fig 3.6: Schematic of an NO sensor (A): Nafion<sup>®</sup> modified active surface

### 3.4.3 H<sub>2</sub>O<sub>2</sub> catalase-based paired biosensor

A pair of Pt<sub>c</sub> electrodes were fabricated and modified by a process previously described (O'Brien *et al.*, 2007). Nafion<sup>®</sup> was applied to both Pt<sub>c</sub> as described in Section 3.5.2 and *o*-PD was then polymerised electrochemically onto the Nafion<sup>®</sup> modified surface of each sensor (see Section 3.5.1). A sensor capable of detecting H<sub>2</sub>O<sub>2</sub> was made by this process [Pt<sub>c</sub>/Nafion<sup>®</sup>/PPD (*Blank*)]. A paired sensor which was modified with catalase was then constructed (see Section 3.5.3). Catalase is an enzyme which degrades H<sub>2</sub>O<sub>2</sub> into water and oxygen. Application of catalase resulted in a paired sensor capable of removing the signal arising from H<sub>2</sub>O<sub>2</sub> without compromising matched selectivity [Pt<sub>c</sub>/Nafion<sup>®</sup>/PPD/Cat-Ga (*Cat*)]. This process yielded two amperometric electrodes one with catalase adhered (*Cat*) and the other without (*Blank*). The H<sub>2</sub>O<sub>2</sub> sensitivity of this biosensor design was derived by subtracting the *Cat* sensor current response from that recorded at the *Blank* sensor. A more detailed description of how the sensitivity of the catalase-based paired biosensor is obtained is described in Section 2.8 (Theory).

## 3.5 Electrode modifications

Electropolymerisation of *o*-PD onto the active surface of the electrode provides an insulating layer of poly-*o*-phenylenediamine (PPD). This technique has previously been used in biosensor design (Lowry *et al.*, 1998). Fundamentally the function of PPD in this case is to provide selectivity over other electroactive species present in the biological milieu. PPD also provides a scaffold for the entrapment of enzymes as has been shown by O'Neill and colleagues (O'Neill *et al.*, 2008). The morphology of the PPD polymer allows the rejection of interfering species e.g. AA, by a size exclusion mechanism. The application of Nafion<sup>®</sup> to the bare metal provides a further interference rejection layer, Nafion<sup>®</sup> is a polyflourinated ionomer permselective membrane and displays effective anionic rejection characteristics (Gerhardt & Hoffman, 2001). A detailed description of the properties of Nafion<sup>®</sup> is provided in Section 2.6 (Theory).

The presence of Nafion<sup>®</sup> also increases the bio-compatibility of the sensor (Borland & Michael, 2007).

### ***3.5.1 PPD-modified electrodes***

The modification of sensors with PPD has been extensively described (O'Neill *et al.*, 2008). Briefly, a 300 mM saturated solution of *o*-PD was freshly prepared as detailed in Section 3.3.2.1. Great care was taken to ensure N<sub>2</sub> saturation of the monomer solution. The electrochemical cell was also purged with N<sub>2</sub> and the electropolymerisation was carried out under N<sub>2</sub> atmospheric conditions. The exclusion of air in this procedure was necessary as the monomer solution is highly susceptible to oxidation. The working electrodes were placed in the monomer solution and a potential of +700 mV vs. SCE was applied to the electrodes for a duration of 30 minutes. The electrodes were removed and allowed to dry for a minimum of 1 hour and stored in the refrigerator at 4 °C when not in use.

### ***3.5.2 Nafion<sup>®</sup> dip-absorption modification***

Nafion<sup>®</sup> was applied to the surface of the electrode by a dip absorption method unless otherwise stated. The electrode was placed in the stock Nafion<sup>®</sup> solution described in 3.3.1.1 for *ca.* 0.5s. The electrode was then removed and allowed to dry for 5 minutes in a vertical position with the active surface of the electrode facing down. This process was repeated a further four times and the electrodes were allowed to dry following modification for a minimum of three hours. This procedure was carried out at room temperature. The electrodes were stored in the refrigerator at 4°C when not in use.

### ***3.5.3 Catalase modification***

A Cat-Ga<sub>(0.25%)</sub> solution as described in 3.3.2.1 was prepared. The *Blank* sensor was placed in the catalase solution for an initial period of five minutes and the electrodes were subsequently allowed to air dry for five minutes. Following this drying period a

further four dips of *ca.* 0.5s duration were carried out with five minutes of air drying in between each immersion. The catalase solution was kept over ice during the modification to maintain the enzyme. This process produced the catalase-based sensor Pt<sub>c</sub>/Nafion<sup>®</sup>/PPD/Cat-Ga (*Cat*).

### 3.6 Electrode treatments

Various parameters were explored to determine the bio-compatibility and stability of the H<sub>2</sub>O<sub>2</sub> biosensor. The effect of proteins and lipids similar to those found in the brain's extracellular environment was examined. The purpose of these experiments is to mimic the type of conditions encountered by the working electrode in the *in-vivo* environment and to examine the effect of these substances on the sensitivity and the selectivity of the paired biosensor. The modified electrodes (sensors) were exposed to bovine serum albumin (BSA), L- $\alpha$ -phosphatidylethanolamine (PEA) and a homogenised sample of *ex-vivo* brain tissue (BT). The procedure for each examination is detailed below.

#### 3.6.1 BSA treated sensors

A complete selectivity characterisation has previously been undertaken by O'Brien *et al.* (O'Brien *et al.*, 2007), however it is necessary to test the sensor for selectivity against AA as it is the most abundantly present interferent in the brain. The sensors were initially tested to determine sensitivity towards H<sub>2</sub>O<sub>2</sub> and selectivity against AA. Once these parameters were established the sensors were submerged in a fresh solution of BSA (see Section 3.3.2.1). The working electrodes remained in solution in the refrigerator at 4 °C for the required time and were intermittently tested. To mimic the constant exposure of the sensor to the biological medium the sensors were immersed in BSA, removed and re-calibrated according to the times specified. Following re-calibration the same sensors were re-immersed in BSA for further testing.

### **3.6.2 PEA treated sensors**

These sensors were treated with PEA (see Section 3.3.2.1) in the same manner as described in Section 3.6.1.

### **3.6.3 BT treated sensors**

A sample of homogenised *ex-vivo* brain tissue (BT) was obtained. The working electrodes were carefully inserted into the tissue to ensure direct contact as would occur when implanted in the brain. Concomitantly the protocol outlined in Section 3.6.1 was adhered to.

### **3.6.4 Long-term sensor stability investigations**

The same protocol was followed as that with the treated sensors, however these sensors were stored in the refrigerator at 4 °C in the absence of any solutions between specified time periods and intermittently tested.

### **3.6.5 Post-implanted sensors**

Following implantation of the working electrodes into the brain over extended periods they were removed and re-calibrated. The purpose of these experiments was a further verification of the long term stability of the sensor in the brain. The stability of the NO sensor has been established in this manner (Finnerty *et al.*, 2012).

### 3.7 Electrochemical experiments

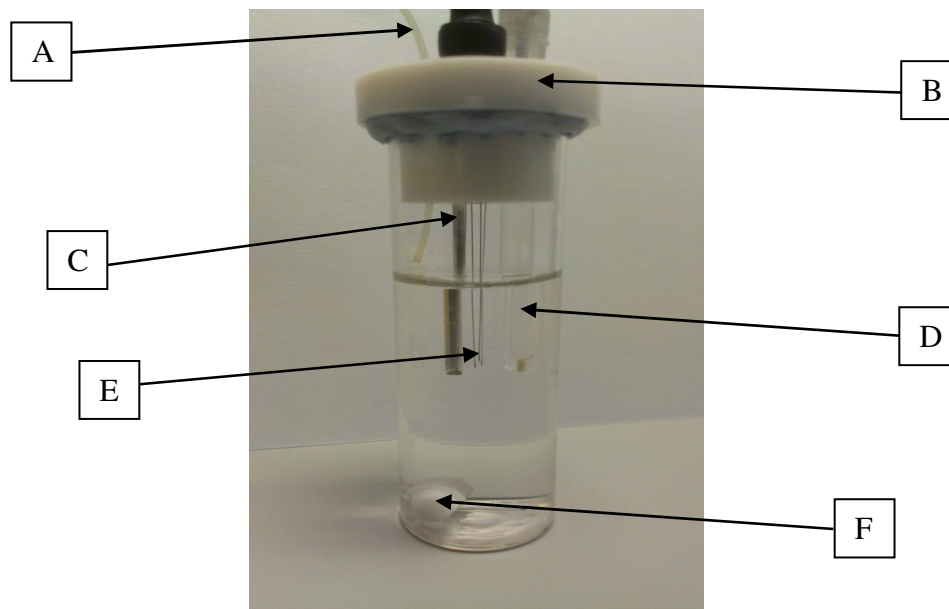


**Fig 3.7: Schematic of an electrochemical cell (A) Gas inlet (B); Teflon<sup>®</sup> cap (C); Auxiliary electrode (D); SCE (E); Working electrodes (sensors) (F); Magnetic stirrer**

#### 3.7.1 Electrochemical cell set-up

All *in-vitro* experiments were carried out at room temperature (*ca.* 25°C). The diagram above demonstrates a typical three electrode set-up. The electrochemical cell consists of a reference electrode, an auxiliary electrode and four working electrodes. The electrochemical changes being investigated take place at the working electrode. The reference electrode has a fixed potential against which the potential of the working electrodes in the cell can be measured. The final electrode is the auxiliary which functions as a source or sink for electrons and completes the electrical circuit. All experiments were performed in PBS (see section 3.3.2.1). The reference electrode used in these experiments was a saturated calomel electrode (SCE). The auxiliary electrode can consist of any conducting metal wire and in our case was a bare silver wire. The cell was covered with a Teflon<sup>®</sup> cap which allows placement of all electrodes, an inlet for

gas and an injection port. The gas supply which may be N<sub>2</sub>, air or O<sub>2</sub> provides a cloud of gas over the solution and is used to control the atmosphere surrounding the PBS, and may be used to saturate the PBS. A glass container holds the solution in which a magnetic stirrer was placed for agitation of the bulk solution. The *in-vivo* set-up utilises a similar methodology and will be discussed in detail in Section 3.10.

### **3.7.2 Experimental techniques**

Throughout this body of work the primary experimental technique utilised was Constant Potential Amperometry (CPA). CPA is an example of a potentiostatic measurement. CPA involves the application of a continuous fixed potential and the corresponding detection of faradaic current changes arising from electroactive target species. This experimental technique allows for the real-time detection of a wide range of electroactive analytes. This technique is not selective however as a range of electroactive species aside from the target analyte may also be detected. The applied voltage will detect all species with oxidation/reduction potentials within the same range as the target species and contribute to the overall faradaic current. Due to the non-selective nature of CPA it is imperative to design a sensor which will exclude interference from other electroactive species. All electrodes were calibrated using CPA at the appropriate potential prior to implantation. All *in-vivo* measurements were determined using CPA.

### **3.7.3 AA calibrations**

20 mL of PBS was N<sub>2</sub> saturated for approximately 30 minutes prior to all calibrations. The atmosphere surrounding the PBS was purged with N<sub>2</sub> during the calibration. A potential of +700 mV vs. SCE was applied to the working electrodes. A capacitance current was immediately observed upon application of the potential. The magnitude of this response is entirely dependent upon the surface characteristics of the individual sensor. The capacitance current was allowed to dissipate prior to commencement of

calibrations and the time required for this procedure varied between sensors. In general the more complex sensor designs require a longer time to achieve a stable baseline and were allowed to settle overnight. Aliquots of AA were introduced into the cell by means of an injection port. Brief agitation of the bulk solution for approximately 3 seconds was achieved via a magnetic stirrer. Once a steady-state response was achieved a subsequent injection of AA was made. The concentration range examined was as follows:

0, 200, 400, 600, 800 and 1000  $\mu\text{M}$

### **3.7.4 NO calibrations**

NO calibrations were carried out in a similar manner to the AA calibrations. In order to detect NO a potential of +900 mV *vs.* SCE was applied to the working electrodes. The concentrations of NO introduced into the cell are outlined below:

0, 0.2, 0.4, 0.6, 0.8 and 1  $\mu\text{M}$

As the *in-vitro* characterisation of the NO sensor has previously been established (Brown *et al.*, 2009), the predominant interference species present in the brain AA was used to establish the selectivity of the NO sensor.

### **3.7.5 H<sub>2</sub>O<sub>2</sub> calibrations**

The H<sub>2</sub>O<sub>2</sub> calibrations were performed utilising air-saturated PBS. A potential of +700 mV *vs.* SCE was applied to the working electrodes. H<sub>2</sub>O<sub>2</sub> was injected into the cell over the concentration range specified below. As the interference rejection characteristics of the H<sub>2</sub>O<sub>2</sub> paired sensor were previously reported (O'Brien *et al.*, 2007) a subsequent AA calibration was sufficient to determine the selectivity properties of the sensor.

0, 1, 2, 5, 10, 20, 50, 100, 150, 250, 350, 550  $\mu\text{M}$

### 3.7.6 Data recording and analysis

All electrochemical experiments carried out used Chart 5 (Windows Version 5.2) and LabChart 6 (AD Instruments Ltd, Gladstone Road, Castle Hill, NSW 2154, Australia). Analysis of all experimental data was performed using Graphpad Prism version 4.02 (GraphPad Software Inc., California U.S.A).

## 3.8 Microdialysis

Microdialysis (MD) is a sampling technique whereby small molecules present in the extracellular fluid in the brain can be recovered by perfusion of a liquid through a semi-permeable dialysis membrane. The perfusate typically used is aCSF and molecules are recovered in the dialysate by the process of diffusion. The technique functions by the diffusion of a higher concentration of analyte in the surrounding tissue across a concentration gradient towards the lower concentration present within the microdialysis probe. The technique can also allow the introduction of substances into the brain which cannot be administered systemically because they can not cross the blood brain barrier (BBB). The dialysate may be analysed by various methods including high performance liquid chromatography (HPLC) (Perry *et al.*, 2009) which provides a highly selective analytical tool. The main disadvantage of MD is the time lag associated with the diffusion of the analyte across the membrane and through the system (O'Neill & Lowry, 2000). Electrochemical techniques yield an advantage over MD however in that they provide real-time localised recordings of electroactive species (Lowry *et al.*, 2006). Electrochemical sensors are also much smaller than microdialysis probes which causes minimal damage to the surrounding tissue (Khan & Michael, 2003). It is also possible to combine sensor technology and MD to ascertain that the designed sensor will correspond to changes in the target analyte as discussed in Section 2.9 (Theory).

### **3.9 Scanning electron microscopy (SEM)**

This technique involves the direction of a focused beam of electrons with energy between 0-30 kV across the surface of a sample. Approximately 1 cm of the active surface end of the sensor was mounted onto an aluminium stub using a carbon dag which restricts the movement of the sample. The sample is then sputtered with a thin layer of gold (20 – 30 nm thickness). The gold layer functions by preventing an electrical charge build up which may be caused by the scanning process. The scanning electron microscope used was a 14 Hitachi S-3200N Variable Pressure SEM and electron beams of 15 kV were utilised. The SEM technique provides a detailed image of the active surface of the sensor.

### **3.10 *In-vivo* experiments**

This section will outline in detail the materials and methods required for the implantation of electrochemical sensors constructed in this body of work into the brain of male Wistar rats. All experiments conducted on animals were performed under license (B100/2205) in accordance with the European Communities Regulations 2002 (Irish Statutory Instrument 566/2002 and U.K. Animals (Scientific procedures) Act 1986).

#### **3.10.1 *Subjects***

Male Wistar rats (Charles River UK Ltd., Manston Rd., Margate, Kent CT9 4LT UK) weighing between 200 and 300 g were group housed in a temperature-controlled (17-23°C), humidity-controlled and light-controlled (12 hr light/12 hr dark) environment with access to food and water *ad libitum* prior to surgery.

#### **3.10.2 *Surgical protocol***

Prior to surgical procedures all equipment and surfaces were thoroughly sterilised. All experiments were conducted in an aseptic manner to minimise any possible infection arising. Anaesthesia was achieved by using the volatile anaesthetic (Isoflurane). The

subject is placed in an induction chamber for 3-4 min, removed and the scalp is then shaved. The animal is subsequently returned to the induction chamber for a further 2-3 min. The animal is then placed in the stereotaxic frame (Kopf) where a nose piece facilitates the administration of Isoflurane during the surgery. Once anaesthesia is established the head is carefully positioned in the nose piece and the head of the subject is levelled between bregma and lambda. Anaesthesia is constantly maintained by the use of a vapouriser (Univentor). The level of anaesthetic provided to the subject is outlined below.

| <b>Anaesthetic</b> | <b>Chamber<br/>(Air)</b> | <b>Chamber<br/>(Isoflurane)</b> | <b>Nose piece<br/>(Air)</b> | <b>Nose piece<br/>(Isoflurane)</b> |
|--------------------|--------------------------|---------------------------------|-----------------------------|------------------------------------|
| Isoflurane         | 700 - 800                | 4 %                             | 400 – 500                   | 1.5 – 3 %                          |

**Table 3.1: The level of anaesthetic and air provided to the subject during surgery.**

The surface of the scalp is sterilised with an iodine solution (Videne<sup>®</sup>). A small incision of approximately 1.5 cm is made to the scalp along the anterior-posterior plane. The scalp is held open using clamps exposing an increased surface area of the skull. Underlying muscle and tissue are removed to allow the positive identification of bregma, which is the point where the sagittal and coronal sutures of the skull meet. Bregma is the reference point upon which the coordinates of various brain regions are established according to the published stereotaxic atlas (Paxinos & Watson, 1998) The specific regions examined in this project are outlined below.

| <b>Brain region</b>       | <b>(A-P)</b> | <b>(M-L)</b> | <b>(D-V)</b> |
|---------------------------|--------------|--------------|--------------|
| <b>Striatum</b>           | + 1.0 mm     | ± 2.5 mm     | - 5.0 mm     |
| <b>Prefrontal Cortex</b>  | + 3.2 mm     | ± 0.8 mm     | - 4.2 mm     |
| <b>Nucleus Accumbens</b>  | + 1.85 mm    | ± 1.3 mm     | - 6.8 mm     |
| <b>Dorsal Hippocampus</b> | -3.6 mm      | ± 3 mm       | - 4.0 mm     |

**Table 3.2: Stereotaxic coordinates for electrode implantation in stated brain regions.**

Anterior–posterior (A-P) and medial-lateral (M-L) coordinates are obtained using bregma as the zero point of reference and dorsal-ventral (D-V) coordinates with respect to the dura. The dura is the outermost layer surrounding the brain. Small burr holes are made in the skull to allow the placement of anchor screws. Once the support screws are in place a hole is drilled for the working electrodes and the reference electrode. Two or four working electrodes may be implanted depending on the purpose of the experiment. Once all electrodes are implanted the electrodes are cemented (Dentalon<sup>®</sup>) at the point of insertion into the skull to ensure no further movement takes place. The gold clips of the electrodes are then placed within a plastic support, a Teflon<sup>®</sup> pedestal (Plastics One Inc.), and cemented into the pedestal while ensuring that no cement enters the cavity of the gold clips. Images of the Teflon<sup>®</sup> pedestal are displayed below in figure 3.8.

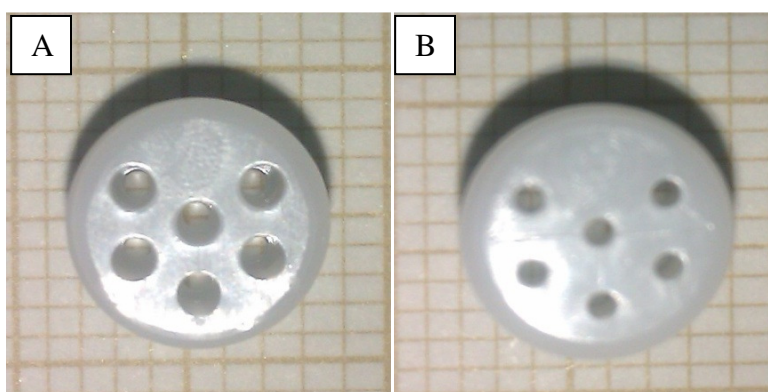


**Fig 3.8: Images of Teflon<sup>®</sup> pedestal (A) Lower surface (B); Upper surface**

This provides a method of connection between the gold clips and potentiostat through a six-pinned cable post surgery. All electrodes are then manipulated to position them close to the surface of the skull with the plastic support positioned centrally and vertically. The entire construct with the exception of the upper surface and sides of the pedestal may then be cemented, eliminating the possibility of damage inflicted by the subject post surgery and avoiding exposure to moisture. The surgical clamps are removed and the skin surrounding the cement is sutured. The animal is removed from the stereotaxic frame and placed in an incubator (27 °C) for 2-4 hours until fully recovered. Post-operative analgesia was provided in the form of a subcutaneous injection (1 mL/kg, s.c.) of Temgesic<sup>®</sup> (Section 3.3.1.2) which was administered after recovery from surgery. The subject is then closely monitored and left to recover for a minimum of 24 hours before any experiments take place. The recovery time of each subject will vary and is also dependent on the volume and length of exposure to the anaesthetic. The animal is monitored regularly post-operatively and if necessary the required procedure was followed to ensure the subject was comfortable and free from pain.

### 3.10.3 *In-vivo* reference and auxiliary electrode

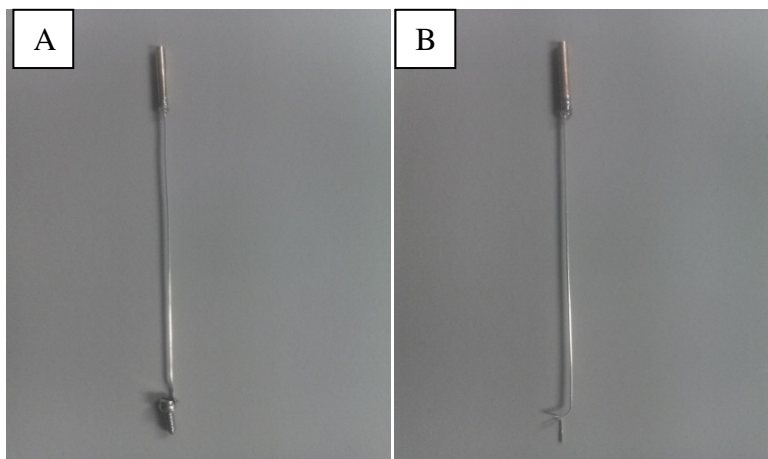


**Fig 3.9:** Images of (A) auxiliary electrode and (B); reference electrode

The images above show the constructed reference and auxiliary electrodes utilised for *in-vivo* experiments. Both were made from 4-5 cm lengths of Teflon<sup>®</sup> coated silver wire (200 µm bare diameter, 270 µm coated diameter (8T), Advent Research Materials, Suffolk, UK). Approximately 3 mm of Teflon<sup>®</sup> was removed from one end of the wire and soldered into a gold electrical contact. The exposed section of wire was glued to provide the flexibility required to manipulate the sensors during the surgery. At the opposite end of the wire *ca.* 3.5 mm of Teflon<sup>®</sup> was removed. To construct a reference electrode the bare wire was twisted in a manner which would allow it to rest on the skull of the subject to control the position of the wire ventrally as can be seen in Figure 3.9. The auxiliary electrode was constructed in a similar manner, however the exposed section of silver wire was soldered to a surgical screw. The auxiliary electrode is attached to a surgical screw to provide a larger surface area and to minimise the invasiveness of the surgical procedure by utilising a pre-existing implant. The reference was implanted into the cortex as has been reported previously (Fillenz & O'Neill, 1986). The potential of the reference utilised *in-vivo* is comparable to that seen by the SCE used in *in-vitro* experiments (O'Neill & Lowry, 2000).

### **3.11 *In-vivo* injections**

#### ***3.11.1 Intraperitoneal injection (i.p.)***

This injection is given into the lower left or right quadrant of the abdomen of the subject. This position is chosen as there are no vital organs present in this area. The injection is given at a 45° angle with the subject positioned on its back in an upright position (Wolfensohn, 2003).

#### ***3.11.2 Subcutaneous injection (s.c.)***

The drug is injected into the scruff of the neck, the skin is gathered using the thumb and first two fingers of the hand and lifted away from the body. The injection is made under the skin parallel to the body to avoid the tissue beneath (Wolfensohn, 2003).

### **3.12 NO Synthesis and UV Spectroscopy**

NO was synthesised in-house using a very reliable and relatively inexpensive method which has previously been described (Brown *et al.*, 2005).

### **3.13 Additional equipment**

#### ***3.13.1 Anaesthesia system***

The set-up consisted of a vaporiser for induction which was a Univentor 400 anaesthesia unit. The air pump in the system was a Stellar S30 and the induction chamber was a 1.4 L Perspex box which were all obtained from Agnthos, Sweden. The entire system was contained within a laminar flow unit supplied by Air Science™.

#### ***3.13.2 Electrode wire***

All platinum and silver wire was sourced from Advent Research Materials, Oxford, UK.

#### ***3.13.3 Incubator***

Following surgery the animal was placed in a heated incubator (Thermacage MKII from Datasand Ltd, UK) at 27 °C until fully recovered.

#### ***3.13.4 Microdialysis pump***

A Univentor 801 syringe pump was used for all microdialysis experiments

#### ***3.13.5 Microdialysis probes***

All probes that were used throughout the project were BR4 brain microdialysis probes supplied from BAS Inc.

#### ***3.13.6 Microscope***

The Microscopes used for all *in-vitro* experiments were the stereomicroscope SZ51 from Olympus America Inc. and the SM 33-745-F from Hund® WETZLER, Germany. *In-Vivo* surgeries utilised an SZ61 microscope from Olympus.

#### ***3.13.7 pH meter***

The pH meter used was the S20 Seveneasy™ from Mettler-Toledo, Switzerland. The device was used to correct the pH of solutions as required.

### ***3.13.8 Sonicator***

The sonicator used was a Fisherbrand FB11002, Leicestershire, UK.

### ***3.13.9 Stereotaxic frame***

The stereotaxic frame (Kopf) allowed the animal to be held in the correct orientation, and to obtain exact coordinates in order to implant sensors into the brain region of interest.

### ***3.13.10 Vortex***

The Vortex (Reax Control from Heidolph) was used for creating homogenous solutions.

## References

- Borland LM & Michael AC. (2007). An Introduction to Electrochemical Methods in Neuroscience. In *Electrochemical Methods for Neuroscience*, ed. Michael ACBLM, pp. 1-15. CRC Press.
- Brown FO, Finnerty NJ, Bolger FB, Millar J & Lowry JP. (2005). Calibration of NO sensors for *in-vivo* voltammetry: laboratory synthesis of NO and the use of UV-visible spectroscopy for determining stock concentrations. *Analytical and Bioanalytical Chemistry* **381**, 964-971.
- Brown FO, Finnerty NJ & Lowry JP. (2009). Nitric oxide monitoring in brain extracellular fluid: characterisation of Nafion<sup>®</sup>-modified Pt electrodes *in vitro* and *in vivo*. *Analyst* **134**, 2012-2020.
- Fillenz M & O'Neill RD. (1986). Effects of light reversal on the circadian pattern of motor-activity and voltammetric signals recorded in rat forebrain. *Journal of Physiology-London* **374**, 91-101.
- Finnerty NJ, O'Riordan SL, Brown FO, Serra PA, O'Neill RD & Lowry JP. (2012). *In vivo* characterisation of a Nafion<sup>®</sup>-modified Pt electrode for real-time nitric oxide monitoring in brain extracellular fluid. *Analytical Methods* **4**, 550-557.
- Gerhardt GA & Hoffman AF. (2001). Effects of recording media composition on the responses of Nafion-coated carbon fiber microelectrodes measured using high-speed chronoamperometry. *Journal of Neuroscience Methods* **109**, 13-21.
- Khan AS & Michael AC. (2003). Invasive consequences of using micro-electrodes and microdialysis probes in the brain. *TrAC Trends in Analytical Chemistry* **22**, 503-508.
- Lowry JP, O'Neill RD & (2006). *Neuroanalytical Chemistry In Vivo Using Biosensors.*, vol. 10. American Scientific Publishers.
- Lowry JP, O'Neill RD, Boutelle MG & Fillenz M. (1998). Continuous monitoring of extracellular glucose concentrations in the striatum of freely moving rats with an implanted glucose biosensor. *Journal of Neurochemistry* **70**, 391-396.
- O'Brien KB, Killoran SJ, O'Neill RD & Lowry JP. (2007). Development and characterization *in vitro* of a catalase-based biosensor for hydrogen peroxide monitoring. *Biosensors & Bioelectronics* **22**, 2994-3000.

- O'Neill RD & Lowry JP. (2000). Voltammetry *In Vivo* for Chemical Analysis of the Living Brain. In *Encyclopedia of Analytical Chemistry*. John Wiley & Sons, Ltd.
- O'Neill RD, Lowry JP, Rocchitta G, McMahon CP & Serra PA. (2008). Designing sensitive and selective polymer/enzyme composite biosensors for brain monitoring *in vivo*. *Trac-Trends in Analytical Chemistry* **27**, 78-88.
- Paxinos G & Watson C. (1998). *The Rat Brain in Stereotaxic Coordinates*. Academic Press.
- Perry M, Li Q & Kennedy RT. (2009). Review of recent advances in analytical techniques for the determination of neurotransmitters. *Analytica Chimica Acta* **653**, 1-22.
- Wolfensohn SL. (2003). *Handbook of Laboratory Animal Management and Welfare*. Blackwell Publishing.

---

**4. *In-vitro* characterisation of a paired  
catalase-based H<sub>2</sub>O<sub>2</sub> biosensor**

---

## 4.1 Introduction

This chapter outlines the development and characterisation of a paired catalase-based hydrogen peroxide (H<sub>2</sub>O<sub>2</sub>) sensor *in-vitro*. Investigations previously carried out by O'Brien *et al.* have demonstrated a highly sensitive and selective dual catalase-based sensor for the detection of H<sub>2</sub>O<sub>2</sub> *in-vitro* (O'Brien *et al.*, 2007). The sensor designs described here are based on these investigations. The primary aim of this chapter is to replicate this dual sensor design to establish the sensitivity, selectivity and stability of the catalase-based paired sensor *in-vitro*. Novel selectivity and stability parameters of this dual sensor design are also presented here.

To date very few reports exist of the real-time detection of H<sub>2</sub>O<sub>2</sub> in the intact living brain. Fluorescent imaging has been used to visualise relative changes in H<sub>2</sub>O<sub>2</sub> in *ex-vivo* brain slices (Avshalumov *et al.*, 2005), however absolute concentrations of H<sub>2</sub>O<sub>2</sub> cannot be determined using this method. Sanford *et al.* have studied H<sub>2</sub>O<sub>2</sub> in brain slice preparations using carbon fibre microelectrodes (CFEs) (Sanford *et al.*, 2010). Many of the techniques employed to detect H<sub>2</sub>O<sub>2</sub> utilise microdialysis (MD) (Hyslop *et al.*, 1995; Lei *et al.*, 1997, 1998), however this analytical tool is restricted by the time delay associated with obtaining samples and by damage caused by insertion of the probe itself (Khan & Michael, 2003).

An implantable biosensor for the detection of H<sub>2</sub>O<sub>2</sub> has previously been reported, however this sensor relies on the presence of a polymer-based mediator and ascorbate oxidase to eliminate interference from ascorbic acid (AA) (Kulagina & Michael, 2003). The H<sub>2</sub>O<sub>2</sub> sensor described here does not require a mediator and consists of a simple modified platinum surface which effectively eliminates interference from AA without compromising sensitivity to the target substrate (H<sub>2</sub>O<sub>2</sub>).

The results obtained from the dual catalase-based sensor described in this chapter demonstrate a high H<sub>2</sub>O<sub>2</sub> sensitivity and exhibit a low limit of detection (LOD). H<sub>2</sub>O<sub>2</sub> has been shown to exist as a tightly regulated diffusible messenger in the brain (Rice, 2011), this would indicate that the presence of H<sub>2</sub>O<sub>2</sub> in the brain may be short-lived as has been suggested previously (Bao *et al.*, 2009) and hence requires a fast method of

detection. The response time of our H<sub>2</sub>O<sub>2</sub> sensor will be investigated in this chapter. The selectivity of the dual sensor design will be clearly established. An investigation into the stability of the paired catalase-based sensor using proteins, lipids and brain tissue samples is also presented. The main focus of this chapter is to develop this paired sensor *in-vitro* in order to detect H<sub>2</sub>O<sub>2</sub> in the *in-vivo* environment.

## 4.2 Experimental

The instrumentation, chemicals, solutions and software used in this section are described in detail in Chapter 3. The working electrodes were manufactured from Pt/Ir wire as outlined in Section 3.4. The various procedures utilised to modify electrodes are presented in Section 3.5. The sensor treatment protocol adhered to is described in Section 3.6. All experiments were performed using Constant Potential Amperometry (CPA). A potential of +700 mV vs. SCE was applied to the working electrodes for all H<sub>2</sub>O<sub>2</sub> and AA calibrations (see Section 3.7).

The data is represented as a Mean  $\pm$  SEM and (n) corresponds to the number of electrodes used in each case. All H<sub>2</sub>O<sub>2</sub> calibration data was linear, in each case the slope value was used to represent the H<sub>2</sub>O<sub>2</sub> sensitivity which is denoted by (nA/ $\mu$ M) or (pA/ $\mu$ M) and an R<sup>2</sup> value is given to express the extent of linearity for each H<sub>2</sub>O<sub>2</sub> calibration.

In the case of a linear AA calibration plot the data is represented in the same manner as H<sub>2</sub>O<sub>2</sub> calibrations. In order to compare non-linear AA responses an alternative analysis method was employed. The corresponding current expressed in nA, attributable to 400  $\mu$ M AA ( $I_{400 \mu\text{M}}$ ) and arising from 1000  $\mu$ M AA ( $I_{1000 \mu\text{M}}$ ) was examined.

Statistical analysis was carried out using paired or unpaired t-tests. One-way ANOVA was used to simultaneously compare results which contained more than two separate groups. These tests were performed using Graphpad Prism and gave a probability value (*P*) which indicates the level of significant or non-significant difference between groups. *P* > 0.05, denotes no significant difference. The extent of significant difference is divided into three parameters (*P* < 0.05,\*), (*P* < 0.01,\*\*) and (*P* < 0.0001,\*\*\*) from the lowest relative level of difference (\*) to the highest (\*\*\*).

### 4.3 Sensitivity of the $H_2O_2$ sensor *in-vitro*

#### 4.3.1 $Pt_c$

In this section the ability of a 1 mm platinum cylinder electrode ( $Pt_c$ ) to detect  $H_2O_2$  *in-vitro* is presented. A bare  $Pt_c$  may be used to detect  $H_2O_2$  *in-vivo*, however this type of sensor will detect other electroactive species present in the brain which oxidise at a similar potential e.g. AA. Consequently it is essential to remove the signal arising from such species and focus on  $H_2O_2$  by modifying the surface of the sensor using permselective membranes (Lowry et al., 1998; Brown & Lowry, 2003). However the required alteration to the  $Pt_c$  surface must not impair the detection of  $H_2O_2$ . Without alteration of the active surface of the electrode, the specificity of the signal arising exclusively from  $H_2O_2$  would be masked by other species present in the biological environment and would furthermore be more susceptible to fouling by lipids and proteins (Bolger et al., 2011).

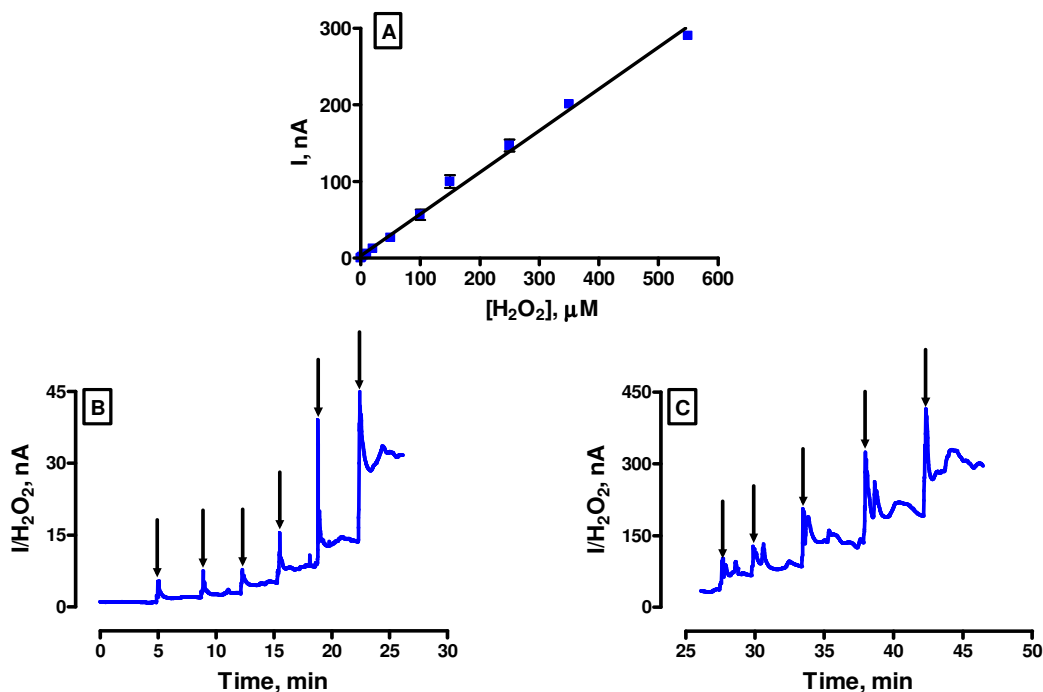


Figure 4.3.1: (A) The current-concentration profile of  $H_2O_2$  at  $Pt_c$  ( $n = 5$ ). (B) A typical raw data trace 0-50  $\mu M$  and (C) 50-550  $\mu M$  for  $H_2O_2$  calibrations. CPA carried out at +700 mV vs. SCE.

Arrows indicate the addition of aliquots of  $H_2O_2$ .

| H <sub>2</sub> O <sub>2</sub> , μM | Mean I, nA | SEM  |
|------------------------------------|------------|------|
| 0                                  | 0          | 0    |
| 1                                  | 0.52       | 0.08 |
| 2                                  | 1.61       | 0.27 |
| 5                                  | 3.56       | 0.63 |
| 10                                 | 5.99       | 0.51 |
| 20                                 | 12.67      | 1.84 |
| 50                                 | 26.51      | 2.63 |
| 100                                | 56.59      | 6.67 |
| 150                                | 99.86      | 8.33 |
| 250                                | 146.84     | 7.72 |
| 350                                | 200.99     | 2.12 |
| 550                                | 290.27     | 3.79 |

**Table 4.3.1: Data obtained from the calibration shown in Figure 4.3.1(A), n = 5. R<sup>2</sup> = 0.9946. Data is represented as a Mean ± standard error of the mean (SEM). Background values subtracted. Mean background current = 0.57 ± 0.1 nA.**

In this section a H<sub>2</sub>O<sub>2</sub> calibration was carried out on a Pt<sub>c</sub> electrode. The purpose of this experiment is to act as a control against which various modifications made to the electrode surface may be compared. It is clear from the data displayed above that it is possible to detect H<sub>2</sub>O<sub>2</sub> at an unmodified Pt<sub>c</sub> electrode. The response is directly proportional to the amount of H<sub>2</sub>O<sub>2</sub> introduced into the cell. Calibrating the Pt<sub>c</sub> over a 0 to 550 μM H<sub>2</sub>O<sub>2</sub> concentration range yielded a sensitivity of 0.54 ± 0.01 nA/μM, n = 5.

#### 4.3.2 Pt<sub>c</sub>/Nafion<sup>®</sup>

Nafion<sup>®</sup> has previously been used in sensor design to improve selectivity over interference species without compromising sensitivity to the target substrate (Gerhardt & Hoffman, 2001; Brown & Lowry, 2003). Nafion<sup>®</sup> is a perfluorinated polymer which is a sulfonated derivative of Teflon<sup>®</sup>; ionic clusters of sulfonic acid groups present in Nafion<sup>®</sup> provide a negatively charged layer which is capable of repelling anionic species such as AA (Park *et al.*, 1998; Brown & Lowry, 2003). The ability of Nafion<sup>®</sup> to protect the exposed surface and to increase the biocompatibility of the sensor has also been shown (Turner *et al.*, 1991; Finnerty *et al.*, 2012). In this instance the detection of H<sub>2</sub>O<sub>2</sub> by adsorption of Nafion<sup>®</sup> (Pt<sub>c</sub>/Nafion<sup>®</sup>) onto the active surface of the electrode was

investigated. Nafion<sup>®</sup> was applied to the surface of the electrode as discussed in Section 3.5.2.

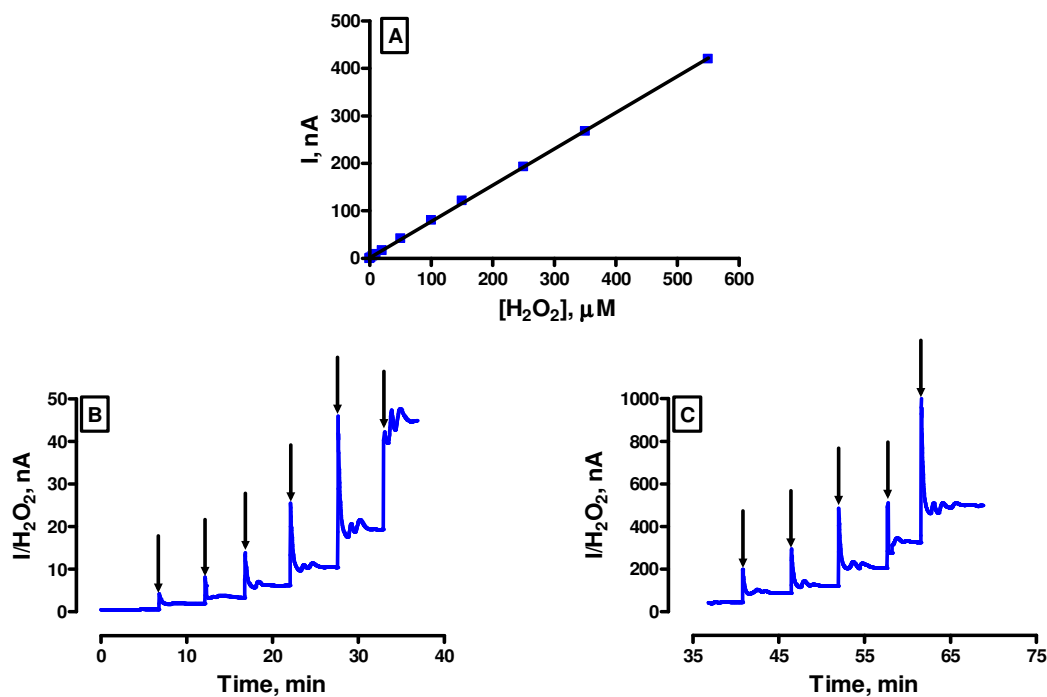


Figure 4.3.2: (A) The current-concentration profile of  $H_2O_2$  at  $Pt_c/Nafion^{\text{®}}$  ( $n = 5$ ). (B) A typical raw data trace 0-50  $\mu M$  and (C) 50-550  $\mu M$  for  $H_2O_2$  calibrations. CPA carried out at +700 mV vs. SCE. Arrows indicate the addition of aliquots of  $H_2O_2$ .

Figure 4.3.2 displays the detection of  $H_2O_2$  by a  $Pt_c$  sensor modified with Nafion<sup>®</sup>. Calibrating the  $Pt_c/Nafion^{\text{®}}$  over a 0 to 550  $\mu M$   $H_2O_2$  range yielded a sensitivity of  $0.76 \pm 0.01$  nA/ $\mu M$ ,  $n = 5$ .

| <b>H<sub>2</sub>O<sub>2</sub>, μM</b> | <b>Mean I, nA</b> | <b>SEM</b> |
|---------------------------------------|-------------------|------------|
| 0                                     | 0                 | 0          |
| 1                                     | 1.00              | 0.08       |
| 2                                     | 2.06              | 0.21       |
| 5                                     | 4.61              | 0.35       |
| 10                                    | 8.85              | 0.45       |
| 20                                    | 16.78             | 0.85       |
| 50                                    | 41.77             | 2.17       |
| 100                                   | 80.09             | 2.29       |
| 150                                   | 121.35            | 5.25       |
| 250                                   | 193.27            | 1.28       |
| 350                                   | 267.84            | 3.58       |
| 550                                   | 419.87            | 3.50       |

**Table 4.3.2:** Data obtained from the calibration shown in Figure 4.3.2(A),  $n = 5$ .  $R^2 = 0.998$ . Data is represented as a Mean  $\pm$  SEM. Background values subtracted. Mean background current =  $0.24 \pm 0.08$  nA.

An increase in H<sub>2</sub>O<sub>2</sub> sensitivity is observed with this sensor design however the response seen at the Pt<sub>c</sub>/Nafion<sup>®</sup> sensor was not significantly different ( $P > 0.05$ ) to that seen at the unmodified Pt<sub>c</sub>.

### 4.3.3 Pt<sub>c</sub>/PPD

A detailed description of the function and properties of poly-*o*-phenylenediamine (PPD) is given in Section 2.5 (Theory). Briefly, selectivity for the desired analyte (H<sub>2</sub>O<sub>2</sub>) over other interferences such as AA can be achieved by the incorporation of permselective membranes such as PPD. The modification of a Pt<sub>c</sub> electrode with PPD does not hinder the detection of H<sub>2</sub>O<sub>2</sub> as is illustrated in Figure 4.3.3.

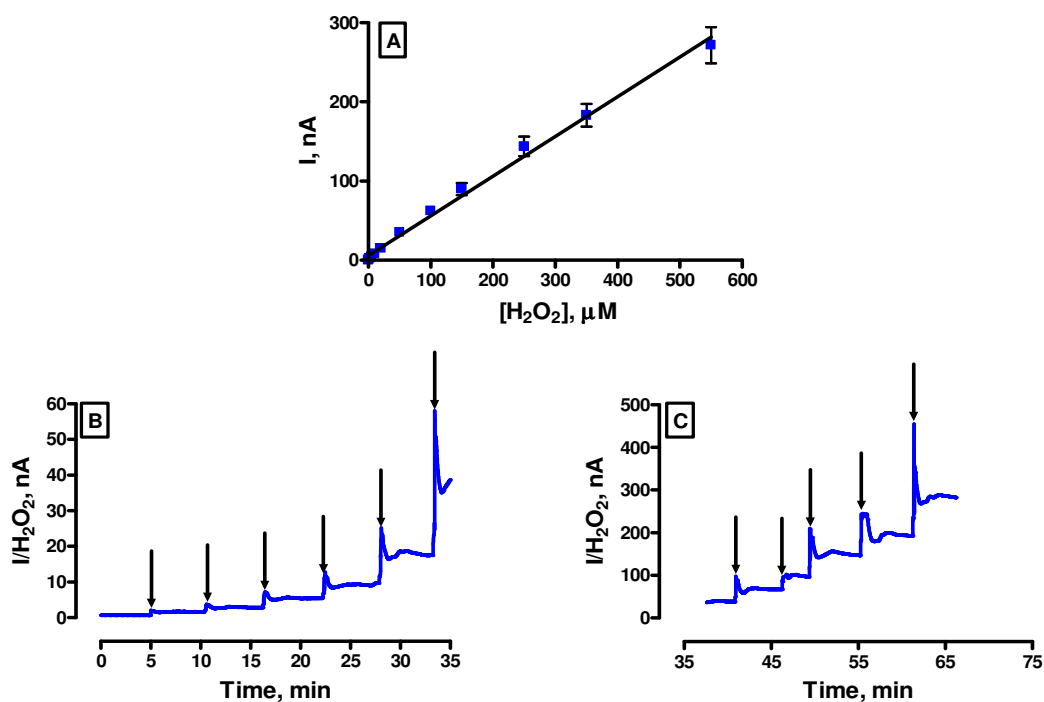


**Figure 4.3.3:** (A) The current-concentration profile of  $H_2O_2$  at  $Pt_c/PPD$  ( $n = 12$ ). (B) A typical raw data trace 0-50  $\mu M$  and (C) 50-550  $\mu M$  for  $H_2O_2$  calibrations. CPA carried out at +700 mV vs. SCE. Arrows indicate the addition of aliquots of  $H_2O_2$ .

Figure 4.3.3 shows the detection of  $H_2O_2$  by a  $Pt_c$  sensor modified with PPD. Calibrating this sensor over a 0 to 550  $\mu M$   $H_2O_2$  range yielded a sensitivity of  $0.50 \pm 0.01$  nA/ $\mu M$ ,  $n = 12$ . The response seen at the  $Pt_c/PPD$  sensor was not significantly different ( $P > 0.05$ ) to that seen at the unmodified  $Pt_c$ . The incorporation of PPD into the biosensor design does not significantly reduce the detection of  $H_2O_2$ . Lowry *et al.* have previously demonstrated that incorporation of PPD into a Pt based sensor design does not obstruct the detection of enzymatically generated  $H_2O_2$  (Lowry *et al.*, 1994).

| H <sub>2</sub> O <sub>2</sub> , μM | Mean I, nA | SEM   |
|------------------------------------|------------|-------|
| 0                                  | 0          | 0     |
| 1                                  | 1.08       | 0.10  |
| 2                                  | 2.33       | 0.22  |
| 5                                  | 4.74       | 0.35  |
| 10                                 | 8.10       | 0.56  |
| 20                                 | 14.79      | 0.88  |
| 50                                 | 35.31      | 2.7   |
| 100                                | 62.43      | 4.98  |
| 150                                | 89.91      | 7.44  |
| 250                                | 143.68     | 12.42 |
| 350                                | 183.09     | 14.4  |
| 550                                | 271.75     | 22.95 |

Table 4.3.3: Data obtained from the calibration shown in Figure 4.3.3(A), n = 12. R<sup>2</sup> = 0.9942. Data is represented as a Mean ± SEM. Background values subtracted. Mean background current = 0.71 ± 0.08 nA.

#### 4.3.4 Pt<sub>c</sub>/Nafion<sup>®</sup>/PPD

In order to maximise the selectivity of the *Blank* sensor design Nafion<sup>®</sup> was utilised in conjunction with PPD to optimise the ability to match the rejection characteristics seen at the catalase-based sensor as previously shown (O'Brien *et al.*, 2007). The ability of this *Blank* sensor to efficiently detect H<sub>2</sub>O<sub>2</sub> must also be considered. There must be no impairment in the sensitivity to the target substrate. This important parameter was maintained and the results are shown below.

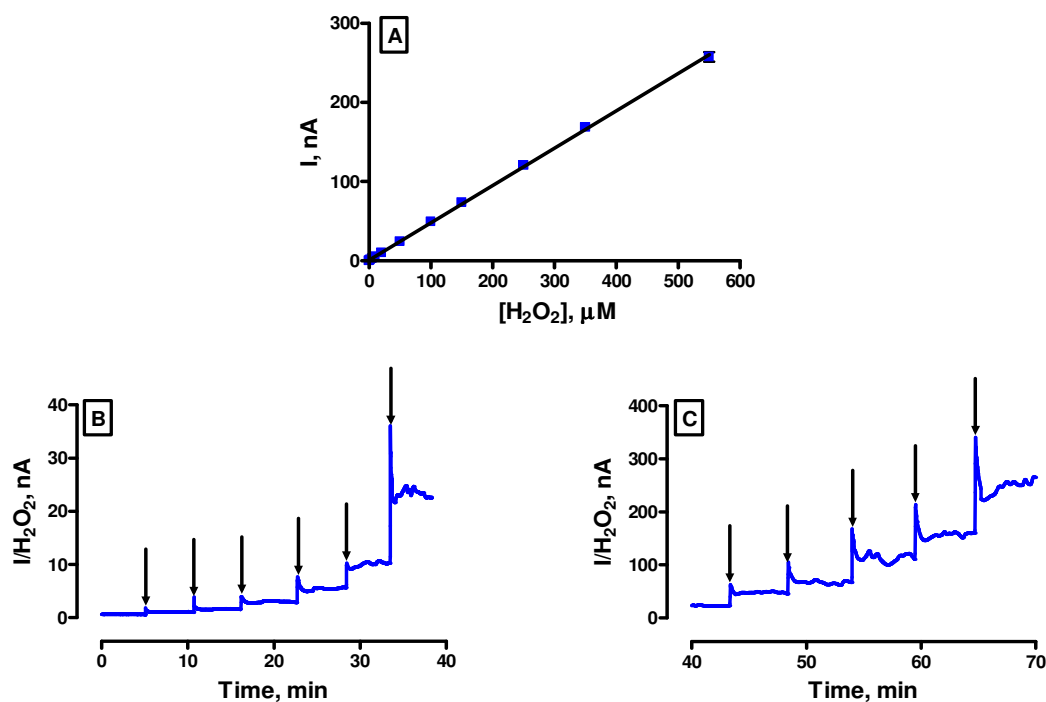


Figure 4.3.4: (A) The current-concentration profile of H<sub>2</sub>O<sub>2</sub> at Pt<sub>c</sub>/Nafion<sup>®</sup>/PPD (n = 24). (B) A typical raw data trace 0-50 μM and (C) 50-550 μM for H<sub>2</sub>O<sub>2</sub> calibrations. CPA carried out at +700 mV vs. SCE. Arrows indicate the addition of aliquots of H<sub>2</sub>O<sub>2</sub>.

| H <sub>2</sub> O <sub>2</sub> , μM | Mean I, nA | SEM  |
|------------------------------------|------------|------|
| 0                                  | 0          | 0    |
| 1                                  | 0.65       | 0.05 |
| 2                                  | 1.31       | 0.09 |
| 5                                  | 2.96       | 0.15 |
| 10                                 | 5.39       | 0.22 |
| 20                                 | 10.36      | 0.32 |
| 50                                 | 24.33      | 0.71 |
| 100                                | 49.32      | 1.37 |
| 150                                | 73.91      | 1.97 |
| 250                                | 120.58     | 3.05 |
| 350                                | 168.66     | 4.07 |
| 550                                | 257.52     | 6.10 |

Table 4.3.4: Data obtained from the calibration shown in Figure 4.3.4(A), n = 24. R<sup>2</sup> = 0.9997. Data is represented as a Mean ± SEM. Background values subtracted. Mean background current = 0.38 ± 0.03 nA.

Figure 4.3.4 shows the detection of H<sub>2</sub>O<sub>2</sub> at a Pt<sub>c</sub> sensor modified with Nafion<sup>®</sup> and subsequently electropolymerised with PPD. Calibrating this modified electrode over a 0 to 550 μM H<sub>2</sub>O<sub>2</sub> concentration range yielded a sensitivity of  $0.47 \pm 0.003$  nA/μM and was linear with an R<sup>2</sup> value of 0.9997, n = 24. The response seen at the Pt<sub>c</sub>/Nafion<sup>®</sup>/PPD sensor was not significantly different ( $P > 0.05$ ) to that seen at the unmodified Pt<sub>c</sub>. The combined incorporation of Nafion<sup>®</sup> and PPD into the biosensor design does not obstruct the detection of H<sub>2</sub>O<sub>2</sub>.

#### **4.3.5 Pt<sub>c</sub>/PPD/Cat-Ga**

The basis of the dual H<sub>2</sub>O<sub>2</sub> biosensor design (see Chapter 2, Section 2.8) requires a second paired sensor which will successfully remove the signal attributed to H<sub>2</sub>O<sub>2</sub>. In order to investigate the simplest possible design achievable a polymerised electrode was modified with catalase (see Section 3.5.3). Catalase is an enzyme which degrades H<sub>2</sub>O<sub>2</sub> into water and oxygen (Simonian & Coyle, 1996). The effect of introducing the enzyme into the design was investigated over the concentration range of 0 to 550 μM H<sub>2</sub>O<sub>2</sub> *in-vitro*. The presence of catalase effectively eliminates the current arising from H<sub>2</sub>O<sub>2</sub> as can be seen below in Figure 4.3.5.

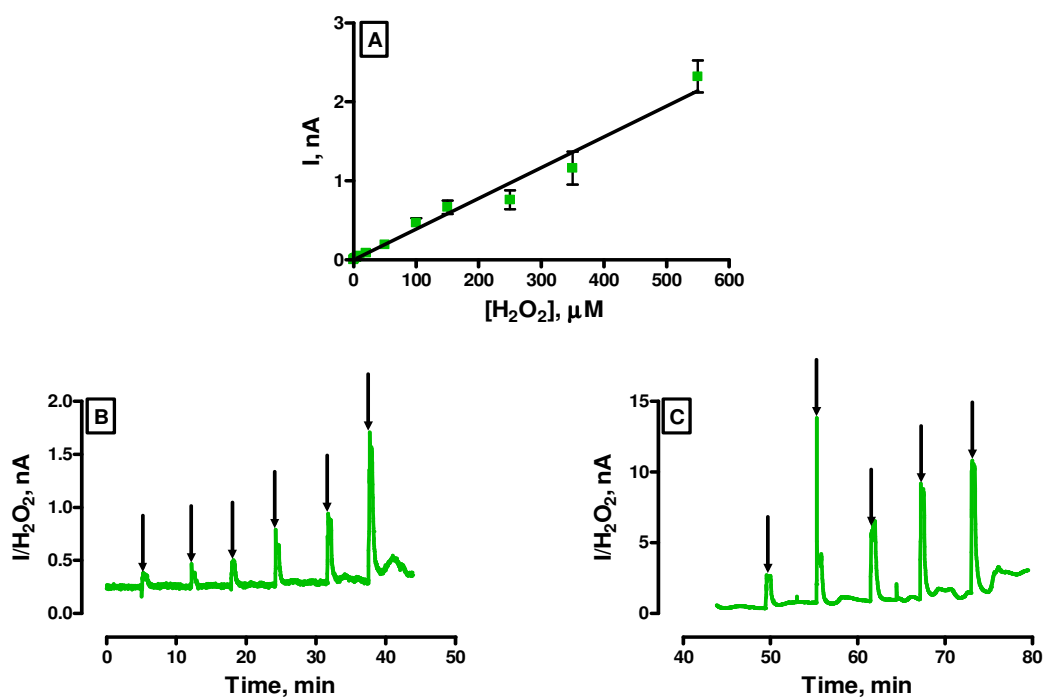


Figure 4.3.5: (A) The current-concentration profile of  $H_2O_2$  at  $Pt_c/PPD/Cat-Ga$  ( $n = 4$ ). (B) A typical raw data trace 0-50  $\mu M$  and (C) 50-550  $\mu M$  for  $H_2O_2$  calibrations. CPA carried out at +700 mV vs. SCE. Arrows indicate the addition of aliquots of  $H_2O_2$ .

| $H_2O_2, \mu M$ | Mean $I, nA$ | SEM   |
|-----------------|--------------|-------|
| 0               | 0            | 0     |
| 1               | 0.01         | 0.003 |
| 2               | 0.02         | 0.003 |
| 5               | 0.03         | 0.004 |
| 10              | 0.05         | 0.01  |
| 20              | 0.09         | 0.01  |
| 50              | 0.19         | 0.02  |
| 100             | 0.47         | 0.06  |
| 150             | 0.67         | 0.08  |
| 250             | 0.76         | 0.12  |
| 350             | 1.16         | 0.21  |
| 550             | 2.32         | 0.20  |

Table 4.3.5: Data obtained from the calibration shown in Figure 4.3.5(A),  $n = 4$ .  $R^2 = 0.9750$ . Data is represented as a Mean  $\pm$  SEM. Background values subtracted. Mean background current =  $0.29 \pm 0.04$  nA.

Figure 4.3.5 shows the detection of H<sub>2</sub>O<sub>2</sub> by a Pt<sub>c</sub> electrode electropolymerised with PPD and subsequently modified with catalase. Calibrating this sensor over a concentration range of 0 to 550 μM H<sub>2</sub>O<sub>2</sub> yielded a sensitivity of  $3.89 \pm 0.20$  pA/μM, n = 4. The response seen at the Pt<sub>c</sub>/PPD/Cat-Ga sensor was significantly different ( $P < 0.05$ ,\*) to that seen at the unmodified Pt<sub>c</sub>. The incorporation of catalase into the biosensor design removes ~99% of the signal attributed to H<sub>2</sub>O<sub>2</sub>.

#### **4.3.6 Pt<sub>c</sub>/Nafion<sup>®</sup>/PPD/Cat-Ga**

It was necessary to utilise Nafion<sup>®</sup> in the construction of the catalase-based sensor to improve the matched selectivity with the *Blank* sensor described in Section 4.3.4. Fluctuations in the level of AA in the extracellular fluid (ECF) under certain circumstances has been observed previously (Miele *et al.*, 1994). It is paramount in the *in-vivo* environment that changes in the concentration of AA will not disrupt the paired detection of H<sub>2</sub>O<sub>2</sub> achievable with the paired biosensor design (see Chapter 2, Section 2.8). Accordingly, the addition of Nafion<sup>®</sup> must not deter the function of the catalase enzyme, i.e. the removal of H<sub>2</sub>O<sub>2</sub>. The results from this section show that the integration of Nafion<sup>®</sup> into the assembly of the catalase-based sensor does not appreciably impact negatively on the function of the enzyme.

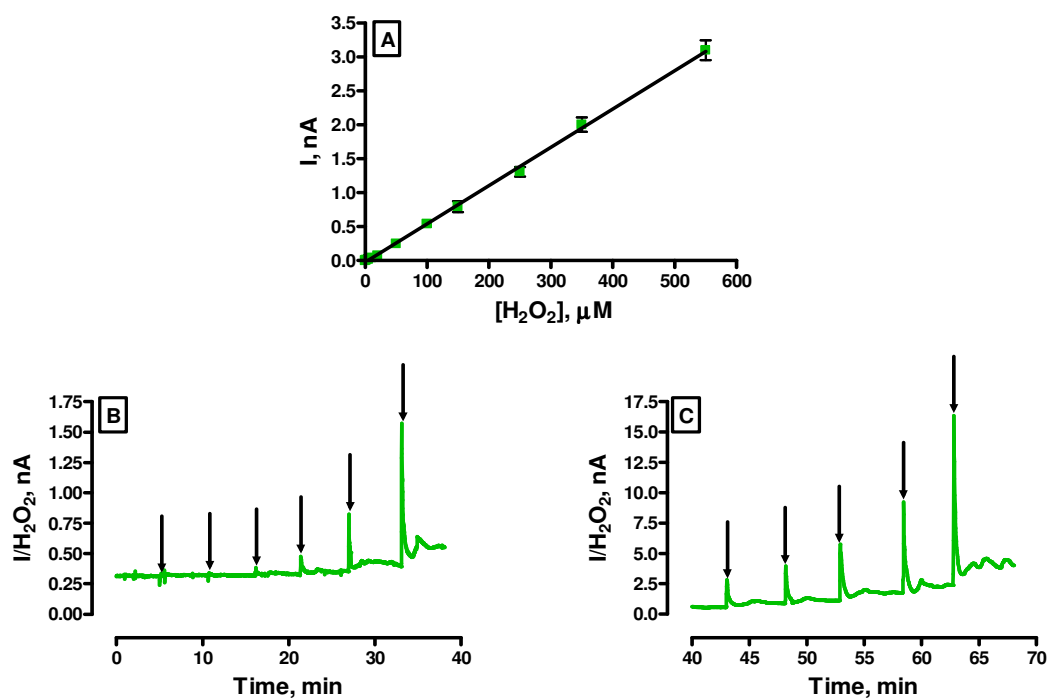


Figure 4.3.6: (A) The current-concentration profile of  $H_2O_2$  at  $Pt_c$ /Nafion<sup>®</sup>/PPD/Cat-Ga ( $n = 24$ ). (B) A typical raw data trace 0-50  $\mu M$  and (C) 50-550  $\mu M$  for  $H_2O_2$  calibrations. CPA carried out at +700 mV vs. SCE. Arrows indicate the addition of aliquots of  $H_2O_2$ .

| $H_2O_2, \mu M$ | Mean $I, nA$ | SEM   |
|-----------------|--------------|-------|
| 0               | 0            | 0     |
| 1               | 0.01         | 0.003 |
| 2               | 0.004        | 0.004 |
| 5               | 0.01         | 0.01  |
| 10              | 0.04         | 0.01  |
| 20              | 0.07         | 0.01  |
| 50              | 0.25         | 0.02  |
| 100             | 0.54         | 0.05  |
| 150             | 0.79         | 0.08  |
| 250             | 1.31         | 0.07  |
| 350             | 2.0          | 0.11  |
| 550             | 3.10         | 0.15  |

Table 4.3.6: Data obtained from the calibration shown in Figure 4.3.6(A),  $n = 24$ .  $R^2 = 0.9989$ . Data is represented as a Mean  $\pm$  SEM. Background values subtracted. Mean background current =  $0.43 \pm 0.03$  nA.

Figure 4.3.6 shows the removal of H<sub>2</sub>O<sub>2</sub> by a Pt<sub>c</sub> sensor modified with Nafion<sup>®</sup>, electropolymerised with PPD and subsequently modified with catalase. Calibrating this sensor over a concentration range of 0 to 550 μM H<sub>2</sub>O<sub>2</sub> yielded a sensitivity of 5.64 ± 0.06 pA/μM, n = 24. The response seen at the Pt<sub>c</sub>/Nafion<sup>®</sup>/PPD/Cat-Ga sensor was significantly different ( $P < 0.05, *$ ) to that seen at the unmodified Pt<sub>c</sub>. The incorporation of catalase into the biosensor design efficiently removes the signal attributable to H<sub>2</sub>O<sub>2</sub>. The trace displayed in Figure 4.3.6 is appreciably closer to baseline levels throughout the calibration and this is an improvement to that seen with the absence of Nafion<sup>®</sup> in the catalase-based sensor design (Figure 4.3.5). The response seen here is not significantly different ( $P > 0.05$ ) when compared with Pt<sub>c</sub>/PPD/Cat-Ga. The improved selectivity of Pt<sub>c</sub>/Nafion<sup>®</sup>/PPD/Cat-Ga over Pt<sub>c</sub>/PPD/Cat-Ga was an essential factor in deciding which sensor would be used as the catalase-based pair and this will be fully discussed in Section 4.5.

#### 4.4 H<sub>2</sub>O<sub>2</sub> sensor sensitivity summary

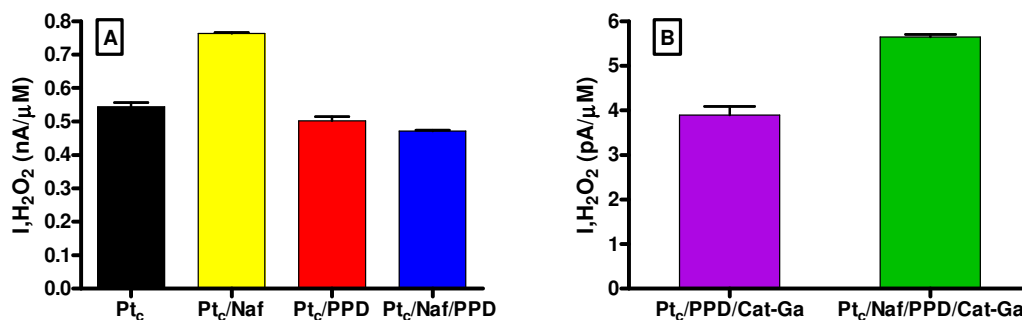


Figure 4.4.1 Comparison of H<sub>2</sub>O<sub>2</sub> sensitivities of modifications to Pt<sub>c</sub> discussed in Section 4.3. Average sensitivity represented as a slope value [(A), nA/μM] and [(B), pA/μM] mean response ± SEM.

| Design                                    | I,<br>(nA/ $\mu$ M) | SEM   | n  |
|---|---------------------|-------|----|
| Pt <sub>c</sub>                           | 0.54                | 0.01  | 5  |
| Pt <sub>c</sub> /Nafion <sup>®</sup>      | 0.76                | 0.004 | 5  |
| Pt <sub>c</sub> /PPD                      | 0.50                | 0.01  | 12 |
| Pt <sub>c</sub> /Nafion <sup>®</sup> /PPD | 0.47                | 0.003 | 24 |

**Table 4.4.1** Comparison of H<sub>2</sub>O<sub>2</sub> sensitivities of stated modifications to Pt<sub>c</sub> shown in Figure 4.4.1 (A)  
Data represented as a mean response  $\pm$  SEM. The number of each sensor type is denoted by (n).

| Design   | I,<br>(pA/ $\mu$ M) | SEM  | n  |
|--|---------------------|------|----|
| Pt <sub>c</sub> /PPD/Cat-Ga                      | 3.89                | 0.20 | 4  |
| Pt <sub>c</sub> /Nafion <sup>®</sup> /PPD/Cat-Ga | 5.64                | 0.06 | 24 |

**Table 4.4.2** Comparison of H<sub>2</sub>O<sub>2</sub> sensitivities of stated modifications to Pt<sub>c</sub> shown in Figure 4.4.1 (B)  
Data represented as a mean response  $\pm$  SEM. The number of each sensor type is denoted by (n).

In summary, various modifications were made to the bare Pt<sub>c</sub> electrode to produce a sensor capable of detecting H<sub>2</sub>O<sub>2</sub> and a paired design, removing H<sub>2</sub>O<sub>2</sub> by inclusion of the enzyme catalase. Each stated alteration, with the exception of catalase adsorption did not negatively effect H<sub>2</sub>O<sub>2</sub> sensitivity and a one-way ANOVA analysis of variance revealed the successive adjustments showed no significant variation  $P > 0.05$ . The sensitivity of each sensor type to the target substrate has been established and summarised in Table 4.4.1.

The inclusion of catalase resulted in ~99% removal of the H<sub>2</sub>O<sub>2</sub> signal in the case of the Pt<sub>c</sub>/PPD/Cat-Ga sensor with respect to the Pt<sub>c</sub>/PPD sensor. A ~98% removal of H<sub>2</sub>O<sub>2</sub> signal occurred with the Pt<sub>c</sub>/Nafion<sup>®</sup>/PPD/Cat-Ga sensor design with respect to the corresponding *Blank* sensor design (Pt<sub>c</sub>/Nafion<sup>®</sup>/PPD). Removal of H<sub>2</sub>O<sub>2</sub> is comparable

with both catalase-based sensor types and is not significantly different ( $P > 0.05$ ). The sensitivity of each catalase-based sensor type to H<sub>2</sub>O<sub>2</sub> has been established and summarised in Table 4.4.2.

In order to establish the correct pair suitable for *in-vivo* applications both sensor types i.e *Blank* and *Cat* must be capable of a matched response for AA. The next Section deals with the selectivity of each sensor in relation to AA, the main interfering species present in the brain.

## 4.5 Selectivity of the H<sub>2</sub>O<sub>2</sub> sensor *in-vitro*

### 4.5.1 Pt<sub>c</sub>

This section examines the response observed at a Pt<sub>c</sub> electrode calibrated at 700 mV vs. SCE following addition of aliquots of AA in the concentration range of 0-1000 μM. The purpose of this experiment is to act as a control against which various modifications to the Pt<sub>c</sub> electrode may be measured.

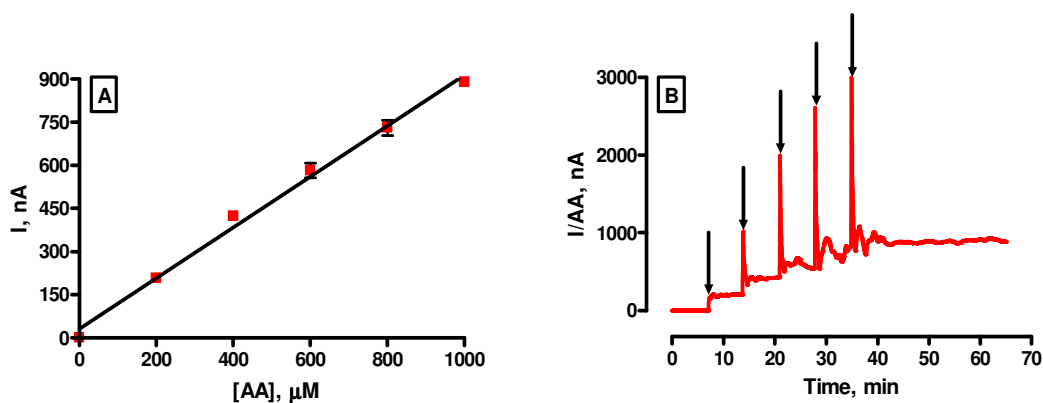


**Figure 4.5.1:** (A) The current-concentration profile of AA at Pt<sub>c</sub> (n = 6). (B) A typical raw data trace 0-1000 μM for AA calibrations. CPA carried out at +700 mV vs. SCE. Arrows indicate the addition of aliquots of AA.

As has been shown with H<sub>2</sub>O<sub>2</sub>, AA is also detectable at +700 mV vs. SCE using a bare Pt<sub>c</sub> (see Figure 4.3.1). The response to AA is proportional to the concentration of AA added to the electrochemical cell with a calculated sensitivity of  $0.88 \pm 0.04$  nA/μM, n = 6. It is not possible to independently detect H<sub>2</sub>O<sub>2</sub> in the presence of AA at the same

potential without further modification of the Pt<sub>c</sub>. For the purpose of *in-vivo* experiments the required H<sub>2</sub>O<sub>2</sub> sensor must be effective at interference rejection.

| AA, $\mu\text{M}$ | Mean I, nA | S.E.M |
|-------------------|------------|-------|
| 0                 | 0          | 0     |
| 200               | 208.39     | 3.63  |
| 400               | 424.46     | 11.80 |
| 600               | 581.87     | 25.63 |
| 800               | 730.09     | 27.06 |
| 1000              | 889.32     | 11.61 |

Table 4.5.1: Data obtained from the calibration shown in Figure 4.3.6(A),  $n = 6$ .  $R^2 = 0.9933$ . Data is represented as a Mean  $\pm$  SEM. Background values subtracted. Mean background current =  $0.86 \pm 0.09$  nA.

#### 4.5.2 Pt<sub>c</sub>/Nafion<sup>®</sup>

This section examines the effect of the incorporation of Nafion<sup>®</sup> onto the electrode surface in terms of the response towards AA. Nafion<sup>®</sup> is a perfluorinated polymer that has been used previously in sensor design to block AA interference (Park *et al.*, 1998).

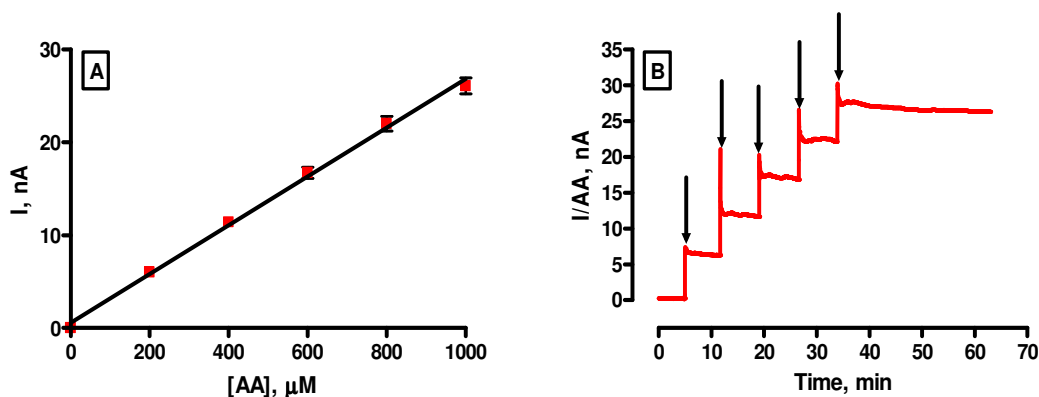


Figure 4.5.2: (A) The current-concentration profile of AA at Pt<sub>c</sub>/Nafion<sup>®</sup> ( $n = 4$ ). (B) A typical raw data trace 0-1000  $\mu\text{M}$  for AA calibrations. CPA carried out at +700 mV vs. SCE. Arrows indicate the addition of aliquots of AA.

| AA, $\mu\text{M}$ | Mean I, nA | S.E.M |
|-------------------|------------|-------|
| 0                 | 0          | 0     |
| 200               | 6.01       | 0.21  |
| 400               | 11.42      | 0.40  |
| 600               | 16.75      | 0.60  |
| 800               | 22.01      | 0.80  |
| 1000              | 26.08      | 0.86  |

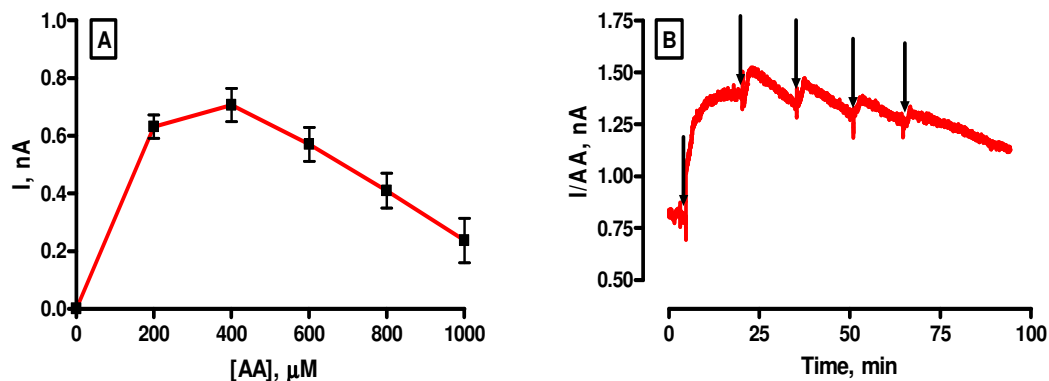
**Table 4.5.2: Data obtained from the calibration shown in Figure 4.3.6(A),  $n = 4$ .  $R^2 = 0.9971$ . Data is represented as a Mean  $\pm$  SEM. Background values subtracted. Mean background current =  $0.29 \pm 0.03$  nA.**

Table 4.5.2 displays data representing the selectivity of this Nafion<sup>®</sup>-modified sensor against AA. It is clear from the tabulated data that this sensor is not sufficiently effective at interference rejection; the response is linear with a sensitivity of  $0.03 \pm 0.001$  nA/ $\mu\text{M}$ ,  $n = 4$ . A significant difference ( $P < 0.0001$ ,\*\*\*) was observed for the current attributable to  $400 \mu\text{M}$  AA ( $I_{400 \mu\text{M}}$ ) and the current arising from  $1000 \mu\text{M}$  AA ( $I_{1000 \mu\text{M}}$ ) with this design when compared to  $\text{Pt}_c$ . However, further alterations were found necessary in order to facilitate efficient interference rejection.

### 4.5.3 $\text{Pt}_c/\text{PPD}$

This section will show the benefit yielded by incorporation of PPD into the H<sub>2</sub>O<sub>2</sub> biosensor design. The interference rejection characteristics of the sensor need to be optimised and for this purpose a film of PPD was grown electrochemically on the surface of the electrode. This method has previously been used in biosensor design (Lowry *et al.*, 1998; O'Neill *et al.*, 2008). The effect of the presence of PPD can clearly be observed in the calibration data below by the presence of the distinguishing bi-phasic calibration curve. As can be seen below an initial peak which reaches a maximum point ( $I_{\text{max}}$ ) occurs at *ca.*  $400 \mu\text{M}$  which is followed by a plateau region and a subsequent return to baseline levels. The plateau region is the result of a phenomenon known as self-blocking where the polymer structure has become saturated with the products of AA oxidation (McAteer & O'Neill, 1996). Figure 4.5.3 below details the AA response observed with the  $\text{Pt}_c/\text{PPD}$  sensor. The two main parameters utilised previously to analyse the AA response at PPD modified electrodes are  $I_{\text{max}}$  and the current observed

due to exposure to 1000  $\mu\text{M}$  AA ( $I_{1000 \mu\text{M}}$ ). However, in this chapter it was decided that as comparisons are made to sensors which lack PPD, and due to linear responses observed with some sensor types, the most comparable aspects from each sensor design are the current attributable to 400  $\mu\text{M}$  AA ( $I_{400 \mu\text{M}}$ ) and the current arising from 1000  $\mu\text{M}$  AA ( $I_{1000 \mu\text{M}}$ ).



**Figure 4.5.3:** (A) The current-concentration profile of AA at Pt/PPD ( $n = 16$ ). (B) A typical raw data trace 0-1000  $\mu\text{M}$  for AA calibrations. CPA carried out at +700 mV vs. SCE. Arrows indicate the addition of aliquots of AA.

| AA, $\mu\text{M}$ | Mean I, nA | S.E.M |
|-------------------|------------|-------|
| 0                 | 0          | 0     |
| 200               | 0.63       | 0.04  |
| 400               | 0.71       | 0.06  |
| 600               | 0.57       | 0.06  |
| 800               | 0.41       | 0.06  |
| 1000              | 0.24       | 0.08  |

**Table 4.5.3:** Data obtained from the calibration shown in Figure 4.3.4(a),  $n = 16$ . Data is represented as a Mean  $\pm$  SEM. Background values subtracted. Mean background current =  $1.02 \pm 0.1\text{nA}$ .

PPD efficiently blocks AA as can be seen from the characteristic non-linear response observed here as demonstrated previously (McAteer & O'Neill, 1996). The AA response of this sensor is comparable to previously published work (O'Neill *et al.*, 2008). However, the utilisation of PPD in isolation as part of the paired H<sub>2</sub>O<sub>2</sub> biosensor design

is not desirable. The rejection characteristics of this sensor can not be matched with the corresponding catalase-based sensor (see Section 4.5.5). Incorporation of a further interference rejection layer is necessary as described in the next Section. It is paramount to reduce the signal attributable to AA as much as possible in order to achieve effective pairing between the chosen *Blank* and *Cat* sensor without affecting sensitivity (see Section 2.8). The  $I_{400\ \mu\text{M}}$  and  $I_{1000\ \mu\text{M}}$  values for these sensors are  $0.71 \pm 0.06\ \text{nA}$  and  $0.24 \pm 0.08\ \text{nA}$  respectively. A significant difference ( $P < 0.0001, ***$ ) was observed between the  $I_{400\ \mu\text{M}}$  and  $I_{1000\ \mu\text{M}}$  values of this sensor design and the Pt<sub>c</sub> electrode (see Section 4.5.1).

#### 4.5.4 Pt<sub>c</sub>/Nafion<sup>®</sup>/PPD

The previous sections have not demonstrated desirable results for the purpose of matching the AA rejection characteristics of both sensors precisely i.e. *Blank* and *Cat* sensor. Investigations into the practical application of the use of the semi-permeable membrane Nafion<sup>®</sup> in conjunction with PPD were therefore carried out. These results compare well with previously published data (O'Brien *et al.*, 2007).

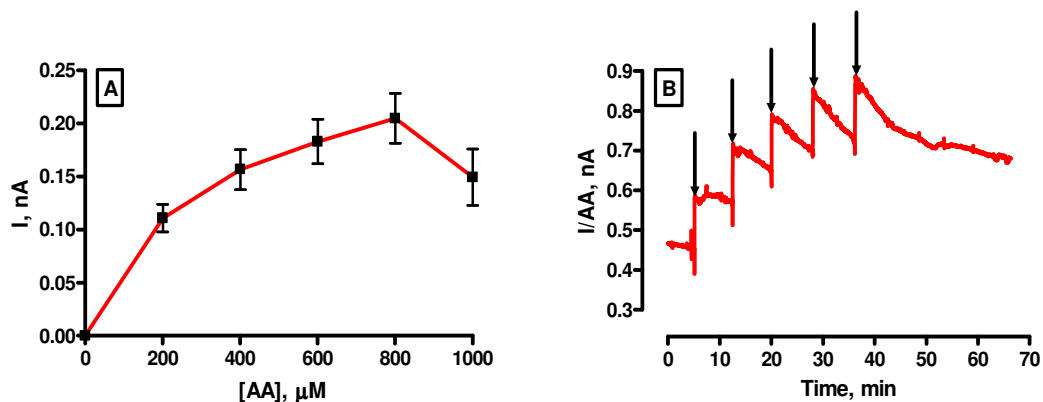


**Figure 4.5.4:** (A) The current-concentration profile of AA at Pt<sub>c</sub>/Nafion<sup>®</sup>/PPD ( $n = 28$ ). (B) A typical raw data trace 0-1000  $\mu\text{M}$  for AA calibrations. CPA carried out at +700 mV vs. SCE. Arrows indicate the addition of aliquots of AA.

| AA, $\mu\text{M}$ | Mean I, nA | SEM  |
|-------------------|------------|------|
| 0                 | 0          | 0    |
| 200               | 0.11       | 0.01 |
| 400               | 0.16       | 0.02 |
| 600               | 0.18       | 0.02 |
| 800               | 0.20       | 0.02 |
| 1000              | 0.15       | 0.03 |

**Table 4.5.4: Data obtained from the calibration shown in Figure 4.3.7(A), n = 28. Data is represented as a Mean  $\pm$  SEM. Background values subtracted. Mean background current =  $0.32 \pm 0.02$  nA.**

The  $I_{400 \mu\text{M}}$  and  $I_{1000 \mu\text{M}}$  values for these sensors are  $0.16 \pm 0.02$  nA and  $0.15 \pm 0.03$  nA respectively. A non-linear response was observed which is in sharp contrast to the response seen with Pt<sub>c</sub> and the  $I_{400 \mu\text{M}}$  and  $I_{1000 \mu\text{M}}$  values of this sensor design were significantly different ( $P < 0.0001, ***$ ) to Pt<sub>c</sub>. The Pt<sub>c</sub>/Nafion<sup>®</sup>/PPD sensor (*Blank*) was chosen as the most suitable candidate for the purpose of *in-vivo* experiments due to very low AA permeability characteristics and a high affinity for the target substrate (H<sub>2</sub>O<sub>2</sub>) as seen in Section 4.3.4

#### 4.5.5 Pt<sub>c</sub>/PPD/Cat-Ga

The objective of this section is to determine whether exclusion of Nafion<sup>®</sup> will affect the selectivity of the desired Catalase-based sensor. The results below illustrate that the AA response of this sensor design (Pt<sub>c</sub>/PPD/Cat-Ga) is not sufficiently low enough for application of this type of sensor in the *in-vivo* environment.

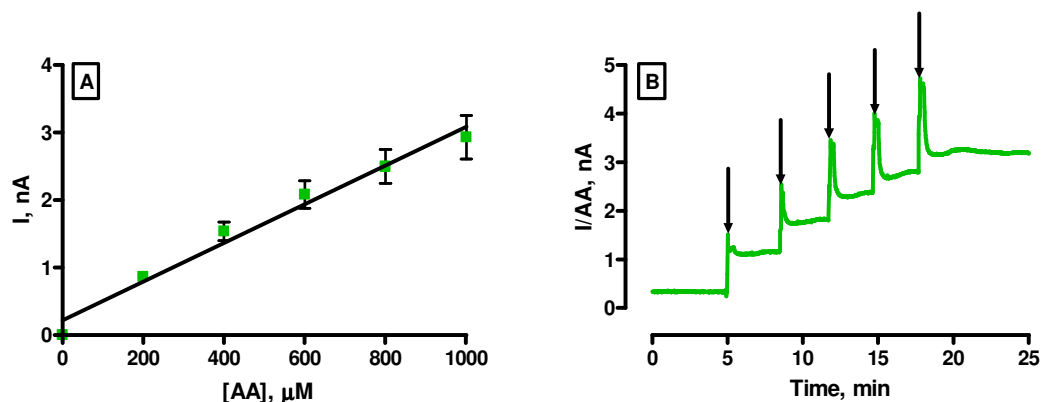


Figure 4.5.5: (A) The current-concentration profile of AA at Pt<sub>c</sub>/PPD/Cat-Ga (n = 5). (B) A typical raw data trace 0-1000 μM for AA calibrations. CPA carried out at +700 mV vs. SCE. Arrows indicate the addition of aliquots of AA.

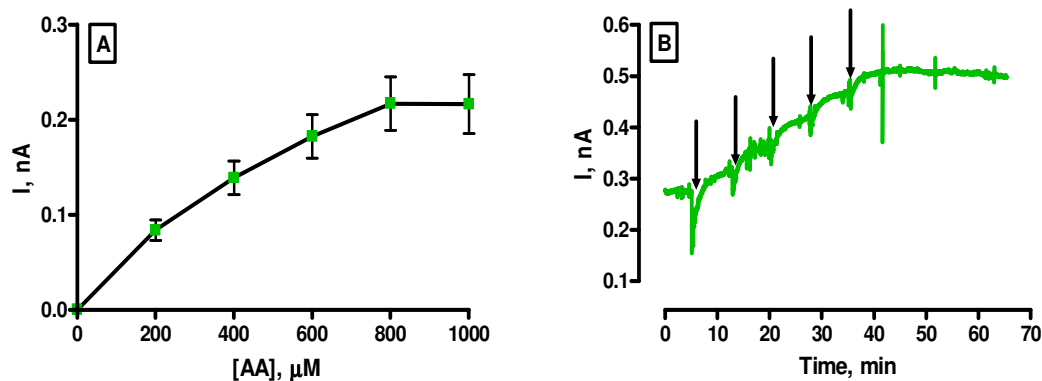
| AA, μM | Mean I, nA | SEM  |
|--------|------------|------|
| 0      | 0          | 0    |
| 200    | 0.87       | 0.06 |
| 400    | 1.54       | 0.14 |
| 600    | 2.08       | 0.20 |
| 800    | 2.50       | 0.25 |
| 1000   | 2.93       | 0.32 |

Table 4.5.5: Data obtained from the calibration shown in Figure 4.3.7(A), n = 5. R<sup>2</sup> = 0.9783. Data is represented as a Mean ± SEM. Background values subtracted. Mean background current = 0.33 ± 0.07 nA.

Despite the inclusion of PPD the characteristic self-blocking response typically seen is not apparent in this case. The response is linear as can be observed in Figure 4.5.5. A sensitivity of  $3.89 \pm 0.20$  pA/μM, n = 5 was recorded. It is clear that this sensor design is not suitable for *in-vivo* use due to a relatively high AA response and the fact that the AA response shown here cannot be successfully matched to the corresponding sensor design which lacks catalase (Pt<sub>c</sub>/PPD) due to the linearity of the response attained here. As stated previously the *Blank* and *Cat* sensor designs must demonstrate matching selectivity parameters.

#### 4.5.6 Pt<sub>c</sub>/Naf/PPD/Cat-Ga

This section deals with the integration of a Nafion<sup>®</sup> layer into the construction of the catalase-based sensor. Nafion<sup>®</sup> was utilised to improve the selectivity in relation to the main endogenous electroactive interference species present in the brain (AA), in order to match AA responses between the *Blank* and *Cat* sensor. The results shown in this section compare well with previous demonstrations of the response towards AA of this sensor design (O'Brien *et al.*, 2007).



**Figure 4.5.6:** (A) The current-concentration profile of AA at Pt<sub>c</sub>/Nafion<sup>®</sup>/PPD/Cat-Ga (n = 28). (B) A typical raw data trace 0-1000 μM for AA calibrations. CPA carried out at +700 mV vs. SCE. Arrows indicate the addition of aliquots of AA.

| AA, μM | Mean I, nA | S.E.M |
|--------|------------|-------|
| 0      | 0          | 0     |
| 200    | 0.08       | 0.01  |
| 400    | 0.14       | 0.02  |
| 600    | 0.18       | 0.02  |
| 800    | 0.22       | 0.03  |
| 1000   | 0.22       | 0.03  |

**Table 4.5.6:** Data obtained from the calibration shown in Figure 4.3.7(A) n = 28. Data is represented as a Mean ± SEM. Background values subtracted. Mean background current = 0.23 ± 0.02 nA.

The I<sub>400 μM</sub> and I<sub>1000 μM</sub> values for these sensors are 0.14 ± 0.02 nA and 0.22 ± 0.03 nA respectively. The incorporation of Nafion<sup>®</sup> into the construction of this sensor successfully achieved a reduction in AA response with respect to Pt<sub>c</sub>/PPD/Cat-Ga with a

significant difference ( $P < 0.0001, ***$ ) observed between  $I_{400 \mu\text{M}}$  and  $I_{1000 \mu\text{M}}$  values. The sensor shown in this section (Pt<sub>c</sub>/Nafion<sup>®</sup>/PPD/Cat-Ga) was chosen as the catalase-based sensor (*Cat*) to use in *in-vivo* experiments due to low AA permeability, efficient removal of H<sub>2</sub>O<sub>2</sub> (Section 4.3.6) and the correlation seen with the AA response when compared to the paired sensor lacking catalase i.e. Pt<sub>c</sub>/Nafion<sup>®</sup>/PPD (Section 4.5.4).

#### 4.6. H<sub>2</sub>O<sub>2</sub> sensor selectivity summary

The  $I_{\text{max}}$  and  $I_{1000 \mu\text{M}}$  values are the parameters which have previously been used to compare selectivity characteristics of biosensor designs which incorporate PPD as discussed in Section 4.5.3. In this section, as comparisons are made to sensors which lack PPD and due to the linear responses observed with certain sensor designs; the most comparable aspects from each sensor design are the current attributable to 400  $\mu\text{M}$  ( $I_{400 \mu\text{M}}$ ) and the current arising from 1000  $\mu\text{M}$  AA ( $I_{1000 \mu\text{M}}$ ). The analysis parameters chosen take into account that the ECF concentration of AA is expected to be between 100 and 500  $\mu\text{M}$  (O'Neill & Lowry, 2000) with fluctuations to higher levels in certain circumstances (Miele *et al.*, 1994).

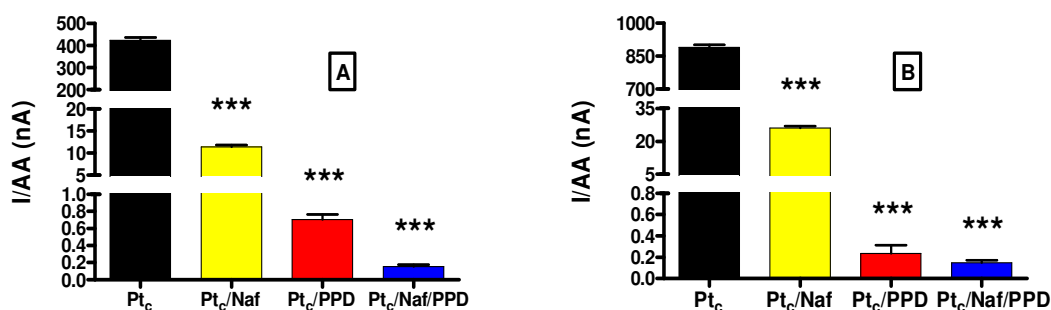


**Figure 4.6.1** Comparison of AA responses following modifications to Pt<sub>c</sub> discussed in Section 4.5. Data represented as a mean response  $\pm$  SEM. (A)  $I_{400 \mu\text{M}}$  and (B)  $I_{1000 \mu\text{M}}$  ( $P < 0.0001, ***$ ), where (*P*) represents the outcome of a unpaired t-test with each design when compared to the response recorded with Pt<sub>c</sub>.

The addition of Nafion<sup>®</sup> to the Pt<sub>c</sub> caused a significant reduction in  $I_{400 \mu\text{M}}$  ( $P < 0.0001, ***$ ) and also in  $I_{1000 \mu\text{M}}$  ( $P < 0.0001, ***$ ). The Pt<sub>c</sub>/PPD sensor also caused a significant reduction in  $I_{400 \mu\text{M}}$  and  $I_{1000 \mu\text{M}}$  with ( $P < 0.0001, ***$ ) and ( $P < 0.0001, ***$ ) respectively

when compared to Pt<sub>c</sub>. A significant decrease in AA response with Pt<sub>c</sub>/Nafion<sup>®</sup>/PPD (*Blank*) was observed in relation to the bare Pt<sub>c</sub> with  $P < 0.0001$ ,\*\*\* for I<sub>400 μM</sub> and  $P < 0.0001$ ,\*\*\* for I<sub>1000 μM</sub>.

The greatest reduction in AA response of the non catalase-based sensors was the Pt<sub>c</sub>/Nafion<sup>®</sup>/PPD (*Blank*). The I<sub>400 μM</sub> of this sensor was significantly less than Pt<sub>c</sub>/Nafion<sup>®</sup> ( $P < 0.0001$ , \*\*\*). A similar finding was seen with the I<sub>1000 μM</sub> response ( $P < 0.0001$ ,\*\*\*). In relation to the polymerised electrode Pt<sub>c</sub>/PPD the Pt<sub>c</sub>/Nafion<sup>®</sup>/PPD (*Blank*) showed a significant improvement in AA rejection capabilities at I<sub>400 μM</sub> ( $P < 0.0001$ ,\*\*\*) and a matched result with the I<sub>1000 μM</sub> response which was shown as not significantly different ( $P > 0.05$ ).

The I<sub>400 μM</sub> and I<sub>1000 μM</sub> response of the Pt<sub>c</sub>/PPD design and the corresponding catalase-based sensor Pt<sub>c</sub>/PPD/Cat-Ga did not correlate well together with significant differences ( $P < 0.0001$ , \*\*\*) recorded for both. A Pt<sub>c</sub>/PPD sensor combined with a Pt<sub>c</sub>/PPD/Cat-Ga sensor would be unsuitable for the detection of H<sub>2</sub>O<sub>2</sub> *in-vivo* as matching AA rejection capabilities cannot be achieved. Figure 4.6.2 below shows how incorporation of Nafion<sup>®</sup> into the catalase-based sensor design improves AA rejection capabilities.

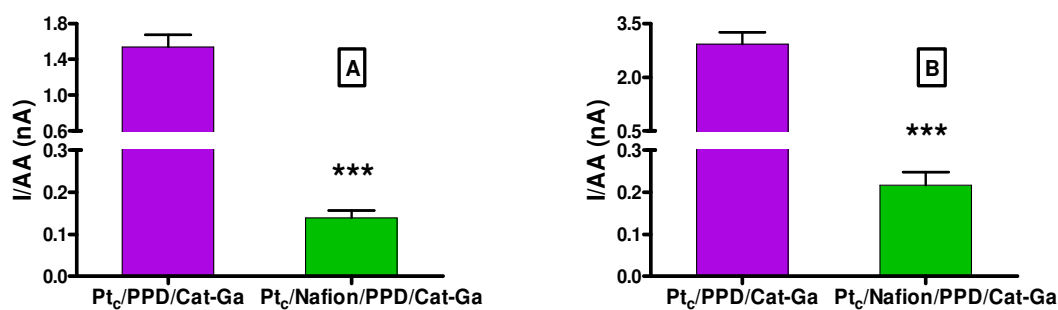


**Figure 4.6.2 Comparison of AA selectivity with alterations to Pt<sub>c</sub> and subsequent modification with catalase as discussed in Section 4.5. Data represented as a mean response  $\pm$  SEM. (A) I<sub>400 μM</sub> and (B) I<sub>1000 μM</sub> ( $P < 0.0001$ , \*\*\*).**

Following incorporation of Nafion<sup>®</sup> into the sensor design Pt<sub>c</sub>/Nafion<sup>®</sup>/PPD/Cat-Ga, a significant difference ( $P < 0.0001, ***$ ) in AA response was observed with respect to the Pt<sub>c</sub>/PPD/Cat-Ga sensor construct for both I<sub>400 μM</sub> and I<sub>1000 μM</sub>. The excellent AA rejection characteristics achieved by the combination of Pt<sub>c</sub>/Nafion<sup>®</sup>/PPD (*Blank*) and Pt<sub>c</sub>/Nafion<sup>®</sup>/PPD/Cat-Ga (*Cat*) are fully discussed in Section 4.8.

| Design   | I, nA<br>(1000 μM) | SEM   | I, nA<br>(400 μM) | SEM  | n  |
|--|--------------------|-------|-------------------|------|----|
| Pt <sub>c</sub>  | 889.32             | 11.61 | 424.46            | 11.8 | 6  |
| Pt <sub>c</sub> /Nafion <sup>®</sup>                           | 26.08              | 0.86  | 11.42             | 0.4  | 4  |
| Pt <sub>c</sub> /PPD   | 0.24               | 0.08  | 0.71              | 0.06 | 16 |
| Pt <sub>c</sub> /Nafion <sup>®</sup> /PPD( <i>Blank</i> )      | 0.15               | 0.03  | 0.16              | 0.02 | 28 |
| Pt <sub>c</sub> /PPD/Cat-Ga                                    | 2.93               | 0.32  | 1.54              | 0.14 | 5  |
| Pt <sub>c</sub> /Nafion <sup>®</sup> /PPD/Cat-Ga( <i>Cat</i> ) | 0.22               | 0.03  | 0.14              | 0.02 | 28 |

**Table 4.6.1 Comparison of AA selectivities following various modifications to Pt<sub>c</sub> discussed in Section 4.5. Data represented as a mean response ± SEM. The number of each sensor type is denoted by (n).**

#### 4.7. Paired H<sub>2</sub>O<sub>2</sub> sensor sensitivity

The detection of H<sub>2</sub>O<sub>2</sub> in this body of work is based on a dual paired sensor design. It is necessary at this point to reiterate that the subtracted current response determined by the paired sensor design is the target of the individual results shown in this chapter. As has been demonstrated in the previous Sections of this chapter Pt<sub>c</sub>/Nafion<sup>®</sup>/PPD was the preferred design chosen for the *Blank* sensor (*Blank*) for application in the *in-vivo* environment. The *Blank* design was determined on balance by the highest H<sub>2</sub>O<sub>2</sub>

sensitivity and the lowest AA permeability. The matched catalase-based biosensor [Pt<sub>c</sub>/Nafion<sup>®</sup>/PPD/Cat-Ga (*Cat*)] was the most appropriate candidate for application *in-vivo*. The *Cat* sensor was identified as suitable due to very similar selectivity characteristics with the *Blank* sensor (see Section 4.8.1). This *Cat* sensor (Pt<sub>c</sub>/Nafion<sup>®</sup>/PPD/Cat-Ga) also showed a high proportion of H<sub>2</sub>O<sub>2</sub> removal (~98%). The results displayed going forward are a representation of the subtracted current response achieved with the paired sensor design i.e. *Blank-Cat*. The sensitivity of the paired H<sub>2</sub>O<sub>2</sub> sensor is discussed in this section.

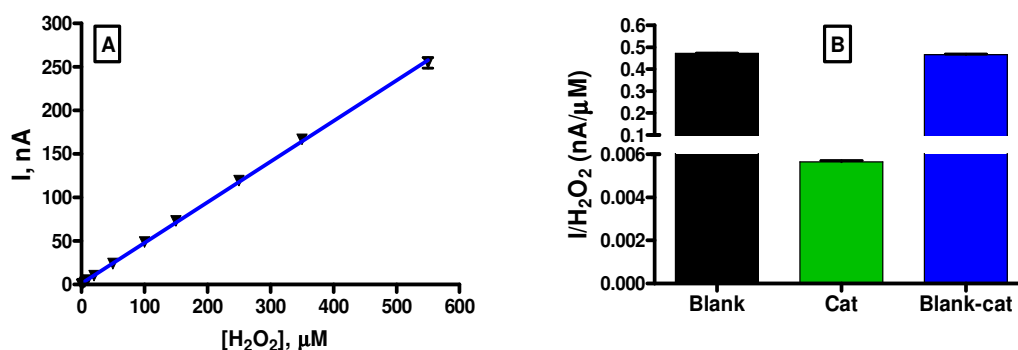


**Figure 4.7.1:** (A) The current-concentration profile of the H<sub>2</sub>O<sub>2</sub> sensitivity of the paired sensor response (*Blank-Cat*) ( $n = 24$ ). CPA carried out at +700 mV vs. SCE. (B) Comparison of the average sensitivity of (*Blank* ( $n = 24$ )), (*Cat* ( $n = 24$ )) and (*Blank-Cat* ( $n = 24+24$ )) represented as a slope value (nA/μM)  $\pm$  SEM.

The overall sensitivity of the dual H<sub>2</sub>O<sub>2</sub> sensor (*Blank-Cat*) is represented above in Figure 4.7.1 (A). The sensitivity of the paired H<sub>2</sub>O<sub>2</sub> sensor is  $0.47 \pm 0.003$  nA/μM and is linear with an R<sup>2</sup> value of 0.9996,  $n = 24+24$ . No significant difference ( $P > 0.05$ ) is observed between the paired sensitivity (*Blank-Cat*) and the H<sub>2</sub>O<sub>2</sub> response at the *Blank* sensor as can be seen in Figure 4.7.1(B). This highly reproducible value is in agreement with previously published data (O'Brien *et al.*, 2007).

### 4.7.1 Limit of detection

The limit of detection (LOD) is the smallest concentration of analyte detectable by a sensor. LOD is defined as the analyte concentration which corresponds to three times the standard deviation of the background current and was calculated as  $0.075 \pm 0.006$   $\mu\text{M}$ ,  $n = 24$  for the *Blank* sensor. The ECF concentration of H<sub>2</sub>O<sub>2</sub> is expected to be between 25 and 50  $\mu\text{M}$  (Hyslop *et al.*, 1995), suggesting that in an *in-vivo* environment our *Blank* sensor can reliably detect low levels of H<sub>2</sub>O<sub>2</sub>. The *Cat* sensor removes ~98% of the H<sub>2</sub>O<sub>2</sub> signal and would therefore have a minimal effect on the overall LOD of the paired sensor design.

### 4.7.2 Response time

The response time of a sensor is defined as the time required to change from 10% to 90% of the maximum response. The response of the *Blank* sensor over time is shown below in Figure 4.7.2.

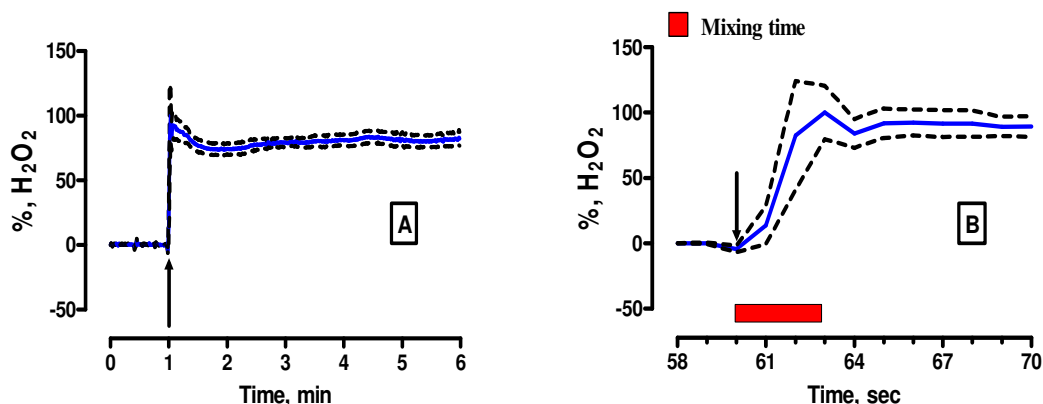


**Figure 4.7.2: The average H<sub>2</sub>O<sub>2</sub> response at the *Blank* sensor design ( $n = 6$ ) for addition of 1  $\mu\text{M}$  H<sub>2</sub>O<sub>2</sub>. Data shown as a percentage with 100% representative of the maximum H<sub>2</sub>O<sub>2</sub> sensitivity, SEM is denoted by the dashed line. The response is plotted vs. minutes (A) and versus seconds (B). Arrows indicate the addition of H<sub>2</sub>O<sub>2</sub>.**

The data shown in Figure 4.7.2 represents the response of the *Blank* sensor over time following the introduction of an aliquot of H<sub>2</sub>O<sub>2</sub> (1  $\mu\text{M}$ ) into the electrochemical cell. The solution is stirred immediately following the injection for approximately 3 seconds. It is clear from Figure 4.7.2 (A) an immediate increase in response occurs as H<sub>2</sub>O<sub>2</sub> is

injected into the cell which reaches a peak value and subsequently exhibits a steady-state behaviour. On closer inspection of this data as presented in Figure 4.7.2 (B) the maximum response of the *Blank* sensor is achieved within the mixing time (~3 s), which has been demonstrated with other polymer-based sensors (Lowry *et al.*, 1994; Ryan *et al.*, 1997). An instantaneous increase in response to H<sub>2</sub>O<sub>2</sub> is observable with this sensor type. The response time of the *Blank* sensor is on the sub-second time scale. The transition from 10 % to 90 % of the maximum response occurs within < 1s. This rapid response time is highly suitable in order to detect H<sub>2</sub>O<sub>2</sub> which is a highly permeable short-lived molecule particularly in the *in-vivo* environment (Bao *et al.*, 2009). As previously stated the overall H<sub>2</sub>O<sub>2</sub> response is based on a paired design (*Blank-Cat*). The *Cat* sensor removes ~98% of the H<sub>2</sub>O<sub>2</sub> signal and therefore has a minimal effect on the response time of the dual sensor design.

#### 4.8. Paired H<sub>2</sub>O<sub>2</sub> sensor selectivity

AA is the primary source of electrochemical interference in the brain. However, other potential sources of interference are possible from various species. These species can be detected over the same potential range as H<sub>2</sub>O<sub>2</sub>. A complete *in-vitro* selectivity characterisation of the H<sub>2</sub>O<sub>2</sub> sensor has been demonstrated by O'Brien *et al.* (O'Brien *et al.*, 2007). In the work presented by O'Brien *et al.* the current arising from the H<sub>2</sub>O<sub>2</sub> paired sensor by introduction of a wide range of relevant chemical species was examined. The effect of introduction of uric acid (UA), serotonin (5-HT), DOPAC, 5-HIAA, dopamine (DA), glutathione, homovanillic acid (HVA), L-tryptophan, L-cysteine and L-tyrosine into the electrochemical cell on the paired H<sub>2</sub>O<sub>2</sub> sensor response was tested. The expected ECF concentration of each analyte was utilised in this examination. The results are displayed in Table 4.8.1.

|                                   | ECF ( $\mu\text{M}$ ) <sup>a</sup> | Paired H <sub>2</sub> O <sub>2</sub> sensor response <sup>b</sup> | n  |
|-----------------------------------|------------------------------------|---|----|
| <b>H<sub>2</sub>O<sub>2</sub></b> | 25-50                              | 0.47 $\pm$ 0.003 (nA/ $\mu\text{M}$ )                             | 24 |
| <b>UA</b>                         | 100                                | < 0.1 % *   | 4  |
| <b>5-HT</b>                       | 0.01                               | < 0.1 % *   | 4  |
| <b>DOPAC</b>                      | 20                                 | < 0.1 % *   | 4  |
| <b>5-HIAA</b>                     | 10                                 | < 0.1 % *   | 4  |
| <b>DA</b>                         | 0.05                               | < 0.1 % *   | 4  |
| <b>Glutathione</b>                | 50                                 | < 0.1 % *   | 4  |
| <b>HVA</b>                        | 20                                 | < 0.1 % *   | 4  |
| <b>L-Tryptophan</b>               | 100                                | < 0.1 % *   | 4  |
| <b>L-Cysteine</b>                 | 50                                 | < 0.1 % *   | 4  |
| <b>L-Tyrosine</b>                 | 100                                | < 0.1 % *   | 4  |

**Table 4.8** *In-vitro* responses of the paired H<sub>2</sub>O<sub>2</sub> sensor to H<sub>2</sub>O<sub>2</sub> and the stated potential interferents. <sup>a</sup> expected ECF concentration. <sup>b</sup> expected response at the stated ECF concentration. \* Less than 0.1 % of H<sub>2</sub>O<sub>2</sub> sensitivity (O'Brien *et al.*, 2007).

The response from each interference species tested was < 0.1 % of the H<sub>2</sub>O<sub>2</sub> sensitivity of the paired sensor. The paired H<sub>2</sub>O<sub>2</sub> sensor is highly selective over the range of interference species tested. It is possible to definitively measure micromolar concentrations of H<sub>2</sub>O<sub>2</sub> in the presence of these interference species.

#### 4.8.1 Paired H<sub>2</sub>O<sub>2</sub> sensor AA selectivity

As the interference rejection characteristics of the H<sub>2</sub>O<sub>2</sub> paired sensor were previously reported (see Section 4.8) a subsequent AA calibration was sufficient to determine the selectivity properties of the sensor.

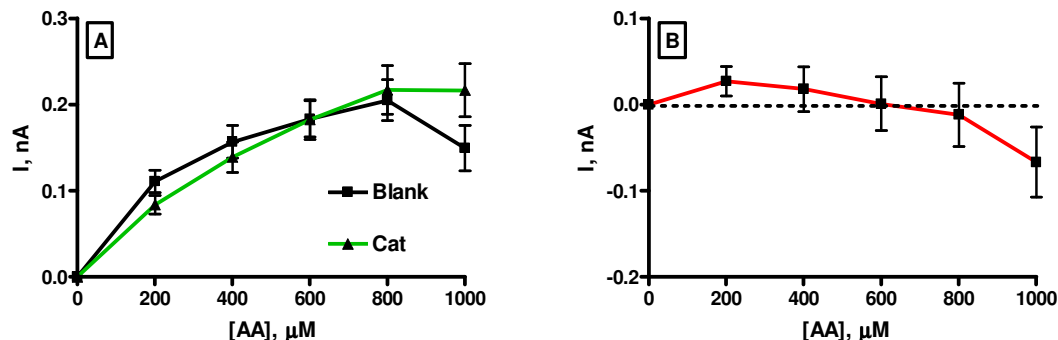


**Figure 4.8.1 : AA response of the paired sensor (*Blank-Cat*). The current-concentration profile of each sensor design (A) *Blank* sensor (n = 28) and *Cat* sensor (n = 28). The current-concentration profile of the paired response *Blank-Cat* (B) (n = 28+28). CPA carried out at +700 mV vs. SCE.**

Figure 4.8.1(A) above shows the current values recorded individually by the *Blank* and *Cat* sensor in response to introduction of 0-1000 μM AA. As discussed previously the response of the H<sub>2</sub>O<sub>2</sub> dual sensor design is obtained by a subtraction method (*Blank-Cat*). As can be seen in Figure 4.8.1(B) the subtracted current does not vary much from baseline levels, denoted by the dashed line. The current remains above basal levels, up to a concentration of 600 μM AA and subsequently a slight drift below baseline is observed. It is clear that the AA response of the dual sensor design is minimised. The small responses to AA are very well matched between the *Blank* and *Cat* sensor as can be observed in Figure 4.8.1(A). The selectivity over AA of the paired sensor is clearly established. The  $I_{400 \mu\text{M}}$  of the *Blank* sensor was found to be  $0.16 \pm 0.02$  nA (n = 28) and this value was not significantly different ( $P > 0.05$ ) when compared to the  $I_{400 \mu\text{M}}$  of the *Cat* sensor ( $0.14 \pm 0.02$  nA, n = 28). Additionally the  $I_{1000 \mu\text{M}}$  AA response of the *Blank* sensor ( $0.15 \pm 0.03$  nA, n = 28) showed no significant variation ( $P > 0.05$ ) from the  $I_{1000 \mu\text{M}}$  of the *Cat* sensor ( $0.22 \pm 0.03$  nA, n = 28).

In conclusion, as the selectivity characteristics of both sensor types are very well matched the interference from AA is successfully eliminated by the paired sensor design (*Blank-Cat*). The  $I_{400\ \mu\text{M}}$  of this dual sensor design is  $0.02 \pm 0.03\ \text{nA}$  ( $n = 28+28$ ) and the  $I_{1000\ \mu\text{M}}$  value recorded was  $-0.07 \pm 0.04\ \text{nA}$  ( $n = 28+28$ ).

#### 4.8.2 H<sub>2</sub>O<sub>2</sub> sensitivity in the presence of AA

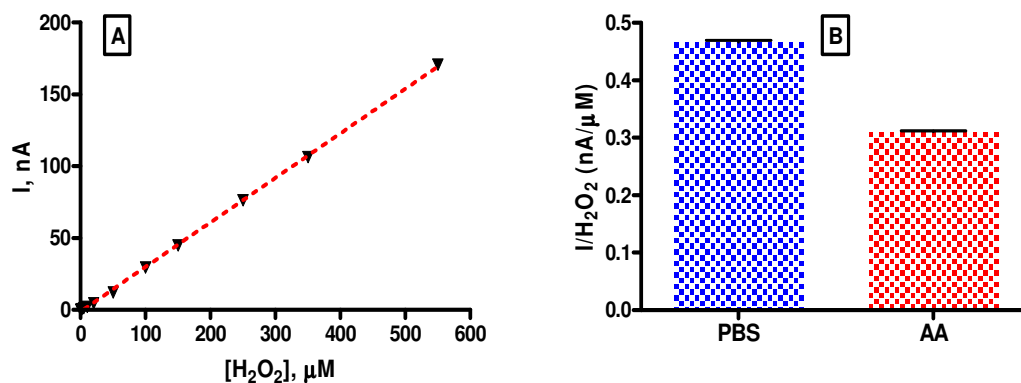


**Figure 4.8.2 : H<sub>2</sub>O<sub>2</sub> sensitivity of the paired sensor in the presence of AA. (A) The current-concentration profile (*Blank-Cat*,  $n = 2+2$ ). CPA carried out at +700 mV vs. SCE. (B) Average paired sensitivity represented as a mean slope  $\pm$  SEM, in normal PBS ( $n = 24+24$ ) and in the presence of AA ( $n = 2+2$ ).**

The basal concentration of AA *in-vivo* has been stated as  $\sim 400\ \mu\text{M}$  (Miele & Fillenz, 1996). In addition the level of AA may fluctuate in response to various stimuli including behavioural, electrical and pharmacological inputs as previously stated (Miele *et al.*, 1994). Taking this factor into account it is intuitive to examine what occurs with a normal H<sub>2</sub>O<sub>2</sub> calibration when AA has been added to the electrochemical cell initially in order to examine conditions encountered in an *in-vivo* environment. An injection of AA ( $500\ \mu\text{M}$ ) was made prior to introduction of the target analyte (H<sub>2</sub>O<sub>2</sub>). In the presence of AA the H<sub>2</sub>O<sub>2</sub> sensitivity was preserved yielding a value of  $0.31 \pm 0.002\ \text{nA}/\mu\text{M}$ ,  $n = 2+2$  with an  $R^2$  value of 0.9996 and this was not significantly different ( $P > 0.05$ ) from a normal H<sub>2</sub>O<sub>2</sub> calibration in PBS. In addition the signal observed following addition of AA was minimal with a maximum increase of  $0.05 \pm 0.04\ \text{nA}$ ,  $n = 2+2$ . This value is significantly different ( $P < 0.0001$ , \*\*\*) than that observed on addition of  $1\ \mu\text{M}$  H<sub>2</sub>O<sub>2</sub> ( $0.47 \pm 0.003\ \text{nA}$ ,  $n = 24+24$ ). To conclude, the pre-existing concentration of AA in the

cell prior to commencement of the H<sub>2</sub>O<sub>2</sub> calibration does not significantly inhibit the sensitivity to the target substrate (H<sub>2</sub>O<sub>2</sub>). The sensitivity of the paired sensor was slightly less than that observed in PBS alone (~ 0.06% per 1 μM of H<sub>2</sub>O<sub>2</sub>).

The interaction between AA and H<sub>2</sub>O<sub>2</sub> *in-vitro* demonstrated here has been studied previously (Lowry & O'Neill, 1992). The reported homogeneous interference of AA has been shown to cause a similar decrease in H<sub>2</sub>O<sub>2</sub> levels when AA is introduced to the cell prior to a H<sub>2</sub>O<sub>2</sub> calibration in the *in-vitro* environment. The homogenous interference of AA described by Lowry *et al.* which is apparent *in-vitro* was demonstrated to be absent in the *in-vivo* environment (Lowry *et al.*, 1994).

#### 4.8.3 H<sub>2</sub>O<sub>2</sub> sensitivity in the presence of DA

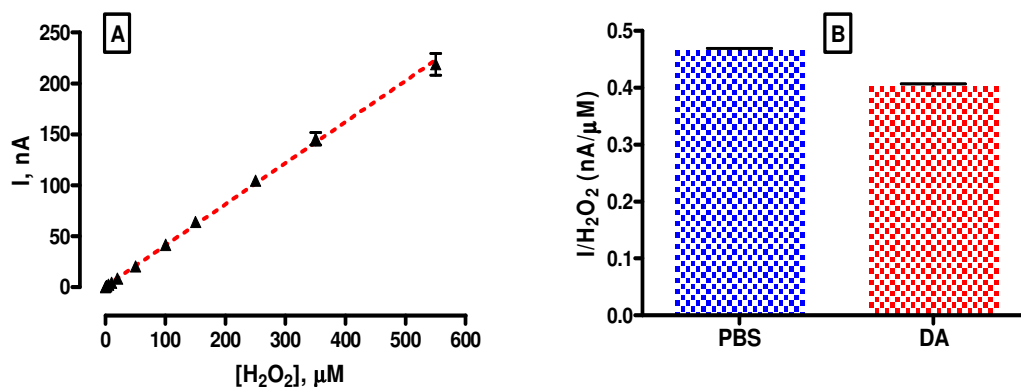


**Figure 4.8.3 : H<sub>2</sub>O<sub>2</sub> sensitivity of the paired sensor in the presence of Dopamine (DA). (A) The current-concentration profile (*Blank-Cat*, n = 3+3). CPA carried out at +700 mV vs. SCE. (B) Average paired sensitivity represented as a mean slope ± SEM, in normal PBS (n = 24+24) and in the presence of DA (n = 3+3).**

In order to mimic physiological conditions it was deemed necessary to investigate the performance of the H<sub>2</sub>O<sub>2</sub> sensor in the presence of dopamine (DA). The basal concentration of DA *in-vivo* is estimated to be between 5 and 50 nM and DA may also be detected at +700 mV vs. SCE. However, the absolute basal concentration of DA *in-vivo* has been much debated due to uptake mechanisms present *in-situ* and a possible trauma layer induced by implantation of a microdialysis probe used to record DA levels (Bungay *et al.*, 2003). A relatively high concentration of DA was chosen (500 nM) to

examine the selectivity of the H<sub>2</sub>O<sub>2</sub> sensor. An injection of DA (500 nM) was added into the electrochemical cell prior to a H<sub>2</sub>O<sub>2</sub> calibration. In the presence of DA the H<sub>2</sub>O<sub>2</sub> sensitivity was retained, yielding a value of  $0.40 \pm 0.004$  nA/ $\mu$ M,  $n = 3+3$  with an  $R^2$  value of 0.9992 and this was not significantly different ( $P > 0.05$ ) from a normal H<sub>2</sub>O<sub>2</sub> calibration in PBS. The response of this sensor towards DA in isolation was negligible ( $0.020 \pm 0.004$  nA,  $n = 3+3$ ). This value is significantly different ( $P < 0.0001$ , \*\*\*) to that observed on addition of 1  $\mu$ M H<sub>2</sub>O<sub>2</sub> ( $0.47 \pm 0.003$  nA,  $n = 24+24$ ). In conclusion, the presence of DA had no significant effect on the subsequent H<sub>2</sub>O<sub>2</sub> calibration.

#### 4.8.4 H<sub>2</sub>O<sub>2</sub> sensitivity in aCSF

As recently discussed by Bolger *et al.* redox reactions of various electroactive species *in-vitro* may depend on the aqueous media conditions utilised to facilitate experiments (Bolger *et al.*, 2011). Specifically a variation in the sensitivity of CFE's to DA, DOPAC and 5-HT has been demonstrated *in-vitro* between different aqueous media including HEPES-buffered saline, PBS and artificial cerebrospinal fluid (aCSF) (Chen & Rice, 1999). For the purpose of normal *in-vitro* H<sub>2</sub>O<sub>2</sub> calibrations all experiments were performed in PBS (see Section 3.7.5). In order to fully investigate the media dependence of H<sub>2</sub>O<sub>2</sub> oxidation at Pt surfaces, the H<sub>2</sub>O<sub>2</sub> sensitivity of an unmodified Pt disc electrode (Pt<sub>d</sub>) was tested in aCSF aqueous media and compared to the H<sub>2</sub>O<sub>2</sub> sensitivity of Pt<sub>d</sub> calibrated in PBS aqueous media (Figure 4.8.4).

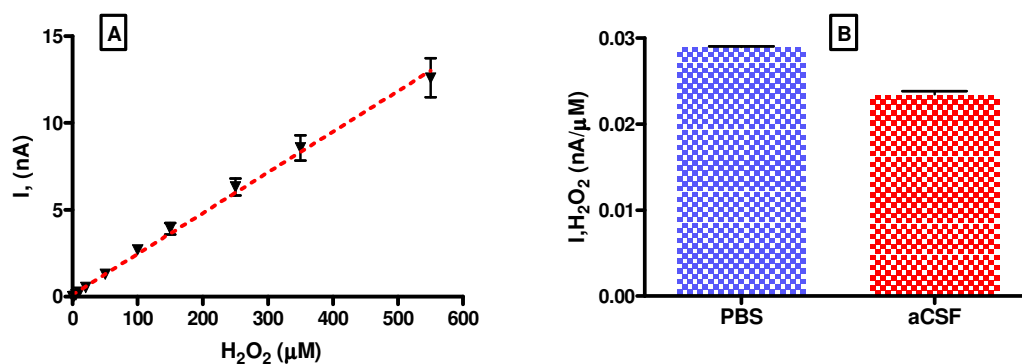


**Figure 4.8.4 :** H<sub>2</sub>O<sub>2</sub> sensitivity of Pt<sub>d</sub> in different aqueous media conditions. (A) The current-concentration profile of Pt<sub>d</sub> in aCSF. CPA carried out at +700 mV vs. SCE. (B) Average H<sub>2</sub>O<sub>2</sub> sensitivity of Pt<sub>d</sub> represented as a mean slope  $\pm$  SEM, in normal PBS ( $n = 4$ ) and in aCSF ( $n = 4$ ).

Under normal conditions in PBS aqueous media the H<sub>2</sub>O<sub>2</sub> sensitivity of Pt<sub>d</sub> was  $0.03 \pm 0.00004$  nA/ $\mu$ M,  $n = 4$  with an  $R^2$  value of 1.000. In aCSF aqueous media the H<sub>2</sub>O<sub>2</sub> sensitivity of Pt<sub>d</sub> was retained, yielding a value of  $0.02 \pm 0.00041$  nA/ $\mu$ M,  $n = 4$  with an  $R^2$  value of 0.9970 and this was not significantly different ( $P > 0.05$ ) from a normal H<sub>2</sub>O<sub>2</sub> calibration in PBS. A small drop in H<sub>2</sub>O<sub>2</sub> sensitivity was seen in aCSF aqueous media however no significant difference ( $P > 0.05$ ) was observed.

For all *in-vitro* experiments H<sub>2</sub>O<sub>2</sub> added to the electrochemical cell was made up in doubly distilled deionised water (H<sub>2</sub>O) (see Section 3.3.2.1). However for the purpose of *in-vivo* experiments; the substrate itself (H<sub>2</sub>O<sub>2</sub>) was diluted in aCSF for local administrations (see Chapter 5). To investigate the viability of H<sub>2</sub>O<sub>2</sub> made up in a solution of aCSF, the target substrate was diluted in aCSF (see Section 3.3.2.2) and the H<sub>2</sub>O<sub>2</sub> sensitivity of Pt<sub>d</sub> was tested *in-vitro* in a PBS aqueous environment; which was compared to that seen with normal substrate (H<sub>2</sub>O<sub>2</sub>) dilution conditions (H<sub>2</sub>O) (Figure 4.8.4.1).

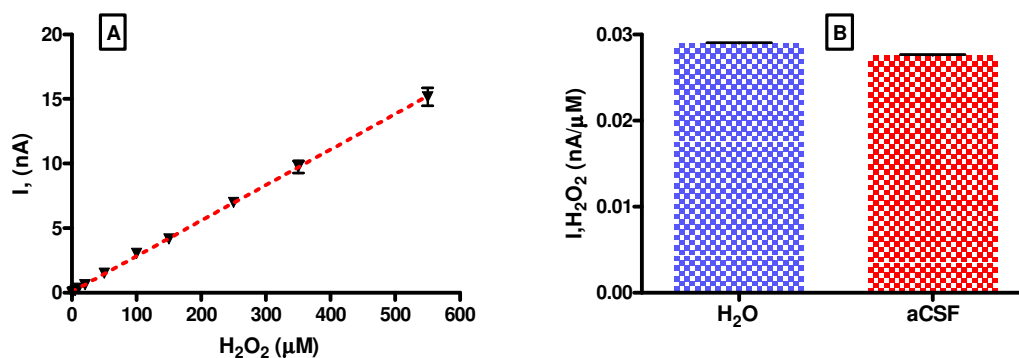


**Figure 4.8.4.1 : H<sub>2</sub>O<sub>2</sub> sensitivity of Pt<sub>d</sub> with different substrate dilution conditions. (A) The current-concentration profile of Pt<sub>d</sub> (Substrate: H<sub>2</sub>O<sub>2</sub> in aCSF). CPA carried out at +700 mV vs. SCE. (B) Average H<sub>2</sub>O<sub>2</sub> sensitivity of Pt<sub>d</sub> represented as a mean slope  $\pm$  SEM, with substrate diluted in H<sub>2</sub>O ( $n = 4$ ) and in aCSF ( $n = 8$ ).**

Under normal conditions where H<sub>2</sub>O<sub>2</sub> is diluted in H<sub>2</sub>O and calibrated in PBS aqueous media the H<sub>2</sub>O<sub>2</sub> sensitivity of Pt<sub>d</sub> was  $0.03 \pm 0.00004$  nA/ $\mu$ M,  $n = 4$  with an  $R^2$  value of 1.000. With aCSF substrate dilution conditions the H<sub>2</sub>O<sub>2</sub> sensitivity of Pt<sub>d</sub> was retained,

yielding a value of  $0.03 \pm 0.00015$  nA/ $\mu$ M,  $n = 8$  with an  $R^2$  value of 0.9997 and this was not significantly different ( $P > 0.05$ ) from normal H<sub>2</sub>O<sub>2</sub> calibration conditions.

#### 4.9 Paired H<sub>2</sub>O<sub>2</sub> sensor stability and biocompatibility

A long-term stability experiment (see Section 3.6.4) was conducted where the stability of the paired sensor over 28 days was investigated in the absence of treatment. The effect of repeated calibrations on the sensitivity and selectivity of the paired H<sub>2</sub>O<sub>2</sub> sensor can be examined in this manner.

The *in-vitro* characteristics of a sensor may not match its properties *in-vivo*. This factor is due in part to how the sensors may be altered by the various constituents of brain tissue and this may be reflected by variations in the sensor's characteristics (O'Neill, 1993). It has been demonstrated previously that when sensors are exposed to biological samples a drop in sensitivity occurs due to fouling of the sensor by proteins and other biomolecules present within the tissue (Garguilo & Michael, 1994).

An examination into the biocompatibility of the paired H<sub>2</sub>O<sub>2</sub> sensor was carried out. In order to mimic the conditions encountered by the H<sub>2</sub>O<sub>2</sub> sensor *in-vivo* the effect of exposure to brain tissue and its components on the sensitivity and selectivity of the *Blank* and *Cat* sensor were investigated. A method previously demonstrated by Brown *et al.* and Bolger *et al.* was used to determine the *in-vitro* biocompatibility of the paired catalase-based sensor (Brown *et al.*, 2009; Bolger *et al.*, 2011). Each sensor (*Blank* and *Cat*) was exposed to samples of homogenised brain tissue (BT), protein (BSA) and lipid (PEA) and tested at specified durations (see Section 3.6) to examine the biocompatibility of the H<sub>2</sub>O<sub>2</sub> sensor.

The intention of these sets of experiments is to gauge the stability of the sensor prior to and during Long Term In-Vivo Electrochemistry (L.I.V.E) recordings. Although these parameters mimic the *in-vivo* medium it must be stated that it is not an entirely correct representation of the response of the sensor, when in contact with intact living brain tissue and only serves as a guide to performance of the paired sensor *in-vivo*.

#### 4.10 Blank stability (long-term)

This section investigates the stability of the *Blank* sensor (Pt<sub>c</sub>/Nafion<sup>®</sup>/PPD) over a four week period (see Section 3.6.4). The experiments outlined in this section also serve as a control against which the biocompatibility of the *Blank* sensor may be compared. The sensitivity of the *Blank* sensor was tested over a 0 to 550 μM H<sub>2</sub>O<sub>2</sub> concentration range. The selectivity of the *Blank* sensor was also assessed over a concentration range of AA (0-1000 μM). These sensors were stored at 4°C in a refrigerator when not in use; the sensitivity and selectivity of the sensors were intermittently tested at the times specified below.

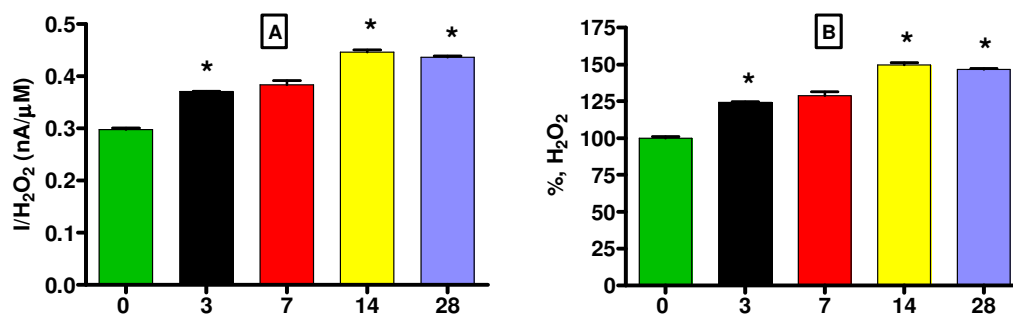


**Figure 4.10.1** H<sub>2</sub>O<sub>2</sub> response of the *Blank* sensor over 28 days the number of days is represented on the x-axis. (A) Data represented as a mean response ± SEM (B) Data shown as a percentage with 100% as the H<sub>2</sub>O<sub>2</sub> sensitivity recorded on the initial day of experiments. ( $P < 0.05, *$ ).

Upon examining the data above in Figure 4.10.1 it is clear that the H<sub>2</sub>O<sub>2</sub> sensitivity of the *Blank* sensor increases over time as part of this long-term stability study with reference to day 0. A significant difference  $P < 0.05, *$  is observed between the first calibration prior to initiation of the shelf-life study and days 3, 14 and 28. No significant difference ( $P > 0.05$ ) is observed between 0 and 7 days. A maximum increase is observed on day 14 which represents a 49.7 % increase. A decrease was observed between day 14 and 28 with a drop in sensitivity of ~3%. Although a gradual increase in sensitivity is observed the magnitude of the response is stymied as the shelf-life study proceeds. A similar sensitivity is observed between day 3 and day 7 and subsequently between 14 and 28 days as shown in Table 4.10.1. A larger exposed Pt surface area would give a higher H<sub>2</sub>O<sub>2</sub> sensitivity value. It is possible that repeated exposure to a

high concentration of the substrate (H<sub>2</sub>O<sub>2</sub>) has caused deterioration in the PPD structure thereby increasing the exposed surface area of the sensor. However, the magnitude of this deterioration does not increase in a linear fashion which supports the overall stability of this sensor.

| Day | Mean I,<br>(nA/ $\mu$ M) | SEM   | %      | SEM (%) | P      | n |
|-----|--------------------------|-------|--------|---------|--------|---|
| 0   | 0.30                     | 0.003 | 100    | 0.94    | n/a    | 4 |
| 3   | 0.37                     | 0.001 | 124.38 | 0.34    | 0.0352 | 4 |
| 7   | 0.38                     | 0.008 | 128.77 | 2.68    | 0.0590 | 4 |
| 14  | 0.45                     | 0.004 | 149.7  | 1.48    | 0.0283 | 4 |
| 28  | 0.44                     | 0.002 | 146.48 | 0.79    | 0.0334 | 4 |

Table 4.10.1 Data obtained from the calibrations shown in Figure 4.10.1. Data represented as a mean response  $\pm$  SEM and as a percentage change (%)  $\pm$  SEM. Where (P) represents the outcome of a paired t-test at each time point (3, 7, 14 and 28 days) when compared to the response recorded with untreated sensors (day = 0). The number of sensors is denoted by (n).

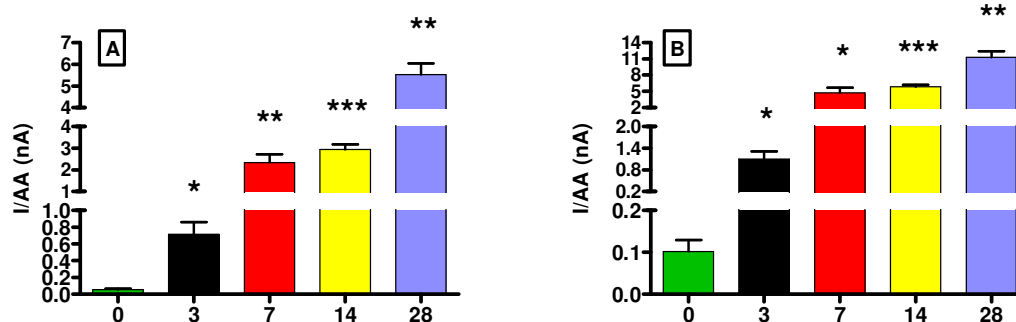


Figure 4.10.2 AA response of the *Blank* sensor over 28 days. Data represented as a mean response  $\pm$  SEM (A) I<sub>400</sub>  $\mu$ M and (B) I<sub>1000</sub>  $\mu$ M

Upon examining the data above in Figure 4.10.2 it is apparent that an increase in AA response is observed by the *Blank* sensor on progression of this stability investigation in comparison to day 0. The level of significant difference is shown in Table 4.10.2. The extent of the increase slows between day 7 and 14 (Figure 4.10.2) in relation to I<sub>400 μM</sub> and I<sub>1000 μM</sub>. This data implicates that a disruption in the polymerised surface has occurred which has created an increased Pt surface area, thereby causing an increase in response to AA. The cause of the stated disruption occurs due to prolonged exposure to H<sub>2</sub>O<sub>2</sub> and due to the necessary repeated physical manipulation of these sensors for each calibration. This structural issue is negated for *in-vivo* experiments as all sensors are calibrated only once immediately prior to implantation.

| Day | I, nA<br>(1000 μM) | SEM  | I, nA<br>(400 μM) | SEM  | n | P<br>(400 μM) | P<br>(1000 μM) |
|-----|--------------------|------|-------------------|------|---|---------------|----------------|
| 0   | 0.10               | 0.03 | 0.06              | 0.01 | 4 | n/a           | n/a            |
| 3   | 1.09               | 0.22 | 0.72              | 0.14 | 4 | 0.0385        | 0.0153         |
| 7   | 4.76               | 0.88 | 2.34              | 0.39 | 4 | 0.0086        | 0.0131         |
| 14  | 5.84               | 0.39 | 2.94              | 0.25 | 4 | < 0.0001      | 0.0007         |
| 28  | 11.31              | 1.11 | 5.52              | 0.52 | 4 | 0.0018        | 0.0020         |

**Table 4.10.2** Data obtained from the calibrations shown in Figure 4.10.2. Data represented as a mean response ± SEM. Where (P) represents the outcome of a paired t-test for I<sub>400 μM</sub> and I<sub>1000 μM</sub> at each time point (3, 7, 14 and 28 days) when compared to the response recorded with untreated sensors (day = 0). The number of sensors is denoted by (n).

### 4.11 *Cat* stability (long-term)

In this section the stability of the *Cat* sensor (Pt<sub>c</sub>/Nafion<sup>®</sup>/PPD/Cat-Ga) was investigated over a four week period (see Section 3.6.4). The experiments outlined in this section also serve as a control against which the biocompatibility of the *Cat* sensor may be compared. The sensitivity of the *Cat* sensor was tested with H<sub>2</sub>O<sub>2</sub> (0-550 μM) concentration range. The selectivity of the *Blank* sensor was assessed over a concentration range of AA (0-1000 μM). These sensors were stored at 4°C in a refrigerator when not in use. The sensitivity and selectivity of the sensors were intermittently tested at the times specified below.

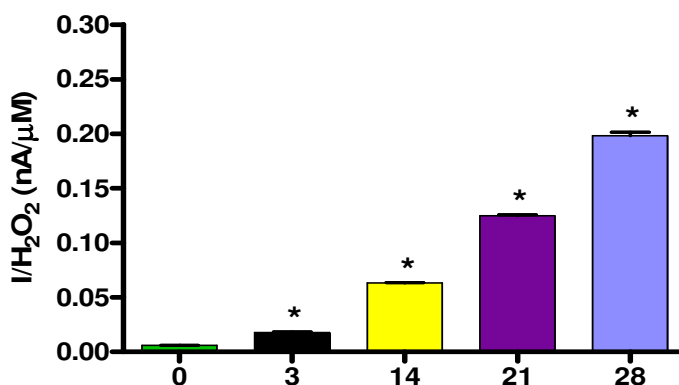


Figure 4.11.1 H<sub>2</sub>O<sub>2</sub> response of the *Cat* sensor over 28 days. Data represented as a mean response  $\pm$  SEM and ( $P < 0.05$ ,\*).

The sensitivity of the *Cat* sensor to H<sub>2</sub>O<sub>2</sub> is shown in Figure 4.11.1 this data shows a consistent pattern, a significant difference ( $P < 0.05$ ,\*) from day 0 is observed at all time points i.e. day 3, 14, 21 and 28. As the function of the catalase enzyme is to remove H<sub>2</sub>O<sub>2</sub>, the data in Figure 4.11.1 signifies a loss in functionality of the catalase-based sensor. The response observed here is typical when compared to other biosensor responses due to constant exposure to high levels of substrate (550 μM H<sub>2</sub>O<sub>2</sub>). The enzyme becomes saturated and does not retain the same function as observed initially on day 0 (Bolger, 2007). On further investigation it was apparent that the relative loss in H<sub>2</sub>O<sub>2</sub> sensitivity was attributable to a variation in sensitivity on introduction of a higher concentration of H<sub>2</sub>O<sub>2</sub> (250-550 μM). As the responses observed here are enzymatic it is

possible to examine and compare *Cat* sensor data obtained at a lower concentration of H<sub>2</sub>O<sub>2</sub> i.e. (0-150  $\mu$ M). No significant variation ( $P > 0.05$ ) was observed at this lower concentration range (0-150  $\mu$ M) between successive time points day 3, 14, 21 and 28 when compared to the sensitivity recorded on day 0. It is apparent that the *Cat* sensor is stable over 28 days up to a concentration of 150  $\mu$ M. As the expected ECF concentration of H<sub>2</sub>O<sub>2</sub> is much lower (25-50  $\mu$ M) the trend shown in Figure 4.11.1 should not be observed *in-vivo*. This factor is supported by evidence provided in Chapter 5 Section 5.11.2, where the baseline of the *Cat* sensor does not show significant changes over an extended period when implanted *in-vivo*. Additionally, all electrodes were calibrated immediately prior to *in-vivo* implantation which excludes long-term stability considerations.

| Mean I, |               |        |        |   |
|---------|---------------|--------|--------|---|
| Day     | (nA/ $\mu$ M) | SEM    | P      | n |
| 0       | 0.01          | 0.0001 | n/a    | 4 |
| 3       | 0.02          | 0.001  | 0.0291 | 4 |
| 14      | 0.06          | 0.001  | 0.0322 | 4 |
| 21      | 0.12          | 0.001  | 0.0310 | 4 |
| 28      | 0.20          | 0.003  | 0.0276 | 4 |

**Table 4.11.1 Data obtained from the calibrations shown in Figure 4.10.1. Data represented as a mean response  $\pm$  SEM. Where (*P*) represents the outcome of a paired t-test at each time point (3, 14, 21 and 28 days) when compared to the response recorded with untreated sensors (day = 0). The number of sensors is denoted by (n).**

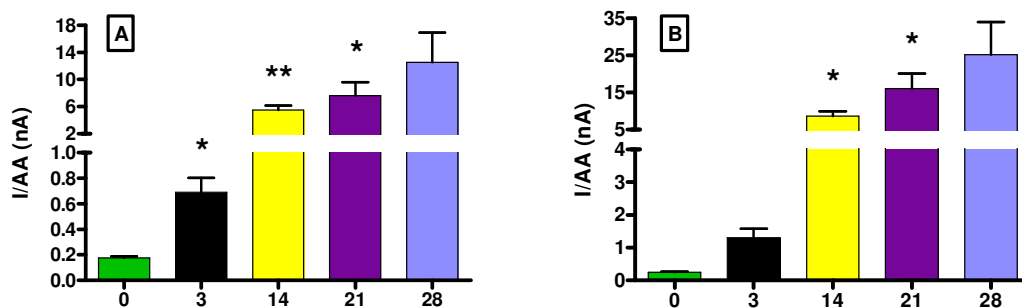


Figure 4.11.2 AA response of the *Cat* sensor over 28 days. Data represented as a mean response  $\pm$  SEM (A)  $I_{400 \mu\text{M}}$  and (B)  $I_{1000 \mu\text{M}}$

On examination of the AA response of the *Cat* sensor shown in Figure 4.11.2 a significant difference ( $P < 0.05, *$ ) in AA response is observed on day 3, 14 and 21 during this long-term stability experiment in comparison to day 0. A similar disruption in the modified surface as seen in Section 4.10 is evident here. As previously stated this structural issue is negated for *in-vivo* experiments as all sensors are calibrated immediately prior to implantation.

| Day | I, nA<br>(1000 $\mu\text{M}$ ) | SEM  | I, nA<br>(400 $\mu\text{M}$ ) | SEM  | n | P<br>(400 $\mu\text{M}$ ) | P<br>(1000 $\mu\text{M}$ ) |
|-----|--------------------------------|------|-------------------------------|------|---|---------------------------|----------------------------|
| 0   | 0.25                           | 0.02 | 0.18                          | 0.01 | 4 | n/a                       | n/a                        |
| 3   | 1.31                           | 0.27 | 0.69                          | 0.11 | 4 | 0.0214                    | 0.0322                     |
| 14  | 8.69                           | 1.28 | 5.49                          | 0.66 | 4 | 0.0040                    | 0.0277                     |
| 21  | 16.17                          | 3.98 | 7.61                          | 2.02 | 4 | 0.0342                    | 0.0277                     |
| 28  | 25.20                          | 8.81 | 12.51                         | 4.4  | 4 | 0.0671                    | 0.0658                     |

Table 4.11.2 Data obtained from the calibrations shown in Figure 4.11.2. Data represented as a mean response  $\pm$  SEM. Where ( $P$ ) represents the outcome of a paired t-test for  $I_{400 \mu\text{M}}$  and  $I_{1000 \mu\text{M}}$  at each time point (3, 14, 21 and 28 days) when compared to the response recorded with untreated sensors (day = 0). The number of sensors is denoted by (n).

### 4.12 Blank biocompatibility (BSA)

The *Blank* sensor (Pt<sub>2</sub>/Nafion<sup>®</sup>/PPD) was exposed to a solution of the protein BSA (see Section 3.6.1) and was tested over a four week period to investigate the effect of protein on the performance of the *Blank* sensor. The sensitivity to the target substrate of the *Blank* sensor was examined (0-550 μM H<sub>2</sub>O<sub>2</sub>). The selectivity of the *Blank* sensor was evaluated with AA (0-1000 μM). These sensors were stored at 4°C in a refrigerator in a 10% (w/v) solution of BSA (see Section 3.6.1) when not in use. The sensitivity and selectivity of the sensors was examined at the times specified below.

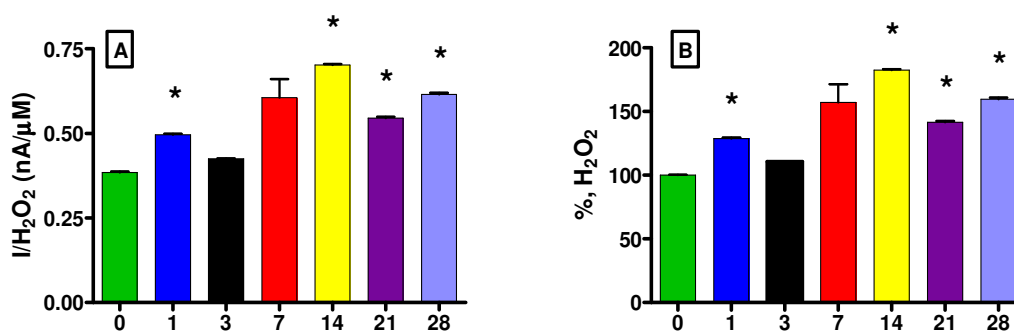


**Figure 4.12.1** H<sub>2</sub>O<sub>2</sub> response of the *Blank* sensor exposed to BSA over 28 days. (A) Data represented as a mean response  $\pm$  SEM (B) Data shown as a percentage with 100% as the H<sub>2</sub>O<sub>2</sub> sensitivity recorded on the initial day of experiments. ( $P < 0.05, *$ ).

The effect of exposure to the protein BSA on the sensitivity of the *Blank* sensor is shown in Figure 4.12.1. An increase in sensitivity is observed after 24 hours (day 1) which is significantly different ( $P < 0.05, *$ ) from the initial calibration. No significant difference can be seen on day 3 and 7 with reference to day 0. Day 1, 14, 21 and 28 show a significant variation ( $P < 0.05, *$ ) from day 0. The maximum increase on addition of H<sub>2</sub>O<sub>2</sub> is observed on day 14 (82.4 %) which falls to a lower level on day 28 (59.8 %). A relative drop in H<sub>2</sub>O<sub>2</sub> response is observed after 14 days. The values are given in Table 4.12.1 and no significant difference ( $P > 0.05$ ) is seen between day 21 and 28. BSA does affect the sensitivity of this sensor type which could be due to a disruption of the modified surface which would result in an increased Pt surface area. The concentration of BSA used here is quite high (10%) which may be more severe than the concentration of protein found *in-vivo*. In an effort to mimic the *in-vivo* environment

more closely the *Blank* sensor was treated with a sample of homogenised brain tissue (see Section 4.16).

| <b>Day</b> | <b>Mean I,<br/>(nA/μM)</b> | <b>SEM</b> | <b>%</b> | <b>SEM (%)</b> | <b>P</b> | <b>n</b> |
|------------|----------------------------|------------|----------|----------------|----------|----------|
| <b>0</b>   | 0.38                       | 0.002      | 100      | 0.61           | n/a      | 4        |
| <b>1</b>   | 0.50                       | 0.003      | 128.92   | 0.69           | 0.0477   | 4        |
| <b>3</b>   | 0.43                       | 0.001      | 110.52   | 0.29           | 0.0650   | 4        |
| <b>7</b>   | 0.61                       | 0.055      | 149.55   | 13.58          | 0.3217   | 4        |
| <b>14</b>  | 0.70                       | 0.003      | 182.41   | 0.85           | 0.0312   | 4        |
| <b>21</b>  | 0.55                       | 0.004      | 151.10   | 1.08           | 0.0210   | 4        |
| <b>28</b>  | 0.62                       | 0.004      | 159.78   | 1.17           | 0.0455   | 4        |

**Table 4.12.1** Data obtained from the calibrations shown in Figure 4.12.1. Data represented as a mean response  $\pm$  SEM. Where (*P*) represents the outcome of a paired t-test at each time point (1, 3, 7, 14, 21 and 28 days) when compared to the response recorded with untreated sensors (day = 0).

The number of sensors is denoted by (n).

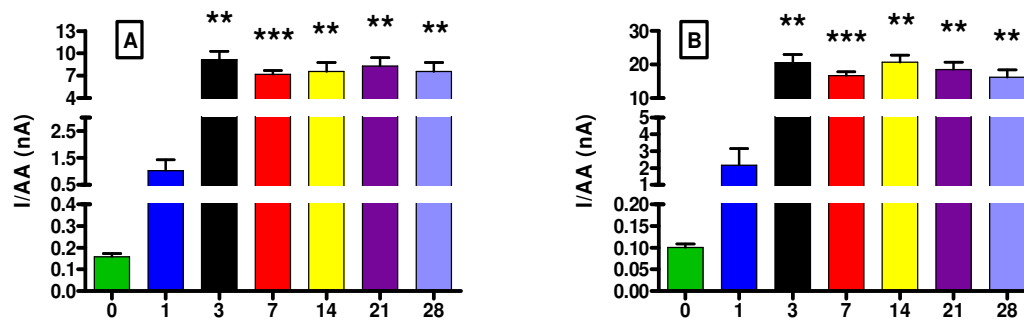


**Figure 4.12.2** AA response of the *Blank* sensor exposed to BSA over 28 days. Data represented as a mean response  $\pm$  SEM (A)  $I_{400 \mu M}$  and (B)  $I_{1000 \mu M}$

No significant difference ( $P > 0.05$ ) in AA response was observed after 24hrs (1) exposure of the *Blank* sensor to a protein solution (BSA). A significant difference ( $P < 0.05$ ,\*) was observed at day 3, 7, 14, 21 and 28, however the magnitude of the increase in AA sensitivity slows following day 3 as can be seen in Figure 4.12.2. The first level of significant difference is observed on day 3. The results represented here suggest that a loss of the integrity of the modified surface has occurred following repeated exposure to BSA. It is possible that the repeated calibration itself may have affected the modified surface of the sensor (see Section 4.10). In order to mimic the *in-vivo* environment more closely the *Blank* sensor was exposed to a sample of homogenised brain tissue (see Section 4.16).

| Day | I, nA          |      | I, nA         |      | n | P             |                |
|-----|----------------|------|---------------|------|---|---------------|----------------|
|     | (1000 $\mu$ M) | SEM  | (400 $\mu$ M) | SEM  |   | (400 $\mu$ M) | (1000 $\mu$ M) |
| 0   | 0.10           | 0.01 | 0.16          | 0.01 | 4 | n/a           | n/a            |
| 1   | 2.16           | 0.99 | 0.01          | 0.41 | 4 | 0.1194        | 0.1287         |
| 3   | 20.51          | 2.44 | 9.16          | 1.10 | 4 | 0.0038        | 0.0036         |
| 7   | 16.66          | 1.09 | 7.17          | 0.53 | 4 | 0.0009        | 0.0006         |
| 14  | 20.68          | 2.05 | 7.58          | 1.20 | 4 | 0.0032        | 0.0021         |
| 21  | 18.48          | 2.24 | 8.31          | 1.07 | 4 | 0.0048        | 0.0038         |
| 28  | 16.2           | 2.22 | 7.58          | 1.20 | 4 | 0.0088        | 0.0054         |

**Table 4.12.2** Data obtained from the calibrations shown in Figure 4.12.2. Data represented as a mean response  $\pm$  SEM. Where (*P*) represents the outcome of a paired *t*-test for  $I_{400 \mu\text{M}}$  and  $I_{1000 \mu\text{M}}$  at each time point (1, 3, 7, 14, 21 and 28 days) when compared to the response recorded with untreated sensors (day = 0). The number of sensors is denoted by (*n*).

### 4.13 *Cat* biocompatibility (BSA)

This section investigates the stability of the *Cat* sensor (Pt<sub>c</sub>/Nafion<sup>®</sup>/PPD/Cat-Ga) over a period of four weeks following exposure to BSA, examining the effect of protein on the function of the *Cat* sensor (see Section 3.6.1). The sensitivity of the *Cat* sensor was tested over a concentration range of H<sub>2</sub>O<sub>2</sub> (0-550  $\mu$ M). The selectivity of the *Cat* sensor was tested over a concentration range of AA (0-1000  $\mu$ M). These sensors were stored at 4°C in a refrigerator in a 10% (w/v) solution of BSA (see Section 3.6.1). The sensitivity and selectivity of the sensors were tested at each time point specified below.

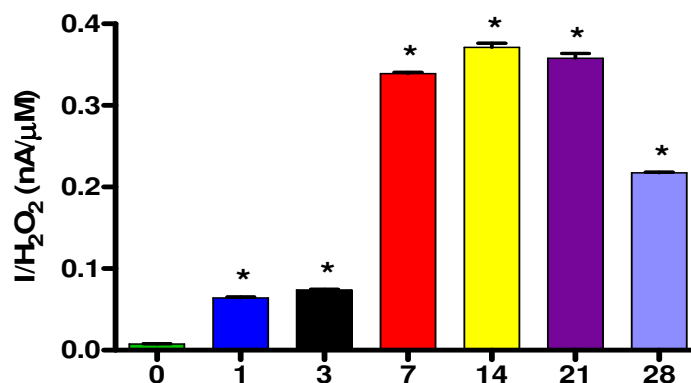


**Figure 4.13.1** H<sub>2</sub>O<sub>2</sub> response of the *Cat* sensor exposed to BSA over 28 days. Data represented as a mean response  $\pm$  SEM and ( $P < 0.05$ ,\*).

The data shown in Figure 4.13.1 shows a definite trend. A significant difference ( $P < 0.05$ ,\*) from day 0 is observed at all time points i.e. 24 hrs day 3, 7, 14, 21 and 28. The ability of the *Cat* sensor to degrade H<sub>2</sub>O<sub>2</sub> is impaired. The maximum loss in sensitivity is seen on day 14 which plateaus on day 21 and is followed by an improved response on day 28. The sensitivity data for each time point is displayed below in Table 4.13.1. As has previously been demonstrated in Section 4.11 the variation in response is more apparent in response to relatively high concentrations of H<sub>2</sub>O<sub>2</sub> (250-550  $\mu$ M). At lower concentrations, i.e. 0-150  $\mu$ M, no significant difference ( $P > 0.05$ ) was observed at any time point (1, 3, 7, 14, 21 and 28 days) with reference to day 0. These results further illustrate that the loss in H<sub>2</sub>O<sub>2</sub> sensitivity is due to saturation of the catalase enzyme by the substrate (H<sub>2</sub>O<sub>2</sub>) and this factor is particularly noticeable in response to high concentrations of H<sub>2</sub>O<sub>2</sub> i.e. 250-550  $\mu$ M.

| Day | Mean I,<br>(nA/ $\mu$ M) | SEM    | P      | n |
|-----|--------------------------|--------|--------|---|
| 0   | 0.01                     | 0.0003 | n/a    | 4 |
| 1   | 0.06                     | 0.0011 | 0.0344 | 4 |
| 3   | 0.07                     | 0.0008 | 0.0357 | 4 |
| 7   | 0.34                     | 0.0014 | 0.0321 | 4 |
| 14  | 0.37                     | 0.0048 | 0.0261 | 4 |
| 21  | 0.36                     | 0.005  | 0.0243 | 4 |
| 28  | 0.22                     | 0.0009 | 0.0292 | 4 |

**Table 4.13.1** Data obtained from the calibrations shown in Figure 4.11.1. Data represented as a mean response  $\pm$  SEM. Where (*P*) represents the outcome of a paired *t*-test at each time point (1, 3, 7, 14, 21 and 28 days) when compared to the response recorded with untreated sensors (day = 0).

The number of sensors is denoted by (n).

In order to minimise the possible saturation of the catalase enzyme, a further investigation was necessary to determine the stability of this sensor design in the presence of BSA. Pt<sub>c</sub>/Nafion<sup>®</sup>/PPD/Cat-Ga sensors were constructed and immersed in a solution of BSA (see Section 3.6.1) for 14 days. These sensors were then removed and re-tested with no intermediate tests undertaken. The expected ECF concentration of H<sub>2</sub>O<sub>2</sub> is 25-50  $\mu$ M which is much lower than that used in the *in-vitro* calibration. This protocol limits repeated exposure of the enzyme to the substrate and minimises saturation of the enzyme. The results of this experiment are displayed below in Figure 4.13.2.

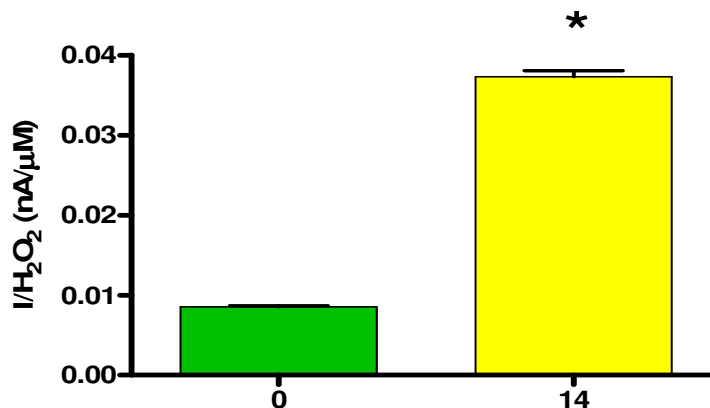
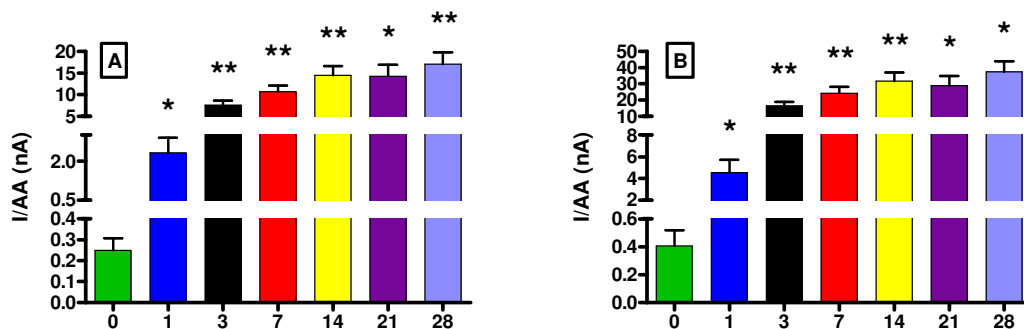


Figure 4.13.2 H<sub>2</sub>O<sub>2</sub> response of the *Cat* sensor exposed to BSA for a constant period of 14 days.

The sensitivity of the *Cat* sensor was tested over a concentration range of H<sub>2</sub>O<sub>2</sub> (0-550  $\mu$ M). The H<sub>2</sub>O<sub>2</sub> sensitivity of the Pt<sub>c</sub>/Nafion<sup>®</sup>/PPD/Cat-Ga sensor prior to emersion in a protein solution (day 0) was  $8.53 \pm 0.13$  pA/ $\mu$ M,  $n = 4$  with an  $R^2$  value of 0.9978. Following 14 days of exposure to BSA the sensors were removed and re-calibrated. On day 14 these sensors displayed a H<sub>2</sub>O<sub>2</sub> sensitivity of  $37.27 \pm 0.78$  pA/ $\mu$ M,  $n = 4$  with an  $R^2$  value of 0.9957. A significant difference ( $P < 0.05, *$ ) was found between day 0 and 14. On day 14 of this stability test a loss in function of the catalase sensor was observed, the loss recorded here is relatively lower than that recorded at the same time-point shown in Table 4.13.1 (day 14). Minimising catalase saturation in this experiment has improved the stability of this sensor design. This factor further supports previous evidence which suggests that saturation of the catalase enzyme with H<sub>2</sub>O<sub>2</sub> is responsible for the apparent loss in ability to degrade H<sub>2</sub>O<sub>2</sub> and not the treatment itself. The loss in sensitivity shown in Figure 4.13.2 is significant ( $P < 0.05, *$ ) but not detrimental to the function of the paired sensor design as a high proportion of function is still retained when compared to an untreated *Blank* sensor (Pt<sub>c</sub>/Nafion<sup>®</sup>/PPD). A ~92% removal in signal at a 550  $\mu$ M concentration of H<sub>2</sub>O<sub>2</sub> is apparent when compared in this manner.



**Figure 4.13.3** AA response of the *Cat* sensor exposed to BSA over 28 days. Data represented as a mean response  $\pm$  SEM (A)  $I_{400 \mu M}$  and (B)  $I_{1000 \mu M}$

On examination of the data shown graphically above in Figure 4.13.3, a significant difference ( $P < 0.05, *$ ) was observed in AA response on day 1 to 28 when compared to day 0. A similar trend was observed with  $I_{400 \mu M}$  and  $I_{1000 \mu M}$  values as can be seen below in Table 4.13.2. The results displayed here suggest a deterioration of the modified surface of the sensor due to exposure to BSA. In order to replicate the *in-vivo* environment more closely the *Blank* sensor was exposed to a sample of homogenised brain tissue (see Section 4.16).

| Day | I, nA          |      | I, nA         |      | n | P             |                |
|-----|----------------|------|---------------|------|---|---------------|----------------|
|     | (1000 $\mu$ M) | SEM  | (400 $\mu$ M) | SEM  |   | (400 $\mu$ M) | (1000 $\mu$ M) |
| 0   | 0.41           | 0.11 | 0.25          | 0.06 | 4 | n/a           | n/a            |
| 1   | 4.55           | 1.17 | 2.32          | 0.58 | 4 | 0.0394        | 0.0448         |
| 3   | 16.33          | 2.47 | 7.57          | 1.08 | 4 | 0.0067        | 0.0081         |
| 7   | 24.21          | 3.83 | 10.68         | 1.47 | 4 | 0.0054        | 0.0081         |
| 14  | 31.64          | 5.39 | 14.41         | 2.19 | 4 | 0.0069        | 0.0097         |
| 21  | 29.05          | 5.76 | 14.23         | 2.63 | 4 | 0.0122        | 0.0149         |
| 28  | 37.45          | 6.38 | 17.03         | 2.74 | 4 | 0.0084        | 0.0101         |

**Table 4.13.2** Data obtained from the calibrations shown in Figure 4.13.3. Data represented as a mean response  $\pm$  SEM. Where (*P*) represents the outcome of a paired t-test for I<sub>400  $\mu$ M</sub> and I<sub>1000  $\mu$ M</sub> at each time point (1, 3, 7, 14, 21 and 28 days) when compared to the response recorded with untreated sensors (day = 0). The number of sensors is denoted by (n).

#### 4.14 Blank biocompatibility (PEA)

The *Blank* sensor (Pt<sub>c</sub>/Nafion<sup>®</sup>/PPD) was treated with a solution of the lipid PEA (see Section 3.6.2) and was tested over 28 days in order to evaluate the effect of this lipid on the characteristics of the *Blank* sensor. The sensitivity to the target analyte of the *Blank* sensor was tested (0-550  $\mu$ M H<sub>2</sub>O<sub>2</sub>). The selectivity of the *Blank* sensor was examined using AA (0-1000  $\mu$ M). These sensors were stored at 4°C in a refrigerator in a 10% (w/v) solution of PEA (see Section 3.6.2) when not in use, the sensitivity and selectivity of the sensors were intermittently tested at the times stated below.

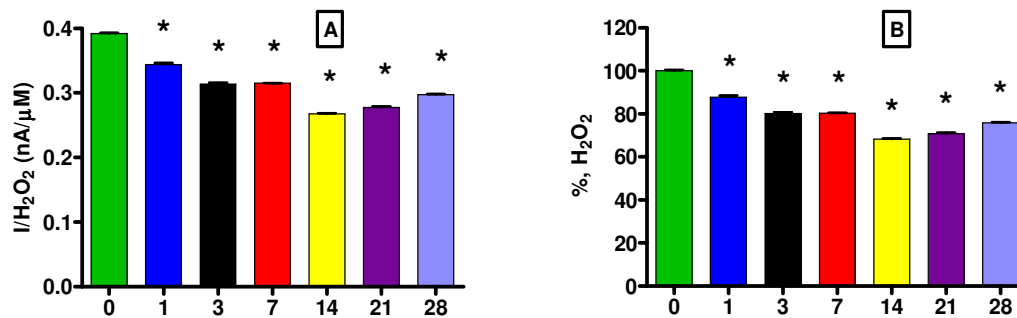


**Figure 4.14.1 H<sub>2</sub>O<sub>2</sub> response of the *Blank* sensor exposed to PEA over 28 days. (A) Data represented as a mean response  $\pm$  SEM (B) Data shown as a percentage with 100% as the H<sub>2</sub>O<sub>2</sub> sensitivity recorded on the initial day of experiments. ( $P < 0.05$ ,\*).**

The effect of exposure to the lipid PEA on the sensitivity of the *Blank* sensor is shown in Figure 4.14.1. It is clear from the data displayed above in Figure 4.14.1 that a gradual decrease in H<sub>2</sub>O<sub>2</sub> sensitivity of the *Blank* sensor is observed over an increased exposure time to the lipid (PEA). A significant difference ( $P < 0.05$ ,\*) from day 0 is observed at all time points i.e. day 1, 3, 7, 14, 21 and 28. A maximum decrease in sensitivity is seen on day 14 (31.8 %) which makes a gradual return towards baseline levels as can be seen from the data displayed in Table 4.14.1. A decrease in sensitivity is observed overall, however after the initial fall in H<sub>2</sub>O<sub>2</sub> sensitivity the effect of PEA on the *Blank* sensor subsides. No significant difference ( $P > 0.05$ ) was observed between day 1 and 28. This indicates that no significant change in sensitivity is apparent on increasing the length of exposure time to the lipid which validates the stability of this sensor design.

| Day | Mean I,<br>(nA/ $\mu$ M) | SEM    | %     | SEM (%) | P      | n |
|-----|--------------------------|--------|-------|---------|--------|---|
| 0   | 0.39                     | 0.002  | 100   | 0.39    | n/a    | 4 |
| 1   | 0.34                     | 0.003  | 87.75 | 0.72    | 0.0146 | 4 |
| 3   | 0.31                     | 0.002  | 80.14 | 0.51    | 0.0235 | 4 |
| 7   | 0.31                     | 0.0004 | 80.34 | 0.11    | 0.0275 | 4 |
| 14  | 0.27                     | 0.001  | 68.22 | 0.29    | 0.0433 | 4 |
| 21  | 0.28                     | 0.002  | 70.85 | 0.44    | 0.0308 | 4 |
| 28  | 0.30                     | 0.001  | 75.87 | 0.33    | 0.0327 | 4 |

**Table 4.14.1** Data obtained from the calibrations shown in Figure 4.12.1. Data represented as a mean response  $\pm$  SEM. Where (*P*) represents the outcome of a paired *t*-test at each time point (1, 3, 7, 14, 21 and 28 days) when compared to the response recorded with untreated sensors (day = 0).

The number of sensors is denoted by (*n*).

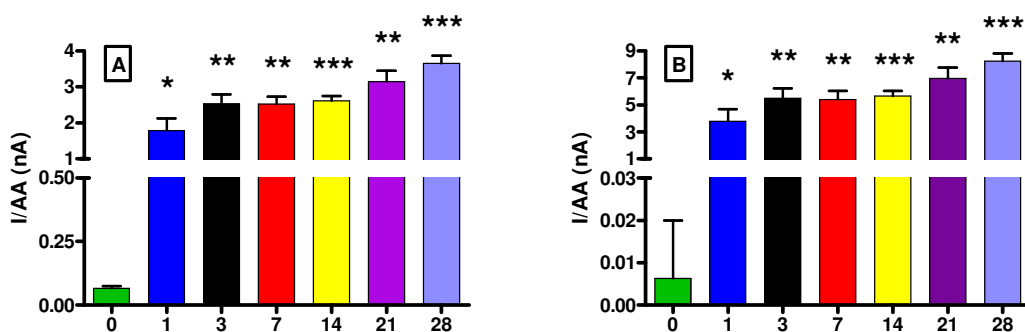


**Figure 4.14.2** AA response of the *Blank* sensor exposed to PEA over 28 days. Data represented as a mean response  $\pm$  SEM (A)  $I_{400 \mu\text{M}}$  and (B)  $I_{1000 \mu\text{M}}$

Figure 4.14.2 displays the AA response of the *Blank* sensor when treated with PEA for a period of four weeks. An increase in AA response can be seen at all time points (1, 3, 7, 14, 21 and 28) with respect to day 0 of treatment. The data shown here would suggest a

deterioration has occurred in the polymer surface. The current responses obtained under these conditions (Table 4.14.2) are not entirely detrimental to the function of the *Blank* sensor. As the high H<sub>2</sub>O<sub>2</sub> sensitivity of the *Blank* sensor is maintained over 28 days a resolution in H<sub>2</sub>O<sub>2</sub> response over AA is still achievable under these conditions.

| Day | I, nA          |       | I, nA         |      | n | P             |                |
|-----|----------------|-------|---------------|------|---|---------------|----------------|
|     | (1000 $\mu$ M) | SEM   | (400 $\mu$ M) | SEM  |   | (400 $\mu$ M) | (1000 $\mu$ M) |
| 0   | 0.006          | 0.014 | 0.07          | 0.01 | 4 | n/a           | n/a            |
| 1   | 3.78           | 0.89  | 1.79          | 0.34 | 4 | 0.0137        | 0.0244         |
| 3   | 5.49           | 0.74  | 2.54          | 0.25 | 4 | 0.0021        | 0.0049         |
| 7   | 5.40           | 0.63  | 2.53          | 0.20 | 4 | 0.0011        | 0.0032         |
| 14  | 5.65           | 0.38  | 2.61          | 0.14 | 4 | 0.0004        | 0.0006         |
| 21  | 6.97           | 0.77  | 3.14          | 0.30 | 4 | 0.0020        | 0.0028         |
| 28  | 8.25           | 0.58  | 3.65          | 0.21 | 4 | 0.0004        | 0.0007         |

**Table 4.14.2** Data obtained from the calibrations shown in Figure 4.14.2. Data represented as a mean response  $\pm$  SEM. Where (*P*) represents the outcome of a paired t-test for I<sub>400  $\mu$ M</sub> and I<sub>1000  $\mu$ M</sub> at each time point (1,3, 7, 14,21 and 28 days) when compared to the response recorded with untreated sensors (day = 0). The number of sensors is denoted by (n).

#### 4.15 *Cat* biocompatibility (PEA)

This section investigates the stability of the *Cat* sensor (Pt<sub>c</sub>/Nafion<sup>®</sup>/PPD/Cat-Ga) over a period of four weeks following continuous exposure to PEA, examining the effect of lipids on the performance of the *Cat* sensor (see Section 3.6.2). The sensitivity of the *Cat* sensor was tested over a concentration range of H<sub>2</sub>O<sub>2</sub> (0-550  $\mu$ M). The selectivity of the *Cat* sensor was tested over a concentration range of AA (0-1000  $\mu$ M). These sensors were stored at 4°C in a refrigerator in a 10% (w/v) solution of PEA (see Section 3.6.2);

the sensitivity and selectivity of the sensors were intermittently tested at the times outlined below.

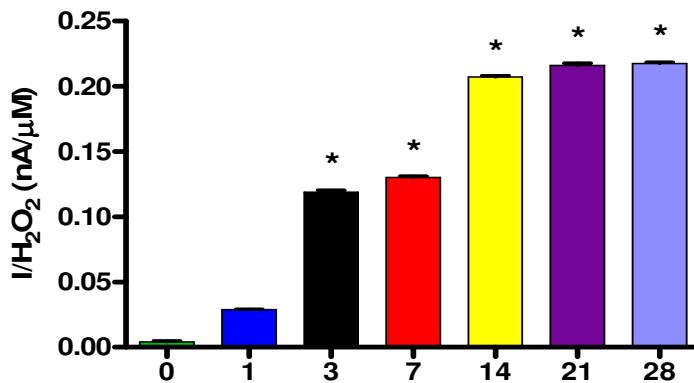


**Figure 4.15.1** H<sub>2</sub>O<sub>2</sub> response of the *Cat* sensor exposed to PEA over 28 days. Data represented as a mean response  $\pm$  SEM and ( $P < 0.05, *$ ).

A significant difference ( $P < 0.05, *$ ) is observed between day 0 and the successive time points 3, 7, 14, 21 and 28 days. The function of the catalase enzyme i.e. to degrade H<sub>2</sub>O<sub>2</sub> into water and oxygen is impacted upon. The maximum loss in sensitivity is observed on day 28 which displays similar current responses to those observed on day 21 and day 14 which can be seen in Table 4.15.1. As has been shown with previous biocompatibility tests with this catalase-based sensor in this chapter, a deterioration in the function of this sensor is observed following exposure to relatively high concentrations of H<sub>2</sub>O<sub>2</sub> (250-550  $\mu$ M). When sensitivities at lower concentrations of H<sub>2</sub>O<sub>2</sub> i.e. 0-150  $\mu$ M are examined no significant differences ( $P > 0.05$ ) are reported at all time points (1, 3, 7, 14, 21 and 28 days) with reference to day 0. The stability of this sensor (Pt<sub>2</sub>/Nafion<sup>®</sup>/PPD/Cat-Ga) is maintained over 28 days when exposed to PEA up to a concentration of 150  $\mu$ M H<sub>2</sub>O<sub>2</sub>. The concentration of PEA used in this experiment (10%) may be less than that encountered under physiological conditions.

| Day | Mean I,<br>(nA/ $\mu$ M) | SEM    | P      | n |
|-----|--------------------------|--------|--------|---|
| 0   | 0.004                    | 0.001  | n/a    | 4 |
| 1   | 0.03                     | 0.0003 | 0.0504 | 4 |
| 3   | 0.12                     | 0.001  | 0.0407 | 4 |
| 7   | 0.13                     | 0.001  | 0.0359 | 4 |
| 14  | 0.21                     | 0.001  | 0.0349 | 4 |
| 21  | 0.22                     | 0.002  | 0.0295 | 4 |
| 28  | 0.22                     | 0.001  | 0.0309 | 4 |

Table 4.15.1 Data obtained from the calibrations shown in Figure 4.13.1. Data represented as a mean response  $\pm$  SEM. Where (*P*) represents the outcome of a paired t-test at each time point (1, 3, 7, 14, 21 and 28 days) when compared to the response recorded with untreated sensors (day = 0).

The number of sensors is denoted by (n).

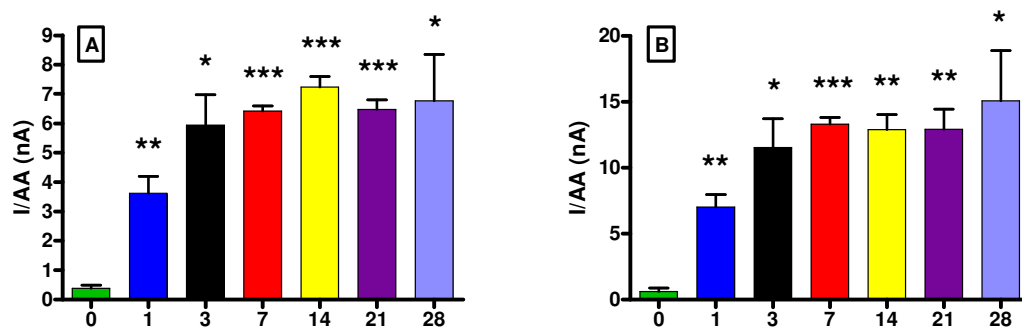


Figure 4.15.2 AA response of the *Cat* sensor exposed to PEA over 28 days. Data represented as a mean response  $\pm$  SEM (A) I<sub>400  $\mu$ M</sub> and (B) I<sub>1000  $\mu$ M</sub>.

Figure 4.15.2 displays the AA response of the *Cat* sensor when treated with PEA for 28 days. A significant difference is observed on day 1, 3, 7, 14, 21 and 28 in comparison to day 0. It appears that the modified surface of the *Cat* sensor is disrupted. This protocol only replicates one aspect of the *in-vivo* environment and it was necessary to expose the *Cat* sensor to a more global representation of the *in-vivo* environment (see Section 4.17).

| Day | I, nA<br>(1000 $\mu$ M) | SEM  | I, nA<br>(400 $\mu$ M) | SEM  | n | P<br>(400 $\mu$ M) | P<br>(1000 $\mu$ M) |
|-----|-------------------------|------|------------------------|------|---|--------------------|---------------------|
| 0   | 0.62                    | 0.27 | 0.38                   | 0.11 | 4 | n/a                | n/a                 |
| 1   | 7.03                    | 0.94 | 3.61                   | 0.57 | 4 | 0.0062             | 0.0027              |
| 3   | 11.54                   | 2.18 | 5.94                   | 1.04 | 4 | 0.0122             | 0.0128              |
| 7   | 13.33                   | 0.47 | 6.41                   | 0.18 | 4 | < 0.0001           | < 0.0001            |
| 14  | 12.90                   | 1.15 | 7.24                   | 0.35 | 4 | 0.0004             | 0.0031              |
| 21  | 12.94                   | 1.52 | 6.47                   | 0.34 | 4 | 0.0008             | 0.0058              |
| 28  | 15.08                   | 3.81 | 6.76                   | 1.59 | 4 | 0.0284             | 0.0328              |

**Table 4.15.2** Data obtained from the calibrations shown in Figure 4.15.2. Data represented as a mean response  $\pm$  SEM. Where (*P*) represents the outcome of a paired t-test for I<sub>400  $\mu$ M</sub> and I<sub>1000  $\mu$ M</sub> at each time point (1,3, 7, 14,21 and 28 days) when compared to the response recorded with untreated sensors (Day = 0). The number of sensors is denoted by (n).

### 4.16 Blank biocompatibility (BT)

In this section the *Blank* sensor (Pt<sub>c</sub>/Nafion<sup>®</sup>/PPD) was exposed to a homogenised sample of *ex-vivo* brain tissue (BT) (see Section 3.6.3) and was tested over 28 days in order to examine the effect of exposure to BT on the sensitivity and selectivity of the sensor. The protocol followed here mimics the conditions encountered in a physiological environment more reliably than the biocompatibility tests discussed in the previous sections. The sensitivity of the *Blank* sensor was tested (0-550 μM H<sub>2</sub>O<sub>2</sub>). The selectivity of the *Blank* sensor was examined using AA (0-1000 μM). These sensors were stored at 4°C in a refrigerator in BT (see Section 3.6.3) when not in use, the sensitivity and selectivity of the sensors were intermittently tested at the times stated below.

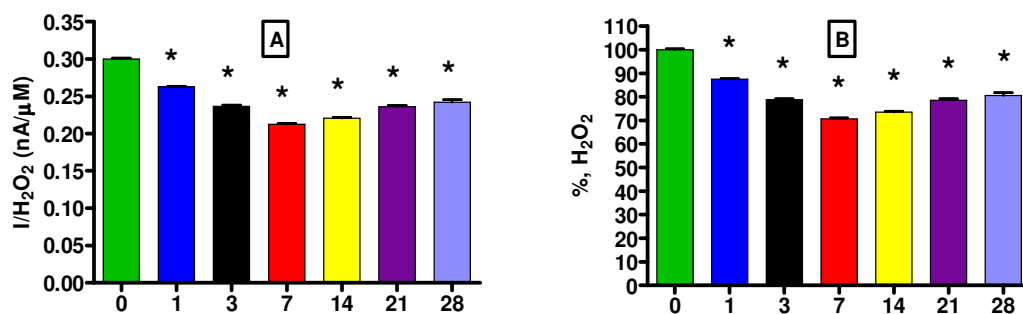


Figure 4.16.1 H<sub>2</sub>O<sub>2</sub> response of the *Blank* sensor exposed to BT over 28 days. (A) Data represented as a mean response  $\pm$  SEM (B) Data shown as a percentage with 100% as the H<sub>2</sub>O<sub>2</sub> sensitivity recorded on the initial day of experiments.

The effect of exposure to BT on the sensitivity of the *Blank* sensor can be seen in Figure 4.16.1. On examining the data displayed in Figure 4.16.1, it is apparent that a gradual decrease in sensitivity of the *Blank* sensor is observed on increasing the duration of exposure to BT. The maximum drop in sensitivity can be seen on day 7 (29.2 %). As the experiment proceeds a return towards the initial sensitivity occurs following continuous BT exposure. The current values are displayed in Table 4.16.1. An initial decrease in sensitivity occurs until day 7, subsequently the sensitivity returns towards control levels

and no significant difference ( $P > 0.05$ ) is observed between the sensitivity on day 28 and that recorded after 24 hours (day 1) of contact with BT. The biocompatibility test shown in this section (BT) is the closest method of mimicking the conditions encountered by the sensor in the *in-vivo* environment. The *in-vitro* results displayed in this section strongly suggest that the *Blank* sensor will remain stable after an initial decrease (*in-vitro*, ~29.2 %). It must be stated at this point that these experiments cannot exactly replicate the *in-vivo* biological medium but serve only as an indication about the stability of a sensor design.

| <b>Day</b> | <b>Mean I,<br/>(nA/μM)</b> | <b>SEM</b> | <b>%</b> | <b>SEM (%)</b> | <b>P</b> | <b>n</b> |
|------------|----------------------------|------------|----------|----------------|----------|----------|
| <b>0</b>   | 0.30                       | 0.001      | 100      | 0.42           | n/a      | 4        |
| <b>1</b>   | 0.26                       | 0.001      | 87.51    | 0.23           | 0.0289   | 4        |
| <b>3</b>   | 0.24                       | 0.002      | 78.75    | 0.53           | 0.0290   | 4        |
| <b>7</b>   | 0.21                       | 0.001      | 70.76    | 0.34           | 0.0313   | 4        |
| <b>14</b>  | 0.22                       | 0.001      | 73.46    | 0.44           | 0.0306   | 4        |
| <b>21</b>  | 0.24                       | 0.002      | 78.49    | 0.75           | 0.0384   | 4        |
| <b>28</b>  | 0.24                       | 0.003      | 80.65    | 1.04           | 0.0417   | 4        |

**Table 4.16.1** Data obtained from the calibrations shown in Figure 4.16.1. Data represented as a mean response  $\pm$  SEM. Where ( $P$ ) represents the outcome of a paired  $t$ -test at each time point (1, 3, 7, 14, 21 and 28 days) when compared to the response recorded with untreated sensors (day = 0).

The number of sensors is denoted by (n).

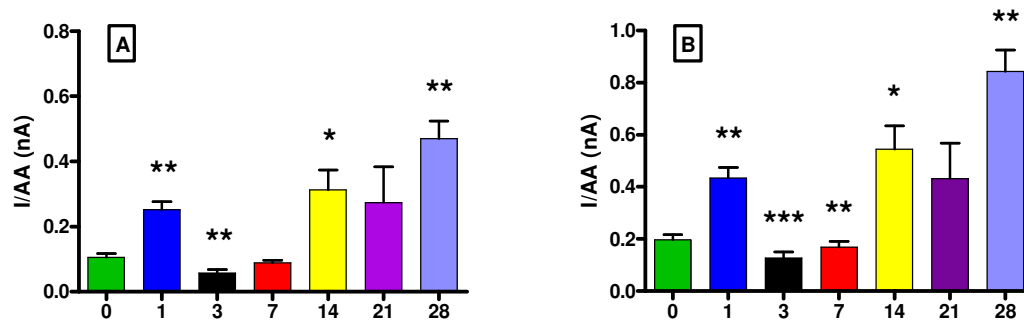


Figure 4.16.2 AA response of the *Blank* sensor exposed to BT over 28 days. Data represented as a mean response  $\pm$  SEM (A) I<sub>400 μM</sub> and (B) I<sub>1000 μM</sub>

Figure 4.16.2 above represents the response of the *Blank* sensor to AA following exposure to BT for a period of 28 days. A decrease in AA response is observed on day 3 and 7 of this protocol. A significant difference in AA signal was recorded on day 1, 14 and 28 in comparison to day 0 (see Table 4.16.2). On examination of the current responses, a massive improvement in the biocompatibility characteristics of the *Blank* sensor is observable with respect to BSA and PEA treatments. The exposure of the sensor to a sample of brain tissue is a far more accurate representation of the *in-vivo* environment. The work presented in this section supports the feasibility of maintaining the stability of this H<sub>2</sub>O<sub>2</sub> detecting sensor during L.I.V.E experiments.

| <b>Day</b> | <b>I, nA<br/>(1000 <math>\mu</math>M)</b> | <b>SEM</b> | <b>I, nA<br/>(400 <math>\mu</math>M)</b> | <b>SEM</b> | <b>n</b> | <b>P,<br/>(400 <math>\mu</math>M)</b> | <b>P,<br/>(1000 <math>\mu</math>M)</b> |
|------------|---|------------|--|------------|----------|---------------------------------------|--|
| <b>0</b>   | 0.20                                      | 0.02       | 0.11                                     | 0.01       | 4        | n/s                                   | n/s                                    |
| <b>1</b>   | 0.43                                      | 0.04       | 0.25                                     | 0.02       | 4        | 0.0022                                | 0.0036                                 |
| <b>3</b>   | 0.13                                      | 0.02       | 0.06                                     | 0.01       | 4        | 0.0039                                | 0.0010                                 |
| <b>7</b>   | 0.17                                      | 0.02       | 0.09                                     | 0.01       | 4        | 0.1589                                | 0.0064                                 |
| <b>14</b>  | 0.54                                      | 0.09       | 0.31                                     | 0.06       | 4        | 0.0385                                | 0.0236                                 |
| <b>21</b>  | 0.43                                      | 0.14       | 0.27                                     | 0.11       | 3        | 0.2707                                | 0.2479                                 |
| <b>28</b>  | 0.84                                      | 0.08       | 0.47                                     | 0.05       | 4        | 0.0081                                | 0.0034                                 |

**Table 4.16.2** Data obtained from the calibrations shown in Figure 4.16.2. Data represented as a mean response  $\pm$  SEM. Where (*P*) represents the outcome of a paired t-test for I<sub>400  $\mu$ M</sub> and I<sub>1000  $\mu$ M</sub> at each time point (1,3, 7, 14,21 and 28 days) when compared to the response recorded with untreated sensors (day = 0). The number of sensors is denoted by (n).

### 4.17 *Cat* biocompatibility (BT)

In this section the stability of the *Cat* sensor (Pt<sub>c</sub>/Nafion<sup>®</sup>/PPD/Cat-Ga) following exposure to BT is examined over a period of 28 days, to investigate the effect of a brain tissue sample on the function of the *Cat* sensor (see Section 3.6.3). The sensitivity of the *Cat* sensor was tested over a concentration range of H<sub>2</sub>O<sub>2</sub> (0-550 μM). The selectivity of the *Cat* sensor was examined using a concentration range of AA (0-1000 μM). These sensors were stored at 4°C in a refrigerator in a sample of BT (see Section 3.6.3); the sensitivity and selectivity of the sensors were intermittently tested at the times shown below.

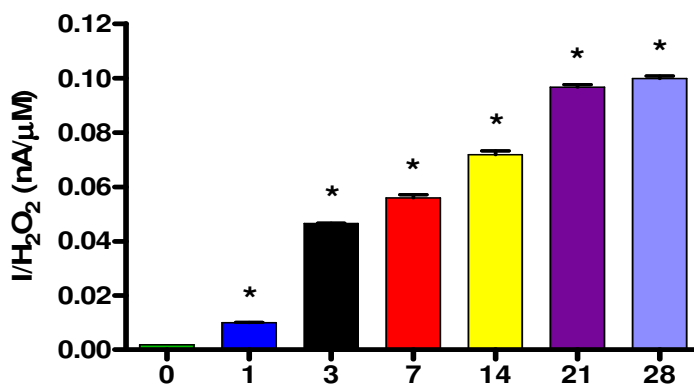


Figure 4.17.1 H<sub>2</sub>O<sub>2</sub> response of the *Cat* sensor exposed to BT over 28 days (0-550 μM H<sub>2</sub>O<sub>2</sub>). Data represented as a mean response ± SEM and ( $P < 0.05, *$ ).

A significant difference ( $P < 0.05, *$ ) is observed between day 0 and the respective days of exposure. The ability of the catalase enzyme to remove H<sub>2</sub>O<sub>2</sub> is compromised. The maximum current response on day 28 is much less than observed with previous biocompatibility tests (see Table 4.17.1). On further examination it was found that at a lower concentration of H<sub>2</sub>O<sub>2</sub> (0-150 μM), the stability of this sensor is maintained (See Section 4.17.2) as has been demonstrated in the previous sections. No significant difference ( $P > 0.05$ ) was observed between days of exposure at this lower concentration.

| Day | Mean I, nA/ $\mu$ M | SEM     | P      | n |
|-----|---------------------|---------|--------|---|
| 0   | 0.002               | 0.0001  | n/a    | 4 |
| 1   | 0.01                | 0.00009 | 0.0374 | 4 |
| 3   | 0.046               | 0.00019 | 0.0325 | 4 |
| 7   | 0.056               | 0.00126 | 0.0373 | 4 |
| 14  | 0.072               | 0.0015  | 0.0355 | 4 |
| 21  | 0.097               | 0.00106 | 0.0294 | 4 |
| 28  | 0.10                | 0.00082 | 0.0267 | 4 |

Table 4.17.1 Data obtained from the calibrations shown in Figure 4.17.1. Data represented as a mean response  $\pm$  SEM. Where (*P*) represents the outcome of a paired t-test at each time point (1, 3, 7, 14, 21 and 28 days) when compared to the response recorded with untreated sensors (day = 0).

The number of sensors is denoted by (n).

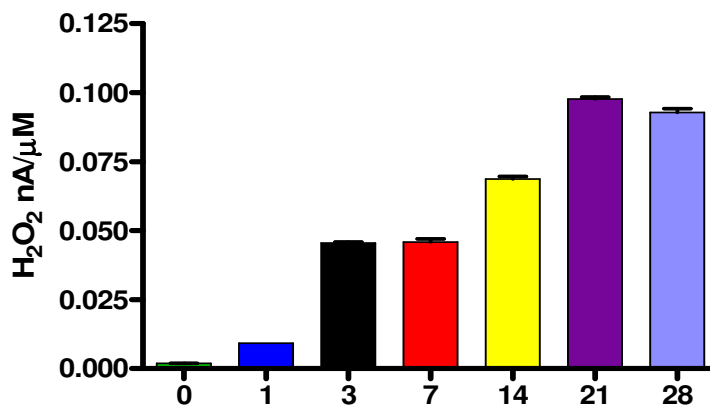


Figure 4.17.2 H<sub>2</sub>O<sub>2</sub> response of the *Cat* sensor exposed to BT over 28 days (0-150  $\mu$ M H<sub>2</sub>O<sub>2</sub>). Data represented as a mean response  $\pm$  SEM and (*P* < 0.05,\*).

| Day | Mean I, nA/ $\mu$ M | SEM     | P      | n |
|-----|---------------------|---------|--------|---|
| 0   | 0.002               | 0.00003 | n/a    | 4 |
| 1   | 0.009               | 0.00004 | 0.0695 | 4 |
| 3   | 0.046               | 0.00032 | 0.0636 | 4 |
| 7   | 0.046               | 0.00117 | 0.0531 | 4 |
| 14  | 0.069               | 0.0008  | 0.0616 | 4 |
| 21  | 0.098               | 0.00067 | 0.0608 | 4 |
| 28  | 0.093               | 0.00134 | 0.0598 | 4 |

**Table 4.17.2** Data obtained from the calibrations shown in Figure 4.17.2. Data represented as a mean response  $\pm$  SEM. Where (*P*) represents the outcome of a paired t-test at each time point (1, 3, 7, 14, 21 and 28 days) when compared to the response recorded with untreated sensors (day = 0).

The number of sensors is denoted by (n).

The same trend was observed here in relation to previous biocompatibility tests on the catalase-based sensor, the stability of this sensor was maintained at relatively lower concentrations (0-150  $\mu$ M) as illustrated in Figure 4.17.2. This factor may be attributable to saturation of the catalase enzyme by the substrate at higher concentrations. This evidence further demonstrates that the deterioration in the function of the catalase-based sensor is dependent on the repeated exposure to high levels of H<sub>2</sub>O<sub>2</sub> (550  $\mu$ M). In order to further investigate this possibility a separate experiment was undertaken. A set of Pt<sub>c</sub>/Nafion<sup>®</sup>/PPD/Cat-Ga sensors were manufactured and left in a sample of BT without removal for 14 days. These sensors were then removed and re-tested with no intermediate tests undertaken. This protocol limits repeated exposure of the enzyme to the substrate and hence should avoid saturation of the enzyme. The results of this experiment are displayed below in Figure 4.17.3.

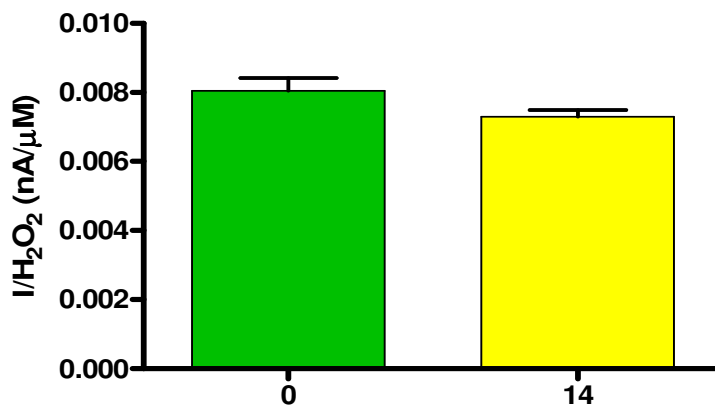


Figure 4.17.3 H<sub>2</sub>O<sub>2</sub> response of the *Cat* sensor exposed to BT for a constant period of 14 days.

The sensitivity of the *Cat* sensor was tested over a concentration range of H<sub>2</sub>O<sub>2</sub> (0-550 μM). The H<sub>2</sub>O<sub>2</sub> sensitivity of the Pt<sub>c</sub>/Nafion<sup>®</sup>/PPD/Cat-Ga sensor prior to BT exposure (day 0) was 8.04 ± 0.38 pA/μM, n = 3 with an R<sup>2</sup> value of 0.9786. Following 14 days of exposure to BT, the sensors were removed and re-calibrated. On day 14 these sensors gave a H<sub>2</sub>O<sub>2</sub> sensitivity of 7.29 ± 0.19 pA/μM, n = 3 with an R<sup>2</sup> value of 0.9929. No significant difference ( $P > 0.05$ ) was found between day 0 and 14. The *Cat* sensor did not show a significant loss in sensitivity due to treatment with BT in this case. This further supports previous evidence which suggests that saturation of the catalase enzyme with H<sub>2</sub>O<sub>2</sub> is responsible for the apparent loss in ability to degrade H<sub>2</sub>O<sub>2</sub> and not the treatment itself. As saturation considerations are effectively eliminated in this instance it is clear that BT does not significantly effect the stability of the *Cat* sensor for up to 14 days.

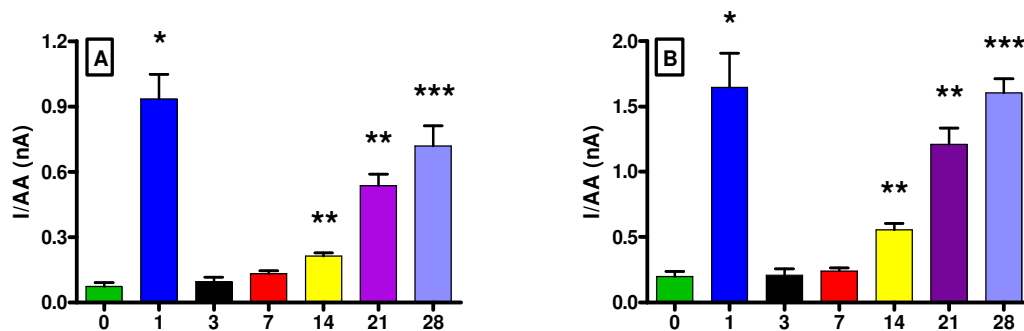


Figure 4.17.4 AA response of the *Cat* sensor exposed to BT over 28 days. Data represented as a mean response  $\pm$  SEM (A) I<sub>400  $\mu$ M</sub> and (B) I<sub>1000  $\mu$ M</sub>

Figure 4.17.4 above illustrates the response of the *Cat* sensor to AA following exposure to BT for 28 days. A similar response is obtained between day 3 and 7 in comparison to day 0 the current values are given in Table 4.17.4. A significant difference ( $P < 0.05$ ) in AA rejection characteristics is seen on day 1, 14, 21 and 28 and the results are summarised in Table 4.17.4. On further inspection of the current responses, a massive improvement in AA rejection capabilities of the *Cat* sensor is evident here in comparison to that seen with BSA and PEA treatments. The treatment of the sensor with a sample of brain tissue is the closest representation of conditions encountered in a physiological environment. The results presented in this section suggest the *Cat* sensor is quite stable in the presence of brain tissue. Many of the parameters of the *in-vivo* environment cannot be replicated *in-vitro*, however these results support the stability of the *Cat* sensor for use in L.I.V.E experiments.

| Day | I, nA<br>(1000 $\mu$ M) | SEM  | I, nA<br>(400 $\mu$ M) | SEM  | n | P<br>(400 $\mu$ M) | P<br>(1000 $\mu$ M) |
|-----|-------------------------|------|------------------------|------|---|--------------------|---------------------|
| 0   | 0.20                    | 0.04 | 0.07                   | 0.02 | 4 | n/a                | n/a                 |
| 1   | 1.65                    | 0.26 | 0.93                   | 0.11 | 3 | 0.0201             | 0.0357              |
| 3   | 0.21                    | 0.05 | 0.1                    | 0.02 | 4 | 0.4315             | 0.8621              |
| 7   | 0.24                    | 0.02 | 0.13                   | 0.01 | 4 | 0.0568             | 0.4013              |
| 14  | 0.56                    | 0.05 | 0.21                   | 0.02 | 3 | 0.0059             | 0.0059              |
| 21  | 1.21                    | 0.12 | 0.54                   | 0.05 | 3 | 0.0048             | 0.0057              |
| 28  | 1.61                    | 0.11 | 0.72                   | 0.09 | 4 | 0.0067             | 0.0009              |

Table 4.17.4 Data obtained from the calibrations shown in Figure 4.17.4. Data represented as a mean response  $\pm$  SEM. Where (P) represents the outcome of a paired t-test for I<sub>400  $\mu$ M</sub> and I<sub>1000  $\mu$ M</sub> at each time point (1,3, 7, 14,21 and 28 days) when compared to the response recorded with untreated sensors (day = 0). The number of sensors is denoted by (n).

#### 4.18 Blank stability and biocompatibility summary

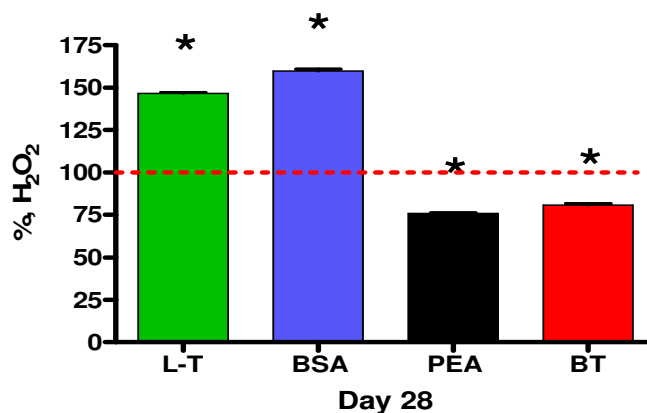
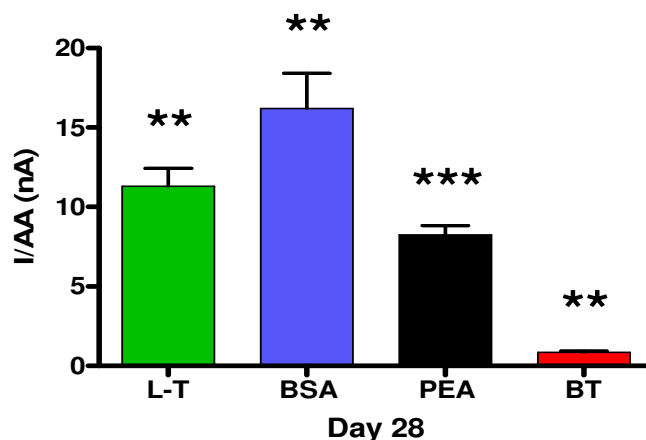


Figure 4.18.1 Comparison of H<sub>2</sub>O<sub>2</sub> responses between long-term stability (L-T) and biocompatibility tests on day 28. Data represented as a percentage change. With 100% as the H<sub>2</sub>O<sub>2</sub> sensitivity recorded on day 0 of each treatment.

The data represented in Figure 4.18.1 compares the effect of the long-term stability test (L-T) and the various biocompatibility tests (PEA, BSA and BT) on the sensitivity of the *Blank* sensor. The H<sub>2</sub>O<sub>2</sub> response of the *Blank* sensor recorded on day 28 is shown. With the long-term stability test (L-T) a significant difference ( $P < 0.05$ ,\*) was observed between day 0 and day 28. The repeated calibration itself has an effect on the *Blank* sensor performance. In each biocompatibility test a significant difference ( $P < 0.05$ ,\*) was observed between day 0 and 28. The concentration of BSA used here is quite high (10%) which may be more severe than the concentration of protein found *in-vivo*. In the case of the PEA test no significant difference ( $P > 0.05$ ) was observed between day 1 and 28. The use of BT is the closest mimic achievable to physiological conditions and the response of the *Blank* sensor on exposure to BT is typical when compared to other sensor designs (Garguilo & Michael, 1994; Finnerty *et al.*, 2012).



**Figure 4.18.2 Comparison of AA responses between long-term stability (L-T) and biocompatibility tests on day 28. Data represented as a mean response  $\pm$  SEM.**

Figure 4.18.2 demonstrates the  $I_{1000 \mu\text{M}}$  of the *Blank* sensor recorded on day 28 of the long term stability test (L-T) and the various biocompatibility tests. A significant difference ( $P < 0.05$ , \*\*) was observed between day 0 and 28 of the long-term stability test. It is likely that a disruption in the polymerised surface has occurred which has created an increased Pt surface area, thereby causing an increase in response to AA. This structural issue is negated for *in-vivo* experiments as all sensors are calibrated immediately prior to implantation. A significant difference was also observed between

day 0 and 28 with the biocompatibility tests. A large reduction in AA response was observed following exposure to BT. The BT biocompatibility test is the closest method of mimicking the conditions encountered by the sensor in the *in-vivo* environment.

#### 4.19 *Cat* stability and biocompatibility summary

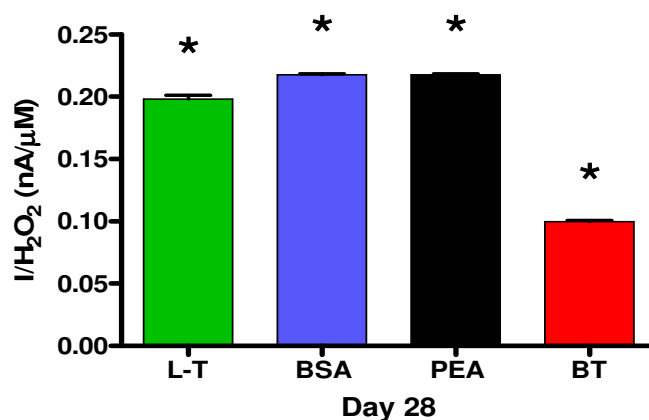


**Figure 4.19.1** Comparison of H<sub>2</sub>O<sub>2</sub> responses between long-term stability (L-T) and biocompatibility tests on day 28. Data represented as a mean response  $\pm$  SEM.

Figure 4.19.1 demonstrates the effect of the long-term stability test (L-T) and the various biocompatibility tests (PEA, BSA and BT) on the function of the catalase enzyme. The ability of the catalase enzyme to remove H<sub>2</sub>O<sub>2</sub> is impaired. With each treatment a significant difference ( $P < 0.05$ ,\*) was demonstrated on day 28 when compared to day 0. However no significant variation ( $P > 0.05$ ) was observed at a lower concentration range of H<sub>2</sub>O<sub>2</sub> (0-150  $\mu$ M) between successive time points when compared to the sensitivity recorded on day 0 with each treatment. This stability of the *Cat* sensor was further supported by the fact that removal of repetitive calibrations improved the performance of this sensor design (see Section 4.13 and 4.17). The stability of the *Cat* sensor following exposure to BT showed an improvement over the other biocompatibility tests.

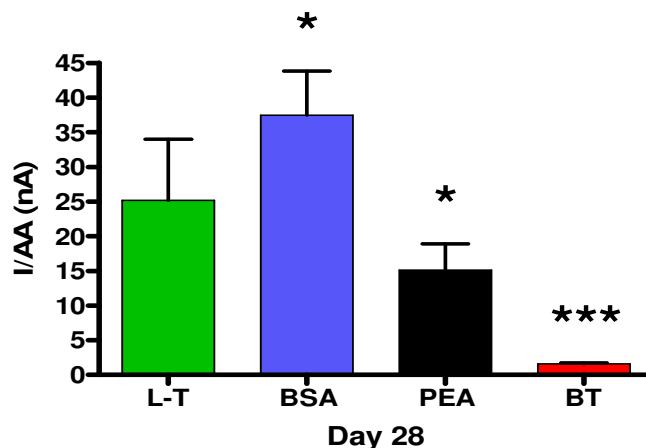


**Figure 4.19.2** Comparison of AA responses between long-term stability (L-T) and biocompatibility tests on day 28. Data represented as a mean response  $\pm$  SEM.

Figure 4.19.2 demonstrates the  $I_{1000 \mu\text{M}}$  of the *Cat* sensor recorded on day 28 of the long term stability test (L-T) and the various biocompatibility tests. No significant difference ( $P > 0.05$ ) was observed between day 0 and 28 of the long-term stability test however an increase in AA response was observed. A corruption in the polymerised surface has occurred which has created an increased Pt surface area, which would increase the response to AA. This damage to the sensor does not impact upon *in-vivo* experiments as all sensors are calibrated immediately prior to implantation. A significant difference ( $P < 0.05$ ) was observed between day 0 and 28 with the biocompatibility tests. A large reduction in AA response was observed following exposure to BT. The BT biocompatibility test is the closest method achievable to mimic physiological conditions.

## 4.20 Post *in-vivo* stability

Following implantation of the paired catalase-based biosensor over an extended period, the sensors were removed and re-calibrated. The sensitivity towards  $H_2O_2$  and selectivity against AA of the sensors was examined. The calibration procedures are outlined in Section 3.7.3 and 3.7.5 respectively. When in contact with biological samples a drop in sensitivity often occurs with Pt based sensors due to fouling of the active surface by proteins and other biomolecules (Garguilo & Michael, 1994; Finnerty *et al.*, 2012). Sensor damage during ex-plantation may also negatively affect the characteristics of the working electrode. The purpose of these experiments is to gauge the stability of the sensors after contact with endogenous lipids and proteins present in the living brain.

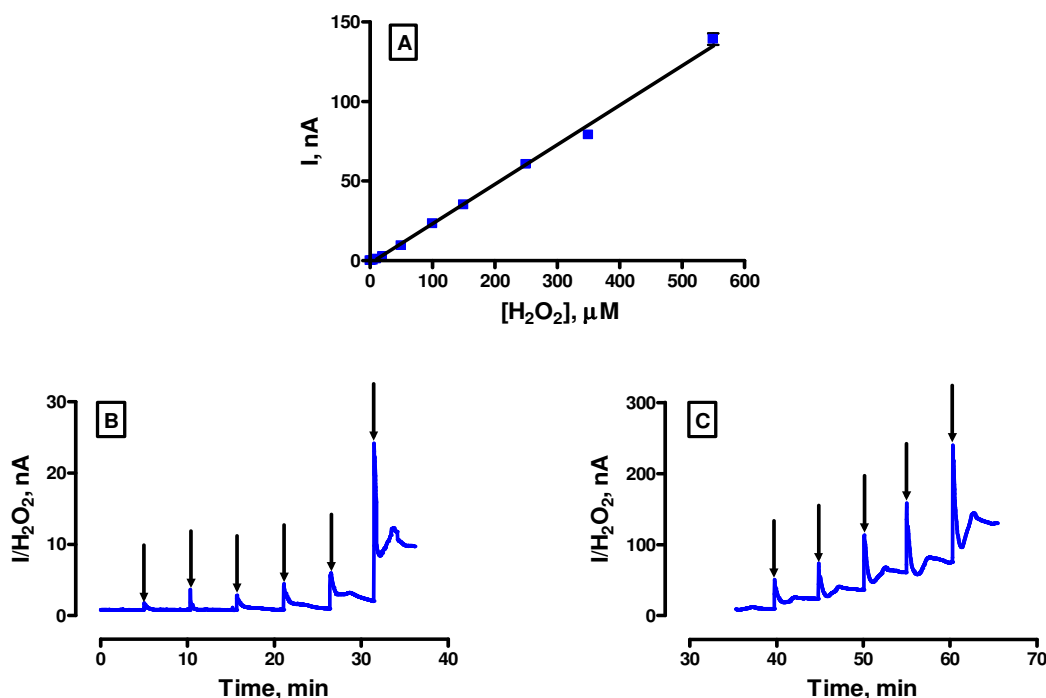


**Figure 4.20.1:** (A) The current-concentration profile of  $H_2O_2$  at the paired sensor following implantation ( $n = 2+2$ ). (B) A typical raw data trace 0-50  $\mu M$  and (C) 50-550  $\mu M$  for  $H_2O_2$  calibrations. CPA carried out at +700 mV vs. SCE. Arrows indicate the addition of aliquots of  $H_2O_2$ .

Figure 4.20.1 (A) demonstrates the average  $H_2O_2$  response of the catalase-based paired sensor following implantation. The sensors described here were implanted over a period

of 16 to 20 days. These sensors were removed following cessation of *in-vivo* experiments. A drop in sensitivity of approximately 46 % was apparent following calibration with H<sub>2</sub>O<sub>2</sub> (0-550 μM). This value is consistent with other reports which have demonstrated a 20 to 50 % loss in sensitivity of sensors following exposure to BT (Garguilo & Michael, 1994; Hu *et al.*, 1994; Finnerty *et al.*, 2012). The paired post-implantation sensitivity obtained was  $0.248 \pm 0.004$  nA/μM and is linear with an R<sup>2</sup> value of 0.9969, n = 2+2. This value is significantly different ( $P < 0.05, *$ ) when compared to average pre-implantation sensitivity of the paired H<sub>2</sub>O<sub>2</sub> sensor. The overall H<sub>2</sub>O<sub>2</sub> response is based on a subtraction value (*Blank-Cat*). The 46% overall loss in H<sub>2</sub>O<sub>2</sub> sensitivity is attributable to the fact that there is an increased response at the *Cat* sensor. The post-implantation sensitivity of the *Cat* sensor is  $0.252 \pm 0.003$  nA/μM (n = 2) and this response is significantly different ( $P < 0.05, *$ ) when compared against pre-implantation data of these sensors. A loss in ability of the *Cat* sensor to remove H<sub>2</sub>O<sub>2</sub> is evident. The post-implantation sensitivity of the *Blank* sensor is  $0.50 \pm 0.01$  nA/μM (n = 2) and this response is not significantly different ( $P > 0.05$ ) when compared against the response of these sensors prior to implantation.

On visual inspection under a microscope and further examination using scanning electron microscopy (SEM) imaging of the *Blank* and *Cat* sensor, it became clear that the PPD layer which is part of each sensor design was corrupted. The catalase enzyme is adhered to the PPD structure as part of the *Cat* sensor design and removal of this PPD layer would lead to a loss in function of the *Cat* sensor. The body's natural response to the presence of a foreign object can also inhibit the sensitivity of an implanted sensor (Wisniewski *et al.*, 2000). A possible explanation of the damaged PPD structure is that following explantation of the sensors the PPD layer is left behind due to encapsulation by gliosis which occurs at the sensor-tissue interface (O'Neill & Lowry, 1995).

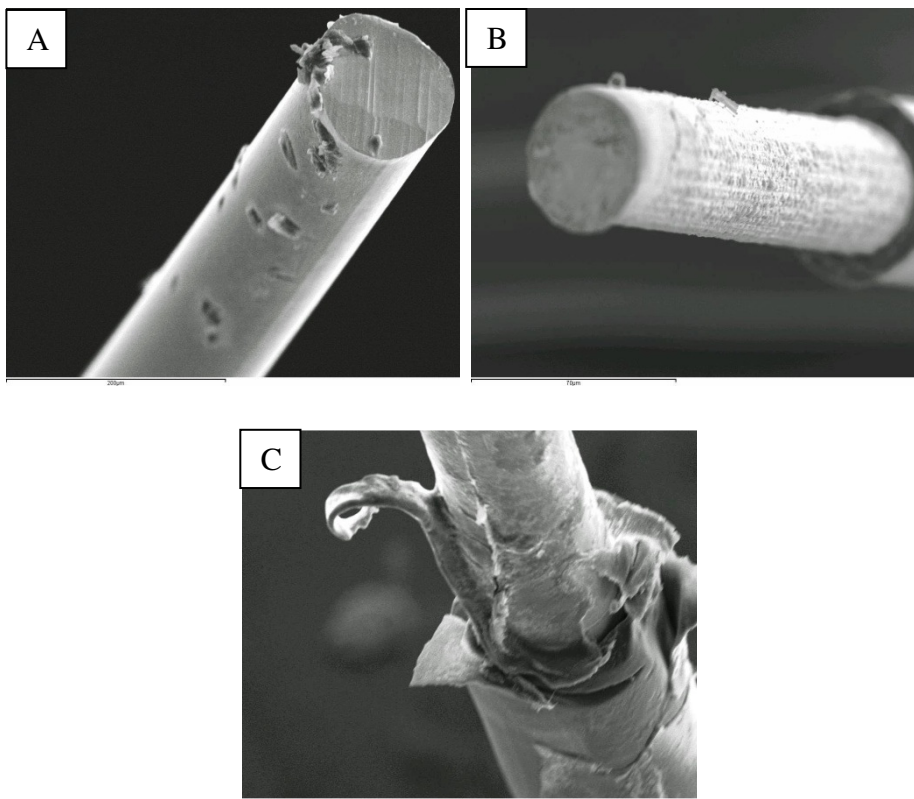


**Figure 4.20.2 SEM images of sensors. (A)  $Pt_c$  electrode [pre-implantation] (x 300), (B)  $Pt_c/PPD$  electrode [pre-implantation] (x 800) and (C)  $Pt_c/Naf/PPD$  sensor (x 120) [following implantation].**

Figure 4.20.2 shows examples of SEM images obtained of (A) an unmodified  $Pt_c$  electrode prior to implantation, (B) a  $Pt_c$  electrode modified with PPD prior to implantation and (C) a  $Pt_c/Naf/PPD$  electrode following implantation for 10 days. The bare  $Pt_c$  has a smooth surface and the striations on the disc surface caused by cutting the electrode can clearly be seen. Following modification with PPD the development of a grainy morphological structure can be seen on the surface of the electrode. Corruption of the PPD surface following ex-plantation is apparent as shown in Figure 4.20.2 (C) a detachment of the outer membrane from the bare Pt surface can be seen.

The disruption of the PPD layer should lead to an increase in  $H_2O_2$  sensitivity as a greater surface area of bare Pt should be present. The loss in  $H_2O_2$  sensitivity observed here is mainly attributable to an increase in sensitivity at the *Cat* sensor. On further examination of the raw data trace in Figure 4.20.1 (A) and (B) an instantaneous increase

in signal is observed following each injection of H<sub>2</sub>O<sub>2</sub>. A decline in response is observed following each injection and the magnitude of this decline is greater than that seen with *in-vitro* H<sub>2</sub>O<sub>2</sub> calibration data of the sensors prior to implantation (see Figure 4.7.2).

It is feasible that proteins and lipids present on the surface of each sensor limit the diffusion of H<sub>2</sub>O<sub>2</sub> in the bulk solution to the active surface of each sensor. The process of stirring following addition of an aliquot of H<sub>2</sub>O<sub>2</sub>, creates forced convection of the analyte to the active surface of the sensor. This explains the initial increase observed in these post *in-vivo* experiments and subsequent decline. In an *in-vitro* H<sub>2</sub>O<sub>2</sub> calibration an immediate plateau in signal is observed following injection of H<sub>2</sub>O<sub>2</sub> (see Figure 4.7.2).

During *in-vivo* experiments however the PPD structure remains intact which is proven by the implanted dual sensor response towards AA as demonstrated in Chapter 5. In order to examine the damage incurred during the process of explantation the selectivity of the sensors in relation to AA was examined as shown below in Figure 4.20.3.

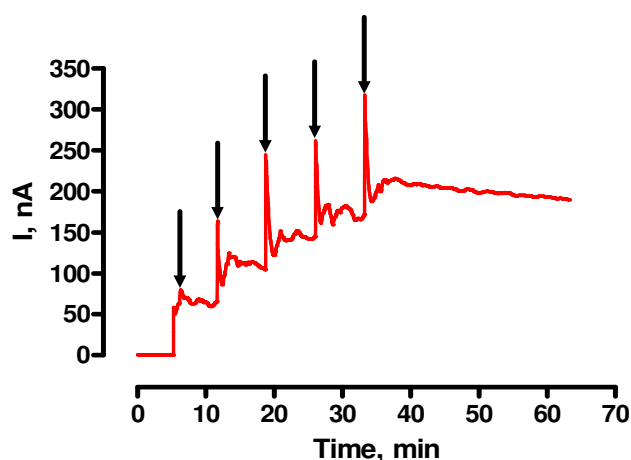


**Figure 4.20.3: Raw data trace 0-1000  $\mu$ M for an AA calibration at the paired H<sub>2</sub>O<sub>2</sub> sensor following implantation. CPA carried out at +700 mV vs. SCE. Arrows indicate the addition of aliquots of AA.**

A large AA response was obtained with these sensors following 16 days of implantation in the striatum of a male wistar rat (see Figure 4.20.3). This would implicate that the PPD structure is disrupted, leading to a larger surface area of Pt and subsequently increasing the AA response. The  $I_{400 \mu\text{M}}$  and  $I_{1000 \mu\text{M}}$  values for the sensors represented in

Figure 4.18.3 are 110.89 nA and 189.6 nA respectively, n=1+1. It is clear that the PPD layer which is an intricate part of each sensor design i.e. *Blank* and *Cat* is damaged during explantation. It is not possible to achieve reliable post *in-vivo* calibration data from this sensor design particularly for the duration of implantation prior to removal of the sensors examined here (16-20 days). The reported damage to the PPD structure during explantation may be caused by gliosis at the sensor-tissue interface. Extensive gliosis has been demonstrated *in-vivo* by O'Neill & Lowry following 7 days of implantation of a fixed cannulae (O'Neill & Lowry, 1995). It is plausible in this case that the process of gliosis has encapsulated the implanted paired H<sub>2</sub>O<sub>2</sub> sensor and upon explantation the PPD layer is removed.

## 4.21 Conclusion

The primary aim of this chapter was to validate the sensitivity and selectivity of the paired catalase-based H<sub>2</sub>O<sub>2</sub> sensor *in-vitro* as demonstrated previously (O'Brien *et al.*, 2007). The H<sub>2</sub>O<sub>2</sub> sensitivity of the dual sensor design was established (see Section 4.7) and reported as  $0.47 \pm 0.003$  nA/ $\mu$ M, n = 24+24. Table 4.21.1 displays the H<sub>2</sub>O<sub>2</sub> response of the relevant sensor designs.

| Design  | H <sub>2</sub> O <sub>2</sub> response                    | R <sup>2</sup> | n            |
|---|---|----------------|--------------|
| Pt <sub>c</sub> /Nafion <sup>®</sup> /PPD ( <i>Blank</i> )      | $0.47 \pm 0.003$ (nA/ $\mu$ M)                            | 0.9997         | 24           |
| Pt <sub>c</sub> /Nafion <sup>®</sup> /PPD/Cat-Ga ( <i>Cat</i> ) | $5.64 \pm 0.06$ (pA/ $\mu$ M)                             | 0.9989         | 24           |
| <b>Paired sensor response (<i>Blank-Cat</i>)</b>                | <b><math>0.47 \pm 0.003</math> (nA/<math>\mu</math>M)</b> | <b>0.9996</b>  | <b>24+24</b> |

**Table 4.21.1 H<sub>2</sub>O<sub>2</sub> sensitivity of the *Blank* sensor, *Cat* sensor and the final paired sensor design (*Blank-Cat*).**

No significant difference ( $P > 0.05$ ) was observed between the H<sub>2</sub>O<sub>2</sub> sensitivity of the paired design presented here and in comparison to that previously reported by O'Brien *et al.* (O'Brien *et al.*, 2007).

The required H<sub>2</sub>O<sub>2</sub> sensor must exhibit a low limit of detection (LOD) and a fast response time in order to detect H<sub>2</sub>O<sub>2</sub> *in-vivo*. The low LOD of the paired H<sub>2</sub>O<sub>2</sub> sensor is demonstrated in Section 4.7.1 which was  $0.075 \pm 0.006$   $\mu$ M, n=24. The LOD of the paired H<sub>2</sub>O<sub>2</sub> sensor is lower than that demonstrated by Sanford *et al.* who reported a detection limit of  $\sim 2$   $\mu$ M for H<sub>2</sub>O<sub>2</sub> using CFEs (Sanford *et al.*, 2010). Kulagina & Michael also demonstrated a higher LOD for H<sub>2</sub>O<sub>2</sub> of approximately 0.3  $\mu$ M using an amperometric microsensor (Kulagina & Michael, 2003).

The response time of the H<sub>2</sub>O<sub>2</sub> sensor is demonstrated in Section 4.7.2 The paired H<sub>2</sub>O<sub>2</sub> sensor displayed a fast response time of  $< 1$ s. This value compares well with previously reported *in-vitro* electrochemical H<sub>2</sub>O<sub>2</sub> detection methods (Li *et al.*, 2010; Sanford *et al.*,

2010). These parameters support the feasibility of utilising the dual H<sub>2</sub>O<sub>2</sub> sensor in the *in-vivo* environment.

The selectivity of the paired sensor against AA, the primary intereferent species in the brain in relation to H<sub>2</sub>O<sub>2</sub> detection was validated (see Section 4.8). The response of our H<sub>2</sub>O<sub>2</sub> sensor to AA was minimal with an I<sub>400 μM</sub> of 0.02 ± 0.03 nA and an I<sub>1000 μM</sub> value of -0.07 ± 0.04 nA (n = 28+28).

| Design  | I, nA<br>(1000 μM)  | I, nA<br>(400 μM)  | n            |
|---|---------------------|--------------------|--------------|
| Pt <sub>c</sub> /Nafion <sup>®</sup> /PPD ( <i>Blank</i> )      | 0.15 ± 0.03         | 0.16 ± 0.02        | 28           |
| Pt <sub>c</sub> /Nafion <sup>®</sup> /PPD/Cat-Ga ( <i>Cat</i> ) | 0.22 ± 0.03         | 0.14 ± 0.02        | 28           |
| Paired sensor response ( <i>Blank-Cat</i> )                     | <b>-0.07 ± 0.04</b> | <b>0.02 ± 0.03</b> | <b>28+28</b> |

**Table 4.21.2 AA response of the *Blank* sensor, *Cat* sensor and the final paired sensor design (*Blank-Cat*).**

The paired H<sub>2</sub>O<sub>2</sub> sensor is also highly selective over a range of other potential interference species as outlined in Section 4.8. The response to each interference species tested was < 0.1 % of the H<sub>2</sub>O<sub>2</sub> sensitivity. The H<sub>2</sub>O<sub>2</sub> sensitivity of the dual sensor is also maintained in the presence of AA (500 μM) and Dopamine (500 nM) as can be seen in Section 4.8.2 and 4.8.3 respectively, no significant difference ( $P > 0.05$ ) was seen in each case when compared to a normal H<sub>2</sub>O<sub>2</sub> calibration in PBS. The H<sub>2</sub>O<sub>2</sub> sensitivity of Pt<sub>d</sub> sensors was retained in aCSF aqueous media conditions in comparison to PBS aqueous conditions. Additionally substrate dilution conditions were examined, the H<sub>2</sub>O<sub>2</sub> added to the electrochemical cell was diluted in aCSF as opposed to H<sub>2</sub>O and no significant difference ( $P > 0.05$ ) in Pt<sub>d</sub> H<sub>2</sub>O<sub>2</sub> sensitivity was observed (see Section 4.8.4).

The stability of the *Blank* and *Cat* sensor was examined as part of a long-term study over 28 days (Section 4.10 and 4.11). It was demonstrated that repeated calibrations in the absence of treatment had a negative effect on the sensitivity and selectivity of each

sensor type. However, the observed loss in function of each sensor *in-vitro* is eliminated for *in-vivo* experiments as all sensors are calibrated immediately prior to implantation.

Biocompatibility characteristics were also examined following treatment with BSA, PEA and BT for each sensor (*Blank* and *Cat*). Variations in the sensitivity and selectivity of the *Blank* and *Cat* sensor design were seen in response to treatment with BSA and PEA and details of these experiments are provided in Sections 4.12 to 4.15. It was determined that the high concentration of protein (BSA) and lipid (PEA) of these treatments had a negative effect on the sensitivity and stability of the *Cat* and *Blank* sensor.

In order to more accurately reflect conditions encountered in the *in-vivo* environment, an *ex-vivo* sample of brain tissue (BT) was utilised as a sensor treatment. The stability of the *Blank* and *Cat* sensor was relatively maintained after exposure to BT with respect to BSA and PEA tests (Section 4.16 and 4.17). The use of BT is the closest method achievable *in-vitro* to mimic physiological conditions.

An examination of sensor characteristics following implantation was discussed in Section 4.20. It was determined that post *in-vivo* sensitivity and selectivity characteristics of the dual sensor could not be reliably obtained due to the unavoidable structural damage inflicted on the PPD based sensor design during explantation of these sensors (Section 4.20).

The *in-vitro* characterisation of the paired catalase-based H<sub>2</sub>O<sub>2</sub> sensor was verified and the *in-vivo* characterisation of this sensor design is shown in Chapter 5.

## References

- Avshalumov MV, Chen BT, Koos T, Tepper JM & Rice ME. (2005). Endogenous hydrogen peroxide regulates the excitability of midbrain dopamine neurons via ATP-sensitive potassium channels. *Journal of Neuroscience* **25**, 4222-4231.
- Bao L, Avshalumov MV, Patel JC, Lee CR, Miller EW, Chang CJ & Rice ME. (2009). Mitochondria Are the Source of Hydrogen Peroxide for Dynamic Brain-Cell Signaling. *Journal of Neuroscience* **29**, 9002-9010.
- Bolger FB. (2007). The *In-Vitro* and *In-Vivo* Characterisation and Application of Real-Time Sensors and Biosensors for Neurochemical Studies of Brain Energy Metabolism., pp. 173-176. NUI Maynooth, PhD Thesis.
- Bolger FB, Bennett R & Lowry JP. (2011). An *in vitro* characterisation comparing carbon paste and Pt microelectrodes for real-time detection of brain tissue oxygen. *Analyst* **136**, 4028-4035.
- Brown FO, Finnerty NJ & Lowry JP. (2009). Nitric oxide monitoring in brain extracellular fluid: characterisation of Nafion<sup>®</sup>-modified Pt electrodes *in vitro* and *in vivo*. *Analyst* **134**, 2012-2020.
- Brown FO & Lowry JP. (2003). Microelectrochemical sensors for *in vivo* brain analysis: an investigation of procedures for modifying Pt electrodes using Nafion<sup>®</sup>. *Analyst* **128**, 700-705.
- Bungay PM, Newton-Vinson P, Isele W, Garris PA & Justice JB. (2003). Microdialysis of dopamine interpreted with quantitative model incorporating probe implantation trauma. *Journal of Neurochemistry* **86**, 932-946.
- Chen BT & Rice ME. (1999). Calibration factors for cationic and anionic neurochemicals at carbon-fiber microelectrodes are oppositely affected by the presence of Ca<sup>2+</sup> and Mg<sup>2+</sup>. *Electroanalysis* **11**, 344-348.
- Finnerty NJ, O'Riordan SL, Brown FO, Serra PA, O'Neill RD & Lowry JP. (2012). *In vivo* characterisation of a Nafion<sup>®</sup>-modified Pt electrode for real-time nitric oxide monitoring in brain extracellular fluid. *Analytical Methods* **4**, 550-557.
- Garguilo MG & Michael AC. (1994). Quantitation of choline in the extracellular fluid of brain-tissue with amperometric microsensors. *Analytical Chemistry* **66**, 2621-2629.
- Gerhardt GA & Hoffman AF. (2001). Effects of recording media composition on the responses of Nafion-coated carbon fiber microelectrodes measured using high-speed chronoamperometry. *Journal of Neuroscience Methods* **109**, 13-21.

- Hu YB, Mitchell KM, Albahadily FN, Michaelis EK & Wilson GS. (1994). Direct measurement of glutamate release in the brain using a dual enzyme-based electrochemical sensor. *Brain Research* **659**, 117-125.
- Hyslop PA, Zhang ZY, Pearson DV & Phebus LA. (1995). Measurement of striatal H<sub>2</sub>O<sub>2</sub> by microdialysis following global forebrain ischemia and reperfusion in the rat - correlation with the cytotoxic potential of H<sub>2</sub>O<sub>2</sub> in-vitro. *Brain Research* **671**, 181-186.
- Khan AS & Michael AC. (2003). Invasive consequences of using micro-electrodes and microdialysis probes in the brain. *TrAC Trends in Analytical Chemistry* **22**, 503-508.
- Kulagina NV & Michael AC. (2003). Monitoring hydrogen peroxide in the extracellular space of the brain with amperometric microsensors. *Analytical Chemistry* **75**, 4875-4881.
- Lei BP, Adachi N & Arai T. (1997). The effect of hypothermia on H<sub>2</sub>O<sub>2</sub> production during ischemia and reperfusion: A microdialysis study in the gerbil hippocampus. *Neuroscience Letters* **222**, 91-94.
- Lei BP, Adachi N & Arai T. (1998). Measurement of the extracellular H<sub>2</sub>O<sub>2</sub> in the brain by microdialysis. *Brain Research Protocols* **3**, 33-36.
- Li X, Liu Y, Zhu A, Luo Y, Deng Z & Tian Y. (2010). Real-Time Electrochemical Monitoring of Cellular H<sub>2</sub>O<sub>2</sub> Integrated with In Situ Selective Cultivation of Living Cells Based on Dual Functional Protein Microarrays at Au-TiO(2) Surfaces. *Analytical Chemistry* **82**, 6512-6518.
- Lowry JP, McAteer K, Elatrash SS, Duff A & O'Neill RD. (1994). Characterisation of glucose oxidase-modified poly(phenylenediamine)-coated electrodes *in-vitro* and *in-vivo*: homogeneous interference by ascorbic acid in hydrogen-peroxide detection. *Analytical Chemistry* **66**, 1754-1761.
- Lowry JP & O'Neill RD. (1992). Homogenous mechanism of ascorbic-acid interference in hydrogen-peroxide detection at enzyme-modified electrodes. *Analytical Chemistry* **64**, 453-456.
- Lowry JP, O'Neill RD, Boutelle MG & Fillenz M. (1998). Continuous monitoring of extracellular glucose concentrations in the striatum of freely moving rats with an implanted glucose biosensor. *Journal of Neurochemistry* **70**, 391-396.
- McAteer K & O'Neill RD. (1996). Strategies for decreasing ascorbate interference at glucose oxidase-modified poly(*o*-phenylenediamine)-coated electrodes. *Analyst* **121**.

- Miele M, Boutelle MG & Fillenz M. (1994). The physiologically induced release of ascorbate in rat-brain is dependent on impulse traffic, calcium influx and glutamate uptake. *Neuroscience* **62**, 87-91.
- Miele M & Fillenz M. (1996). *In vivo* determination of extracellular brain ascorbate. *Journal of Neuroscience Methods* **70**, 15-19.
- O'Brien KB, Killoran SJ, O'Neill RD & Lowry JP. (2007). Development and characterization *in vitro* of a catalase-based biosensor for hydrogen peroxide monitoring. *Biosensors & Bioelectronics* **22**, 2994-3000.
- O'Neill RD. (1993). Sensor-tissue interactions in neurochemical analysis with carbon paste electrodes *in vivo*. *Analyst* **118**, 433-438.
- O'Neill RD & Lowry JP. (1995). On the significance of brain extracellular uric acid detected with *in-vivo* monitoring techniques: A review. *Behavioural Brain Research* **71**, 33-49.
- O'Neill RD & Lowry JP. (2000). Voltammetry *In Vivo* for Chemical Analysis of the Living Brain. In *Encyclopedia of Analytical Chemistry*. John Wiley & Sons, Ltd.
- O'Neill RD, Lowry JP, Rocchitta G, McMahon CP & Serra PA. (2008). Designing sensitive and selective polymer/enzyme composite biosensors for brain monitoring *in vivo*. *Trac-Trends in Analytical Chemistry* **27**, 78-88.
- Park JK, Tran PH, Chao JKT, Ghodadra R, Rangarajan R & Thakor NV. (1998). *In vivo* nitric oxide sensor using non-conducting polymer-modified carbon fiber. *Biosensors & Bioelectronics* **13**, 1187-1195.
- Rice ME. (2011). H<sub>2</sub>O<sub>2</sub>: A Dynamic Neuromodulator. *Neuroscientist* **17**, 389-406.
- Ryan MR, Lowry JP & Oneill RD. (1997). Biosensor for neurotransmitter L-glutamic acid designed for efficient use of L-glutamate oxidase and effective rejection of interference. *Analyst* **122**, 1419-1424.
- Sanford AL, Morton SW, Whitehouse KL, Oara HM, Lugo-Morales LZ, Roberts JG & Sombors LA. (2010). Voltammetric Detection of Hydrogen Peroxide at Carbon Fiber Microelectrodes. *Analytical Chemistry* **82**, 5205-5210.
- Simonian NA & Coyle JT. (1996). Oxidative stress in neurodegenerative diseases. *Annual Review of Pharmacology and Toxicology* **36**, 83-106.
- Turner RFB, Harrison DJ & Rajotte RV. (1991). Preliminary *in vivo* biocompatibility studies on perfluorosulfonic acid polymer membranes for biosensor applications. *Biomaterials* **12**, 361-368.

Wisniewski N, Moussy F & Reichert WM. (2000). Characterization of implantable biosensor membrane biofouling. *Fresenius Journal of Analytical Chemistry* **366**, 611-621.

---

**5. *In-vivo* characterisation of a paired  
catalase-based H<sub>2</sub>O<sub>2</sub> biosensor**

---

## 5.1 Introduction

The *in-vitro* characterisation of the paired hydrogen peroxide (H<sub>2</sub>O<sub>2</sub>) catalase-based sensor has been demonstrated in the previous Chapter. This chapter outlines the characterisation of the dual H<sub>2</sub>O<sub>2</sub> sensor design in the biological environment. The paired H<sub>2</sub>O<sub>2</sub> sensor was implanted into the brain of Wistar rats. The effect of local and systemic administration of known inducers and inhibitors of H<sub>2</sub>O<sub>2</sub> on the performance of the dual H<sub>2</sub>O<sub>2</sub> sensor response is investigated in this chapter.

A variation between an electrochemical sensor's characteristics observed *in-vitro* can often be seen *in-vivo*. Commonly, a discrepancy in the characteristics of the sensor can be seen when utilised in the biological milieu (O'Neill, 1993). This observed variation is attributable to factors inherent to a complex physiological environment such as the brain. Brain tissue consists of lipids and proteins which may affect the properties of the sensor *in-vivo* (Garguilo & Michael, 1994). The reaction of the body to the presence of a foreign object can also negatively affect the properties of a sensor (Wisniewski *et al.*, 2000). Mass transport of the analyte to an electrochemical sensor may also be restricted by the brain tissue itself (Cheng *et al.*, 1979; Dayton *et al.*, 1983).

Additionally, potential interferent species are present in the brain, principally ascorbic acid (AA) which can fluctuate under certain circumstances (Miele *et al.*, 1994; Miele & Fillenz, 1996). It is therefore necessary to investigate the function of the dual H<sub>2</sub>O<sub>2</sub> sensor when utilised in the biological environment. Various procedures outlined in this chapter were used to establish sensitivity, selectivity and stability of the catalase-based H<sub>2</sub>O<sub>2</sub> sensor when implanted in the brain.

Currently few methods exist to detect H<sub>2</sub>O<sub>2</sub> in the brain, most of these methods rely on the use of microdialysis (Lei *et al.*, 1997, 1998) which suffers from poor temporal and spatial resolution. Electrochemical methods have an advantageous distinction in that they provide long-term real-time measurements of neurochemical species of interest. The detection of H<sub>2</sub>O<sub>2</sub> in the anaesthetised animal has been previously reported (Kulagina & Michael, 2003), however the sensor described in this publication requires a

mediator and an additional method to remove interference from AA; which is not required with the dual H<sub>2</sub>O<sub>2</sub> sensor presented in this work.

H<sub>2</sub>O<sub>2</sub> is a reactive oxygen species (ROS) which has recently been indicated to act as a neuromodulator (Rice, 2011) and as a signalling molecule (Stone & Yang, 2006). Synaptic dopamine release has been shown to be regulated by H<sub>2</sub>O<sub>2</sub>. Avshalumov and Bao have investigated the effect of exogenously applied and endogenously altered H<sub>2</sub>O<sub>2</sub> on the evoked production of dopamine in *ex-vivo* brain slices (Avshalumov *et al.*, 2003; Bao *et al.*, 2009). H<sub>2</sub>O<sub>2</sub> is neutral and membrane permeable and it is also a relatively stable ROS which makes it suitable as a diffusible signalling molecule (Rice, 2011).

H<sub>2</sub>O<sub>2</sub> is implicated in a variety of normal cellular functions and also in the pathophysiology of disease states (Andersen, 2004; Rhee, 2006). An over production of ROS/H<sub>2</sub>O<sub>2</sub> has been implicated in neurodegenerative diseases such as Parkinson's and Alzheimer's disease (Valko *et al.*, 2007; Melo *et al.*, 2011). Additionally, many biosensors rely on the detection of enzymatically produced H<sub>2</sub>O<sub>2</sub> to measure substrates such as glucose (Lowry *et al.*, 1998b), choline (Garguilo & Michael, 1996) and glutamate (Hu *et al.*, 1994) in the brain.

As H<sub>2</sub>O<sub>2</sub> is implicated in a number of neurochemical processes and electrochemical analytical techniques the real-time detection of H<sub>2</sub>O<sub>2</sub> *in-vivo* would provide a major advancement in the field of neurochemistry.

## 5.2 Experimental

The instrumentation, chemicals, solutions and software used in this section are described in detail in Chapter 3. Details of the manufacture of the working electrodes are outlined in Section 3.4. All experiments outlined in this chapter were performed using Constant Potential Amperometry (CPA). A potential of +700 mV *vs.* Ag wire (see Section 3.10.3) was applied to the working electrodes for all *in-vivo* experiments.

Chronic *in-vivo* experiments were carried out in freely-moving animals where long-term recordings were obtained and this protocol is discussed in Section 3.10. An alternative experimental procedure was utilised to obtain acute *in-vivo* data which is derived from

short-term recordings. A similar protocol to the chronic preparation is used to conduct an acute experiment. However acute experiments were carried out over a shorter time frame while the animal is under anaesthesia and held in the stereotaxic frame. The same protocol for implantation of the catalase-based paired H<sub>2</sub>O<sub>2</sub> sensor was followed for chronic and acute *in-vivo* experiments. The catalase-based paired H<sub>2</sub>O<sub>2</sub> sensor was glued to a microdialysis probe and the entire construct was implanted into the striatum of a male Wistar rat.

The number of implanted dual catalase-based H<sub>2</sub>O<sub>2</sub> sensors is denoted by (n) i.e. a *Blank* and a *Cat* sensor in the same number of animals. In the case where the number of administrations included in the data exceeds the number of sensors/animals the value is given and denoted by (adm).

The average data is represented as a Mean  $\pm$  SEM. The maximum current response was used to analyse the response to the addition of each perfusate and the administration of each physiologically relevant substance. Reported *in-vivo* H<sub>2</sub>O<sub>2</sub> concentration changes are based on the average *in-vitro* pre-implantation calibration data.

Statistical analysis was carried out using paired or unpaired t-tests. One-way ANOVA was used to simultaneously compare results which contained more than two separate groups. These tests were performed using Graphpad Prism and gave a probability value (*P*) which indicates the level of significant or non-significant difference between groups. *P* > 0.05, denotes no significant difference. The extent of significant difference is divided into three parameters (*P* < 0.05,\*), (*P* < 0.01,\*\*) and (*P* < 0.0001,\*\*\*) from the lowest relative level of difference (\*) to the highest (\*\*\*).

### 5.3 Local and systemic control experiments (freely-moving)

The data displayed in this section was obtained from freely-moving male Wistar rats. This section outlines the control experiments conducted in freely-moving animals. The effect of the local perfusion of artificial cerebrospinal fluid (aCSF) and the systemic administration of saline on the H<sub>2</sub>O<sub>2</sub> sensor response is described here. The effect of the local administration of H<sub>2</sub>O<sub>2</sub> and the addition of substances of interest to the perfusate on the paired H<sub>2</sub>O<sub>2</sub> sensor response may be compared against the local addition of aCSF (Section 5.3.1). The effect of systemic administration of various physiologically relevant substances on the paired H<sub>2</sub>O<sub>2</sub> sensor response may be compared against that observed upon systemic administration of saline (Section 5.3.2).

#### 5.3.1 Local aCSF Administration

As a control experiment aCSF was perfused through the microdialysis (MD) probe. A typical example of the outcome of this perfusion on the paired catalase-based H<sub>2</sub>O<sub>2</sub> sensor response is shown below in Figure 5.3.1.

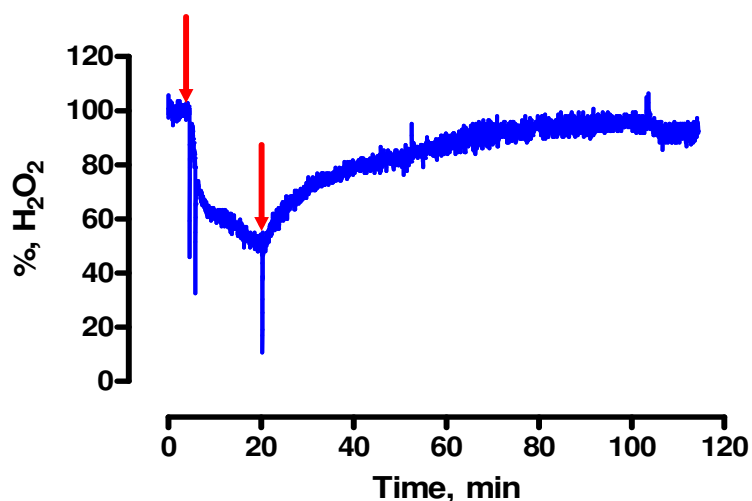


**Figure 5.3.1** A typical example of an aCSF perfusion detected by the paired H<sub>2</sub>O<sub>2</sub> sensor implanted in the striatum of a freely-moving Wistar rat. The arrows indicate the duration of the perfusion.

An immediate decrease in H<sub>2</sub>O<sub>2</sub> signal is apparent upon commencement of the aCSF perfusion. A decrease of  $-361.6 \pm 161.7$  pA ( $n = 3$ ) was observed which corresponds to a concentration change of  $-775.2 \pm 346.6$  nM H<sub>2</sub>O<sub>2</sub> ( $n = 3$ ). The aCSF perfusion decreased

the H<sub>2</sub>O<sub>2</sub> sensor response to  $58.5 \pm 6.2$  % (n = 3) of basal levels following  $13.3 \pm 0.2$  mins (n = 3) from the start of each perfusion. A return to a baseline level is apparent after  $70.2 \pm 5.5$  mins (n = 3). No significant difference ( $P > 0.05$ ) was observed between the pre-perfusion baseline  $823.3 \pm 297.3$  pA (n = 3) and the post-perfusion baseline  $790.7 \pm 283.2$  pA (n = 3). The decrease observed here is due to diffusion of H<sub>2</sub>O<sub>2</sub> through the microdialysis membrane and into the dialysate thus reducing the concentration of H<sub>2</sub>O<sub>2</sub> surrounding the sensor. On cessation of the perfusion H<sub>2</sub>O<sub>2</sub> diffuses back in the extracellular fluid (ECF) towards the implanted sensor and hence an increase in H<sub>2</sub>O<sub>2</sub> signal is observed. The response recorded here was used as a control against which various perfusions which were carried out in freely-moving animals were compared in this chapter.

| Analyte | Current change (pA) | Baseline change (%) | Conc. change (nM)  | Max response (mins) | Return (mins)  | Pre-perfusion baseline (pA) | Post-perfusion baseline (pA) |
|---------|---------------------|---------------------|--------------------|---------------------|----------------|-----------------------------|------------------------------|
| aCSF    | $-361.6 \pm 161.7$  | $58.5 \pm 6.2$      | $-775.2 \pm 346.6$ | $13.3 \pm 0.2$      | $70.2 \pm 5.5$ | $823.3 \pm 297.3$           | $790.7 \pm 283.2$            |

Table 5.3.1: Summary of results obtained on perfusion of aCSF. Data obtained from 3 paired H<sub>2</sub>O<sub>2</sub> sensors implanted in the striatum of 3 Wistar rats.

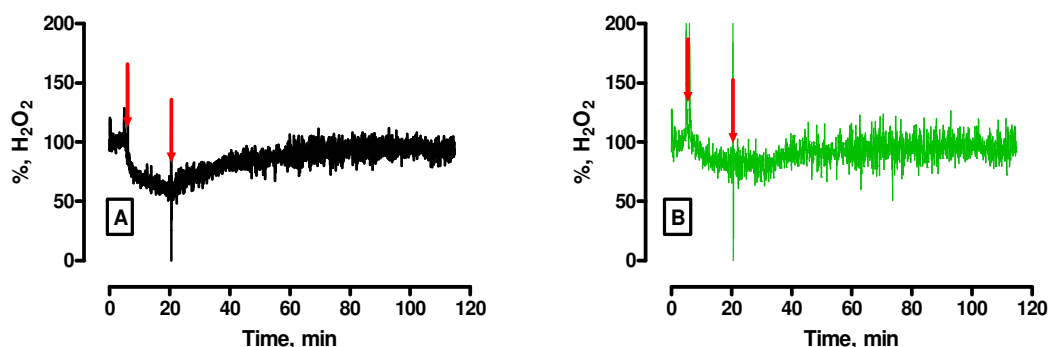


Figure 5.3.1.1 A typical example of an aCSF perfusion detected by (A) *Blank* sensor and (B) *Cat* sensor; implanted in the striatum of a Wistar rat. The arrows indicate the duration of the perfusion.

An immediate decrease in response by the *Blank* (A) and *Cat* (B) sensor is apparent upon perfusion of aCSF as can be seen in Figure 5.3.1.1 A decrease in current was observed at the *Blank* sensor of  $-467.4 \pm 163.1$  pA ( $n = 3$ ) and a decrease was also observed at the *Cat* sensor of  $-105.3 \pm 18.1$  pA ( $n = 3$ ). The aCSF perfusion causes a decrease in current response detected by the *Blank* sensor to  $66.7 \pm 3.8$  % ( $n = 3$ ) of basal levels following  $13.3 \pm 0.2$  mins ( $n = 3$ ) from the start of each perfusion. Similarly a decrease in response was detected by the *Cat* sensor ( $84.6 \pm 2.8$  %,  $n = 3$ ). A return to a baseline level is apparent subsequently which was complete on both sensor types after  $70.2 \pm 5.5$  mins ( $n = 3$ ). No significant difference ( $P > 0.05$ ) was observed between the pre-perfusion baseline and the post-perfusion baseline of the *Cat* and *Blank* sensor. Additionally, no significant difference ( $P > 0.05$ ) was seen between the maximum current response of the *Cat* and *Blank* sensor.

| <b>aCSF</b>  | <b>Current change (pA)</b> | <b>Baseline change (%)</b> | <b>Max response (mins)</b> | <b>Return (mins)</b> | <b>Pre-perfusion baseline (pA)</b> | <b>Post-perfusion baseline (pA)</b> |
|--------------|----------------------------|----------------------------|----------------------------|----------------------|------------------------------------|-------------------------------------|
| <i>Blank</i> | $-467.4 \pm 163.1$         | $66.7 \pm 3.8$             | $13.3 \pm 0.2$             | $70.2 \pm 5.5$       | $1341.3 \pm 323.5$                 | $1272.4 \pm 317.3$                  |
| <i>Cat</i>   | $-105.3 \pm 18.1$          | $84.6 \pm 2.8$             | -                          | -                    | $518 \pm 35.7$                     | $481.5 \pm 37.9$                    |

**Table 5.3.1.1: Summary of results obtained on perfusion of aCSF. Data obtained from 3 paired H<sub>2</sub>O<sub>2</sub> sensors implanted in the striatum of 3 Wistar rats.**

### 5.3.2 Systemic (s.c.) Saline Administration

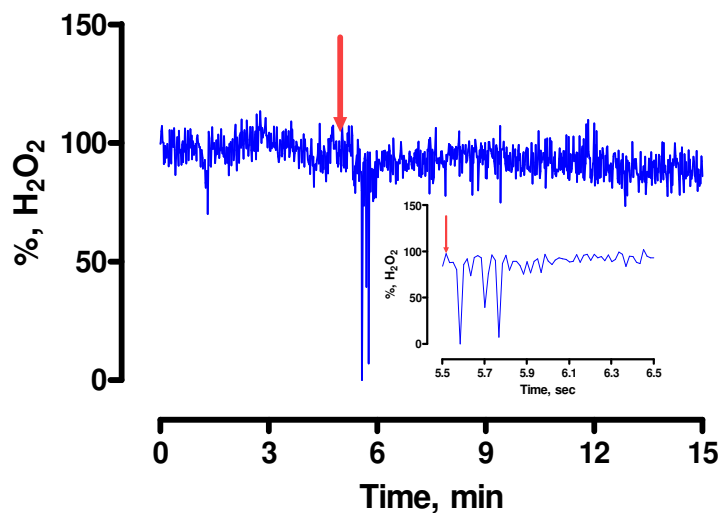


**Figure 5.3.2** A typical example of a 2 mL/kg s.c. injection of saline detected by the paired  $H_2O_2$  sensor implanted in the striatum of a freely-moving Wistar rat. The arrow indicates the point of administration. Inset: Initial 60 sec of response.

As a control experiment saline (Section 3.3.3.2) was administered subcutaneously (s.c.) (Section 3.11.2) and the effect on the  $H_2O_2$  signal was measured. Immediately following the injection a brief fluctuation in  $H_2O_2$  response is observed which is due to the physical manipulation of the subject. A small increase was observed ( $155.3 \pm 123.9$  pA,  $n = 3$ ) following  $7.9 \pm 0.9$  mins ( $n = 3$ ) and a return to a steady baseline was recorded after  $12.7 \pm 0.4$  mins ( $n = 3$ ). The purpose of the experiments shown in this section is to demonstrate the response observed which is attributed to the injection itself. The administration of various substances in this manner (s.c.) may be compared against the saline response. It is clear that a transient fluctuation in  $H_2O_2$  signal is observed following injection of saline and quickly returns to a baseline level. The immediate brief response due to the injection is demonstrated by the inset graph in Figure 5.3.2. No significant difference ( $P > 0.05$ ) was observable between the pre and post-injection baseline levels. No lasting effect on the  $H_2O_2$  response can be seen following saline administration.

| Analyte | Current change (pA) | Change (%) | Conc. change (nM) | Max response (mins) | Return (mins) | Pre-injection baseline (pA) | Post-injection baseline (pA) |
|---------|---------------------|------------|-------------------|---------------------|---------------|-----------------------------|------------------------------|
| Saline  | 155.3 ± 123.9       | 1.0 ± 4.4  | 69.3 ± 55.3       | 7.9 ± 0.9           | 12.7 ± 0.4    | 842.6 ± 749.9               | 1390.2 ± 699.9               |

Table 5.3.2: Summary of results obtained on injection of saline. Data obtained from 3 paired H<sub>2</sub>O<sub>2</sub> sensors implanted in the striatum of 3 Wistar rats.

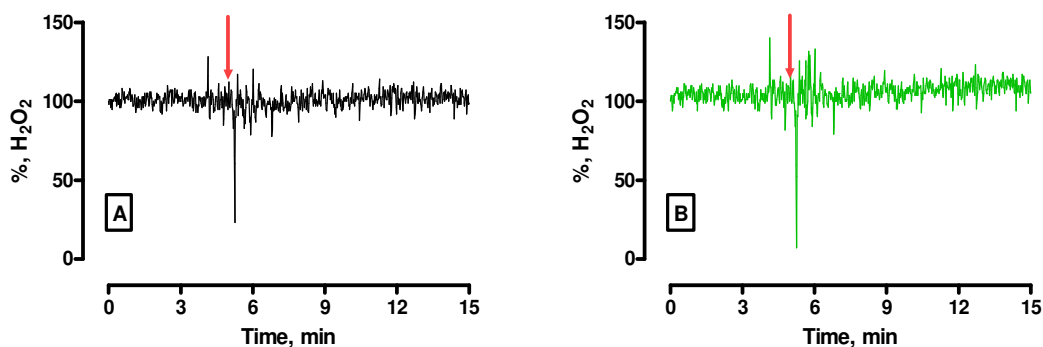


Figure 5.3.2.1 A typical example of a 2 ml/kg s.c. injection of saline detected by (A) *Blank* sensor and (B) *Cat* sensor; implanted in the striatum of a Wistar rat. The arrow indicates the point of administration.

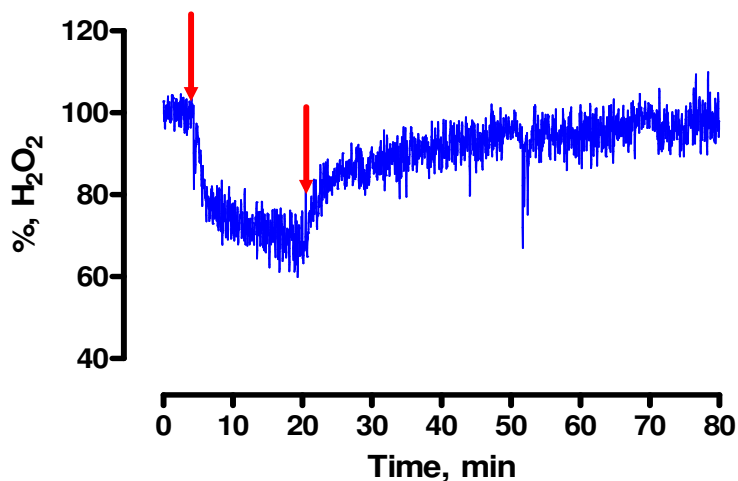
A brief fluctuation in response by the *Blank* (A) and *Cat* (B) sensor is apparent immediately following the injection of saline as can be seen in Figure 5.3.2. A small increase in current was observed at the *Blank* sensor of  $79.4 \pm 68.1$  pA ( $n = 3$ ) and a similar change was observed at the *Cat* sensor of  $10.1 \pm 21.7$  pA ( $n = 3$ ). No significant difference ( $P > 0.05$ ) was observed between the pre-injection baseline and the post-injection baseline of the *Cat* and *Blank* sensor. Additionally, no significant difference ( $P > 0.05$ ) was seen between the maximum current response of the *Cat* and *Blank* sensor.

| <b>Saline</b> | <b>Current change (pA)</b> | <b>Change (%)</b> | <b>Max response (mins)</b> | <b>Return (mins)</b> | <b>Pre-injection baseline (pA)</b> | <b>Post-injection baseline (pA)</b> |
|---------------|----------------------------|-------------------|----------------------------|----------------------|------------------------------------|-------------------------------------|
| <i>Blank</i>  | 79.4 ± 68.1                | 3.0 ± 2.2         | 7.9 ± 0.9                  | 12.7 ± 0.4           | 2176.6 ± 595.2                     | 2240.6 ± 636.6                      |
| <i>Cat</i>    | 10.1 ± 21.7                | 2.2 ± 3.0         | -                          | -                    | 818.2 ± 137.7                      | 850.4 ± 130.7                       |

**Table 5.3.2.1: Summary of results obtained on injection of saline. Data obtained from 3 paired H<sub>2</sub>O<sub>2</sub> sensors implanted in the striatum of 3 Wistar rats.**

#### **5.4 Local H<sub>2</sub>O<sub>2</sub> Administration (freely-moving)**

This section demonstrates the response of the paired H<sub>2</sub>O<sub>2</sub> sensor to the local perfusion of various concentrations of H<sub>2</sub>O<sub>2</sub> in freely-moving animals. The experimental condition utilised here is otherwise termed as a chronic preparation. The animal is allowed to recover from anaesthetic (Section 3.10) prior to commencement of experiments in order to enable long-term recording of the analyte of interest. Various concentrations of H<sub>2</sub>O<sub>2</sub> were added to the perfusate in order to examine the response of the H<sub>2</sub>O<sub>2</sub> sensor in the *in-vivo* environment (Section 3.3.2.2). The vehicle used for perfusion of each concentration of substrate was aCSF. The response of the dual sensor to each dilution of H<sub>2</sub>O<sub>2</sub> was compared against aCSF as shown in Figure 5.3.1. The method utilised to deliver the target substrate to the implanted paired H<sub>2</sub>O<sub>2</sub> sensor is termed retrodialysis (RD) as discussed in Section 2.9.

5.4.1 25  $\mu\text{M}$  H<sub>2</sub>O<sub>2</sub>

**Figure 5.4.1:** A typical example of a 25  $\mu\text{M}$  H<sub>2</sub>O<sub>2</sub> perfusion detected by the paired H<sub>2</sub>O<sub>2</sub> sensor implanted in the striatum of a freely-moving Wistar rat. The arrows indicate the duration of the perfusion.

An immediate decrease was observed on perfusion of 25  $\mu\text{M}$  H<sub>2</sub>O<sub>2</sub> (Figure 5.3.1). A decrease of  $-311.6 \pm 172.6$  pA ( $n = 2$ ) was recorded which corresponds to a concentration change of  $-668.0 \pm 370.0$  nM H<sub>2</sub>O<sub>2</sub> ( $n = 2$ ). The presence of 25  $\mu\text{M}$  H<sub>2</sub>O<sub>2</sub> in the perfusate caused a reduction in the paired sensor response to  $66.2 \pm 5.0$  % ( $n = 2$ ) of baseline levels which was observed after  $13.4 \pm 0.7$  mins ( $n = 2$ ). A subsequent return to a baseline level was observed which occurred  $66.1 \pm 3.1$  mins ( $n = 2$ ) following the start of the perfusion. The percentage change recorded here is quite similar to that observed on perfusion with aCSF (Figure 5.3.1) and was not significantly different  $P > 0.05$ . No significant difference ( $P > 0.05$ ) was observed between the baseline current pre-perfusion  $866 \pm 382.2$  pA ( $n = 2$ ) and the new post-perfusion basal level  $816.7 \pm 339.2$  pA ( $n = 2$ ).

| Analyte                                  | Current change (pA) | Baseline change (%) | Conc. change (nM)  | Max response (mins) | Return (mins)  | Pre-perfusion baseline (pA) | Post-perfusion baseline (pA) |
|--|---------------------|---------------------|--------------------|---------------------|----------------|-----------------------------|------------------------------|
| 25 $\mu$ M H <sub>2</sub> O <sub>2</sub> | -311.6 $\pm$ 172.6  | 66.2 $\pm$ 5.0      | -668.0 $\pm$ 370.0 | 13.4 $\pm$ 0.7      | 66.1 $\pm$ 3.1 | 866 $\pm$ 382.2             | 816.7 $\pm$ 339.2            |

Table 5.4.1: Summary of results obtained on perfusion of 25  $\mu$ M H<sub>2</sub>O<sub>2</sub>. Data obtained from 2 paired H<sub>2</sub>O<sub>2</sub> sensors implanted in the striatum of 2 Wistar rats.

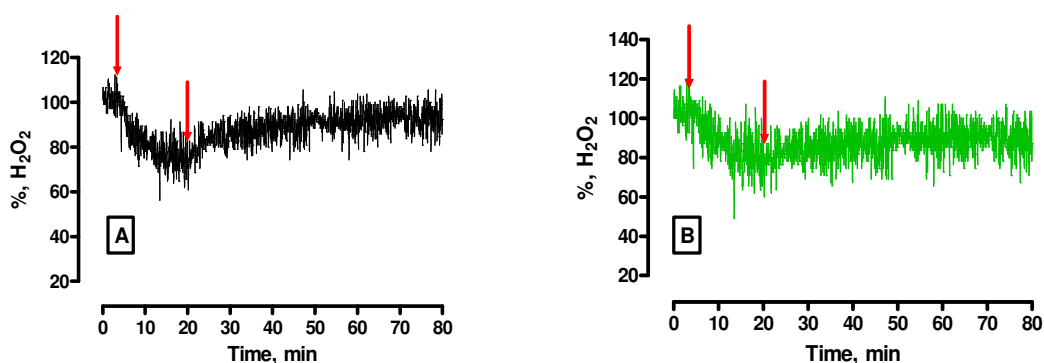


Figure 5.4.1.1: A typical example of a 25  $\mu$ M H<sub>2</sub>O<sub>2</sub> perfusion detected by (A) *Blank* sensor and (B) *Cat* sensor; implanted in the striatum of a Wistar rat. The arrows indicate the duration of the perfusion.

An immediate decrease in response by the *Blank* (A) and *Cat* (B) sensor can be seen following perfusion of 25  $\mu$ M H<sub>2</sub>O<sub>2</sub> (Figure 5.4.1.1). A decrease in current was observed at the *Blank* sensor of  $-414.0 \pm 158.7$  pA ( $n = 2$ ) and a similar decrease was observed at the *Cat* sensor of  $-102.4 \pm 13.9$  pA ( $n = 2$ ). No significant difference ( $P > 0.05$ ) was observed between the pre-perfusion baseline and the post-perfusion baseline of the *Cat* and *Blank* sensor. Additionally, no significant difference ( $P > 0.05$ ) was seen between the maximum current response of the *Cat* and *Blank* sensor.

| <b>25 <math>\mu</math>M<br/>H<sub>2</sub>O<sub>2</sub></b> | <b>Current<br/>change<br/>(pA)</b> | <b>Baseline<br/>change<br/>(%)</b> | <b>Max<br/>response<br/>(mins)</b> | <b>Return<br/>(mins)</b> | <b>Pre-<br/>perfusion<br/>baseline<br/>(pA)</b> | <b>Post-<br/>perfusion<br/>baseline<br/>(pA)</b> |
|--|------------------------------------|------------------------------------|------------------------------------|--------------------------|---|--|
| <i>Blank</i>   | -414.0 $\pm$<br>158.7              | 71.7 $\pm$ 3.9                     | 13.4 $\pm$ 0.7                     | 66.1 $\pm$ 3.1           | 1412.8 $\pm$<br>364.9                           | 1332.2 $\pm$<br>352.4                            |
| <i>Cat</i>   | -102.4 $\pm$<br>13.9               | 81.3 $\pm$ 1.9                     | -                                  | -                        | 546.9 $\pm$<br>17.4                             | 515.6 $\pm$<br>13.0                              |

**Table 5.3.1.1: Summary of results obtained on perfusion of 25  $\mu$ M H<sub>2</sub>O<sub>2</sub>. Data obtained from 2 paired H<sub>2</sub>O<sub>2</sub> sensors implanted in the striatum of 2 Wistar rats.**

#### 5.4.2 100 $\mu$ M H<sub>2</sub>O<sub>2</sub>

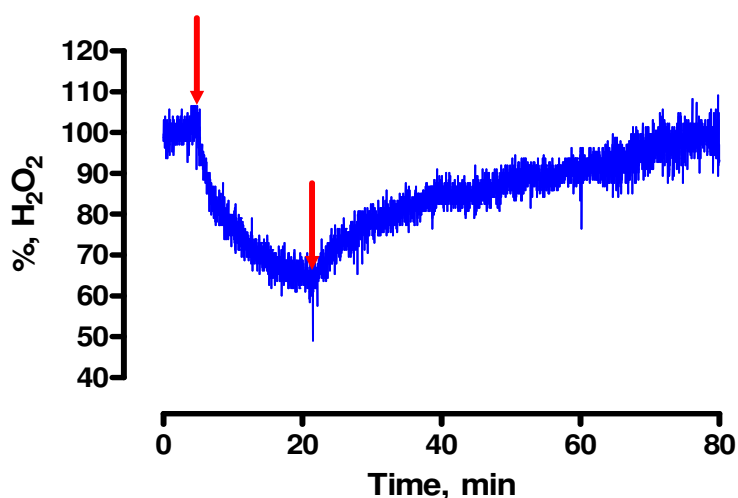


**Figure 5.4.2: A typical example of a 100  $\mu$ M H<sub>2</sub>O<sub>2</sub> perfusion detected by the paired H<sub>2</sub>O<sub>2</sub> sensor implanted in the striatum of a freely-moving Wistar rat. The arrows indicate the duration of the perfusion.**

A decrease was observed following the perfusion of 100  $\mu$ M H<sub>2</sub>O<sub>2</sub> to 71.8  $\pm$  5.3 % (n = 2) of basal levels as can be seen in Figure 5.4.2. A recorded decrease of -243.0  $\pm$  146.8 pA (n = 2) which corresponds to a concentration change of -520.8  $\pm$  314.6 nM H<sub>2</sub>O<sub>2</sub> (n = 2) was observed. The magnitude of this decrease is not as pronounced as that seen with perfusion of aCSF however no significant difference was observed ( $P > 0.05$ ). The maximum change observed here occurred 10.9  $\pm$  1.1 mins (n = 2) following the start of

the perfusion and returned to a baseline level  $45.5 \pm 3.0$  mins ( $n = 2$ ) subsequently. No significant difference ( $P > 0.05$ ) was observed between pre-perfusion and post-perfusion baseline levels. A summary of this data is provided in Table 5.4.2.

| Analyte                                   | Current change (pA) | Baseline change (%) | Conc. change (nM)  | Max response (mins) | Return (mins)  | Pre-perfusion baseline (pA) | Post-perfusion baseline (pA) |
|---|---------------------|---------------------|--------------------|---------------------|----------------|-----------------------------|------------------------------|
| 100 $\mu$ M H <sub>2</sub> O <sub>2</sub> | $-243.0 \pm 146.8$  | $71.8 \pm 5.3$      | $-520.8 \pm 314.6$ | $10.9 \pm 1.1$      | $45.5 \pm 3.0$ | $791.5 \pm 372.4$           | $756.7 \pm 281.6$            |

Table 5.4.2: Summary of results obtained on perfusion of 100  $\mu$ M H<sub>2</sub>O<sub>2</sub>. Data obtained from 2 paired H<sub>2</sub>O<sub>2</sub> sensors implanted in the striatum of 2 Wistar rats.

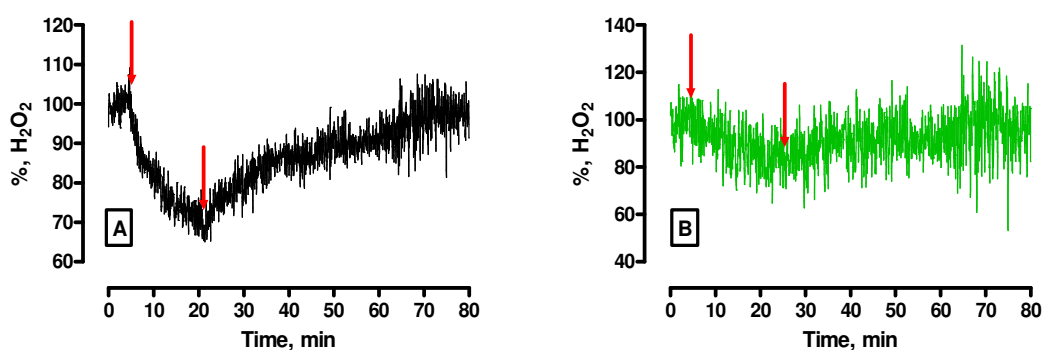


Figure 5.4.2.1: A typical example of a 100  $\mu$ M H<sub>2</sub>O<sub>2</sub> perfusion detected by (A) *Blank* sensor and (B) *Cat* sensor; implanted in the striatum of a Wistar rat. The arrows indicate the duration of the perfusion.

Figure 5.4.2.1 demonstrates the response of the *Blank* (A) and *Cat* (B) sensor following perfusion of 100  $\mu$ M H<sub>2</sub>O<sub>2</sub>. A clear decrease in current was observed at the *Blank* sensor of  $-414.0 \pm 158.7$  pA ( $n = 2$ ) and similarly a decrease was observed at the *Cat* sensor of  $-102.4 \pm 13.9$  pA ( $n = 2$ ). No significant difference ( $P > 0.05$ ) was observed between the pre-perfusion baseline and the post-perfusion baseline of the *Cat* and *Blank* sensor. Additionally, no significant difference ( $P > 0.05$ ) was observed between the maximum current response of the *Cat* and *Blank* sensor.

| <b>100 <math>\mu</math>M H<sub>2</sub>O<sub>2</sub></b> | <b>Current change (pA)</b> | <b>Baseline change (%)</b> | <b>Max response (mins)</b> | <b>Return (mins)</b> | <b>Pre-perfusion baseline (pA)</b> | <b>Post-perfusion baseline (pA)</b> |
|---|----------------------------|----------------------------|----------------------------|----------------------|------------------------------------|-------------------------------------|
| <i>Blank</i>  | -330.5 $\pm$ 120.8         | 75.0 $\pm$ 2.2             | 10.9 $\pm$ 1.1             | 45.5 $\pm$ 3.0       | 1291.8 $\pm$ 371.1                 | 756.7 $\pm$ 281.6                   |
| <i>Cat</i>  | -88.3 $\pm$ 26.6           | 82.4 $\pm$ 5.3             | -                          | -                    | 500.2 $\pm$ 1.0                    | 503.5 $\pm$ 47.7                    |

Table 5.4.2.1: Summary of results obtained on perfusion of 100  $\mu$ M H<sub>2</sub>O<sub>2</sub>. Data obtained from 2 paired H<sub>2</sub>O<sub>2</sub> sensors implanted in the striatum of 2 Wistar rats.

### 5.4.3 200 $\mu$ M H<sub>2</sub>O<sub>2</sub>

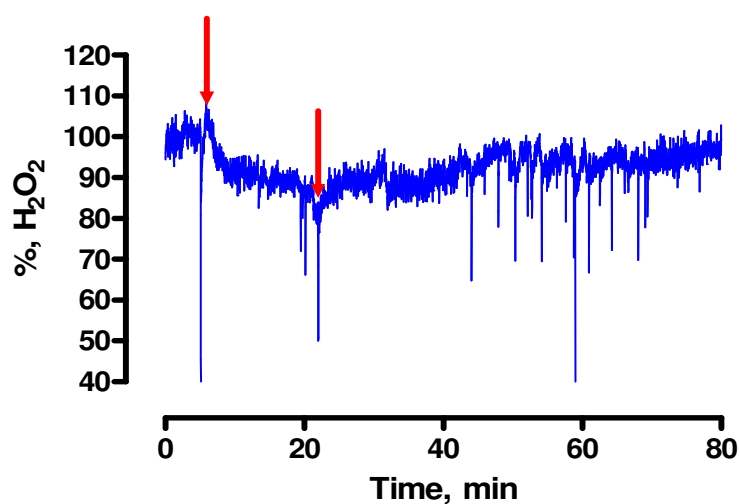


Figure 5.4.3: A typical example of a 200  $\mu$ M H<sub>2</sub>O<sub>2</sub> perfusion detected by the paired H<sub>2</sub>O<sub>2</sub> sensor implanted in the striatum of a freely-moving Wistar rat. The arrows indicate the duration of the perfusion.

As can be seen in Figure 5.4.3 a relatively small decrease in the paired sensor response was observed following perfusion of 200  $\mu$ M H<sub>2</sub>O<sub>2</sub> to 86.9  $\pm$  8.2 % (n = 3, 4adm). The percentage change observed here is significantly less (P < 0.05,\*) than the change observed in the control experiment with the perfusion of aCSF (Figure 5.3.1). A decrease of -179.7  $\pm$  91.5 pA (n = 3, 4adm) was observed which corresponds to a concentration change of -385.1  $\pm$  196.1 nM H<sub>2</sub>O<sub>2</sub> (n = 3, 4adm). The maximum change

recorded in this instance was seen  $11.8 \pm 0.7$  mins ( $n = 3$ , 4adm) from the start of the perfusion and returned  $59.1 \pm 4.2$  mins ( $n = 3$ , 4adm) after the initiation of the perfusion. No significant difference ( $P > 0.05$ ) was observed between pre-perfusion ( $1589.3 \pm 428.2$  pA,  $n = 3$ , 4adm) and post-perfusion H<sub>2</sub>O<sub>2</sub> levels ( $1389.7 \pm 302.4$  pA,  $n = 3$ , 4adm).

| Analyte                                   | Current change (pA) | Baseline change (%) | Conc. change (nM)  | Max response (mins) | Return (mins)  | Pre-perfusion baseline (pA) | Post-perfusion baseline (pA) |
|---|---------------------|---------------------|--------------------|---------------------|----------------|-----------------------------|------------------------------|
| 200 $\mu$ M H <sub>2</sub> O <sub>2</sub> | $-179.7 \pm 91.5$   | $86.9 \pm 8.2$      | $-385.1 \pm 196.1$ | $11.8 \pm 0.7$      | $59.1 \pm 4.2$ | $1589.3 \pm 428.2$          | $1389.7 \pm 302.4$           |

**Table 5.4.3: Summary of results obtained on perfusion of 200  $\mu$ M H<sub>2</sub>O<sub>2</sub>. Data obtained from 3 paired H<sub>2</sub>O<sub>2</sub> sensors implanted in the striatum of 3 Wistar rats. The average data includes 4 administrations.**

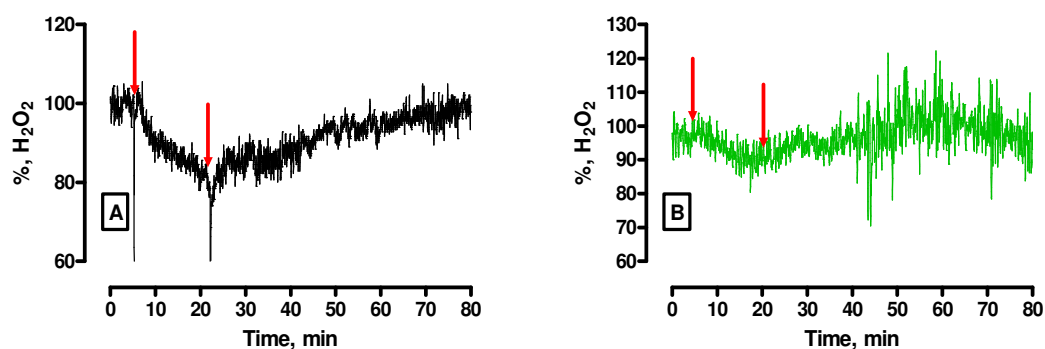


**Figure 5.4.3.1: A typical example of a 200  $\mu$ M H<sub>2</sub>O<sub>2</sub> perfusion detected by (A) *Blank* sensor and (B) *Cat* sensor; implanted in the striatum of a Wistar rat. The arrows indicate the duration of the perfusion.**

Figure 5.4.3.1 demonstrates the response of the *Blank* (A) and *Cat* (B) sensor following the addition of a higher concentration of H<sub>2</sub>O<sub>2</sub> to the perfusate (200  $\mu$ M). A clear decrease in current was observed at the *Blank* sensor of  $-237.5 \pm 94.1$  pA ( $n = 3$ , 4ad) and a decrease was also observed at the *Cat* sensor ( $-57.9 \pm 28.0$  pA,  $n = 3$ , 4ad). No significant difference ( $P > 0.05$ ) was observed between the pre-perfusion baseline and

the post-perfusion baseline of the *Cat* and *Blank* sensor. Additionally, no significant difference ( $P > 0.05$ ) was observed between the maximum current response of the *Cat* and *Blank* sensor.

| <b>200 <math>\mu</math>M H<sub>2</sub>O<sub>2</sub></b> | <b>Current change (pA)</b> | <b>Baseline change (%)</b> | <b>Max response (mins)</b> | <b>Return (mins)</b> | <b>Pre-perfusion baseline (pA)</b> | <b>Post-perfusion baseline (pA)</b> |
|---|----------------------------|----------------------------|----------------------------|----------------------|------------------------------------|-------------------------------------|
| <i>Blank</i>  | $-237.5 \pm 94.1$          | $87.3 \pm 6.2$             | $11.8 \pm 0.7$             | $59.1 \pm 4.2$       | $2045.0 \pm 381.0$                 | $1853.3 \pm 261.0$                  |
| <i>Cat</i>  | $-57.9 \pm 28.0$           | $89.2 \pm 3.7$             | -                          | -                    | $455.7 \pm 77.9$                   | $463.6 \pm 75.0$                    |

**Table 5.4.3.1:** Summary of results obtained on perfusion of 200  $\mu$ M H<sub>2</sub>O<sub>2</sub>. Data obtained from 3 paired H<sub>2</sub>O<sub>2</sub> sensors implanted in the striatum of 3 Wistar rats. The average data includes 4 administrations.

#### 5.4.4 500 $\mu$ M H<sub>2</sub>O<sub>2</sub>

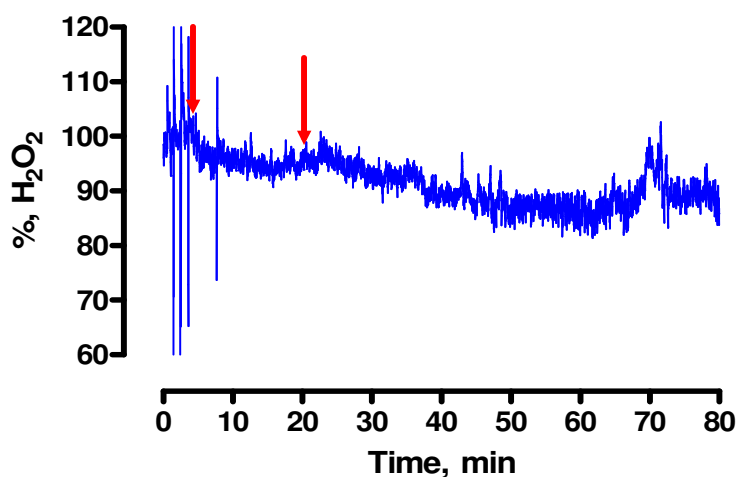


**Figure 5.4.4:** A typical example of a 500  $\mu$ M H<sub>2</sub>O<sub>2</sub> perfusion detected by the paired H<sub>2</sub>O<sub>2</sub> sensor implanted in the striatum of a freely-moving Wistar rat. The arrows indicate the duration of the perfusion.

As can be seen in Figure 5.4.4 a minor decrease in the paired catalase-based sensor response was observed on perfusion of 500  $\mu$ M H<sub>2</sub>O<sub>2</sub> to  $91.8 \pm 2.6$  % ( $n = 2$ , 3ad). A current decrease of  $-127.8 \pm 35.0$  pA ( $n = 2$ , 3ad) was recorded and this value

corresponds to a concentration change of  $-274.0 \pm 75.0$  nM H<sub>2</sub>O<sub>2</sub> (n = 2, 3ad). The maximum change in signal was observed  $12.2 \pm 0.7$  mins (n = 2, 3ad) following commencement of the perfusion and returned to a steady baseline  $70.5 \pm 2.7$  mins (n = 2, 3ad) after the perfusion. The change in H<sub>2</sub>O<sub>2</sub> signal observed here was significantly different ( $P < 0.01, **$ ) from that observed on perfusion of aCSF. No significant difference ( $P > 0.05$ ) was observed between pre-perfusion ( $1834.9 \pm 765.3$  pA, n = 2, 3ad) and post-perfusion H<sub>2</sub>O<sub>2</sub> levels ( $1748.3 \pm 697.1$  pA, n = 2, 3ad).

| Analyte                                   | Current change (pA) | Baseline change (%) | Conc. change (nM) | Max response (mins) | Return (mins)  | Pre-perfusion baseline (pA) | Post-perfusion baseline (pA) |
|---|---------------------|---------------------|-------------------|---------------------|----------------|-----------------------------|------------------------------|
| 500 $\mu$ M H <sub>2</sub> O <sub>2</sub> | $-127.8 \pm 35.0$   | $91.8 \pm 2.6$      | $-274.0 \pm 75.0$ | $12.2 \pm 0.7$      | $70.5 \pm 2.7$ | $1834.9 \pm 765.3$          | $1748.3 \pm 697.1$           |

**Table 5.4.4: Summary of results obtained on perfusion of 500  $\mu$ M H<sub>2</sub>O<sub>2</sub>. Data obtained from 2 paired H<sub>2</sub>O<sub>2</sub> sensors implanted in the striatum of 2 Wistar rats. The average data includes 3 administrations.**

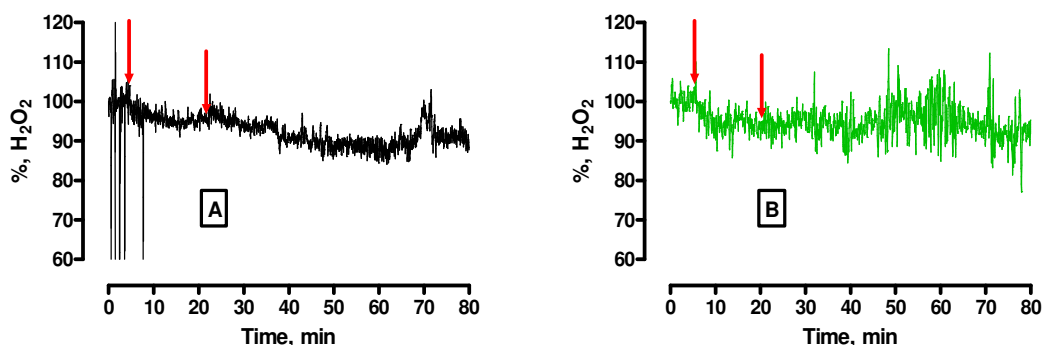


**Figure 5.4.4.1: A typical example of a 500  $\mu$ M H<sub>2</sub>O<sub>2</sub> perfusion detected by (A) *Blank* sensor and (B) *Cat* sensor; implanted in the striatum of a Wistar rat. The arrows indicate the duration of the perfusion.**

The response of the *Blank* (A) and *Cat* (B) sensor following perfusion of 500  $\mu$ M H<sub>2</sub>O<sub>2</sub> is demonstrated in Figure 5.4.4.1. A relatively small decrease in current was recorded by the *Blank* sensor of  $-166.7 \pm 36.3$  pA (n = 2, 3ad) and a minor deviation from baseline

level was recorded by the *Cat* sensor ( $-39.1 \pm 71.5$  pA,  $n = 2$ , 3ad). No significant difference ( $P > 0.05$ ) was observed between the pre-perfusion baseline and the post-perfusion baseline of the *Cat* and *Blank* sensor. Additionally, no significant difference ( $P > 0.05$ ) was observed between the maximum current response of the *Cat* and *Blank* sensor.

| <b>500 <math>\mu</math>M H<sub>2</sub>O<sub>2</sub></b> | <b>Current change (pA)</b> | <b>Baseline change (%)</b> | <b>Max response (mins)</b> | <b>Return (mins)</b> | <b>Pre-perfusion baseline (pA)</b> | <b>Post-perfusion baseline (pA)</b> |
|---|----------------------------|----------------------------|----------------------------|----------------------|------------------------------------|-------------------------------------|
| <i>Blank</i>  | $-166.7 \pm 36.3$          | $91.2 \pm 2.9$             | $12.2 \pm 0.7$             | $70.5 \pm 2.7$       | $2322.8 \pm 653.8$                 | $2261.3 \pm 641.0$                  |
| <i>Cat</i>  | $-39.1 \pm 71.5$           | $102.6 \pm 16.9$           | -                          | -                    | $488.0 \pm 179.3$                  | $513.1 \pm 125.3$                   |

**Table 5.4.4.1: Summary of results obtained on perfusion 500  $\mu$ M H<sub>2</sub>O<sub>2</sub>. Data obtained from 2 paired H<sub>2</sub>O<sub>2</sub> sensors implanted in the striatum of 2 Wistar rats. The average data includes 3 administrations.**

#### 5.4.5 1000 $\mu$ M H<sub>2</sub>O<sub>2</sub>

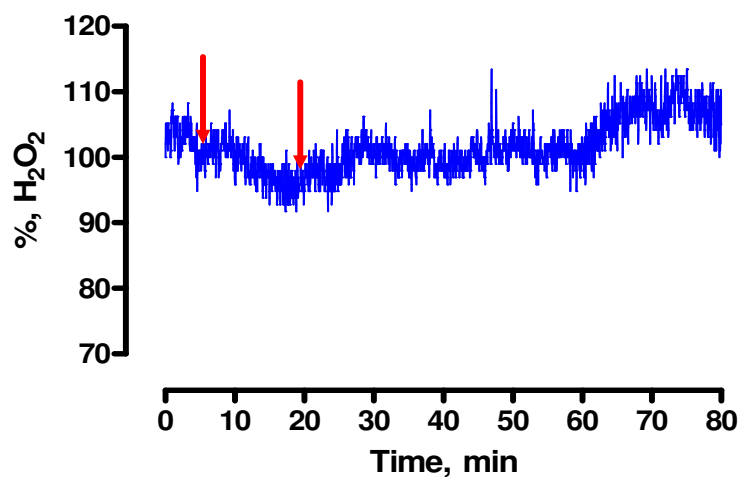


**Figure 5.4.5: A typical example of a 1000  $\mu$ M H<sub>2</sub>O<sub>2</sub> perfusion detected by the paired H<sub>2</sub>O<sub>2</sub> sensor implanted in the striatum of a freely-moving Wistar rat. The arrows indicate the duration of the perfusion.**

As seen in Figure 5.4.4 a slight change in the paired sensor response was observed on perfusion of 1000  $\mu\text{M}$  H<sub>2</sub>O<sub>2</sub> (Figure 5.4.5) which on further inspection was found to be not significantly different ( $P > 0.05$ ) from pre-perfusion baseline levels. A decrease of  $17.6 \pm 88.3$  pA ( $n = 2$ ) was recorded which corresponds to a concentration change of  $37.7 \pm 189.3$  nM H<sub>2</sub>O<sub>2</sub> ( $n = 2$ ). The magnitude of this decrease was  $98.3 \pm 5.3$  % ( $n = 2$ ) of baseline levels. The change in H<sub>2</sub>O<sub>2</sub> signal observed here was significantly different ( $P < 0.01, **$ ) from that observed on perfusion of aCSF. No significant difference ( $P > 0.05$ ) was observed between the pre-perfusion ( $929.7 \pm 73.85$  pA,  $n = 2$ ) and post-perfusion baseline levels ( $919.3 \pm 46.0$  pA,  $n = 2$ ).

| Analyte   | Current change (pA) | Baseline change (%) | Conc. change (nM) | Max response (mins) | Return (mins)   | Pre-perfusion baseline (pA) | Post-perfusion baseline (pA) |
|---|---------------------|---------------------|-------------------|---------------------|-----------------|-----------------------------|------------------------------|
| <b>1000 <math>\mu\text{M}</math> H<sub>2</sub>O<sub>2</sub></b> | $17.6 \pm 88.3$     | $98.3 \pm 5.3$      | $37.7 \pm 189.3$  | $11.8 \pm 0.1$      | $53.0 \pm 11.9$ | $929.7 \pm 73.9$            | $919.3 \pm 46.0$             |

**Table 5.4.5: Summary of results obtained on perfusion of 1000  $\mu\text{M}$  H<sub>2</sub>O<sub>2</sub>. Data obtained from 2 paired H<sub>2</sub>O<sub>2</sub> sensors implanted in the striatum of 2 Wistar rats.**

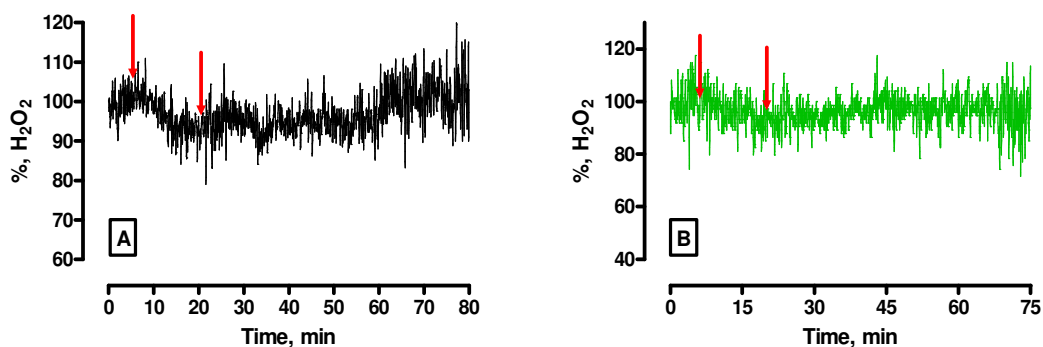


Figure 5.4.5.1: A typical example of a 1000  $\mu\text{M}$  H<sub>2</sub>O<sub>2</sub> perfusion detected by (A) *Blank* sensor and (B) *Cat* sensor; implanted in the striatum of a Wistar rat. The arrows indicate the duration of the perfusion.

Figure 5.4.3.1 demonstrates the response of the *Blank* (A) and *Cat* (B) sensor following the addition of a higher concentration of H<sub>2</sub>O<sub>2</sub> to the perfusate (1000  $\mu\text{M}$ ). A small deviation in response was recorded by the *Blank* sensor of  $-31.5 \pm 60.7$  pA ( $n = 2$ ) and a minor deviation from baseline was recorded by the *Cat* sensor  $-49.1 \pm 27.6$  pA,  $n = 2$ ). No significant difference ( $P > 0.05$ ) was observed between the pre-perfusion baseline and the post-perfusion baseline of the *Cat* and *Blank* sensor. Additionally, no significant difference ( $P > 0.05$ ) was observed between the maximum current response of the *Cat* and *Blank* sensor.

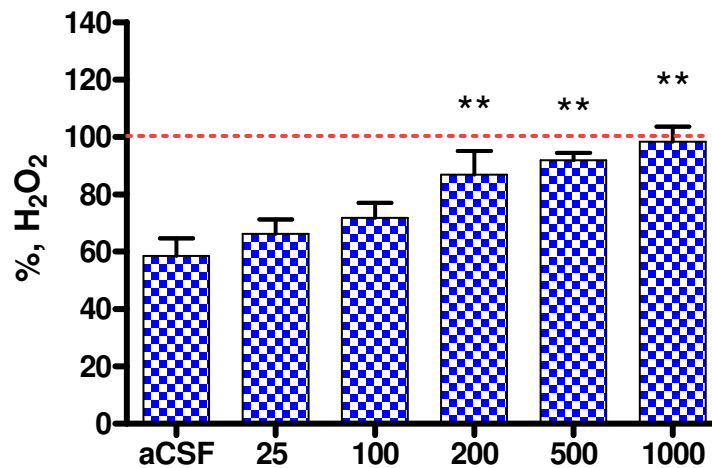
| <b>1000 <math>\mu\text{M}</math><br/>H<sub>2</sub>O<sub>2</sub></b> | <b>Current<br/>change<br/>(pA)</b> | <b>Baseline<br/>change<br/>(%)</b> | <b>Max<br/>response<br/>(mins)</b> | <b>Return<br/>(mins)</b> | <b>Pre-<br/>perfusion<br/>baseline<br/>(pA)</b> | <b>Post-<br/>perfusion<br/>baseline<br/>(pA)</b> |
|---|------------------------------------|------------------------------------|------------------------------------|--------------------------|---|--|
| <i>Blank</i>  | $-31.5 \pm 60.7$                   | $97.2 \pm 3.6$                     | $11.8 \pm 0.1$                     | $53.0 \pm 11.9$          | $2586.4 \pm 1128.8$                             | $2541.1 \pm 1179.8$                              |
| <i>Cat</i>  | $-49.1 \pm 27.6$                   | $92.6 \pm 2.7$                     | -                                  | -                        | $605.7 \pm 151.6$                               | $549.8 \pm 153.8$                                |

Table 5.4.5.1: Summary of results obtained on perfusion of 1000  $\mu\text{M}$  H<sub>2</sub>O<sub>2</sub>. Data obtained from 2 paired H<sub>2</sub>O<sub>2</sub> sensors implanted in the striatum of 2 Wistar rats.

## 5.5 Local H<sub>2</sub>O<sub>2</sub> administration summary (freely-moving)

This section provides a summary of the data presented in Section 5.4. The maximum change recorded due to the local administration of H<sub>2</sub>O<sub>2</sub> by the paired H<sub>2</sub>O<sub>2</sub> sensor (*Blank-Cat*), the *Blank* sensor and the *Cat* sensor is compared against the corresponding aCSF response.

### 5.5.1 Paired H<sub>2</sub>O<sub>2</sub> sensor summary (freely-moving)



**Figure 5.5.1: Paired H<sub>2</sub>O<sub>2</sub> sensor response following perfusions as discussed in Section 5.4. Data shown as an average percentage change, with 100 % as the pre-perfusion H<sub>2</sub>O<sub>2</sub> baseline signal.**

The effect of the local administration of H<sub>2</sub>O<sub>2</sub> on the maximum response of the paired H<sub>2</sub>O<sub>2</sub> sensor (*Blank-Cat*) is demonstrated in Figure 5.5.1. It is clear from the data illustrated above in Figure 5.5.1 and that shown in Table 5.5.1 that the local administration of H<sub>2</sub>O<sub>2</sub> does not cause an obvious increase in the paired catalase-based H<sub>2</sub>O<sub>2</sub> sensor response. The effect of the local administration of aCSF can be used as a control against which the perfusion of each concentration of H<sub>2</sub>O<sub>2</sub> can be measured. No significant difference ( $P > 0.05$ ) was observed following administration of 25  $\mu$ M and 100  $\mu$ M H<sub>2</sub>O<sub>2</sub> when compared to the addition aCSF to the perfusate. A significant difference ( $P < 0.01$ ,\*\*) was observed following perfusion of 200, 500 and 1000  $\mu$ M H<sub>2</sub>O<sub>2</sub> when compared to the response seen with aCSF (Section 5.3.1).

When compared to the perfusion of aCSF the addition of H<sub>2</sub>O<sub>2</sub> to the perfusate reduces the deviation below basal levels in a concentration dependent manner. As the concentration of H<sub>2</sub>O<sub>2</sub> in the perfusate increases with each experiment the H<sub>2</sub>O<sub>2</sub> signal remains appreciably closer to baseline levels in each case. The H<sub>2</sub>O<sub>2</sub> sensor is responding to a change in exogenously applied H<sub>2</sub>O<sub>2</sub>. A definitive trend is observed here and the lack of an increase by the H<sub>2</sub>O<sub>2</sub> sensor may be due to the effect of an inherent mechanism of the *in-vivo* environment.

A network of antioxidant mechanisms regulate the level of H<sub>2</sub>O<sub>2</sub>/ROS in the brain which consist of the peroxidase enzymes, primarily catalase and glutathione peroxidase (Rice, 2011). Homeostasis of the level of ROS and peroxidase activity must be maintained to prevent oxidative damage (Simonian & Coyle, 1996; Valko *et al.*, 2007). It is possible that the effect of the local addition of H<sub>2</sub>O<sub>2</sub> on the catalase-based H<sub>2</sub>O<sub>2</sub> sensor is dampened by this network of control mechanisms. The ECF concentration of H<sub>2</sub>O<sub>2</sub> has been estimated to be between 25-50  $\mu$ M (Hyslop *et al.*, 1995). However it is possible that the local addition of H<sub>2</sub>O<sub>2</sub> of concentrations higher than that estimated to be present in the ECF can be controlled by the antioxidant network. The data presented here would indicate that the robust antioxidant network can tolerate the presence of a high concentration of H<sub>2</sub>O<sub>2</sub>.

A one-way ANOVA analysis of variance revealed no significant difference ( $P > 0.05$ ) in the maximum response time of each perfusion and similarly in the subsequent time required to return to baseline levels following each perfusion with ( $P > 0.05$ ). No significant difference ( $P > 0.05$ ) was observed for the pre-perfusion and post-perfusion baseline level for each change in concentration of H<sub>2</sub>O<sub>2</sub> added to the perfusate which was determined by a one-way ANOVA analysis of variance.

| Analyte                               | Current change (pA) | Baseline change (%) | Conc. change (nM) | Max response (mins) | Return (mins) | Pre-perfusion baseline (pA) | Post-perfusion baseline (pA) | n | P      |
|---------------------------------------|---------------------|---------------------|-------------------|---------------------|---------------|-----------------------------|------------------------------|---|--------|
| aCSF                                  | -361.6 ± 161.7      | 58.5 ± 6.2          | -775.2 ± 346.6    | 13.3 ± 0.2          | 70.2 ± 5.5    | 823.3 ± 297.3               | 790.7 ± 283.2                | 3 | n/a    |
| 25 μM H <sub>2</sub> O <sub>2</sub>   | -311.6 ± 172.6      | 66.2 ± 5.0          | -668.0 ± 370.0    | 13.4 ± 0.7          | 66.1 ± 3.1    | 866 ± 382.2                 | 816.7 ± 339.2                | 2 | 0.4436 |
| 100 μM H <sub>2</sub> O <sub>2</sub>  | -243.0 ± 146.8      | 71.8 ± 5.3          | -520.8 ± 314.6    | 10.9 ± 1.1          | 45.5 ± 3.0    | 791.5 ± 372.4               | 756.7 ± 281.6                | 2 | 0.2311 |
| 200 μM H <sub>2</sub> O <sub>2</sub>  | -179.7 ± 91.5       | 86.9 ± 8.2          | -385.1 ± 196.1    | 11.8 ± 0.7          | 59.1 ± 4.2    | 1589.3 ± 428.2              | 1389.7 ± 302.4               | 4 | 0.0494 |
| 500 μM H <sub>2</sub> O <sub>2</sub>  | -127.8 ± 35.0       | 91.8 ± 2.6          | -274.0 ± 75.0     | 12.2 ± 0.7          | 70.5 ± 2.7    | 1834.9 ± 765.3              | 1748.3 ± 697.1               | 2 | 0.0075 |
| 1000 μM H <sub>2</sub> O <sub>2</sub> | 17.6 ± 88.3         | 98.3 ± 5.3          | 37.7 ± 189.3      | 11.8 ± 0.1          | 53.0 ± 11.9   | 929.7 ± 73.9                | 919.3 ± 46.0                 | 2 | 0.0015 |

Table 5.5.1: Summary of paired H<sub>2</sub>O<sub>2</sub> sensor results obtained following perfusions in freely-moving animals as discussed in Section 5.4.

### 5.5.2 Blank sensor summary (freely-moving)

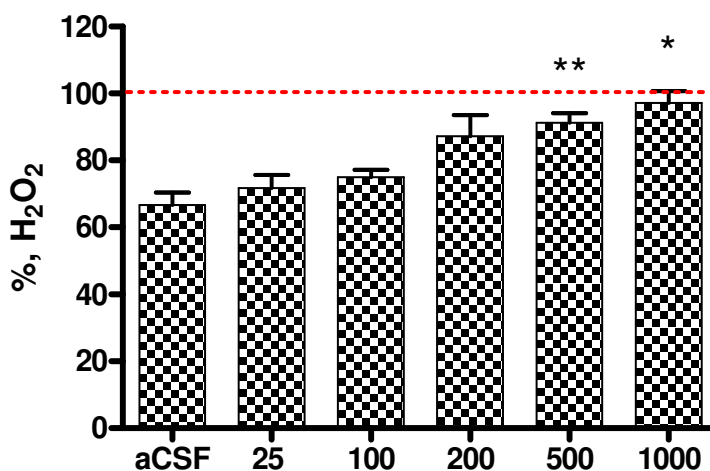


Figure 5.5.2: *Blank* sensor response following perfusions as discussed in Section 5.4. Data shown as an average percentage change, with 100 % as the pre-perfusion baseline signal.

The effect of the local administration of H<sub>2</sub>O<sub>2</sub> on the maximum response of the *Blank* sensor is demonstrated in Figure 5.5.2. It is apparent that the addition of H<sub>2</sub>O<sub>2</sub> to the perfusate does not induce a clear increase in the *Blank* sensor response above basal levels as denoted by the dashed line in Figure 5.5.2. The effect of the local

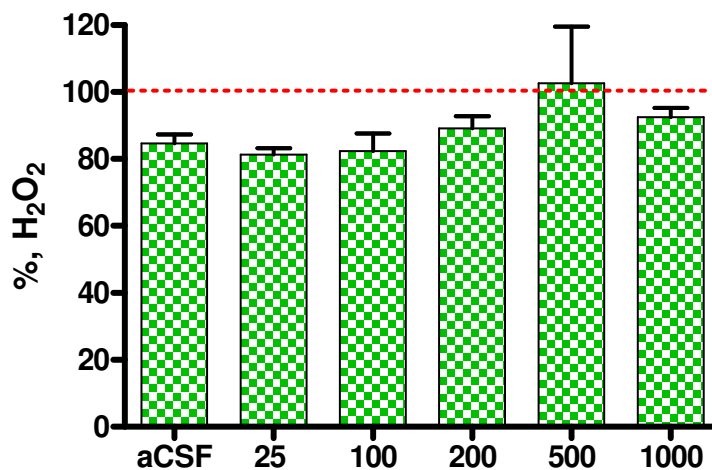
administration of aCSF may be compared against the perfusion of each concentration of H<sub>2</sub>O<sub>2</sub>. No significant difference ( $P > 0.05$ ) in response was observed following administration of 25  $\mu$ M, 100  $\mu$ M and 200  $\mu$ M H<sub>2</sub>O<sub>2</sub> when compared to the addition of aCSF to the perfusate. A significant difference ( $P < 0.05$ ) was observed following perfusion of 500 and 1000  $\mu$ M H<sub>2</sub>O<sub>2</sub> when compared to the response seen with aCSF (Section 5.3.1).

No significant difference ( $P > 0.05$ ) was observed between the maximum response of the *Blank* sensor, following the local administration of aCSF and the various concentrations of H<sub>2</sub>O<sub>2</sub> when compared to the paired H<sub>2</sub>O<sub>2</sub> sensor response (Section 5.5.1). This finding means that the contribution to the overall signal by the *Cat* sensor is negligible due to the efficiency of H<sub>2</sub>O<sub>2</sub> removal by the catalase-modified electrode which is demonstrated in the next Section (5.5.3).

| Analyte                                    | Current change (pA) | Baseline change (%) | Max response (mins) | Return (mins)   | Pre-perfusion baseline (pA) | Post-perfusion baseline (pA) | n | P      |
|--|---------------------|---------------------|---------------------|-----------------|-----------------------------|------------------------------|---|--------|
| aCSF                                       | -467.4 $\pm$ 163.1  | 66.7 $\pm$ 3.8      | 13.3 $\pm$ 0.2      | 70.2 $\pm$ 5.5  | 1341.3 $\pm$ 323.5          | 1272.4 $\pm$ 317.3           | 3 | n/a    |
| 25 $\mu$ M H <sub>2</sub> O <sub>2</sub>   | -414.0 $\pm$ 158.7  | 71.7 $\pm$ 3.9      | 13.4 $\pm$ 0.7      | 66.1 $\pm$ 3.1  | 1412.8 $\pm$ 364.9          | 1332.2 $\pm$ 352.4           | 2 | 0.4414 |
| 100 $\mu$ M H <sub>2</sub> O <sub>2</sub>  | -330.5 $\pm$ 120.8  | 75.0 $\pm$ 2.2      | 10.9 $\pm$ 1.1      | 45.5 $\pm$ 3.0  | 1291.8 $\pm$ 371.1          | 756.7 $\pm$ 281.6            | 2 | 0.2013 |
| 200 $\mu$ M H <sub>2</sub> O <sub>2</sub>  | -237.5 $\pm$ 94.1   | 87.3 $\pm$ 6.2      | 11.8 $\pm$ 0.7      | 59.1 $\pm$ 4.2  | 2045.0 $\pm$ 381.0          | 1853.3 $\pm$ 261.0           | 4 | 0.0503 |
| 500 $\mu$ M H <sub>2</sub> O <sub>2</sub>  | -166.7 $\pm$ 36.3   | 91.2 $\pm$ 2.9      | 12.2 $\pm$ 0.7      | 70.5 $\pm$ 2.7  | 2322.8 $\pm$ 653.8          | 2261.3 $\pm$ 641.0           | 2 | 0.0067 |
| 1000 $\mu$ M H <sub>2</sub> O <sub>2</sub> | -31.5 $\pm$ 60.7    | 97.2 $\pm$ 3.6      | 11.8 $\pm$ 0.1      | 53.0 $\pm$ 11.9 | 2586.4 $\pm$ 1128.8         | 2541.1 $\pm$ 1179.8          | 2 | 0.0117 |

**Table 5.5.2: Summary of *Blank* sensor results obtained following perfusions in freely-moving animals as discussed in Section 5.4.**

### 5.5.3 *Cat* sensor summary (freely-moving)



**5.5.3:** *Cat* sensor response following perfusions as discussed in Section 5.4. Data shown as an average percentage change, with 100 % as the pre-perfusion baseline signal.

The effect of the local administration of H<sub>2</sub>O<sub>2</sub> on the maximum response of the *Cat* sensor is demonstrated in Figure 5.5.3. A consistent pattern is evident following the addition of H<sub>2</sub>O<sub>2</sub> to the perfusate. No significant difference ( $P > 0.05$ ) in response was observed following administration of each concentration of H<sub>2</sub>O<sub>2</sub> (25-1000  $\mu$ M) when compared to the addition of aCSF to the perfusate. The *Cat* sensor effectively eliminates a contribution to the overall response by removing the signal attributable to H<sub>2</sub>O<sub>2</sub>. As can be seen in Figure 5.5.2 the *Cat* sensor response remains below baseline levels (dashed line) following each perfusion. A clear increase in the *Cat* sensor response above baseline levels would indicate a disruption in the function of the catalase-based sensor.

| Analyte                               | Current change (pA) | Baseline change (%) | Max response (mins) | Return (mins) | Pre-perfusion baseline (pA) | Post-perfusion baseline (pA) | n | P      |
|---------------------------------------|---------------------|---------------------|---------------------|---------------|-----------------------------|------------------------------|---|--------|
| aCSF                                  | -105.3 ± 18.1       | 84.6 ± 2.8          | 13.3 ± 0.2          | 70.2 ± 5.5    | 518 ± 35.7                  | 481.5 ± 37.9                 | 3 | n/a    |
| 25 μM H <sub>2</sub> O <sub>2</sub>   | -102.4 ± 13.9       | 81.3 ± 1.9          | 13.4 ± 0.7          | 66.1 ± 3.1    | 546.9 ± 17.4                | 515.6 ± 13.0                 | 2 | 0.4524 |
| 100 μM H <sub>2</sub> O <sub>2</sub>  | -88.3 ± 26.6        | 82.4 ± 5.3          | 10.9 ± 1.1          | 45.5 ± 3.0    | 500.2 ± 1.0                 | 503.5 ± 47.7                 | 2 | 0.6954 |
| 200 μM H <sub>2</sub> O <sub>2</sub>  | -57.9 ± 28.0        | 89.2 ± 3.7          | 11.8 ± 0.7          | 59.1 ± 4.2    | 455.7 ± 77.9                | 463.6 ± 75.0                 | 4 | 0.4015 |
| 500 μM H <sub>2</sub> O <sub>2</sub>  | -39.1 ± 71.5        | 102.6 ± 16.9        | 12.2 ± 0.7          | 70.5 ± 2.7    | 488.0 ± 179.3               | 513.1 ± 125.3                | 2 | 0.3529 |
| 1000 μM H <sub>2</sub> O <sub>2</sub> | -49.1 ± 27.6        | 92.6 ± 2.7          | 11.8 ± 0.1          | 53.0 ± 11.9   | 605.7 ± 151.6               | 549.8 ± 153.8                | 2 | 0.1474 |

Table 5.5.3: Summary of *Cat* sensor results obtained following perfusions in freely-moving animals as discussed in Section 5.4.

## 5.6 Local sodium azide (SA) administration

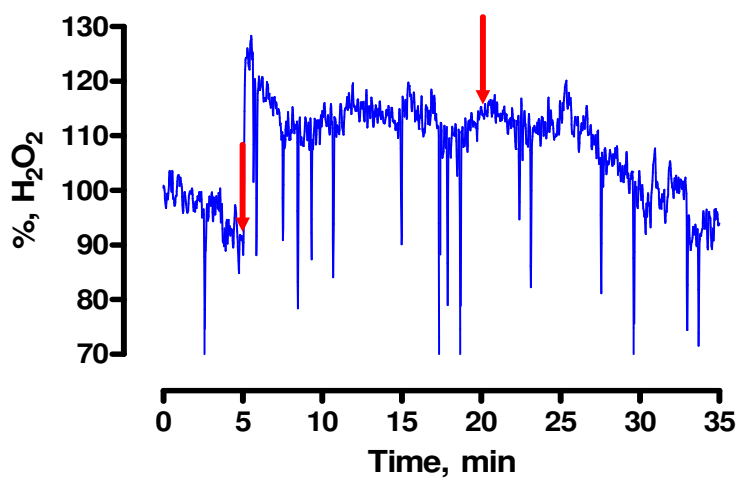


Figure 5.6.1: A typical example of a 10 mM SA perfusion detected by the paired H<sub>2</sub>O<sub>2</sub> sensor implanted in the striatum of a freely-moving Wistar rat. The arrows indicate the duration of the perfusion.

Catalase is one of the primary peroxidase enzymes present in the brain (Cohen, 1994; Dringen *et al.*, 2005), the function of this enzyme is to convert potentially harmful H<sub>2</sub>O<sub>2</sub>

into water and oxygen. Sodium azide (SA) inhibits the function of catalase in the brain (Zimatkin *et al.*, 2006). As catalase is an enzyme which degrades H<sub>2</sub>O<sub>2</sub>; impairment in the activity of catalase in the brain should lead to an increase in H<sub>2</sub>O<sub>2</sub> levels. A current increase of  $219.8 \pm 108.7$  pA ( $n = 1$ , 2ad) was recorded which corresponds to a concentration change of  $471.1 \pm 232.9$  nM H<sub>2</sub>O<sub>2</sub> ( $n = 1$ , 2ad). An elevated H<sub>2</sub>O<sub>2</sub> response was observed following perfusion of SA of  $118.4 \pm 0.8$  % ( $n = 1$ , 2ad). This value was significantly different ( $P < 0.01, **$ ) from perfusion of aCSF. No significant difference ( $P > 0.05$ ) was observed between the pre-perfusion ( $1170.8 \pm 541.5$  pA,  $n = 1$ , 2ad) and post-perfusion baseline levels ( $1182.3 \pm 547.5$  pA,  $n = 1$ , 2ad) in this case. The maximum change in signal was observed  $1.3 \pm 0.2$  mins ( $n = 1$ , 2ad) following perfusion of this concentration of SA (10 mM) and returned to a steady baseline  $25.5 \pm 1.7$  mins ( $n = 1$ , 2ad) post perfusion. Additionally no significant difference ( $P > 0.05$ ) was observed between the baseline and maximum current response of the catalase-based sensor (*Cat*) following perfusion of SA. Therefore the local administration of SA does not increase the *Cat* sensor response.

| Analyte | Current change (pA) | Baseline change (%) | Conc. change (nM) | Max response (mins) | Return (mins)  | Pre-perfusion baseline (pA) | Post-perfusion baseline (pA) |
|---------|---------------------|---------------------|-------------------|---------------------|----------------|-----------------------------|------------------------------|
| SA      | $219.8 \pm 108.7$   | $118.4 \pm 0.8$     | $471.1 \pm 232.9$ | $1.3 \pm 0.2$       | $25.5 \pm 1.7$ | $1170.8 \pm 541.5$          | $1182.3 \pm 547.5$           |

**Table 5.6.1: Summary of results obtained on perfusion of sodium azide (10 mM). Data obtained from 1 paired H<sub>2</sub>O<sub>2</sub> sensor implanted in the striatum of 1 Wistar rat. The average data includes 2 administrations.**

## 5.6.1 Systemic SA administration

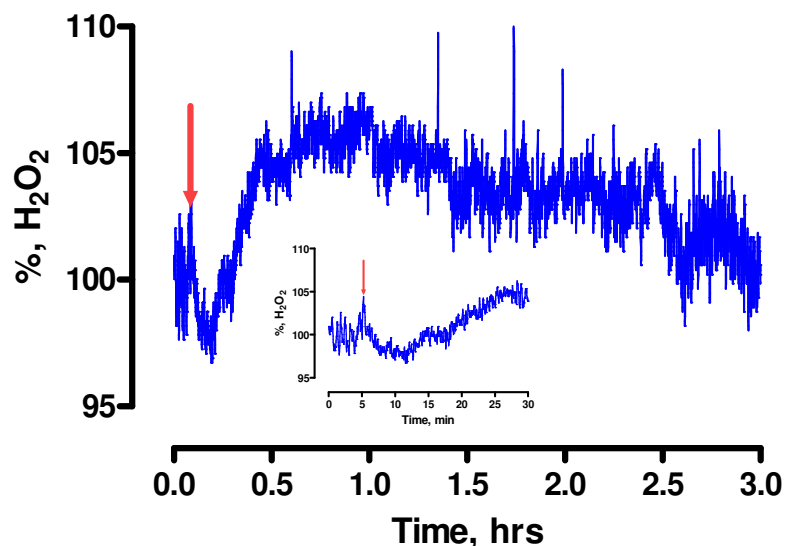


**Figure 5.6.1:** A 20mg/kg s.c. injection of SA detected by the paired  $H_2O_2$  sensor implanted in the striatum of a freely-moving Wistar rat. The arrow indicates the point of administration. *Inset:* Initial 30 min of response.

As previously stated sodium azide (SA) inhibits the function of catalase in the brain (Zimatkin *et al.*, 2006; Jamal *et al.*, 2007). A disruption in the function of the catalase enzyme should lead to an elevation in the level of  $H_2O_2$ . An increase in  $H_2O_2$  signal was observed following injection of sodium azide (SA) the maximum current increase recorded was 0.3 nA which corresponds to a change of 5.7% which occurred after 49 mins following the injection and returned to a steady baseline after 193 mins. The data represented in Figure 5.6.1 is preliminary, however, it does suggest that an increased production in  $H_2O_2$  occurs following the systemic introduction of SA. Following on from this work the effect of this systemic administration on the local administration of  $H_2O_2$  was investigated (Section 5.6.2).

### 5.6.2 The effect of systemic SA administration on the local administration of H<sub>2</sub>O<sub>2</sub>

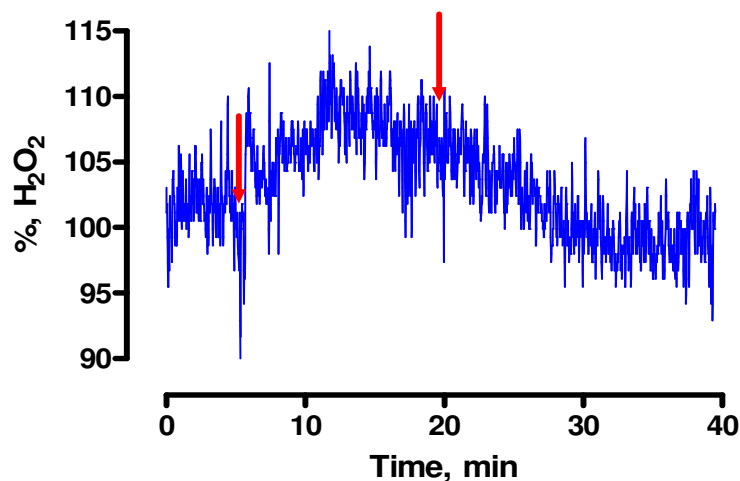


**Figure 5.6.2:** A typical example of a 1 mM H<sub>2</sub>O<sub>2</sub> perfusion detected by the paired H<sub>2</sub>O<sub>2</sub> sensor implanted in the striatum of a freely-moving Wistar rat following pre-administration with sodium azide (SA). The arrows indicate the duration of the perfusion.

This section investigates the effect of systemic pre-administration of SA (20 mg/kg) on the local administration of H<sub>2</sub>O<sub>2</sub>. SA was injected approximately 30 mins prior to perfusion of H<sub>2</sub>O<sub>2</sub>. The addition of 500  $\mu$ M and 1 mM H<sub>2</sub>O<sub>2</sub> to the perfusate following pre-administration with SA was examined. As previously stated (Section 5.6.1) SA inhibits the function of catalase and inhibition of this peroxidase enzyme should increase H<sub>2</sub>O<sub>2</sub> levels. The local perfusion of 500  $\mu$ M H<sub>2</sub>O<sub>2</sub> following pre-administration of SA was investigated which resulted in a reduction in H<sub>2</sub>O<sub>2</sub> levels to  $94.6 \pm 2.3$  %,  $n = 2$  of baseline. The control value for local administration of 500  $\mu$ M (Section 5.4.4) resulted in a minor decrease to  $91.8 \pm 2.6$  % ( $n = 2$ , 3ad) of basal H<sub>2</sub>O<sub>2</sub> levels. The effect of pre-treatment with SA on the perfusion of 500  $\mu$ M H<sub>2</sub>O<sub>2</sub> was not significant ( $P > 0.05$ ), however the magnitude of the maximum decrease recorded was reduced. In order to further investigate the effect of pre-administration with SA further a higher concentration of H<sub>2</sub>O<sub>2</sub> was added to perfusate (1 mM) following pre-treatment with SA.

The recorded change following perfusion of 1mM H<sub>2</sub>O<sub>2</sub> following pre-treatment (SA) is shown in Figure 5.6.2. A clear increase above basal levels of H<sub>2</sub>O<sub>2</sub> (100 %) can be seen

which is markedly different to that seen with the control experiment (Section 5.4.5). An increase of 0.2 nA (109.3%) was observed due to this perfusion (1 mM H<sub>2</sub>O<sub>2</sub>). This preliminary experiment suggests pre-administration with SA appears to have a negative effect on the robust peroxidase enzyme catalase.

Other mechanisms exist to maintain redox homeostasis in the brain such as the peroxidase enzyme glutathione peroxidase (GPx) (Dringen *et al.*, 2005). Previous work has demonstrated that catalase and GPx play a dual role in the prevention of H<sub>2</sub>O<sub>2</sub> mediated toxicity in brain preparations (Avshalumov *et al.*, 2004; Baud *et al.*, 2004). It is likely that although the function of catalase can be challenged by the inhibitor SA, the overall mechanisms which prevent oxidative stress induced by ROS/H<sub>2</sub>O<sub>2</sub> may not be completely compromised. The next Section (5.7) investigates the effect of GPx inhibition on endogenous levels of H<sub>2</sub>O<sub>2</sub> in the brain.

### **5.7 Local mercaptosuccinate (MCS) administration**

The aim of this section is to investigate the effect of local perfusion of mercaptosuccinate (MCS) on the H<sub>2</sub>O<sub>2</sub> sensor response when implanted in the freely-moving animal. MCS is a glutathione peroxidase (GPx) inhibitor (Dringen *et al.*, 1998; Avshalumov *et al.*, 2003; Avshalumov *et al.*, 2005). GPx is the primary enzyme responsible for regulation of neuronal ROS/H<sub>2</sub>O<sub>2</sub> levels. The local perfusion of MCS should disrupt H<sub>2</sub>O<sub>2</sub> removal and hence lead to an increase in H<sub>2</sub>O<sub>2</sub> levels in the brain. The preliminary data shown in this section is a dose response study from one animal. 0.1 mM and 1 mM MCS were added to the perfusate and the H<sub>2</sub>O<sub>2</sub> response was measured by the dual H<sub>2</sub>O<sub>2</sub> sensor.

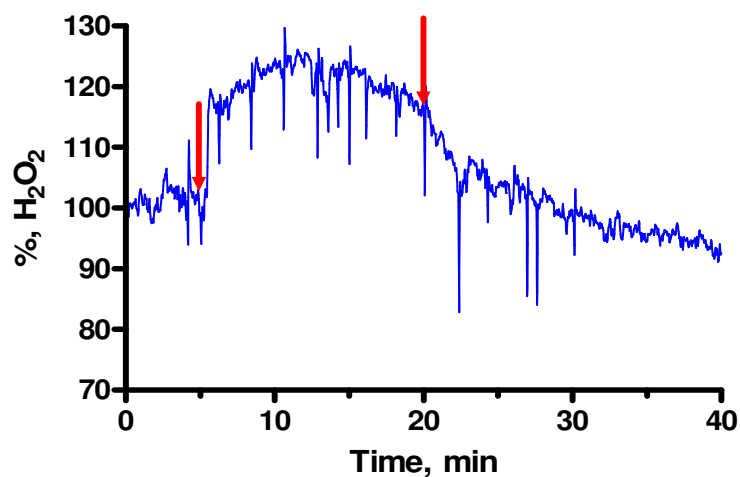


Figure 5.7.1: An example of a 1 mM MCS perfusion detected by the paired  $H_2O_2$  sensor implanted in the striatum of a freely-moving Wistar rat. The arrows indicate the duration of the perfusion.

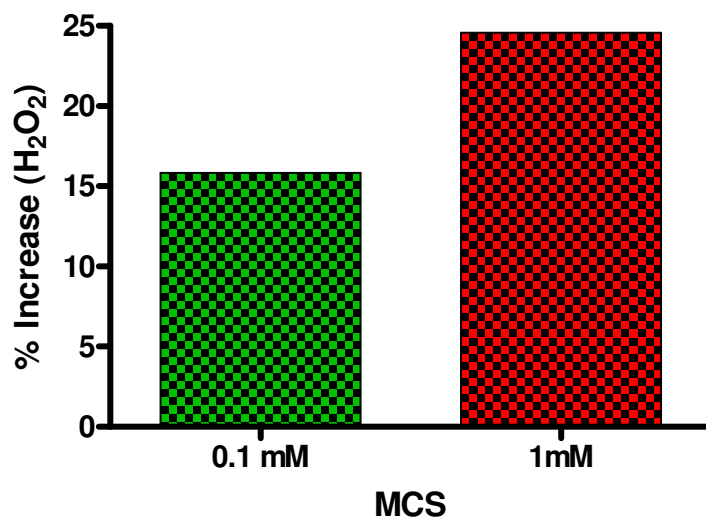


Figure 5.7.2: Preliminary dose response comparison of MCS perfusion on  $H_2O_2$  response implanted in the striatum of a freely-moving Wistar rat. Data represented as a percentage increase above baseline.

| Analyte | Current change (pA) | Baseline change (%) | Conc. change (nM) | Max response (mins) | Return (mins) | Pre-perfusion baseline (pA) | Post-perfusion baseline (pA) |
|---------|---------------------|---------------------|-------------------|---------------------|---------------|-----------------------------|------------------------------|
| 0.1 mM  | 212.6               | 115.8               | 455.7             | 10.9                | 24.7          | 1344.3                      | 1339.5                       |
| 1 mM    | 449.9               | 124.6               | 964.4             | 6.2                 | 23.5          | 1830.8                      | 1724.3                       |

**Table 5.7.1: Summary of results obtained on perfusion of MCS. Data obtained from 1 paired  $H_2O_2$  sensor implanted in the striatum of 1 Wistar rat.**

Preliminary findings indicate that the local administration of MCS in a dose dependent manner produces a dose related increase in  $H_2O_2$  as is summarised in Table 5.7.1. Future work may involve the simultaneous inhibition of catalase and GPx using SA and MCS respectively in order to suppress the anti-oxidant network and increase the endogenous level of  $H_2O_2$  in the brain.

## 5.8 Local ascorbic acid (AA) administration

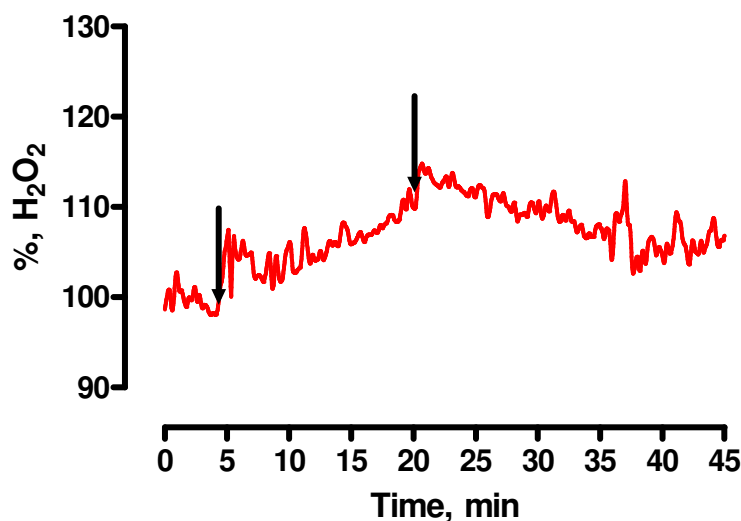


**Figure 5.8.1: A typical example of a 1 mM AA perfusion detected by the paired  $H_2O_2$  sensor implanted in the striatum of a freely-moving Wistar rat. The arrows indicate the duration of the perfusion.**

Ascorbic acid is the primary interference species in the brain, with an estimated concentration of between 100 and 500  $\mu\text{M}$  in the ECF (Lowry *et al.*, 1996). It is necessary to test the selectivity of the H<sub>2</sub>O<sub>2</sub> sensor against this potential interferent. In order to determine whether the presence of AA would interfere with the detection of H<sub>2</sub>O<sub>2</sub> in the brain 1 mM AA was added to the perfusate and locally introduced. A maximum current increase of  $245.3 \pm 38.4$  pA ( $n = 2$ ) which corresponds to  $117.9 \pm 7.8$  % ( $n = 2$ ) was recorded by the H<sub>2</sub>O<sub>2</sub> sensor following perfusion of 1 mM AA. The response was slow to achieve a maximum response ( $10.3 \pm 3.3$  mins,  $n = 2$ ) and no significant difference ( $P > 0.05$ ) was observed between pre-perfusion ( $1780.6 \pm 966.6$  pA) and post-perfusion baseline levels ( $1828.4 \pm 1105.5$  pA).

Carbon paste electrodes (CPEs) have been previously utilised to demonstrate changes in ECF ascorbate (Lowry *et al.*, 1996; Miele & Fillenz, 1996; Lowry *et al.*, 1998a). Miele *et al.* demonstrated a sharp immediate increase in current detected by the CPE upon local administration of ascorbate which was attenuated for the duration of the perfusion (Miele & Fillenz, 1996). In this instance a comparatively slower and minimal current change was observed (Figure 5.8.1) it is probable that the PPD layer which is part of the H<sub>2</sub>O<sub>2</sub> sensor design slows the access of AA to the active surface of the sensor and effectively eliminates interference as seen previously (Lowry *et al.*, 1998b; O'Neill *et al.*, 2008). The expected rapid fluctuation of H<sub>2</sub>O<sub>2</sub> *in-vivo* (Rice, 2011) should exclude contributions to the signal by slow fluctuations in basal concentrations of AA which are expected to be much lower than the concentration added to the perfusate here (1 mM) (Miele *et al.*, 1994; Miele & Fillenz, 1996).

| Analyte | Current change (pA) | Baseline change (%) | Max response (mins) | Return (mins)  | Pre-perfusion baseline (pA) | Post-perfusion baseline (pA) |
|---------|---------------------|---------------------|---------------------|----------------|-----------------------------|------------------------------|
| AA      | $245.3 \pm 38.4$    | $117.9 \pm 7.8$     | $10.3 \pm 3.3$      | $29.8 \pm 2.0$ | $1780.6 \pm 966.6$          | $1828.4 \pm 1105.5$          |

**Table 5.6.1: Summary of results obtained on perfusion of AA. Data obtained from 2 paired H<sub>2</sub>O<sub>2</sub> sensors implanted in the striatum of 2 Wistar rats.**

## 5.8.1 Systemic AA administration

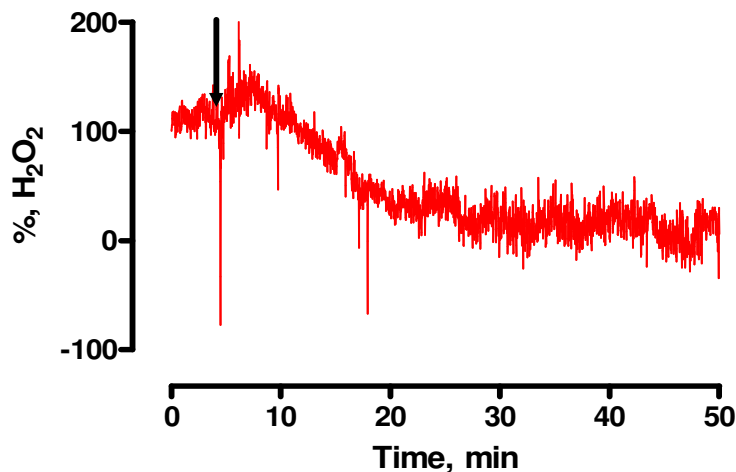


**Figure 5.8.1.1:** An intraperitoneal injection (i.p) of AA (2 g/kg) detected by the paired H<sub>2</sub>O<sub>2</sub> sensor implanted in the striatum of a freely-moving Wistar rat. The arrows indicate the duration of the perfusion.

In this section the selectivity of the H<sub>2</sub>O<sub>2</sub> sensor against systemically introduced ascorbate (2 g/kg, s.c.) was investigated which has previously been demonstrated with PPD based sensors (Lowry *et al.*, 1998a). Sodium ascorbate was the preferred choice as an interference test *in-vivo* as AA, even with pH adjustment, causes significant discomfort to the animal. An immediate decrease in H<sub>2</sub>O<sub>2</sub> signal was observed following the injection. The maximum decrease recorded was 170.0 pA in this case which corresponds to a current change of -95.0 %. As previously stated the overall response of the H<sub>2</sub>O<sub>2</sub> sensor design is based on a subtraction value i.e. *Blank-Cat*. The recorded decrease here is seen due to an increase in signal detected by the *Cat* sensor of 30.8 % however the response at the *Blank* sensor remained steady with a maximum increase of 7.1 % (see Figure 5.8.1.2).

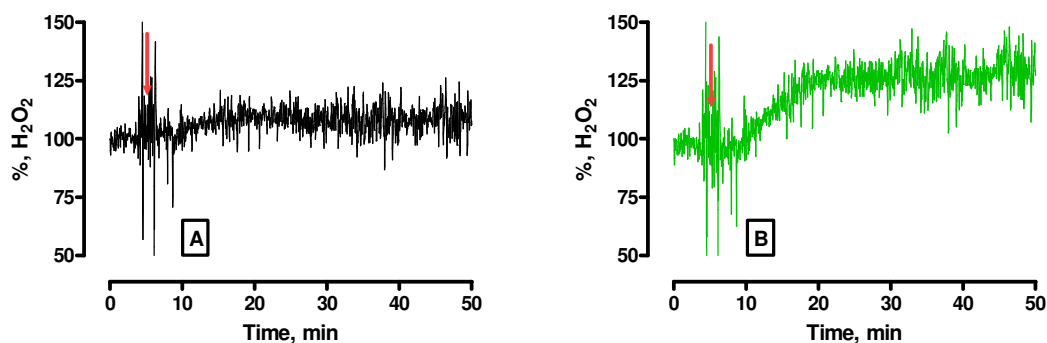


**Figure 5.8.1.2: An intraperitoneal injection (i.p) of AA (2 g/kg) detected by (A) *Blank* sensor and (B) *Cat* sensor; implanted in the striatum of a freely-moving Wistar rat. The arrows indicate the duration of the perfusion.**

From *in-vitro* calibration data it is feasible that the current at the *Cat* sensor attributable to the presence of a high concentration of AA (1000  $\mu$ M) may be slightly higher than that recorded at the *Blank* sensor. The *in-vitro* AA response of the paired sensor is low however and no significant difference is observed between the *Blank* and *Cat* sensor (Section 4.8). No distinct increase in the *Blank* sensor response was observed following this systemic administration of ascorbate. The baseline current values of the *Blank* sensor are higher than the *Cat* sensor *in-vivo* (Section 5.11), therefore the response towards basal concentrations of AA of the paired sensor does not have a negative effect on the sensitivity of the paired design. It must be stated that the work presented in this section is preliminary and further examination of the response to systemically introduced ascorbate needs to be carried out.

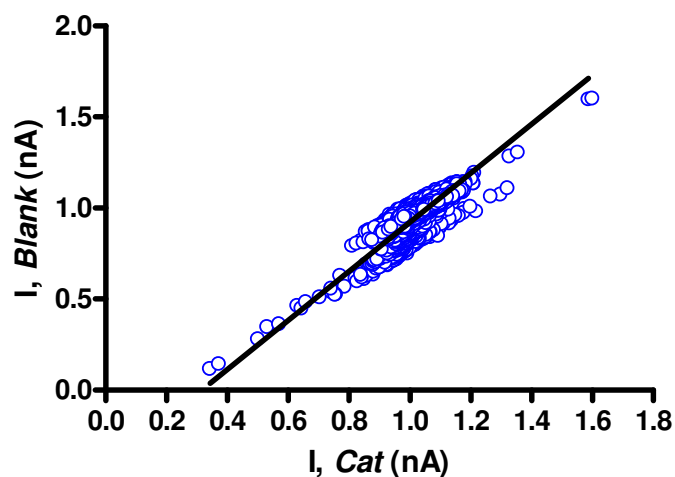


**Figure 5.8.1.3: A bivariate scattergram of changes in the *Blank* and *Cat* sensor currents following the systemic administration of AA.**

Figure 5.8.1.3 illustrates a correlation analysis of the changes in current recorded by the *Blank* and *Cat* sensor following the systemic administration of AA (2 g/kg, s.c.). There is a high correlation between both sensor designs with a calculated correlation coefficient of 0.8314 ( $p < 0.0001$ ).

## 5.9 Local H<sub>2</sub>O<sub>2</sub> administration (acute preparation)

This section demonstrates the response of the paired H<sub>2</sub>O<sub>2</sub> sensor to the local perfusion of various concentrations of H<sub>2</sub>O<sub>2</sub> in the “Acute” preparation. An acute preparation is where the recording takes place while the animal is still under anaesthetic and held in the stereotaxic frame. Additionally the acute preparation facilitates the perfusion of high concentrations of H<sub>2</sub>O<sub>2</sub> (10 and 100 mM) which would likely not be tolerated in the freely-moving animal.

### 5.9.1 aCSF

As a control experiment aCSF was perfused through the microdialysis probe. A typical example of the outcome of this perfusion on the paired catalase-based H<sub>2</sub>O<sub>2</sub> sensor response is shown below in Figure 5.9.1.

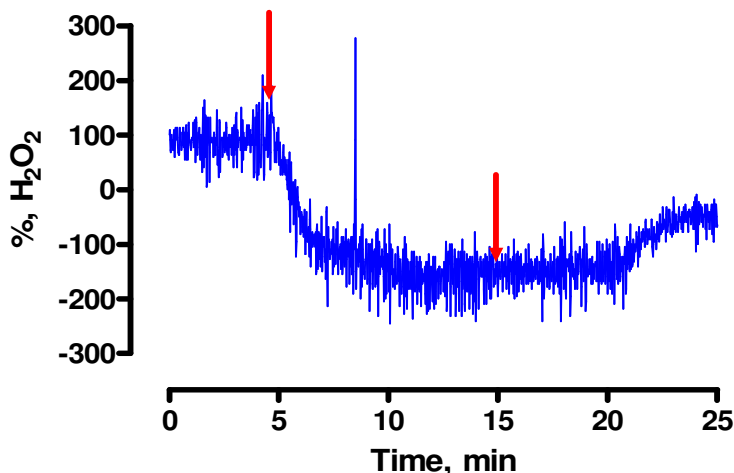


**Figure 5.9.1:** A typical example of an aCSF perfusion detected by the paired H<sub>2</sub>O<sub>2</sub> sensor implanted in the striatum of an anaesthetised Wistar rat. The arrows indicate the duration of the perfusion.

Figure 5.9.1 represents the paired H<sub>2</sub>O<sub>2</sub> sensor response following aCSF perfusion in the anaesthetised animal. The average paired current response following aCSF perfusion demonstrated a decrease in current ( $-76.7 \pm 24.6$  pA,  $n = 2$ ) which corresponds to a concentration change of  $-164.4 \pm 52.7$  nM H<sub>2</sub>O<sub>2</sub> ( $n = 2$ ). In the anaesthetised animal the pre-perfusion baseline of the *Cat* and *Blank* sensor are not significantly different ( $P > 0.05$ ) (Table 5.9.1.1). This observation contrasts greatly to the baseline current values

for the *Cat* and *Blank* sensor seen in the freely-moving animal. The *Blank* sensor baseline is consistently much higher than the *Cat* sensor in the freely-moving animal (see Section 5.5.2 and 5.5.3). Additionally the maximum current response obtained by both sensors (*Blank* and *Cat*) following perfusion of aCSF in the anaesthetised animal was not significantly different ( $P > 0.05$ ). Therefore difficulty arises in representing the overall paired response (*Blank-Cat*). The individual response of the *Cat* and *Blank* sensor following perfusion of aCSF is shown in Figure 5.9.1.1. The discrepancy in the baseline level of the paired H<sub>2</sub>O<sub>2</sub> sensor between the freely-moving and the acute preparation is fully discussed in Section 5.12.

The aCSF perfusion decreased the paired H<sub>2</sub>O<sub>2</sub> sensor response to  $-105.7 \pm 52.9 \%$  ( $n = 2$ ) of basal levels following  $13.2 \pm 0.3$  mins ( $n = 2$ ) from the start of each perfusion. A return to a baseline level is apparent after  $20.7 \pm 0.6$  mins ( $n = 2$ ). No significant difference ( $P > 0.05$ ) was observed between the pre-perfusion and post-perfusion baseline levels.

| Analyte | Current change (pA) | Baseline change (%) | Conc. change (nM) | Max response (mins) | Return (mins)  | Pre-perfusion baseline (pA) | Post-perfusion baseline (pA) |
|---------|---------------------|---------------------|-------------------|---------------------|----------------|-----------------------------|------------------------------|
| aCSF    | $-76.7 \pm 24.6$    | $-105.7 \pm 52.9$   | $-164.4 \pm 52.7$ | $13.2 \pm 0.3$      | $20.7 \pm 0.6$ | $117.2 \pm 97.3$            | $39.0 \pm 47.6$              |

**Table 5.9.1: Summary of results obtained on perfusion of aCSF. Data obtained from 2 paired H<sub>2</sub>O<sub>2</sub> sensors implanted in the striatum of 2 Wistar rats.**

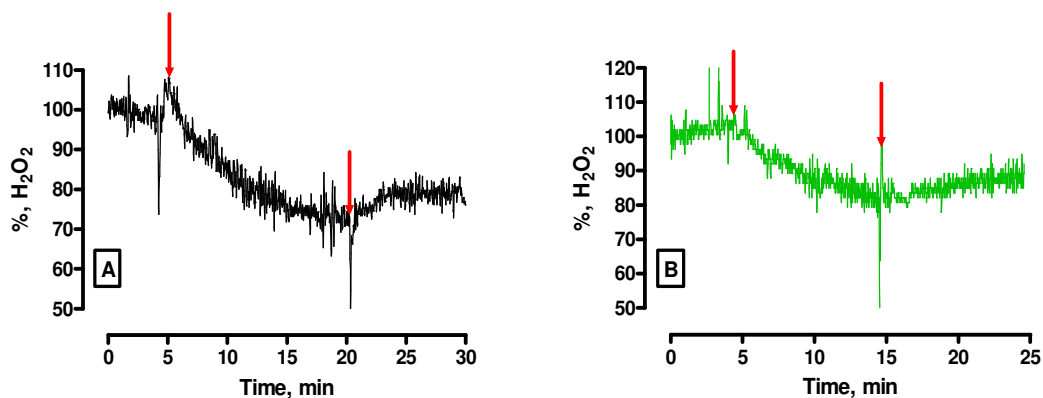


**Figure 5.9.1.1: A typical example of an aCSF perfusion detected by (A) *Blank* sensor and (B) *Cat* sensor; implanted in the striatum of an anaesthetised Wistar rat. The arrows indicate the duration of the perfusion.**

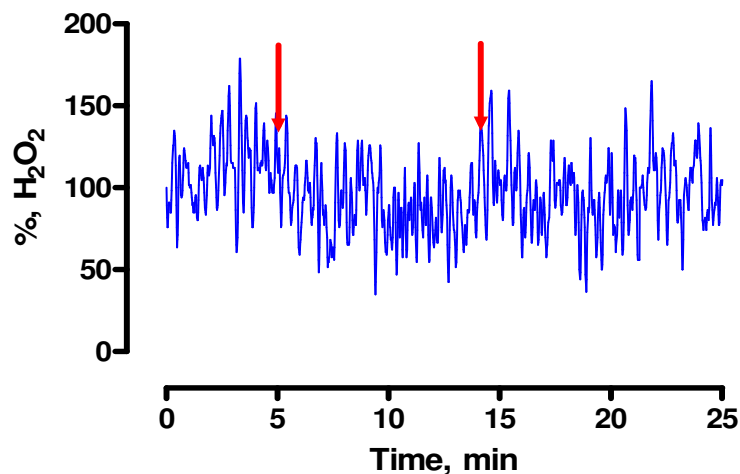
An immediate decrease in response by the *Cat* (A) and *Blank* (B) sensor is apparent on commencement of the aCSF perfusion. The aCSF perfusion decreased the current of the *Blank* sensor to  $69.4 \pm 4.4 \%$  ( $n = 2$ ) of basal levels after  $13.2 \pm 0.3$  mins ( $n = 2$ ) from the start of each perfusion. Similarly a decrease was detected by the *Cat* sensor ( $80.6 \pm 8.1 \%$ ,  $n = 2$ ). A return to a baseline level occurred on both sensor designs after  $20.7 \pm 0.6$  mins ( $n = 2$ ). No significant difference ( $P > 0.05$ ) was observed between the pre-perfusion baseline and the post-perfusion baseline of the *Cat* and *Blank* sensors. Additionally no significant difference  $P > 0.05$  was observed between the maximum current response of the *Blank* and *Cat* sensor following perfusion with aCSF.

The decrease observed here by both sensor designs is due to diffusion of  $H_2O_2$  through the microdialysis membrane and into the dialysate thus reducing the concentration of  $H_2O_2$  surrounding the sensor. On cessation of the perfusion  $H_2O_2$  diffuses back towards the implanted sensors and hence an increase in  $H_2O_2$  signal is observed.

| <b>aCSF</b>  | <b>Current change (pA)</b> | <b>Baseline Change (%)</b> | <b>Max response (mins)</b> | <b>Return (mins)</b> | <b>Pre-perfusion baseline (pA)</b> | <b>Post-perfusion baseline (pA)</b> |
|--------------|----------------------------|----------------------------|----------------------------|----------------------|------------------------------------|-------------------------------------|
| <i>Blank</i> | -142.1 ± 54.6              | 69.4 ± 4.4                 | 13.2 ± 0.3                 | 20.7 ± 0.6           | 447.7 ± 114.1                      | 305.6 ± 59.5                        |
| <i>Cat</i>   | -65.4 ± 30.0               | 80.6 ± 8.1                 | -                          | -                    | 330.6 ± 16.9                       | 277.6 ± 6.3                         |

**Table 5.9.1.1: Summary of results obtained on perfusion of aCSF. Data obtained from 2 paired H<sub>2</sub>O<sub>2</sub> sensors implanted in the striatum of 2 Wistar rats.**

As can be seen in Figure 5.9.1.1 a decrease is observed in the *Cat* and *Blank* sensor response following perfusion of aCSF. However the overall subtracted response is masked by the proximity of the baseline levels of the *Cat* and *Blank* sensor prior to perfusion of the analyte. The overall H<sub>2</sub>O<sub>2</sub> response is based on a subtraction value (*Blank*–*Cat*). Due to the similarity of the initial baselines of the *Cat* and *Blank* sensor the decrease in current response detected individually by both sensor designs is not clearly represented by an overall paired response. The maximum current response obtained by both sensors following perfusion of aCSF is quite similar. Hence, a difficulty arises when the overall maximum change in H<sub>2</sub>O<sub>2</sub> response is represented by subtraction. This finding was fully investigated and the outcome is discussed in Section 5.12.

5.9.2  $50 \mu M H_2O_2$ 

**Figure 5.9.2:** A typical example of a  $50 \mu M H_2O_2$  perfusion detected by the paired  $H_2O_2$  sensor implanted in the striatum of an anaesthetised Wistar rat. The arrows indicate the duration of the perfusion.

The response of the paired  $H_2O_2$  sensor following perfusion of  $50 \mu M H_2O_2$  is shown in Figure 5.9.2. The signal remains close to baseline levels for the duration of the perfusion. As mentioned previously (Section 5.9.1) with the concentration used in this case, the pre-perfusion baseline and the maximum current response of the *Cat* and *Blank* sensor are not significantly different ( $P > 0.05$ ). The individual response of the *Cat* and *Blank* sensor following perfusion of  $50 \mu M H_2O_2$  is shown in Figure 5.9.3.1.

A slight deviation from baseline levels following the perfusion of  $50 \mu M H_2O_2$  ( $55.7 \pm 63.6$  pA,  $n = 3$ ) was apparent. No significant difference ( $P > 0.05$ ) was observed between the baseline current pre-perfusion  $-28.8 \pm 64.8$  pA ( $n = 3$ ) and the new post-perfusion basal level  $-18.2 \pm 48.1$  pA ( $n = 3$ ).

| Analyte                                  | Current change (pA) | Baseline change (%) | Conc. change (nM) | Max response (mins) | Return (mins)  | Pre-perfusion baseline (pA) | Post-perfusion baseline (pA) |
|--|---------------------|---------------------|-------------------|---------------------|----------------|-----------------------------|------------------------------|
| 50 $\mu$ M H <sub>2</sub> O <sub>2</sub> | 55.7 $\pm$ 63.6     | 87.9 $\pm$ 17.8     | 119.5 $\pm$ 136.4 | 11.3 $\pm$ 2.0      | 20.6 $\pm$ 1.5 | -28.8 $\pm$ 64.8            | -18.2 $\pm$ 48.1             |

**Table 5.9.2:** Summary of results obtained on perfusion of 50  $\mu$ M H<sub>2</sub>O<sub>2</sub>. Data obtained from 3 paired H<sub>2</sub>O<sub>2</sub> sensors implanted in the striatum of 3 Wistar rats.

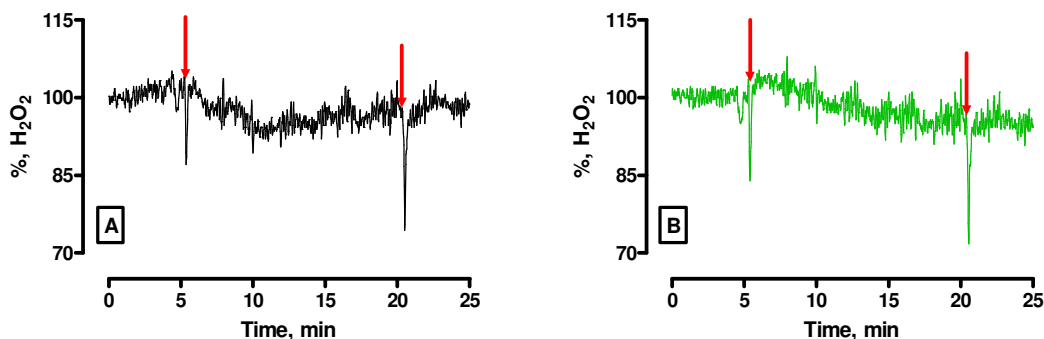


**Figure 5.9.2.1:** A typical example of a 50  $\mu$ M H<sub>2</sub>O<sub>2</sub> perfusion detected by (A) *Blank* sensor and (B) *Cat* sensor; implanted in the striatum of an anaesthetised Wistar rat. The arrows indicate the duration of the perfusion.

The concentration of H<sub>2</sub>O<sub>2</sub> in the perfusate was increased to 50  $\mu$ M H<sub>2</sub>O<sub>2</sub> and a decrease in response by the *Cat* (A) and *Blank* (B) sensor was recorded. This perfusion decreased the *Blank* sensor current response to 93.3  $\pm$  3.0 % (n = 3) of basal levels following 11.3  $\pm$  2.0 mins (n = 3) from the start of each perfusion. A similar decrease was detected by the *Cat* sensor (92.5  $\pm$  1.8 %, n = 3). A return to the pre-perfusion baseline level can be seen following the end of the perfusion which was complete on both sensor designs after 20.6  $\pm$  1.5 mins (n = 3). No significant difference ( $P > 0.05$ ) was observed between the pre-perfusion baseline and the post-perfusion baseline of the *Cat* and *Blank* sensor. Additionally, no significant difference ( $P > 0.05$ ) was determined between the *Cat* and *Blank* sensor maximum current response.

| <b>50 <math>\mu</math>M H<sub>2</sub>O<sub>2</sub></b> | <b>Current change (pA)</b> | <b>Baseline Change (%)</b> | <b>Max response (mins)</b> | <b>Return (mins)</b> | <b>Pre-perfusion baseline (pA)</b> | <b>Post-perfusion baseline (pA)</b> |
|--|----------------------------|----------------------------|----------------------------|----------------------|------------------------------------|-------------------------------------|
| <i>Blank</i>   | -21.5 $\pm$ 10.9           | 93.3 $\pm$ 3.0             | 11.3 $\pm$ 2.0             | 20.6 $\pm$ 1.5       | 300.4 $\pm$ 22.7                   | 278.9 $\pm$ 11.9                    |
| <i>Cat</i>   | -26.0 $\pm$ 9.3            | 92.5 $\pm$ 1.8             | -                          | -                    | 329.2 $\pm$ 55.2                   | 301.0 $\pm$ 42.4                    |

**Table 5.9.2.1: Summary of results obtained on perfusion of 50  $\mu$ M H<sub>2</sub>O<sub>2</sub>. Data obtained from 3 paired H<sub>2</sub>O<sub>2</sub> sensors implanted in the striatum of 3 Wistar rats.**

The pre-perfusion baseline level prior to administration and the maximum current change recorded by both sensors (*Blank* and *Cat*) following perfusion of 50  $\mu$ M are not significantly different ( $P > 0.05$ ). Therefore it is difficult to represent the overall maximum change in H<sub>2</sub>O<sub>2</sub> response by subtraction. This factor is discussed in Section 5.12.

### 5.9.3 100 $\mu$ M H<sub>2</sub>O<sub>2</sub>

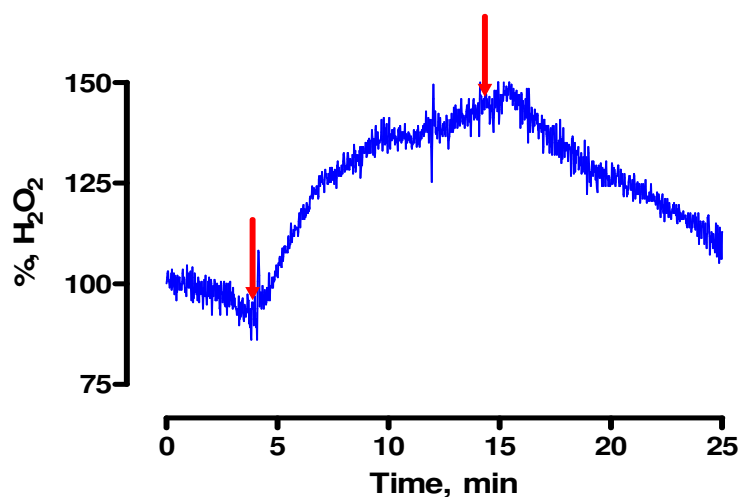


**Figure 5.9.3: A typical example of a 100  $\mu$ M H<sub>2</sub>O<sub>2</sub> perfusion detected by the paired H<sub>2</sub>O<sub>2</sub> sensor implanted in the striatum of an anaesthetised Wistar rat. The arrows indicate the duration of the perfusion.**

An immediate increase in response ( $93.3 \pm 42.4$  pA,  $n = 3$ ) was observed due to the perfusion of  $100 \mu\text{M}$  H<sub>2</sub>O<sub>2</sub> which corresponds to a  $142.9 \pm 11.5$  %,  $n = 3$  change from baseline. A continuous increase in response is apparent on progression of the perfusion. Once the perfusion is stopped as indicated by the arrows in Figure 5.9.3, an immediate decrease in response can be seen. The maximum change observed occurred after  $8.6 \pm 2.0$  mins ( $n = 3$ ) following the start of the perfusion and returned to a baseline level  $21.2 \pm 1.4$  mins ( $n = 3$ ) subsequently. No significant difference ( $P > 0.05$ ) was observed between pre-perfusion and post-perfusion baseline levels. A summary of the data is provided below in Table 5.9.4.

| Analyte  | Current change (pA) | Baseline change (%) | Conc. change (nM) | Max response (mins) | Return (mins)  | Pre-perfusion baseline (pA) | Post-perfusion baseline (pA) |
|--|---------------------|---------------------|-------------------|---------------------|----------------|-----------------------------|------------------------------|
| <b>100 <math>\mu\text{M}</math> H<sub>2</sub>O<sub>2</sub></b> | $93.3 \pm 42.4$     | $142.9 \pm 11.5$    | $200.1 \pm 91.0$  | $8.6 \pm 2.0$       | $21.2 \pm 1.4$ | $-192.4 \pm 48.2$           | $-116.3 \pm 25.2$            |

**Table 5.9.3.1: Summary of results obtained on perfusion of  $100 \mu\text{M}$  H<sub>2</sub>O<sub>2</sub>. Data obtained from 3 paired H<sub>2</sub>O<sub>2</sub> sensors implanted in the striatum of 3 Wistar rats.**

A greater discrepancy in the maximum current response could be seen between the *Cat* and *Blank* sensor following addition of  $100 \mu\text{M}$  H<sub>2</sub>O<sub>2</sub> and higher concentrations to the perfusate. The *Blank* sensor responded to an increased concentration of H<sub>2</sub>O<sub>2</sub> added to the perfusate (Figure 5.9.3.1).

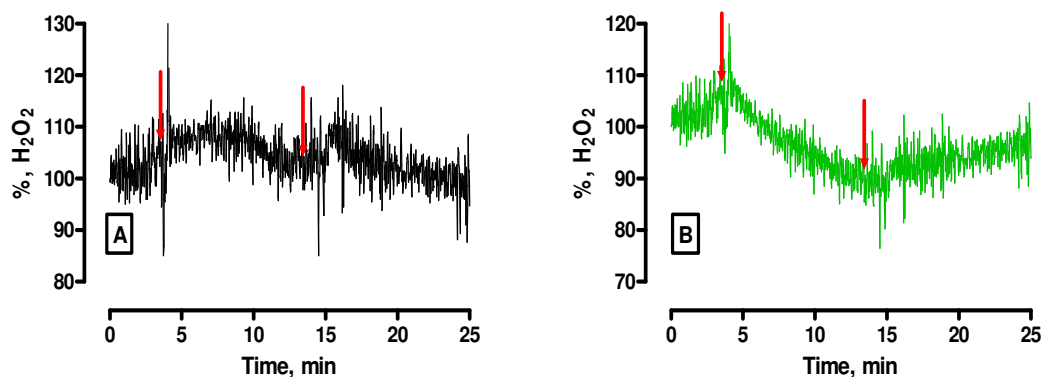


**Figure 5.9.3.1:** A typical example of a 100  $\mu\text{M}$  H<sub>2</sub>O<sub>2</sub> perfusion detected by (A) *Blank* sensor and (B) *Cat* sensor; implanted in the striatum of an anaesthetised Wistar rat. The arrows indicate the duration of the perfusion.

An overall increase in response was detected by the paired H<sub>2</sub>O<sub>2</sub> sensor due to the addition of 100  $\mu\text{M}$  H<sub>2</sub>O<sub>2</sub> to the perfusate. This perfusion decreased the response of the *Blank* sensor (A) to  $89.2 \pm 7.2$  % ( $n = 3$ ) of basal levels after  $8.6 \pm 2.0$  mins ( $n = 3$ ) from the start of each perfusion. A greater decrease was detected by the *Cat* sensor (B) ( $83.1 \pm 9.5$  %,  $n = 3$ ). No significant difference ( $P > 0.05$ ) was observed between the pre-perfusion baseline and the post-perfusion baselines of the *Cat* and *Blank* sensors.

| <b>100 <math>\mu\text{M}</math> H<sub>2</sub>O<sub>2</sub></b> | <b>Current change (pA)</b> | <b>Baseline Change (%)</b> | <b>Max response (mins)</b> | <b>Return (mins)</b> | <b>Pre-perfusion baseline (pA)</b> | <b>Post-perfusion baseline (pA)</b> |
|--|----------------------------|----------------------------|----------------------------|----------------------|------------------------------------|-------------------------------------|
| <i>Blank</i>   | $-67.4 \pm 52.7$           | $89.2 \pm 7.2$             | $8.6 \pm 2.0$              | $21.2 \pm 1.4$       | $509.6 \pm 99.1$                   | $420.2 \pm 41.8$                    |
| <i>Cat</i>   | $-144.2 \pm 101.2$         | $83.1 \pm 9.5$             | -                          | -                    | $632.8 \pm 199.8$                  | $474.3 \pm 109.8$                   |

**Table 5.9.3.1:** Summary of results obtained on perfusion of 50  $\mu\text{M}$  H<sub>2</sub>O<sub>2</sub>. Data obtained from 3 paired H<sub>2</sub>O<sub>2</sub> sensors implanted in the striatum of 3 Wistar rats.

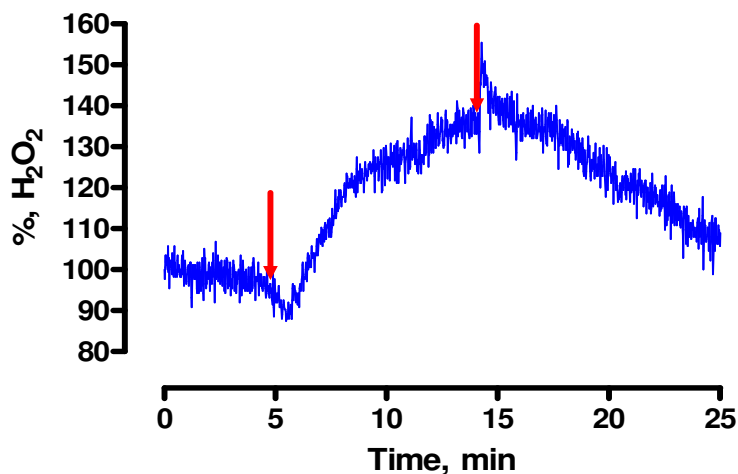
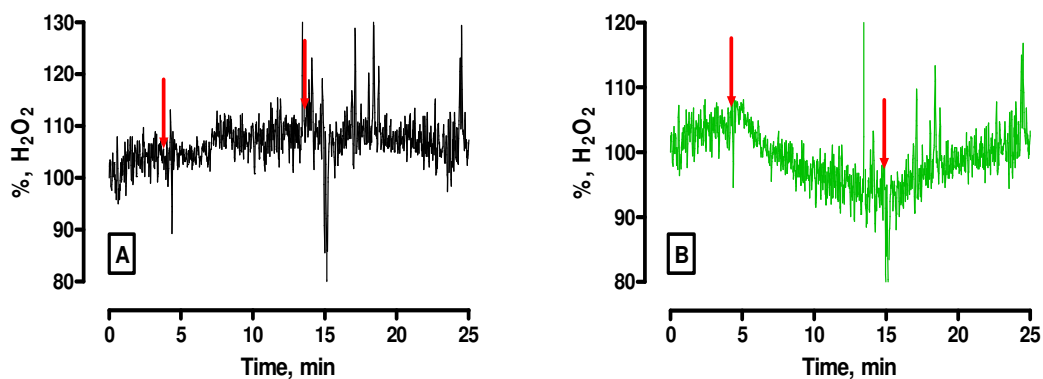
5.9.4 200  $\mu\text{M}$  H<sub>2</sub>O<sub>2</sub>

Figure 5.9.4: A typical example of a 200  $\mu\text{M}$  H<sub>2</sub>O<sub>2</sub> perfusion detected by the paired H<sub>2</sub>O<sub>2</sub> sensor implanted in the striatum of an anaesthetised Wistar rat. The arrows indicate the duration of the perfusion.

The concentration of H<sub>2</sub>O<sub>2</sub> in the perfusate was increased to 200  $\mu\text{M}$ . An increase in current response was recorded ( $47.9 \pm 10$  pA,  $n = 4$ , 5adm) due to the perfusion. The maximum change observed here occurred  $5.0 \pm 0.4$  mins ( $n = 4$ , 5adm) following the start of the perfusion and returned to a baseline level  $19.7 \pm 1.1$  mins ( $n = 4$ , 5adm) subsequently. No significant difference ( $P > 0.05$ ) was observed between pre-perfusion and post-perfusion baseline levels. A summary of the data is provided below in Table 5.9.4.

| Analyte   | Current change (pA) | Baseline change (%) | Conc. change (nM) | Max response (mins) | Return (mins)  | Pre-perfusion baseline (pA) | Post-perfusion baseline (pA) |
|---|---------------------|---------------------|-------------------|---------------------|----------------|-----------------------------|------------------------------|
| 200 $\mu\text{M}$ H <sub>2</sub> O <sub>2</sub> | $47.9 \pm 10.0$     | $135.9 \pm 7.6$     | $102.6 \pm 21.5$  | $5.0 \pm 0.4$       | $19.7 \pm 1.1$ | $19.7 \pm 1.1$              | $-72.7 \pm 52.8$             |

Table 5.9.4: Summary of results obtained on perfusion of 200  $\mu\text{M}$  H<sub>2</sub>O<sub>2</sub>. Data obtained from 4 paired H<sub>2</sub>O<sub>2</sub> sensors implanted in the striatum of 4 Wistar rats. The average data includes 5 administrations.



**Figure 5.9.4.1** A typical example of a 200  $\mu\text{M}$  H<sub>2</sub>O<sub>2</sub> perfusion detected by (A) *Blank* sensor and (B) *Cat* sensor; implanted in the striatum of an anaesthetised Wistar rat. The arrows indicate the duration of the perfusion.

The *Blank* sensor (A) response remained close to baseline levels following the perfusion of 200  $\mu\text{M}$  H<sub>2</sub>O<sub>2</sub>, a maximum current response of  $(-15.1 \pm 31.2 \text{ pA}, n = 4, 5\text{adm})$  was recorded by the *Blank* sensor which corresponds to a  $97.6 \pm 9.3 \%$ ,  $n = 4, 5\text{adm}$  change. A decrease in current response was detected by the *Cat* sensor  $(-63.0 \pm 22.3 \text{ pA}, n = 4, 5\text{adm})$ . Due to the proximity of the pre-perfusion baseline of both sensor designs (Table 5.9.5.1) an overall maximum increase was detected by the paired H<sub>2</sub>O<sub>2</sub> sensor following addition of 200  $\mu\text{M}$  H<sub>2</sub>O<sub>2</sub> to the perfusate. No significant difference ( $P > 0.05$ ) was observed between the pre-perfusion baseline and the post-perfusion baselines of the *Cat* and *Blank* sensors.

| <b>200 <math>\mu</math>M H<sub>2</sub>O<sub>2</sub></b> | <b>Current change (pA)</b> | <b>Baseline Change (%)</b> | <b>Max response (mins)</b> | <b>Return (mins)</b> | <b>Pre-perfusion baseline (pA)</b> | <b>Post-perfusion baseline (pA)</b> |
|---|----------------------------|----------------------------|----------------------------|----------------------|------------------------------------|-------------------------------------|
| <i>Blank</i>  | -15.1 $\pm$ 31.2           | 97.6 $\pm$ 9.3             | 5.0 $\pm$ 0.4              | 19.7 $\pm$ 1.1       | 370.9 $\pm$ 31.5                   | 353.0 $\pm$ 22.2                    |
| <i>Cat</i>  | -63.0 $\pm$ 22.3           | 85.3 $\pm$ 6.5             | -                          | -                    | 472.4 $\pm$ 64.4                   | 444.6 $\pm$ 57.9                    |

Table 5.9.4.1: Summary of results obtained on perfusion of 200  $\mu$ M H<sub>2</sub>O<sub>2</sub>. Data obtained from 4 paired H<sub>2</sub>O<sub>2</sub> sensors implanted in the striatum of 4 Wistar rats. The average data includes 5 administrations.

### 5.9.5 500 $\mu$ M H<sub>2</sub>O<sub>2</sub>

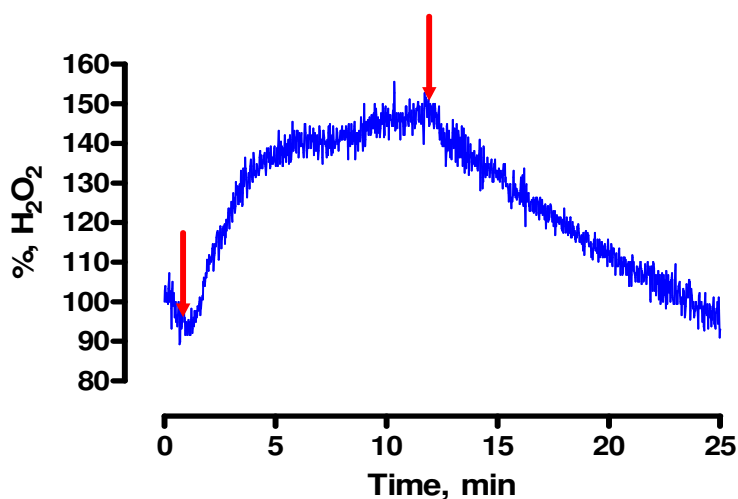


Figure 5.9.5: A typical example of a 500  $\mu$ M H<sub>2</sub>O<sub>2</sub> perfusion detected by the paired H<sub>2</sub>O<sub>2</sub> sensor implanted in the striatum of an anaesthetised Wistar rat. The arrows indicate the duration of the perfusion.

The concentration of H<sub>2</sub>O<sub>2</sub> in the perfusate was increased to 500  $\mu$ M. An immediate increase in response (161.3  $\pm$  17.6 %, n = 3) was observed due to the perfusion of 500  $\mu$ M H<sub>2</sub>O<sub>2</sub>. There was an immediate increase in H<sub>2</sub>O<sub>2</sub> response and a subsequent return to baseline levels as shown in Figure 5.9.5. The maximum change observed here occurred 9.9  $\pm$  0.8 mins (n = 3) following the start of the perfusion and returned to a baseline level 20.3  $\pm$  1.4 mins (n = 3) subsequently. No significant difference ( $P > 0.05$ ) was

observed between pre-perfusion and post-perfusion baseline levels. A summary of the data is provided below in Table 5.9.5.

| Analyte                                   | Current change (pA) | Baseline change (%) | Conc. change (nM) | Max response (mins) | Return (mins)  | Pre-perfusion baseline (pA) | Post-perfusion baseline (pA) |
|---|---------------------|---------------------|-------------------|---------------------|----------------|-----------------------------|------------------------------|
| 500 $\mu$ M H <sub>2</sub> O <sub>2</sub> | 72.1 $\pm$ 25.3     | 161.3 $\pm$ 17.6    | 154.5 $\pm$ 54.2  | 9.9 $\pm$ 0.8       | 20.3 $\pm$ 1.4 | -115.4 $\pm$ 37.4           | -43.3 $\pm$ 28.0             |

**Table 5.9.5:** Summary of results obtained on perfusion of 500  $\mu$ M H<sub>2</sub>O<sub>2</sub>. Data obtained from 3 paired H<sub>2</sub>O<sub>2</sub> sensors implanted in the striatum of 3 Wistar rats.

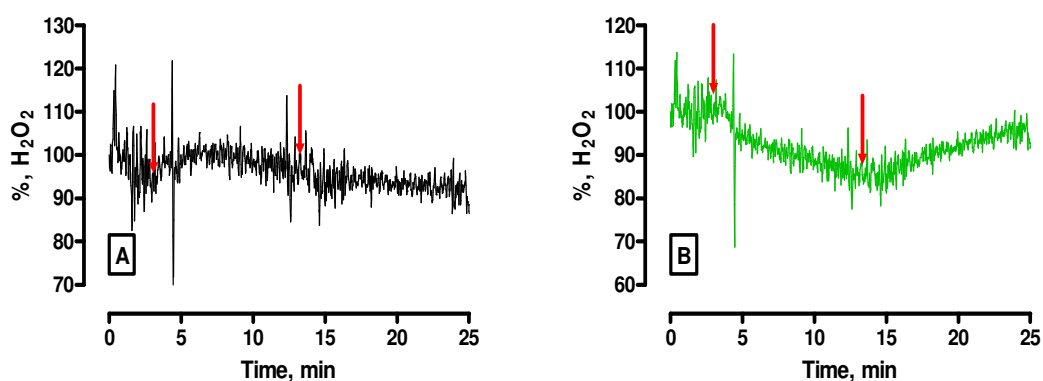


**Figure 5.9.5.1:** A typical example of a 500  $\mu$ M H<sub>2</sub>O<sub>2</sub> perfusion detected by (A) *Blank* sensor and (B) *Cat* sensor; implanted in the striatum of an anaesthetised Wistar rat. The arrows indicate the duration of the perfusion.

Following the perfusion of 500  $\mu$ M H<sub>2</sub>O<sub>2</sub> the *Blank* sensor (A) response remained close to baseline levels, a maximum current response of  $(-25.0 \pm 17.0$  pA,  $n = 3$ ) was recorded by the *Blank* sensor which corresponds to a  $93.3 \pm 4.6$  %,  $n = 3$  change. A deviation from baseline in current response was detected by the *Cat* sensor of  $-24.7 \pm 48.7$  pA,  $n = 3$ . As observed with the 200  $\mu$ M perfusion, due to the proximity of the pre-perfusion baseline of both sensor designs (Table 5.9.5.1) an overall maximum increase was detected by the paired H<sub>2</sub>O<sub>2</sub> sensor following addition of 500  $\mu$ M H<sub>2</sub>O<sub>2</sub> to the perfusate. No significant difference ( $P > 0.05$ ) was observed between the pre-perfusion baseline and the post-perfusion baselines of the *Cat* and *Blank* sensors.

| <b>500 <math>\mu</math>M<br/>H<sub>2</sub>O<sub>2</sub></b> | <b>Current<br/>change<br/>(pA)</b> | <b>Baseline<br/>Change<br/>(%)</b> | <b>Max<br/>response<br/>(mins)</b> | <b>Return<br/>(mins)</b> | <b>Pre-<br/>perfusion<br/>baseline<br/>(pA)</b> | <b>Post-<br/>perfusion<br/>baseline<br/>(pA)</b> |
|---|------------------------------------|------------------------------------|------------------------------------|--------------------------|---|--|
| <i>Blank</i>  | -25.0 $\pm$<br>17.0                | 93.3 $\pm$ 4.6                     | 9.9 $\pm$ 0.8                      | 20.3 $\pm$ 1.4           | 382.1 $\pm$<br>8.9                              | 351.2 $\pm$<br>10.9                              |
| <i>Cat</i>  | -24.7 $\pm$<br>48.7                | 98.6 $\pm$<br>13.8                 | -                                  | -                        | 422.5 $\pm$<br>84.9                             | 383.5 $\pm$<br>90.1                              |

Table 5.9.5.1: Summary of results obtained on perfusion of 500  $\mu$ M H<sub>2</sub>O<sub>2</sub>. Data obtained from 3 paired H<sub>2</sub>O<sub>2</sub> sensors implanted in the striatum of 3 Wistar rats.

### 5.9.6 1000 $\mu$ M H<sub>2</sub>O<sub>2</sub>

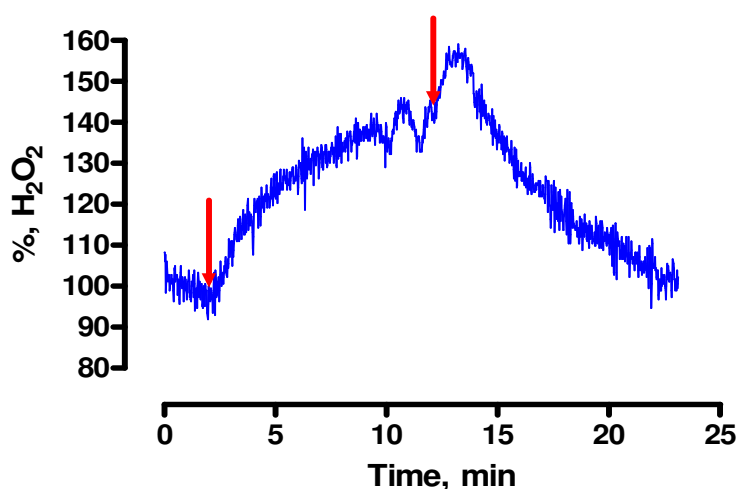


Figure 5.9.6: A typical example of a 1000  $\mu$ M H<sub>2</sub>O<sub>2</sub> perfusion detected by the paired H<sub>2</sub>O<sub>2</sub> sensor implanted in the striatum of an anaesthetised Wistar rat. The arrows indicate the duration of the perfusion.

In this case a relatively high concentration of H<sub>2</sub>O<sub>2</sub> was added to the perfusate (1000  $\mu$ M). An immediate increase in response was observed due to the perfusion (162.7  $\pm$  12.0 %, n = 3). There was a sharp immediate increase in H<sub>2</sub>O<sub>2</sub> response and a subsequent return to baseline levels as shown in Figure 5.9.7. The change observed here was not significantly different (P > 0.05) from that seen on introduction of 500  $\mu$ M H<sub>2</sub>O<sub>2</sub> (Figure 5.9.5). However a plateau region is not evident in this case when compared to Figure 5.9.5. The increase in response outlasts the duration of the perfusion. It is

possible that this concentration of H<sub>2</sub>O<sub>2</sub> (1000 μM) has more of a detrimental effect on mechanisms which exist *in-vivo* to remove exogenously applied H<sub>2</sub>O<sub>2</sub>. The maximum change detected here occurred  $5.4 \pm 1.8$  mins ( $n = 3$ ) following the start of the perfusion and returned to a baseline level  $18.6 \pm 0.9$  mins ( $n = 3$ ) subsequently. No significant difference ( $P > 0.05$ ) was found between pre-perfusion and post-perfusion baseline levels. A summary of the data is provided below in Table 5.9.6.

| Analyte                               | Current change (pA) | Baseline change (%) | Conc. change (nM) | Max response (mins) | Return (mins)  | Pre-perfusion baseline (pA) | Post-perfusion baseline (pA) |
|---------------------------------------|---------------------|---------------------|-------------------|---------------------|----------------|-----------------------------|------------------------------|
| 1000 μM H <sub>2</sub> O <sub>2</sub> | $56.5 \pm 14.7$     | $162.7 \pm 12.0$    | $121.1 \pm 31.5$  | $5.4 \pm 1.8$       | $18.6 \pm 0.9$ | $-48.3 \pm 76.2$            | $-41.0 \pm 75.7$             |

Table 5.9.6: Summary of results obtained on perfusion of 1000 μM H<sub>2</sub>O<sub>2</sub>. Data obtained from 3 paired H<sub>2</sub>O<sub>2</sub> sensors implanted in the striatum of 3 Wistar rats.

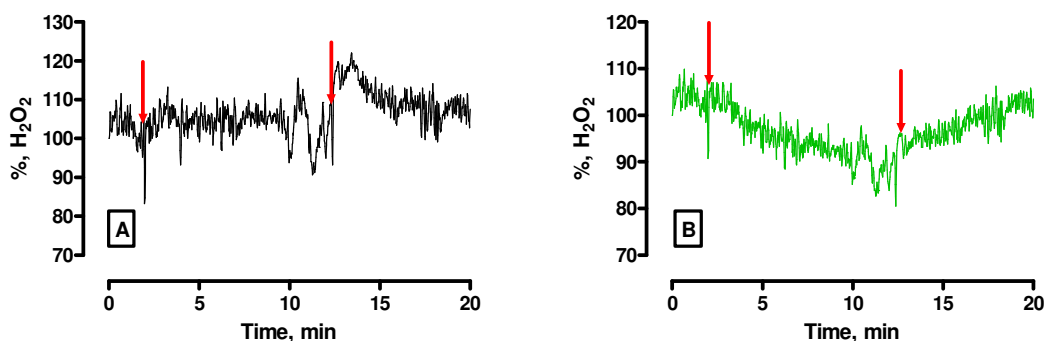


Figure 5.9.6.1: A typical example of a 1000 μM H<sub>2</sub>O<sub>2</sub> perfusion detected by (A) *Blank* sensor and (B) *Cat* sensor; implanted in the striatum of an anaesthetised Wistar rat. The arrows indicate the duration of the perfusion.

An average increase was detected by the *Blank* sensor (A) following the perfusion of 1000 μM H<sub>2</sub>O<sub>2</sub>, a maximum current response of  $(26.9 \pm 37.9$  pA,  $n = 3$ ) was recorded by the *Blank* sensor which corresponds to a  $(110.7 \pm 13.9$  %,  $n = 3$ ) change. A decrease in current response was detected by the *Cat* sensor ( $-29.6 \pm 33.4$ ,  $n = 3$ ) which corresponds

to  $(97.6 \pm 10.7 \%, n = 3)$ . An overall increase was detected by the paired H<sub>2</sub>O<sub>2</sub> sensor following addition of 1000  $\mu\text{M}$  H<sub>2</sub>O<sub>2</sub> to the perfusate. No significant difference ( $P > 0.05$ ) was observed between the pre-perfusion baseline and the post-perfusion baselines of the *Cat* and *Blank* sensors.

| <b>1000 <math>\mu\text{M}</math> H<sub>2</sub>O<sub>2</sub></b> | <b>Current change (pA)</b> | <b>Baseline Change (%)</b> | <b>Max response (mins)</b> | <b>Return (mins)</b> | <b>Pre-perfusion baseline (pA)</b> | <b>Post-perfusion baseline (pA)</b> |
|---|----------------------------|----------------------------|----------------------------|----------------------|------------------------------------|-------------------------------------|
| <i>Blank</i>  | $26.9 \pm 37.9$            | $110.7 \pm 13.9$           | $5.4 \pm 1.8$              | $18.6 \pm 0.9$       | $327.6 \pm 31.3$                   | $325.4 \pm 24.9$                    |
| <i>Cat</i>  | $-29.6 \pm 33.4$           | $97.6 \pm 10.7$            | -                          | -                    | $375.9 \pm 106.0$                  | $366.5 \pm 100.5$                   |

**Table 5.9.6.1: Summary of results obtained on perfusion of 1000  $\mu\text{M}$  H<sub>2</sub>O<sub>2</sub>. Data obtained from 3 paired H<sub>2</sub>O<sub>2</sub> sensors implanted in the striatum of 3 Wistar rats.**

### 5.9.7 10 mM H<sub>2</sub>O<sub>2</sub>

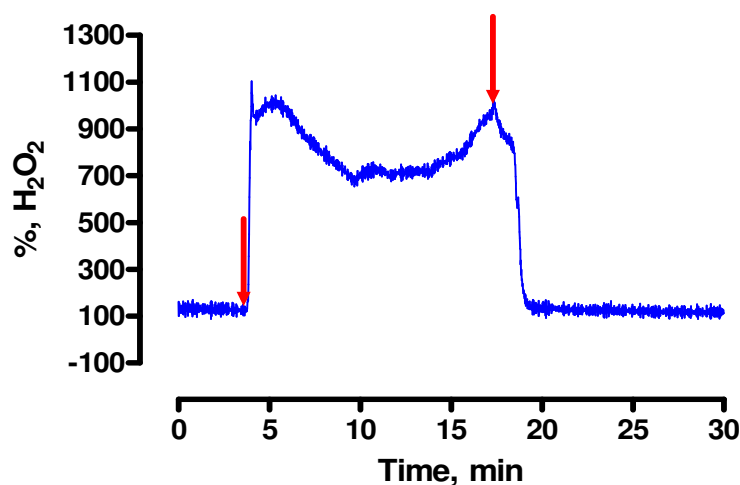


**Figure 5.9.7: A typical example of a 10 mM H<sub>2</sub>O<sub>2</sub> perfusion detected by the paired H<sub>2</sub>O<sub>2</sub> sensor implanted in the striatum of an anaesthetised Wistar rat. The arrows indicate the duration of the perfusion.**

A high concentration of H<sub>2</sub>O<sub>2</sub> (10 mM) was introduced to the perfusate. An immediate increase in response ( $1696.2 \pm 80.0 \text{ pA}, n = 2$ ) was observed due to the perfusion which reached a distinct maximum increase of  $932.7 \pm 157.8 \%$  ( $n = 2$ ) above basal levels. The

maximum change detected here occurred  $10.6 \pm 1.4$  mins ( $n = 2$ ) following the start of the perfusion and returned to a baseline level  $16.6 \pm 2.1$  mins ( $n = 2$ ) following the perfusion. No significant difference ( $P > 0.05$ ) was found between pre-perfusion and post-perfusion baseline levels. A summary of the data is provided in Table 5.9.7.

| Analyte                             | Current change (pA) | Baseline change (%) | Conc. change (nM)  | Max response (mins) | Return (mins)  | Pre-perfusion baseline (pA) | Post-perfusion baseline (pA) |
|-------------------------------------|---------------------|---------------------|--------------------|---------------------|----------------|-----------------------------|------------------------------|
| 10 mM H <sub>2</sub> O <sub>2</sub> | $1696.2 \pm 80.0$   | $932.7 \pm 157.8$   | $3636.0 \pm 171.5$ | $10.6 \pm 1.4$      | $16.6 \pm 2.1$ | $-58.9 \pm 60.0$            | $-58.9 \pm 59.4$             |

Table 5.9.7: Summary of results obtained on perfusion of 10 mM H<sub>2</sub>O<sub>2</sub>. Data obtained from 2 paired H<sub>2</sub>O<sub>2</sub> sensors implanted in the striatum of 2 Wistar rats.

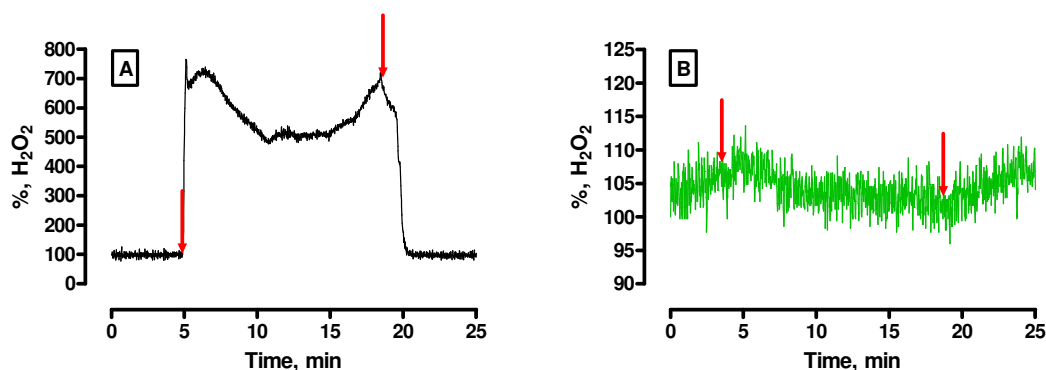


Table 5.9.7.1: A typical example of a 10 mM H<sub>2</sub>O<sub>2</sub> perfusion detected by (A) *Blank* sensor and (B) *Cat* sensor; implanted in the striatum of an anaesthetised Wistar rat. The arrows indicate the duration of the perfusion.

Following the perfusion of 10 mM H<sub>2</sub>O<sub>2</sub> a clear increase in response of ( $1374.4 \pm 39.3$  pA,  $n = 2$ ) was detected by the *Blank* sensor (A), which corresponds to a percentage change of ( $626.5 \pm 53.6$  %,  $n = 3$ ). A slight deviation from baseline levels was detected by the *Cat* sensor ( $0.7 \pm 1.3$  pA,  $n = 3$ ) which corresponds to ( $100.3 \pm 0.4$  %,  $n = 3$ ). An overall increase was detected by the paired H<sub>2</sub>O<sub>2</sub> sensor following addition of 10 mM H<sub>2</sub>O<sub>2</sub> to the perfusate. No significant difference ( $P > 0.05$ ) was observed between the pre-perfusion baseline and the post-perfusion baselines of the *Cat* and *Blank* sensors.

Additionally a significant difference ( $P < 0.05, *$ ) was determined between the *Cat* and *Blank* sensor maximum current response.

| <b>10 mM H<sub>2</sub>O<sub>2</sub></b> | <b>Current change (pA)</b> | <b>Baseline Change (%)</b> | <b>Max response (mins)</b> | <b>Return (mins)</b> | <b>Pre-perfusion baseline (pA)</b> | <b>Post-perfusion baseline (pA)</b> |
|---|----------------------------|----------------------------|----------------------------|----------------------|------------------------------------|-------------------------------------|
| <i>Blank</i>                            | 1374.4 ± 39.3              | 626.5 ± 53.6               | 10.6 ± 1.4                 | 16.6 ± 2.1           | 263.0 ± 19.3                       | 260.9 ± 16.4                        |
| <i>Cat</i>                              | 0.7 ± 1.3                  | 100.3 ± 0.4                | -                          | -                    | 321.9 ± 40.7                       | 319.8 ± 42.9                        |

Table 5.9.7.1: Summary of results obtained on perfusion of 10 mM H<sub>2</sub>O<sub>2</sub>. Data obtained from 2 paired H<sub>2</sub>O<sub>2</sub> sensors implanted in the striatum of 2 Wistar rats.

### 5.9.8 100 mM H<sub>2</sub>O<sub>2</sub>

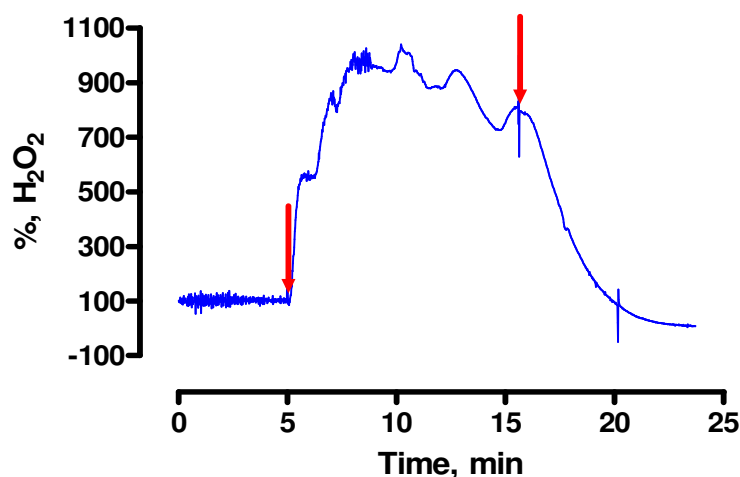


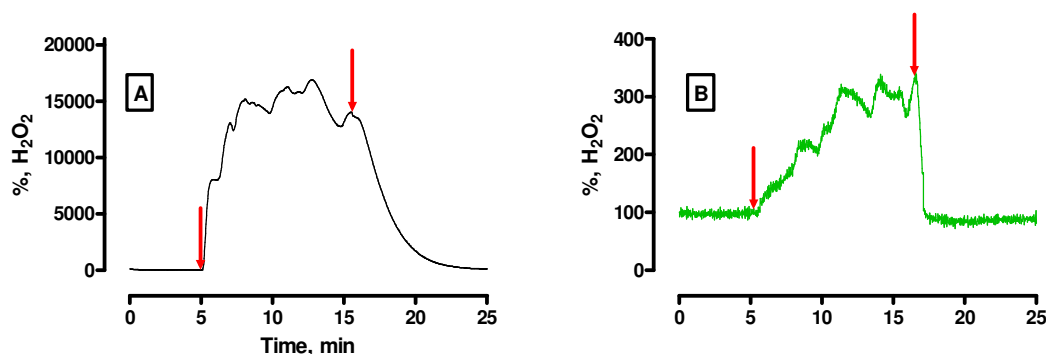
Figure 5.9.8: A typical example of a 100 mM H<sub>2</sub>O<sub>2</sub> perfusion detected by the paired H<sub>2</sub>O<sub>2</sub> sensor implanted in the striatum of an anaesthetised Wistar rat. The arrows indicate the duration of the perfusion.

Figure 5.9.8 demonstrates the typical response recorded following the perfusion of 100 mM H<sub>2</sub>O<sub>2</sub>. An immediate increase in response ( $2725.1 \pm 1011.5$  pA,  $n = 3$ ) was seen following the perfusion. There was an instantaneous increase in H<sub>2</sub>O<sub>2</sub> response followed by a plateau region and a subsequent return to baseline levels as shown in Figure 5.9.8. The highest concentration of H<sub>2</sub>O<sub>2</sub> used in these sets of experiments (100 mM) exerts

the highest overall effect on H<sub>2</sub>O<sub>2</sub> detection by the paired H<sub>2</sub>O<sub>2</sub> sensor in the acute preparation. The maximum change in signal detected here occurred  $3.7 \pm 0.7$  mins ( $n = 3$ ) following the start of the perfusion and returned to a baseline level  $15.5 \pm 2.8$  mins ( $n = 3$ ) following the perfusion. No significant difference ( $P > 0.05$ ) was found between pre-perfusion and post-perfusion baseline levels of the paired H<sub>2</sub>O<sub>2</sub> sensor. A summary of the data is provided in Table 5.9.8.

| Analyte                              | Current change (pA) | Baseline change (%) | Conc. change (nM)   | Max response (mins) | Return (mins)  | Pre-perfusion baseline (pA) | Post-perfusion baseline (pA) |
|--------------------------------------|---------------------|---------------------|---------------------|---------------------|----------------|-----------------------------|------------------------------|
| 100 mM H <sub>2</sub> O <sub>2</sub> | $2725.1 \pm 1011.5$ | $1078 \pm 408.4$    | $5841.6 \pm 2168.3$ | $3.7 \pm 0.7$       | $15.5 \pm 2.8$ | $-309.3 \pm 115.5$          | $5841.6 \pm 2168.3$          |

**Table 5.9.8: Summary of results obtained on perfusion of 100 mM H<sub>2</sub>O<sub>2</sub>. Data obtained from 3 paired H<sub>2</sub>O<sub>2</sub> sensors implanted in the striatum of 3 Wistar rats.**



**Table 5.9.8.1: A typical example of a 100 mM H<sub>2</sub>O<sub>2</sub> perfusion detected by (A) *Blank* sensor and (B) *Cat* sensor; implanted in the striatum of an anaesthetised Wistar rat. The arrows indicate the duration of the perfusion.**

An immediate increase in response of ( $3280.1 \pm 1100.6$  pA,  $n = 3$ ) was detected by the *Blank* sensor (A) following the perfusion of 100 mM H<sub>2</sub>O<sub>2</sub>, which corresponds to a percentage change of ( $16055 \pm 8930.6$  %,  $n = 3$ ). A slight deviation from baseline levels was detected by the *Cat* sensor ( $0.7 \pm 1.3$  pA,  $n = 3$ ) which corresponds to ( $100.3 \pm 0.4$  %,  $n = 3$ ). An overall increase was detected by the paired H<sub>2</sub>O<sub>2</sub> sensor following

addition of 100 mM H<sub>2</sub>O<sub>2</sub> to the perfusate. No significant difference ( $P > 0.05$ ) was observed between the pre-perfusion baseline and the post-perfusion baselines of the *Cat* and *Blank* sensors.

| <b>100 mM H<sub>2</sub>O<sub>2</sub></b> | <b>Current change (pA)</b> | <b>Baseline Change (%)</b> | <b>Max response (mins)</b> | <b>Return (mins)</b> | <b>Pre-perfusion baseline (pA)</b> | <b>Post-perfusion baseline (pA)</b> |
|--|----------------------------|----------------------------|----------------------------|----------------------|------------------------------------|-------------------------------------|
| <i>Blank</i>                             | 3280.1 ± 1100.6            | 16055 ± 8930.6             | 3.7 ± 0.7                  | 15.5 ± 2.8           | 126.5 ± 105.6                      | 137.5 ± 119.2                       |
| <i>Cat</i>                               | 555 ± 291.5                | 258.4 ± 95.8               | -                          | -                    | 352.4 ± 79.1                       | 2499.2 ± 998.4                      |

**Table 5.9.8.1:** Summary of results obtained on perfusion of 100 mM H<sub>2</sub>O<sub>2</sub>. Data obtained from 3 paired H<sub>2</sub>O<sub>2</sub> sensors implanted in the striatum of 3 Wistar rats.

## 5.10 Local H<sub>2</sub>O<sub>2</sub> administration summary (acute preparation)

This section provides a summary of the data presented in Section 5.9. The maximum change recorded due to the local administration of H<sub>2</sub>O<sub>2</sub> by the paired H<sub>2</sub>O<sub>2</sub> sensor (*Blank-Cat*), the *Blank* sensor and the *Cat* sensor is compared against the corresponding aCSF response.

### 5.10.1 Paired H<sub>2</sub>O<sub>2</sub> sensor summary (acute)

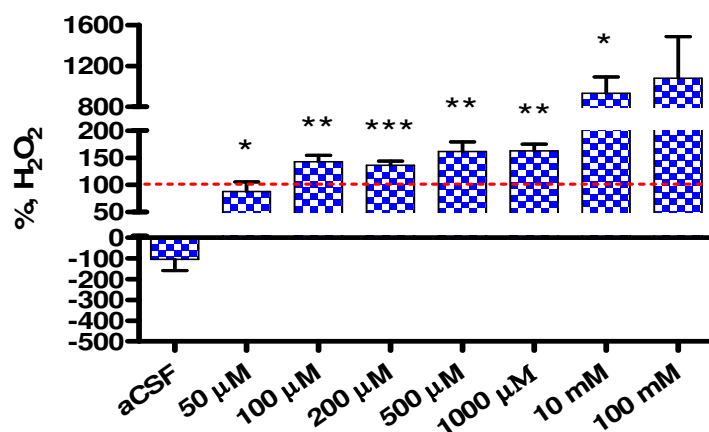


**Figure 5.10.1:** Paired H<sub>2</sub>O<sub>2</sub> sensor response following perfusions as discussed in Section 5.9. Data shown as an average percentage change, with 100 % as the pre-perfusion H<sub>2</sub>O<sub>2</sub> baseline signal.

| Analyte                               | Current change (pA) | Baseline change (%) | Conc. change (nM) | Max response (mins) | Return (mins) | Pre-perfusion baseline (pA) | Post-perfusion baseline (pA) | n | P      |
|---------------------------------------|---------------------|---------------------|-------------------|---------------------|---------------|-----------------------------|------------------------------|---|--------|
| aCSF                                  | -76.7 ± 24.6        | -105.7 ± 52.9       | -164.4 ± 52.7     | 13.2 ± 0.3          | 20.7 ± 0.6    | 117.2 ± 97.3                | 39.0 ± 47.6                  | 2 | n/a    |
| 50 µM H <sub>2</sub> O <sub>2</sub>   | 55.7 ± 63.6         | 87.9 ± 17.8         | 119.5 ± 136.4     | 11.3 ± 2.0          | 20.6 ± 1.5    | -28.8 ± 64.8                | -18.2 ± 48.1                 | 3 | 0.0240 |
| 100 µM H <sub>2</sub> O <sub>2</sub>  | 93.3 ± 42.4         | 142.9 ± 11.5        | 200.1 ± 91.0      | 8.6 ± 2.0           | 21.2 ± 1.4    | -192.4 ± 48.2               | -116.3 ± 25.2                | 3 | 0.0097 |
| 200 µM H <sub>2</sub> O <sub>2</sub>  | 47.9 ± 10.0         | 135.9 ± 7.6         | 102.6 ± 21.5      | 5.0 ± 0.4           | 19.7 ± 1.1    | 19.7 ± 1.1                  | -72.7 ± 52.8                 | 4 | 0.0005 |
| 500 µM H <sub>2</sub> O <sub>2</sub>  | 72.1 ± 25.3         | 161.3 ± 17.6        | 154.5 ± 54.2      | 9.9 ± 0.8           | 20.3 ± 1.4    | -115.4 ± 37.4               | -43.3 ± 28.0                 | 3 | 0.0099 |
| 1000 µM H <sub>2</sub> O <sub>2</sub> | 56.5 ± 14.7         | 162.7 ± 12.0        | 121.1 ± 31.5      | 5.4 ± 1.8           | 18.6 ± 0.9    | -48.3 ± 76.2                | -41.0 ± 75.7                 | 3 | 0.0080 |
| 10 mM H <sub>2</sub> O <sub>2</sub>   | 1696.2 ± 80.0       | 932.7 ± 157.8       | 3636.0 ± 171.5    | 10.6 ± 1.4          | 16.6 ± 2.1    | -58.9 ± 60.0                | -58.9 ± 59.4                 | 2 | 0.0247 |
| 100 mM H <sub>2</sub> O <sub>2</sub>  | 2725.1 ± 1011.5     | 1078 ± 408.4        | 5841.6 ± 2168.3   | 3.7 ± 0.7           | 15.5 ± 2.8    | -309.3 ± 115.5              | 5841.6 ± 2168.3              | 3 | 0.1111 |

**Table 5.10.1: Summary of paired H<sub>2</sub>O<sub>2</sub> sensor results obtained following perfusions in anaesthetised animals as discussed in Section 5.9.**

Figure 5.10.1 and Table 5.10.1 summarises the paired H<sub>2</sub>O<sub>2</sub> sensor data discussed in Section 5.9. The effect of the local administration of aCSF can be used as a control against which the perfusion of each concentration of H<sub>2</sub>O<sub>2</sub> can be measured. A significant difference ( $P < 0.05$ ,\*) was observed between the local aCSF and 50 µM perfusion of H<sub>2</sub>O<sub>2</sub>. A significant difference ( $P < 0.05$ ) was observed on perfusion of a higher concentration range of H<sub>2</sub>O<sub>2</sub> which was observed at each incremental stage from 100 µM to 10 mM H<sub>2</sub>O<sub>2</sub> when compared to the response observed with aCSF (Section 5.9.1) and the details of these statistical tests are presented in Table 5.10.1. At each intermediate increase in the concentration of H<sub>2</sub>O<sub>2</sub>, a proportional increase in H<sub>2</sub>O<sub>2</sub> response was detected by the dual catalase-based H<sub>2</sub>O<sub>2</sub> sensor. No significant difference ( $P > 0.05$ ) was observed between the 100 mM perfusion and the local administration of aCSF, however a clear increase above baseline levels of H<sub>2</sub>O<sub>2</sub> is apparent.

A one-way ANOVA analysis of variance revealed a significant difference ( $P < 0.01$ ,\*\*) between the maximum response time of each perfusion. The time required to reach a maximum response generally decreased as the concentration of H<sub>2</sub>O<sub>2</sub> added to the

perfusate increased. The time required to return to baseline levels following each perfusion was not significantly different ( $P > 0.05$ ) as determined by one-way ANOVA. A significant difference ( $P < 0.01, ***$ ) for the pre-perfusion and post-perfusion baseline level for each change in concentration of H<sub>2</sub>O<sub>2</sub> added to the perfusate was observed as determined by a one-way ANOVA analysis of variance. The difference observed with pre and post-perfusion baseline levels between different H<sub>2</sub>O<sub>2</sub> concentrations locally introduced, is due to the proximity of the *Blank* and *Cat* sensor baseline response in the anaesthetised animal which is further discussed in Section 5.12.

A contrasting H<sub>2</sub>O<sub>2</sub> response was observed here in comparison to that observed in the freely-moving animal data. A clear increase above baseline levels of H<sub>2</sub>O<sub>2</sub> was detected by the dual H<sub>2</sub>O<sub>2</sub> sensor at each stage from a concentration of 100  $\mu$ M to 100 mM H<sub>2</sub>O<sub>2</sub> in the acute experimental set-up. The disparity in the results between the acute and freely-moving animal data may be due to the constant use of anaesthetic in the acute procedure. Anaesthesia has been shown to cause an alteration of various mechanisms and levels of neurotransmitters in the central nervous system (CNS) which has been extensively reviewed by O'Neill *et al.* (O'Neill *et al.*, 1998). A limited amount of *in-vivo* data is available on the effect of volatile anesthetics such as Isoflurane on electroactive species such as H<sub>2</sub>O<sub>2</sub> in the brain.

Generally anaesthesia causes systemic CNS depression and hence a decrease in neuronal activity (Mueller *et al.*, 2011). It is possible that the network of antioxidant mechanisms which regulate the level of H<sub>2</sub>O<sub>2</sub>/ROS in the brain cannot function normally due to the effect of anaesthesia. In which case exogenously applied H<sub>2</sub>O<sub>2</sub> may not be efficiently removed and therefore an increase in H<sub>2</sub>O<sub>2</sub> levels in the ECF surrounding the implanted paired sensor occurs and a corresponding increase in current due to the presence of H<sub>2</sub>O<sub>2</sub> is detected by the sensor.

## 5.10.2 Blank sensor summary (acute)

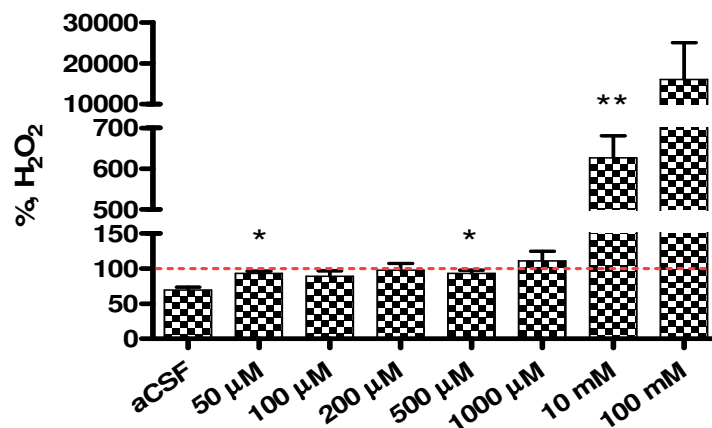


Figure 5.10.2: Blank sensor response following perfusions as discussed in Section 5.9. Data shown as an average percentage change, with 100 % as the pre-perfusion baseline signal.

| Analyte                               | Current change (pA) | Baseline change (%) | Max response (mins) | Return (mins) | Pre-perfusion baseline (pA) | Post-perfusion baseline (pA) | n | P      |
|---------------------------------------|---------------------|---------------------|---------------------|---------------|-----------------------------|------------------------------|---|--------|
| aCSF                                  | -142.1 ± 54.6       | 69.4 ± 4.4          | 13.2 ± 0.3          | 20.7 ± 0.6    | 447.7 ± 114.1               | 305.6 ± 59.5                 | 2 | n/a    |
| 50 μM H <sub>2</sub> O <sub>2</sub>   | -21.5 ± 10.9        | 93.3 ± 3.0          | 11.3 ± 2.0          | 20.6 ± 1.5    | 300.4 ± 22.7                | 278.9 ± 11.9                 | 3 | 0.0177 |
| 100 μM H <sub>2</sub> O <sub>2</sub>  | -67.4 ± 52.7        | 89.2 ± 7.2          | 8.6 ± 2.0           | 21.2 ± 1.4    | 509.6 ± 99.1                | 420.2 ± 41.8                 | 3 | 0.1369 |
| 200 μM H <sub>2</sub> O <sub>2</sub>  | -15.1 ± 31.2        | 97.6 ± 9.3          | 5.0 ± 0.4           | 19.7 ± 1.1    | 370.9 ± 31.5                | 353.0 ± 22.2                 | 4 | 0.1339 |
| 500 μM H <sub>2</sub> O <sub>2</sub>  | -25.0 ± 17.0        | 93.3 ± 4.6          | 9.9 ± 0.8           | 20.3 ± 1.4    | 382.1 ± 8.9                 | 351.2 ± 10.9                 | 3 | 0.1339 |
| 1000 μM H <sub>2</sub> O <sub>2</sub> | 26.9 ± 37.9         | 110.7 ± 13.9        | 5.4 ± 1.8           | 18.6 ± 0.9    | 327.6 ± 31.3                | 325.4 ± 24.9                 | 3 | 0.1075 |
| 10 mM H <sub>2</sub> O <sub>2</sub>   | 1374.4 ± 39.3       | 626.5 ± 53.6        | 10.6 ± 1.4          | 16.6 ± 2.1    | 263.0 ± 19.3                | 260.9 ± 16.4                 | 2 | 0.0092 |
| 100 mM H <sub>2</sub> O <sub>2</sub>  | 3280.1 ± 1100.6     | 16055 ± 8930.6      | 3.7 ± 0.7           | 15.5 ± 2.8    | 126.5 ± 105.6               | 137.5 ± 119.2                | 3 | 0.2597 |

Table 5.10.2: Summary of Blank sensor results obtained following perfusions in anaesthetised animals as discussed in Section 5.9.

Figure 5.10.2 and Table 5.10.2 summarises the *Blank* sensor data discussed in Section 5.9. At relatively lower concentrations of H<sub>2</sub>O<sub>2</sub> added to the perfusate (50-1000  $\mu$ M H<sub>2</sub>O<sub>2</sub>) the *Blank* sensor response remains close to baseline levels. However a significant difference ( $P < 0.05, *$ ) was observed following perfusion of 50 and 500  $\mu$ M H<sub>2</sub>O<sub>2</sub> when compared to the response observed following aCSF perfusion (Section 5.9.1). In relation to the freely-moving animal data a higher response was detected by the *Blank* sensor in the acute preparation on perfusion of these concentrations of H<sub>2</sub>O<sub>2</sub> (50-1000  $\mu$ M H<sub>2</sub>O<sub>2</sub>). Following perfusion of 100 mM H<sub>2</sub>O<sub>2</sub> in the anaesthetised animal no significant difference ( $P > 0.05$ ) in the *Blank* sensor response was seen in comparison to the effect of aCSF administration however a clear increase above baseline levels can be seen (Figure 5.10.2).

### 5.10.3 Cat sensor summary (acute)

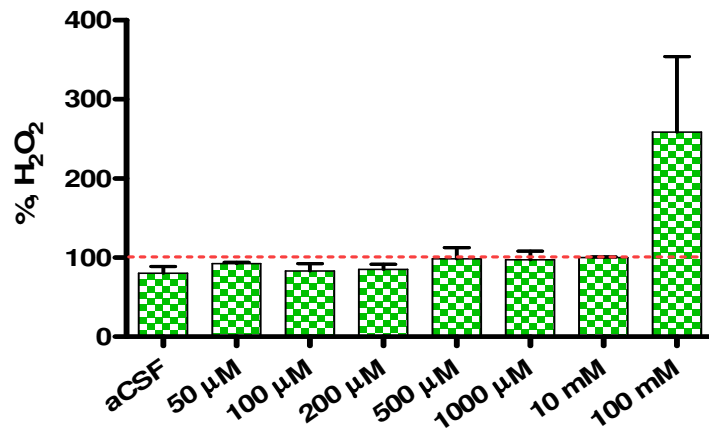


Figure 5.10.3: *Cat* sensor response following perfusions as discussed in Section 5.9. Data shown as an average percentage change, with 100 % as the pre-perfusion baseline signal.

| Analyte                               | Current change (pA) | Baseline change (%) | Max response (mins) | Return (mins) | Pre-perfusion baseline (pA) | Post-perfusion baseline (pA) | n | P      |
|---------------------------------------|---------------------|---------------------|---------------------|---------------|-----------------------------|------------------------------|---|--------|
| aCSF                                  | -65.4 ± 30.0        | 80.6 ± 8.1          | 13.2 ± 0.3          | 20.7 ± 0.6    | 330.6 ± 16.9                | 277.6 ± 6.3                  | 2 | n/a    |
| 50 µM H <sub>2</sub> O <sub>2</sub>   | -26.0 ± 9.3         | 92.5 ± 1.8          | 11.3 ± 2.0          | 20.6 ± 1.5    | 329.2 ± 55.2                | 301.0 ± 42.4                 | 3 | 0.1633 |
| 100 µM H <sub>2</sub> O <sub>2</sub>  | -144.2 ± 101.2      | 83.1 ± 9.5          | 8.6 ± 2.0           | 21.2 ± 1.4    | 632.8 ± 199.8               | 474.3 ± 109.8                | 3 | 0.8690 |
| 200 µM H <sub>2</sub> O <sub>2</sub>  | -63.0 ± 22.3        | 85.3 ± 6.5          | 5.0 ± 0.4           | 19.7 ± 1.1    | 472.4 ± 64.4                | 444.6 ± 57.9                 | 4 | 0.7059 |
| 500 µM H <sub>2</sub> O <sub>2</sub>  | -24.7 ± 48.7        | 98.6 ± 13.8         | 9.9 ± 0.8           | 20.3 ± 1.4    | 422.5 ± 84.9                | 383.5 ± 90.1                 | 3 | 0.4095 |
| 1000 µM H <sub>2</sub> O <sub>2</sub> | -29.6 ± 33.4        | 97.6 ± 10.7         | 5.4 ± 1.8           | 18.6 ± 0.9    | 375.9 ± 106.0               | 366.5 ± 100.5                | 3 | 0.3402 |
| 10 mM H <sub>2</sub> O <sub>2</sub>   | 0.7 ± 1.3           | 100.3 ± 0.4         | 10.6 ± 1.4          | 16.6 ± 2.1    | 321.9 ± 40.7                | 319.8 ± 42.9                 | 2 | 0.1361 |
| 100 mM H <sub>2</sub> O <sub>2</sub>  | 555 ± 291.5         | 258.4 ± 95.8        | 3.7 ± 0.7           | 15.5 ± 2.8    | 352.4 ± 79.1                | 2499.2 ± 998.4               | 3 | 0.2466 |

**Table 5.10.3: Summary of *Cat* sensor results obtained following perfusions in anaesthetised animals as discussed in Section 5.9.**

Figure 5.10.3 and Table 5.10.3 summarises the *Cat* sensor data discussed in Section 5.9. When compared to the corresponding aCSF perfusion no significant difference ( $P > 0.05$ ) in the *Cat* sensor response was seen following each perfusion of H<sub>2</sub>O<sub>2</sub> (50 µM-100 mM) in the anaesthetised animal. Although no significant difference ( $P > 0.05$ ) was observed between the 100 mM H<sub>2</sub>O<sub>2</sub> perfusion and the addition of aCSF to the perfusate a clear increase above baseline levels can be seen (Figure 5.10.3). The observed increase above baseline levels due to the local addition of the highest concentration of H<sub>2</sub>O<sub>2</sub> used in these experiments (100 mM) causes saturation of the catalase enzyme which is part of the *Cat* sensor design. Therefore an increased response occurs due to the local addition of a comparatively high concentration of H<sub>2</sub>O<sub>2</sub>. However it is clear from Figure 5.10.3 and Table 5.10.3 that the *Cat* sensor effectively eliminates a contribution to the overall response by removing the signal attributable to H<sub>2</sub>O<sub>2</sub> up to a concentration of 10 mM H<sub>2</sub>O<sub>2</sub>. The *Cat* sensor data obtained in the acute set-up compares well with that observed in the freely-moving animal experiments. In both scenarios no significant difference ( $P > 0.05$ ) can be seen following each concentration of H<sub>2</sub>O<sub>2</sub> locally introduced in comparison to the corresponding aCSF response.

### 5.11 Baseline stability (freely-moving)

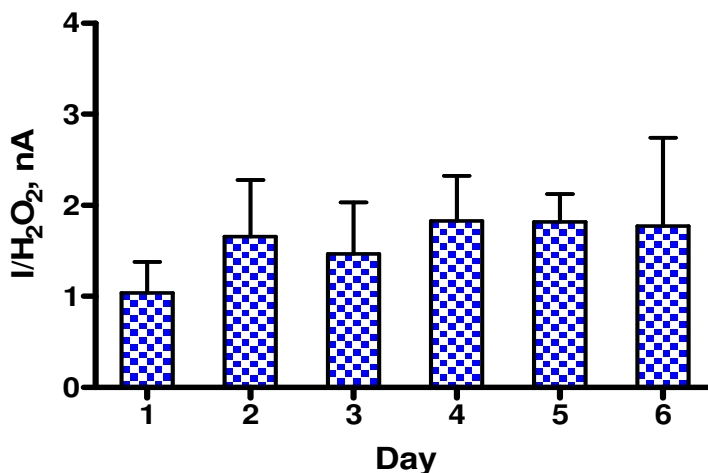


**Figure 5.11.1:** The average baseline recorded by the paired H<sub>2</sub>O<sub>2</sub> sensor *in-vivo* over a consecutive period of six days in freely-moving animals. Data represented as a mean response  $\pm$  SEM and  $n = 3$ .

A decrease in sensitivity of an electrochemical sensor can often be observed following contact with a biological sample (Garguilo & Michael, 1994). It was necessary to investigate any effect the physiological environment may have on the paired H<sub>2</sub>O<sub>2</sub> sensor when implanted. The mean baseline current of the paired H<sub>2</sub>O<sub>2</sub> sensor was examined over a consecutive period of six days and recordings were taken following an initial period of *ca.* 24 hrs following implantation.

The mean baseline current recorded by the paired H<sub>2</sub>O<sub>2</sub> sensor *in-vivo* over the stated successive period is shown in Figure 5.11.1. Each paired H<sub>2</sub>O<sub>2</sub> sensor was implanted in the striatum of a freely-moving rat. A one-way ANOVA analysis of variance revealed that the baseline current showed no significant variation  $P > 0.05$  over the stated duration of implantation. No significant difference  $P > 0.05$  in sensitivity was apparent on the sixth day when compared to the initial day of implantation. These results support the stability of the H<sub>2</sub>O<sub>2</sub> sensor design for the purpose of long-term *in-vivo* recording.

| Day | Mean I, (nA ± SEM) | n |
|-----|--------------------|---|
| 1   | 1.04 ± 0.34        | 3 |
| 2   | 1.66 ± 0.62        | 3 |
| 3   | 1.47 ± 0.56        | 3 |
| 4   | 1.83 ± 0.5         | 3 |
| 5   | 1.82 ± 0.31        | 3 |
| 6   | 1.77 ± 0.97        | 3 |

**Table 5.11.1: Summary of data shown in Figure 5.11.1. Data represented as a mean response ± SEM.**

Additionally the average basal H<sub>2</sub>O<sub>2</sub> concentration in the striatum can be derived from the data displayed in Table 5.11.1. This value was calculated from the average *in-vitro* calibration data of the paired H<sub>2</sub>O<sub>2</sub> sensor design. The average *in-vitro* sensitivity of the catalase-based H<sub>2</sub>O<sub>2</sub> paired sensor is 0.47 ± 0.003 nA/μM, n = 24 (Chapter 4 Section 4.7).

The average baseline current response obtained from *in-vivo* experiments over a period of six days is 1.60 ± 0.30 nA, n = 3. This value corresponds to a H<sub>2</sub>O<sub>2</sub> ECF basal concentration of 3.42 ± 0.27 μM. Current literature suggests that the ECF H<sub>2</sub>O<sub>2</sub> concentration is in the region of 25-50 μM (Hyslop *et al.*, 1995). As previously stated a competing network of antioxidants are present in the brain which regulate ROS/H<sub>2</sub>O<sub>2</sub> levels (Rice, 2011). These antioxidants may cause the basal level of H<sub>2</sub>O<sub>2</sub> to be much lower than previously expected. Electrochemical methods provide increased temporal and spatial resolution which may explain the disparity in the ECF basal concentration estimated here and that determined by Hyslop *et al.* (Hyslop *et al.*, 1995). However it must be stated that the capacitance current of the paired H<sub>2</sub>O<sub>2</sub> sensor will contribute to the overall baseline current value. Additionally, the diffusional constraints of brain

tissue itself may restrict mass transport of the analyte to the sensor (Cheng *et al.*, 1979; Dayton *et al.*, 1983).

From the results presented in this chapter it is clear that mechanisms present in the physiological environment which remove H<sub>2</sub>O<sub>2</sub> are robust. The evidence presented in this chapter would suggest that the basal ECF concentration of H<sub>2</sub>O<sub>2</sub> is in fact much lower than previously reported.

### 5.11.2 *Blank sensor baseline stability (freely-moving)*

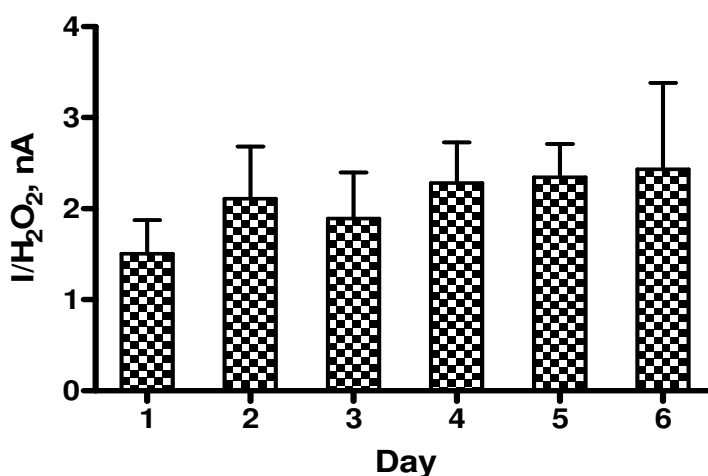


**Figure 5.11.2:** The average baseline recorded by the *Blank* sensor *in-vivo* over a consecutive period of six days. Data represented as a mean response  $\pm$  SEM and  $n = 6$ .

The data shown in Figure 5.11.2 shows the mean baseline current recorded by the *Blank* sensor *in-vivo* over six successive days. Each *Blank* sensor was implanted in the striatum of a freely-moving rat. A one-way ANOVA analysis of variance revealed that the baseline current showed no significant variation  $P > 0.05$  over the stated duration of implantation. The current detected by the *Blank* sensor remains consistent over six days. Any deterioration in the PPD structure which is part of this sensor design would lead to an increased current response as the period of implantation increases. No significant change ( $P > 0.05$ ) in current response was detected by the *Blank* sensor over the stated duration of implantation. These results validate the stability of *Blank* sensor design for the purpose of obtaining long-term *in-vivo* recordings.

| Day | Mean I, (nA ± SEM) | n |
|-----|--------------------|---|
| 1   | 1.51 ± 0.37        | 3 |
| 2   | 2.11 ± 0.57        | 3 |
| 3   | 1.89 ± 0.51        | 3 |
| 4   | 2.28 ± 0.45        | 3 |
| 5   | 2.35 ± 0.36        | 3 |
| 6   | 2.44 ± 0.95        | 3 |

Table 5.11.2: Summary of data shown in Figure 5.11.2. Data represented as a mean response ± SEM.

### 5.11.3 Cat sensor baseline stability (freely-moving)

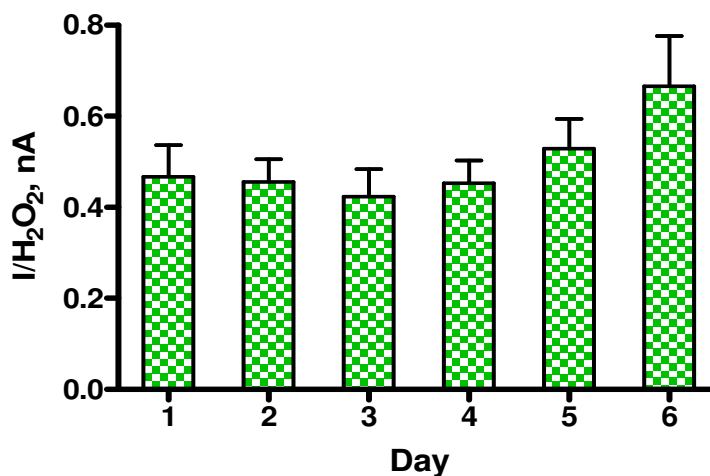


Figure 5.11.3: The average baseline recorded by the *Cat* sensor *in-vivo* over a consecutive period of six days. Data represented as a mean response ± SEM and n = 6.

The data shown in Figure 5.11.3 displays the mean baseline current recorded by the catalase-based sensor (*Cat*) *in-vivo* over six successive days. Each *Cat* sensor was

implanted in the striatum of a freely-moving rat. A one-way ANOVA analysis of variance revealed that the baseline current showed no significant variation  $P > 0.05$  over six days of implantation. The catalase enzyme remains stable over the specified duration of time in the *in-vivo* environment. Impairment in the function of the enzyme would lead to a distinct increase in current as the duration of implantation increases. No significant difference  $P > 0.05$  in the response of the catalase sensor is observed over six days of implantation however a small increase is observed on day 5 and 6. Previous work by Hu *et al.* has demonstrated a loss in viability of an enzyme based sensor which typically occurs following initial exposure to brain tissue (Hu *et al.*, 1994). The *Cat* sensor response is stable over six days of recording. The results shown in this Section validate the stability of *Cat* sensor design for the purpose of obtaining long-term *in-vivo* recordings.

| <b>Day</b> | <b>Mean I, (nA ± SEM)</b> | <b>n</b> |
|------------|---------------------------|----------|
| <b>1</b>   | 0.47 ± 0.07               | 3        |
| <b>2</b>   | 0.46 ± 0.05               | 3        |
| <b>3</b>   | 0.42 ± 0.06               | 3        |
| <b>4</b>   | 0.45 ± 0.05               | 3        |
| <b>5</b>   | 0.53 ± 0.07               | 3        |
| <b>6</b>   | 0.67 ± 0.11               | 3        |

**Table 5.11.3: Summary of data shown in Figure 5.11.2. Data represented as a mean response ± SEM.**

### 5.12 Baseline comparison (acute and freely-moving)

A variation in the baseline level of H<sub>2</sub>O<sub>2</sub> was observable between the acute and freely-moving animal data. The average baseline response of the paired H<sub>2</sub>O<sub>2</sub> sensor was  $1.60 \pm 0.30$  nA  $n = 3$  in freely-moving animals however the corresponding value obtained from the acute preparation was  $-0.27 \pm 0.04$  nA  $n = 3$ . No significant difference ( $P > 0.05$ ) between baseline levels in both experimental conditions was observed however a discrepancy is clearly apparent.

In the anaesthetised animal the pre-perfusion baseline of the *Cat* and *Blank* sensor are in close proximity (see Section 5.10.2 and 5.10.3). This observation contrasts greatly to the baseline current values for the *Cat* and *Blank* sensor seen in the freely-moving animal. The *Blank* sensor baseline is consistently much higher than the *Cat* sensor in the freely-moving animal (see Section 5.5.2 and 5.5.3). The lack of resolution of the *Blank* sensor baseline current over the *Cat* sensor baseline in the acute set-up leads to difficulty in obtaining an overall subtracted response.

A limited amount of time is available to conduct an acute experiment due to the nature of the experimental conditions. It is possible that in the acute set-up the capacitance of the paired H<sub>2</sub>O<sub>2</sub> sensor does not have sufficient time to dissipate. In order to fully investigate this possibility the time required to reach a steady baseline level from the application of potential in the acute preparation was calculated ( $100.67 \pm 11.92$  mins  $n = 3$ ). A new baseline was obtained from the freely-moving animal data following a similar elapsed amount of time from the application of potential ( $102.67 \pm 3.18$   $n = 3$ ). At this revised time point the current response of the paired H<sub>2</sub>O<sub>2</sub> sensor in the freely-moving animals was  $1.22 \pm 0.70$   $n = 3$ . A discrepancy in baseline levels between the acute and freely-moving preparations was still apparent following a similar time-frame from the application of the potential to the working electrodes. These results suggest that the disparity in baseline levels in each scenario is due to a different experimental parameter and not due to time considerations.

It has previously been demonstrated that neuronal activity is globally decreased during the use of general anaesthesia (Mueller *et al.*, 2011). A drop in neuronal activity

corresponds to a decrease demand for regional cerebral blood flow and hence a matched reduction in oxygen levels (Li *et al.*, 2011). The primary source of  $H_2O_2$  in the brain is derived from the action of the enzyme superoxide dismutase (SOD) on the highly reactive compound superoxide which is derived from the mitochondrial reduction of molecular  $O_2$ . The production of  $H_2O_2$  is linked to increased neuronal activity due to an increased level of  $O_2$  consumption which generates  $H_2O_2$  (Rice, 2011). This phenomenon may be a contributing factor in the reduction of the baseline level of  $H_2O_2$  seen here in the anaesthetised animal, as the neuronal activity of the animal is suppressed by the effect of the anaesthesia.

### 5.13 Conclusion

The aim of this chapter was to characterise the paired catalase-based H<sub>2</sub>O<sub>2</sub> sensor in the *in-vivo* environment. The sensitivity of the H<sub>2</sub>O<sub>2</sub> sensor was examined when implanted in the striatum of the freely-moving animal by the local perfusion of various concentrations of H<sub>2</sub>O<sub>2</sub> (Section 5.4). These perfusions were compared to the local addition of aCSF which was introduced in the same manner (Section 5.3.1). Addition of H<sub>2</sub>O<sub>2</sub> to the perfusate caused no significant difference  $P > 0.05$  to the sensor response at a low concentration (25  $\mu$ M) in relation to perfusion of aCSF. However a significant difference with respect to aCSF was observed at a higher concentration of exogenously applied H<sub>2</sub>O<sub>2</sub> (100  $\mu$ M to 1000  $\mu$ M). At each subsequent stage (100  $\mu$ M to 1000  $\mu$ M) the H<sub>2</sub>O<sub>2</sub> sensor showed a difference in response which was proportional to an increase in the concentration of locally introduced H<sub>2</sub>O<sub>2</sub> (Section 5.5). Interestingly no distinct increase above basal H<sub>2</sub>O<sub>2</sub> levels was observed following introduction of H<sub>2</sub>O<sub>2</sub> to the perfusate in freely-moving animals.

A robust network of antioxidant mechanisms control the level of H<sub>2</sub>O<sub>2</sub>/ROS in the brain, which are responsible for the prevention of the development of oxidative stress. The variety of processes which maintain oxidant homeostasis in the brain has been extensively reviewed (Dringen *et al.*, 2005; Valko *et al.*, 2007). These mechanisms consist of various enzymatic and non-enzymatic control mechanisms (Simonian & Coyle, 1996) and the consequences of a disruption in the balance between antioxidants and ROS has been implicated in a variety of neurological diseases and dysfunctions (Barnham *et al.*, 2004; Melo *et al.*, 2011). It is therefore possible that exogenously applied H<sub>2</sub>O<sub>2</sub> may be efficiently controlled by the inherent mechanisms of the intact living brain.

Additionally the delivery of H<sub>2</sub>O<sub>2</sub> to the implanted catalase-based paired H<sub>2</sub>O<sub>2</sub> sensor may be restricted by recovery issues associated with the MD/RD technique as discussed in Section 2.9.

The selectivity of the implanted sensor in the striatum of the freely-moving animal was addressed by the local perfusion and systemic administration of the primary interferent

species present in the brain (Lowry *et al.*, 2006). The local perfusion of AA had no effect on the H<sub>2</sub>O<sub>2</sub> sensor response, no significant difference  $P > 0.05$  was observed between the maximum current response and baseline levels (Section 5.8). The preliminary results from the systemic administration of AA on the H<sub>2</sub>O<sub>2</sub> sensor response exhibited an overall decrease. The protracted gradual decrease caused by the systemic administration of AA should not affect the detection of H<sub>2</sub>O<sub>2</sub>. H<sub>2</sub>O<sub>2</sub> is a highly permeable short-lived molecule (Bao *et al.*, 2009) and would demonstrate more rapid fluctuations when compared to AA. These results indicate that the sensor is selective over AA *in-vivo* as has been demonstrated *in-vitro* (Section 4.8).

| Administration | Current change (pA) | Baseline change (%) | Max response    | Return          | Pre-perfusion baseline (pA) | Post-perfusion baseline (pA) |
|----------------|---------------------|---------------------|-----------------|-----------------|-----------------------------|------------------------------|
| Local AA       | 245.3 ± 38.4        | 117.9 ± 7.8         | 10.3 ± 3.3 mins | 29.8 ± 2.0 mins | 1780.6 ± 966.6              | 1828.4 ± 1105.5              |
| Systemic AA    | -170.0              | 4.95                | 6 hr 14 mins    | 14 hr 38 mins   | 177.8                       | 48.9                         |

**Table 5.13.1: Summary of results obtained upon local perfusion and systemic administration of AA, as discussed in Section 5.8 and 5.8.1.**

The primary enzymes responsible for the degradation of H<sub>2</sub>O<sub>2</sub> in the brain, catalase and glutathione peroxidase (GPx) were inhibited by the use of sodium azide (SA) and mercaptosuccinate (MCS) respectively. MCS and GPx have been used previously for the same purpose (Dringen *et al.*, 1998; Avshalumov *et al.*, 2005). The intention of these experiments (Section 5.6 and 5.7) was to inhibit the antioxidant network responsible for the regulation of H<sub>2</sub>O<sub>2</sub> in an attempt to show an increase in the endogenous production of H<sub>2</sub>O<sub>2</sub>. The local perfusion of MCS and SA caused an increase in the paired catalase-based H<sub>2</sub>O<sub>2</sub> sensor response, this would indicate that the implanted sensor is responding to an endogenous increase in H<sub>2</sub>O<sub>2</sub> levels and is selective to the target substrate (H<sub>2</sub>O<sub>2</sub>). Preliminary data presented in this chapter indicates that GPx inhibition of endogenous H<sub>2</sub>O<sub>2</sub> production by use of MCS, exhibits its affect in a dose dependent manner (Section 5.7) as has been demonstrated previously in brain preparations (Avshalumov *et al.*,

2005). A higher concentration of SA was added to the perfusate with respect to MCS and caused a similar percentage increase in H<sub>2</sub>O<sub>2</sub> response. Previous work has suggested that catalase has a higher overall activity in the brain than GPx (Avshalumov *et al.*, 2004). Further work is required to elucidate the role of SA (catalase inhibition) and MCS (GPx inhibition) on the downstream endogenous elevation of H<sub>2</sub>O<sub>2</sub>.

| Analyte    | Current change (pA) | Baseline change (%) | Conc. change (nM) | Max response (mins) | Return (mins) | Pre-perfusion baseline (pA) |
|------------|---------------------|---------------------|-------------------|---------------------|---------------|-----------------------------|
| SA (10 mM) | 219.8 ± 108.7       | 118.4 ± 0.8         | 471.1 ± 232.9     | 1.3 ± 0.2           | 25.5 ± 1.7    | 1170.8 ± 541.5              |
| MCS (1 mM) | 449.9               | 124.6               | 964.4             | 6.2                 | 23.5          | 1830.8                      |

**Table 5.13.2: Summary of results obtained upon local perfusion of SA and MCS, as discussed in Section 5.6 and 5.7.**

The stability of the dual H<sub>2</sub>O<sub>2</sub> sensor was assessed over a continuous period of six days while implanted in the striatum of a freely-moving animal (Section 5.11). No significant difference  $P > 0.05$  was seen in the H<sub>2</sub>O<sub>2</sub> sensor response for the duration of these recordings. These results support the feasibility of using the H<sub>2</sub>O<sub>2</sub> sensor in the attainment of long-term electrochemical recordings as has been previously demonstrated using electrochemical sensors (Lowry *et al.*, 1998a; Bolger *et al.*, 2011; Finnerty *et al.*, 2012).

Following the local administration of H<sub>2</sub>O<sub>2</sub>, a difference in the paired H<sub>2</sub>O<sub>2</sub> sensor response was observed in the anaesthetised animal (Section 5.9) in comparison to the response observed in the freely-moving animal (Section 5.4). A clear increase above basal levels of H<sub>2</sub>O<sub>2</sub> was observed at a higher concentration range of exogenously applied H<sub>2</sub>O<sub>2</sub> (100 µM to 100 mM) in the anaesthetised animal (Section 5.10.1). The local administration of H<sub>2</sub>O<sub>2</sub> in the freely-moving animal does not cause an obvious increase in the paired catalase-based H<sub>2</sub>O<sub>2</sub> sensor response (Section 5.5.1). The disparity in response of the dual H<sub>2</sub>O<sub>2</sub> sensor in the acute and freely-moving preparation may be due to a suppression in neuronal activity due to anaesthesia (Mueller *et al.*, 2011). This factor is fully discussed in Section 5.10.

The role of H<sub>2</sub>O<sub>2</sub> as a neuromodulator may be fully understood by its real-time detection in the brain. The effect of this signalling molecule on inhibitory and excitatory processes which regulate dopamine has been thoroughly researched by Rice *et al.* in brain tissue preparations (Avshalumov *et al.*, 2005; Rice, 2011). The real-time detection of H<sub>2</sub>O<sub>2</sub> in the intact living brain presented in this chapter could provide novel information on this proposed neuromodulatory role.

The highly effective anti-oxidant network present in the brain serves as a mop-up mechanism which removes potentially harmful reactive oxygen species such as H<sub>2</sub>O<sub>2</sub> (Simonian & Coyle, 1996; Valko *et al.*, 2007). An insult to this controlled redox homeostasis is dealt with efficiently under normal circumstances (Droge, 2002). The results demonstrated in this chapter suggest that the effect of exogenously applied H<sub>2</sub>O<sub>2</sub> is controlled to some extent by these mop-up mechanisms *in-situ*. Additionally, these results indicate that anaesthesia has a negative effect on the normal function of the anti-oxidant network. Preliminary findings presented in this chapter demonstrate that inhibition of specific peroxidase enzymes induces an elevation of endogenous H<sub>2</sub>O<sub>2</sub>.

As previously stated a disruption in the maintenance of levels of ROS in the brain can lead to oxidative stress. Oxidative stress is implicated in the pathology of many neurological disorders such as Alzheimer's disease, Parkinson's disease and amyotrophic lateral sclerosis (Barnham *et al.*, 2004; Melo *et al.*, 2011). As H<sub>2</sub>O<sub>2</sub> is indicative of the production of ROS (Simonian & Coyle, 1996), the real-time detection of H<sub>2</sub>O<sub>2</sub> in the physiological environment may provide an understanding and more importantly an advancement in the therapeutic approach to a broad spectrum of neurodegenerative diseases.

## References

- Andersen JK. (2004). Oxidative stress in neurodegeneration: cause or consequence? *Nature Medicine* **10**, S18-S25.
- Avshalumov MV, Chen BT, Koos T, Tepper JM & Rice ME. (2005). Endogenous hydrogen peroxide regulates the excitability of midbrain dopamine neurons via ATP-sensitive potassium channels. *Journal of Neuroscience* **25**, 4222-4231.
- Avshalumov MV, Chen BT, Marshall SP, Pena DM & Rice ME. (2003). Glutamate-dependent inhibition of dopamine release in striatum is mediated by a new diffusible messenger, H<sub>2</sub>O<sub>2</sub>. *Journal of Neuroscience* **23**, 2744-2750.
- Avshalumov MV, MacGregor DG, Sehgal LM & Rice ME. (2004). The glial antioxidant network and neuronal ascorbate: protective yet permissive for H(2)O(2) signaling. *Neuron Glia Biology* **1**, 365-376.
- Bao L, Avshalumov MV, Patel JC, Lee CR, Miller EW, Chang CJ & Rice ME. (2009). Mitochondria Are the Source of Hydrogen Peroxide for Dynamic Brain-Cell Signaling. *Journal of Neuroscience* **29**, 9002-9010.
- Barnham KJ, Masters CL & Bush AI. (2004). Neurodegenerative diseases and oxidative stress. *Nature Reviews Drug Discovery* **3**, 205-214.
- Baud O, Greene AE, Li JR, Wang H, Volpe JJ & Rosenberg PA. (2004). Glutathione peroxidase-catalase cooperativity is required for resistance to hydrogen peroxide by mature rat oligodendrocytes. *Journal of Neuroscience* **24**, 1531-1540.
- Bolger FB, Bennett R & Lowry JP. (2011). An *in vitro* characterisation comparing carbon paste and Pt microelectrodes for real-time detection of brain tissue oxygen. *Analyst* **136**, 4028-4035.
- Cheng HY, Schenk J, Huff R & Adams RN. (1979). *In vivo* electrochemistry: behavior of micro electrodes in brain tissue. *Journal of Electroanalytical Chemistry and Interfacial Electrochemistry* **100**, 23-31.
- Cohen G. (1994). Enzymatic nonenzymatic sources of oxyradicals and regulation of antioxidant defences. In *Neurobiology of NO and OH*, ed. Chiueh CCGDLCCA, pp. 8-14.
- Dayton MA, Ewing AG & Wightman RM. (1983). Diffusion processes measured at microvoltammetric electrodes in brain tissue. *Journal of Electroanalytical Chemistry and Interfacial Electrochemistry* **146**, 189-200.

- Dringen R, Kussmaul L & Hamprecht B. (1998). Rapid clearance of tertiary butyl hydroperoxide by cultured astroglial cells via oxidation of glutathione. *Glia* **23**, 139-145.
- Dringen R, Pawlowski PG & Hirrlinger J. (2005). Peroxide detoxification by brain cells. *Journal of Neuroscience Research* **79**, 157-165.
- Droge W. (2002). Free radicals in the physiological control of cell function. *Physiological Reviews* **82**, 47-95.
- Finnerty NJ, O'Riordan SL, Brown FO, Serra PA, O'Neill RD & Lowry JP. (2012). *In vivo* characterisation of a Nafion<sup>®</sup>-modified Pt electrode for real-time nitric oxide monitoring in brain extracellular fluid. *Analytical Methods* **4**, 550-557.
- Garguilo MG & Michael AC. (1994). Quantitation of choline in the extracellular fluid of brain-tissue with amperometric microsensors. *Analytical Chemistry* **66**, 2621-2629.
- Garguilo MG & Michael AC. (1996). Amperometric microsensors for monitoring choline in the extracellular fluid of brain. *Journal of Neuroscience Methods* **70**, 73-82.
- Hu YB, Mitchell KM, Albahadily FN, Michaelis EK & Wilson GS. (1994). Direct measurement of glutamate release in the brain using Aa dual enzyme-based electrochemical sensor. *Brain Research* **659**, 117-125.
- Hyslop PA, Zhang ZY, Pearson DV & Phebus LA. (1995). Measurement of striatal H<sub>2</sub>O<sub>2</sub> by microdialysis following global forebrain ischemia and reperfusion in the rat - correlation with the cytotoxic potential of H<sub>2</sub>O<sub>2</sub> *in-vitro*. *Brain Research* **671**, 181-186.
- Jamal M, Ameno K, Uekita I, Kumihashi M, Wang W & Ijiri I. (2007). Catalase mediates acetaldehyde formation in the striatum of free-moving rats. *Neurotoxicology* **28**, 1245-1248.
- Kulagina NV & Michael AC. (2003). Monitoring hydrogen peroxide in the extracellular space of the brain with amperometric microsensors. *Analytical Chemistry* **75**, 4875-4881.
- Lei BP, Adachi N & Arai T. (1997). The effect of hypothermia on H<sub>2</sub>O<sub>2</sub> production during ischemia and reperfusion: A microdialysis study in the gerbil hippocampus. *Neuroscience Letters* **222**, 91-94.
- Lei BP, Adachi N & Arai T. (1998). Measurement of the extracellular H<sub>2</sub>O<sub>2</sub> in the brain by microdialysis. *Brain Research Protocols* **3**, 33-36.

- Li J, Bravo DS, Upton AL, Gilmour G, Tricklebank MD, Fillenz M, Martin C, Lowry JP, Bannerman DM & McHugh SB. (2011). Close temporal coupling of neuronal activity and tissue oxygen responses in rodent whisker barrel cortex. *European Journal of Neuroscience* **34**, 1983-1996.
- Lowry JP, Boutelle MG, O'Neill RD & Fillenz M. (1996). Characterization of carbon paste electrodes *in vitro* for simultaneous amperometric measurement of changes in oxygen and ascorbic acid concentrations *in vivo*. *Analyst* **121**, 761-766.
- Lowry JP, Miele M, O'Neill RD, Boutelle MG & Fillenz M. (1998a). An amperometric glucose-oxidase/poly(*o*-phenylenediamine) biosensor for monitoring brain extracellular glucose: *in vivo* characterisation in the striatum of freely-moving rats. *Journal of Neuroscience Methods* **79**, 65-74.
- Lowry JP, O'Neill RD & (2006). *Neuroanalytical Chemistry In Vivo Using Biosensors.*, vol. 10. American Scientific Publishers.
- Lowry JP, O'Neill RD, Boutelle MG & Fillenz M. (1998b). Continuous monitoring of extracellular glucose concentrations in the striatum of freely moving rats with an implanted glucose biosensor. *Journal of Neurochemistry* **70**, 391-396.
- Melo A, Monteiro L, Lima RMF, Oliveira DMd, Cerqueira MDd & El-Bacha RS. (2011). Oxidative stress in neurodegenerative diseases: mechanisms and therapeutic perspectives. *Oxidative medicine and cellular longevity* **2011**, 467180.
- Miele M, Boutelle MG & Fillenz M. (1994). The physiologically induced release of ascorbate in rat-brain is dependent on impulse traffic, calcium influx and glutamate uptake. *Neuroscience* **62**, 87-91.
- Miele M & Fillenz M. (1996). *In vivo* determination of extracellular brain ascorbate. *Journal of Neuroscience Methods* **70**, 15-19.
- Mueller CP, Pum ME, Amato D, Schuettler J, Huston JP & Silva MADS. (2011). The *in vivo* neurochemistry of the brain during general anesthesia. *Journal of Neurochemistry* **119**, 419-446.
- O'Neill RD. (1993). Sensor-tissue interactions in neurochemical analysis with carbon paste electrodes *in vivo*. *Analyst* **118**, 433-438.
- O'Neill RD, Lowry JP & Mas M. (1998). Monitoring brain chemistry *in vivo*: Voltammetric techniques, sensors, and behavioral applications. *Critical Reviews in Neurobiology* **12**, 69-127.

- O'Neill RD, Lowry JP, Rocchitta G, McMahon CP & Serra PA. (2008). Designing sensitive and selective polymer/enzyme composite biosensors for brain monitoring *in vivo*. *Trac-Trends in Analytical Chemistry* **27**, 78-88.
- Rhee SG. (2006). H<sub>2</sub>O<sub>2</sub>, a necessary evil for cell signaling. *Science* **312**, 1882-1883.
- Rice ME. (2011). H<sub>2</sub>O<sub>2</sub>: A Dynamic Neuromodulator. *Neuroscientist* **17**, 389-406.
- Simonian NA & Coyle JT. (1996). Oxidative stress in neurodegenerative diseases. *Annual Review of Pharmacology and Toxicology* **36**, 83-106.
- Stone JR & Yang SP. (2006). Hydrogen peroxide: A signaling messenger. *Antioxidants & Redox Signaling* **8**, 243-270.
- Valko M, Leibfritz D, Moncol J, Cronin MTD, Mazur M & Telser J. (2007). Free radicals and antioxidants in normal physiological functions and human disease. *International Journal of Biochemistry & Cell Biology* **39**, 44-84.
- Wisniewski N, Moussy F & Reichert WM. (2000). Characterization of implantable biosensor membrane biofouling. *Fresenius Journal of Analytical Chemistry* **366**, 611-621.
- Zimatkin SM, Pronko SP, Vasiliou V, Gonzalez FJ & Deitrich RA. (2006). Enzymatic mechanisms of ethanol oxidation in the brain. *Alcoholism-Clinical and Experimental Research* **30**, 1500-1505.

---

**6. *In-vitro* and *in-vivo* characterisation of  
a nitric oxide sensor**

---

## 6.1 Introduction

The physiological role of nitric oxide (NO) as the endothelium derived relaxing factor (EDRF), involved in the process of vasodilation and regulation of blood pressure was discovered in the late 1980's (Ignarro *et al.*, 1987). Since then much interest has developed around the role of NO in the body.

NO is derived from three main NO synthase enzymes (NOS). These consist of inducible NOS (iNOS), endothelial NOS (eNOS) and neuronal NOS (nNOS) (Kiechle & Malinski, 1993; Bruckdorfer, 2005; Guix *et al.*, 2005). The source of NOS in the body determines the specific type of NO produced. The global physiological function of NO has been extensively studied in processes such as the immune response (Bogdan *et al.*, 2000), anti-microbial activity (Fang, 2004) and penile erection (Mas *et al.*, 2002). Of the three isoforms of NOS, nNOS is present in the most abundance in the brain. Neuronal NO has been implicated in a variety of neurological processes, specifically sleep and appetite regulation (Williams *et al.*, 2002; Cavas & Navarro, 2006) synaptic plasticity, neurotransmission and learning and memory (Wass *et al.*, 2006a; Wass *et al.*, 2006b; Nugent *et al.*, 2007). Hence the detection of NO in the central nervous system (CNS) provides an insight into a variety of vital neurological functions.

A range of analytical techniques enable the detection of NO. However these techniques rely on indirect detection methods, by measuring nitrite and other markers of NO production using spectroscopic methods (Hetrick & Schoenfisch, 2009). The poor sensitivity of these techniques are not suitable for the detection of NO *in-vivo*, due to the short half-life of NO in the biological environment which is typically less than 10 seconds (Kelm, 1999). Additionally, the concentration of NO in biological samples is within the pico to micromolar range (Wink & Mitchell, 1998), which requires a highly sensitive detection method. Also the selectivity of these spectroscopic methods are questionable due to interference from nitrite and nitrate from sources other than NO (Finnerty *et al.*, 2012a). Electrochemical techniques provide the appropriate temporal and spatial resolution necessary to detect NO in the physiological environment to enable long-term *in-vivo* NO recordings.

The electrochemical reduction of NO has previously been shown (Meulemans, 1993; Maskus *et al.*, 1996; Liu *et al.*, 2003), however a significant amount of interference from oxygen is possible due to the required operating potential. The electro-oxidation of NO is the most suitable monitoring technique and a variety of electrode materials modified with permselective polymers such as Nafion<sup>®</sup>, operating between 0.6 and 1.0 V have been used for this purpose. They are predominantly carbon fibre (Friedemann *et al.*, 1996; Park *et al.*, 1998; Heinzen & Pollack, 2002), glassy carbon (Pallini *et al.*, 1998), and Pt electrodes (Park *et al.*, 2010; Park *et al.*, 2012).

Our research group has demonstrated a highly sensitive, selective and stable NO sensor for the purpose of *in-vivo* NO monitoring (Brown & Lowry, 2003; Brown *et al.*, 2009). This NO sensor also possesses the required operational characteristics i.e. a highly suitable response time and detection limit to enable the detection of NO *in-vivo* (Brown *et al.*, 2009). Furthermore the application of this NO sensor in the physiological environment for the continuous real-time detection of NO in the brain has been extensively characterised (Finnerty *et al.*, 2012a; Finnerty *et al.*, 2012b).

The NO sensor utilised here was constructed as previously described in detail by Brown *et al.* (Brown *et al.*, 2009). A detailed procedure for the laboratory synthesis of NO; which was used to determine the sensitivity of the NO sensor has previously been shown (Brown *et al.*, 2005). Finnerty *et al.* have recently published a detailed *in-vivo* characterisation of the NO sensor implanted in the striatum (Finnerty *et al.*, 2012a). Additionally an extensive regional characterisation of the NO sensor was carried out in the striatum, prefrontal cortex (PFC) and nucleus accumbens (NA) of freely-moving animals (Finnerty *et al.*, 2012b). This chapter demonstrates the *in-vitro* and *in-vivo* characterisation of the NO sensor with reference to this recently published work (Finnerty *et al.*, 2012a; Finnerty *et al.*, 2012b).

At normal levels NO exhibits a neuroprotective effect, through maintaining cognitive function in the brain by regulating synaptic plasticity and neurotransmission (Calabrese *et al.*, 2007). However, abnormally high concentrations of NO and the resulting further production of other reactive nitrogen species (RNS), leads to nitrosative stress in the CNS and exerts a damaging toxic effect (Valko *et al.*, 2007). Nitrosative stress occurs

when the production of RNS surpasses the ability of the antioxidant network to suppress NO/RNS production. NO carries out its toxic effect in a pro-oxidant environment predominantly by interaction with superoxide, leading to the formation of peroxynitrite (Pacher *et al.*, 2007). Nitrosative stress due to abnormal production of RNS such as NO has been implicated in a variety of neurodegenerative disorders such as Alzheimer's disease (Pacher *et al.*, 2007) and Parkinson's disease (Andersen, 2004).

The aim of this chapter is to replicate the *in-vitro* and *in-vivo* characterisation of the NO sensor as previously shown, in order to further illustrate the application of this sensor for the real-time detection of NO in animal models of neurological disease and dysfunction (see Chapter 7 and 8).

## 6.2 Experimental

A detailed description of the instrumentation, chemicals, solutions and software used in this section is given in Chapter 3. A detailed description of the manufacture of the NO sensor is outlined in Section 3.4. All experiments outlined in this chapter were performed using Constant Potential Amperometry (CPA). For all *in-vitro* and *in-vivo* experiments a potential of +900 mV vs. SCE and Ag wire (see Section 3.10.3) respectively was applied to the working electrodes.

The number of implanted NO sensors is denoted by (n) and the number of animals indicated. In the case where the number of administrations included in the data exceeds the number of sensors/animals the value is given and denoted by (adm). Reported *in-vivo* NO concentration changes are based on the average *in-vitro* pre-implantation calibration data.

Statistical analysis was carried out using paired or unpaired t-tests. One-way ANOVA was used to simultaneously compare results which contained more than two separate groups. These tests were performed using Graphpad Prism and gave a probability value ( $P$ ) which indicates the level of significant or non-significant difference between groups.  $P > 0.05$ , denotes no significant difference. The extent of significant difference is divided into three parameters ( $P < 0.05$ ,\*), ( $P < 0.01$ ,\*\*) and ( $P < 0.0001$ ,\*\*\*) from the lowest relative level of difference (\*) to the highest (\*\*\*)

### 6.3 *In-vitro* characterisation of the NO sensor

A detailed description of the *in-vitro* characterisation of the Nafion<sup>®</sup>-modified Platinum disc (Pt<sub>d</sub>) (5 pre-coats, 2 applications) NO sensor has been described by Brown *et al.* (Brown & Lowry, 2003; Brown *et al.*, 2009). In the initial development of the NO sensor a Nafion<sup>®</sup> thermal annealing procedure of Pt microelectrodes was described that allowed the electrochemical detection of gaseous neurochemical species such as NO (Brown & Lowry, 2003). Brown & Lowry demonstrated the optimum Nafion<sup>®</sup> thermal annealing procedure required to enable sensitivity towards the target analyte and optimise interference rejection. Additional preliminary stability studies were conducted to demonstrate a sensor suitable for Long Term In-Vivo Electrochemistry (L.I.V.E) NO recordings (Brown & Lowry, 2003).

The initial *in-vitro* development of the Nafion<sup>®</sup>-modified Pt<sub>d</sub> sensor was extended further to focus on the ability of the NO sensor design to detect NO in the *in-vivo* environment (Brown *et al.*, 2009). In this work Brown *et al.* demonstrate the optimum applied potential for the detection of NO (+900 mV *vs.* SCE), the selectivity of the sensor over a range of interference species and the stability of the sensor design was also presented. The required operational characteristics of the Nafion<sup>®</sup>-modified sensor for the detection of NO in the physiological environment were validated and preliminary *in-vivo* research presented the reliable detection of NO in the physiological environment (Brown *et al.*, 2009).

The *in-vivo* stability of the NO sensor following implantation has recently been published (Finnerty *et al.*, 2012a) and these results are shown in Section 6.6. An extensive *in-vivo* characterisation of the Nafion<sup>®</sup>-modified NO sensor has been demonstrated (Finnerty *et al.*, 2012a; Finnerty *et al.*, 2012b) and these findings are discussed in Section 6.8.

The *in-vitro* characterisation of the Nafion<sup>®</sup>-modified NO sensor presented in this chapter is a validation of the previously established sensitivity and selectivity of this sensor design (Brown & Lowry, 2003; Brown *et al.*, 2009; Finnerty *et al.*, 2012a). Recently published work regarding the stability of the Nafion<sup>®</sup>-modified sensor

determined *in-vitro* following implantation for a prolonged period is also presented in this chapter (Finnerty *et al.*, 2012a).

#### 6.4 Sensitivity of the NO sensor *in-vitro*

A Nafion<sup>®</sup>-modified Platinum disc (Pt<sub>d</sub>) (5 pre-coats, 2 applications) sensor was constructed as previously described in detail by Brown *et al.* (Brown *et al.*, 2009). This section will outline the sensitivity of the NO sensor to the target substrate *in-vitro*.

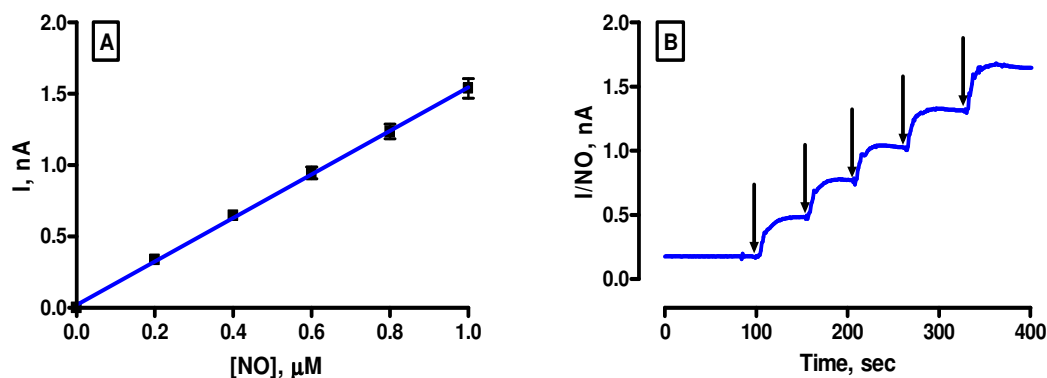


**Figure 6.4.1:** (A) The current-concentration profile of NO at Nafion<sup>®</sup>-modified Pt<sub>d</sub> (5 pre-coats, 2 applications) sensors (n = 16). (B) A typical raw data trace 0-1 μM for NO calibrations. CPA carried out at +900 mV vs. SCE. Arrows indicate the addition of 0.2 μM aliquots of NO.

Figure 6.4.1 represents the response of the NO sensor with respect to the stock administration of NO (0 to 1 μM). The response demonstrated here is directly proportional to the amount of NO introduced into the electrochemical cell. Calibrating the NO sensor over a 0 to 1 μM NO concentration range yielded a sensitivity of  $1.53 \pm 0.02$  nA/μM, n = 16. No significant difference ( $P > 0.05$ ) was observed between the NO sensitivity of the Nafion<sup>®</sup>-modified Pt<sub>d</sub> sensor reported here in comparison to that previously reported by Finnerty *et al.* (Finnerty *et al.*, 2012a).

| <b>NO, <math>\mu\text{M}</math></b> | <b>Mean I, nA</b> | <b>SEM</b>  |
|-------------------------------------|-------------------|-------------|
| <b>0</b>                            | <b>0</b>          | <b>0</b>    |
| <b>0.2</b>                          | <b>0.34</b>       | <b>0.03</b> |
| <b>0.4</b>                          | <b>0.65</b>       | <b>0.03</b> |
| <b>0.6</b>                          | <b>0.95</b>       | <b>0.04</b> |
| <b>0.8</b>                          | <b>1.24</b>       | <b>0.05</b> |
| <b>1.0</b>                          | <b>1.54</b>       | <b>0.07</b> |

**Table 6.4.1: Data obtained from the calibration shown in Figure 4.6.1(A),  $n = 16$ .  $R^2 = 0.9994$ . Data is represented as a Mean  $\pm$  standard error of the mean (SEM). Background values subtracted.**

**Mean background current =  $0.13 \pm 0.02$  nA.**

#### ***6.4.2 Limit of detection of the NO sensor in-vitro***

The limit of detection (LOD) of the NO sensor was calculated from *in-vitro* data. The LOD is defined as the smallest concentration of analyte detectable by a given sensor. The LOD value corresponds to three times the standard deviation of the background current and was calculated as  $2.73 \pm 0.34$  nM,  $n = 12$  for the NO sensor. The LOD of the Nafion<sup>®</sup>-modified NO sensor is consistent with previous findings for the same sensor design (Brown *et al.*, 2009). The ECF concentration of NO is expected to be within the pico to micromolar range (Shibuki, 1990; Wink & Mitchell, 1998). In an *in-vivo* environment the LOD of our sensor is sufficient to detect the expected neuronal concentration.

### 6.4.3 Response time of the NO sensor in-vitro

The response time of a sensor is defined as the time required to change from 10% to 90% of the maximum response. The *in-vitro* response of the NO sensor over time is shown below in Figure 6.4.3.

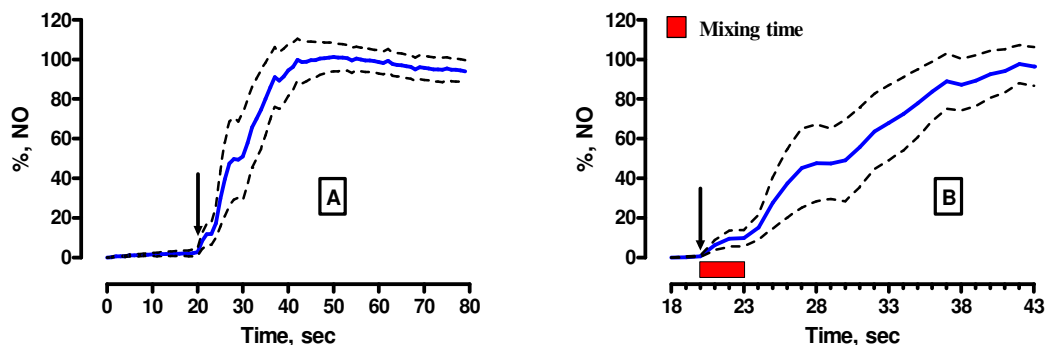


**Figure 6.4.3: The average NO response at the Nafion®-modified Pt<sub>d</sub> (5 pre-coats, 2 applications) sensor design (n = 7) for addition of 1 μM NO. Data shown as a percentage with 100% representative of the maximum NO sensitivity, SEM is denoted by the dashed line. The entire response is plotted vs. seconds (A) and the immediate response (B). Arrows indicate the addition of 1 μM NO.**

Following the introduction of 1 μM NO into the cell a gradual increase in the sensor response was observed. The response time of the NO sensor was calculated as  $12.21 \pm 1.83$  secs,  $n = 7$ . The solution was stirred immediately following the injection for approximately 3 seconds as outlined in Figure 6.3.3 (B). The increase in response observed here due to the introduction of NO outlasted the period of agitation of the bulk solution. The response time of the Nafion®-modified NO sensor is consistent with previous findings (Brown *et al.*, 2009). The response time of this NO sensor design is sufficient to determine NO which has a short lifetime in tissue (Kiechle & Malinski, 1993; Kelm, 1999). Additionally, it has previously been demonstrated that the response time of the NO sensor improves when tested under physiological temperature conditions of 37°C (Brown *et al.*, 2009).

### 6.5 Selectivity of the NO sensor *in-vitro*

The most abundantly present interference species in the brain is ascorbic acid (AA), which has a reported concentration of *ca.* 500  $\mu\text{M}$  in the ECF (Miele & Fillenz, 1996). However other potential sources of interference are possible from a wide range of species. These interferents can be detected at similar potentials to NO.

A detailed *in-vitro* selectivity characterisation of the NO sensor has been demonstrated by *Brown et al.* (Brown *et al.*, 2009). In this work presented by *Brown et al.* the current arising from the NO sensor by introduction of a wide range of chemical species was examined. The effect of uric acid (UA), serotonin (5-HT), DOPAC, 5-HIAA, dopamine (DA), glutathione, homovanillic acid (HVA), nitrite ( $\text{NO}_2^-$ ) and hydrogen peroxide ( $\text{H}_2\text{O}_2$ ) on the NO sensor response was tested. The expected ECF concentration of each analyte was utilised in this examination. The selectivity of the NO sensor over these interference species was established in these investigations (Brown *et al.*, 2009).

The sensitivity of the NO sensor was also maintained in the presence of AA (500  $\mu\text{M}$ ), DA (0.05  $\mu\text{M}$ ) and  $\text{O}_2$  (50  $\mu\text{M}$ ) (Brown *et al.*, 2009). As the interference rejection properties of the NO sensor had previously been examined a subsequent AA calibration was sufficient to elucidate the selectivity of the NO sensor.

## 6.5.1 AA Selectivity of the NO sensor

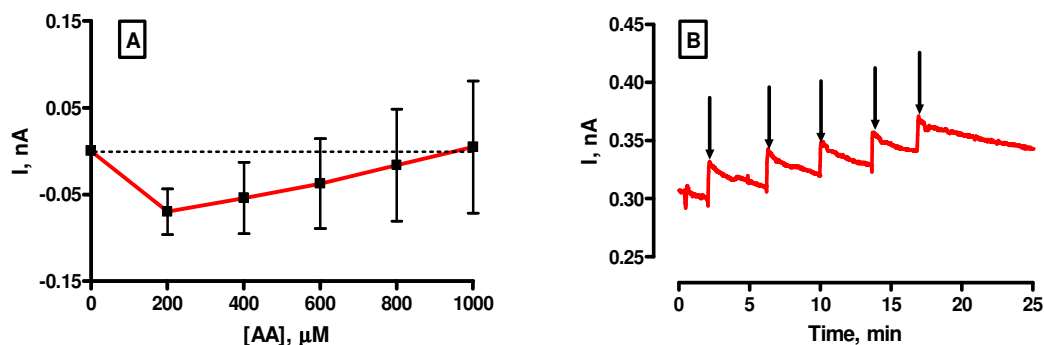


Figure 6.5.1: (A) The current-concentration profile of AA at Nafion<sup>®</sup>-modified Pt<sub>4</sub> (5 pre-coats, 2 applications) sensors (n = 16). (B) A typical raw data trace 0-1000 μM for AA calibrations. CPA carried out at +900 mV vs. SCE. Arrows indicate the addition of 200 μM aliquots of AA.

| AA, μM | Mean I, nA | S.E.M |
|--------|------------|-------|
| 0      | 0          | 0     |
| 200    | -0.07      | 0.03  |
| 400    | -0.05      | 0.04  |
| 600    | -0.04      | 0.05  |
| 800    | -0.02      | 0.06  |
| 1000   | 0.005      | 0.08  |

Table 6.5.1: Data obtained from the calibration shown in Figure 6.4.1(A). Data is represented as a Mean ± SEM. Background values subtracted. Mean background current =  $0.30 \pm 0.03$  nA.

Figure 6.5.1(A) above shows the current values recorded by the NO sensor in response to the addition of AA (0-1000 μM). As can be seen in Figure 6.5.1(A) the average NO sensor response exhibits an initial gradual drift below baseline levels, denoted by the dashed line. The current remains in close proximity to basal levels, up to a concentration of 1000 μM. No significant difference ( $P > 0.05$ ) was observed between baseline levels and the maximum response of the NO sensor due to addition of AA. Figure 6.5.1(B) demonstrates the typical response of the NO sensor to AA and the proximity of the response to baseline levels is apparent. The selectivity over AA of the NO sensor is clearly evident. It is clear that the AA response of the NO sensor design is negligible with a calculated sensitivity of  $0.03 \pm 0.04$  pA/μM, n = 16. This response is diminutive

when compared to the response observed at an unmodified sensor as demonstrated in the next Section (6.5.2).

### 6.5.2 AA $Pt_d$

This section examines the response observed at an unmodified  $Pt_d$  electrode calibrated at 900 mV vs. SCE following the addition of aliquots of AA in the concentration range of 0-1000  $\mu\text{M}$ . The purpose of this experiment is to act as a control against which the AA response of the Nafion<sup>®</sup>-modified NO sensor may be measured.

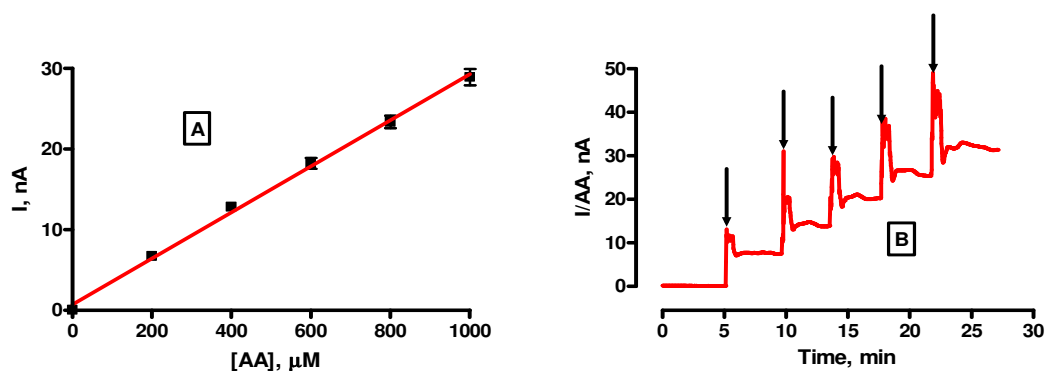


Figure 6.5.2: (A) The current-concentration profile of AA at an unmodified  $Pt_d$  electrode ( $n = 20$ ). (B) A typical raw data trace 0-1000  $\mu\text{M}$  for AA calibrations. CPA carried out at +900 mV vs. SCE. Arrows indicate the addition of 200  $\mu\text{M}$  aliquots of AA.

| AA, $\mu\text{M}$ | Mean I, nA | S.E.M |
|-------------------|------------|-------|
| 0                 | 0          | 0     |
| 200               | 6.68       | 0.25  |
| 400               | 12.82      | 0.44  |
| 600               | 18.22      | 0.66  |
| 800               | 23.37      | 0.79  |
| 1000              | 28.94      | 1.00  |

Table 6.5.2: Data obtained from the calibration shown in Figure 6.4.2(A),  $n = 20$ .  $R^2 = 0.9977$ . Data is represented as a Mean  $\pm$  standard error of the mean (SEM). Background values subtracted.

Mean background current =  $0.23 \pm 0.05$  nA.

Table 6.5.2 displays data representing the AA response of the unmodified  $Pt_d$  electrode. The response to AA is proportional to the concentration of AA added to the electrochemical cell with a calculated sensitivity of  $28.6 \pm 0.04$  pA/ $\mu\text{M}$ ,  $n = 20$ .

### 6.5.3 AA response comparison

This section compares the AA response of the Pt<sub>d</sub> electrode to the Nafion<sup>®</sup>-modified Pt<sub>d</sub> NO sensor. It is clear from Figure 6.5.3 below that the Nafion<sup>®</sup> thermal annealing procedure as previously demonstrated (Brown *et al.*, 2009), has greatly reduced the AA response observed at an unmodified Pt<sub>d</sub> electrode.

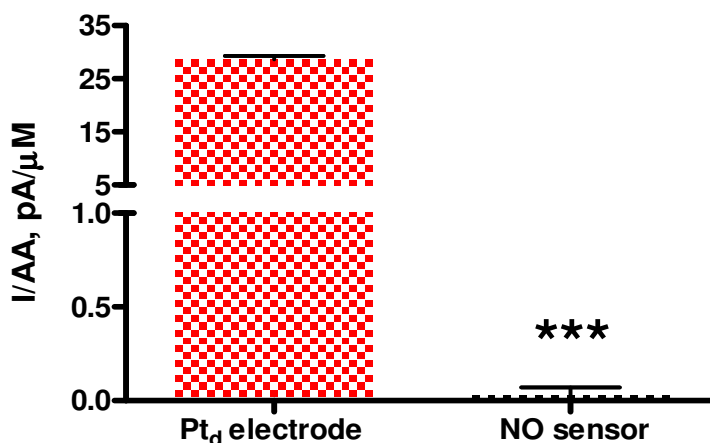


**Figure 6.5.3:** Comparison between AA responses of Pt<sub>d</sub> and the NO sensor. Average response represented as a slope value (pA/μM) mean response ± SEM and ( $P < 0.0001$ , \*\*\*).

A significant difference ( $P < 0.0001$ , \*\*\*) in AA response was seen with the Nafion<sup>®</sup>-modified Pt<sub>d</sub> NO sensor when compared to an unmodified electrode (Pt<sub>d</sub>). The AA response of the Pt<sub>d</sub> electrode was  $28.6 \pm 0.04$  pA/μM,  $n = 20$  and a sensitivity to AA of  $0.03 \pm 0.04$  pA/μM,  $n = 16$  was obtained with the NO sensor. It is clear that the modification of the bare electrode has effectively eliminated the detection of AA at the active surface of the electrode. It is paramount that the modification of the working electrode in order to reject interference from AA does not hinder the detection of NO and this is demonstrated in the next Section (6.6).

## 6.6 In-Vitro Sensitivity and Selectivity of the NO sensor summary

The *in-vitro* sensitivity to NO and the AA rejection characteristics of the NO sensor have been demonstrated in Sections (6.4 and 6.5) respectively. This section compares the sensitivity of the Nafion<sup>®</sup>-modified sensor to these two analytes (NO and AA).

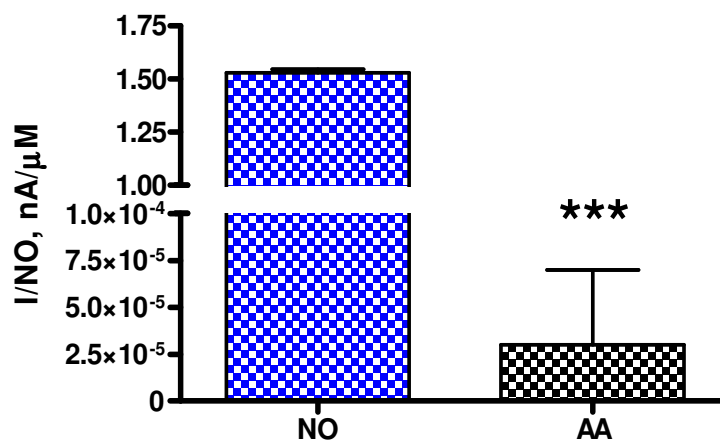


**Figure 6.6.1:** Comparison between sensitivities of the Nafion<sup>®</sup>-modified Pt<sub>4</sub> (5 pre-coats, 2 applications) sensor to NO and AA. Average response represented as a slope value (nA/μM) mean response ± SEM and ( $P < 0.0001$ , \*\*\*).

The *in-vitro* NO sensitivity ( $1.53 \pm 0.02$  nA/μM,  $n = 16$ ) was significantly different ( $P < 0.0001$ , \*\*\*) to the recorded *in-vitro* AA response ( $0.03 \pm 0.04$  pA/μM,  $n = 16$ ) of the NO sensor. These results substantiate the suitability of the Nafion<sup>®</sup>-modified NO sensor for the detection of NO in the *in-vivo* environment.

## 6.7 Post *in-vivo* stability

The NO sensor was implanted into the brain of Wistar rats over an extended period, subsequently the sensors were removed and re-calibrated. The sensors sensitivity towards NO and selectivity over AA was examined following implantation. The calibration procedures are outlined in Section 3.7.4 and 3.7.3 respectively. The *in-vitro* characteristics of a sensor may differ from that observed *in-vivo*. The influence of the *in-vivo* environment on the properties of a sensor is due in part to how the sensor may be altered by the various constituents of brain tissue. When in contact with a biological sample a drop in sensitivity of the sensor may occur due to fouling of the sensor by proteins and other biomolecules present within the tissue (Garguilo & Michael, 1994; Hu *et al.*, 1994). The natural defence mechanism of the body to the presence of a foreign object can also inhibit the sensitivity of an implanted sensor (Wisniewski *et al.*, 2000).

The effect of the environment may be reflected by variations in the sensors characteristics. The aim of this section is to examine the stability of the NO sensor following exposure to the physiological environment.

The following section is a discussion of the post *in-vivo* stability results of the NO sensor; which we have recently published (Finnerty *et al.*, 2012a).

### 6.7.1 Post *in-vivo* NO sensitivity

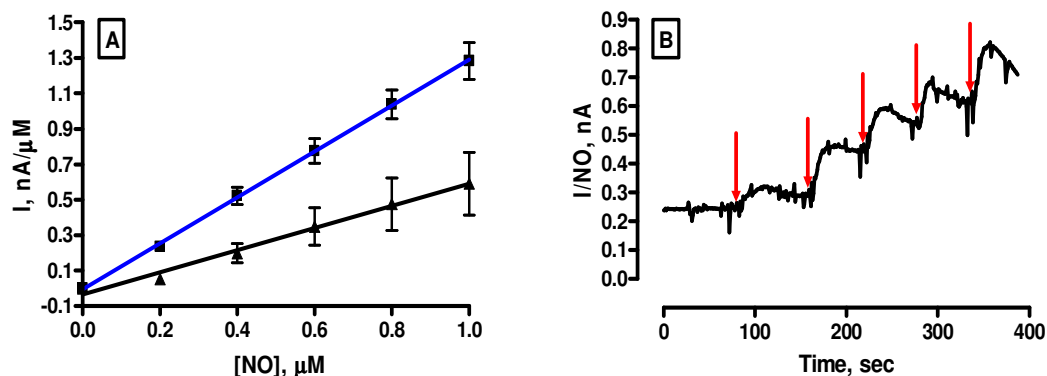


**Figure 6.7.1:** (A) The current-concentration profile of NO at Nafion<sup>®</sup>-modified Pt<sub>4</sub> (5 pre-coats, 2 applications) sensors; pre *in-vivo* (■) and post *in-vivo* (▲) ( $n = 7$ ). (B) A typical raw data trace 0-1  $\mu$ M for post *in-vivo* NO calibrations. CPA carried out at +900 mV vs. SCE. Arrows indicate the addition of 0.2  $\mu$ M aliquots of NO.

Figure 6.7.1 demonstrates the average NO sensitivity of the Nafion<sup>®</sup>-modified Pt<sub>4</sub> (5 pre-coats, 2 applications) sensors prior to and following implantation. The sensors represented here were implanted over a period of 11 to 23 days. The pre *in-vivo* NO sensitivity of these sensors which was determined from *in-vitro* calibration data was  $1.30 \pm 0.01$  nA/ $\mu$ M,  $n = 7$ . These sensors were removed following cessation of *in-vivo* experiments and the post *in-vivo* sensitivity to NO of these sensors was determined as  $0.62 \pm 0.03$  nA/ $\mu$ M,  $n = 7$ . This value is significantly different ( $P < 0.0001$ , \*\*\*) when compared to the pre-implantation sensitivity of the same sensors.

A drop in sensitivity of approximately 48 % was apparent following calibration with NO. This value is consistent with other reports which have demonstrated a 20 to 50 % loss in sensitivity of sensors following exposure to biological samples (Garguilo &

Michael, 1994; Hu *et al.*, 1994). The loss in sensitivity recorded here is also comparable to previous *in-vitro* bio-compatibility determinations by Brown *et al.* of the same sensor design (Brown *et al.*, 2009). In this work a 38 % loss in sensitivity was recorded due to exposure to lipid and protein, however the loss observed was seen within an initial 24 hr period and no significant difference was apparent subsequently (Brown *et al.*, 2009).

On further inspection of the raw data trace in Figure 6.7.1 (B) an increase in response is observed following each addition of NO. A decline in response is observed following each injection and this contrasts greatly when compared to the response seen with the average *in-vitro* NO calibration data prior to implantation (see Figure 6.4.1 (B)). It is possible that the adhesion of proteins and lipids to the surface of each sensor creates a diffusional barrier which limits the movement of NO added to the bulk solution to the active surface of each sensor. The process of stirring following addition of NO creates forced convection of the analyte to the active surface of the sensor. This is a possible explanation for the initial increase and subsequent decline in response observed with the post *in-vivo* calibration which is not apparent with these sensors prior to implantation.

Additionally the process of ex-plantation can cause damage to the modified sensor which may negatively affect the characteristics of the working electrode. However during *in-vivo* experiments the Nafion<sup>®</sup>-modified active surface of the NO sensor remains intact which is proven by the sensor's response towards systemically introduced ascorbate while implanted (Finnerty *et al.*, 2012a). Also the mean baseline current of the Nafion<sup>®</sup>-modified Pt<sub>d</sub> NO sensor is largely unaffected *in-vivo* over a chronic period of continuous recording (Finnerty *et al.*, 2012a).

| NO, $\mu\text{M}$ | Mean I, nA | SEM  |
|-------------------|------------|------|
| 0                 | 0          | 0    |
| 0.2               | 0.24       | 0.02 |
| 0.4               | 0.52       | 0.05 |
| 0.6               | 0.78       | 0.07 |
| 0.8               | 1.04       | 0.08 |
| 1.0               | 1.28       | 0.10 |

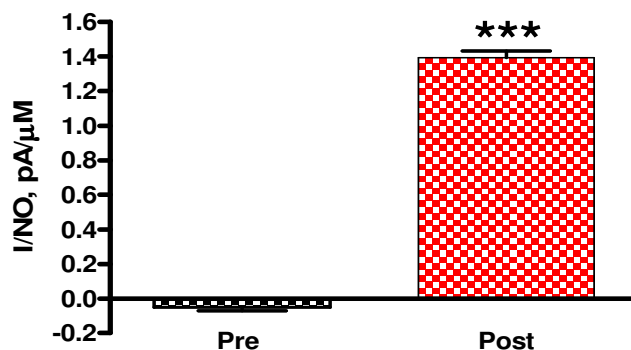
**Table 6.7.1:** Pre-implantation NO data shown in Figure 4.6.1(A), ( $\blacksquare$ );  $n = 7$ .  $R^2 = 0.9996$ . Data is represented as a Mean  $\pm$  standard error of the mean (SEM). Background values subtracted. Mean background current =  $0.12 \pm 0.02$  nA.

| NO, $\mu\text{M}$ | Mean I, nA | SEM  |
|-------------------|------------|------|
| 0                 | 0          | 0    |
| 0.2               | 0.05       | 0.01 |
| 0.4               | 0.20       | 0.05 |
| 0.6               | 0.35       | 0.11 |
| 0.8               | 0.48       | 0.15 |
| 1.0               | 0.59       | 0.18 |

**Table 6.7.2:** Post-implantation NO data shown in Figure 4.6.1(A), ( $\blacktriangle$ );  $n = 7$ .  $R^2 = 0.9889$ . Data is represented as a Mean  $\pm$  standard error of the mean (SEM). Background values subtracted. Mean background current =  $0.26 \pm 0.06$  nA.

| NO sensor                       | NO sensitivity (nA/ $\mu\text{M}$ ) | $R^2$  | n |
|---------------------------------|-------------------------------------|--------|---|
| Pre <i>in-vivo</i> sensitivity  | $1.30 \pm 0.01$                     | 0.9996 | 7 |
| Post <i>in-vivo</i> sensitivity | $0.62 \pm 0.03$                     | 0.9889 | 7 |

**Table 6.7.3:** Comparison between sensitivities of NO sensors prior to and following implantation for 11 to 23 days

6.7.2 Post *in-vivo* AA selectivity

**Figure 6.7.2:** Comparison between pre *in-vivo* and post *in-vivo* AA sensitivities of the NO sensor. Average response represented as a slope value (pA/μM) mean response ± SEM and ( $P < 0.0001$ , \*\*\*).

Figure 6.7.2 represents the AA response of the NO sensor prior to and following an implantation period of 11 to 23 days. The pre *in-vivo* AA sensitivity of these sensors which was determined from *in-vitro* calibration data was  $-0.05 \pm 0.02$  pA/μM,  $n = 7$ . The post *in-vivo* sensitivity of these sensors to AA which was determined from *in-vitro* data was  $1.39 \pm 0.04$  pA/μM,  $n = 7$ . This value is significantly different ( $P < 0.0001$ , \*\*\*) when compared to the pre-implantation AA response of the same sensors.

A clear increase in AA sensitivity of the NO sensor following implantation is apparent. However, when the post *in-vivo* AA response of the sensor is compared to an unmodified Pt<sub>d</sub> a significant difference ( $P < 0.01$ , \*\*) is observed. This supports the stability of the modified Pt active surface of the NO sensor, a disruption to the surface would lead to a larger exposed surface area of Pt and hence a higher sensitivity to AA as seen in Figure 6.5.2.

## 6.8 *In-vivo* characterisation of the NO sensor

The *in-vitro* characterisation of the NO sensor has been discussed (Section 6.4 to 6.6). The results displayed in the remainder of this chapter demonstrate the viability of the NO sensor performance in the physiological environment. Our research group has previously conducted a detailed *in-vivo* characterisation of the Nafion<sup>®</sup>-modified NO sensor which was carried out in the striatum of freely-moving Wistar rats (Finnerty *et al.*, 2012a). An extensive regional characterisation of the NO sensor has also been conducted in the striatum, nucleus accumbens (NA) and prefrontal cortex (P.F.C) (Finnerty *et al.*, 2012b).

As demonstrated by Finnerty *et al.* the implanted Nafion<sup>®</sup>-modified Pt<sub>d</sub> sensor demonstrates significant changes from baseline following the local and systemic administration of known inducers and inhibitors of NO production (Finnerty *et al.*, 2012a; Finnerty *et al.*, 2012b). Additionally, the NO sensor displayed no significant response following the systemic administration of sodium ascorbate which demonstrates the selectivity of the NO sensor over AA which is discussed in Section 6.8.4.

The remainder of this chapter will demonstrate the NO sensor response to the systemic administration of saline and the relevant substances which induce and inhibit NO production. The results in this section demonstrate the sensitivity, selectivity and stability of the NO sensor implanted in the nucleus accumbens (NA) of freely-moving male Wistar rats.

### 6.8.1 Systemic administration of saline (i.p.)

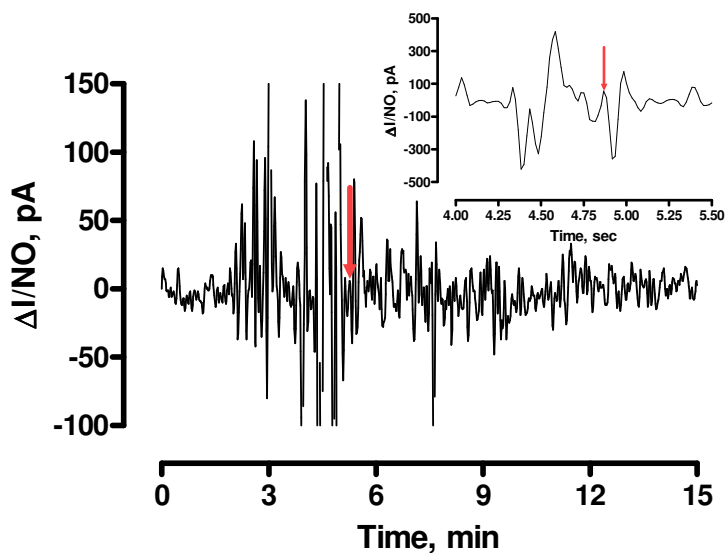


**Figure 6.8.1:** A typical example of a 1mL injection of saline (i.p.) detected by the NO sensor implanted in the NA of a freely-moving Wistar rat. *Inset:* Immediate response following injection (secs). The arrow indicates the point of administration.

All systemic administrations shown in this chapter were carried out by intraperitoneal injection (i.p.) in 1 mL of saline. As a control experiment saline (see Section 3.3.3.2) was administered (i.p.) (see Section 3.11.1) and the effect on the NO signal was measured (see Figure 6.8.1). Upon the injection of saline a brief fluctuation in NO is observable which is due to the physical manipulation of the subject as can be seen in Figure 6.8.2 (inset). The animal must be positioned on its back to facilitate an i.p. injection (see Section 3.11.1) which requires more physical movement than a subcutaneous injection (s.c.). A disparity in the NO signal due to the extent of movement can be observed with an s.c. injection (see Section 7.3.1). However, the NO response with each administration (s.c. and i.p.) is minimal and short-lived. A small increase was found following the i.p. injection of saline in this case, which was  $12.3 \pm 3.9$  pA ( $n = 9$ ) following  $2.5 \pm 0.3$  mins ( $n = 9$ ) and a return to pre-injection baseline levels was seen  $7.5 \pm 0.2$  mins ( $n = 9$ ) subsequently. The recorded change in current corresponds to a concentration change of  $7.8 \pm 2.5$  nM NO ( $n = 9$ ). However, this NO

concentration change is short lived. The aim of the experiments shown in this section is to demonstrate the NO response which is attributable to the injection itself which is minor. No significant difference ( $P > 0.05$ ) was observed between pre and post-injection baseline levels. No lasting effect on the NO response of the Nafion<sup>®</sup>-modified NO sensor was observed following this injection. The data presented in this section is consistent with previous findings of the effect of systemic administration of saline on the response of this NO sensor design monitored in the NA (Finnerty *et al.*, 2012b).

| Analyte | Current change (pA) | Change (%) | Conc. change (nM) | Max response (mins) | Return (mins) | Pre-injection baseline (pA) | Post-injection baseline (pA) |
|---------|---------------------|------------|-------------------|---------------------|---------------|-----------------------------|------------------------------|
| Saline  | 12.3 ± 3.9          | 3.2 ± 1.0  | 7.8 ± 2.5         | 2.5 ± 0.3           | 7.5 ± 0.2     | 378.6 ± 137.8               | 389.6 ± 142.7                |

**Table 6.8.1: Summary of results shown in Section 6.8.1. Data obtained from 9 sensors implanted in the NA of 3 Wistar rats.**

### 6.8.2 Systemic administration of L-arginine

The amino acid L-arginine is the precursor to NO production in the body (Kiechle & Malinski, 1993; Guix *et al.*, 2005). The reaction of molecular oxygen with L-arginine in the presence of nitric oxide synthase and other co-factors produces NO and L-citrulline in equimolar quantities. L-citrulline can then be converted back to L-arginine as part of the normal nitrogen metabolism of the body (Bruckdorfer, 2005). This section demonstrates the effect of systemic administration of the substrate for NO production (L-arginine) on the NO sensor response while implanted in the NA of freely-moving rats.

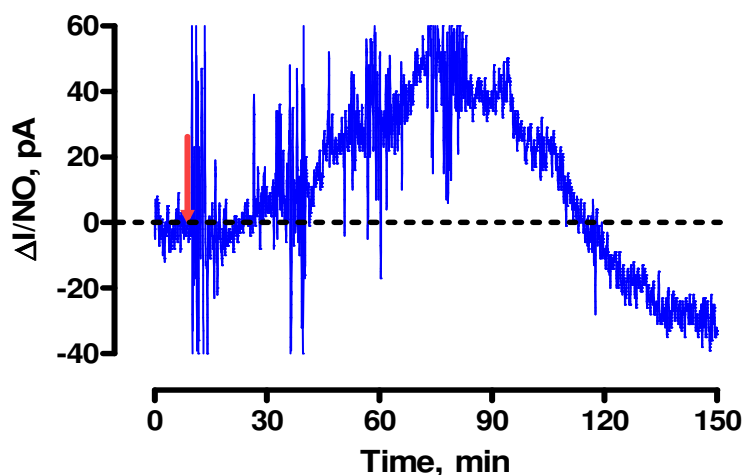


**Figure 6.8.2:** A typical example of an L-arginine (300 mg/kg) injection (i.p.) monitored in the NA of a freely-moving Wistar rat. The arrow indicates the point of administration.

Following the injection of L-arginine (300 mg/kg) (see Section 3.3.2.2) a clear increase in NO above baseline levels denoted by the dashed line was apparent as can be seen in Figure 6.8.2. A significant change in current above baseline levels ( $59.4 \pm 10.2$  pA,  $P < 0.05, *$ ), ( $n = 4$ , 6ad) was observed which corresponds to a concentration change of  $37.6 \pm 6.4$  nM ( $n = 4$ , 6ad). The maximum increase was recorded  $82.6 \pm 10.2$  mins ( $n = 4$ , 6ad) following the administration. A return to a baseline level was observed  $159.4 \pm 12.7$  mins ( $n = 4$ , 6ad) subsequently. A drift below baseline can be seen in Figure 6.8.2 however no significant difference ( $P > 0.05$ ) was observed between pre and post-injection baseline levels.

| Analyte    | Current change (pA) | Change (%)     | Conc. change (nM) | Max response (mins) | Return (mins)    | Pre-injection baseline (pA) | Post-injection baseline (pA) |
|------------|---------------------|----------------|-------------------|---------------------|------------------|-----------------------------|------------------------------|
| L-arginine | $59.4 \pm 10.2$     | $16.6 \pm 2.8$ | $37.6 \pm 6.4$    | $82.6 \pm 10.2$     | $159.4 \pm 12.7$ | $358.3 \pm 115.7$           | $390.4 \pm 110.3$            |

**Table 6.8.2:** Summary of results shown in Section 6.8.2. Data obtained from 4 sensors implanted in the NA of 3 Wistar rats. Average data from 6 administrations.

The data presented in this section is consistent with previous findings of the effect of systemic injection of L-arginine on the response of the NO sensor implanted in the NA

(Finnerty *et al.*, 2012b). Furthermore this data further supports work demonstrated by our research group on the effect of local and systemic administration of L-arginine on the response of this NO sensor design (Brown *et al.*, 2009; Finnerty *et al.*, 2012a). It is evident that the NO sensor is responding to an increase in endogenous levels of NO. Additionally the data outlined in this section validates finding by other research groups who have reported an increase in NO due to the administration of L-arginine (Heinzen & Pollack, 2002; Mas *et al.*, 2002).

#### 6.8.2.1 Systemic administration of L-arginine vs. saline

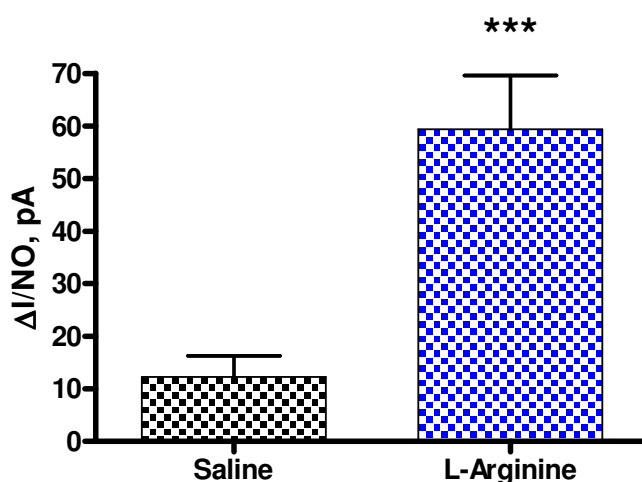


**Figure 6.8.2.1: Comparison between systemic (i.p.) saline (1ml) and L-arginine (300 mg/kg in 1mL saline) administration. Data represented as meant current change from baseline.  $P < 0.0001$ ,\*\*\*.**

The effect of saline administration (see Section 6.8.1) may be used as a control against which the systemic injection of L-arginine (300 mg/kg) may be compared. It is clear from Figure 6.8.2.1 that the effect of L-arginine administration ( $n = 4$ , 6ad) on the NO sensor response is significantly different ( $P < 0.0001$ ,\*\*\*) from the control experiment. These results demonstrate that following L-arginine administration the NO sensor responds to an endogenous elevation of NO and that the observed response is not attributable to injection stress.

### 6.8.3 Systemic administration of L-NAME

In this section the effect of L-NAME, a known inhibitor of NO production on NO levels monitored in the NA is investigated. L-NAME is a non-selective NO inhibitor and it carries out its action by competing with L-arginine for its binding site on the NOS enzyme (Alderton *et al.*, 2001; Salerno *et al.*, 2002). Therefore the systemic administration of L-NAME results in a decreased production of NO, thereby causing a reduction in the NO sensor response.

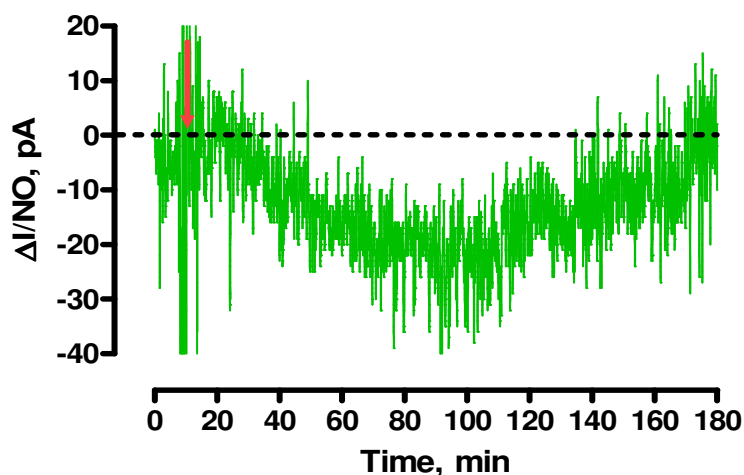


**Figure 6.8.3:** A typical example of an L-NAME (30 mg/kg) injection (i.p.) monitored in the NA of a freely-moving Wistar rat. The arrow indicates the point of administration.

Figure 6.8.3 demonstrates the effect of systemic L-NAME (30 mg/kg) administration on the NO sensor response monitored in the NA. Following systemic administration of L-NAME a clear decrease in NO levels below baseline levels (dashed line) was evident. A significant current decrease below baseline levels ( $-23.2 \pm 2.7$  pA,  $P < 0.0001$ ,\*\*\*), ( $n = 7$ , 5ad) was observed which corresponds to a concentration change of  $-15.2 \pm 1.8$  nM ( $n = 7$ , 5ad). The maximum decrease was recorded  $72.6 \pm 19.6$  mins ( $n = 7$ , 5ad) following the administration. A return to a baseline level was observed  $176.0 \pm 12.6$  mins ( $n = 7$ , 5ad) following the injection. No significant difference ( $P > 0.05$ ) was observed between pre and post-injection baseline levels.

| Analyte | Current change (pA) | Change (%) | Conc. change (nM) | Max response (mins) | Return (mins) | Pre-injection baseline (pA) | Post-injection baseline (pA) |
|---------|---------------------|------------|-------------------|---------------------|---------------|-----------------------------|------------------------------|
| L-NAME  | -23.2 ± 2.7         | -7.6 ± 0.9 | -15.2 ± 1.8       | 72.6 ± 19.6         | 176.0 ± 12.6  | 304.4 ± 32.2                | 318.5 ± 23.3                 |

**Table 6.8.3: Summary of results shown in Section 6.8.2. Data obtained from 7 sensors implanted in the NA of 2 Wistar rats. Average data from 5 administrations.**

The results presented in this section are consistent with previously published work on the effect of systemic injection of L-NAME on the response of the NO sensor implanted in the NA (Finnerty *et al.*, 2012a; Finnerty *et al.*, 2012b). It is clear from the data presented here that inhibition of endogenous NO production is represented by a decrease in NO sensor response.

#### 6.8.3.1 Systemic administration of L-NAME vs. saline

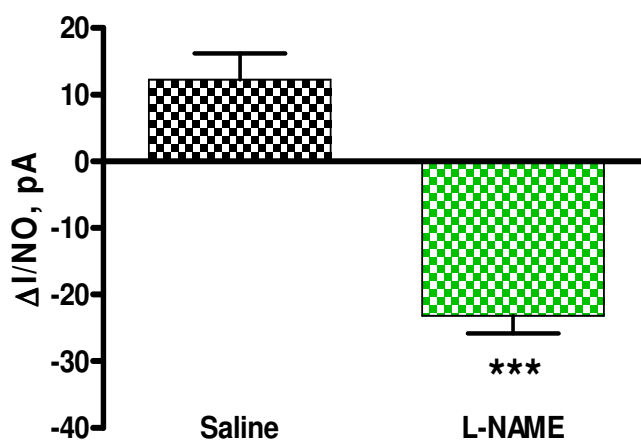


**Figure 6.8.3.1: Comparison between systemic (i.p.) saline (1ml) and L-NAME (30 mg/kg in 1mL saline) administration. Data represented as meant current change from baseline.  $P < 0.0001$ ,\*\*\*.**

In Figure 6.8.3.1 the systemic administration of L-NAME (30 mg/kg) on NO levels detected by the NO sensor implanted in the NA is compared against the corresponding saline response (see Section 6.8.1). It is evident that the effect of L-NAME administration (n = 7, 5ad) on the NO sensor response is significantly different ( $P < 0.0001$ ,\*\*\*) from systemic saline administration. These results demonstrate that

following L-NAME administration the NO sensor responds to an endogenous reduction in NO production. The observed response is not attributable to injection stress but to the NOS inhibitory effect of L-NAME.

#### 6.8.4 Systemic administration of sodium ascorbate

Ascorbic acid is the primary interference species in the brain, with an estimated concentration of between 100 and 500  $\mu\text{M}$  in the ECF (Miele & Fillenz, 1996). Sodium ascorbate was utilised as an interference test *in-vivo* since AA, even with pH adjustment, causes significant discomfort to the animal. Ascorbate can be easily detected using voltametric methods *in-vivo* due to the high concentration of this molecule and relative ease of oxidation (O'Neill *et al.*, 1998; Lowry *et al.*, 2006). Therefore it is necessary to verify the selectivity of the NO sensor against this possible interferent. In order to determine whether the presence of this interferent would affect the NO sensor response sodium ascorbate was systemically administered and the current was monitored.

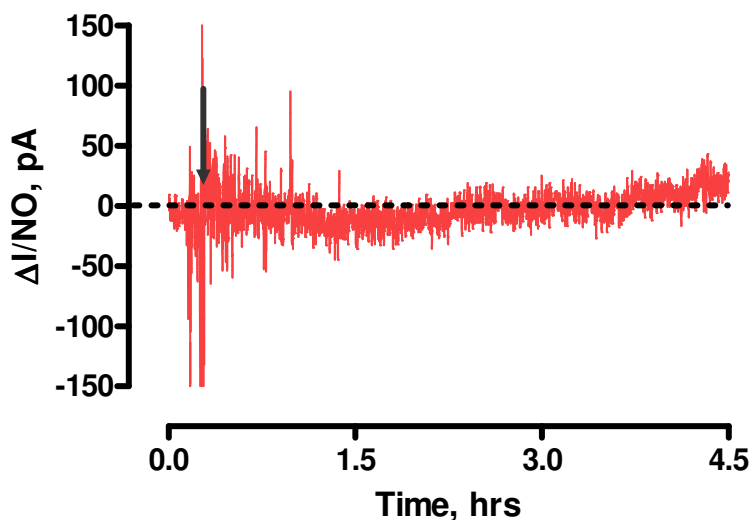


**Figure 6.8.4:** A typical example of a (2 g/kg) sodium ascorbate injection (i.p.) monitored in the NA of a freely-moving Wistar rat. The arrow indicates the point of administration.

Figure 6.8.4 demonstrates the effect of systemic ascorbate administration on the NO sensor response. Previous investigations utilising a carbon paste sensor to monitor ascorbate have demonstrated a maximal effect due to systemic ascorbate administration within 60 minutes (Lowry *et al.*, 1996; Finnerty *et al.*, 2012b). It is quite clear from

Figure 6.8.4 that the current response of the NO sensor remains close to basal levels for the initial 60 min period. A slight deviation from baseline levels was observed however no significant difference ( $P > 0.05$ ) was observed between the maximum current response ( $-23.2 \pm 13.9$  pA,  $n = 8$ , 5ad) and pre-injection baseline levels ( $342.3 \pm 93.6$  pA,  $n = 8$ , 5ad) in these experiments. The current remained in close proximity to baseline levels for the duration of the recording period (Figure 6.8.4). The minimal response of the NO sensor due to the introduction of ascorbate demonstrates the integrity of the Nafion<sup>®</sup>-modified surface of the NO sensor design. These findings further demonstrate the selectivity of the NO sensor over AA as has previously been successfully demonstrated *in-vivo* (Finnerty *et al.*, 2012a; Finnerty *et al.*, 2012b).

| Analyte          | Current change (pA) | Change (%)      | Conc. change (nM) | Max response (mins) | Return (mins)    | Pre-injection baseline (pA) | Post-injection baseline (pA) |
|------------------|---------------------|-----------------|-------------------|---------------------|------------------|-----------------------------|------------------------------|
| Sodium ascorbate | $-23.2 \pm 13.9$    | $-6.8 \pm 23.7$ | $-14.7 \pm 8.8$   | $118.3 \pm 10.1$    | $267.8 \pm 16.5$ | $342.3 \pm 93.6$            | $343.3 \pm 96.1$             |

Table 6.8.4: Summary of results shown in Section 6.8.4. Data obtained from 8 sensors implanted in the NA of 3 Wistar rats. Average data includes 5 administrations.

#### 6.8.4.1 Systemic administration of Sodium ascorbate vs. saline

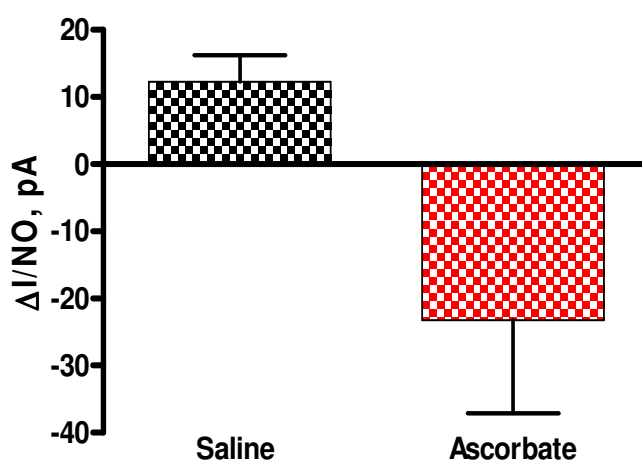


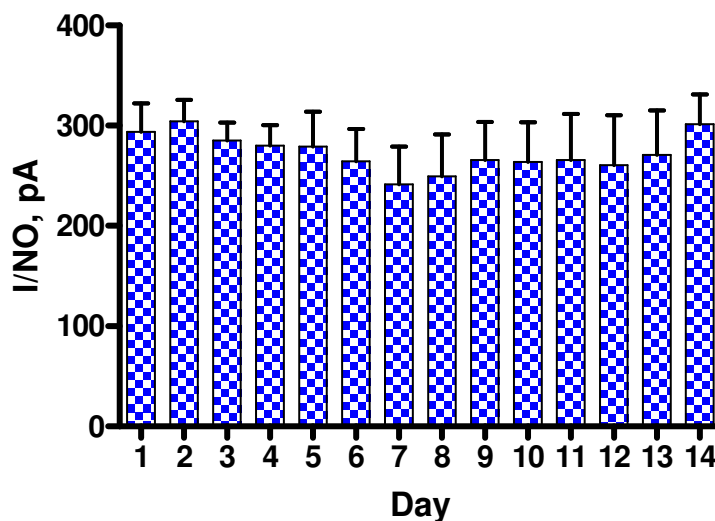
Figure 6.8.4.1: Comparison between systemic (i.p.) saline (1ml) and sodium ascorbate (2 g/kg in 1mL saline) administration. Data represented as meant current change from baseline.

Figure 6.8.4.1 compares the effect of systemic administration of sodium ascorbate against the administration of saline. No significant difference ( $P = 0.0653$ ) was observed between the control experiments conducted using saline (see Section 6.8.1) and the response of the NO sensor following injection of ascorbate. These results re-establish that the NO sensor is selective over AA *in-vivo* and stable in the physiological environment. A disruption to the Nafion<sup>®</sup>-modified Pt active surface of the sensor would lead to an increased surface area of exposed Pt and an increase in AA detection which is clearly absent (see Figures 6.8.4 and 6.8.4.1).

### **6.8.5 Baseline stability of the NO sensor**

The mean *in-vivo* baseline current of the NO sensor was examined over a consecutive period of 14 days of implantation. A decrease in sensitivity of an electrochemical sensor can often be observed following contact with a biological sample due to fouling of the sensor by proteins and other biomolecules present within the tissue (Garguilo & Michael, 1994). The normal reaction of the body to the presence of a foreign object may also negatively affect the sensitivity of an implanted sensor (Wisniewski *et al.*, 2000).

It has previously been demonstrated that the baseline current value of the implanted NO sensor remains consistent for a consecutive period of 8 days (Finnerty *et al.*, 2012a). These findings indicate that the NO sensor is stable over a prolonged period in the *in-vivo* environment. Any disruption to the modified active surface of the NO sensor should lead to an increase in baseline current values as the period of implantation progresses. It was necessary to investigate any effect the physiological environment may have on the stability of the NO sensor while implanted. The data presented in this section is taken from NO sensors implanted in the NA.



**Figure 6.8.5.1: Baseline stability of the NO sensor implanted in the NA for a consecutive period of 14 days (n = 2-6, 2-5 animals).**

The data shown in Figure 6.8.5.2 demonstrates the mean baseline current recorded by the NO sensor *in-vivo* over fourteen consecutive days. The baseline value was calculated from the same time point for each day of implantation and recordings were taken following an initial period of *ca.* 24 hrs following implantation. The data represented here is from NO sensors implanted in the NA of freely-moving rats. A one-way ANOVA analysis of variance revealed that the baseline current showed no significant variation  $P > 0.05$  over the stated duration of implantation. The current detected by the NO sensor remains consistent over fourteen days. Any deterioration in the Nafion<sup>®</sup>-modified active surface which is part of this sensor design would lead to an increased current response as the duration of implantation progresses. No significant change ( $P > 0.05$ ) was observed in current response detected by the NO sensor over the stated duration of implantation. These results verify the stability of the NO sensor for the purpose of obtaining L.I.V.E recordings.

| <b>Day</b> | <b>Mean I,<br/>(pA ± SEM)</b> | <b>n</b> | <b>Day</b> | <b>Mean I,<br/>(pA ± SEM)</b> | <b>n</b> |
|------------|-------------------------------|----------|------------|-------------------------------|----------|
| <b>1</b>   | 293.8 ± 28.3                  | 6        | <b>8</b>   | 249.6 ± 41.4                  | 4        |
| <b>2</b>   | 304.5 ± 21.2                  | 6        | <b>9</b>   | 265.9 ± 37.8                  | 4        |
| <b>3</b>   | 285.2 ± 18                    | 6        | <b>10</b>  | 263.7 ± 39.8                  | 4        |
| <b>4</b>   | 280.3 ± 20.3                  | 5        | <b>11</b>  | 265.8 ± 45.9                  | 3        |
| <b>5</b>   | 279.3 ± 34.7                  | 5        | <b>12</b>  | 260.6 ± 49.8                  | 3        |
| <b>6</b>   | 264.5 ± 32.4                  | 4        | <b>13</b>  | 270.8 ± 44.4                  | 3        |
| <b>7</b>   | 241.6 ± 37.5                  | 4        | <b>14</b>  | 301.4 ± 29.7                  | 2        |

**Table 6.8.5.1: Summary of the data provided in Figure 6.8.5.1. Day 1-3: (n = 6, 5 animals), Day 4-5: (n = 5, 5 animals), Day 6-10: (n = 4, 4 animals), Day 11-13: (n = 3, 3 animals) and Day 14 (n = 2, 2 animals).**

## 6.9 Conclusion

The primary aim of this chapter was to verify the *in-vitro* and *in-vivo* characterisation of the NO sensor as previously demonstrated by our research group (Brown & Lowry, 2003; Brown *et al.*, 2009; Finnerty *et al.*, 2012a; Finnerty *et al.*, 2012b).

The *in-vitro* NO sensitivity was established (see Section 6.4) and reported as  $1.53 \pm 0.02$  nA/ $\mu$ M,  $n = 16$ . No significant difference ( $P > 0.05$ ) was observed between the NO sensitivity of the NO sensor design presented here in comparison to that previously demonstrated by Finnerty *et al* (Finnerty *et al.*, 2012b). The sensitivity of the NO sensor is highly suitable for the detection of NO *in-vivo*, as NO has a short half-life in biological tissues (Kelm, 1999). Additionally the concentration of NO in biological samples is within the pico-micromolar range (Wink & Mitchell, 1998).

The NO sensor must exhibit a fast response time and low limit of detection (LOD) in order to detect physiological NO, due to the afore mentioned low concentration and short lifetime of NO *in-vivo*. The operational characteristics of the NO sensor, i.e. the response time (see Section 6.4.3) and LOD (see Section 6.4.2) were calculated as  $12.21 \pm 1.83$  secs, ( $n = 7$ ) and  $2.73 \pm 0.34$  nM, ( $n = 12$ ) respectively. The response time and LOD of the NO sensor reported in this chapter are consistent with previous reports of the operational characteristics of the NO sensor (Brown *et al.*, 2009) and are efficient for the detection of NO *in-vivo*.

The *in-vitro* selectivity of the NO sensor against AA, the primary interferent species in the brain in relation to NO detection was validated (see Section 6.5) and reported as  $0.03 \pm 0.04$  pA/ $\mu$ M,  $n = 16$ . No significant difference ( $P > 0.05$ ) was observed between baseline levels and the maximum response of the NO sensor due to addition of AA (see Section 6.5). The selectivity characteristics of the NO sensor reported here are consistent with previous findings (Brown *et al.*, 2009), where it was determined that AA had no effect on the NO sensor response *in-vitro*. Additionally Brown *et al.* have previously described the excellent rejection characteristics of the NO sensor, the sensor was tested over a wide range of potential interferent species (see Section 6.5) and the unaffected response of the NO sensor was shown. The sensitivity of the NO sensor was also

preserved in the presence of AA (500  $\mu$ M), DA (0.05  $\mu$ M) and O<sub>2</sub> (50  $\mu$ M) (Brown *et al.*, 2009).

An examination of NO sensor characteristics following implantation was discussed in Section 6.7. It was determined that the post *in-vivo* sensitivity of the NO sensor was approximately 48 % less than the pre-implantation sensitivity of the same sensors. Details of the post-implantation sensitivity of the NO sensor have recently been published (Finnerty *et al.*, 2012a). The AA selectivity characteristics of the NO sensor following implantation were described in Section 6.7.2. An increased response to AA following implantation of the NO sensor was observed which was significantly different ( $P < 0.0001, ***$ ) to the pre *in-vivo* response of the same sensors. However, the Nafion<sup>®</sup>-modified active surface of the NO sensor remains intact when implanted as proven by the sensor response to systemically introduced ascorbate *in-vivo* as shown in Section 6.8.4.

The *in-vitro* characterisation of the NO sensor was discussed in Section 6.4 to Section 6.7. The next step was to establish the sensitivity, selectivity and stability of the NO sensor in the *in-vivo* environment. As a control experiment the effect of systemic administration of saline on the implanted NO sensor was examined in Section 6.8.1. The *in-vivo* functionality of the NO sensor was then confirmed while implanted in the nucleus accumbens (NA) of the freely-moving animal (see Sections 6.8.2 and 6.8.3). The precursor to NO production in the body (L-arginine) was systemically administered and NO levels in the NA were monitored (see Section 6.8.2). A significant increase ( $P < 0.0001, ***$ ) in the NO sensor response was observed following the administration of L-arginine with respect to the injection of saline (see Section 6.8.2.1).

Additionally the effect of the non-selective NOS inhibitor (L-NAME) on the response of the NO sensor was determined in the NA (see Section 6.8.3). A significant decrease in the NO sensor response was observed following the administration of L-NAME with respect to the corresponding saline response (see Section 6.8.3.1).

To verify the selectivity of the NO sensor over AA in the physiological environment sodium ascorbate was administered systemically (see Section 6.8.4). No significant

difference ( $P > 0.05$ ) was observed between the maximum current response and pre-injection baseline levels of the NO sensor following the injection of ascorbate. The main results from the *in-vivo* characterisation of the NO sensor in the NA, as previously determined by Finnerty *et al.* are summarised in Table 6.9.1 (Finnerty *et al.*, 2012b).

| Analyte          | Current change (pA) | Change (%)  | Conc. change (nM) | Max response (mins) | Return (mins) | Pre-injection baseline (pA) | Post-injection baseline (pA) | <i>P</i> |
|------------------|---------------------|-------------|-------------------|---------------------|---------------|-----------------------------|------------------------------|----------|
| Saline           | 12.3 ± 3.9          | 3.2 ± 1.0   | 7.8 ± 2.5         | 2.5 ± 0.3           | 7.5 ± 0.2     | 378.6 ± 137.8               | 389.6 ± 142.7                | n/a      |
| L-Arginine       | 59.4 ± 10.2         | 16.6 ± 2.8  | 37.6 ± 6.4        | 82.6 ± 10.2         | 159.4 ± 12.7  | 358.3 ± 115.7               | 390.4 ± 110.3                | ↑,***    |
| L-NAME           | -23.2 ± 2.7         | -7.6 ± 0.9  | -15.2 ± 1.8       | 72.6 ± 19.6         | 176.0 ± 12.6  | 304.4 ± 32.2                | 318.5 ± 23.3                 | ↓,***    |
| Sodium ascorbate | -23.2 ± 13.9        | -6.8 ± 23.7 | -14.7 ± 8.8       | 118.3 ± 10.1        | 267.8 ± 16.5  | 342.3 ± 93.6                | 343.3 ± 96.1                 | > 0.05   |

**Table 6.9.1.: Summary of *in-vivo* NO sensor results from systemic administrations discussed in Section 6.8. Where (*P*) represents the outcome of an unpaired t-test of the maximum response following each administration vs. saline response. Where (↑) denotes an increase and (↓) denotes a decrease in NO monitored in the NA.**

The sensitivity of the NO sensor in the NA of the freely-moving animal was established as summarised in Table 6.9.1. No significant difference ( $P > 0.05$ ) was observed between the maximum current response following each administration (saline, L-arginine, L-NAME and sodium ascorbate) when compared to the corresponding *in-vivo* results previously shown by Finnerty *et al.* in the NA (Finnerty *et al.*, 2012b). Additionally, the maximum response time and subsequent time required to return to a baseline level following the administration of saline, L-arginine and L-NAME showed no significant difference ( $P > 0.05$ ) to that previously presented by Finnerty *et al.* (Finnerty *et al.*, 2012b).

The baseline stability of the NO sensor while implanted in the NA for a consecutive period of 14 days was shown in Section 6.8.5. Previous investigations have demonstrated the stability of the NO sensor implanted in the brain for a continuous period of 8 days (Finnerty *et al.*, 2012a). No significant variation  $P > 0.05$  was observed

in the baseline current of the NO sensor over the stated duration of implantation (see Section 6.8.5). These results further verify the stability of the NO sensor for the purpose of obtaining long-term *in-vivo* recordings.

In summary the *in-vitro* and *in-vivo* characterisation of the NO sensor was verified. The application of this NO sensor for the real-time detection of NO in animal models of neurological disease and dysfunction is presented in Chapter 7 and Chapter 8.

## References

- Alderton WK, Cooper CE & Knowles RG. (2001). Nitric oxide synthases: structure, function and inhibition. *Biochemical Journal* **357**, 593-615.
- Andersen JK. (2004). Oxidative stress in neurodegeneration: cause or consequence? *Nature Medicine* **10**, S18-S25.
- Bogdan C, Rollingshoff M & Diefenbach A. (2000). Reactive oxygen and reactive nitrogen intermediates in innate and specific immunity. *Current Opinion in Immunology* **12**, 64-76.
- Brown FO, Finnerty NJ, Bolger FB, Millar J & Lowry JP. (2005). Calibration of NO sensors for *in-vivo* voltammetry: laboratory synthesis of NO and the use of UV-visible spectroscopy for determining stock concentrations. *Analytical and Bioanalytical Chemistry* **381**, 964-971.
- Brown FO, Finnerty NJ & Lowry JP. (2009). Nitric oxide monitoring in brain extracellular fluid: characterisation of Nafion<sup>®</sup>-modified Pt electrodes *in vitro* and *in vivo*. *Analyst* **134**, 2012-2020.
- Brown FO & Lowry JP. (2003). Microelectrochemical sensors for *in vivo* brain analysis: an investigation of procedures for modifying Pt electrodes using Nafion<sup>®</sup>. *Analyst* **128**, 700-705.
- Bruckdorfer R. (2005). The basics about nitric oxide. *Molecular Aspects of Medicine* **26**, 3-31.
- Calabrese V, Mancuso C, Calvani M, Rizzarelli E, Butterfield DA & Stella AMG. (2007). Nitric oxide in the central nervous system: neuroprotection versus neurotoxicity. *Nature Reviews Neuroscience* **8**, 766-775.
- Cavas M & Navarro JF. (2006). Effects of selective neuronal nitric oxide synthase inhibition on sleep and wakefulness in the rat. *Progress in Neuro-Psychopharmacology & Biological Psychiatry* **30**, 56-67.
- Fang FC. (2004). Antimicrobial reactive oxygen and nitrogen species: Concepts and controversies. *Nature Reviews Microbiology* **2**, 820-832.
- Finnerty NJ, O'Riordan SL, Brown FO, Serra PA, O'Neill RD & Lowry JP. (2012a). *In vivo* characterisation of a Nafion<sup>®</sup>-modified Pt electrode for real-time nitric oxide monitoring in brain extracellular fluid. *Analytical Methods* **4**, 550-557.

- Finnerty NJ, O’Riordan SL, Palsson E & Lowry JP. (2012b). Brain nitric oxide: Regional characterisation of a real-time microelectrochemical sensor. *Journal of Neuroscience Methods* **209**, 13-21.
- Friedemann MN, Robinson SW & Gerhardt GA. (1996). *o*-phenylenediamine-modified carbon fiber electrodes for the detection of nitric oxide. *Analytical Chemistry* **68**, 2621-2628.
- Garguilo MG & Michael AC. (1994). Quantitation of choline in the extracellular fluid of brain-tissue with amperometric microsensors. *Analytical Chemistry* **66**, 2621-2629.
- Guix FX, Uribealago I, Coma M & Munoz FJ. (2005). The physiology and pathophysiology of nitric oxide in the brain. *Progress in Neurobiology* **76**, 126-152.
- Heinzen EL & Pollack GM. (2002). Use of an electrochemical nitric oxide sensor to detect neuronal nitric oxide production in conscious, unrestrained rats. *Journal of Pharmacological and Toxicological Methods* **48**, 139-146.
- Hetrick EM & Schoenfisch MH. (2009). Analytical Chemistry of Nitric Oxide. In *Annual Review of Analytical Chemistry*, pp. 409-433.
- Hu YB, Mitchell KM, Albahadily FN, Michaelis EK & Wilson GS. (1994). Direct measurement of glutamate release in the brain using a dual enzyme-based electrochemical sensor. *Brain Research* **659**, 117-125.
- Ignarro LJ, Buga GM, Wood KS, Byrns RE & Chaudhuri G. (1987). Endothelium-derived relaxing factor produced and released from artery and vein is nitric-oxide. *Proceedings of the National Academy of Sciences of the United States of America* **84**, 9265-9269.
- Kelm M. (1999). Nitric oxide metabolism and breakdown. *Biochimica Et Biophysica Acta-Bioenergetics* **1411**, 273-289.
- Kiechle FL & Malinski T. (1993). Nitric-oxide - biochemistry, pathophysiology, and detection. *American Journal of Clinical Pathology* **100**, 567-575.
- Liu XJ, Shang LB, Pang JT & Li GX. (2003). A reagentless nitric oxide biosensor based on haemoglobin/polyethyleneimine film. *Biotechnology and Applied Biochemistry* **38**, 119-122.
- Lowry JP, Boutelle MG, O’Neill RD & Fillenz M. (1996). Characterization of carbon paste electrodes *in vitro* for simultaneous amperometric measurement of changes in oxygen and ascorbic acid concentrations *in vivo*. *Analyst* **121**, 761-766.

- Lowry JP, O'Neill RD & (2006). *Neuroanalytical Chemistry In Vivo Using Biosensors.*, vol. 10. American Scientific Publishers.
- Mas M, Escrig A & Gonzalez-Mora JL. (2002). *In vivo* electrochemical measurement of nitric oxide in corpus cavernosum penis. *Journal of Neuroscience Methods* **119**, 143-150.
- Maskus M, Pariente F, Wu Q, Toffanin A, Shapleigh JP & Abruna HD. (1996). Electrocatalytic reduction of nitric oxide at electrodes modified with electropolymerized films of Cr(v-tpy)(2) (3+) and their application to cellular NO determinations. *Analytical Chemistry* **68**, 3128-3134.
- Meulemans A. (1993). Continuous monitoring of n-nitroso-l-arginine using microcarbon electrode in rat brain. *Neuroscience Letters* **157**, 7-12.
- Miele M & Fillenz M. (1996). *In vivo* determination of extracellular brain ascorbate. *Journal of Neuroscience Methods* **70**, 15-19.
- Nugent FS, Penick EC & Kauer JA. (2007). Opioids block long-term potentiation of inhibitory synapses. *Nature* **446**, 1086-1090.
- O'Neill RD, Lowry JP & Mas M. (1998). Monitoring brain chemistry *in vivo*: Voltammetric techniques, sensors, and behavioral applications. *Critical Reviews in Neurobiology* **12**, 69-127.
- Pacher P, Beckman JS & Liaudet L. (2007). Nitric oxide and peroxynitrite in health and disease. *Physiological Reviews* **87**, 315-424.
- Pallini M, Curulli A, Amine A & Palleschi G. (1998). Amperometric nitric oxide sensors: a comparative study. *Electroanalysis* **10**, 1010-1016.
- Park JK, Tran PH, Chao JKT, Ghodadra R, Rangarajan R & Thakor NV. (1998). *In vivo* nitric oxide sensor using non-conducting polymer-modified carbon fiber. *Biosensors & Bioelectronics* **13**, 1187-1195.
- Park SS, Hong M, Song C-K, Jhon G-J, Lee Y & Suh M. (2010). Real-Time *in vivo* Simultaneous Measurements of Nitric Oxide and Oxygen Using an Amperometric Dual Microsensor. *Analytical Chemistry* **82**, 7618-7624.
- Park SS, Kim J & Lee Y. (2012). Improved Electrochemical Microsensor for the Real-Time Simultaneous Analysis of Endogenous Nitric Oxide and Carbon Monoxide Generation. *Analytical Chemistry* **84**, 1792-1796.
- Salerno L, Sorrenti V, Di Giacomo C, Romeo G & Siracusa MA. (2002). Progress in the development of selective nitric oxide synthase (NOS) inhibitors. *Current Pharmaceutical Design* **8**, 177-200.

- Shibuki K. (1990). An electrochemical microprobe for detecting nitric-oxide release in brain-tissue. *Neuroscience Research* **9**, 69-76.
- Valko M, Leibfritz D, Moncol J, Cronin MTD, Mazur M & Telser J. (2007). Free radicals and antioxidants in normal physiological functions and human disease. *International Journal of Biochemistry & Cell Biology* **39**, 44-84.
- Wass C, Archer T, Palsson E, Fejgin K, Alexandersson A, Klamer D, Engel JA & Svensson L. (2006a). Phencyclidine affects memory in a nitric oxide-dependent manner: Working and reference memory. *Behavioural Brain Research* **174**, 49-55.
- Wass C, Archer T, Palsson E, Fejgin K, Klamer D, Engel JA & Svensson L. (2006b). Effects of phencyclidine on spatial learning and memory: Nitric oxide-dependent mechanisms. *Behavioural Brain Research* **171**, 147-153.
- Williams IL, Wheatcroft SB, Shah AM & Kearney MT. (2002). Obesity, atherosclerosis and the vascular endothelium: mechanisms of reduced nitric oxide bioavailability in obese humans. *International Journal of Obesity* **26**, 754-764.
- Wink DA & Mitchell JB. (1998). Chemical biology of nitric oxide: Insights into regulatory, cytotoxic, and cytoprotective mechanisms of nitric oxide. *Free Radical Biology and Medicine* **25**, 434-456.
- Wisniewski N, Moussy F & Reichert WM. (2000). Characterization of implantable biosensor membrane biofouling. *Fresenius Journal of Analytical Chemistry* **366**, 611-621.

---

## **7. The detection of nitric oxide in an animal model of autism**

---

## 7.1 Introduction

The *in-vitro* and *in-vivo* characterisation of the Nafion<sup>®</sup>-modified Platinum disc (Pt<sub>d</sub>) (5 pre-coats, 2 applications) nitric oxide (NO) sensor has been established as discussed in Chapter 6. The purpose of this chapter is to utilise the NO sensor in detecting changes in NO levels in the brain of freely-moving rats following systemic administration of Propionic acid (PPA).

PPA is endogenous to the body and exists as an intermediate of normal cellular metabolism and is a product of bacterial metabolism in the human gut (Al-Lahham *et al.*, 2010). MacFabe *et al.* have demonstrated that PPA may be used in rats to mimic the behavioural changes and neuroinflammatory responses which are associated with autism spectrum disorders (ASDs) (MacFabe *et al.*, 2008; Shultz *et al.*, 2009).

ASDs consist of related neurodevelopmental disorders which are characterised by a varying degree of social impairment, difficulties with communication, repetitive behaviours and restricted interests (Rapin & Tuchman, 2008). These symptoms may be debilitating in certain individuals depending on the severity of the condition. However the characteristics of ASDs can display positive attributes in some individuals such as enhanced memory, heightened skills in areas such as mathematics and a superior ability to concentrate (Walsh *et al.*, 2011). To date the relationship between the brain and the behavioural characteristics which are symptomatic of ASDs are not fully understood. The pathogenesis of ASDs has a strong genetic basis, however the exact cause of ASDs is not entirely explained by genetic factors (Folstein & Rosen-Sheidley, 2001). A variety of environmental agents have been indicated in the development of autism such as prenatal exposure to infection (Meyer *et al.*, 2011), ethanol and valproic acid (Arndt *et al.*, 2005).

Current research indicates that the development of ASDs is the result of contributing factors. Gastrointestinal (GI) disturbances have been strongly associated with ASDs, specifically due to an abnormal composition of enteric microbiota in autistic individuals (Parracho *et al.*, 2005; de Theije *et al.*, 2011). Evidence has been shown that treatment of these GI abnormalities in ASDs patients with antibiotics has resulted primarily in

alleviating local symptoms and additionally in a short-term improvement of cognitive skills (Sandler *et al.*, 2000). Research and anecdotal evidence has been reported that the symptoms of ASDs may be exacerbated by the ingestion of wheat and dairy food products (Jyonouchi *et al.*, 2002). These combined reports indicate that a gut derived factor may contribute to the pathogenesis of ASDs. Among other short-chain fatty acids PPA is produced by opportunistic enteric bacteria such as *clostridial* species in the gut and elevated levels of these bacteria have been found in ASDs individuals (Finegold *et al.*, 2002). PPA is also commonly found in wheat and dairy food products (Brock & Buckel, 2004). A dysfunction in normal short-chain fatty acid metabolism can result in access of PPA to the bloodstream. PPA can readily cross the blood-brain barrier by passive or active means and gain access to the central nervous system (Conn *et al.*, 1983). PPA and other short-chain fatty acids have been shown to negatively affect processes such as lipid metabolism (Hara *et al.*, 1999), immune function (Le Poul *et al.*, 2003) and neurotransmitter release (DeCastro *et al.*, 2005) all of which have been implicated in the etiology of ASDs.

Increased oxidative stress in ASDs may contribute to development of the disorder. A variety of underlying contributing factors combined with oxidative stress have been proposed as a causative factor in ASDs (Chauhan & Chauhan, 2006). Reactive oxygen species (ROS) and reactive nitrogen species (RNS) production is regulated by a robust anti-oxidant network. A disruption in normal ROS (e.g. H<sub>2</sub>O<sub>2</sub>) and RNS (e.g. NO) homeostasis leads to oxidative/nitrosative stress and consequently mitochondrial dysfunction, inflammation and cell injury (Valko *et al.*, 2007). Several studies have shown a decrease in anti-oxidant enzyme activity in ASDs including catalase (Zoroglu *et al.*, 2004), and superoxide dismutase (Yorbik *et al.*, 2002) in the blood. Elevated levels of oxidative stress markers have also been measured in ASDs brain tissue preparations (Chauhan *et al.*, 2012; Rose *et al.*, 2012). Haematological studies undertaken by Sogut *et al.* have demonstrated that a decreased level of anti-oxidant activity and an elevated level of NO is found in individuals with ASDs (Sogut *et al.*, 2003). NO has been shown to exert neuroprotective effects at normal concentrations, however NO can become neurotoxic at high concentrations (Calabrese *et al.*, 2007). Evidence has been shown that treatment with PPA has resulted in a reduction in anti-

oxidant enzyme levels and increased oxidative stress markers in brain homogenates of rats (El-Ansary *et al.*, 2012). Additionally chronic administration with ascorbic acid prevents behavioural alterations associated with the administration of PPA in rats (Pettenuzzo *et al.*, 2002). Recent work conducted by MacFabe *et al.* has demonstrated that intracerebroventricular infusions of PPA produced behavioural, biochemical, electrophysiological and pathological effects in rats consistent with that found in ASDs (MacFabe *et al.*, 2007; MacFabe *et al.*, 2008; MacFabe *et al.*, 2011).

The novel investigations discussed in this chapter present the real-time detection of NO in the nucleus accumbens (NA) and dorsal hippocampus (DH) of male Wistar rats in response to the systemic administration of PPA. The NA and DH are part of the limbic system which plays a role in emotional and social cognitive processing. It has been postulated that the social and behavioural impairments which manifest in ASDs may reflect a dysfunction in the limbic system (MacFabe *et al.*, 2008). The NA has been shown to play a role in processes such as reward emotion and addiction (Saulskaya & Fofonova, 2006; Saul'skaya *et al.*, 2008). Functional magnetic resonance imaging has indicated that a general reward dysfunction is implicated in ASDs (Dichter *et al.*, 2012; Kohls *et al.*, 2012). The hippocampus is strongly associated with learning and memory and abnormalities in this brain region have been indicated in ASDs individuals (Goh & Peterson, 2012). NO has been shown to play an important role in synaptic plasticity (Garthwaite, 2008) and plays a vital role in learning and memory (Wass *et al.*, 2006a; Wass *et al.*, 2006b; Nugent *et al.*, 2007). The main aim of this chapter is to demonstrate the effect of PPA on NO levels in the central nervous system (CNS) of freely-moving animals.

## 7.2 Experimental

A detailed description of the instrumentation, chemicals, solutions and software used during these experiments is given in Chapter 3. A detailed description of the manufacture of the NO sensor is outlined in Section 3.4. The surgical protocol followed for the implantation of NO sensors is provided in Section 3.10.2. All experiments outlined in this chapter were performed using Constant Potential Amperometry (CPA). A potential of +900 mV vs. Ag wire (see Section 3.10.3) was applied to the working electrodes for all *in-vivo* experiments. For systemic administration a stock solution of PPA was prepared by dissolving 0.5 g of sodium propionate in 1 mL saline which was subsequently injected at 1 mL/kg (500 mg/kg) twice daily at 12.00 hrs and 15.00 hrs.

The number of implanted NO sensors is denoted by (n) and the number of animals utilised is provided. In the case where the number of administrations included in the data exceeds the number of sensors/animals the value is given and denoted by (adm). NO sensors were implanted in two different regions of the brain, the dorsal hippocampus (DH) and the nucleus accumbens (NA).

Reported *in-vivo* NO concentration changes are based on the average *in-vitro* pre-implantation calibration data. Area under the curve (AUC) analysis was utilised to determine the overall NO response following administration of PPA. The net AUC value is represented in this chapter i.e. the average AUC value was calculated for peaks below and above baseline levels. AUC provides an integrated measurement of a measurable effect or phenomenon. AUC determines the overall change in NO before returning to a baseline level which is relative to the effect of PPA administration.

Statistical analysis was carried out using paired or unpaired t-tests. These tests were performed using Graphpad Prism and gave a probability value ( $P$ ) which indicates the level of significant or non-significant difference between groups.  $P > 0.05$ , denotes no significant difference. The extent of significant difference is divided into three parameters ( $P < 0.05$ ,\*), ( $P < 0.01$ ,\*\*) and ( $P < 0.0001$ ,\*\*\*) from the lowest relative level of difference (\*) to the highest (\*\*\*).

### 7.3 Systemic control experiments (s.c.)

The data displayed in this section was obtained from freely-moving rats. This section outlines the control experiments conducted in freely-moving animals. The effect of the systemic administration of saline on the NO sensor response is described within. The systemic administration of various physiologically relevant substances on the NO sensor response may be compared against the control experiments shown in this section.

#### 7.3.1 Systemic (s.c.) saline administration (NA)

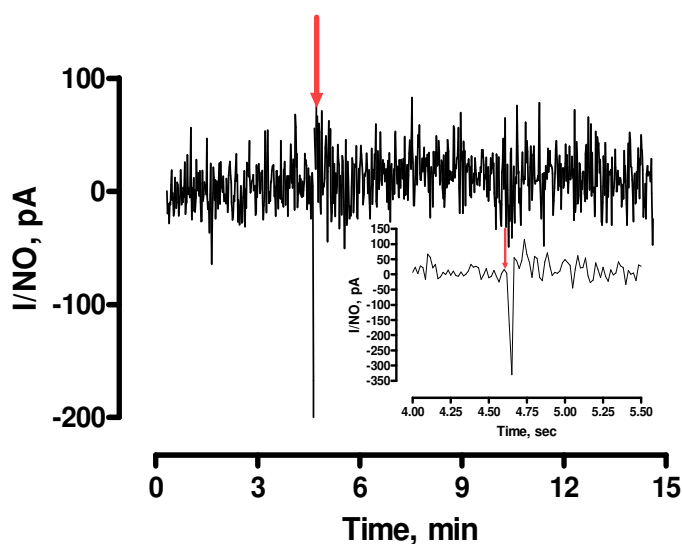


**Figure 7.3.1** A typical example of a 1mL/kg s.c. injection of saline detected by the NO sensor implanted in the nucleus accumbens (NA) of a freely-moving Wistar rat. *Inset:* Immediate response following injection (secs). The arrow indicates the point of administration.

All systemic administrations shown in this chapter were carried out in 1 mL/kg of saline by subcutaneous injection (s.c.). As a control experiment saline (Section 3.3.3.2) was administered subcutaneously (s.c.) (Section 3.11.2) and the effect on the NO signal was measured. Upon the administration of saline a brief fluctuation in NO is observed which is due to the physical manipulation of the subject as can be seen in Figure 7.3.1 (inset). A small increase was found subsequently of  $10.5 \pm 1.9$  pA ( $n = 6$ , 10ad) after  $3.0 \pm 0.3$  mins ( $n = 6$ , 10ad) and a return to pre-injection baseline levels was seen  $7.4 \pm 0.4$  mins ( $n = 6$ , 10ad) following the injection. The recorded change in current corresponds to a concentration change of  $6.9 \pm 1.2$  nM NO ( $n = 6$ , 10ad). However this NO concentration

change is short lived. The aim of the experiments shown in this section is to demonstrate the NO response which is attributable to the injection itself is minimal. No significant difference ( $P > 0.05$ ) was observed between pre and post-injection baseline levels. No lasting effect on the response of the NO sensor was observed following the systemic administration of saline. The data presented in this section is consistent with previous findings of the effect of systemic administration of saline on the response of this sensor design monitored in the NA (Finnerty *et al.*, 2012).

| Analyte | Current change (pA) | Change (%) | Conc. change (nM) | Max response (mins) | Return (mins) | Pre-injection baseline (pA) | Post-injection baseline (pA) |
|---------|---------------------|------------|-------------------|---------------------|---------------|-----------------------------|------------------------------|
| Saline  | 10.5 ± 1.9          | 1.9 ± 0.3  | 7.0 ± 1.0         | 3.0 ± 0.3           | 7.4 ± 0.4     | 550.7 ± 104.3               | 554.6 ± 104.8                |

**Table 7.3.1: Summary of results shown in Section 7.3.1. Data obtained from 6 sensors implanted in the nucleus accumbens of 3 Wistar rats. Average data includes 10 administrations.**

## 7.4 Propionic acid (PPA) administration dose response

The preliminary results in this section demonstrate the response of the NO sensor implanted in the nucleus accumbens (NA) following the systemic administration of PPA. A dose response study was conducted and the NO response attributable to the administration of 1  $\mu\text{M/g}$ , 2  $\mu\text{M/g}$  and 4  $\mu\text{M/g}$  PPA was examined.

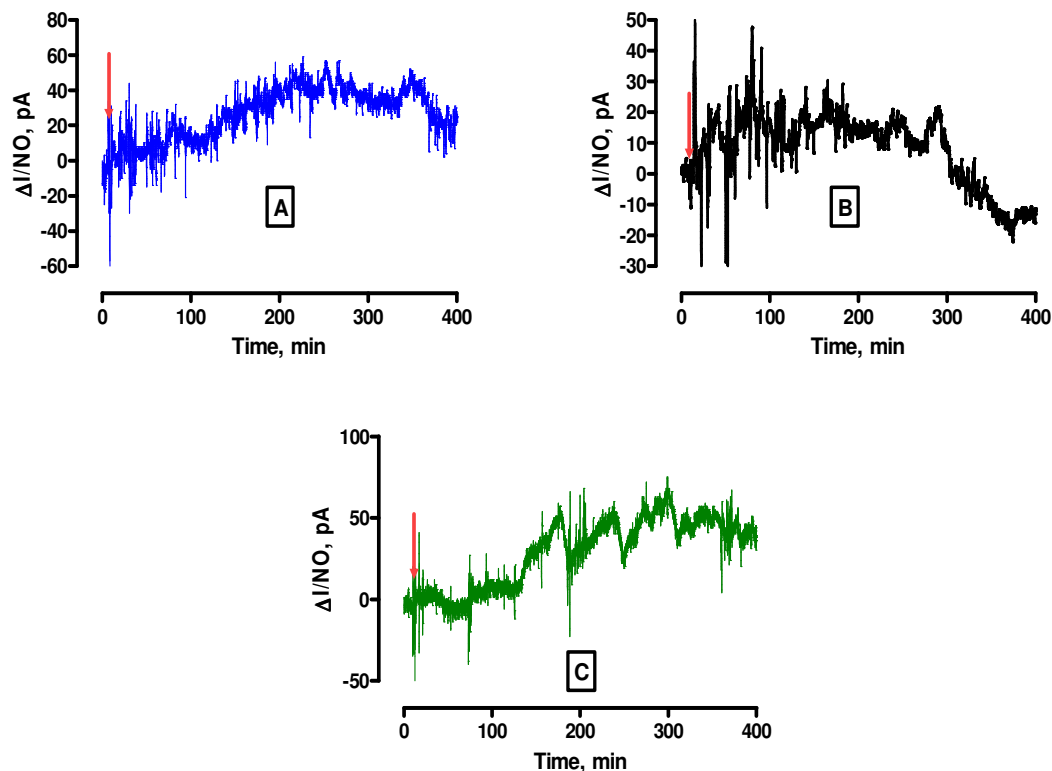


**Figure 7.4.1** The effect of each dose of systemically administered PPA on the NO sensor response monitored in the Nucleus Accumbens (NA) of freely-moving Wistar rats. An example of each dose is represented as follows (A) 1  $\mu\text{M/g}$ , (B) 2  $\mu\text{M/g}$  and (C) 4  $\mu\text{M/g}$ . Arrows indicates the point of administration.

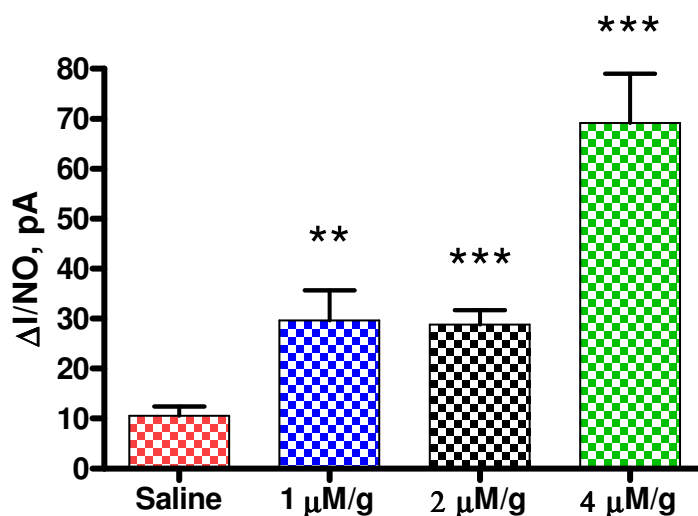


**Figure 7.4.2** Dose response comparison of PPA systemic administration vs. saline on the NO sensor response implanted in the nucleus accumbens (NA) of a freely-moving Wistar rat. Data represented as the maximum current response  $\pm$  SEM (pA) above baseline.

The data represented in Figure 7.4.2 demonstrates the maximum current response of the NO sensor implanted in the nucleus accumbens (NA) of freely-moving animals following the systemic administration of PPA. A clear increase above baseline levels of NO was observed following the administration of each dose of PPA (1  $\mu$ M/g, 2  $\mu$ M/g and 4  $\mu$ M/g). The 1  $\mu$ M/g dose of PPA resulted in a recorded maximal current increase of  $29.67 \pm 6.03$  pA ( $n = 3$ ). The systemic administration of a higher dose of PPA (2  $\mu$ M/g) resulted in a similar increase of  $28.80 \pm 2.91$  pA ( $n = 3$ ) which was not significantly different ( $P > 0.05$ ) to the lower dose (1  $\mu$ M/g). The highest dose of PPA administered resulted in the highest observed current change of  $69.15 \pm 9.85$  pA ( $n = 2$ ) and was significantly different ( $P < 0.05$ ,\*) from the NO response recorded following injection of the lowest dose of PPA (1  $\mu$ M/g). With each dose a significant difference ( $P < 0.05$ ) in the current response was observed compared to the NO response seen upon administration of saline recorded in the NA (Section 7.3.2). The results are summarised in Table 7.4.1. Similar maximum response times were observed with the 1  $\mu$ M/g, 2  $\mu$ M/g and 4  $\mu$ M/g dose of PPA and the time required to return to a baseline level following the injection was similar in each case. However the NO response recorded following the administration of 4  $\mu$ M/g PPA is much more attenuated when compared to

the lower doses (Figure 7.4.1). It is possible that PPA exerts its effects on the NO response in a dose independent manner. However it must be stated at this point that the experiments shown in this section are preliminary. Further work is required to elucidate the effect of different systemically administered doses of PPA on the NO sensor response. The increase in NO levels due to administration of 4  $\mu\text{M/g}$  PPA may be due to an accumulation of PPA as the previous lower doses (1  $\mu\text{M/g}$  and 2  $\mu\text{M/g}$ ) had been administered to the same animal. Future work may involve the extension of the time allowed between the injection of each dose of PPA in order to fully examine the long-term effect of each systemically administered dose. PPA has been shown to accumulate within cells and induce intracellular acidification (Shultz *et al.*, 2008). The pilot study demonstrated in this section indicates that the systemic administration of PPA induces the production of NO in the NA. In order to elucidate the possible accumulative effect of PPA on NO levels, PPA was administered to the subject at a different dose (500 mg/kg), more frequently and over an extended period and these results are outlined in the next Section (Section 7.5).

| PPA               | Current change (pA) | Change (%)     | Conc. change (nM) | Max response (mins) | Return (mins)     | Pre-injection baseline (pA) | Post-injection baseline (pA) | n |
|-------------------|---------------------|----------------|-------------------|---------------------|-------------------|-----------------------------|------------------------------|---|
| 1 $\mu\text{M/g}$ | 29.7 $\pm$ 6.0      | 9.2 $\pm$ 3.0  | 19.4 $\pm$ 3.9    | 111.0 $\pm$ 35.0    | 271.0 $\pm$ 112.0 | 359.5 $\pm$ 70.4            | 355.3 $\pm$ 58.2             | 3 |
| 2 $\mu\text{M/g}$ | 28.8 $\pm$ 2.9      | 8.2 $\pm$ 1.8  | 18.8 $\pm$ 1.9    | 284.7 $\pm$ 8.3     | 436.3 $\pm$ 54.7  | 383.0 $\pm$ 65.9            | 373.7 $\pm$ 64.8             | 3 |
| 4 $\mu\text{M/g}$ | 69.2 $\pm$ 9.8      | 20.8 $\pm$ 3.8 | 45.3 $\pm$ 6.4    | 270                 | 375               | 334.5 $\pm$ 14.4            | 392.2 $\pm$ 4.0              | 2 |

**Table 7.4.1: Summary of results shown in Section 7.4. With n = the number of sensors implanted in 2 animals (1  $\mu\text{M/g}$ ), 2 animals (2  $\mu\text{M/g}$ ) and 1 animal (4  $\mu\text{M/g}$ ).**

## 7.5 Chronic Propionic acid (PPA) administration (NA)

This section outlines the effect of chronic repetitive administration of PPA on NO levels in the NA of freely-moving animals. Each animal was administered PPA (500 mg/kg) twice daily (see Section 3.3.2.2) for a continuous period of 12 days and the corresponding changes in NO levels on each day were monitored by the NO sensor.

### 7.5.1 24 hr Control NO data (NA)

The results in this section demonstrate the response detected by the NO sensor for a continuous period of 24 hrs while implanted in the nucleus accumbens (NA). The administration of saline has no lasting effect on the NO sensor response as has been demonstrated in Section 7.3.2. The results shown in this section act as a control against which the NO response due to the long term administration of PPA, recorded in the NA for a period of 24 hrs may be compared.

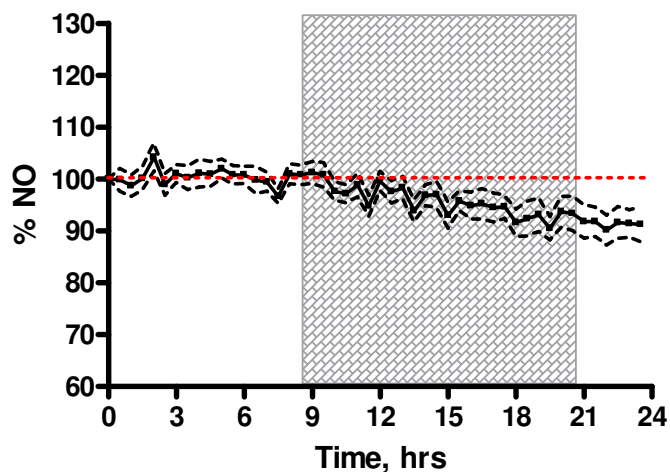


**Figure 7.5.1** The recorded NO response in the NA over a continuous period of 24 hrs. Data represented as a percentage current change  $\pm$  SEM. SEM represented by dashed line (black).

Figure 7.5.1 represents the NO levels recorded in the NA over a continuous period of 24 hrs for an average of 8 days ( $n = 3$ , 2 animals). The data represents the long-term NO response recorded in the NA. It is clear that the NO response remains close to baseline levels for the duration of the recording period. The dark phase of the light cycle is

represented by the hatched box in Figure 7.5.1. A slight drift below baseline levels of NO which is denoted by the dashed line is apparent within the dark phase of the light cycle and a return to a stable baseline level of NO can be seen subsequently. In order to examine the overall change in NO over a 24 hr period for an average of 8 days AUC analysis was performed which gave a response of  $-22.4 \pm 9.7$  pA/hr ( $n = 3$ ).

Recordings were taken after an initial period of *ca.* 24 hrs following the application of potential to the working electrodes. Therefore the contribution of the capacitance current to the overall NO sensor response represented in Figure 7.5.1 is greatly reduced. Additionally the baseline stability of the NO sensor is maintained while implanted in the NA for a consecutive period of 14 days (see Section 6.8.5). However it is possible that some remaining capacitance may contribute to the overall NO response presented in Figure 7.5.1. Therefore the small variation in NO response recorded over the 24 hr period demonstrated in Figure 7.5.1 is likely attributable to a combination of residual capacitance (signal drift) and contributions to the NO response from the circadian rhythms of the animal.

The role of NO in the maintenance of the sleep-wake cycle has been extensively reviewed (Gautier-Sauvigne *et al.*, 2005; Cespuglio *et al.*, 2012). The influence of NOS inhibitors and inducers on the sleep-wake cycle in rats has been demonstrated by Gautier-Sauvigne *et al.* (Gautier-Sauvigne *et al.*, 2005). Nycthemeral variations i.e. changes pertaining to the duration of a day (24 hrs), in NO levels have been demonstrated by Cespuglio *et al.* using voltametric methods in freely-moving rats. A variation in the level of NO was determined between episodes of waking and sleep in the animal within a 24 hr period by this research group. Additionally regional deviations were determined where opposite nycthemeral changes in NO within the light and dark phase were detected (Cespuglio *et al.*, 2012). These combined findings may contribute to the small variations in the long-term NO response recorded in the NA (Figure 7.5.1). However the overall contribution of previously determined sleep/wake effects and possible residual capacitance on the level of NO over a 24 hr period are effectively eliminated from the overall signal attributable to administration of PPA (see Section 7.5.2) by the control data presented in this section.

## 7.5.2 Chronic PPA administration (NA) day 1-6

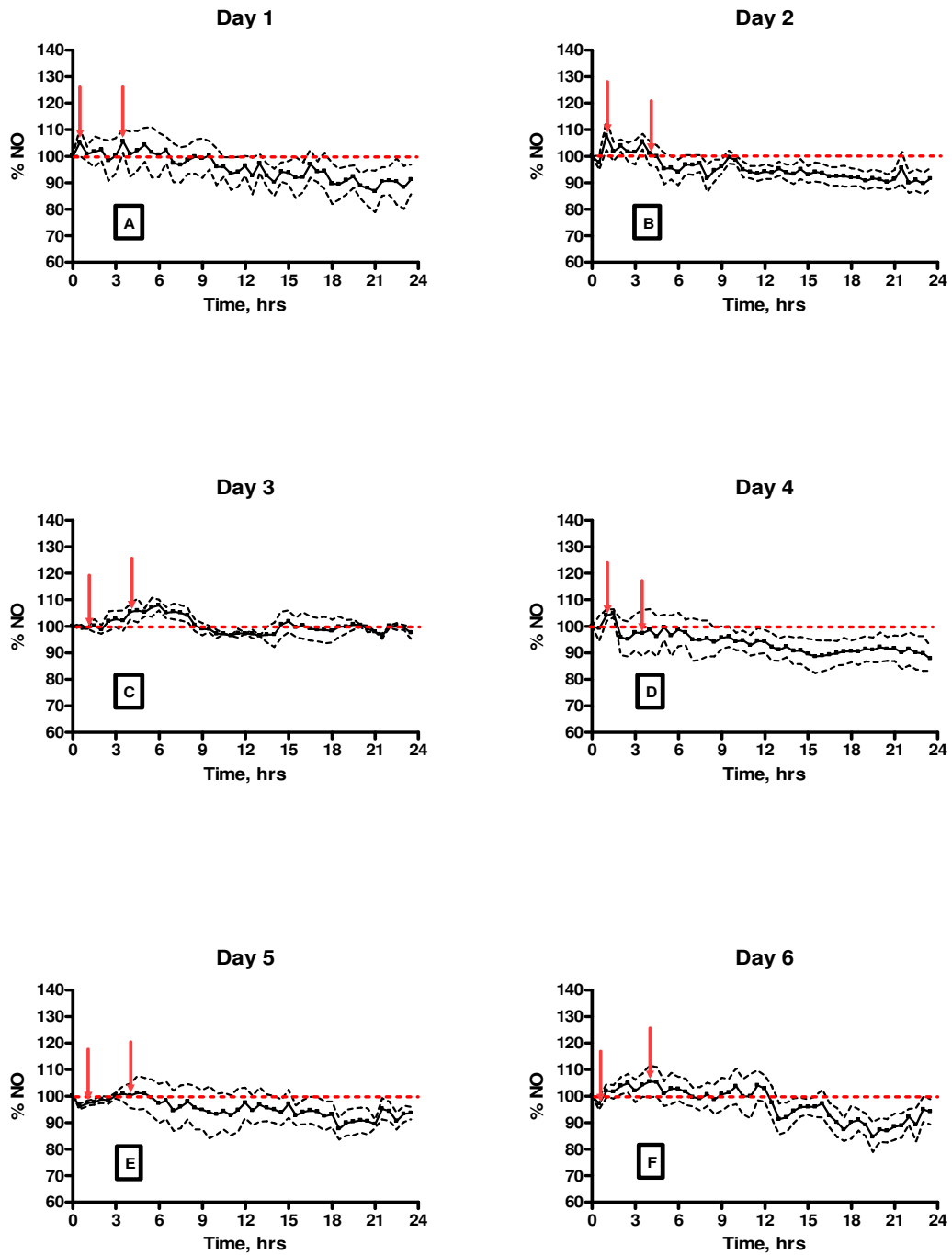


**Figure 7.5.2** The average NO response recorded in the NA over a continuous period of 24 hrs following systemic administration of PPA. (A) 1 day of PPA treatment (B) 2 days, (C) 3 days, (D) 4 days, (E) 5 days and (F) 6 days. Data represented as a percentage change  $\pm$  SEM. Arrows indicate the injection of PPA.

This section presents NO levels in the nucleus accumbens (NA) monitored by the NO sensor following the administration (s.c.) of PPA (Section 3.3.2.2) for an initial period of 1 to 6 days. PPA was administered twice daily, the first injection was given at 12.00 hrs and the second injection was administered at 15.00 hrs as indicated by the arrows shown in Figure 7.5.2. The NO response was monitored for a continuous period of 24 hrs. The results demonstrated in this chapter represent the novel detection of NO in the freely-moving animal following treatment with PPA. It was deemed necessary to investigate the long-term effect of PPA over 24 hrs on the level of NO in the NA as the effect of PPA on NO levels in the brain of freely-moving animals has not previously been demonstrated.

AUC analysis was utilised in determining the overall effect of PPA on the NO current response. The NO response in the NA remained close to baseline levels upon the initial exposure to PPA on day 1 as can be seen in Figure 7.5.2(A). The maximum NO response was achieved within  $9.1 \pm 2.0$  hrs,  $n = 4$  and a return to pre-injection basal levels was observed  $14.3 \pm 2.1$  hrs,  $n = 4$  subsequently. The pre-injection ( $318.1 \pm 33$  pA,  $n = 4$ ) and post-injection baseline values ( $313.5 \pm 38.4$  pA,  $n = 4$ ) were not significantly different ( $P > 0.05$ ). Day 1 of the PPA administration protocol resulted in an AUC value of  $-12.2 \pm 14.0$  pA/hr, this value was not significantly different ( $P > 0.05$ ) to the control experiments outlined in Section 7.5.1.

The AUC determined for day 2 of the PPA administration protocol was  $-13.7 \pm 8.7$  pA/hr ( $n = 5$ ). This value was not significantly different ( $P > 0.05$ ) to the control experiments outlined in Section 7.5.1. No significant difference was observed between the pre and post-injection basal levels on day 2 and the results are summarised in Table 7.5.2. No significant difference ( $P > 0.05$ ) was observed between the maximum response time and the time required to return to a baseline level on day 2 with respect to day 1.

As can be seen in Figure 7.5.2(C) an increase above baseline levels of NO occurred on day 3 of PPA treatment which gave an AUC value of  $5.3 \pm 5.3$  pA/hr ( $n = 4$ ). The AUC value determined for day 3 was not significantly different ( $P > 0.05$ ) to the corresponding AUC value calculated for day 0 (see Section 7.5.1). No significant

difference ( $P > 0.05$ ) was observed between the baseline level recorded prior to administration of PPA ( $278.3 \pm 20.4$  pA,  $n = 4$ ) and the subsequent return to baseline levels ( $281.5 \pm 22.1$  pA,  $n = 4$ ) on day 3. The time required to achieve a maximum NO current response on day 3 ( $5.4 \pm 0.1$  hrs,  $n = 4$ ) was less than that seen on day 1 ( $9.1 \pm 2.0$  hrs,  $n = 4$ ) and day 2 ( $6.4 \pm 0.7$  hrs,  $n = 5$ ). However the maximum response time recorded on day 3 was not significantly different  $P > 0.05$  when compared to day 1 and similarly the time required to return to a baseline level was not significantly different ( $P > 0.05$ ).

The AUC determined for days 4 and 5 of PPA treatment was  $-16.7 \pm 11.8$  pA/hr ( $n = 4$ ) and  $-11.1 \pm 12.2$  ( $n = 4$ ) respectively. No significant difference  $P > 0.05$  was observed on day 4 and 5 of PPA administration when compared to the NO response determined by AUC on day 0. The pre and post-injection baseline levels recorded on day 4 and 5 were not significantly different ( $P > 0.05$ ) and the results are summarised in Table 7.5.2. No significant difference ( $P > 0.05$ ) was observed between the maximum response time and subsequent return to baseline levels on day 4 and 5 when compared to day 1.

A similar trend was observed on day 6 of the PPA administration protocol. AUC analysis revealed a response of  $-5.8 \pm 8.0$  pA/hr ( $n = 4$ ) on day 6. When compared to the AUC value determined on day 0 no significant difference ( $P > 0.05$ ) was observed on day 6. The pre and post-injection baseline levels recorded on day 6 revealed no significant difference ( $P > 0.05$ ). A summary of these results is provided in Table 7.5.2. The maximum response time and the time required to reach a subsequent baseline level on day 6 did not significantly differ,  $P > 0.05$ , from day 1 of PPA administration.

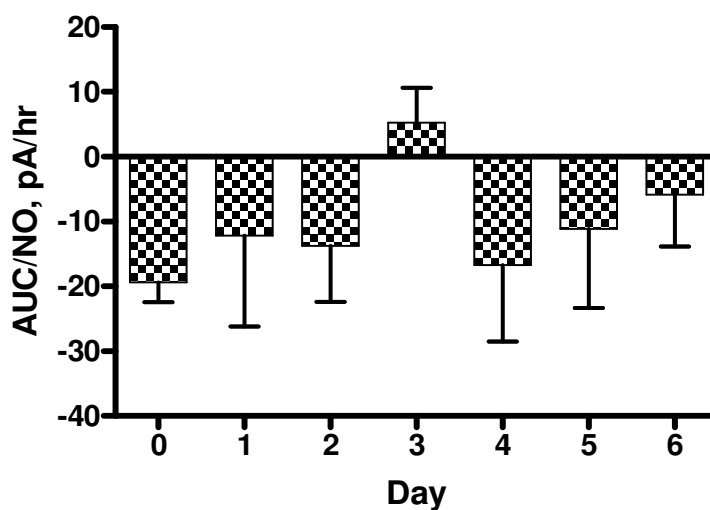


**Figure 7.5.2.1 Comparison between control NO response recorded in the NA and the response following systemic administration of PPA. Control data (day 0) and day 1-7 of PPA administration. Data represented as Mean AUC  $\pm$  SEM (pA/hr).**

Figure 7.5.2.1 represents the average NO response recorded on day 1 to 6 of PPA treatment determined by AUC analysis. The control NO response calculated by AUC (Section 7.5.1) is represented by day 0. The NO response recorded on day 1 to day 6 of the PPA treatment protocol is not significantly different ( $P > 0.05$ ) on each day when compared to the NO response determined for day 0. An increase in NO levels in the NA has occurred due to the systemic administration of PPA. However no significant difference ( $P > 0.05$ ) in NO response was determined by AUC analysis on each day between day 1 and 6 of the PPA administration protocol when compared to day 0. It was necessary to extend the administration of PPA to fully examine the effect of PPA administration on the NO response. Day 7 to day 12 of the systemic administration of PPA is shown in the next Section (7.5.3).

| PPA          | Current change (pA) | Change (%)  | Conc. change (nM) | Max response (mins) | Return (mins) | AUC (pA/hr)  | Pre-injection baseline (pA) | Post-injection baseline (pA) | n |
|--------------|---------------------|-------------|-------------------|---------------------|---------------|--------------|-----------------------------|------------------------------|---|
| <b>Day 0</b> | n/a                 | n/a         | n/a               | n/a                 | n/a           | -22.4 ± 9.7  | n/a                         | n/a                          | 3 |
| <b>Day 1</b> | 17.6 ± 32.6         | 5.5 ± 10.2  | 11.1 ± 20.6       | 9.1 ± 2.0           | 14.3 ± 2.1    | -12.2 ± 14.0 | 318.1 ± 33.0                | 313.5 ± 38.4                 | 4 |
| <b>Day 2</b> | -23.1 ± 16.6        | -7.5 ± 5.4  | -14.6 ± 10.5      | 6.4 ± 0.7           | 14.6 ± 0.6    | -13.7 ± 8.7  | 306.9 ± 25.8                | 284.8 ± 23.4                 | 5 |
| <b>Day 3</b> | 24.3 ± 3.6          | 8.7 ± 1.3   | 15.4 ± 2.3        | 5.4 ± 0.1           | 12.3 ± 0.8    | 5.3 ± 5.3    | 278.3 ± 20.4                | 281.5 ± 22.1                 | 4 |
| <b>Day 4</b> | -7.0 ± 45.3         | -2.4 ± 15.7 | -4.4 ± 28.7       | 10.1 ± 2.0          | 15.4 ± 1.9    | -16.7 ± 11.8 | 287.7 ± 24.4                | 280.5 ± 34.4                 | 4 |
| <b>Day 5</b> | -2.1 ± 31.4         | -0.7 ± 11.2 | -1.3 ± 19.8       | 7.3 ± 1.2           | 14.3 ± 0.9    | -11.1 ± 12.2 | 279.3 ± 34.7                | 268.8 ± 36.9                 | 4 |
| <b>Day 6</b> | 60.2 ± 43.8         | 22.0 ± 16.0 | 38.1 ± 27.7       | 7.1 ± 1.6           | 15.5 ± 0.5    | -5.8 ± 8.0   | 274.1 ± 26.9                | 256.3 ± 31.5                 | 5 |

**Table 7.5.2 Summary of the NO data recorded between day 1 and 6 of chronic PPA administration (NA). With n = the number of sensors implanted in 2 animals (day 0), 4 animals (day 1-5) and 5 animals (day 6).**

## 7.5.3 Chronic PPA administration (NA) day 7-12

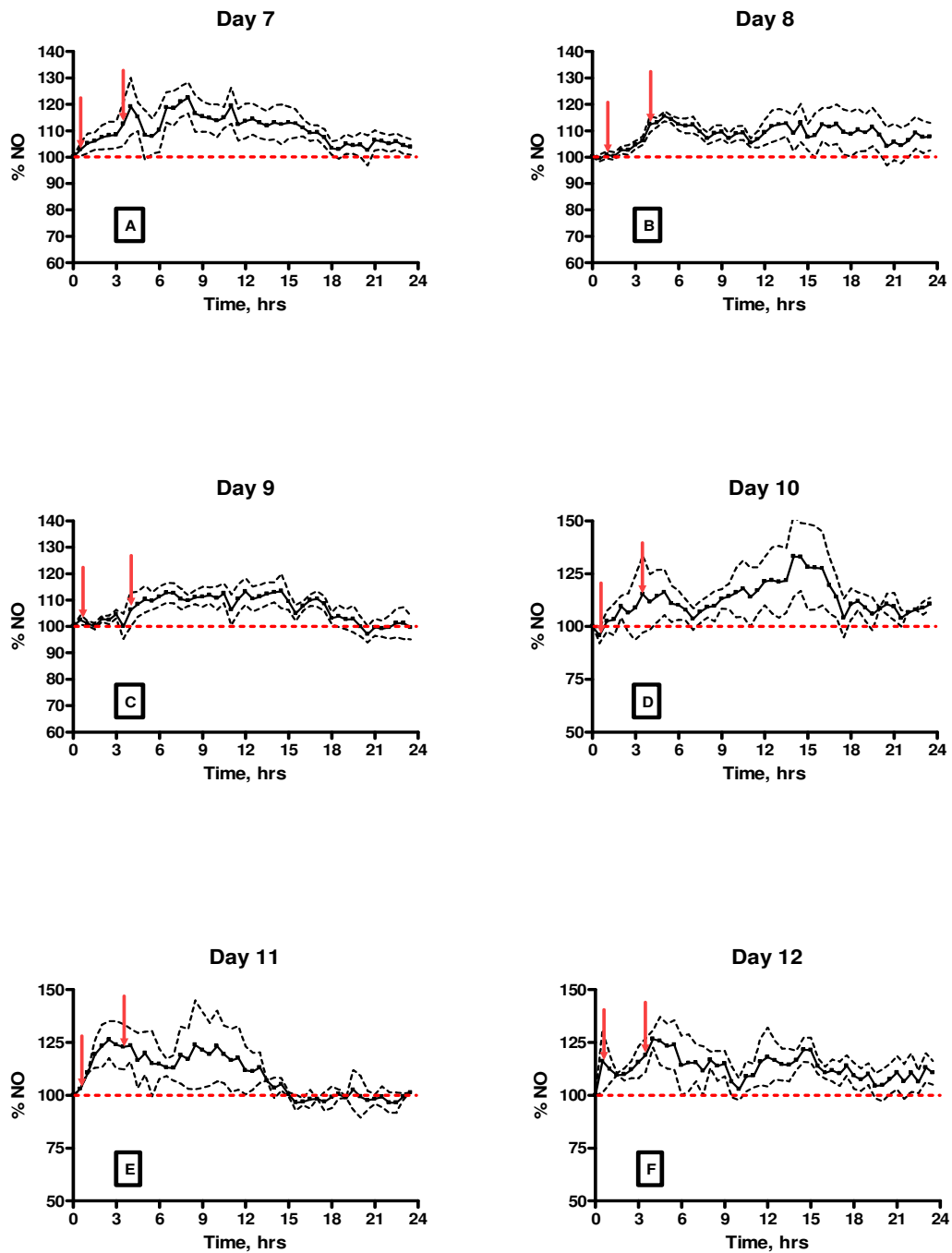


Figure 7.5.3 The average NO response recorded in the NA over a continuous period of 24 hrs following systemic administration of PPA. (A) 7 days of PPA treatment (B) 8 days, (C) 9 days, (D) 10 days, (E) 11 days and (F) 12 days. Data represented as a percentage change  $\pm$  SEM. Arrows indicate the injection of PPA.

The results demonstrated in this section examine the extension of the PPA administration protocol discussed in Section 7.5.2 (1 to 6 days). This section represents NO levels monitored in the NA by the NO sensor following the administration (s.c.) of PPA (Section 3.3.2.2) for a subsequent period of 7 to 12 days. PPA was administered twice daily, the first injection was given at 12.00 hrs and the second injection was administered at 15.00 hrs as indicated by the arrows shown in Figure 7.5.3.

Figure 7.5.3(A) demonstrates the average NO response recorded following 7 days of systemic PPA administration. An increase in NO was observed following the administration of PPA. AUC analysis revealed a significant difference ( $P < 0.05, *$ ) between the overall NO response on day 7 ( $24.1 \pm 7.4$  pA/hr,  $n = 3$ ) when compared to day 0. The pre-injection ( $225.4 \pm 47.8$  pA,  $n = 3$ ) and post-injection baseline values ( $238.1 \pm 51.5$  pA,  $n = 3$ ) on day 7 did not significantly differ ( $P > 0.05$ ). As had been observed on day 2 to day 6 of PPA treatment the maximum response time and the time required to achieve a subsequent baseline level on day 7 did not significantly differ ( $P > 0.05$ ) from day 1 of PPA administration.

Figure 7.5.3(B) illustrates the NO response recorded by the NO sensor implanted in the NA following the systemic administration of PPA for a total of 8 days. A clear increase in NO above baseline levels was observed, the calculated AUC analysis of the NO response on day 8 was  $23.4 \pm 7.5$  pA/hr,  $n = 5$ . A significant difference ( $P < 0.01, **$ ) was observed between the AUC of day 8 and day 0. The maximum NO response was achieved within  $5.2 \pm 0.7$  hrs,  $n = 5$  and a return to pre-injection basal levels occurred  $17.6 \pm 0.8$  hrs,  $n = 5$  subsequently. No significant difference  $P > 0.05$  was observed between the baseline level recorded prior to administration of PPA ( $384.9 \pm 152.8$  pA,  $n = 5$ ) and the subsequent return to baseline levels ( $406.1 \pm 152.1$  pA,  $n = 5$ ) on day 8.

Day 9 of the PPA administration protocol resulted in an increase in NO above baseline levels and the AUC of this response was  $20.2 \pm 4.8$  pA/hr ( $n = 5$ ). The response on day 9 was significantly different ( $P < 0.01, **$ ) from the NO response determined by AUC on day 0. No significant difference was observed between the pre and post-injection basal levels of NO on day 9 and the results are summarised in Table 7.5.3. The

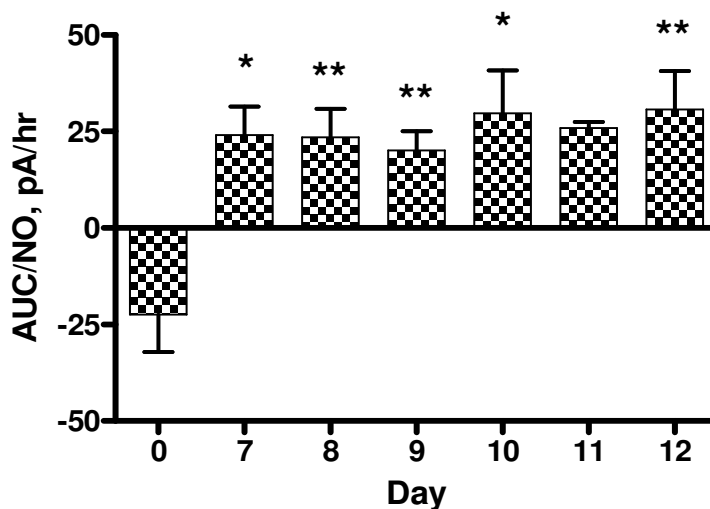
maximum response time and the time required to return to a baseline was not significantly different  $P > 0.05$  on day 9 with respect to day 1.

The AUC determined for day 10 of the PPA administration protocol was  $29.7 \pm 11.1$  pA/hr ( $n = 3$ ). A similar trend was observed to that seen on day 8 and 9. An increase in NO response was observed with respect to day 0 and this response was significantly different ( $P < 0.05, *$ ). No significant difference ( $P > 0.05$ ) was observed between the baseline level recorded prior to administration of PPA ( $278.6 \pm 26.5$  pA,  $n = 3$ ) and the subsequent return to baseline levels ( $300.3 \pm 24.9$  pA,  $n = 3$ ) on day 10. The maximum response time and the baseline return time period was not significantly different ( $P > 0.05$ ) from day 1.

The calculated AUC for day 11 of the PPA administration protocol was  $25.8 \pm 1.6$  pA/hr ( $n = 2$ ). A similar trend was observed on day 11 when compared to that seen from day 7 to 10. An increase in NO response was observed with respect to day 0, however in this case the response was not significantly different ( $P > 0.05$ ). The statistical abnormality determined on day 11 is likely due to a discrepancy in the number of sensors examined in the data ( $n = 2$ ) (see Table 7.6.2). Future work may include the repetition of the PPA administration protocol for a period of 11 days in order to fully examine this possibility. However an overall increase was observed on day 11 in relation to day 0. No significant difference  $P > 0.05$  was observed between the NO baseline level recorded prior to administration of PPA ( $278.6 \pm 26.5$  pA,  $n = 2$ ) and the subsequent return to baseline levels ( $271.7 \pm 8.6$  pA,  $n = 2$ ) on day 11. The maximum response time and the time required to return to baseline was not significantly different  $P > 0.05$  from day 1.

Figure 7.5.3(F) demonstrates the average NO response recorded in the NA following 12 days of systemic PPA administration. A clear attenuated increase in NO was observed following the administration of PPA. As seen previously a significant difference ( $P < 0.01, **$ ) in response was observed on day 12 ( $30.7 \pm 9.9$  pA/hr,  $n = 4$ ) when compared to the AUC determined on day 0. The pre-injection ( $258.1 \pm 35.3$  pA,  $n = 4$ ) and post-injection baseline values ( $276.5 \pm 36.0$  pA,  $n = 4$ ) on day 12 were not significantly different  $P > 0.05$ . As had been observed on day 2 to day 11 of PPA treatment, the

maximum response time and the time required to achieve a subsequent baseline level on day 12 did not significantly differ  $P > 0.05$  from day 1 of PPA administration.



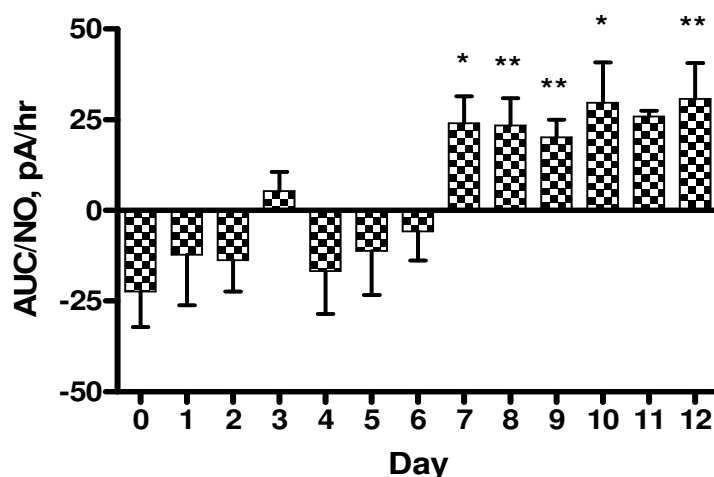
**Figure 7.5.3.1 Comparison between control NO response recorded in the NA and the response following systemic administration of PPA. Control data (day 0) and day 8-14 of PPA administration. Data represented as Mean AUC  $\pm$  SEM (pA/hr) with ( $P < 0.05$ ,\*) and ( $P < 0.01$ ,\*\*).**

Figure 7.5.3.1 demonstrates the average NO response monitored in the NA on day 7 to 12 of systemic PPA administration determined by AUC analysis. The control NO response calculated by AUC (Section 7.5.1) is displayed and denoted by day 0. It is clear that the NO response recorded on day 7 to day 12 of the PPA treatment protocol is significantly different ( $P < 0.05$ ) on each day with the exception of day 11 when compared to the NO response recorded on day 0. A discussion of the effect of each day of PPA treatment (day 1 to 12) monitored in the NA by the Nafion<sup>®</sup>-modified NO sensor is discussed in the next Section (7.5.4).

| PPA           | Current change (pA) | Change (%)  | Conc. change (nM) | Max response (mins) | Return (mins) | AUC (pA/hr) | Pre-injection baseline (pA) | Post-injection baseline (pA) | n |
|---------------|---------------------|-------------|-------------------|---------------------|---------------|-------------|-----------------------------|------------------------------|---|
| <b>Day 0</b>  | n/a                 | n/a         | n/a               | n/a                 | n/a           | -22.4 ± 9.7 | n/a                         | n/a                          | 3 |
| <b>Day 7</b>  | 52.3 ± 18.2         | 23.2 ± 8.1  | 33.1 ± 11.5       | 7.0 ± 0.5           | 17.0 ± 0.5    | 24.1 ± 7.4  | 225.4 ± 47.8                | 238.1 ± 51.5                 | 3 |
| <b>Day 8</b>  | 61.4 ± 20.2         | 16.0 ± 5.2  | 38.9 ± 12.8       | 5.2 ± 0.7           | 17.6 ± 0.8    | 23.4 ± 7.5  | 384.9 ± 152.8               | 406.1 ± 152.1                | 5 |
| <b>Day 9</b>  | 50.5 ± 7.7          | 12.6 ± 2.0  | 50.2 ± 7.9        | 5.3 ± 0.9           | 16.3 ± 0.9    | 20.2 ± 4.8  | 459 ± 168.3                 | 289.4 ± 19.0                 | 5 |
| <b>Day 10</b> | 92.7 ± 29.1         | 33.3 ± 10.4 | 58.6 ± 18.4       | 7.0 ± 2.8           | 15.3 ± 1.2    | 29.7 ± 11.1 | 278.6 ± 26.5                | 300.3 ± 24.9                 | 3 |
| <b>Day 11</b> | 104.2 ± 24.9        | 38.0 ± 9.1  | 65.9 ± 15.7       | 6.5 ± 1.5           | 15.8 ± 0.7    | 25.8 ± 1.6  | 274.4 ± 12.5                | 271.7 ± 8.6                  | 2 |
| <b>Day 12</b> | 86.1 ± 19.9         | 22.3 ± 3.7  | 59.4 ± 9.7        | 7.0 ± 0.7           | 16.4 ± 0.6    | 30.7 ± 9.9  | 258.1 ± 35.3                | 276.5 ± 36                   | 4 |

**Table 7.6.2 Summary of the NO data recorded between day 7 to 12 of chronic PPA administration (NA). With n = the number of sensors implanted in 2 animals (day 0), 3 animals (day 7), 4 animals (day 8-9), 3 animals (day 10), 2 animals (day 11) and 4 animals (day 12).**

## 7.5.4 AUC comparison chronic PPA administration (NA) day 1-12



**Figure 7.5.4** Comparison between the NO responses recorded in the NA on day 0 and day 1-12 of PPA administration. Data represented as Mean AUC  $\pm$  SEM (pA/hr). With ( $P < 0.05$ ,\*) and ( $P < 0.01$ ,\*\*).

Figure 7.5.4 represents the overall NO response before returning to baseline (AUC) recorded in the NA on day 0 (Section 7.5.1) against the AUC values obtained on day 1 to 14 of the PPA administration protocol. It is clear that an increase in NO response occurs as the experimental protocol proceeds from day 7 through to day 12 and the level of exposure to PPA is increased. It can be deduced that the observed increases in NO due to the administration of PPA are incurred by an accumulative effect of the presence of PPA. The more prolonged the exposure time to PPA the more attenuated and maximal the NO response in the NA becomes. The results presented in this section are summarised in Table 7.5.4.

No significant difference  $P > 0.05$  was observed between the maximum response time and the time required to return to baseline on each day of PPA treatment when compared to day 1. No significant difference  $P > 0.05$  was observed between the pre and post-injection basal levels of NO on each day of PPA treatment (day 1 to 12).

A significant difference ( $P < 0.05$ ) in NO response was determined by AUC analysis on day 8 and 9 following the administration of PPA when compared to day 1 of PPA treatment. Similarly a significant difference ( $P < 0.05$ ) was observed between the AUC

value determined on day 12 when compared to day 1. With (day 8,  $P = 0.0484$ ), (day 9,  $P = 0.0472$ ) and (day 12,  $P = 0.0464$ ) when compared to the AUC value calculated for day 1 of PPA treatment.

| Day         | 0           | 1            | 2           | 3         | 4            | 5            | 6          |
|-------------|-------------|--------------|-------------|-----------|--------------|--------------|------------|
| AUC (pA/hr) | -22.4 ± 9.7 | -12.2 ± 14.0 | -13.7 ± 8.7 | 5.3 ± 5.3 | -16.7 ± 11.8 | -11.1 ± 12.2 | -5.8 ± 8.0 |
| <i>P</i>    | n/a         | 0.5677       | 0.5655      | 0.0984    | 0.7402       | 0.5164       | 0.2750     |
| <i>n</i>    | 3           | 4            | 5           | 4         | 4            | 4            | 5          |

| Day         | 0           | 7          | 8          | 9          | 10          | 11         | 12         |
|-------------|-------------|------------|------------|------------|-------------|------------|------------|
| AUC (pA/hr) | -22.4 ± 9.7 | 24.1 ± 7.4 | 23.4 ± 7.5 | 20.2 ± 4.8 | 29.7 ± 11.1 | 25.8 ± 1.6 | 30.7 ± 9.9 |
| <i>P</i>    | n/a         | 0.0262     | 0.0077     | 0.0093     | 0.0175      | 0.0518     | 0.0074     |
| <i>n</i>    | 3           | 3          | 5          | 5          | 3           | 2          | 4          |

**Table 7.5.4 Comparison of the NO data (NA), Data represented as AUC ± SEM (pA/hr), recorded on day 0 against day 1-12 of chronic PPA administration.**

From the results presented in this section, it is clear that the systemic administration of PPA, which has previously been used in the development of an animal model of autism, leads to an increased production of NO in the NA. The PPA induced elevation of NO levels is particularly evident towards the end of the experimental procedure i.e. day 7-12 (see Figure 7.5.4). The evidence of a PPA induced increase in NO presented here is further supported by the previous detection of increased oxidative stress markers in brain homogenates of PPA treated rats (MacFabe *et al.*, 2008; El-Ansary *et al.*, 2012).

Increased oxidative stress has been implicated in the development of autism as reviewed by Chauhan and Chauhan (Chauhan & Chauhan, 2006). A disruption in anti-oxidant enzyme levels in autism has been demonstrated, specifically by a reduction in catalase and superoxide dismutase (SOD) in erythrocytes of autistic individuals (Yorbik *et al.*, 2002; Zoroglu *et al.*, 2004). Additionally the impairment of glutathione redox homeostasis which maintains the primary anti-oxidant defence systems in the CNS has been demonstrated in post mortem ASDs brain preparations (Chauhan *et al.*, 2012).

An elevated level of NO has previously been demonstrated in blood samples of autistic persons (Sogut *et al.*, 2003). Indirect markers of elevated NO production i.e. nitrite and nitrate have been demonstrated in the plasma of autistic individuals (Zoroglu *et al.*, 2003; Sweeten *et al.*, 2004). Additionally an elevation of oxidative stress markers has been presented in PPA treated rat brain tissue preparations (MacFabe *et al.*, 2008; El-Ansary *et al.*, 2012). It is well established that a disruption to the robust anti-oxidant network leads to an increased production of oxidative (e.g. H<sub>2</sub>O<sub>2</sub>) and nitrosative stress markers (e.g. NO) (Andersen, 2004; Valko *et al.*, 2007). The downstream effects of an abnormally high concentration of NO in the CNS is the formation of peroxynitrite which is highly neurotoxic (Calabrese *et al.*, 2007). These combined reports indicate that oxidative/nitrosative stress is highly implicated in the pathophysiology of ASDs.

### **7.6 Chronic Propionic acid (PPA) administration (DH)**

The results displayed in this section outline the effect of chronic repetitive administration of PPA on NO levels in the dorsal hippocampus (DH) of freely-moving animals. Each animal was administered PPA twice daily (Section 3.3.2.2) for a continuous period of 12 days and the corresponding changes in NO levels on each day were monitored by the NO sensor. The first injection of PPA was given at 12.00 hrs and the second injection was administered at 15.00 hrs.

### 7.6.1 24 hr Control NO data (DH)

The results in this section demonstrate the response of the NO sensor implanted in the DH for a continuous period of 24 hrs. The administration of saline has no lasting effect on the NO sensor response as can be seen in Section 7.3.1. The results shown in this section act as a control against which the NO response due to the long term administration of PPA recorded in the DH may be compared.

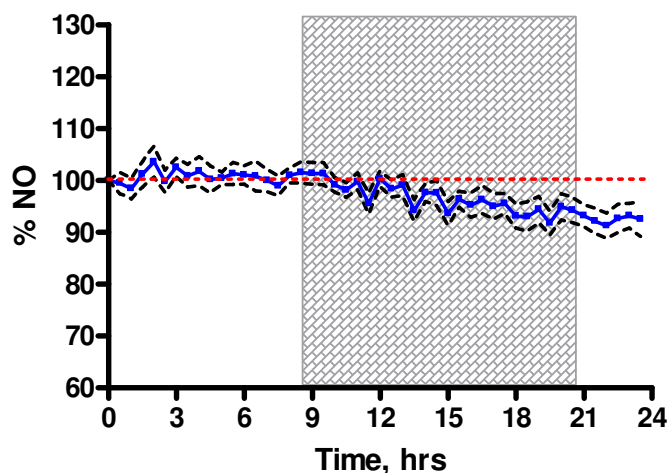


**Figure 7.6.1** The recorded NO response in the DH over a continuous period of 24 hrs. Data represented by a mean response  $\pm$  SEM (pA). SEM represented by dashed line (black).

Figure 7.6.1 presents the NO levels recorded in the DH over a continuous period of 24 hrs for an average of 8 days ( $n = 2$ , 2 animals). It can be seen that the level of NO remains close to baseline levels for the duration of the recording period. A small drift below baseline levels of NO which is denoted by the dashed line was apparent. The AUC determined for the overall change in NO in the DH over a 24 hr period was  $-23.6 \pm 10.5$  pA/hr ( $n = 2$ ) and this value is not significantly different ( $P > 0.05$ ) when compared to the NO response obtained in the NA on day 0.

The variation in NO levels between different brain regions following the administration of known inducers and inhibitors of NO production has previously been demonstrated (see Section 7.7). A relative lack of information is available on the comparison between long-term changes in NO in different brain regions in the absence of pharmacological treatment. However a time-dependent variation in the level of NO monitored in the

hippocampus has previously been demonstrated using electrochemical recordings (Heinzen & Pollack, 2002). This research group demonstrated changes of NO over a chronic recording period in saline treated rats which they attribute to the circadian rhythms of the animal (Heinzen & Pollack, 2002).

A strong correlation was observed in these experiments between changes in baseline levels of NO monitored over a 24 hr recording period in the DH when compared to the corresponding NO levels in the NA. The time-dependent minor variation in NO which is mirrored closely in both regions over the recorded time frame which suggests a contribution to the signal from a circadian variation in the level of NO.

As previously discussed (see Section 7.5.1) capacitance contributions to the overall NO signal as presented in Figure 7.6.1 are greatly reduced as recordings were taken following an initial period of *ca.* 24 hrs following implantation. Additionally the baseline stability of the NO sensor is maintained while implanted for a consecutive period of 14 days (see Section 6.8.5). As seen in the NA the small variation in the NO response recorded over 24 hrs in the DH is likely mainly attributed to the circadian rhythms of the animal, which is supported by research previously conducted by Cespuglio *et al.* as discussed in Section 7.5.1 (Cespuglio *et al.*, 2012).

## 7.6.2 Chronic PPA administration (DH) day 1-6

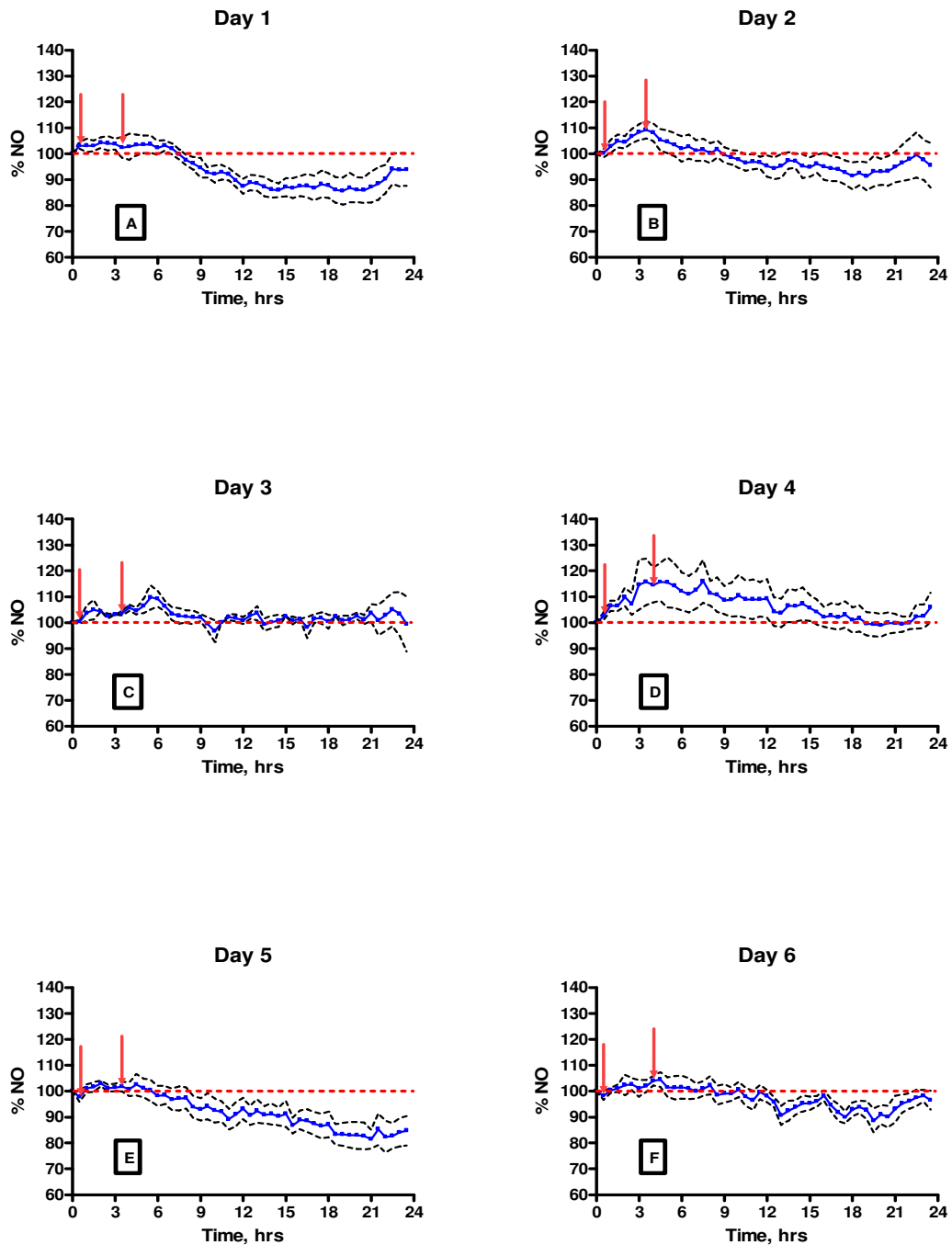


Figure 7.5.2 The average NO response recorded in the DH over a continuous period of 24 hrs following systemic administration of PPA. (A) 1 day of PPA treatment (B) 2 days, (C) 3 days, (D) 4 days, (E) 5 days and (F) 6 days. Data represented as a percentage change  $\pm$  SEM. Arrows indicate the injection of PPA.

The NO response recorded in the DH remained close to baseline levels on the initial day of PPA treatment (day 1) as can be seen in Figure 7.6.2(A). The maximum NO response was achieved within  $16.9 \pm 1.5$  hrs,  $n = 5$  and a subsequent decline in NO levels was observed which reached a baseline level  $21.8 \pm 0.5$  hrs,  $n = 5$  following the initial injection. The pre ( $455.1 \pm 104.2$  pA,  $n = 5$ ) and post-injection baseline values ( $428.4 \pm 114.7$  pA,  $n = 5$ ) showed no significant difference ( $P > 0.05$ ). Day 1 of PPA treatment resulted in an AUC value of  $-25.4 \pm 6.0$  pA/hr ( $n = 4$ ) and this value was not significantly different ( $P > 0.05$ ) to the control experiments outlined in Section 7.6.1.

The AUC determined for day 2 of the PPA administration protocol was  $-12.8 \pm 11.7$  pA/hr ( $n = 5$ ) and this response was not significantly different  $P > 0.05$  from the NO response determined by AUC on day 0. No significant difference was observed between the pre and post injection basal levels on day 2 and the results are summarised in Table 7.6.2. A significant difference ( $P < 0.05$ ) was observed between the maximum response time and the time required to return to a baseline level on day 2 when compared to day 1.

The NO response on day 3 of the PPA administration protocol is represented in Figure 7.6.2(C). AUC analysis revealed a response of  $15.2 \pm 7.5$  pA/hr ( $n = 4$ ) on day 3. When compared to the AUC value determined on day 0 no significant difference ( $P > 0.05$ ) was observed. The pre and post-injection baseline levels recorded on day 3 revealed no significant difference  $P > 0.05$ , a summary of these results is provided in Table 7.6.2. The maximum response time and the time required to achieve a subsequent baseline level on day 3 were significantly different ( $P < 0.05$ ) from day 1 of PPA administration.

The AUC determined for day 4 and 5 of PPA treatment was  $13.5 \pm 15.8$  pA/hr ( $n = 4$ ) and  $-35.5 \pm 18.2$  ( $n = 6$ ) respectively. No significant difference  $P > 0.05$  was observed on day 4 and 5 of PPA administration when compared to the NO response determined by AUC on day 0 (Section 7.6.1). The pre and post-injection baseline levels recorded on day 4 and 5 were not significantly different  $P > 0.05$  and the results are summarised in Table 7.6.2. A significant difference ( $P < 0.05$ ) was observed between the maximum response time and subsequent return to baseline levels on day 4 when compared to day 1. The maximum response time and the time required to achieve a subsequent baseline

level on day 5 did not significantly differ  $P > 0.05$  when compare to day 1 of PPA administration.

AUC analysis revealed a response of  $-11.7 \pm 7.9$  pA/hr ( $n = 6$ ) on day 6. When compared to the AUC value determined on day 0 no significant difference ( $P > 0.05$ ) was observed on day 6. The pre and post-injection baseline levels recorded on day 6 revealed no significant difference  $P > 0.05$  and a summary of these results is provided in Table 7.6.2. The maximum response time and the time required to achieve a subsequent baseline level on day 6 did not significantly differ  $P > 0.05$  from day 1 of PPA administration.

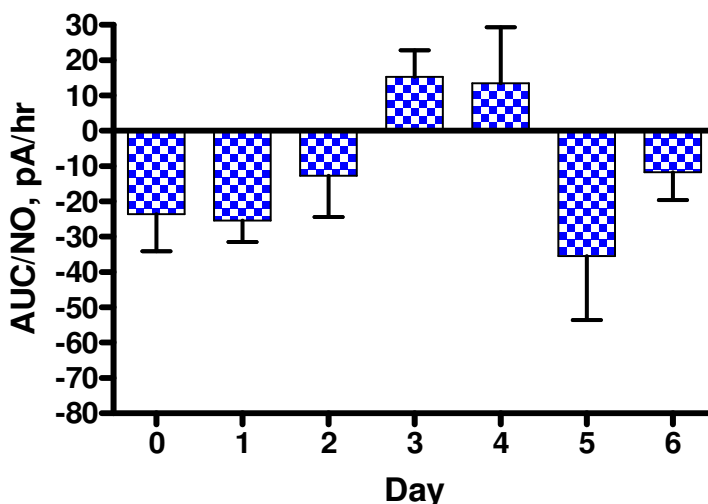


**Figure 7.6.2.1 Comparison between control NO response recorded in the DH and the response following systemic administration of PPA. Control data (day 0) and day 1-6 of PPA administration.**

**Data represented as Mean AUC  $\pm$  SEM (pA/hr).**

Figure 7.6.2.1 represents the average NO response recorded in the DH on day 1 to 6 of PPA treatment which was determined by AUC analysis. The control NO response calculated by AUC (Section 7.6.1) is represented by day 0. The NO response recorded on day 1 to day 6 of the PPA treatment protocol is not significantly different  $P > 0.05$  on each day when compared to the NO response recorded on day 0. It is clear that the systemic administration of PPA has caused an increase in NO levels in the DH on day 3 and day 4 of PPA administration. However no significant difference  $P > 0.05$  in NO

response was determined by AUC analysis on day 3 and 4 of the PPA administration protocol when compared to day 0. It was necessary to extend the administration of PPA to fully examine the effect of PPA administration on the NO response. Day 7 to day 12 of systemic administration of PPA is shown in the next Section (7.6.3).

| PPA          | Current change (pA) | Change (%)   | Conc. change (nM) | Max response (mins) | Return (mins) | AUC (pA/hr)  | Pre-injection baseline (pA) | Post-injection baseline (pA) | n |
|--------------|---------------------|--------------|-------------------|---------------------|---------------|--------------|-----------------------------|------------------------------|---|
| <b>Day 0</b> | n/a                 | n/a          | n/a               | n/a                 | n/a           | -23.6 ± 10.5 | n/a                         | n/a                          | 2 |
| <b>Day 1</b> | -74.7 ± 13.0        | -16.4 ± 2.9  | -47.3 ± 8.3       | 16.9 ± 1.5          | 21.8 ± 0.5    | -25.4 ± 6.0  | 455.1 ± 104.2               | 428.4 ± 114.7                | 5 |
| <b>Day 2</b> | -20.4 ± 25.0        | -4.0 ± 4.9   | -12.9 ± 15.8      | 7.0 ± 1.3           | 15.0 ± 1.7    | -12.8 ± 11.7 | 515.7 ± 124.5               | 492.2 ± 131.0                | 5 |
| <b>Day 3</b> | -18.6 ± 30.0        | -3.7 ± 6.0   | -11.8 ± 19        | 6.3 ± 0.5           | 14.2 ± 1.4    | 15.2 ± 7.5   | 499.6 ± 132.7               | 414.3 ± 116.8                | 4 |
| <b>Day 4</b> | 54.1 ± 15.6         | 12.6 ± 3.6   | 34.2 ± 9.9        | 4.8 ± 0.8           | 13.5 ± 0.9    | 13.5 ± 15.8  | 428.7 ± 121.8               | 429.0 ± 109.2                | 4 |
| <b>Day 5</b> | -111.3 ± 27.4       | -17.7 ± 4.4  | -70.5 ± 17.4      | 15.9 ± 2.1          | 20.1 ± 0.9    | -35.5 ± 18.2 | 629.6 ± 228.5               | 542.4 ± 218.9                | 6 |
| <b>Day 6</b> | -83.8 ± 52.9        | -16.2 ± 10.2 | -53.0 ± 33.5      | 14.8 ± 2.7          | 19.8 ± 0.8    | -11.7 ± 7.9  | 516.8 ± 191.3               | 488.3 ± 184.9                | 6 |

**Table 7.6.2 Summary of the NO data recorded between day 1 and 6 of chronic PPA administration (DH). With n = the number of sensors implanted in 2 animals (day 0), 3 animals (day 1), 4 animals (day 2-3), 3 animals (day 4), 4 animals (day 5) and 5 animals (day 6).**

## 7.6.3 Chronic PPA administration (DH) day 7-12

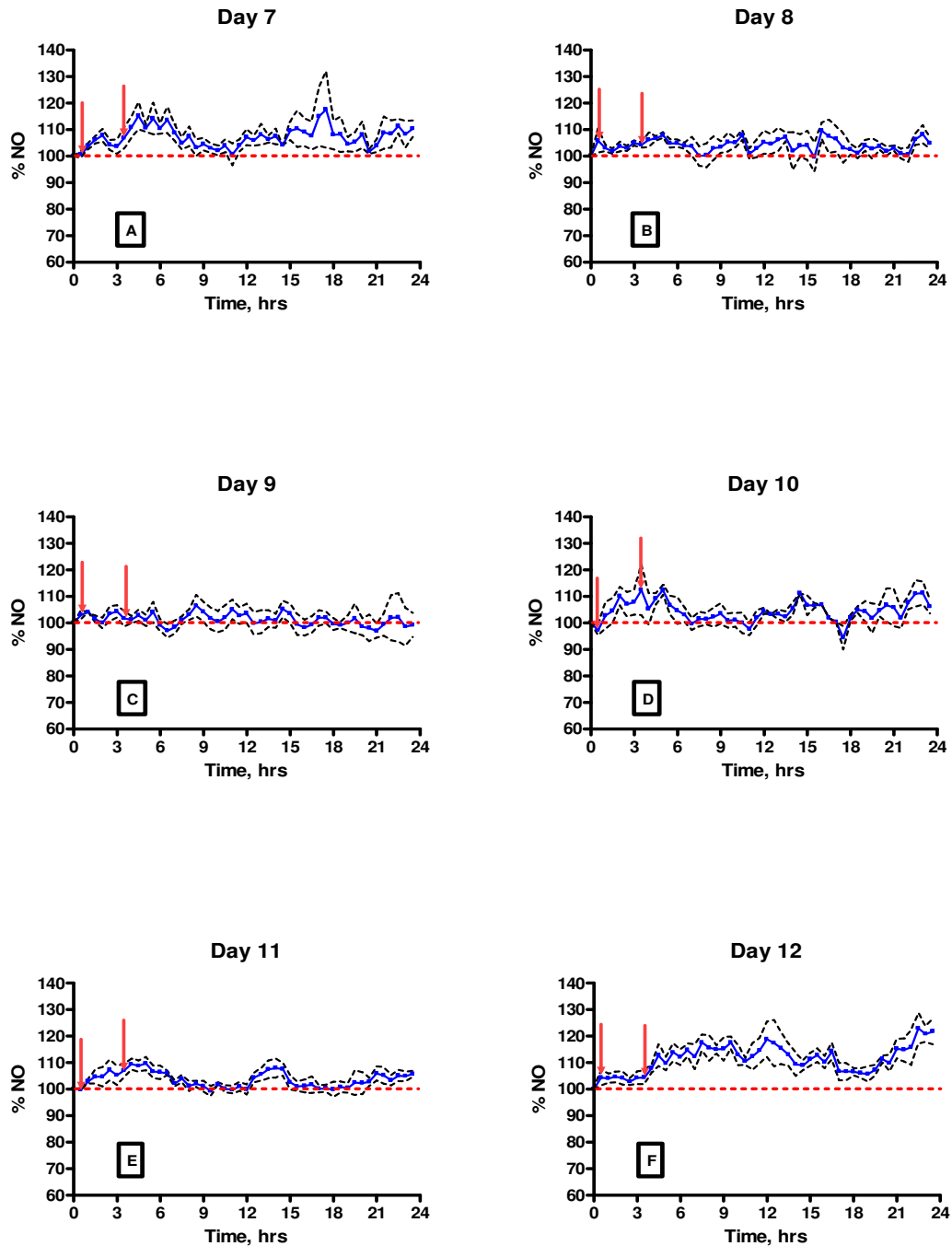


Figure 7.6.3 The average NO response recorded in the DH over a continuous period of 24 hrs following systemic administration of PPA. (A) 7 days of PPA treatment (B) 8 days, (C) 9 days, (D) 10 days, (E) 11 days and (F) 12 days. Data represented as a percentage change  $\pm$  SEM. Arrows indicate the injection of PPA.

The results demonstrated in this section examine the extension of the PPA administration protocol discussed in Section 7.6.2 (1 to 6 days). This section represents NO levels monitored in the DH by the NO sensor following the administration (s.c.) of PPA (Section 3.3.2.2) for a subsequent period of 7 to 12 days. PPA was administered twice daily, the first injection was given at 12.00 hrs and the second injection was administered at 15.00 hrs as indicated by the arrows shown in Figure 7.6.3.

Figure 7.5.3(A) demonstrates the average NO response recorded following 7 days of systemic PPA administration. An increase in NO can be seen following the administration of PPA. AUC analysis revealed a significant difference ( $P < 0.05, *$ ) between the overall NO response on day 7 ( $19.0 \pm 4.5$  pA/hr,  $n = 3$ ) when compared to day 0. The pre-injection ( $323.0 \pm 62.9$  pA,  $n = 3$ ) and post-injection baseline values ( $334.3 \pm 57.9$  pA,  $n = 3$ ) on day 7 did not significantly differ  $P > 0.05$ . The maximum response time and the time required to achieve a subsequent baseline level on day 7 did not significantly differ  $P > 0.05$  from day 1 of PPA administration.

Figure 7.6.3(B) illustrates the NO response recorded by the Nafion<sup>®</sup>-modified NO sensor implanted in the NA following the systemic administration of PPA for a total of 8 days. An increase in NO above baseline levels can be seen. The AUC analysis of the NO response on day 8 was  $11.1 \pm 3.9$  pA/hr,  $n = 4$ . A significant difference ( $P < 0.05, *$ ) was observed when the AUC on day 8 was compared to day 0. The maximum NO response was achieved within  $5.75 \pm 0.6$  hrs,  $n = 4$  and a return to pre-injection basal levels was observed  $18.0 \pm 2.1$  hrs,  $n = 4$  subsequently. No significant difference ( $P > 0.05$ ) was observed between the baseline level recorded prior to administration of PPA ( $560.1 \pm 303.8$  pA,  $n = 4$ ) and the subsequent return to baseline levels ( $568.0 \pm 300.4$  pA,  $n = 4$ ) on day 8.

The AUC determined for day 9 of the PPA administration protocol was  $8.7 \pm 3.6$  pA/hr ( $n = 4$ ), this response did not significantly differ  $P > 0.05$  from the NO response determined by AUC on day 0. However a relative increase in NO is apparent. No significant difference was observed between the pre and post injection basal levels on day 9 and the results are summarised below in Table 7.6.3. A significantly different ( $P <$

0.05) maximum response time and return to baseline level was observed on day 9 with respect to day 1.

The AUC determined for day 10 and 11 of PPA treatment was  $11.2 \pm 5.9$  pA/hr ( $n = 3$ ) and  $10.6 \pm 1.9$  ( $n = 4$ ) respectively. When compared to the AUC value determined on day 0 no significant difference ( $P > 0.05$ ) was observed on day 10 however a relative increase in NO is apparent. A significant difference ( $P < 0.05, *$ ) was observed between the AUC determined on day 11 and day 0. The pre and post-injection baseline levels recorded on day 10 and 11 revealed no significant difference  $P > 0.05$ , a summary of these results is provided in Table 7.6.3. The maximum response time and the time required to achieve a subsequent baseline level on day 10 and 11 were significantly different  $P < 0.05$  from day 1 of PPA administration.

As can be seen in Figure 7.5.3(F) a clear increase above baseline levels of NO occurred on day 12 of PPA treatment which gave an AUC value of  $34.4 \pm 7.2$  pA/hr ( $n = 3$ ). The AUC value determined for day 12 is significantly different ( $P < 0.05, *$ ) to that recorded on day 0. Although a continuation of the increase in NO is observed at the end of the recording period in Figure 7.5.3(F), the pre-injection ( $301.1 \pm 32.2$ ,  $n = 3$ ) and post-injection baseline values ( $322.2 \pm 23.7$  pA,  $n = 3$ ) did not significantly differ ( $P > 0.05$ ). Additionally a significantly different ( $P < 0.05, *$ ) maximum response time and return to baseline level was observed on day 12 with respect to day 1.

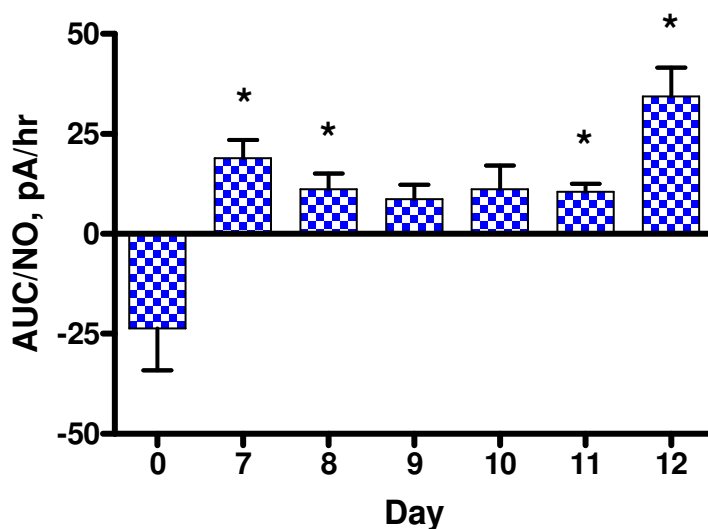


**Figure 7.6.3.1 Comparison between control NO response recorded in the DH and the response following systemic administration of PPA. Control data (day 0) and day 7-12 of PPA administration. Data represented as Mean AUC  $\pm$  SEM (pA/hr) with ( $P < 0.05$ , \*).**

Figure 7.6.3.1 demonstrates the average NO response recorded on day 7 to 12 due to the systemic administration of PPA determined by AUC analysis. The control NO response calculated by AUC (Section 7.6.1) is displayed and denoted by day 0. The NO response recorded on day 7, 8, 11 and 12 of the PPA treatment protocol is significantly different ( $P < 0.05$ ) on each day when compared to the NO response recorded on day 0. No significant difference was determined on day 9 and 10 in comparison to day 0; however a relative increase in NO is apparent. A discussion of the effect of each day of PPA treatment (day 1 to 12) on the response of the NO sensor implanted in the DH is discussed in the next Section (7.6.4).

| PPA           | Current change (pA) | Change (%) | Conc. change (nM) | Max response (mins) | Return (mins) | AUC (pA/hr)  | Pre-injection baseline (pA) | Post-injection baseline (pA) | n |
|---------------|---------------------|------------|-------------------|---------------------|---------------|--------------|-----------------------------|------------------------------|---|
| <b>Day 0</b>  | n/a                 | n/a        | n/a               | n/a                 | n/a           | -23.6 ± 10.5 | n/a                         | n/a                          | 2 |
| <b>Day 7</b>  | 52.8 ± 14.2         | 16.4 ± 4.4 | 33.4 ± 9.0        | 8.8 ± 3.9           | 18.0 ± 2.1    | 19.0 ± 4.5   | 323.0 ± 62.9                | 334.3 ± 57.9                 | 3 |
| <b>Day 8</b>  | 35.2 ± 30.6         | 6.3 ± 5.5  | 22.3 ± 19.4       | 5.75 ± 0.6          | 17.13 ± 0.9   | 11.1 ± 3.9   | 560.1 ± 303.8               | 568.0 ± 300.4                | 4 |
| <b>Day 9</b>  | 34.4 ± 8.6          | 11.7 ± 2.9 | 21.8 ± 5.4        | 7.4 ± 0.8           | 16.5 ± 0.6    | 8.7 ± 3.6    | 294.5 ± 32.2                | 299.3 ± 28.1                 | 4 |
| <b>Day 10</b> | 37.9 ± 9.4          | 13.1 ± 3.2 | 24.0 ± 6.0        | 6.0 ± 1.0           | 15.5 ± 2.5    | 11.2 ± 5.9   | 289.5 ± 45.4                | 300.4 ± 45.1                 | 3 |
| <b>Day 11</b> | 34.6 ± 5.2          | 10.9 ± 1.6 | 21.9 ± 3.3        | 3.9 ± 0.2           | 17.3 ± 0.9    | 10.6 ± 1.9   | 316.3 ± 33.0                | 321.8 ± 30.9                 | 4 |
| <b>Day 12</b> | 73.7 ± 17.9         | 24.5 ± 5.9 | 46.6 ± 11.3       | 7.7 ± 2.2           | 19.2 ± 0.7    | 34.4 ± 7.2   | 301.1 ± 32.2                | 322.2 ± 23.7                 | 3 |

**Table 7.6.3 Summary of the NO data recorded between day 7 and 12 of chronic PPA administration (DH). With n = the number of sensors implanted in 2 animals (day 0), 3 animals (day 7), 4 animals (day 8), 3 animals (day 9-11) and 2 animals (day 12).**

## 7.6.4 AUC comparison chronic PPA administration (DH) day 1-14

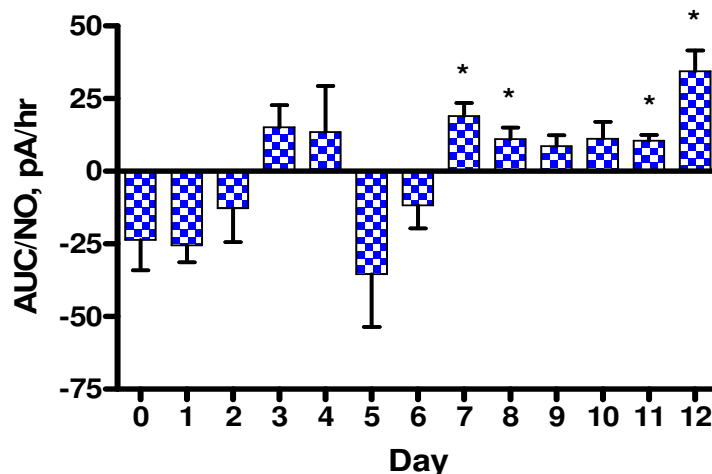


Figure 7.6.4 Comparison between the NO responses recorded in the DH on day 0 and day 1-12 of PPA administration. Data represented as Mean AUC  $\pm$  SEM (pA/hr) and ( $P < 0.05$ ,\*).

Figure 7.6.4 represents the overall NO response recorded in the DH (AUC) on day 0 against the AUC values obtained on day 1 to 12 of the PPA administration protocol. It can be seen that an overall increase in NO response above baseline levels occurs on day 3 and 4 of systemic PPA administration. Generally as the exposure time to PPA is increased the NO response in the DH becomes more maximal. As discussed in Section 7.6.3 day 7, 8, 11 and 12 of PPA treatment results in an NO response which is significantly different  $P < 0.05$  to the control experiments outlined in Section 7.6.1. Therefore the presence of systemically introduced PPA causes an increase in the level of NO in the DH.

As observed in the NA it can be seen that an increase in NO response occurs as the experimental protocol proceeds from day 7 through to day 12 and the level of exposure to PPA is increased. It can be determined that the observed increase in NO due to the administration of PPA is incurred by an accumulative effect of the presence of PPA. The more prolonged the exposure time to PPA the more attenuated and maximal the NO response in the DH becomes. However the magnitude of the increase in NO is lower in the DH in comparison to the NA and this observation is discussed in Section 7.6.4. The results presented in this section are summarised in Table 7.6.4.

No significant difference  $P > 0.05$  was observed between the pre and post-injection basal levels of NO on each day of PPA treatment (day 1 to 12). A significant difference  $P < 0.05$  was observed between the maximum response time and the time required to return to baseline on day 2-4 and day 8-12 of PPA treatment when compared to day 1. Generally a decrease in the maximum response time and the subsequent time required to achieve a stable baseline was observed where a relative increase in NO was determined by AUC analysis in relation to day 0.

A significant difference ( $P < 0.05$ ) in NO response was determined by AUC analysis on day 3, 7, 8, 9, 10 and 11 following the administration of PPA when compared to day 1 of PPA treatment. Similarly a significant difference ( $P < 0.05$ ) was observed between the AUC value determined on day 12 when compared to day 1. With (day 3,  $P = 0.0079$ ), (day 7,  $P = 0.0027$ ), (day 8,  $P = 0.0023$ ), (day 9,  $P = 0.0028$ ), (day 10,  $P = 0.0082$ ), (day 11,  $P = 0.0013$ ) and (day 12,  $P = 0.0014$ ) when compared to the AUC value calculated for day 1 of PPA treatment.

| Day         | 0            | 1           | 2            | 3          | 4           | 5            | 6           |
|-------------|--------------|-------------|--------------|------------|-------------|--------------|-------------|
| AUC (pA/hr) | -23.6 ± 10.5 | -25.4 ± 6.0 | -12.8 ± 11.7 | 15.2 ± 7.5 | 13.5 ± 15.8 | -35.5 ± 18.2 | -11.7 ± 7.9 |
| <i>P</i>    | n/a          | 0.9100      | 0.5177       | 0.0621     | 0.0737      | 0.5539       | 0.4120      |
| <i>n</i>    | 2            | 5           | 5            | 4          | 4           | 6            | 6           |

| Day         | 0            | 7          | 8          | 9         | 10         | 11         | 12         |
|-------------|--------------|------------|------------|-----------|------------|------------|------------|
| AUC (pA/hr) | -23.6 ± 10.5 | 19.0 ± 4.5 | 11.1 ± 3.9 | 8.7 ± 3.6 | 11.2 ± 5.9 | 10.6 ± 1.9 | 34.4 ± 7.2 |
| <i>P</i>    | n/a          | 0.0414     | 0.0484     | 0.0622    | 0.0860     | 0.0493     | 0.0110     |
| <i>n</i>    | 2            | 3          | 4          | 4         | 3          | 4          | 3          |

**Table 7.6.4 Comparison of the NO data (DH) AUC ± SEM (pA/hr) recorded on day 1 of PPA treatment against day 1-12 of chronic PPA administration**

A similar effect was observed with the NO response monitored in the DH following the chronic systemic administration of PPA in comparison to the response recorded in the NA. The administration of PPA for a continuous period of 12 days leads to an increased production of NO in the DH. The PPA induced elevation of NO levels is particularly

noticeable towards the end of the experimental procedure i.e. day 7-12 (see Figure 7.6.4). PPA has been utilised previously in the development of an animal model of autism as previously discussed (MacFabe *et al.*, 2008; MacFabe *et al.*, 2011). The detection of elevated NO levels presented in this section is further supported by the detection of increased oxidative stress markers measured in PPA treated rodent brain tissue preparations (El-Ansary *et al.*, 2012).

### 7.7 Regional comparison (Chronic PPA administration) DH and NA

This section demonstrates a comparative analysis of the effect of chronic repetitive administration of PPA for 12 days on NO levels in the NA and DH of freely-moving animals. Each animal was administered PPA twice daily (Section 3.3.2.2) for a continuous period of 12 days and the corresponding changes in NO levels on each day were monitored by the NO sensor. The AUC of the NO response calculated on each day of PPA administration in the NA and the DH is compared in this section.

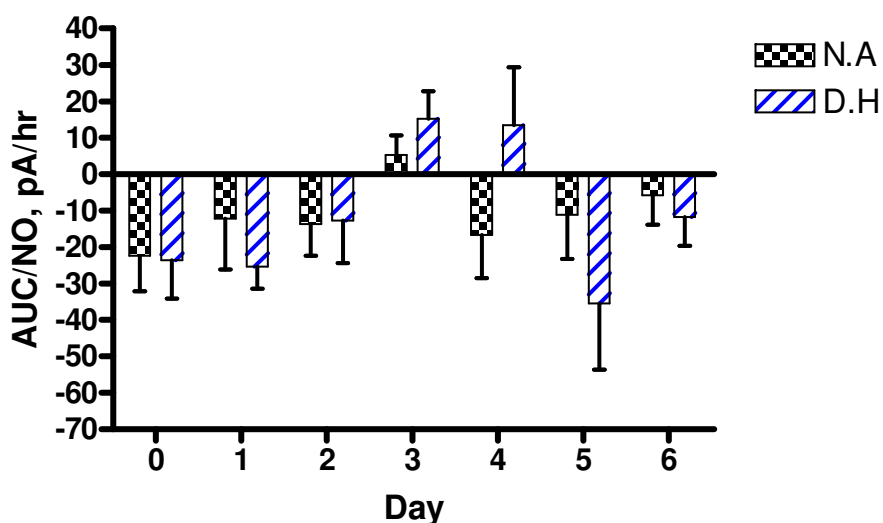


**Figure 7.7.1 Comparison between the NO responses recorded in the NA and the DH following systemic administration of PPA. Data includes day 0-6 of PPA administration. Data represented as Mean AUC ± SEM (pA/hr).**

A similar trend was observed in the NA and the DH on day 1-6 of the PPA administration protocol. No significant difference ( $P > 0.05$ ) in NO response, which was determined by AUC analysis, was observed between day 1-6 inclusively in comparison to the corresponding value determined for day 0 in both regions. Additionally no significant difference ( $P > 0.05$ ) was observed between both regions on day 0-6 of PPA administration as shown in Table 7.7.1.

| Day             | 0            | 1            | 2            | 3          | 4            | 5            | 6           |
|-----------------|--------------|--------------|--------------|------------|--------------|--------------|-------------|
| NA, AUC (pA/hr) | -22.4 ± 9.7  | -12.2 ± 14.0 | -13.7 ± 8.7  | 5.3 ± 5.3  | -16.7 ± 11.8 | -11.1 ± 12.2 | -5.8 ± 8.0  |
| DH, AUC (pA/hr) | -23.6 ± 10.5 | -25.4 ± 6.0  | -12.8 ± 11.7 | 15.2 ± 7.5 | 13.5 ± 15.8  | -35.5 ± 18.2 | -11.7 ± 7.9 |
| <i>P</i>        | 0.4187       | 0.1841       | 0.3326       | 0.2386     | 0.2295       | 0.1507       | 0.0616      |
| NA (n)          | 3            | 4            | 5            | 4          | 4            | 4            | 5           |
| DH (n)          | 2            | 3            | 4            | 4          | 3            | 4            | 3           |

**Table 7.7.1 Comparison between NO levels monitored in NA and DH. Data represented as AUC ± SEM (pA/hr), recorded on day 0-6 of chronic PPA administration.**

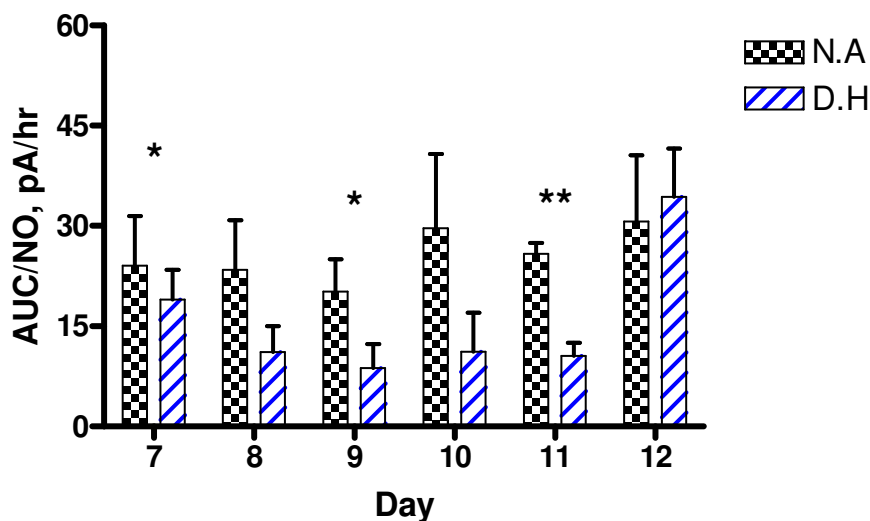


**Figure 7.7.2 Comparison between the NO responses recorded in the NA and the DH following systemic administration of PPA. Data includes day 7-12 of PPA administration. Data represented as Mean AUC ± SEM (pA/hr).**

A disparity was observed between NO levels recorded in the NA and the DH on day 7-12 of the PPA administration protocol. In both regions a relative increase in NO was determined by AUC analysis between day 7-12 and day 0 (see Section 7.5.4 and 7.6.4). However a relatively higher NO response was determined in the NA in comparison to the DH on day 7-12 of the PPA administration as shown in Figure 7.7.2. A significantly higher ( $P < 0.05$ ) PPA induced NO response was observed in the NA on day 7, 9 and 11 when compared to the corresponding values obtained from sensors implanted in the DH.

| Day                | 7             | 8             | 9             | 10             | 11            | 12            |
|--------------------|---------------|---------------|---------------|----------------|---------------|---------------|
| NA, AUC<br>(pA/hr) | 24.1 ±<br>7.4 | 23.4 ±<br>7.5 | 20.2 ±<br>4.8 | 29.7 ±<br>11.1 | 25.8 ±<br>1.6 | 30.7 ±<br>9.9 |
| DH, AUC<br>(pA/hr) | 19.0 ±<br>4.5 | 11.1 ±<br>3.9 | 8.7 ±<br>3.6  | 11.2 ±<br>5.9  | 10.6 ±<br>1.9 | 34.4 ±<br>7.2 |
| <i>P</i>           | 0.0445        | 0.3878        | 0.0349        | 0.1586         | 0.0036        | 0.0992        |
| NA (n)             | 3             | 5             | 5             | 3              | 2             | 4             |
| DH (n)             | 3             | 4             | 4             | 3              | 4             | 3             |

**Table 7.7.2 Comparison between NO levels monitored in NA and DH. Data represented as AUC ± SEM (pA/hr), recorded on day 7-12 of chronic PPA administration.**

It is difficult to draw direct comparisons between NO levels in different regions of the CNS as previously discussed by Finnerty *et al.* (Finnerty *et al.*, 2012). NO is derived from three main NO synthase enzymes (NOS), these consist of inducible NOS (iNOS), endothelial NOS (eNOS) and neuronal NOS (nNOS) (Kiechle & Malinski, 1993; Bruckdorfer, 2005; Guix *et al.*, 2005). The distribution of nNOS within the CNS is abundant, the activity and inhibition of nNOS by interaction with a variety of proteins may contribute to a disparity in the level of NO in different brain regions (Garthwaite, 2008).

The previous detection of indirect markers of NO production (i.e. nitrite and nitrate) obtained by microdialysis has revealed a regional difference in L-arginine induced NO production in the hippocampus and striatum (Hara *et al.*, 2004). Interestingly Hara *et al.* reported no significant change in markers of NO production in the striatum following the systemic administration of L-arginine. These findings contradict that published by other researchers who utilised similar detection methods to measure L-arginine induced NO production in the cerebellum (Yamada & Nabeshima, 1997). Additionally the detection of cGMP, an indirect marker of NO production, was found to be unchanged following the administration of the NOS inhibitors L-NAME and L-NARG in the prefrontal cortex (Laitinen *et al.*, 1994; Pepicelli *et al.*, 2004). This contrasts with other reports of an L-NAME induced inhibition of NO production in the hippocampus and cerebellum determined via cGMP detection and retrodialysis administration (Fedele & Raiteri, 1999). These combined reports may reflect an underlying disparity in the extent of exogenously altered NO production between different brain regions. This may lead to

conflicting experimental results depending on the sensitivity of the NO detection method utilised and the region investigated. These combined afore mentioned findings rely on indirect detection methods which lack the specificity and improved time resolution of direct electrochemical NO recordings demonstrated by our research group (Finnerty *et al.*, 2012). The NO precursor L-Arginine and NOS inhibitor L-NAME produce regional differences in the respective elevation and inhibition of NO in the striatum, prefrontal cortex and NA (Finnerty *et al.*, 2012). These previously determined regional differences may explain the disparity between PPA induced NO production in the NA and DH.

The activity of the constitutive isoforms of NOS in the CNS i.e. nNOS and eNOS on the level of NO in different regions of the brain must be considered. The expression of iNOS is rarely present at tonic levels in the brain and is normally produced in pathological conditions in response to an inflammatory insult (Guix *et al.*, 2005). It is well established that the expression of iNOS is a hallmark of neurodegenerative disorders such as Parkinson's and Alzheimer's disease (Calabrese *et al.*, 2007). Specifically in a pro-oxidant environment NO produced from either nNOS or iNOS can interact with superoxide and lead to the production of peroxynitrite which can damage cells (Calabrese *et al.*, 2007). The expression of iNOS has been implicated in the development of autism however the exact mechanism of NO production in autistic individuals is yet to be elucidated (Chauhan & Chauhan, 2006).

However a general similarity is observed in the DH and NA on day 7-12 of chronic PPA administration. An increase in NO production was determined in both regions following repeated injections of PPA. Increased susceptibility to oxidative stress may contribute to the development of autism (Chauhan & Chauhan, 2006). The global elevated NO production induced by the systemic administration of PPA may be derived from a disruption in normal redox homeostasis which would result in nitrosative stress and hence an increase in NO (Valko *et al.*, 2007).

## 7.8 Behavioural observations

MacFabe *et al.* have previously demonstrated a detailed description of the behavioural abnormalities induced in freely-moving rats by repeated intracerebroventricular (ICV) administrations of PPA (MacFabe *et al.*, 2007). In research conducted by Shultz *et al.* an impairment in the social behaviour of the animal has been demonstrated following ICV treatment with PPA (Shultz *et al.*, 2008). The chronic systemic administration (s.c.) of PPA has been shown to cause cognitive deficits in rats (Pettenuzzo *et al.*, 2002) and a conditioned place avoidance (Ossenkopp *et al.*, 2012). Repetitive systemic administration of PPA has also been demonstrated to reduce social interaction, increase anxiety-like behaviour and hypoactivity in rats (Shams *et al.*, 2009). Additionally the development of increased locomotor activity and repetitive dystonic or neurological movement disorders due to exposure to PPA has been demonstrated (MacFabe *et al.*, 2007; MacFabe *et al.*, 2008).

The reported behavioural outcomes due to repetitive administration of PPA consist of four main behavioural abnormalities including retropulsion, a snake-like posture, repetitive turning and limb dystonia (MacFabe *et al.*, 2007). The main characteristics of ASDs include social impairment, difficulties with communication, repetitive behaviours and restricted interests (Rapin & Tuchman, 2008). The social impairment and the repetitive and restricted behavioural characteristics of PPA treated rodents are consistent with the expectations for an animal model of autism (MacFabe *et al.*, 2011).

As seen previously in PPA treated rats abnormal behavioural characteristics were noted in the subjects utilised in these sets of experiments. As previously observed with systemic administrations of PPA, the subjects remained healthy for the duration of the PPA administration protocol outlined here (Pettenuzzo *et al.*, 2002). In the absence of detailed behavioural testing the most noticeable change in behaviour of the subjects utilised in this study occurred towards the end of the experimental protocol. The behaviour of the animal was consistently normal during the initial 5 days of PPA administration.

Upon the extension of the level of PPA administration (day 6-12), the animal manifested a propensity to turn repeatedly in a 360 degree manner in the housing bowl and postural abnormalities were observed. The observed PPA induced behavioural changes mirror the behavioural abnormalities previously demonstrated by MacFabe *et al.* in PPA treated rats (MacFabe *et al.*, 2007). In the study outlined in this chapter the observed abnormal behavioural traits of the PPA treated animal were particularly noticeable following 8 days of systemic administration and were exacerbated towards the end of the experimental procedure. Additionally the behavioural changes incurred by the administration of PPA were prominent within a few hours of the injection itself. The effect of PPA on the behavioural traits of the animal has previously been shown to exert a maximal effect within 30 mins following ICV infusion (MacFabe *et al.*, 2007). The discrepancy in the time required to induce a behavioural change seen in the subjects used in these experiments may be explained by the route of PPA administration i.e. s.c.

Interestingly the observed behavioural abnormalities in the subjects utilised in this chapter were more prominent where an increase in NO was recorded. In the absence of a detailed behavioural analysis of the subjects presented in this chapter, it is difficult to draw accurate correlations between the recorded changes in NO and the observed abnormal behaviours caused by the systemic administration of PPA. However, in general the manifestation of the behavioural abnormalities observed towards the end of the experimental protocol in this study were consistent with an increased production of NO.

## 7.9 Conclusion

The primary aim of this chapter was to demonstrate the novel detection of NO in an animal model of autism. The *in-vitro* and *in-vivo* characterisation of the NO sensor utilised in this chapter was verified with respect to previous work conducted by our research group in Chapter 6. The PPA induced animal model of autism described in this chapter has previously been extensively researched by MacFabe *et al.* (MacFabe *et al.*, 2007; MacFabe *et al.*, 2008; MacFabe *et al.*, 2011).

As a control experiment the effect of systemic administration of saline (s.c.) on the implanted NO sensor was examined in Section 7.3.2. No lasting effect on the NO sensor response was observed following the systemic administration of saline. These results are consistent with previous findings of the effect of systemic administration of saline on the response of this NO sensor design (Finnerty *et al.*, 2012).

An initial pilot study was conducted as presented in Section 7.4. The relative short-term effect of PPA administration on the level of NO in the NA was examined. A significant increase ( $P < 0.05$ ) in NO response was determined following the administration of each dose of PPA (1  $\mu\text{M/g}$ , 2  $\mu\text{M/g}$  and 4  $\mu\text{M/g}$ ) with respect to the administration of saline. A summary of the results presented in Section 7.4 is shown in Table 7.8.1.

| PPA               | Current change (pA) | Change (%)     | Conc. change (nM) | Max response (mins) | Return (mins)     | Pre-injection baseline (pA) | Post-injection baseline (pA) | n |
|-------------------|---------------------|----------------|-------------------|---------------------|-------------------|-----------------------------|------------------------------|---|
| 1 $\mu\text{M/g}$ | 29.7 $\pm$ 6.0      | 9.2 $\pm$ 3.0  | 19.4 $\pm$ 3.9    | 111.0 $\pm$ 35.0    | 271.0 $\pm$ 112.0 | 359.5 $\pm$ 70.4            | 355.3 $\pm$ 58.2             | 3 |
| 2 $\mu\text{M/g}$ | 28.8 $\pm$ 2.9      | 8.2 $\pm$ 1.8  | 18.8 $\pm$ 1.9    | 284.7 $\pm$ 8.3     | 436.3 $\pm$ 54.7  | 383.0 $\pm$ 65.9            | 373.7 $\pm$ 64.8             | 3 |
| 4 $\mu\text{M/g}$ | 69.2 $\pm$ 9.8      | 20.8 $\pm$ 3.8 | 45.3 $\pm$ 6.4    | 270                 | 375               | 334.5 $\pm$ 14.4            | 392.2 $\pm$ 4.0              | 2 |

**Table 7.4.1: Summary of results shown in Section 7.4.**

Previous demonstrations of a PPA induced animal model of autism involved the long-term systemic administration of PPA (500mg/kg) (Shams *et al.*, 2009). It was deemed necessary to investigate the long-term effect of PPA over 24 hrs on the level of NO in

the NA and DH. The effect of repetitive chronic PPA administration on NO levels in the intact living brain of freely-moving animals has not previously been demonstrated. As a control experiment the response of the NO sensor implanted in the NA for a continuous period of 24 hrs was examined in Section 7.5.1. A small variation in the NO response was observed over the 24 hr period which is likely attributable to the circadian rhythms of the animal (Heinzen & Pollack, 2002; Cespuglio *et al.*, 2012).

Additionally the corresponding level of NO in the DH was examined over a continuous period of 24 hrs (see Section 7.6.1). No significant difference ( $P > 0.05$ ) was observed between the 24 hr control data response, determined by AUC analysis, in the NA and the DH. However minor differences were observed in the recorded NO signal in both regions (see Figure 7.5.1 and 7.6.1). These small changes in NO over the specified time period may be attributed to the circadian rhythms of the animal as discussed in Section 7.5.1. However, the overall contribution of natural processes on the level of NO are effectively eliminated from the overall signal attributable to administration of PPA by the control data presented in Section 7.5.1 and 7.6.1.

NO levels in the NA and DH monitored by the NO sensor following the systemic administration of PPA for an initial period of 1 to 6 days are presented in Sections 7.5.2 and 7.6.2 respectively. A similar trend was observed in the NA and the DH on day 1-6 of the PPA administration protocol. No significant difference ( $P > 0.05$ ) in NO response, determined by AUC analysis, was observed between day 1-6 inclusively in comparison to the corresponding value determined for the 24 hr control data in both regions. A robust network of antioxidant mechanisms regulate the level of RNS such as NO in the CNS (Calabrese *et al.*, 2007). These mechanisms are responsible for the prevention of the development of nitrosative stress and consequently maintain cognitive function. The variety of processes which maintain this vital balance in the brain has been extensively reviewed (Droge, 2002; Valko *et al.*, 2007). It is therefore plausible that the initial exposure to PPA (day 1-6) is dealt with effectively by these control mechanisms.

The effect of the extension of the PPA administration protocol (day 7-12) on the level of NO monitored in the NA and DH is represented in Section 7.5.3 and 7.6.3 respectively.

A general trend emerged in the NO response recorded in both regions following the systemic administration of PPA after 7 days of repetitive PPA administration. An increase in NO was detected in both regions from day 7-12 inclusively when compared to the corresponding control data. The results are summarised in Section 7.5.4 and 7.6.4. The consistent over production of NO due to the development of oxidative/nitrosative stress has previously been implicated in the development of autism (Chauhan & Chauhan, 2006). Elevated levels of NO and indirect markers of NO production have been demonstrated in biological samples of autistic individuals (Sogut *et al.*, 2003; Sweeten *et al.*, 2004). Additionally increased oxidative stress markers have been detected in post-mortem autistic brain preparations (Chauhan *et al.*, 2012; Rose *et al.*, 2012). Also increased oxidative stress markers have been determined in brain preparations of a PPA induced animal model of autism (MacFabe *et al.*, 2007; MacFabe *et al.*, 2008).

The exact neuropharmacological role of PPA in the induced elevation of NO in the brain has yet to be fully elucidated. Previous *ex-vivo* brain preparation studies have indicated that PPA acts through a glutamatergic pathway. Specifically the incubation of brain slice preparations with PPA has been shown to stimulate the phosphorylation of cytoskeletal proteins. The use of specific N-methyl-D-aspartate (NMDA) receptor agonists has been shown to mimic the stated effect following brain slice exposure to PPA (de Mattos-Dutra *et al.*, 2000). Additionally PPA has previously been shown to promote intracellular calcium ( $\text{Ca}^{2+}$ ) release (Nakao *et al.*, 1992). It is known that activation of NMDA receptors which are abundantly present in the NA (Monaghan & Cotman, 1985), by glutamate or by other agonists result in an influx of  $\text{Ca}^{2+}$  and leads to depolarisation of the cell. The constitutive forms of NOS (eNOS and nNOS) are activated by  $\text{Ca}^{2+}$  followed by binding with calmodulin which leads directly to the production of NO (Alderton *et al.*, 2001; Saulskaya & Fofonova, 2006).

As previously stated the exact mechanism of NO production in the animal model of autism presented here remains to be elucidated. The role of iNOS in the expression of NO has been demonstrated in neurodegenerative disease states such as Parkinson's and

Alzheimer's disease (Calabrese *et al.*, 2007). Additionally the expression of iNOS has been implicated in the development of autism (Chauhan & Chauhan, 2006).

PPA itself is not cytotoxic as determined by a lack of apoptotic cell death or loss in brain tissue analysis of PPA treated rats (MacFabe *et al.*, 2007). Neuropathological investigations of PPA treated rat brain tissue and post mortem autistic brain preparations have indicated the presence of activated microglia and astrocytes (Vargas *et al.*, 2005; MacFabe *et al.*, 2011). Cytokines produced by this process lead to an inflammatory process which is known to activate iNOS and hence elicit an increase in NO (Guix *et al.*, 2005). Also the time required for iNOS expression and a subsequent production of NO due to an inflicted inflammatory response may be extended (Guix *et al.*, 2005). Specifically iNOS induced NO production by astrocytes and macrophages challenged with inflammatory cytokines may take up to three days to elicit a response (Ding & Merrill, 1997). This process may be a possible explanation for the observed time delay i.e. 7 days for the clear increase in NO production presented following continuous systemic administration of PPA.

The behavioural abnormalities found in the animal model of autism presented in this chapter are discussed in Section 7.8. The administration of the primary anti-oxidant species in the brain, ascorbic acid, in conjunction with PPA results in suppression of the cognitive deficits observed following PPA administration (Pettenuzzo *et al.*, 2002). Future work may involve the pre-administration or combined administration of ascorbic acid or other antioxidants in an effort to elucidate the proposed nitrosative stress mediation of autism. Additional research may involve the use of specific NOS inhibitors (Alderton *et al.*, 2001), to elucidate the exact mechanism of NO production in the PPA animal model of autism. This proposed research may further support the proposed role of oxidative/nitrosative stress in the etiology of ASDs. Current research and the results presented in this chapter indicate that oxidative/nitrosative stress is a major contributing factor in the etiology of ASDs.

The further detection of NO in an animal model of autism may lead to a better understanding of the etiology of ASDs and hence the development of potential therapeutic strategies.

## References

- Al-Lahham SaH, Peppelenbosch MP, Roelofsen H, Vonk RJ & Venema K. (2010). Biological effects of propionic acid in humans; metabolism, potential applications and underlying mechanisms. *Biochimica Et Biophysica Acta-Molecular and Cell Biology of Lipids* **1801**, 1175-1183.
- Alderton WK, Cooper CE & Knowles RG. (2001). Nitric oxide synthases: structure, function and inhibition. *Biochemical Journal* **357**, 593-615.
- Andersen JK. (2004). Oxidative stress in neurodegeneration: cause or consequence? *Nature Medicine* **10**, S18-S25.
- Arndt TL, Stodgell CJ & Rodier PM. (2005). The teratology of autism. *International Journal of Developmental Neuroscience* **23**, 189-199.
- Brock M & Buckel W. (2004). On the mechanism of action of the antifungal agent propionate - Propionyl-CoA inhibits glucose metabolism in *Aspergillus nidulans*. *European Journal of Biochemistry* **271**, 3227-3241.
- Bruckdorfer R. (2005). The basics about nitric oxide. *Molecular Aspects of Medicine* **26**, 3-31.
- Calabrese V, Mancuso C, Calvani M, Rizzarelli E, Butterfield DA & Stella AMG. (2007). Nitric oxide in the central nervous system: neuroprotection versus neurotoxicity. *Nature Reviews Neuroscience* **8**, 766-775.
- Cespuglio R, Amrouni D, Meiller A, Buguet A & Gautier-Sauvigne S. (2012). Nitric oxide in the regulation of the sleep-wake states. *Sleep Medicine Reviews* **16**, 265-279.
- Chauhan A, Audhya T & Chauhan V. (2012). Brain region-specific glutathione redox imbalance in autism. *Neurochemical research* **37**, 1681-1689.
- Chauhan A & Chauhan V. (2006). Oxidative stress in autism. *Pathophysiology : the official journal of the International Society for Pathophysiology / ISP* **13**, 171-181.
- Conn AR, Fell DI & Steele RD. (1983). Characterisation of alpha-keto acid transport across blood-brain-barrier in rats. *American Journal of Physiology* **245**, E253-E260.
- de Mattos-Dutra A, Meirelles R, da Rocha BB, Kommers T, Wofchuk ST, Wajner M & Pessoa-Pureur R. (2000). Methylmalonic and propionic acids increase the *in vitro* incorporation of P-32 into cytoskeletal proteins from cerebral cortex of young rats through NMDA glutamate receptors. *Brain Research* **856**, 111-118.

- de Theije CGM, Wu J, da Silva SL, Kamphuis PJ, Garsen J, Korte SM & Kraneveld AD. (2011). Pathways underlying the gut-to-brain connection in autism spectrum disorders as future targets for disease management. *European Journal of Pharmacology* **668**, S70-S80.
- DeCastro M, Nankova BB, Shah P, Patel P, Mally PV, Mishra R & La Gamma EF. (2005). Short chain fatty acids regulate tyrosine hydroxylase gene expression through a cAMP-dependent signaling pathway. *Molecular Brain Research* **142**, 28-38.
- Dichter GS, Richey JA, Rittenberg AM, Sabatino A & Bodfish JW. (2012). Reward Circuitry Function in Autism During Face Anticipation and Outcomes. *Journal of Autism and Developmental Disorders* **42**, 147-160.
- Ding M & Merrill JE. (1997). The kinetics and regulation of the induction of type II nitric oxide synthase and nitric oxide in human fetal glial cell cultures. *Molecular Psychiatry* **2**, 117-119.
- Droge W. (2002). Free radicals in the physiological control of cell function. *Physiological Reviews* **82**, 47-95.
- El-Ansary AK, Ben Bacha A & Kotb M. (2012). Etiology of autistic features: the persisting neurotoxic effects of propionic acid. *J Neuroinflammation* **9**, 74.
- Fedele E & Raiteri M. (1999). *In vivo* studies of the cerebral glutamate receptor NO cGMP pathway. *Progress in Neurobiology* **58**, 89-120.
- Finegold SM, Molitoris D, Song YL, Liu CX, Vaisanen ML, Bolte E, McTeague M, Sandler R, Wexler H, Marlowe EM, Collins MD, Lawson PA, Summanen P, Baysallar M, Tomzynski TJ, Read E, Johnson E, Rolfe R, Nasir P, Shah H, Haake DA, Manning P & Kaul A. (2002). Gastrointestinal microflora studies in late-onset autism. *Clinical Infectious Diseases* **35**, S6-S16.
- Finnerty NJ, O'Riordan SL, Palsson E & Lowry JP. (2012). Brain nitric oxide: Regional characterisation of a real-time microelectrochemical sensor. *Journal of Neuroscience Methods* **209**, 13-21.
- Folstein SE & Rosen-Sheidley B. (2001). Genetics of autism: Complex aetiology for a heterogeneous disorder. *Nature Reviews Genetics* **2**, 943-955.
- Garthwaite J. (2008). Concepts of neural nitric oxide-mediated transmission. *European Journal of Neuroscience* **27**, 2783-2802.
- Gautier-Sauvigne S, Colas D, Parmantier P, Clement P, Gharib A, Sarda N & Cespuglio R. (2005). Nitric oxide and sleep. *Sleep Medicine Reviews* **9**, 101-113.

- Goh S & Peterson BS. (2012). Imaging evidence for disturbances in multiple learning and memory systems in persons with autism spectrum disorders. *Developmental Medicine and Child Neurology* **54**, 208-213.
- Guix FX, Uribealago I, Coma M & Munoz FJ. (2005). The physiology and pathophysiology of nitric oxide in the brain. *Progress in Neurobiology* **76**, 126-152.
- Hara H, Haga S, Aoyama Y & Kiriya S. (1999). Short-chain fatty acids suppress cholesterol synthesis in rat liver and intestine. *Journal of Nutrition* **129**, 942-948.
- Hara S, Mukai T, Kurosaki K, Mizukami H, Kuriwa F & Endo T. (2004). Different response to exogenous L-arginine in nitric oxide production between hippocampus and striatum of conscious rats: a microdialysis study. *Neuroscience Letters* **366**, 302-307.
- Heinzen EL & Pollack GM. (2002). Use of an electrochemical nitric oxide sensor to detect neuronal nitric oxide production in conscious, unrestrained rats. *Journal of Pharmacological and Toxicological Methods* **48**, 139-146.
- Jyonouchi H, Sun SN & Itokazu N. (2002). Innate immunity associated with inflammatory responses and cytokine production against common dietary proteins in patients with autism spectrum disorder. *Neuropsychobiology* **46**, 76-84.
- Kiechle FL & Malinski T. (1993). Nitric-oxide - biochemistry, pathophysiology, and detection. *American Journal of Clinical Pathology* **100**, 567-575.
- Kohls G, Schulte-Ruther M, Nehr Korn B, Muller K, Fink GR, Kamp-Becker I, Herpertz-Dahlmann B, Schultz RT & Konrad K. (2012). Reward system dysfunction in autism spectrum disorders. *Soc Cogn Affect Neurosci* **11**, 11.
- Laitinen JT, Laitinen KS, Tuomisto L & Airaksinen MM. (1994). Differential regulation of cyclic GMP levels in the frontal cortex and the cerebellum of anesthetized rats by nitric oxide: an *in vivo* microdialysis study. *Brain Res* **668**, 117-121.
- Le Poul E, Loison C, Struyf S, Springael JY, Lannoy V, Decobecq ME, Brezillon S, Dupriez V, Vassart G, Van Damme J, Parmentier M & Detheux M. (2003). Functional characterization of human receptors for short chain fatty acids and their role in polymorphonuclear cell activation. *Journal of Biological Chemistry* **278**, 25481-25489.
- MacFabe DF, Cain DP, Rodriguez-Capote K, Franklin AE, Hoffman JE, Boon F, Taylor AR, Kavaliers M & Ossenkopp K-P. (2007). Neurobiological effects of intraventricular propionic acid in rats: Possible role of short chain fatty acids on

- the pathogenesis and characteristics of autism spectrum disorders. *Behavioural Brain Research* **176**, 149-169.
- MacFabe DF, Cain NE, Boon F, Ossenkopp K-P & Cain DP. (2011). Effects of the enteric bacterial metabolic product propionic acid on object-directed behavior, social behavior, cognition, and neuroinflammation in adolescent rats: Relevance to autism spectrum disorder. *Behavioural Brain Research* **217**, 47-54.
- MacFabe DF, Rodríguez-Capote K, Franklin JE, Kavaliers M, Possmayer F, Ossenkopp K-P & Franklin AE. (2008). A Novel Rodent Model of Autism: Intraventricular Infusions of Propionic Acid Increase Locomotor Activity and Induce Neuroinflammation and Oxidative Stress in Discrete Regions of Adult Rat Brain. *American Journal of Biochemistry and Biotechnology* **4**, 146-166.
- Meyer U, Feldon J & Dammann O. (2011). Schizophrenia and Autism: Both Shared and Disorder-Specific Pathogenesis Via Perinatal Inflammation? *Pediatric Research* **69**, 26R-33R.
- Monaghan DT & Cotman CW. (1985). Distribution of N-methyl-D-aspartate-sensitive L-[3H]glutamate-binding sites in rat brain. *J Neurosci* **5**, 2909-2919.
- Nakao S, Fujii A & Niederman R. (1992). Alteration of cytoplasmic Ca<sup>2+</sup> in resting and stimulated human neutrophils by short-chain carboxylic acids at neutral pH. *Infect Immun* **60**, 5307-5311.
- Nugent FS, Penick EC & Kauer JA. (2007). Opioids block long-term potentiation of inhibitory synapses. *Nature* **446**, 1086-1090.
- Ossenkopp K-P, Foley KA, Gibson J, Fudge MA, Kavaliers M, Cain DP & MacFabe DF. (2012). Systemic treatment with the enteric bacterial fermentation product, propionic acid, produces both conditioned taste avoidance and conditioned place avoidance in rats. *Behavioural Brain Research* **227**, 134-141.
- Parracho H, Bingham MO, Gibson GR & McCartney AL. (2005). Differences between the gut microflora of children with autistic spectrum disorders and that of healthy children. *Journal of Medical Microbiology* **54**, 987-991.
- Pepicelli O, Brescia A, Gherzi E, Raiteri M & Fedele E. (2004). GABA(A), but not NMDA, receptors modulate *in vivo* NO-mediated cGMP synthesis in the rat cerebral cortex. *Neuropharmacology* **46**, 480-489.
- Pettenuzzo LF, Schuck PF, Fontella F, Wannmacher CMD, Wyse AT, Dutra CS, Netto CA & Wajner M. (2002). Ascorbic acid prevents cognitive deficits caused by chronic administration of propionic acid to rats in the water maze. *Pharmacology Biochemistry and Behavior* **73**, 623-629.

- Rapin I & Tuchman RF. (2008). Autism: Definition, Neurobiology, Screening, Diagnosis. *Pediatric Clinics of North America* **55**, 1129-+.
- Rose S, Melnyk S, Pavliv O, Bai S, Nick TG, Frye RE & James SJ. (2012). Evidence of oxidative damage and inflammation associated with low glutathione redox status in the autism brain. *Translational psychiatry* **2**, e134.
- Sandler RH, Finegold SM, Bolte ER, Buchanan CP, Maxwell AP, Vaisanen ML, Nelson MN & Wexler HM. (2000). Short-term benefit from oral vancomycin treatment of regressive-onset autism. *Journal of Child Neurology* **15**, 429-435.
- Saul'skaya NB, Fofonova NV & Savel'ev SA. (2008). Glutamatergic regulation of extracellular citrulline levels in the nucleus accumbens during an emotional conditioned reflex. *Neuroscience and behavioral physiology* **38**, 487-492.
- Saul'skaya NB & Fofonova NV. (2006). Effects of N-methyl-D-aspartate on extracellular citrulline level in the rat nucleus accumbens. *Neuroscience Letters* **407**, 91-95.
- Shams S, Kavaliers M, Foley KA, Ossenkopp KP & MacFabe DF. (2009). Reduced social interaction, anxiety-like behavior and hypoactivity following systemic administrations of propionic acid in juvenile male rats. *Society for Neuroscience Abstract Viewer and Itinerary Planner* **39**.
- Shultz SR, MacFabe DE, Ossenkopp K-P, Scratch S, Whelan J, Taylor R & Cain DP. (2008). Intracerebroventricular injection of propionic acid, an enteric bacterial metabolic end-product, impairs social behavior in the rat: Implications for an animal model of autism. *Neuropharmacology* **54**, 901-911.
- Shultz SR, MacFabe DF, Martin S, Jackson J, Taylor R, Boon F, Ossenkopp K-P & Cain DP. (2009). Intracerebroventricular injections of the enteric bacterial metabolic product propionic acid impair cognition and sensorimotor ability in the Long-Evans rat: Further development of a rodent model of autism. *Behavioural Brain Research* **200**, 33-41.
- Sogut S, Zoroglu SS, Ozyurt H, Yilmaz HR, Ozugurlu F, Sivasli E, Yetkin O, Yanik M, Tutkun H, Savas HA, Tarakcioglu M & Akyol O. (2003). Changes in nitric oxide levels and antioxidant enzyme activities may have a role in the pathophysiological mechanisms involved in autism. *Clinica Chimica Acta* **331**, 111-117.
- Sweeten TL, Posey DJ, Shankar S & McDougale CJ. (2004). High nitric oxide production in autistic disorder: A possible role for interferon-gamma. *Biological Psychiatry* **55**, 434-437.

- Valko M, Leibfritz D, Moncol J, Cronin MTD, Mazur M & Telser J. (2007). Free radicals and antioxidants in normal physiological functions and human disease. *International Journal of Biochemistry & Cell Biology* **39**, 44-84.
- Vargas DL, Nascimbene C, Krishnan C, Zimmerman AW & Pardo CA. (2005). Neuroglial activation and neuroinflammation in the brain of patients with autism. *Annals of Neurology* **57**, 67-81.
- Walsh P, Elsabbagh M, Bolton P & Singh I. (2011). In search of biomarkers for autism: scientific, social and ethical challenges. *Nature Reviews Neuroscience* **12**, 603-612.
- Wass C, Archer T, Palsson E, Fejgin K, Alexandersson A, Klamer D, Engel JA & Svensson L. (2006a). Phencyclidine affects memory in a nitric oxide-dependent manner: Working and reference memory. *Behavioural Brain Research* **174**, 49-55.
- Wass C, Archer T, Palsson E, Fejgin K, Klamer D, Engel JA & Svensson L. (2006b). Effects of phencyclidine on spatial learning and memory: Nitric oxide-dependent mechanisms. *Behavioural Brain Research* **171**, 147-153.
- Yamada K & Nabeshima T. (1997). Simultaneous measurement of nitrite and nitrate levels as indices of nitric oxide release in the cerebellum of conscious rats. *Journal of Neurochemistry* **68**, 1234-1243.
- Yorbik O, Sayal A, Akay C, Akbiyik DI & Sohmen T. (2002). Investigation of antioxidant enzymes in children with autistic disorder. *Prostaglandins Leukotrienes and Essential Fatty Acids* **67**, 341-343.
- Zoroglu SS, Armutcu F, Ozen S, Gurel A, Sivasli E, Yetkin O & Meram I. (2004). Increased oxidative stress and altered activities of erythrocyte free radical scavenging enzymes in autism. *European Archives of Psychiatry and Clinical Neuroscience* **254**, 143-147.
- Zoroglu SS, Yurekli M, Meram I, Sogut S, Tutkun H, Yetkin O, Sivasli E, Savas HA, Yanik M, Herken H & Akyol O. (2003). Pathophysiological role of nitric oxide and adrenomedullin in autism. *Cell Biochemistry and Function* **21**, 55-60.

---

**8. The detection of NO and H<sub>2</sub>O<sub>2</sub> in an animal model of Parkinson's disease**

---

## 8.1 Introduction

Parkinson's disease (PD) is a severe progressive neurodegenerative movement disorder. The neuropathological feature of PD is dopamine (DA) cell degeneration in an area of the midbrain known as the substantia nigra pars compacta (SNc) which leads to an insufficient availability of striatal DA (Olanow & Tatton, 1999; Schapira & Jenner, 2011). Dopaminergic neurons project from the SNc and terminate in the striatum where they maintain the normal physiological level of DA. The role of this dopaminergic nigrostriatal system in the maintenance of striatal DA and the subsequent control of voluntary movement has previously been described by Obeso *et al.* (Obeso *et al.*, 2008).

Neuropathological investigations of PD have routinely demonstrated the presence of intracytoplasmic inclusions known as 'Lewy bodies' that are composed of several proteins including  $\alpha$ -synuclein and parkin (Olanow & Tatton, 1999; Lotharius & Brundin, 2002; Schapira & Jenner, 2011). The protein  $\alpha$ -synuclein has been hypothesised to play a role in the normal physiological intracellular storage of DA within the presynaptic terminal (Lotharius & Brundin, 2002). Additionally  $\alpha$ -synuclein has also been postulated to play a role in synaptic plasticity (Clayton & George, 1998). Various familial forms of PD exist which have been linked to genetic mutations in specific proteins including  $\alpha$ -synuclein and parkin (Olanow & Tatton, 1999; Lotharius & Brundin, 2002; Schapira & Jenner, 2011). However familial forms of PD are relatively uncommon and count for less than 10 % of all PD cases (Maguire-Zeiss *et al.*, 2005).

Sporadic idiopathic PD is the predominant form of the neurodegenerative disease, it is largely associated with advancing age and has been linked to certain environmental factors including exposure to pesticides, herbicides and toxins (Olanow & Tatton, 1999; Schapira & Jenner, 2011). The role of various toxins including rotenone, paraquat (PQ) and MPTP in the development of PD has previously been examined and utilised to study PD in animal models (Beal, 2001; McCormack *et al.*, 2005; McCormack *et al.*, 2006).

The degeneration of dopaminergic cells in the SNc which is a pathological hallmark of PD has been attributed to oxidative stress specifically as a result of DA metabolism

(Lotharius & Brundin, 2002; Andersen, 2004; Chinta & Andersen, 2008). DA may be metabolised enzymatically or auto-oxidised to form hydrogen peroxide (H<sub>2</sub>O<sub>2</sub>). The metabolism of DA leads to the formation of the primary reactive oxygen species (ROS) superoxide (O<sub>2</sub><sup>•-</sup>), DA-quinone species and hydroxy radicals. The over production of ROS and subsequent production of reactive nitrogen species (RNS) leads to oxidative/nitrosative stress which leads to damage to cell structures, DNA, lipids and proteins (Valko *et al.*, 2007). A detailed description of DA metabolism related oxidative stress and the postulated role of this pathway in the degeneration of dopaminergic cells in the SNc is discussed in detail in Section 1.7.

The herbicide paraquat (PQ) otherwise known as methyl viologen dichloride hydrate is an environmental toxin which has previously been linked to the development of PD in humans (Tanner *et al.*, 2011). PQ is structurally similar to the parkinsonism inducing toxin MPP<sup>+</sup> (Dinis-Oliveira *et al.*, 2006; Bove & Perier, 2012). The repeated systemic administration of PQ has previously been utilised to develop an animal model of PD (McCormack *et al.*, 2005; McCormack *et al.*, 2006).

The ability of PQ to cross the blood brain barrier (BBB) has previously been questioned, PQ is a charged hydrophilic molecule which is unlikely to cross the BBB by passive means (Di Monte, 2003). Additionally non-human primate studies have indicated that the BBB impedes the access of PQ to the brain (Bartlett *et al.*, 2009). However PQ has been shown to reach the brain in rodents following systemic administration in a dose dependent manner (Corasaniti *et al.*, 1998; Shimizu *et al.*, 2001; McCormack & Di Monte, 2003). The systemic co-administration of simple amino acids (e.g. L-valine and L-phenylalanine) in addition to PQ has previously been shown to reduce the access of PQ to the brain in a rodent model (Shimizu *et al.*, 2001; McCormack & Di Monte, 2003). Therefore PQ may gain access to the CNS via the BBB neutral amino acid transporter supporting the role of active transport of PQ across the BBB (Shimizu *et al.*, 2001; McCormack & Di Monte, 2003).

Systemic PQ administration has been shown to selectively induce neurodegeneration of dopaminergic cells in the SNc of rodents primarily via oxidative stress (McCormack *et al.*, 2005; McCormack *et al.*, 2006). It has been postulated that PQ may be transported

directly into dopaminergic neurons by the dopamine transporter (DAT). The local co-administration of GBR-12909, a selective DAT inhibitor, reduced paraquat uptake into the striatal tissue of rats (Shimizu *et al.*, 2003a). This process may explain PQ mediated specific dopaminergic neurodegeneration as demonstrated by other research groups (McCormack *et al.*, 2005; McCormack *et al.*, 2006). Alternatively Richardson *et al.* have excluded the role of DAT in the active uptake of PQ. This research group has suggested that the loss of dopaminergic neurons following systemic administration of PQ is attributable to the unique susceptibility of the DA neurons to PQ mediated oxidative stress (Richardson *et al.*, 2005).

As previously stated the loss of striatal DA and the presence of 'Lewy bodies' are the major characteristics of the pathology of PD. Shimizu *et al.* have previously demonstrated that repeated subcutaneous injections of PQ to rodents resulted in a significant decrease in DA and its metabolites in the striatum (Shimizu *et al.*, 2003a). Additionally systemic PQ administration has been shown to induce the up-regulation of  $\alpha$ -synuclein the major constituent of 'Lewy bodies' (Manning-Bog *et al.*, 2002). The systemic administration of PQ has been shown to cause a decrease in locomotor activity in rodents due to a proposed decline in striatal dopamine nerve terminal density (Brooks *et al.*, 1999).

Intracellular PQ may lead to oxidative stress through indirect mitochondrial dysfunction (MTdys) via redox cycling and by direct MTdys via inhibition of Complex I of the mitochondrial ETC known as NADH-ubiquinone oxidoreductase. The exact mechanism of PQ induced MTdys has been disputed (Richardson *et al.*, 2005; Miller, 2007; Cory-Slechta *et al.*, 2008; LoPachin & Gavin, 2008). Direct PQ mediated mitochondrial (Complex I) inhibition has been indicated by several research groups (Castello *et al.*, 2007; Cocheme & Murphy, 2008; Czerniczyniec *et al.*, 2011). Equally indirect MTdys due to the cytosolic redox cycling of PQ has been postulated as a causative factor in PQ mediated oxidative stress (Bonneh-Barkay *et al.*, 2005a; Bonneh-Barkay *et al.*, 2005b; McCormack *et al.*, 2006; Berry *et al.*, 2010). However both direct and indirect MTdys initiated by PQ leads to the development of oxidative/nitrosative stress and the subsequent deleterious process of neuronal cell damage (Lin & Beal, 2006).

Under normal physiological conditions Complex I of the mitochondrial ETC accepts electrons from NADH (Uversky, 2004). However, when PQ is present PQ preferentially accepts these electrons and leads to Complex I inhibition, the production of (O<sub>2</sub><sup>•-</sup>) and subsequent MTdys (Dinis-Oliveira *et al.*, 2006; Cocheme & Murphy, 2008).

The process of cytosolic redox cycling of PQ is facilitated by intracellular enzymes (cellular diaphorases) such as NADPH oxidase, NADPH-cytochrome *c* reductase and nitric oxide synthase (NOS) (Day *et al.*, 1999; Dinis-Oliveira *et al.*, 2006; Purisai *et al.*, 2007). This pathway leads to the production of O<sub>2</sub><sup>•-</sup> and hence the development of oxidative/nitrosative stress. PQ may be reduced in the cytosol to form a PQ monocation free radical (PQ<sup>•+</sup>) by cellular diaphorases (e.g. NOS), which are enzymes that transfer electrons from NADPH to small molecules such as PQ (Day *et al.*, 1999). PQ<sup>•+</sup> is rapidly re-oxidised in the presence of molecular oxygen thereby generating O<sub>2</sub><sup>•-</sup> and reformed PQ which initiates the processes which lead to oxidative/nitrosative stress and subsequently indirect MTdys (Day *et al.*, 1999; Dinis-Oliveira *et al.*, 2006; Bove & Perier, 2012).

It has previously been demonstrated that dose dependent PQ treatment stimulates transient striatal glutamate release (Shimizu *et al.*, 2003a). It is known that activation of N-methyl-D-aspartate (NMDA) receptors which are abundantly present in the NA (Monaghan & Cotman, 1985), by glutamate or by other agonists results in an influx of Ca<sup>2+</sup> and leads to depolarisation of the cell. The constitutive forms of NOS (eNOS and nNOS) are activated by Ca<sup>2+</sup> followed by binding with calmodulin which leads directly to the production of NO (Alderton *et al.*, 2001; Saulskaya & Fofonova, 2006).

The PQ evoked release of NO may diffuse to dopaminergic terminals leading to MTdys mediated by reactive nitrogen species (RNS) and consequently the overproduction of dopamine (Shimizu *et al.*, 2003a; Dinis-Oliveira *et al.*, 2006). The non-selective NOS inhibitor L-NAME has previously been shown to block PQ mediated dopamine overflow *in-vivo* (Shimizu *et al.*, 2003b). In a pro-oxidant environment NO can interact directly with (O<sub>2</sub><sup>•-</sup>) and lead to the formation of the main secondary highly toxic reactive nitrogen species (RNS) peroxynitrite (ONOO<sup>-</sup>) (Ramalingam & Kim, 2012). NOS itself

may act as a diaphorase in conjunction with PQ and ‘uncoupling’ of the NOS enzyme may lead to the preferential formation of O<sub>2</sub><sup>•-</sup> over NO (Day *et al.*, 1999; Margolis *et al.*, 2000). It is unclear whether L-NAME exerts a protective effect via inhibition of NOS mediated NO production or by inhibition of O<sub>2</sub><sup>•-</sup> formation from NOS ‘uncoupling’ (Dinis-Oliveira *et al.*, 2006; Moran *et al.*, 2010). As previously discussed the redox cycling of PQ is known to result in the production of O<sub>2</sub><sup>•-</sup> which is the main source of H<sub>2</sub>O<sub>2</sub> production in the brain. An increase in striatal H<sub>2</sub>O<sub>2</sub> determined by a fluorescent method has been shown by Czerniczyniec *et al.* following the systemic administration of PQ (Czerniczyniec *et al.*, 2011).

The characteristics of PQ, MPP<sup>+</sup> and rotenone as Complex I inhibitors and oxidative stressors have enabled the successful replication of certain aspects of the pathophysiology of PD in animal models (Beal, 2001; McCormack *et al.*, 2005; McCormack *et al.*, 2006). A variety of reports indicate that changes in NO and H<sub>2</sub>O<sub>2</sub> occur in the neuronal environment following systemic injections of PQ as determined by indirect methods of analysis. The main aim of this chapter is to demonstrate the novel direct *in-vivo* electrochemical detection of NO and H<sub>2</sub>O<sub>2</sub> following the systemic administration of PQ in order to examine PQ mediated oxidative/nitrosative stress.

## 8.2 Experimental

The instrumentation, chemicals, solutions and software used in this section are described in detail in Chapter 3. Details of the manufacture of the working electrodes are outlined in Section 3.4. All experiments outlined in this chapter were performed using Constant Potential Amperometry (CPA). A potential of +700 mV and +900 mV vs. Ag wire (see Section 3.10.3) was applied to the working electrodes for the detection of H<sub>2</sub>O<sub>2</sub> and NO respectively for all *in-vivo* experiments. The number of implanted NO sensors is denoted by (n) and the number of animals indicated. NO sensors were implanted ipsilaterally (same side). The number of implanted dual catalase-based H<sub>2</sub>O<sub>2</sub> sensors is denoted by (n) i.e. a *Blank* and a *Cat* sensor in the same number of animals. The *Blank* and *Cat* sensor were implanted ipsi-laterally to each other and contra-laterally to NO sensors. All sensors (NO/H<sub>2</sub>O<sub>2</sub>) were implanted in the nucleus accumbens (NA).

For systemic administration of PQ varying doses including 5, 10, 20 and 30 mg/kg were prepared in normal saline and injected in a volume of 2 mL/kg. Each injection of PQ was given at 12.00 hrs followed by a 72 hr recording period.

Reported *in-vivo* NO concentration changes are based on the average *in-vitro* pre-implantation calibration data. Area under the curve (AUC) analysis was utilised to determine the overall NO response following administration of PQ. The net AUC value is represented in this chapter i.e. the average AUC value was calculated for peaks below and above baseline levels. AUC provides an integrated measurement of a measurable effect or phenomenon. AUC determines the overall change in NO before returning to a baseline level which is relative to the effect of PQ administration.

Statistical analysis was carried out using paired or unpaired t-tests. These tests were performed using Graphpad Prism and gave a probability value (*P*) which indicates the level of significant or non-significant difference between groups. *P* > 0.05, denotes no significant difference. The extent of significant difference is divided into three parameters (*P* < 0.05,\*), (*P* < 0.01,\*\*) and (*P* < 0.0001,\*\*\*) from the lowest relative level of difference (\*) to the highest (\*\*\*).

### 8.3 Systemic control experiments

All systemic administrations shown in this chapter were carried out in 2 mL/kg of saline by subcutaneous injection (s.c.). The effect of systemically administered saline on the NO sensor and paired H<sub>2</sub>O<sub>2</sub> sensor response has previously been demonstrated in Section 7.3.1 and 5.3.2 respectively. For the purpose of clarity the response of each sensor design NO/H<sub>2</sub>O<sub>2</sub> following the systemic administration of saline is presented in Figure 8.3.1.

#### 8.3.1 Systemic (s.c.) saline administration

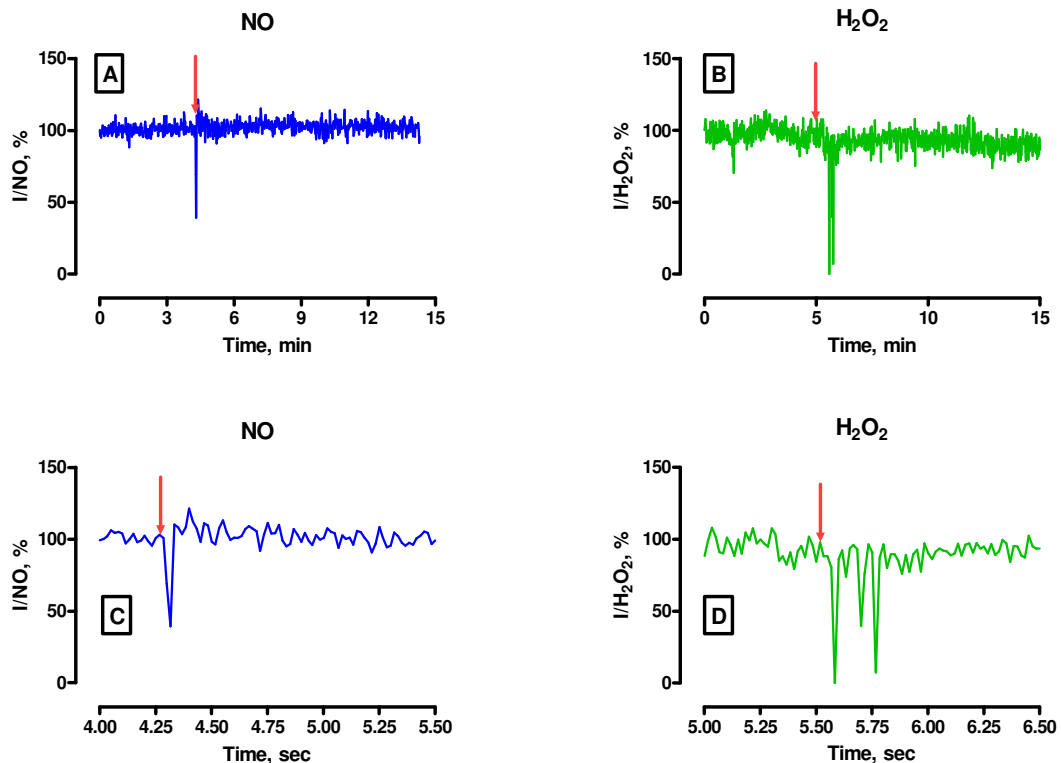


**Figure 8.3.1** Typical example of an s.c. injection of saline detected by the NO and H<sub>2</sub>O<sub>2</sub> sensor. *Top panel:* NO sensor (A) and H<sub>2</sub>O<sub>2</sub> sensor (B), response monitored in the brain of a freely-moving Wistar rat following injection of saline. *Bottom panel:* Immediate response following injection (secs); NO sensor (C) and H<sub>2</sub>O<sub>2</sub> sensor (D). The arrow indicates the point of administration.

| <b>Saline</b>                     | <b>Current change (pA)</b> | <b>Change (%)</b> | <b>Conc. change (nM)</b> | <b>Max response (mins)</b> | <b>Return (mins)</b> | <b>Pre-injection baseline (pA)</b> | <b>Post-injection baseline (pA)</b> |
|-----------------------------------|----------------------------|-------------------|--------------------------|----------------------------|----------------------|------------------------------------|-------------------------------------|
| <b>NO</b>                         | 10.5 ± 1.9                 | 1.9 ± 0.3         | 7.0 ± 1.0                | 3.0 ± 0.3                  | 7.4 ± 0.4            | 550.7 ± 104.3                      | 554.6 ± 104.8                       |
| <b>H<sub>2</sub>O<sub>2</sub></b> | 155.3 ± 123.9              | 1.0 ± 4.4         | 69.3 ± 55.3              | 7.9 ± 0.9                  | 12.7 ± 0.4           | 842.6 ± 749.9                      | 1390.2 ± 699.9                      |

**Table 8.3.1: Summary of NO/H<sub>2</sub>O<sub>2</sub> data monitored in freely-moving animals obtained on injection of saline. NO Data obtained from 6 sensors; average data includes 10 administrations. H<sub>2</sub>O<sub>2</sub> Data obtained from 3 paired H<sub>2</sub>O<sub>2</sub> sensors. All data obtained from sensors implanted in the brain of 6 Wistar rats.**

As a control experiment saline (Section 3.3.3.2) was administered subcutaneously (s.c.) (Section 3.11.2) and the effect on the NO/H<sub>2</sub>O<sub>2</sub> signal was measured. The NO response following the injection of saline has previously been shown in Section 7.3.1 and the corresponding H<sub>2</sub>O<sub>2</sub> response is discussed in Section 5.3.2. Briefly, in each case no significant difference ( $P > 0.05$ ) was observed between the pre and post-injection baseline levels of NO/H<sub>2</sub>O<sub>2</sub>. A short lived change in NO/H<sub>2</sub>O<sub>2</sub> concentration was measured following the injection of saline. However, no lasting effect on the NO or paired H<sub>2</sub>O<sub>2</sub> sensor response was observed and no significant difference ( $P > 0.05$ ) was observed between the maximum percentage change and the baseline level recorded by the NO and H<sub>2</sub>O<sub>2</sub> sensor following the injection of saline.

## 8.4. Chronic Paraquat (PQ) dose response (NA)

The results presented in this section demonstrate the long term effect of paraquat (PQ) administration on the level of NO monitored in the NA. The response of the NO sensor was examined following the systemic injection of a low dose of PQ (5 mg/kg) and a relatively high dose of PQ (30 mg/kg) for a period of 72 hrs. The long-term response of the NO sensor over 72 hrs in the absence of treatment is also presented in this section. Additionally the preliminary simultaneous detection of H<sub>2</sub>O<sub>2</sub> and NO in the same animal following each administered dose of PQ (5 and 30 mg/kg) is shown.

### 8.4.1 Control NO data (NA)

The results presented in this section demonstrate the response detected by the NO sensor for a continuous period of 72 hrs while implanted in the NA. The administration of saline has no lasting effect on the NO/H<sub>2</sub>O<sub>2</sub> sensor response as has been demonstrated in Section 8.3.1. The results presented in this section act as a control against which the NO response due to the administration of PQ, recorded in the NA for a period of 72 hrs may be compared.

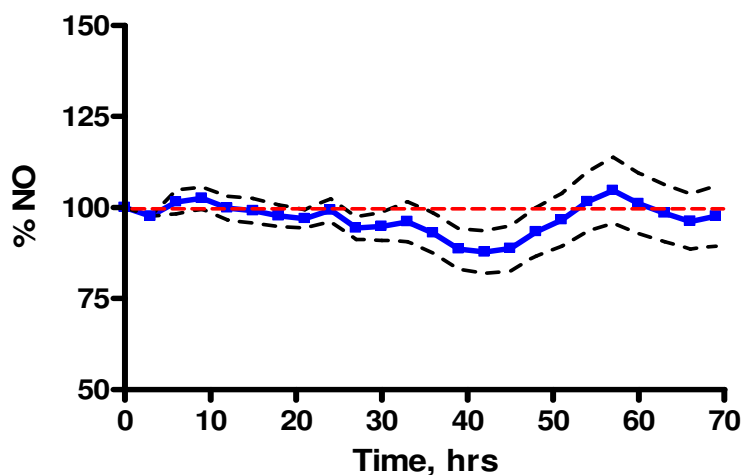


**Figure 8.4.1** The average NO response in the NA over a continuous period of 72 hrs. Data represented as a percentage current change  $\pm$  SEM. SEM represented by dashed line (black).

Figure 8.4.1 represents the NO levels recorded in the NA over a continuous period of 72 hrs ( $n = 10$ , 3 animals). It is clear that the NO response remains close to baseline levels

for the duration of the recording period. A slight deviation from baseline levels of NO, which is denoted by the dashed line, can be seen, however a return to stable baseline levels of NO can be seen subsequently. In order to examine the overall change in NO over a 72 hr period AUC analysis was performed which gave a response of  $-96.2 \pm 92.9$  pA/hr (n = 10).

The NO recordings presented in Figure 8.4.1 were taken after an initial period of *ca.* 24 hrs following the application of the potential to the working electrodes. Therefore the contribution of the capacitance current to the overall NO sensor response represented in Figure 8.4.1 is greatly reduced. The minor variation in NO levels recorded over a continuous period of 72 hrs is likely attributable to the circadian rhythms of the animal which is supported by work conducted by other research groups.

Heinzen & Pollack have previously demonstrated a time dependent variation in the level of NO in saline treated animals. This research group recorded brain NO over an extended time period via electrochemical methods and found time dependent fluctuations; which they attributed to a circadian variation in the production of NO (Heinzen & Pollack, 2002). Additionally, Cespuglio *et al.* have previously demonstrated circadian dependent changes in the level of NO, as determined by long-term electrochemical recordings in freely-moving animals (Cespuglio *et al.*, 2012). However the overall contribution of sleep-wake effects or possible residual capacitance to the NO response following the administration of PQ may be compared to the control data presented in Figure 8.4.1.

#### **8.4.2 PQ dose response (NO)**

The aim of this section is to investigate the effect of the systemic administration of paraquat (PQ) on the NO sensor response while implanted in the NA of freely-moving animals. A dose response study was conducted and the long-term NO response attributable to the administration of a low dose of PQ (5 mg/kg) and a relatively high dose of PQ (30 mg/kg) was examined.

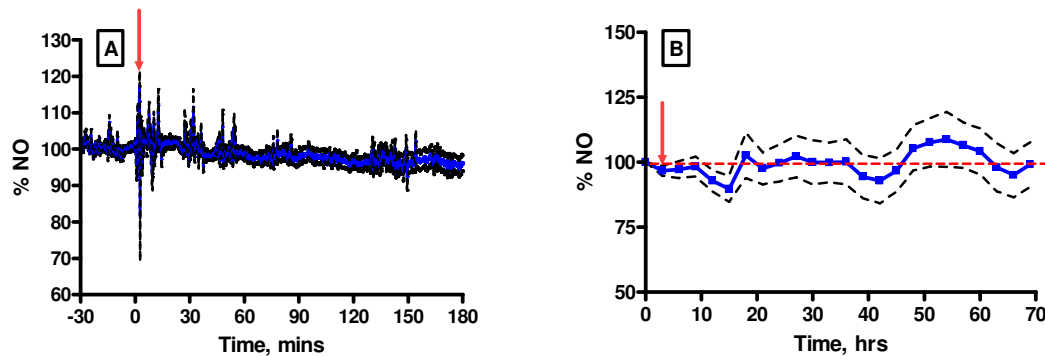


**Figure 8.4.2.1** The average NO response recorded in the NA following the systemic administration of PQ (5 mg/kg) (A) Initial 3 hr average NO response recorded following injection (5 mg/kg PQ) (B) The average NO response recorded over a continuous period of 72 hrs following injection (5 mg/kg PQ). Data represented as a percentage change  $\pm$  SEM. SEM represented by dashed line (black).

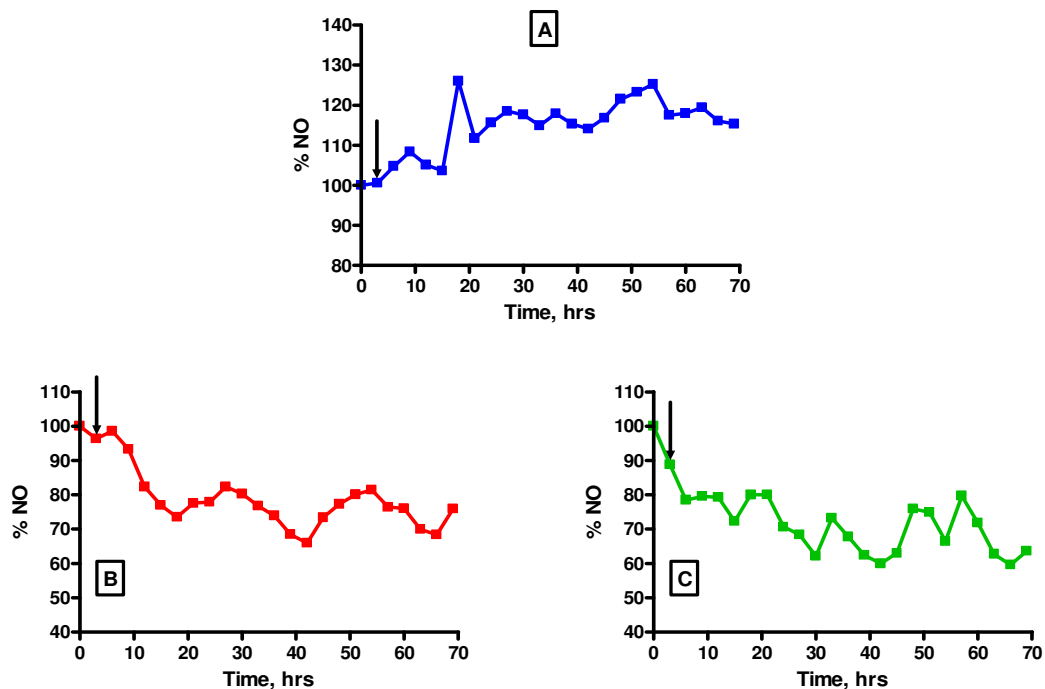
Arrow indicates the injection of PQ.

Figure 8.4.2.1 represents the average NO response ( $n = 9$ , 3 animals) recorded in the NA following the administration of a low dose of PQ (5 mg/kg). The animals included in the data presented in Figure 8.4.2.1 were not previously exposed to PQ. Figure 8.4.2.1 (A) demonstrates the average NO response monitored for a period of 3 hrs immediately following the systemic administration of PQ (5 mg/kg). It is clear that the NO response remains close to baseline levels for the duration of this initial recording period (3 hrs), it was therefore necessary to examine the NO response over an extended time-frame following PQ exposure and this extended NO response (72 hrs) can be seen in Figure 8.4.2.1 (B).

Shimizu *et al.* and Hara *et al.* have previously demonstrated a lasting increase in indirect markers of NO production following PQ exposure as determined by a microdialysis method (Hara *et al.*, 2001; Shimizu *et al.*, 2003a). The effect of systemic PQ administration on the direct electrochemical detection of NO levels in the brain of freely-moving animals has not previously been reported. Therefore it was deemed necessary to investigate the long-term influence (72 hrs) of PQ administration on the level of NO monitored in the NA. It is apparent that a slight deviation in the average NO response above and below baseline levels occurred for a period of 72 hrs following the systemic administration of PQ (5 mg/kg) as can be seen in Figure 8.4.2.1 (B).

In this case it was not possible to definitively measure a maximum NO current response following the injection of 5 mg/kg PQ due to conflicting NO responses mediated by administration of this low dose of toxin (5 mg/kg) as presented in Figure 8.4.2.1. AUC analysis was utilised to determine the overall effect of 5 mg/kg PQ on the NO current response monitored in the NA. The systemic administration of 5 mg/kg PQ resulted in an AUC value of  $-15.0 \pm 36.7$  pA/hr ( $n = 9$ ) and this value was not significantly different ( $P > 0.05$ ) to the control experiments outlined in Section 8.4.1. The pre-injection ( $458.1 \pm 66.6$  pA,  $n = 9$ ) and post-injection baseline values ( $429.3 \pm 57.0$  pA,  $n = 9$ ) were not significantly different ( $P > 0.05$ ).

It is evident from Figure 8.4.2.1 that a deviation from basal levels of NO does occur following the administration of 5 mg/kg PQ. Although no significant difference ( $P > 0.05$ ) was observed between the NO response following administration of this low dose of PQ and the corresponding control data, the variation in the average NO response as represented by the dashed line (black) is clear in Figure 8.4.2.1 and is due to inter-animal variability. Conflicting deviations above and below baseline levels of NO were observed between the different animals utilised in this study following the administration of this low dose of PQ (5 mg/kg) as presented in Figure 8.4.2.2.



**Figure 8.4.2.2** Typical examples of the NO response recorded in the NA of independent animals over a continuous period of 72 hrs following systemic administration of PQ (5 mg/kg). (A) Animal 1 (B) Animal 2 and (C) Animal 3.

It is clear from Figure 8.4.2.2 that the systemic administration of 5 mg/kg PQ leads to an increase in NO response in Animal 1 (A) and a contrasting decrease in Animal 2 (B) and Animal 3 (C). This discrepancy may reflect the susceptibility of a given animal to the influence of PQ as an oxidative stressor. The development of PD has been postulated to be partially as a consequence of an underlying weakened energy metabolism (Wellstead & Cloutier, 2011). This pre-condition may be a considerable influence on the subsequent susceptibility of neurons to progressive degeneration which is a pathological characteristic of PD.

In relation to the studies presented in this section this factor may lead to a variation in the vulnerability of a given animal to the subsequent PQ mediated development of oxidative/nitrosative stress. Additionally, this process may partly replicate the variable underlying susceptibility of individuals to the development of PD due to advancing age and exposure to various environmental toxins (Lotharius & Brundin, 2002; Tanner *et*

*al.*, 2011; Wirdefeldt *et al.*, 2011). Therefore these results further support the use of PQ to develop a suitable animal model of PD. The effect of the low administered dose of PQ (5 mg/kg) utilised in these sets of experiments, may be efficiently regulated by the robust antioxidant network which maintains redox homeostasis in the intact living brain. The effect of a higher administered dose of PQ (30 mg/kg) on the level of NO in the NA is shown in Figure 8.4.2.2.

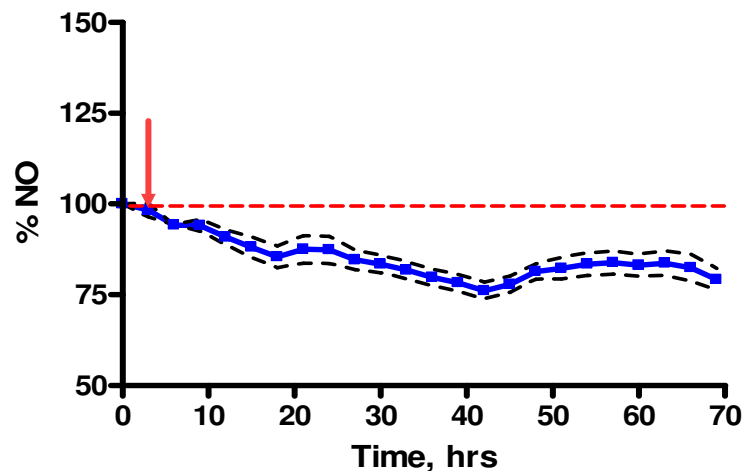


**Figure 8.4.2.3** The average NO response recorded in the NA over a continuous period of 72 hrs following systemic administration of PQ (30 mg/kg). Data represented as a percentage change  $\pm$  SEM. SEM represented by dashed line (black). Arrow indicates the injection of PQ.

Figure 8.4.2.3 represents the average NO response ( $n = 13$ , 5 animals) recorded in the NA following the administration of a relatively higher dose of PQ (30 mg/kg). The animals included in the data presented in Figure 8.4.2.3 were naive to previous PQ exposure. Following the systemic administration of PQ (30 mg/kg) a clear decrease in NO levels below baseline levels (dashed line) was evident as can be seen in Figure 8.4.3.

AUC analysis was utilised to determine the overall effect of 30 mg/kg PQ systemic administration on the NO current response monitored in the NA. It was possible to determine a maximum current change following the administration of 30 mg/kg PQ due to the recorded reproducible distinct decrease in NO. The maximum NO response was achieved within  $47.1 \pm 2.1$  hrs ( $n = 13$ ) following the injection and a return to a stable

baseline level was observed  $62.5 \pm 1.0$  hrs ( $n = 13$ ) subsequently. The pre-injection ( $482.9 \pm 62.6$  pA,  $n = 13$ ) and post-injection baseline values ( $423.5 \pm 44.0$  pA,  $n = 13$ ) were not significantly different ( $P > 0.05$ ). However, it is clear from Figure 8.4.3 that the level of NO fails to completely return to pre-injection baseline levels for the duration of the recording period.

The systemic administration of 30 mg/kg PQ resulted in an AUC value of  $-193.9 \pm 43.4$  pA/hr ( $n = 9$ ). This value was not significantly different ( $P > 0.05$ ) to the control experiments outlined in Section 8.4.1. However a significant difference ( $P < 0.01, **$ ) was observed between the AUC value calculated for the 30 mg/kg and 5 mg/kg PQ NO response. No significant difference ( $P > 0.05$ ) was observed between the maximum response time and subsequent return to baseline levels following the administration of 5 mg/kg PQ and the relatively higher administered dose (30 mg/kg PQ). It is clear that PQ exhibits its effect on NO levels in the neuronal environment in a dose dependent manner. It has previously been demonstrated by Corasaniti *et al.* that the systemic administration of a moderate and high dose of PQ in rats (20 mg/kg and 100 mg/kg) leads to induced tremors, rearing and occasional wet-dog shakes. Whereas a relatively low dose of PQ failed to replicate these behavioural abnormalities (Corasaniti *et al.*, 1998).

Following systemic administration of 30 mg/kg PQ a pronounced attenuated decrease in NO levels below baseline levels (dashed line) was apparent for a continuous period of 72 hrs as can be seen in Figure 8.4.3. This response contrasts greatly to that seen following the systemic administration of a relatively low dose of PQ, i.e. 5 mg/kg (see Figure 8.4.2). The highly reproducible marked decrease in NO levels following the systemic administration of 30 mg/kg PQ may be explained by the diaphorase activity of the NOS enzyme. NOS is an example of a cellular diaphorase which are a class of enzymes that can transfer electrons from NADPH to small molecules such as PQ (Day *et al.*, 1999; Dinis-Oliveira *et al.*, 2006).

It has previously been demonstrated that NOS can preferentially produce  $O_2^{\cdot-}$  upon exposure to PQ by a process known as ‘uncoupling’ of the NOS enzyme (Day *et al.*, 1999; Margolis *et al.*, 2000). NOS may transfer electrons to PQ at the reductase domain

of the enzyme which leads to the increased production of O<sub>2</sub><sup>-</sup> at the expense of NO from NOS (Margolis *et al.*, 2000). Day *et al.* have previously demonstrated a PQ related decrease in indirect markers of NO production from NOS *in-vitro* and a corresponding increase in NOS mediated O<sub>2</sub><sup>-</sup> production markers (Day *et al.*, 1999). Additionally, NOS ‘uncoupling’ was more pronounced upon increasing the concentration of PQ (Day *et al.*, 1999). Margolis *et al.* have also demonstrated the proportional concentration dependent PQ induced preferential production of O<sub>2</sub><sup>-</sup> over NO from NOS *in-vitro* (Margolis *et al.*, 2000). The ‘uncoupling’ of NOS would explain the highly reproducible distinct depletion in NO levels following the systemic administration of 30 mg/kg PQ as presented in Figure 8.4.3.

| PQ       | Current change (pA) | Change (%)  | Conc. change (nM) | Max response (hrs) | Return (hrs) | AUC (pA/hr)   | Pre-injection baseline (pA) | Post-injection baseline (pA) | n  |
|----------|---------------------|-------------|-------------------|--------------------|--------------|---------------|-----------------------------|------------------------------|----|
| 5 mg/kg  | n/a                 | n/a         | n/a               | n/a                | n/a          | -15.0 ± 36.7  | 458.1 ± 66.6                | 429.3 ± 57.0                 | 9  |
| 30 mg/kg | -349.9 ± 80.2       | -22.7 ± 5.2 | -229.0 ± 52.5     | 47.1 ± 2.1         | 62.5 ± 1.0   | -193.9 ± 43.4 | 482.9 ± 62.6                | 423.5 ± 44.0                 | 13 |

Table 8.4.1: Summary of the NO data recorded following PQ administration. With n = the number of sensors implanted in the NA of 3 animals (5 mg/kg) and 5 animals (30 mg/kg).

#### 8.4.3 Preliminary PQ dose response (NO and H<sub>2</sub>O<sub>2</sub>)

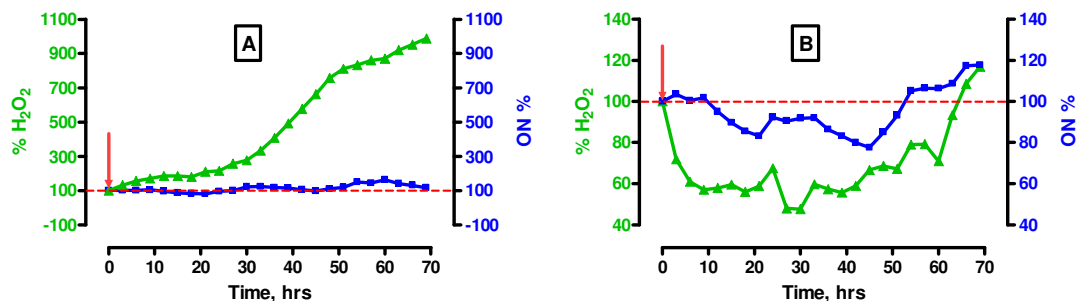


Figure 8.4.4 The dual NO (■; blue) and H<sub>2</sub>O<sub>2</sub> (▲; green) response recorded in the NA over a continuous period of 72 hrs. Following the systemic administration of (A) PQ (5 mg/kg) and (B) PQ (30 mg/kg). Data represented as a percentage change ± SEM. Arrow indicates the injection of PQ.

The results presented in this section demonstrate the preliminary simultaneous long-term detection of H<sub>2</sub>O<sub>2</sub> and NO in the same animal following the administration of PQ. The animals included in the data presented in Figure 8.4.4 were naive to previous PQ exposure. Figure 8.4.4(A) demonstrates the dual NO and H<sub>2</sub>O<sub>2</sub> response in the NA following the systemic injection of a low dose of PQ (5 mg/kg). A slight deviation in baseline levels of NO was observed following this injection and a large attenuated increase in H<sub>2</sub>O<sub>2</sub> can be seen following the administration of 5 mg/kg PQ. It is possible that this relatively low dose of PQ is not sufficient to induce ‘uncoupling’ of the NOS enzyme as discussed in Section 8.4.2. Therefore the level of NO remains largely unaffected following the administration of this dose of PQ. It has previously been demonstrated that the redox cycling of PQ produces O<sub>2</sub><sup>•-</sup> (Dinis-Oliveira *et al.*, 2006; Bove & Perier, 2012). As O<sub>2</sub><sup>•-</sup> is the main source of H<sub>2</sub>O<sub>2</sub> production in the neuronal environment (see Section 2.10.2). The redox cycling of PQ may explain the large increase in H<sub>2</sub>O<sub>2</sub> response following the injection of PQ. An increased *in-vitro* mitochondrial production of H<sub>2</sub>O<sub>2</sub> has previously been shown following exposure to PQ as determined by flourometric methods *in-vitro* (Cocheme & Murphy, 2008).

The preliminary simultaneous detection of NO and H<sub>2</sub>O<sub>2</sub> in the NA following the systemic administration of a moderate dose of PQ (30 mg/kg) is presented in Figure 8.4.4(B). As previously demonstrated in Section 8.4.2 a protracted distinct decrease in NO below baseline levels was observed following the administration of 30 mg/kg PQ which may be attributed to the diaphorase activity of the NOS enzyme as discussed in Section 8.4.2. The large decrease in H<sub>2</sub>O<sub>2</sub> levels may reflect the formation of <sup>•</sup>OH from H<sub>2</sub>O<sub>2</sub> in a pro-oxidant environment (see Section 2.10.2). It must be stated at this point that the experiments outlined in this section are preliminary, however, the future simultaneous detection of H<sub>2</sub>O<sub>2</sub>/NO in a paraquat model of PD may provide an insight into the independent role of oxidative/nitrosative stress in the process of PQ mediated dopaminergic neurodegeneration which is characteristic of PD.

### 8.5 PQ additive dose response (NO)

This section demonstrates the effect of an additive dose sequence of PQ administration on the NO sensor response implanted in the NA. The aim of this section is to investigate the effect of systemic pre-administration of PQ (10 mg/kg) followed by the administration of a higher dose of PQ (20 mg/kg) 72 hrs subsequently, on the NO sensor response while implanted in the brain of freely-moving animals.

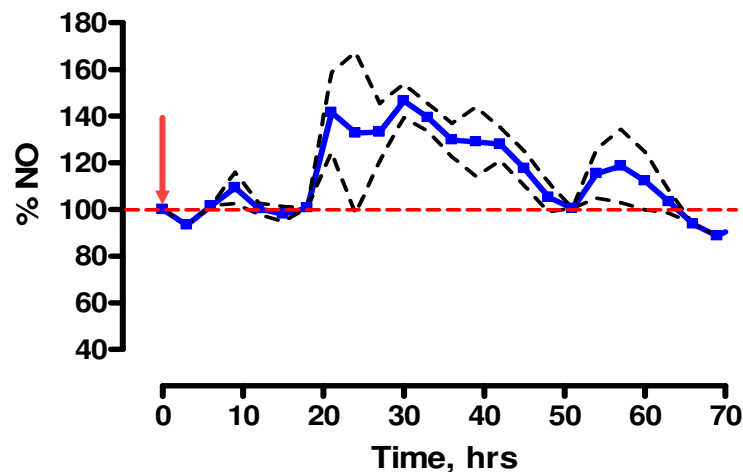


**Figure 8.5.1** The average NO response recorded in the NA over a continuous period of 72 hrs following systemic administration of PQ (20 mg/kg) with pre-administration of PQ (10 mg/kg). Data represented as a percentage change  $\pm$  SEM. SEM represented by dashed line (black). Arrow indicates the injection of PQ (20 mg/kg).

This section investigates the effect of systemic pre-administration of PQ (10 mg/kg) followed by the systemic injection of a higher dose of PQ (20 mg/kg) on the NO response ( $n = 2$ , 2 animals) monitored in the NA. Following systemic administration of PQ (20 mg/kg) a clear increase above basal levels of NO (dashed line) was apparent as can be seen in Figure 8.5.1. The calculated AUC value for the administration of PQ (20 mg/kg) following pre-treatment with a lower dose of PQ (10 mg/kg) was  $58.6 \pm 27.6$  pA/hr ( $n = 2$ ). The maximum NO response was achieved within  $34.5 \pm 4.5$  hrs ( $n = 2$ ) and a return to pre-injection basal levels was observed  $61.5 \pm 1.5$  hrs ( $n = 2$ ) subsequently. The pre-injection ( $392.0 \pm 41.7$  pA,  $n = 2$ ) and post-injection baseline values ( $409.3 \pm 59.5$  pA,  $n = 2$ ) were not significantly different ( $P > 0.05$ ).

The AUC value calculated from this additive dose response was not significantly different ( $P > 0.05$ ) to the AUC value determined for the control experiments outlined in Section 8.4.1. However, an increase above baseline levels of NO was observed following the additive PQ dose response (see Figure 8.5.1). Following on from this pilot study the effect of the repetitive administration of a moderate dose of PQ (30 mg/kg) on NO levels in the NA was examined as shown in Section 8.6.

Shimizu *et al.* have previously demonstrated that the local administration of PQ results in a transient release of glutamate in the striatum (Shimizu *et al.*, 2003a). Additionally, this research group has shown a concentration dependent elevated level of indirect markers of striatal NO production following the local addition of PQ (Shimizu *et al.*, 2003a). It is known that activation of NMDA receptors which are abundantly present in the NA (Monaghan & Cotman, 1985), by glutamate or by other agonists results in an intracellular influx of Ca<sup>2+</sup> and initiates the process of excitotoxicity (Garthwaite, 2008).

This glutamate mediated Ca<sup>2+</sup> influx may then activate the constitutive forms of NOS (eNOS and nNOS) and lead to the production of NO (Alderton *et al.*, 2001; Saulskaya & Fofonova, 2006). It is plausible in this case that the diaphorase activity of NOS as previously discussed is overcome by the PQ stimulated glutamatergic production of NO thereby leading to an increase in NO. This process would explain the substantial increase in NO levels following the administration of 20 mg/kg with the pre-treatment of a lower dose of PQ (10 mg/kg). The subsequent fall in NO levels may be attributed to the known interaction between NO and O<sub>2</sub><sup>-</sup> in a pro-oxidant environment induced in this case by PQ which leads to the production of the highly toxic RNS peroxynitrite (ONOO<sup>-</sup>) (Calabrese *et al.*, 2007; Ramalingam & Kim, 2012).

In order to further examine the PQ stimulated production of NO as seen in Figure 8.5.1 a moderate dose of PQ (30 mg/kg) was administered to the animal repetitively in a sequential manner and the results are presented in Section 8.6.

## 8.6 PQ repetitive dose response (NO)

This section examines the effect of the repeated administration of a moderate dose of PQ (30 mg/kg) on the NO sensor response monitored in the NA. Three systemic administrations of PQ (30 mg/kg) were administered to each animal and were interspersed with a 72 hr recording period. The animals included in the data presented in Figure 8.5.1 were naive to PQ exposure prior to initiation of these experiments. It has previously been demonstrated that the repeated systemic administration of a moderate dose of PQ is necessary to replicate the characteristics of PD in an animal model; including dopaminergic cell degeneration and the production of increased markers of oxidative/nitrosative stress (McCormack *et al.*, 2005; McCormack *et al.*, 2006).

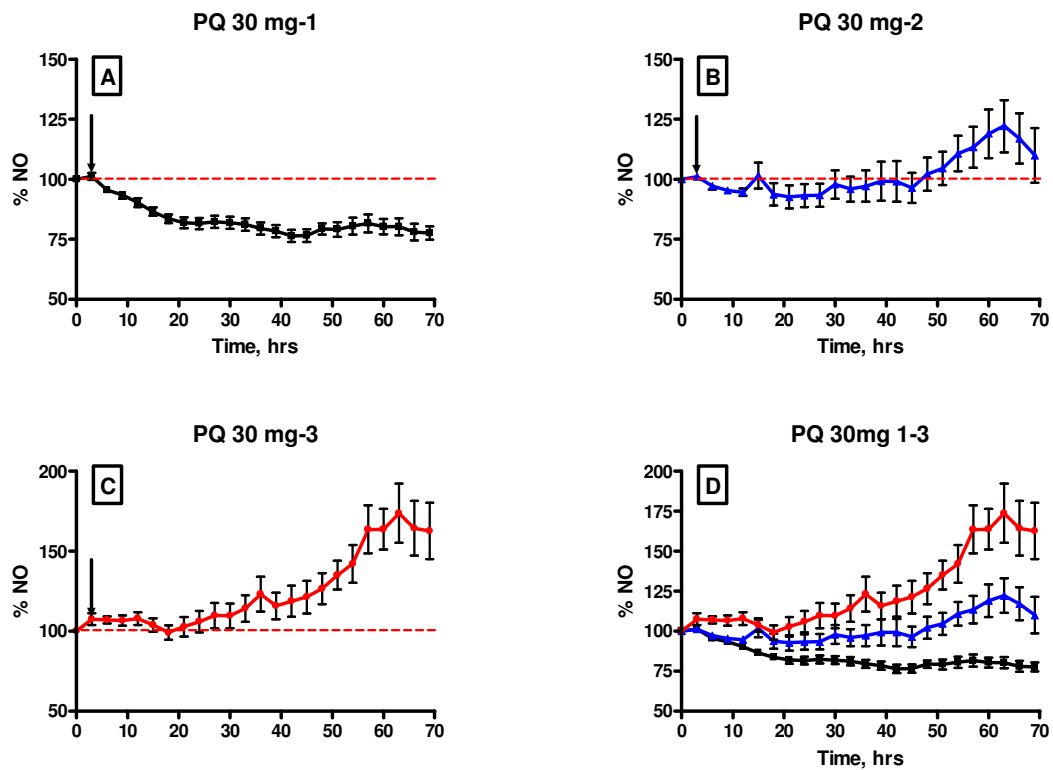


**Figure 8.6.1** The average NO response recorded in the NA over a continuous period of 72 hrs following the systemic administration of PQ (30 mg/kg) (A) 1<sup>st</sup> injection (B) 2<sup>nd</sup> injection and (C) 3<sup>rd</sup> (D) Overlay of all 3 injections of PQ (30 mg/kg). Data represented as a percentage change  $\pm$  SEM.

Arrow indicates the injection of PQ (30 mg/kg).

Figure 8.6.1(A) demonstrates the NO response monitored in the NA following the initial systemic administration of a moderate dose of PQ (30 mg/kg). As previously seen in Section 8.4.2 this moderate dose of PQ is sufficient to induce a prolonged decrease in NO levels for a continuous period of 72 hrs. The maximum NO response ( $-339.0 \pm 71.2$  pA,  $n = 10$ ) was achieved within  $47.1 \pm 4.1$  hrs ( $n = 10$ ) and a return to pre-injection basal levels was observed  $65.7 \pm 1.0$  hrs ( $n = 10$ ) subsequently. The pre-injection ( $1370.4 \pm 269$  pA,  $n = 10$ ) and post-injection baseline values ( $1043.9 \pm 202.5$  pA,  $n = 10$ ) were not significantly different ( $P > 0.05$ ). However it is clear from Figure 8.5.1 that the NO response does not fully return to pre-injection baseline NO levels following the injection of this initial dose of PQ (30 mg/kg).

The systemic administration of this initial moderate dose of toxin (30 mg/kg PQ) resulted in an AUC value of  $-236.8 \pm 55.2$  pA/hr ( $n = 10$ ). As previously discussed this marked decrease in NO levels detected following the initial administration of PQ (30 mg/kg) may be explained by the diaphorase activity of the NOS enzyme. PQ exposure results in ‘uncoupling’ of the NOS enzyme in a dose dependent manner (Day *et al.*, 1999; Margolis *et al.*, 2000; Moran *et al.*, 2010). Therefore, following the initial exposure to PQ (30 mg/kg) as demonstrated in Figure 8.6.1(A)  $O_2^{\cdot-}$  may be preferentially produced by the NOS enzyme at the expense of the production of NO leading to a decrease in NO monitored by the sensor implanted in the NA.

Following the second administration of PQ (30 mg/kg) as presented in 8.6.1(B) the NO levels initially remain close to pre-injection baseline levels. A maximum increase in NO levels ( $134.5 \pm 117.2$  pA,  $n = 10$ ) was then observed  $51.0 \pm 4.2$  hrs ( $n = 10$ ) following this injection which corresponds to a  $12.7 \pm 11.1$  %,  $n = 10$  change. The AUC value determined for this administration of PQ was  $-29.0 \pm 51.8$  pA/hr ( $n = 10$ ). No significant difference ( $P > 0.05$ ) was observed between this AUC response and the corresponding value obtained from the control data presented in Figure 8.4.1. However, a significant difference ( $P < 0.05, *$ ) was observed between the AUC value determined between the initial administration of PQ (30 mg/kg) and that following the second administration of PQ (30 mg/kg). It can be seen in Figure 8.6.1(B) that a delayed increase in the level of brain NO occurs following the second administration of 30 mg/kg PQ. It is possible that

this second injection (30 mg/kg PQ) leads to a stimulated glutamate efflux and a subsequent increase in the level of NO above baseline levels due to an influx of intracellular Ca<sup>2+</sup> which may cause an increase in brain NO as previously discussed in Section 8.4.3 (Alderton *et al.*, 2001; Shimizu *et al.*, 2003a).

The second administration of PQ was not sufficient to lead to an uncontrolled production of NO however. The level of NO returns towards pre-injection baseline levels prior to the third injection of 30 mg/kg PQ. This may reflect the ability of the opposing anti-oxidant network to dampen the production of ROS/RNS (see Section 2.10). The subsequent decline in NO levels following the transient increase in NO as seen in Figure 8.6.1(B) may also be explained by the interaction between NO and O<sub>2</sub><sup>-</sup> in a pro-oxidant environment which leads to the formation of the highly toxic nitrogen species ONOO<sup>-</sup> (Calabrese *et al.*, 2007; Ramalingam & Kim, 2012). It has been postulated that NO produced from the action of PQ may diffuse to dopaminergic nerve terminals where it can exhibit deleterious effects primarily by the formation of the highly toxic RNS, ONOO<sup>-</sup> and subsequently lead to dopamine release (Shimizu *et al.*, 2003a; Moran *et al.*, 2010).

Following the administration of the third moderate dose of PQ (30 mg/kg) as shown in Figure 8.6.1(C), an elevated production of NO can be seen which is substantially larger than that observed following the initial and secondary dose of systemic PQ administration (30 mg/kg). A prolonged attenuated increase in the level of NO was recorded which remained above baseline levels for the duration of the recording period. The AUC value determined for this third administration of PQ (30 mg/kg) was 237.6 ± 74.8 pA/hr (n = 10). The maximum NO current response (894.6 ± 253.6 pA, n = 10) following the administration of the third dose of PQ was achieved within 53.7 ± 4.3 hrs (n = 10) and a return to pre-injection basal levels was observed 62.4 ± 2.5 hrs (n = 10) following this administration. The pre-injection (988.6 ± 136.6 pA, n = 10) and post-injection baseline values (1648.5 ± 307.4 pA, n = 10) were not significantly different (*P* > 0.05), however it is clear from Figure 8.6.1(C) that the NO response fails to return completely to pre-injection baseline levels. It is possible that the proposed glutamatergic pathway of NO production due to repetitive moderate PQ administration suppresses the

diaphorase activity of the NOS enzyme and the opposing anti-oxidant network which leads to an unrecoverable elevation of brain NO levels (Shimizu *et al.*, 2003a; Dinis-Oliveira *et al.*, 2006; Moran *et al.*, 2010). No significant difference ( $P > 0.05$ ) was observed between the maximum response time and subsequent return to baseline levels following the administration of each systemically administered dose of 30 mg/kg PQ. A summary of the main results discussed in this section is provided for in Table 8.6.1.

| <b>PQ<br/>(30<br/>mg/kg)</b> | <b>Current<br/>change<br/>(pA)</b> | <b>Change<br/>(%)</b> | <b>Conc.<br/>change<br/>(nM)</b> | <b>Max<br/>response<br/>(hrs)</b> | <b>Return<br/>(hrs)</b> | <b>AUC<br/>(pA/hr)</b> | <b>Pre-<br/>injection<br/>baseline<br/>(pA)</b> | <b>Post-<br/>injection<br/>baseline<br/>(pA)</b> |
|------------------------------|------------------------------------|-----------------------|----------------------------------|-----------------------------------|-------------------------|------------------------|---|--|
| <b>1<sup>st</sup></b>        | -339.0<br>± 71.2                   | -19.2 ±<br>4.0        | -221.8<br>± 46.6                 | 47.1 ±<br>4.1                     | 65.7 ±<br>1.0           | -236.8<br>± 55.2       | 1370.4<br>± 269                                 | 1043.9<br>± 202.5                                |
| <b>2<sup>nd</sup></b>        | 134.5 ±<br>117.2                   | 12.7 ±<br>11.1        | 88.0 ±<br>76.7                   | 51.0 ±<br>4.2                     | 65.1 ±<br>1.1           | -29.0 ±<br>51.8        | 1059.6<br>± 208.9                               | 1091.9<br>± 162.7                                |
| <b>3<sup>rd</sup></b>        | 894.6 ±<br>253.6                   | 90.5 ±<br>25.6        | 588.5 ±<br>166.8                 | 53.7 ±<br>4.3                     | 62.4 ±<br>2.5           | 237.6<br>± 74.8        | 988.6<br>± 136.6                                | 1648.5<br>± 307.4                                |

**Table 8.6.1: Summary of the NO data recorded following the repetitive administration of 30 mg/kg PQ. With n = 10 sensors implanted in the NA of 3 animals in each case.**

### 8.7 Preliminary PQ ascending dose response (NO and H<sub>2</sub>O<sub>2</sub>)

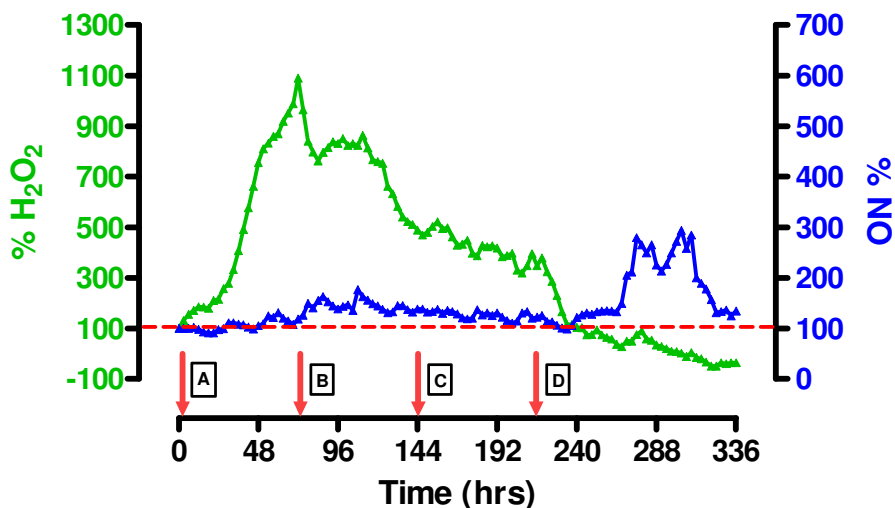


**Figure 8.7.1** The dual NO (■; blue) and H<sub>2</sub>O<sub>2</sub> (▲; green) response recorded in the NA over a continuous period of 336 hrs. Following the systemic administration of (A) PQ (5 mg/kg), (B) PQ (10 mg/kg), (C) PQ (20 mg/kg) and (D) PQ (30mg/kg). Data represented as a percentage change ± SEM. Arrow indicates the injection of PQ.

This section demonstrates the preliminary simultaneous detection of NO and H<sub>2</sub>O<sub>2</sub> following the repetitive systemic administration of paraquat (PQ) in a sequential manner of ascending doses. A PQ induced animal model of PD has previously been successfully demonstrated by McCormack *et al.* following the repetitive systemic administration of a moderate dose of PQ (McCormack *et al.*, 2005; McCormack *et al.*, 2006). The purpose of this section is to investigate the effect of an ascending administered level of PQ on the preliminary simultaneous measurement of NO and H<sub>2</sub>O<sub>2</sub> in the freely-moving animal.

An initial low dose of PQ was injected (s.c.) as represented in Figure 8.7.1(A). This dose of PQ was sufficient to initiate a marked increase in the production of H<sub>2</sub>O<sub>2</sub> in the NA. Following the administration of this initial dose of PQ the level of PQ administered was increased sequentially from 10 mg/kg (Figure 8.7.1(B)) to 20 mg/kg Figure 8.7.1(C) and finally 30 mg/kg Figure 8.7.1(D) with an allowed intervening period of 72 hrs in each case and a subsequent 120 hr recording period following cessation of the ascending PQ

dose response. The initial substantial elevation of H<sub>2</sub>O<sub>2</sub> may be explained by the redox cycling of PQ which is known to produce O<sub>2</sub><sup>•-</sup>, the main source of H<sub>2</sub>O<sub>2</sub> in the neuronal environment (see Section 2.10.2). As the level of H<sub>2</sub>O<sub>2</sub> remains elevated the NO response remains close to PQ naive pre-injection baseline levels. It has previously been demonstrated in Section 8.4.2 that a relatively low dose of PQ is not sufficient to induce an overall substantial change in the level of NO.

As the ascending dose response progresses a deviation above pre-injection baseline levels of NO can be seen following the administration of 10 and 20 mg/kg PQ which increases after the injection of 30 mg/kg PQ. A corresponding decrease in the level of H<sub>2</sub>O<sub>2</sub> was observed following the fourth and final injection (30 mg/kg PQ). The opposite correlation between NO and H<sub>2</sub>O<sub>2</sub> levels seen towards the end of the ascending PQ dose response may be explained by the interaction between O<sub>2</sub><sup>•-</sup> and NO which leads to ONOO<sup>-</sup> production (Calabrese *et al.*, 2007; Ramalingam & Kim, 2012). This process may lead to an insufficient availability of O<sub>2</sub><sup>•-</sup> which is required for the formation of H<sub>2</sub>O<sub>2</sub> (see Section 2.10). It is important to state at this point that these results are preliminary, however, they do suggest a potential role for the simultaneous detection of NO and H<sub>2</sub>O<sub>2</sub> in a PQ mediated animal model of PD in order to further knowledge surrounding the role of oxidative/nitrosative stress in the development of PD.

## 8.7 Behavioural observations

Brooks *et al.* have previously demonstrated the development of a neurobehavioral syndrome in freely-moving rodents following the repeated systemic administration of a moderate dose of PQ (Brooks *et al.*, 1999). This behavioural syndrome was primarily characterised by a PQ induced reduction in locomotor activity which the authors attribute to PQ mediated dopaminergic cell degeneration (Brooks *et al.*, 1999).

Additionally, Hara *et al.* have reported the appearance of shaking behaviour known as wet dog shakes (WDS) in a dose dependent manner in rodents following the systemic administration of PQ. Furthermore the appearance of WDS was ameliorated by the pre-administration of NOS inhibitors which suggests that NO may be involved in the development of this PQ related behavioural characteristic (Hara *et al.*, 2001). However

the correlation between WDS and NO production could not be substantiated by this research group, the authors suggest that this finding may be due to the insufficient sensitivity of the microdialysis NO detection method utilised (Hara *et al.*, 2001).

It has previously been demonstrated by Corasaniti *et al.* that the systemic administration of a moderate and high dose of PQ in rats (20 mg/kg and 100 mg/kg) leads to induced tremors, rearing, salivation and occasional WDS. It was found that a relatively low dose of PQ (5 mg/kg) was not sufficient to produce these same behavioural abnormalities (Corasaniti *et al.*, 1998). The abnormal motor characteristics previously reported in PQ treated rodents demonstrated by several research groups supports the use of PQ in an animal model of PD.

As seen previously in PQ treated rodents abnormal behavioural characteristics were noted in the subjects utilised in these sets of experiments including temporary tremors and a reduction in general movement. In the absence of detailed behavioural testing the most noticeable change in behaviour of the subjects utilised in this study occurred following the administration of a relatively high dose of PQ (30 mg/kg). The injection of a low dose of PQ (5 mg/kg) did not elicit any gross behavioural changes in all animals utilised in this study as noted previously by Corasaniti *et al.* (Corasaniti *et al.*, 1998). The administration of 30 mg/kg PQ elicited occasional shaking behaviour, piloerection and transient tremors in the subjects and the repetitive administration of this dose of PQ (30 mg/kg) was sufficient to increase this abnormal motor behaviour. Additionally the PQ mediated change in behavioural characteristics were prominent within a few hours of the injection itself.

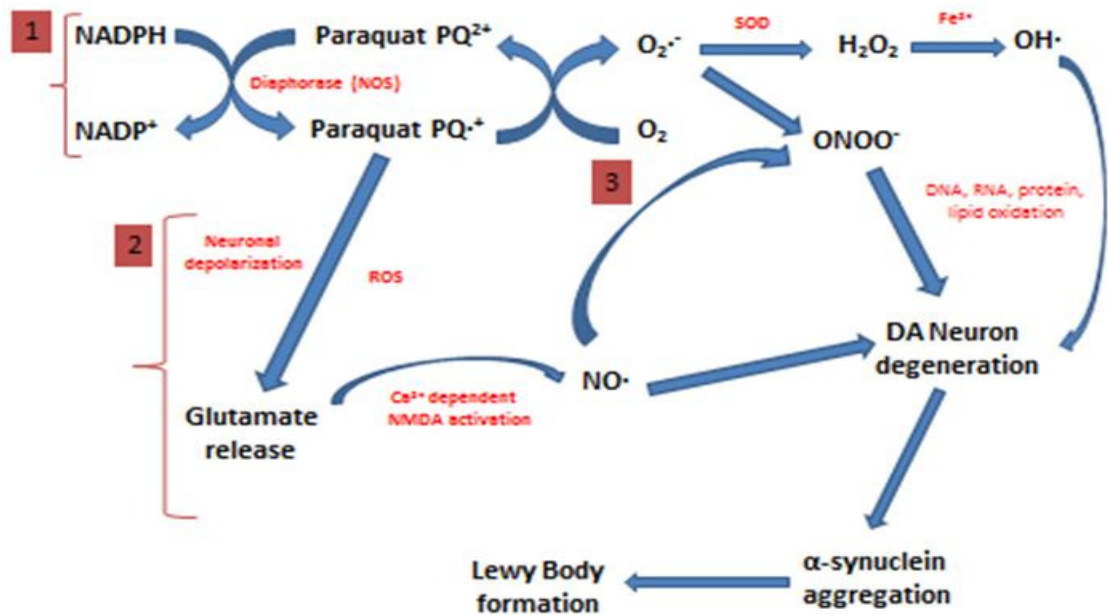
8.8 PQ mediated toxicity *in-vivo*

Figure 8.8.1 Proposed neurochemical pathway of PQ mediated toxicity *in-vivo*.  
(Schematic courtesy of Dr. Niall Finnerty).

Figure 8.8.1 demonstrates the proposed mechanism of PQ mediated neuronal toxicity as studied in this chapter. It has previously been proposed that the redox cycling properties of PQ facilitates direct MTdys via inhibition of Complex I of the ETC leading to the production of superoxide  $O_2^{\cdot-}$  (Castello *et al.*, 2007; Cocheme & Murphy, 2008; Czerniczyniec *et al.*, 2011). Additionally redox cycling of PQ may be mediated by cellular diaphorases which are enzymes that transfer electrons from NADPH to small molecules such as PQ (Day *et al.*, 1999; Purisai *et al.*, 2007; Berry *et al.*, 2010). NOS is an example of a cellular diaphorase (Day *et al.*, 1999). PQ may be reduced in the cytosol in this manner to form a PQ monocation free radical ( $PQ^{\cdot+}$ ). Subsequently  $PQ^{\cdot+}$  is rapidly re-oxidised in the presence of molecular oxygen leading to the production of  $O_2^{\cdot-}$  and reformed PQ which initiates the processes which lead to oxidative/nitrosative stress (see Figure 8.8.1[1]) (Dinis-Oliveira *et al.*, 2006; Berry *et al.*, 2010).

It has previously been demonstrated that NOS can preferentially produce O<sub>2</sub><sup>•-</sup> upon exposure to PQ and is termed ‘uncoupling’ of the NOS enzyme (Day *et al.*, 1999; Margolis *et al.*, 2000). NOS may transfer electrons to PQ at the reductase domain of the enzyme resulting in the increased production of O<sub>2</sub><sup>•-</sup> at the expense of NO from NOS (Margolis *et al.*, 2000). The proposed ‘uncoupling’ of the NOS enzyme due to PQ exposure and the resulting decrease in brain NO levels is supported by the response detected by the NO sensor implanted in the NA following the administration of 30 mg/kg PQ (see Section 8.4.2 and Figure 8.6.1(A)). The production of O<sub>2</sub><sup>•-</sup> leads to the formation of the secondary reactive oxygen species (ROS), H<sub>2</sub>O<sub>2</sub>, which is primarily facilitated by the superoxide dismutase enzyme (SOD) (see Section 2.10). It has previously been demonstrated via indirect detection methods that the systemic injection of PQ leads to the production of H<sub>2</sub>O<sub>2</sub> *in-vitro* and in *ex-vivo* brain preparations (Cocheme & Murphy, 2008; Czerniczyniec *et al.*, 2011). The preliminary detection of elevated H<sub>2</sub>O<sub>2</sub> levels following the administration of a relatively low dose of PQ (5 mg/kg) is demonstrated in Section 8.4.3.

The interaction between NO and O<sub>2</sub><sup>•-</sup> in a PQ mediated pro-oxidant environment leads to the production of the highly toxic RNS; ONOO<sup>-</sup> as represented in Figure 8.8.1[3] (see Section 2.10.3). The proposed glutamatergic pathway of NO production due to PQ exposure is represented in Figure 8.8.1[2]. As previously discussed the systemic administration of PQ has been shown to lead to a transient increase in brain glutamate levels (Shimizu *et al.*, 2003a). Glutamate mediated activation of non-NMDA receptors leads to the hyperactivation of NMDA receptor channels and subsequently an intracellular influx of Ca<sup>2+</sup> (Shimizu *et al.*, 2003a; Garthwaite, 2008; Moran *et al.*, 2010). This glutamate mediated Ca<sup>2+</sup> influx may then activate the constitutive forms of NOS (eNOS and nNOS) and lead to the production of NO (Alderton *et al.*, 2001; Saulskaya & Fofonova, 2006). It has previously been postulated that NO produced from this PQ induced glutamatergic pathway diffuses to dopaminergic terminals and leads to MTdys primarily via interaction between NO and O<sub>2</sub><sup>•-</sup> and the subsequent formation of the highly toxic species ONOO<sup>-</sup> (Shimizu *et al.*, 2003a; Moran *et al.*, 2010) This process may explain the degeneration of dopaminergic neurons following the systemic

administration of PQ as previously demonstrated by McCormack *et al.* in a rodent model (McCormack *et al.*, 2005; McCormack *et al.*, 2006). In addition the prolonged attenuated production of NO recorded in the NA following the repetitive administration of PQ may support this hypothesis (see Figure 8.6.1(A)). Additionally PQ mediated production of  $\cdot\text{OH}$  from H<sub>2</sub>O<sub>2</sub> (see Section 2.10.2) among other ROS/RNS due to PQ exposure as represented in Figure 8.8.1, may lead to damage to cell structures, DNA and lipids (Valko *et al.*, 2007).

It has previously been demonstrated that the systemic administration of PQ leads to the up-regulation of the  $\alpha$ -synuclein protein which is the main constituent of the PD related intracytoplasmic inclusions commonly known as 'Lewy bodies' (Manning-Bog *et al.*, 2002). It has been postulated that the development of oxidative/nitrosative stress may contribute to  $\alpha$ -synuclein accumulation by altering the protein itself or by the interruption of processes involved in protein degradation (Ostrerova-Golts *et al.*, 2000; Butterfield & Kanski, 2001).

The combined results presented in this chapter suggest that the administration of a relatively low dose of PQ leads to the induction of the diaphorase activity of the NOS enzyme and a decrease in brain NO due to the preferential production of O<sub>2</sub> $\cdot^-$  (see Figure 8.8.1[1]). Further exposure to PQ may lead to a transient increase in brain NO mediated by the proposed glutamatergic pathway (Figure 8.8.1[2]) which is recoverable due to a decline in NO facilitated by the production of ONOO $^-$  (see Figure 8.8.1[3]). Above a certain threshold of PQ exposure glutamate mediated production overcomes these processes and leads to an unrecoverable elevation of NO levels amongst other ROS/RNS species.

## 8.9 Conclusion

The primary aim of this chapter was to demonstrate the novel detection of NO in a paraquat (PQ) induced animal model of Parkinson's disease (PD). Additionally, the preliminary simultaneous detection of NO and H<sub>2</sub>O<sub>2</sub> in the brain of freely-moving animals following the systemic administration of PQ was demonstrated in this chapter. The systemic administration of PQ has previously been demonstrated to elicit dopaminergic cell degeneration, the increased production of brain oxidative/nitrosative stress markers, behavioural motor abnormalities and the up-regulation of  $\alpha$ -synuclein in rodents (Corasaniti *et al.*, 1998; Hara *et al.*, 2001; Manning-Bog *et al.*, 2002; Shimizu *et al.*, 2003a; McCormack *et al.*, 2005; Dinis-Oliveira *et al.*, 2006; McCormack *et al.*, 2006). All of these afore mentioned characteristics are successfully displayed following PQ exposure in rodents and are consistent with the main pathophysiological consequences of PD development in humans (Olanow & Tatton, 1999; Lotharius & Brundin, 2002; Schapira & Jenner, 2011).

As a control experiment the effect of the systemic administration of saline (s.c.) on the implanted NO and H<sub>2</sub>O<sub>2</sub> sensors was examined in Section 7.3.2. No lasting effect on the NO sensor response was observed following the systemic administration of saline. These results are consistent with previous findings of the effect of systemic administration of saline on the response of this NO sensor design (Finnerty *et al.*, 2012). Additionally no lasting effect on the H<sub>2</sub>O<sub>2</sub> response can be seen following the systemic administration of saline (see Section 8.3).

As an additional control experiment the response of the NO sensor implanted in the NA for a continuous period of 72 hrs was examined in Section 8.4.1. The NO response remained close to baseline levels for the duration of the recording period. A slight deviation from baseline levels of NO was apparent, which is likely attributable to the previously reported circadian variation in the level of brain NO recorded over an extended time-frame (Heinzen & Pollack, 2002; Cespuglio *et al.*, 2012). However a return to a stable baseline level of NO was observed within the recording period (see Figure 8.4.1).

A PQ dose response study was conducted in Section 8.4.2 and the long-term NO response attributable to the administration of a low dose of PQ (5 mg/kg) and a relatively high dose of PQ (30 mg/kg) was examined. Following the administration of a relatively low dose of PQ (5 mg/kg) the recorded level of brain NO remained close to pre-injection baseline levels for a continuous period of 72 hrs. However individual conflicting minor deviations above and below baseline levels of NO were noted following the administration of this low dose of PQ (5 mg/kg) due to inter-animal variability. This response may reflect the susceptibility of a given animal to the influence of PQ as an oxidative stressor. The previously hypothesised influence of an underlying weakened energy metabolism to the development of PD, mediated by oxidative/nitrosative stress, gives credence to the variation in the recorded NO response between animals following the administration of this low dose of PQ (Wellstead & Cloutier, 2011).

The systemic administration of 30 mg/kg PQ elicited a contrasting NO response in comparison to the administration of a relatively lower dose of the toxin (5 mg/kg). Following the systemic administration of PQ (30 mg/kg) a clear decrease in NO levels below pre-injection baseline levels was evident (see Figure 8.4.3). This marked reproducible decrease in brain NO may be explained by the diaphorase activity of the NO producing enzyme nitric oxide synthase (NOS). It has previously been demonstrated that NOS as a cellular diaphorase can preferentially produce O<sub>2</sub><sup>•-</sup> over NO upon exposure to PQ and is termed ‘uncoupling’ of the NOS enzyme (Day *et al.*, 1999; Margolis *et al.*, 2000). NOS may transfer electrons to PQ at the reductase domain of the enzyme resulting in the increased production of O<sub>2</sub><sup>•-</sup> at the expense of NO from NOS (Margolis *et al.*, 2000). The previously determined ‘uncoupling’ of the NOS enzyme provides an explanation for the decrease in NO observed following the initial exposure to a moderate level of PQ (30 mg/kg). A summary of the main PQ dose response NO results is displayed in Table 8.9.1.

In addition, the preliminary simultaneous detection of changes in H<sub>2</sub>O<sub>2</sub> and NO by the paired catalase-based H<sub>2</sub>O<sub>2</sub> sensor and the previously characterised NO sensor following the administration of a low (5 mg/kg) and moderate dose (30 mg/kg) of PQ was

examined in Section 8.4.3. It has previously been demonstrated that the redox cycling of PQ results in the production of O<sub>2</sub><sup>•-</sup> (Dinis-Oliveira *et al.*, 2006; Bove & Perier, 2012). O<sub>2</sub><sup>•-</sup> is the primary source of H<sub>2</sub>O<sub>2</sub> production in the neuronal environment (Ramalingam & Kim, 2012). An increase in H<sub>2</sub>O<sub>2</sub> was detected following the administration of 5 mg/kg PQ possibly due to the redox cycling properties of PQ. Additionally an attenuated decrease in H<sub>2</sub>O<sub>2</sub> levels was recorded following the administration of a moderate dose of PQ (30 mg/kg) which may be attributable to the formation of <sup>•</sup>OH from H<sub>2</sub>O<sub>2</sub> in a pro-oxidant environment (see Section 2.10.2).

| <b>PQ</b>       | <b>Current change (pA)</b> | <b>Change (%)</b> | <b>Conc. change (nM)</b> | <b>Max response (hrs)</b> | <b>Return (hrs)</b> | <b>AUC (pA/hr)</b> | <b>Pre-injection baseline (pA)</b> | <b>Post-injection baseline (pA)</b> | <b>n</b> |
|-----------------|----------------------------|-------------------|--------------------------|---------------------------|---------------------|--------------------|------------------------------------|-------------------------------------|----------|
| <b>5 mg/kg</b>  | n/a                        | n/a               | n/a                      | n/a                       | n/a                 | -15.0 ± 36.7       | 458.1 ± 66.6                       | 429.3 ± 57.0                        | 9        |
| <b>30 mg/kg</b> | -349.9 ± 80.2              | -22.7 ± 5.2       | -229.0 ± 52.5            | 47.1 ± 2.1                | 62.5 ± 1.0          | -193.9 ± 43.4      | 482.9 ± 62.6                       | 423.5 ± 44.0                        | 13       |

**Table 8.9.1: Summary of NO results shown in Section 8.4.2**

Following on from the initial PQ exposure dose response the effect of an additive sequential dose of PQ on the implanted NO sensor was examined in Section 8.5. It has previously been demonstrated by McCormack *et al.* that the repetitive administration of a moderate dose of PQ is required to induce an increased production of nitrotyrosine-containing proteins in *ex-vivo* brain preparations, which is an indication of oxidative/nitrosative stress (McCormack *et al.*, 2005). An increase in NO above baseline levels was determined following the injection of 20 mg/kg PQ with pre-administration of 10 mg/kg PQ. This pilot study demonstrates that repetitive exposure to PQ is a necessary requirement in the development of PQ mediated NO production in the neuronal environment.

The increase in NO recorded following the administration of a sequential additive dose of PQ may occur via a glutamatergic pathway. It has previously been demonstrated that the local administration of PQ results in a transient release of glutamate in the striatum (Shimizu *et al.*, 2003a). Glutamate mediated activation of non-NMDA receptors leads to

the hyperactivation of NMDA receptor channels and subsequently an intracellular influx of Ca<sup>2+</sup> (Shimizu *et al.*, 2003a; Garthwaite, 2008; Moran *et al.*, 2010). This glutamate mediated Ca<sup>2+</sup> influx may then activate brain NOS and lead directly to the production of NO (Alderton *et al.*, 2001; Saulskaya & Fofonova, 2006).

The effect of the repeated systemic administration of PQ (30 mg/kg) on the level of NO monitored in the NA is presented in Section 8.6. The initial administration of 30 mg/kg PQ leads to an attenuated decrease in NO levels below baseline levels (see Figure 8.6.1(A)). As previously discussed this marked decrease in brain NO induced by the initial exposure to a moderate dose of PQ (30 mg/kg) may be explained by the diaphorase activity of the NOS enzyme which leads to the preferential production of O<sub>2</sub><sup>-</sup> over NO from NOS (Day *et al.*, 1999; Margolis *et al.*, 2000).

Following the second administration of PQ (30 mg/kg) the initial NO response monitored in the NA remains close to pre-injection baseline levels followed by a delayed increase in brain NO (see Figure 8.6.1(B)). The increase in NO detected following this injection may be explained by a glutamate mediated production of NO as previously discussed. The subsequent return of elevated NO to pre-injection baseline levels may be explained by the interaction between NO and PQ mediated O<sub>2</sub><sup>-</sup> production which is known to lead to the formation of ONOO<sup>-</sup> which would result in a decline in brain NO production.

The systemic administration of the third dose of 30 mg/kg PQ leads to an elevated attenuated production of brain NO (see Figure 8.6.1(C)). This finding suggests that beyond a certain level of PQ exposure an unrecoverable elevation of brain NO occurs. It has been postulated that NO produced from the action of PQ may diffuse to dopaminergic nerve terminals where it can exert deleterious effects primarily by the formation of the highly toxic RNS, ONOO<sup>-</sup> (Shimizu *et al.*, 2003a; Moran *et al.*, 2010). This process may lead to progressive dopaminergic cell degeneration which is characteristic of the pathology of PD. The overall proposed mechanism of PQ induced neuronal toxicity is discussed in detail in Section 8.8. A summary of the results presented in Section 8.6 is shown in Table 8.9.2.

| <b>PQ<br/>(30<br/>mg/kg)</b> | <b>Current<br/>change<br/>(pA)</b> | <b>Change<br/>(%)</b> | <b>Conc.<br/>change<br/>(nM)</b> | <b>Max<br/>response<br/>(hrs)</b> | <b>Return<br/>(hrs)</b> | <b>AUC<br/>(pA/hr)</b> | <b>Pre-<br/>injection<br/>baseline<br/>(pA)</b> | <b>Post-<br/>injection<br/>baseline<br/>(pA)</b> |
|------------------------------|------------------------------------|-----------------------|----------------------------------|-----------------------------------|-------------------------|------------------------|---|--|
| <b>1<sup>st</sup></b>        | -339.0<br>± 71.2                   | -19.2 ±<br>4.0        | -221.8<br>± 46.6                 | 47.1 ±<br>4.1                     | 65.7 ±<br>1.0           | -236.8<br>± 55.2       | 1370.4<br>± 269                                 | 1043.9<br>± 202.5                                |
| <b>2<sup>nd</sup></b>        | 134.5 ±<br>117.2                   | 12.7 ±<br>11.1        | 88.0 ±<br>76.7                   | 51.0 ±<br>4.2                     | 65.1 ±<br>1.1           | -29.0 ±<br>51.8        | 1059.6<br>± 208.9                               | 1091.9<br>± 162.7                                |
| <b>3<sup>rd</sup></b>        | 894.6 ±<br>253.6                   | 90.5 ±<br>25.6        | 588.5 ±<br>166.8                 | 53.7 ±<br>4.3                     | 62.4 ±<br>2.5           | 237.6<br>± 74.8        | 988.6<br>± 136.6                                | 1648.5<br>± 307.4                                |

**Table 8.9.2: Summary of NO results shown in Section 8.6.**

The preliminary simultaneous detection of NO and H<sub>2</sub>O<sub>2</sub> following the repetitive systemic administration of paraquat (PQ) in a sequential manner of ascending doses is presented in Section 8.7. An initial substantial elevation of H<sub>2</sub>O<sub>2</sub> was recorded following the administration of a low dose of PQ (5 mg/kg). This increase in brain H<sub>2</sub>O<sub>2</sub> may be explained by the redox cycling of PQ in the neuronal environment which is known to lead to the production of O<sub>2</sub><sup>•-</sup> and sequential H<sub>2</sub>O<sub>2</sub> formation (see Section 2.10.2) (Dinis-Oliveira *et al.*, 2006; Bove & Perier, 2012). The corresponding level of NO remained close to baseline levels upon the initial exposure to PQ (see Figure 8.7.1).

An opposite correlation was observed between NO and H<sub>2</sub>O<sub>2</sub> levels towards the end of the ascending PQ dose response. This observation may be explained by the interaction between O<sub>2</sub><sup>•-</sup> and NO which leads to ONOO<sup>-</sup> production (Calabrese *et al.*, 2007; Ramalingam & Kim, 2012). The NO mediated formation of ONOO<sup>-</sup> may lead to an insufficient availability of O<sub>2</sub><sup>•-</sup> which is required for the formation of H<sub>2</sub>O<sub>2</sub> (see Section 2.10). The dual detection of NO and H<sub>2</sub>O<sub>2</sub> presented in Section 8.7 is preliminary however and the future detection of these species in the neuronal environment following the administration of PQ may facilitate an examination of the role of oxidative/nitrosative stress in PQ mediated neurotoxicity.

The behavioural changes induced in rodents by PQ exposure are discussed in Section 8.7. The main behavioural abnormalities observed in this study included a general

reduction in movement, occasional shaking behaviour and transient tremors. These behavioural traits were more noticeable at higher doses of administered PQ (30 mg/kg) and following repeated exposure. In the absence of detailed behavioural testing it is difficult to correlate changes in NO with PQ elicited behavioural abnormalities. Future work may focus on a possible link between these PQ mediated behavioural responses and changes in brain NO as previously examined (Hara *et al.*, 2001).

The further real-time detection of NO, along with other RNS and ROS, including H<sub>2</sub>O<sub>2</sub>, in a PQ induced animal model of PD may provide previously undetermined information surrounding the etiology and pathophysiology of PD. An understanding of the role of oxidative/nitrosative stress in the initiation and development of PD may hopefully lead to the development of novel PD therapeutic strategies.

## References

- Alderton WK, Cooper CE & Knowles RG. (2001). Nitric oxide synthases: structure, function and inhibition. *Biochemical Journal* **357**, 593-615.
- Andersen JK. (2004). Oxidative stress in neurodegeneration: cause or consequence? *Nature Medicine* **10**, S18-S25.
- Bartlett RM, Holden JE, Nickles RJ, Murali D, Barbee DL, Barnhart TE, Christian BT & DeJesus OT. (2009). Paraquat is excluded by the blood brain barrier in rhesus macaque: An *in vivo* pet study. *Brain Research* **1259**, 74-79.
- Beal MF. (2001). Experimental models of Parkinson's disease. *Nat Rev Neurosci* **2**, 325-334.
- Berry C, La Vecchia C & Nicotera P. (2010). Paraquat and Parkinson's disease. *Cell Death and Differentiation* **17**, 1115-1125.
- Bonneh-Barkay D, Langston WJ & Di Monte DA. (2005a). Toxicity of redox cycling pesticides in primary mesencephalic cultures. *Antioxid Redox Signal* **7**, 649-653.
- Bonneh-Barkay D, Reaney SH, Langston WJ & Di Monte DA. (2005b). Redox cycling of the herbicide paraquat in microglial cultures. *Brain Res Mol Brain Res* **134**, 52-56.
- Bove J & Perier C. (2012). Neurotoxin-based models of Parkinson's disease. *Neuroscience* **211**, 51-76.
- Brooks AI, Chadwick CA, Gelbard HA, Cory-Slechta DA & Federoff HJ. (1999). Paraquat elicited neurobehavioral syndrome caused by dopaminergic neuron loss. *Brain Research* **823**, 1-10.
- Butterfield DA & Kanski J. (2001). Brain protein oxidation in age-related neurodegenerative disorders that are associated with aggregated proteins. *Mechanisms of Ageing and Development* **122**, 945-962.
- Calabrese V, Mancuso C, Calvani M, Rizzarelli E, Butterfield DA & Stella AMG. (2007). Nitric oxide in the central nervous system: neuroprotection versus neurotoxicity. *Nature Reviews Neuroscience* **8**, 766-775.
- Castello PR, Drechsel DA & Patel M. (2007). Mitochondria are a major source of paraquat-induced reactive oxygen species production in the brain. *Journal of Biological Chemistry* **282**, 14186-14193.

- Cespuglio R, Amrouni D, Meiller A, Buguet A & Gautier-Sauvigne S. (2012). Nitric oxide in the regulation of the sleep-wake states. *Sleep Medicine Reviews* **16**, 265-279.
- Chinta SJ & Andersen JK. (2008). Redox imbalance in Parkinson's disease. *Biochimica Et Biophysica Acta-General Subjects* **1780**, 1362-1367.
- Clayton DF & George JM. (1998). The synucleins: a family of proteins involved in synaptic function, plasticity, neurodegeneration and disease. *Trends in Neurosciences* **21**, 249-254.
- Cocheme HM & Murphy MP. (2008). Complex I is the major site of mitochondrial superoxide production by paraquat. *Journal of Biological Chemistry* **283**, 1786-1798.
- Corasaniti MT, Strongoli MC, Rotiroti D, Bagetta G & Nistico G. (1998). Paraquat: A useful tool for the *in vivo* study of mechanisms of neuronal cell death. *Pharmacology & Toxicology* **83**, 1-7.
- Cory-Slechta DA, Thiruchelvam M & Di Monte DA. (2008). Letter regarding: "Paraquat: The Red Herring of Parkinson's Disease Research". *Toxicological Sciences* **103**, 215-216.
- Czerniczyniec A, Karadayian AG, Bustamante J, Cutrera RA & Lores-Arnaiz S. (2011). Paraquat induces behavioral changes and cortical and striatal mitochondrial dysfunction. *Free Radical Biology and Medicine* **51**, 1428-1436.
- Day BJ, Patel M, Calavetta L, Chang LY & Stamler JS. (1999). A mechanism of paraquat toxicity involving nitric oxide synthase. *Proceedings of the National Academy of Sciences of the United States of America* **96**, 12760-12765.
- Di Monte DA. (2003). The environment and Parkinson's disease: is the nigrostriatal system preferentially targeted by neurotoxins? *Lancet Neurol* **2**, 531-538.
- Dinis-Oliveira RJ, Remiao F, Carmo H, Duarte JA, Navarro AS, Bastos ML & Carvalho F. (2006). Paraquat exposure as an etiological factor of Parkinson's disease. *Neurotoxicology* **27**, 1110-1122.
- Finnerty NJ, O'Riordan SL, Palsson E & Lowry JP. (2012). Brain nitric oxide: Regional characterisation of a real-time microelectrochemical sensor. *Journal of Neuroscience Methods* **209**, 13-21.
- Garthwaite J. (2008). Concepts of neural nitric oxide-mediated transmission. *European Journal of Neuroscience* **27**, 2783-2802.

- Hara S, Mukai T, Kurosaki K, Kuriiwa F, Yanase T, Kano S & Endo T. (2001). No parallel relationship between nitric oxide production and wet dog shakes susceptible to nitric oxide synthase inhibitors following systemic administration of paraquat in rats. *Archives of Toxicology* **74**, 775-782.
- Heinzen EL & Pollack GM. (2002). Use of an electrochemical nitric oxide sensor to detect neuronal nitric oxide production in conscious, unrestrained rats. *Journal of Pharmacological and Toxicological Methods* **48**, 139-146.
- Lin MT & Beal MF. (2006). Mitochondrial dysfunction and oxidative stress in neurodegenerative diseases. *Nature* **443**, 787-795.
- LoPachin RM & Gavin T. (2008). Response to "Paraquat: The Red Herring of Parkinson's Disease Research". *Toxicological Sciences* **103**, 219-221.
- Lotharius J & Brundin P. (2002). Pathogenesis of Parkinson's disease: Dopamine, vesicles and alpha-synuclein. *Nature Reviews Neuroscience* **3**, 932-942.
- Maguire-Zeiss KA, Short DW & Federoff HJ. (2005). Synuclein, dopamine and oxidative stress: co-conspirators in Parkinson's disease? *Molecular Brain Research* **134**, 18-23.
- Manning-Bog AB, McCormack AL, Li J, Uversky VN, Fink AL & Di Monte DA. (2002). The herbicide paraquat causes up-regulation and aggregation of alpha-synuclein in mice - Paraquat and alpha-synuclein. *Journal of Biological Chemistry* **277**, 1641-1644.
- Margolis AS, Porasuphatana S & Rosen GM. (2000). Role of paraquat in the uncoupling of nitric oxide synthase. *Biochimica Et Biophysica Acta-General Subjects* **1524**, 253-257.
- McCormack AL, Atienza JG, Johnston LC, Andersen JK, Vu S & Di Monte DA. (2005). Role of oxidative stress in paraquat-induced dopaminergic cell degeneration. *Journal of Neurochemistry* **93**, 1030-1037.
- McCormack AL, Atienza JG, Langston JW & Di Monte DA. (2006). Decreased susceptibility to oxidative stress underlies the resistance of specific dopaminergic cell populations to paraquat-induced degeneration. *Neuroscience* **141**, 929-937.
- McCormack AL & Di Monte DA. (2003). Effects of L-dopa and other amino acids against paraquat-induced nigrostriatal degeneration. *Journal of Neurochemistry* **85**, 82-86.
- Miller GW. (2007). Paraquat: The red herring of Parkinson's disease research. *Toxicological Sciences* **100**, 1-2.

- Monaghan DT & Cotman CW. (1985). Distribution of N-methyl-D-aspartate-sensitive L-[<sup>3</sup>H]glutamate-binding sites in rat brain. *J Neurosci* **5**, 2909-2919.
- Moran JM, Ortiz-Ortiz MA, Ruiz-Mesa LM & Fuentes JM. (2010). Nitric Oxide in Paraquat-Mediated Toxicity: A Review. *Journal of Biochemical and Molecular Toxicology* **24**, 402-409.
- Obeso JA, Marin C, Rodriguez-Oroz C, Blesa J, Benitez-Temino B, Mena-Segovia J, Rodriguez M & Olanow CW. (2008). The Basal Ganglia in Parkinson's Disease: Current Concepts and Unexplained Observations. *Annals of Neurology* **64**, S30-S46.
- Olanow CW & Tatton WG. (1999). Etiology and pathogenesis of Parkinson's disease. *Annual Review of Neuroscience* **22**, 123-144.
- Ostrerova-Golts N, Petrucelli L, Hardy J, Lee JM, Farer M & Wolozin B. (2000). The A53T alpha-synuclein mutation increases iron-dependent aggregation and toxicity. *Journal of Neuroscience* **20**, 6048-6054.
- Purisai MG, McCormack AL, Cumine S, Li J, Isla MZ & Di Monte DA. (2007). Microglial activation as a priming event leading to paraquat-induced dopaminergic cell degeneration. *Neurobiology of Disease* **25**, 392-400.
- Ramalingam M & Kim S-J. (2012). Reactive oxygen/nitrogen species and their functional correlations in neurodegenerative diseases. *Journal of Neural Transmission* **119**, 891-910.
- Richardson JR, Quan Y, Sherer TB, Greenamyre JT & Miller GW. (2005). Paraquat neurotoxicity is distinct from that of MPTP and rotenone. *Toxicological Sciences* **88**, 193-201.
- Saulskaya NB & Fofonova NV. (2006). Effects of N-methyl-D-aspartate on extracellular citrulline level in the rat nucleus accumbens. *Neuroscience Letters* **407**, 91-95.
- Schapira AH & Jenner P. (2011). Etiology and Pathogenesis of Parkinson's Disease. *Movement Disorders* **26**, 1049-1055.
- Shimizu K, Matsubara K, Ohtaki K, Fujimaru S, Saito O & Shiono H. (2003a). Paraquat induces long-lasting dopamine overflow through the excitotoxic pathway in the striatum of freely moving rats. *Brain Research* **976**, 243-252.
- Shimizu K, Matsubara K, Ohtaki K & Shiono H. (2003b). Paraquat leads to dopaminergic neural vulnerability in organotypic midbrain culture. *Neuroscience Research* **46**, 523-532.

- Shimizu K, Ohtaki K, Matsubara K, Aoyama K, Uezono T, Saito O, Suno M, Ogawa K, Hayase N, Kimura K & Shiono H. (2001). Carrier-mediated processes in blood-brain barrier penetration and neural uptake of paraquat. *Brain Research* **906**, 135-142.
- Tanner CM, Kamel F, Ross GW, Hoppin JA, Goldman SM, Korell M, Marras C, Bhudhikanok GS, Kasten M, Chade AR, Comyns K, Richards MB, Meng C, Priestley B, Fernandez HH, Cambi F, Umbach DM, Blair A, Sandler DP & Langston JW. (2011). Rotenone, Paraquat, and Parkinson's Disease. *Environmental Health Perspectives* **119**, 866-872.
- Uversky VN. (2004). Neurotoxicant-induced animal models of Parkinson's disease: understanding the role of rotenone, maneb and paraquat in neurodegeneration. *Cell and Tissue Research* **318**, 225-241.
- Valko M, Leibfritz D, Moncol J, Cronin MTD, Mazur M & Telser J. (2007). Free radicals and antioxidants in normal physiological functions and human disease. *International Journal of Biochemistry & Cell Biology* **39**, 44-84.
- Wellstead P & Cloutier M. (2011). An energy systems approach to Parkinson's disease. *Wiley Interdisciplinary Reviews-Systems Biology and Medicine* **3**, 1-6.
- Wirdefeldt K, Adami HO, Cole P, Trichopoulos D & Mandel J. (2011). Epidemiology and etiology of Parkinson's disease: a review of the evidence. *Eur J Epidemiol* **26**, 28.

---

## **9. General Conclusions**

---

The detection of chemical changes in the extracellular fluid (ECF) of the brain using Long Term *In-Vivo* Electrochemistry (L.I.V.E) provides an insight into the processes which underlie cognitive function. In addition information regarding the pathophysiology of a variety of neurodegenerative diseases and disorders may be yielded by this technique. The fundamental basis of L.I.V.E is the implantation of an electrochemical sensor into the brain, the application of a suitable potential and the subsequent detection of a faradaic current which is proportional to the concentration of the target species.

Monitoring neurochemicals using L.I.V.E in the ECF is complicated by a variety of technical obstacles. A range of neurotransmitters (NTs) in the ECF are not electroactive and many species oxidise at similar potentials. Additionally, brain tissue consists of lipids and proteins which may affect the properties of the sensor *in-vivo* (Garguilo & Michael, 1994). The reaction of the body to the presence of a foreign object can also negatively affect the characteristics of a sensor (Wisniewski *et al.*, 2000). Mass transport of the analyte to an electrochemical sensor may also be restricted by the brain tissue itself (Cheng *et al.*, 1979; Dayton *et al.*, 1983).

In recent years various strategies have been utilised in order to improve the sensitivity, selectivity and stability of implanted electrochemical sensors. The incorporation of a biological recognition unit, usually an enzyme into the design of the sensor facilitates the detection of non-electroactive species (Hu *et al.*, 1994; Lowry *et al.*, 1994; Garguilo & Michael, 1996; Ryan *et al.*, 1997). The application of a suitable potential and the modification of the electrode surface with various permselective membranes has improved the selectivity and stability of the L.I.V.E technique (McAteer & O'Neill, 1996; Lowry *et al.*, 1998; Brown *et al.*, 2009). The primary aim of this thesis is to authoritatively establish the detection of hydrogen peroxide (H<sub>2</sub>O<sub>2</sub>) and nitric oxide (NO) in the *in-vitro* environment and to demonstrate the detection of these species in the ECF of the brain.

An extensive *in-vitro* and *in-vivo* characterisation of a highly suitable electrochemical sensor for the purpose of the chronic real-time detection of NO has previously been demonstrated by our research group (Finnerty *et al.*, 2012a; Finnerty *et al.*, 2012b). The

initial *in-vitro* characterisation of the paired catalase-based  $\text{H}_2\text{O}_2$  sensor utilised in this body of work has previously been reported (O'Brien *et al.*, 2007). A validation of the previous *in-vitro* and *in-vivo* characterisation of the NO sensor with the inclusion of new *in-vitro* stability attributes is presented in this thesis. Novel *in-vitro* characteristics of the paired catalase-based  $\text{H}_2\text{O}_2$  sensor are also demonstrated in this thesis. The previously unreported *in-vivo* characterisation of the paired  $\text{H}_2\text{O}_2$  sensor in the anaesthetised and freely-moving animal is also presented.

Following on from this work the novel detection of NO in an animal model of autism spectrum disorders (ASDs) is shown. Additionally, the dual detection of NO and  $\text{H}_2\text{O}_2$  in an animal model of Parkinson's disease (PD) is presented. In both instances the specific focus is on the role of oxidative/nitrosative stress in the pathophysiology of these conditions. The aim of this novel contribution to the field of neurochemistry is the further advancement of knowledge surrounding the etiology and progression of ASDs and PD which may yield new therapeutic advancements.

Chapter 4 demonstrates the replication of the catalase-based dual  $\text{H}_2\text{O}_2$  sensor design to establish the sensitivity, selectivity and stability of the  $\text{H}_2\text{O}_2$  sensor in the *in-vitro* environment. Novel selectivity and stability parameters of the dual  $\text{H}_2\text{O}_2$  sensor design are also presented in Chapter 4. Specifically the long-term stability (28 days) of the sensor is addressed following exposure to lipids, proteins and *ex-vivo* brain tissue.

As shown in Chapter 4 the detection of  $\text{H}_2\text{O}_2$  in the *in-vitro* environment is not impaired in the presence of other electroactive species including dopamine (DA) and ascorbic acid (AA). Aqueous and substrate *in-vitro* media conditions were changed to artificial cerebrospinal fluid (aCSF) in order to mimic *in-vivo* characterisation parameters. The oxidation of  $\text{H}_2\text{O}_2$  at platinum electrodes ( $\text{Pt}_d$ ) was not significantly different under either of these conditions. The operational characteristics of the paired  $\text{H}_2\text{O}_2$  sensor are also demonstrated. The catalase-based paired  $\text{H}_2\text{O}_2$  sensor possesses the required response time and limit of detection for the purpose of *in-vivo*  $\text{H}_2\text{O}_2$  monitoring.  $\text{H}_2\text{O}_2$  is a highly permeable short-lived molecule which may be particularly prevalent in the *in-vivo* environment (Maier & Chan, 2002; Bao *et al.*, 2009).

The characterisation of the H<sub>2</sub>O<sub>2</sub> sensor in the *in-vivo* environment is demonstrated in Chapter 5. The paired H<sub>2</sub>O<sub>2</sub> sensor was implanted into the brain of anaesthetised and freely-moving Wistar rats. The effect of local and systemic administration of known inducers and inhibitors of H<sub>2</sub>O<sub>2</sub> on the performance of the dual H<sub>2</sub>O<sub>2</sub> sensor response was investigated.

Following the local administration of H<sub>2</sub>O<sub>2</sub> (100 µM to 1000 µM) in the freely-moving animal a significant difference was observed with respect to the perfusion of aCSF. However no distinct increase above basal levels of endogenous H<sub>2</sub>O<sub>2</sub> was observed following introduction of H<sub>2</sub>O<sub>2</sub> to the perfusate. It is plausible that exogenously applied H<sub>2</sub>O<sub>2</sub> may be efficiently controlled by the inherent mechanisms of the intact living brain. A variety of enzymatic/non-enzymatic processes regulate the production of reactive oxygen species (ROS) such as H<sub>2</sub>O<sub>2</sub> in order to prevent the development of oxidative stress and subsequent deleterious processes (Barnham *et al.*, 2004; Valko *et al.*, 2007; Melo *et al.*, 2011; Ramalingam & Kim, 2012). It is therefore possible that exogenously applied H<sub>2</sub>O<sub>2</sub> is capably dealt with by the extensive antioxidant network. This observation is further supported by the recorded response of the H<sub>2</sub>O<sub>2</sub> sensor following the local administration of H<sub>2</sub>O<sub>2</sub> in the anaesthetised animal.

The effect of the local administration of H<sub>2</sub>O<sub>2</sub> on the paired sensor response was relatively more pronounced in the anaesthetised animal. A clear increase above basal levels of H<sub>2</sub>O<sub>2</sub> was observed at a higher concentration range of exogenously applied H<sub>2</sub>O<sub>2</sub> (100 µM to 100 mM). It is possible that the robust network of antioxidant mechanisms which regulate the level of H<sub>2</sub>O<sub>2</sub>/ROS in the brain cannot function normally due to the effect of anaesthesia; consequently an increase was recorded by the implanted H<sub>2</sub>O<sub>2</sub> sensor following the local administration of H<sub>2</sub>O<sub>2</sub> (100 µM to 100 mM) in the acute experimental set-up.

Additionally, a lower baseline level of H<sub>2</sub>O<sub>2</sub> was recorded in the acute preparation, where anaesthesia is constantly administered to the animal, in comparison to the freely-moving regime. Suppressed neuronal activity corresponds to a decrease demand for regional cerebral blood flow and hence a matched reduction in oxygen levels (Li *et al.*, 2011). Neuronal H<sub>2</sub>O<sub>2</sub> is primarily derived through the action of the enzyme superoxide

dismutase (SOD) on superoxide ( $O_2^{\cdot-}$ ) which is derived from the mitochondrial reduction of molecular  $O_2$ . The endogenous production of  $H_2O_2$  is linked to increased neuronal activity due to an increased level of  $O_2$  consumption which generates  $H_2O_2$  (Rice, 2011). Therefore, a drop in neuronal activity due to anaesthesia may explain a reduction in  $H_2O_2$  baseline levels.

The next step in the *in-vivo* characterisation of the  $H_2O_2$  sensor was to inhibit the antioxidant network responsible for the regulation of  $H_2O_2$  in an attempt to show an increase in the endogenous production of  $H_2O_2$ . The primary enzymes responsible for the degradation of  $H_2O_2$  in the brain are catalase and glutathione peroxidase (GPx) which are inhibited by sodium azide (SA) and mercaptosuccinate (MCS) respectively. The local perfusion of MCS and SA caused an increase in the paired catalase-based  $H_2O_2$  sensor response, this preliminary data would indicate that the implanted sensor is responding to an endogenous increase in  $H_2O_2$  levels and is therefore selective towards  $H_2O_2$ . Additionally, the *in-vivo* selectivity of the paired  $H_2O_2$  sensor over locally introduced AA was demonstrated and the preliminary selectivity of the sensor over systemically administered AA was shown.

Chapter 6 demonstrates the *in-vitro* and *in-vivo* characterisation of the NO sensor as previously shown; in order to further illustrate the application of this sensor for the real-time detection of NO in animal models of neurological disease and dysfunction. The sensitivity and selectivity of the NO sensor in the *in-vitro* environment were in agreement with previously published demonstrations (Finnerty *et al.*, 2012a; Finnerty *et al.*, 2012b). Additionally, the operational characteristics of the sensor including the response time and the limit of detection were consistent with previous reports (Brown *et al.*, 2009). The required *in-vitro* characteristics of the NO sensor were established, which are needed to detect NO in the physiological environment, due to the relatively low concentration and short half-life of the target species *in-vivo* (Kiechle & Malinski, 1993; Wink & Mitchell, 1998; Kelm, 1999).

An examination of NO sensor characteristics following implantation was presented in Chapter 6 as has been published recently (Finnerty *et al.*, 2012a). It was determined that the post *in-vivo* sensitivity of the NO sensor was approximately 48 % less than the pre-

implantation sensitivity of the same sensors. The AA selectivity characteristics of the NO sensor following implantation were also described. An increased response to AA following implantation of the NO sensor was observed. However, the Nafion<sup>®</sup>-modified active surface of the NO sensor remains intact while implanted as proven by the sensor response to systemically administered ascorbate *in-vivo* as shown in Chapter 6. An explanation for the altered *in-vitro* NO sensitivity and AA selectivity of the NO sensor following implantation may be that the process of ex-plantation causes damage to the active surface of the sensor.

The sensitivity, selectivity and stability of the NO sensor while implanted in the nucleus accumbens (NA) of the freely-moving animal was validated in Chapter 6. The response of the implanted NO sensor to systemically administered saline was established and no lasting effect on the NO response of the Nafion<sup>®</sup>-modified NO sensor was observed following this injection. The precursor to NO production in the body (L-arginine) was systemically administered and NO levels in the NA were monitored. A significant increase in the NO sensor response was observed following the administration of L-arginine with respect to the injection of saline. The effect of the non-selective nitric oxide synthase (NOS) inhibitor (L-NAME) on the response of the NO sensor was determined in the NA. A significant decrease in the NO sensor response was observed following the administration of L-NAME with respect to the corresponding saline response.

The *in-vivo* selectivity of the NO sensor over ascorbate, the primary interference species present in the brain was examined. No significant difference was observed between the maximum current response and pre-injection baseline levels of the NO sensor following the injection of ascorbate. These results further support the proficient sensitivity, selectivity and stability of the NO sensor in the *in-vivo* environment as previously demonstrated (Finnerty *et al.*, 2012a; Finnerty *et al.*, 2012b).

The *in-vivo* characterisation results recorded by the NO sensor as presented in this thesis are consistent with recently published data. No significant difference ( $P > 0.05$ ) was observed between the maximum current response following each administration (saline, L-arginine, L-NAME and sodium ascorbate) when compared to the corresponding *in-*

*vivo* results previously shown by Finnerty *et al.* in the NA of freely-moving animals (Finnerty *et al.*, 2012b). Additionally the baseline stability of the NO sensor while implanted in the NA for a consecutive period of 14 days was shown in Chapter 6. Previous investigations have demonstrated the stability of the NO sensor implanted in the brain for a consecutive period of 8 days (Finnerty *et al.*, 2012a). No significant variation was observed in the baseline current of the NO sensor over this extended duration of implantation (14 days). These results further verify the stability of the NO sensor for the purpose of obtaining long-term *in-vivo* recordings.

Chapter 7 demonstrates the novel electrochemical detection of NO in an animal model of autism. The previously characterised NO sensor was implanted in the NA and dorsal hippocampus (DH) of freely-moving animals. The long-term detection of NO was recorded by the sensor prior to and following the chronic systemic administration of Propionic acid (PPA). MacFabe *et al.* have previously demonstrated that PPA may be used in rats to mimic the behavioural changes and neuroinflammatory responses which are associated with autism spectrum disorders (ASDs) (MacFabe *et al.*, 2007; MacFabe *et al.*, 2008; MacFabe *et al.*, 2011).

As a control experiment the level of NO in the NA and DH was examined over a continuous period of 24 hrs in the absence of treatment. A small variation in the NO response was observed over the 24 hr period which is likely attributable to the circadian rhythms of the animal (see Section 7.5.1 and 7.6.1). Also no significant difference was observed between the 24 hr control data response recorded in the NA and the DH as determined by area under the curve (AUC) analysis. Time dependent changes in the level of NO recorded over a 24 hr period have previously been demonstrated by Cespuglio *et al.* using voltametric methods in freely-moving rats (Cespuglio *et al.*, 2012). The time-dependent minor variation in NO over 24 hrs as presented in Chapter 7, which is mirrored closely in both regions suggests a contribution to the signal from a diurnal variation in the level of NO. The overall contribution of natural processes and possible residual capacitance of the sensor to the recorded level of NO are effectively eliminated from the overall signal attributable to administration of PPA by this control data.

An initial pilot study determined the relative short-term effect of PPA administration on the level of NO in the NA. A significant increase in NO response was determined following the administration of each dose of PPA (1  $\mu$ M/g, 2  $\mu$ M/g and 4  $\mu$ M/g) with respect to the administration of saline. Previous demonstrations of a PPA induced animal model of autism involved the long-term systemic administration of PPA (500mg/Kg) (Shams *et al.*, 2009). Following on from the pilot study presented in Chapter 7 the PPA administration protocol was extended and the dose of PPA administered was changed (500 mg/kg). Each animal was administered PPA (500 mg/Kg) twice daily for a continuous period of 12 days and the corresponding changes in NO levels in the NA and DH on each day were monitored by the NO sensor.

A similar trend was observed in the NA and the DH on Day 1-6 of the PPA administration protocol. No significant difference in NO response, as determined by AUC analysis, was observed between Day 1-6 inclusively in comparison to the corresponding value determined for the 24 hr control data in both regions.

A robust network of antioxidant mechanisms regulate the level of reactive nitrogen species (RNS) such as NO in the CNS (Calabrese *et al.*, 2007; Valko *et al.*, 2007). The antioxidant network is responsible for the prevention of the development of oxidative/nitrosative stress and exists to maintain normal cognitive function. It is therefore plausible that the initial exposure to PPA (Day 1-6) is dealt with effectively by these robust control mechanisms inherent to the intact living brain and suppresses the over production of NO. Therefore no significant difference in NO response was recorded in both regions on Day 1-6 of the PPA administration protocol in comparison to the corresponding control data.

Following the extension of the PPA administration protocol (Day 7-12) a general trend emerged in the NO response recorded in the NA and the DH. Following 7 days of chronic PPA administration, an increase in NO was detected in both regions from Day 7-12 inclusively when compared to the corresponding control data.

The unregulated overproduction of NO due to the development of oxidative/nitrosative stress has previously been implicated in the development of autism (Chauhan &

Chauhan, 2006). An increase in the level of NO and indirect markers of NO production have been demonstrated in biological samples of autistic individuals (Sogut *et al.*, 2003; Sweeten *et al.*, 2004). Additionally, increased oxidative stress markers have been detected in pathological studies of autistic brain preparations (Chauhan *et al.*, 2012; Rose *et al.*, 2012). Also, increased oxidative stress markers have been determined in brain preparations of a PPA induced animal model of autism (MacFabe *et al.*, 2007; MacFabe *et al.*, 2008). The recorded elevation of NO levels in the animal model of autism presented in Chapter 7 would support this research. Neuropathological investigations of ASDs brain preparations have indicated the presence of activated microglia and astrocytes (Vargas *et al.*, 2005). Cytokines produced by this process lead to an inflammatory process which is known to activate iNOS and hence induce an increase in NO (Guix *et al.*, 2005). The observed PPA induced increase in NO levels may be attributable to iNOS or alternatively is derived from the constitutive forms of NOS (eNOS and nNOS).

Previous studies conducted with *ex-vivo* brain preparations have indicated that PPA may act through a glutamatergic pathway. This research demonstrates that the incubation of brain slice preparations with PPA has been shown to stimulate the phosphorylation of cytoskeletal proteins. The use of specific N-methyl-D-aspartate (NMDA) receptor agonists has been shown to mimic the stated effect following brain slice exposure to PPA (de Mattos-Dutra *et al.*, 2000). PPA has also previously been shown to promote intracellular calcium ( $\text{Ca}^{2+}$ ) release (Nakao *et al.*, 1992). It is known that activation of NMDA receptors, abundantly present in the NA (Monaghan & Cotman, 1985), by glutamate or by other agonists results in an influx of  $\text{Ca}^{2+}$  and leads to depolarisation of the cell. eNOS and nNOS are activated by  $\text{Ca}^{2+}$  followed by binding with calmodulin which leads directly to the production of NO (Alderton *et al.*, 2001; Saulskaya & Fofonova, 2006).

However, the exact neuropharmacological role of PPA in the induced elevation of NO in the brain as presented in Chapter 7 has yet to be fully elucidated. Future work may involve the use of specific NOS inhibitors (Alderton *et al.*, 2001), to elucidate the exact mechanism of NO production in the PPA animal model of autism presented in Chapter

7. The further detection of NO in an animal model of autism with a specific focus on the role of nitrosative stress may lead to a better understanding of the etiology and pathophysiology of ASDs. This research may lead to the development of novel potential therapeutic strategies for incidences of severe impairment by debilitating restricted and repetitive traits seen in certain ASDs cases.

Chapter 8 demonstrates the novel electrochemical detection of brain NO in a paraquat (PQ) induced animal model of Parkinson's disease (PD). Additionally the preliminary simultaneous detection of NO and H<sub>2</sub>O<sub>2</sub> in the same animal following the systemic administration of PQ is presented in Chapter 8. NO was monitored in the NA using the previously extensively characterised NO sensor (Finnerty *et al.*, 2012a; Finnerty *et al.*, 2012b) and the level of H<sub>2</sub>O<sub>2</sub> in the NA was recorded using the catalase-based H<sub>2</sub>O<sub>2</sub> sensor (see Chapter 4 and 5). The role of various toxins including rotenone, PQ and MPTP in the development of PD has previously been examined and utilised to study PD in animal models (Beal, 2001; McCormack *et al.*, 2005; McCormack *et al.*, 2006).

The structural similarity of PQ to the parkinsonism inducing toxin MPP<sup>+</sup> (Davis *et al.*, 1979; Langston *et al.*, 1983; Dinis-Oliveira *et al.*, 2006; Bove & Perier, 2012) has led to the development of an animal model of PD by the repeated systemic administration of PQ in rodents (McCormack *et al.*, 2005; McCormack *et al.*, 2006). Systemically administered PQ has been shown to cross the blood brain barrier (BBB) in rodents via a neutral amino acid transporter (Corasaniti *et al.*, 1998; Shimizu *et al.*, 2001; McCormack & Di Monte, 2003) and subsequently leads to dopaminergic cell degeneration, behavioural motor abnormalities and the up-regulation of  $\alpha$ -synuclein which is the major constituent of 'Lewy bodies' which are cytoplasmic inclusions commonly found in pathological studies of PD (Brooks *et al.*, 1999; Manning-Bog *et al.*, 2002; McCormack *et al.*, 2005).

It has been postulated that the degeneration of dopaminergic cells which is a pathological hallmark of PD is mediated by oxidative/nitrosative stress specifically as a result of DA metabolism (Lotharius & Brundin, 2002; Andersen, 2004; Chinta & Andersen, 2008). The main focus of Chapter 8 is the detection of NO as a marker of

nitrosative stress and the preliminary detection of  $\text{H}_2\text{O}_2$  as an indication of the development of oxidative stress in a PQ induced animal model of PD.

As long-term changes in NO were examined in Chapter 8 following the systemic administration of PQ, a control experiment was conducted, where the level of NO in the NA was monitored over a continuous period of 70 hrs in the absence of treatment. Minor deviations in the baseline level of NO were apparent over the recorded time period which are largely attributable to a circadian variation in the level of NO as previously demonstrated (Heinzen & Pollack, 2002; Cespuglio *et al.*, 2012).

The neurotoxic effect of PQ is primarily mediated by the redox cycling properties of this molecule (see Section 8.8) which leads to direct and indirect mitochondrial dysfunction (MTdys) and the deleterious consequences of oxidative/nitrosative stress. A PQ dose response study was conducted in Chapter 8 and the long-term NO response attributable to the administration of a low dose of PQ (5 mg/kg) and a relatively high dose of PQ (30 mg/kg) was examined. The recorded NO response monitored in the NA following the administration of 5 mg/kg PQ displayed inter-animal variability. Conflicting NO responses above and below baseline levels of NO were observed between animals following this administration (5 mg/kg PQ). The discrepancy observed between the animals utilised in this study (5 mg/kg PQ) may reflect an underlying susceptibility to oxidative/nitrosative stress mediated by PQ. It is postulated that this variable NO response is consistent with a previously hypothesised underlying weakened energy metabolism and vulnerability to oxidative/nitrosative stress processes leading to the development of PD (Wellstead & Cloutier, 2011).

The systemic administration of 30 mg/kg PQ elicited a contrasting NO response in comparison to the administration of a relatively lower dose of the toxin (5 mg/kg). Following the systemic administration of PQ (30 mg/kg) a clear decrease in NO levels below pre-injection baseline levels was evident. This decrease in NO may be attributed to the diaphorase activity of the NO producing enzyme NOS. It has previously been demonstrated that NOS may act as a cellular diaphorase in that it may donate electrons to PQ and lead to ‘uncoupling’ of NOS which results in the preferential formation of  $\text{O}_2^{\cdot-}$  over NO from NOS (Day *et al.*, 1999; Margolis *et al.*, 2000).

The preliminary detection of an increased level of  $\text{H}_2\text{O}_2$  in the NA was demonstrated following the administration of 5 mg/kg PQ. This can be attributed to the formation of the primary source of  $\text{H}_2\text{O}_2$  production;  $\text{O}_2^{\cdot-}$  due to PQ redox cycling in the neuronal environment (see Section 8.8). Additionally, a preliminary decrease in  $\text{H}_2\text{O}_2$  was recorded following the administration of a relatively higher dose of PQ (30 mg/kg) which may be due to the formation of  $\cdot\text{OH}$  from  $\text{H}_2\text{O}_2$  in a PQ mediated pro-oxidant environment (see Section 2.10.2). The preliminary simultaneous detection of  $\text{H}_2\text{O}_2$  and NO following an extended sequential additive administration of PQ is demonstrated in Section 8.7. Following a relatively low exposure to PQ, a substantial increase in  $\text{H}_2\text{O}_2$  was recorded in the NA and the corresponding NO levels remained close to baseline levels. Following increased exposure to PQ an opposite correlation was observed between NO and  $\text{H}_2\text{O}_2$  levels which may be explained by the interaction between  $\text{O}_2^{\cdot-}$  and NO which leads to  $\text{ONOO}^-$  production (Calabrese *et al.*, 2007; Ramalingam & Kim, 2012). This process may lead to an insufficient availability of  $\text{O}_2^{\cdot-}$  which is required for the formation of  $\text{H}_2\text{O}_2$  and a corresponding decrease in NO levels (see Section 2.10). However, future work is required to ascertain changes in neuronal  $\text{H}_2\text{O}_2$  levels following the administration of PQ.

The additive (see Section 8.5) and repetitive (see Section 8.6) systemic administration of PQ (30 mg/kg) resulted in an increase in brain NO above baseline levels. It is postulated that the PQ mediated increase in NO levels is facilitated by a glutamatergic pathway. It has previously been demonstrated that PQ exposure in rodents leads to a transient increase in glutamate levels in the neuronal environment (Shimizu *et al.*, 2003). Glutamate mediated activation of non-NMDA receptors leads to the hyperactivation of NMDA receptor channels and subsequently an intracellular influx of  $\text{Ca}^{2+}$  (Shimizu *et al.*, 2003; Garthwaite, 2008; Moran *et al.*, 2010). This glutamate mediated  $\text{Ca}^{2+}$  influx may then activate brain NOS and lead directly to the production of NO (Alderton *et al.*, 2001; Saulskaya & Fofonova, 2006). Additionally, this proposed glutamatergic pathway of NO production may exceed the proposed ‘uncoupling’ of the NOS enzyme and the opposing anti-oxidant network at high levels of PQ exposure. This process may lead to an unrecoverable elevation of brain NO levels as demonstrated in Section 8.6 following

the repetitive administration of PQ (30 mg/kg). A detailed description of this glutamatergic NO producing pathway is provided for in Section 8.8.

The further real-time detection of NO amongst other RNS and reactive oxygen species (ROS) including H<sub>2</sub>O<sub>2</sub> in a PQ induced animal model of PD may provide previously undetermined information surrounding the etiology and pathophysiology of PD. An understanding of the role of oxidative/nitrosative stress in the initiation and development of PD may hopefully lead to the development of novel PD therapeutic strategies.

Progression of this body of work may include the further detection of H<sub>2</sub>O<sub>2</sub> *in-vivo* combined with NO as a method of simultaneous oxidative/nitrosative stress detection in a PQ induced animal model of PD amongst other neurodegenerative diseases and dysfunctions. As NO and H<sub>2</sub>O<sub>2</sub> are relatively stable RNS/ROS species in the neuronal environment they present suitable markers for the detection of neurodegenerative disease initiation and progression mediated by oxidative/nitrosative stress (Maier & Chan, 2002; Valko *et al.*, 2007; Rice, 2011). The real-time electrochemical detection of NO and H<sub>2</sub>O<sub>2</sub> *in-vivo* provides an advantageous distinction over currently available analytical techniques. It facilitates the temporal analysis of the initiation and progression of oxidative/nitrosative stress, which has been implicated in the pathophysiology of a variety of neurodegenerative diseases and dysfunctions and its role is currently not fully understood (Andersen, 2004; Barnham *et al.*, 2004; Chauhan & Chauhan, 2006; Obeso *et al.*, 2010; Melo *et al.*, 2011; Walsh *et al.*, 2011).

## References

- Alderton WK, Cooper CE & Knowles RG. (2001). Nitric oxide synthases: structure, function and inhibition. *Biochemical Journal* **357**, 593-615.
- Andersen JK. (2004). Oxidative stress in neurodegeneration: cause or consequence? *Nature Medicine* **10**, S18-S25.
- Bao L, Avshalumov MV, Patel JC, Lee CR, Miller EW, Chang CJ & Rice ME. (2009). Mitochondria Are the Source of Hydrogen Peroxide for Dynamic Brain-Cell Signaling. *Journal of Neuroscience* **29**, 9002-9010.
- Barnham KJ, Masters CL & Bush AI. (2004). Neurodegenerative diseases and oxidative stress. *Nature Reviews Drug Discovery* **3**, 205-214.
- Bove J & Perier C. (2012). Neurotoxin-based models of Parkinson's disease. *Neuroscience* **211**, 51-76.
- Brooks AI, Chadwick CA, Gelbard HA, Cory-Slechta DA & Federoff HJ. (1999). Paraquat elicited neurobehavioral syndrome caused by dopaminergic neuron loss. *Brain Research* **823**, 1-10.
- Brown FO, Finnerty NJ & Lowry JP. (2009). Nitric oxide monitoring in brain extracellular fluid: characterisation of Nafion<sup>®</sup>-modified Pt electrodes *in vitro* and *in vivo*. *Analyst* **134**, 2012-2020.
- Calabrese V, Mancuso C, Calvani M, Rizzarelli E, Butterfield DA & Stella AMG. (2007). Nitric oxide in the central nervous system: neuroprotection versus neurotoxicity. *Nature Reviews Neuroscience* **8**, 766-775.
- Cespuglio R, Amrouni D, Meiller A, Buguet A & Gautier-Sauvigne S. (2012). Nitric oxide in the regulation of the sleep-wake states. *Sleep Medicine Reviews* **16**, 265-279.
- Chauhan A, Audhya T & Chauhan V. (2012). Brain region-specific glutathione redox imbalance in autism. *Neurochemical research* **37**, 1681-1689.
- Chauhan A & Chauhan V. (2006). Oxidative stress in autism. *Pathophysiology : the official journal of the International Society for Pathophysiology / ISP* **13**, 171-181.
- Cheng HY, Schenk J, Huff R & Adams RN. (1979). *In vivo* electrochemistry: behavior of micro electrodes in brain tissue. *Journal of Electroanalytical Chemistry and Interfacial Electrochemistry* **100**, 23-31.

- Chinta SJ & Andersen JK. (2008). Redox imbalance in Parkinson's disease. *Biochimica Et Biophysica Acta-General Subjects* **1780**, 1362-1367.
- Davis GC, Williams AC, Markey SP, Ebert MH, Caine ED, Reichert CM & Kopin IJ. (1979). Chronic parkinsonism secondary to intravenous-injection of meperidine analogs. *Psychiatry Research* **1**, 249-254.
- Day BJ, Patel M, Calavetta L, Chang LY & Stamler JS. (1999). A mechanism of paraquat toxicity involving nitric oxide synthase. *Proceedings of the National Academy of Sciences of the United States of America* **96**, 12760-12765.
- Dayton MA, Ewing AG & Wightman RM. (1983). Diffusion processes measured at microvoltammetric electrodes in brain tissue. *Journal of Electroanalytical Chemistry and Interfacial Electrochemistry* **146**, 189-200.
- de Mattos-Dutra A, Meirelles R, da Rocha BB, Kommers T, Wofchuk ST, Wajner M & Pessoa-Pureur R. (2000). Methylmalonic and propionic acids increase the *in vitro* incorporation of P-32 into cytoskeletal proteins from cerebral cortex of young rats through NMDA glutamate receptors. *Brain Research* **856**, 111-118.
- Dinis-Oliveira RJ, Remiao F, Carmo H, Duarte JA, Navarro AS, Bastos ML & Carvalho F. (2006). Paraquat exposure as an etiological factor of Parkinson's disease. *Neurotoxicology* **27**, 1110-1122.
- Finnerty NJ, O'Riordan SL, Brown FO, Serra PA, O'Neill RD & Lowry JP. (2012a). *In vivo* characterisation of a Nafion<sup>®</sup>-modified Pt electrode for real-time nitric oxide monitoring in brain extracellular fluid. *Analytical Methods* **4**, 550-557.
- Finnerty NJ, O'Riordan SL, Palsson E & Lowry JP. (2012b). Brain nitric oxide: Regional characterisation of a real-time microelectrochemical sensor. *Journal of Neuroscience Methods* **209**, 13-21.
- Garguilo MG & Michael AC. (1994). Quantitation of choline in the extracellular fluid of brain-tissue with amperometric microsensors. *Analytical Chemistry* **66**, 2621-2629.
- Garguilo MG & Michael AC. (1996). Amperometric microsensors for monitoring choline in the extracellular fluid of brain. *Journal of Neuroscience Methods* **70**, 73-82.
- Garthwaite J. (2008). Concepts of neural nitric oxide-mediated transmission. *European Journal of Neuroscience* **27**, 2783-2802.
- Guix FX, Uribealago I, Coma M & Munoz FJ. (2005). The physiology and pathophysiology of nitric oxide in the brain. *Progress in Neurobiology* **76**, 126-152.

- Heinzen EL & Pollack GM. (2002). Use of an electrochemical nitric oxide sensor to detect neuronal nitric oxide production in conscious, unrestrained rats. *Journal of Pharmacological and Toxicological Methods* **48**, 139-146.
- Hu YB, Mitchell KM, Albahadily FN, Michaelis EK & Wilson GS. (1994). Direct measurement of glutamate release in the brain using a dual enzyme-based electrochemical sensor. *Brain Research* **659**, 117-125.
- Kelm M. (1999). Nitric oxide metabolism and breakdown. *Biochimica Et Biophysica Acta-Bioenergetics* **1411**, 273-289.
- Kiechle FL & Malinski T. (1993). Nitric-oxide - biochemistry, pathophysiology, and detection. *American Journal of Clinical Pathology* **100**, 567-575.
- Langston JW, Ballard P, Tetrud JW & Irwin I. (1983). Chronic Parkinsonism in humans due to a product of meperidine-analog synthesis. *Science* **219**, 979-980.
- Li J, Bravo DS, Upton AL, Gilmour G, Tricklebank MD, Fillenz M, Martin C, Lowry JP, Bannerman DM & McHugh SB. (2011). Close temporal coupling of neuronal activity and tissue oxygen responses in rodent whisker barrel cortex. *European Journal of Neuroscience* **34**, 1983-1996.
- Lotharius J & Brundin P. (2002). Pathogenesis of Parkinson's disease: Dopamine, vesicles and alpha-synuclein. *Nature Reviews Neuroscience* **3**, 932-942.
- Lowry JP, McAteer K, Elatrash SS, Duff A & O'Neill RD. (1994). Characterisation of glucose oxidase-modified poly(phenylenediamine)-coated electrodes *in-vitro* and *in-vivo*: homogeneous interference by ascorbic acid in hydrogen-peroxide detection. *Analytical Chemistry* **66**, 1754-1761.
- Lowry JP, Miele M, O'Neill RD, Boutelle MG & Fillenz M. (1998). An amperometric glucose-oxidase/poly(*o*-phenylenediamine) biosensor for monitoring brain extracellular glucose: *in vivo* characterisation in the striatum of freely-moving rats. *Journal of Neuroscience Methods* **79**, 65-74.
- MacFabe DF, Cain DP, Rodriguez-Capote K, Franklin AE, Hoffman JE, Boon F, Taylor AR, Kavaliers M & Ossenkopp K-P. (2007). Neurobiological effects of intraventricular propionic acid in rats: Possible role of short chain fatty acids on the pathogenesis and characteristics of autism spectrum disorders. *Behavioural Brain Research* **176**, 149-169.
- MacFabe DF, Cain NE, Boon F, Ossenkopp K-P & Cain DP. (2011). Effects of the enteric bacterial metabolic product propionic acid on object-directed behavior, social behavior, cognition, and neuroinflammation in adolescent rats: Relevance to autism spectrum disorder. *Behavioural Brain Research* **217**, 47-54.

- MacFabe DF, Rodríguez-Capote K, Franklin JE, Kavaliers M, Possmayer F, Ossenkopp K-P & Franklin AE. (2008). A Novel Rodent Model of Autism: Intraventricular Infusions of Propionic Acid Increase Locomotor Activity and Induce Neuroinflammation and Oxidative Stress in Discrete Regions of Adult Rat Brain. *American Journal of Biochemistry and Biotechnology* **4**, 146-166.
- Maier CM & Chan PH. (2002). Role of superoxide dismutases in oxidative damage and neurodegenerative disorders. *Neuroscientist* **8**, 323-334.
- Manning-Bog AB, McCormack AL, Li J, Uversky VN, Fink AL & Di Monte DA. (2002). The herbicide paraquat causes up-regulation and aggregation of alpha-synuclein in mice - Paraquat and alpha-synuclein. *Journal of Biological Chemistry* **277**, 1641-1644.
- Margolis AS, Porasuphatana S & Rosen GM. (2000). Role of paraquat in the uncoupling of nitric oxide synthase. *Biochimica Et Biophysica Acta-General Subjects* **1524**, 253-257.
- McAteer K & O'Neill RD. (1996). Strategies for decreasing ascorbate interference at glucose oxidase-modified poly(*o*-phenylenediamine)-coated electrodes. *Analyst* **121**.
- McCormack AL, Atienza JG, Johnston LC, Andersen JK, Vu S & Di Monte DA. (2005). Role of oxidative stress in paraquat-induced dopaminergic cell degeneration. *Journal of Neurochemistry* **93**, 1030-1037.
- Melo A, Monteiro L, Lima RMF, Oliveira DMd, Cerqueira MDd & El-Bacha RS. (2011). Oxidative stress in neurodegenerative diseases: mechanisms and therapeutic perspectives. *Oxidative medicine and cellular longevity* **2011**, 467180.
- Monaghan DT & Cotman CW. (1985). Distribution of N-methyl-D-aspartate-sensitive L-[3H]glutamate-binding sites in rat brain. *J Neurosci* **5**, 2909-2919.
- Moran JM, Ortiz-Ortiz MA, Ruiz-Mesa LM & Fuentes JM. (2010). Nitric Oxide in Paraquat-Mediated Toxicity: A Review. *Journal of Biochemical and Molecular Toxicology* **24**, 402-409.
- Nakao S, Fujii A & Niederman R. (1992). Alteration of cytoplasmic Ca<sup>2+</sup> in resting and stimulated human neutrophils by short-chain carboxylic acids at neutral pH. *Infect Immun* **60**, 5307-5311.
- O'Brien KB, Killoran SJ, O'Neill RD & Lowry JP. (2007). Development and characterization *in vitro* of a catalase-based biosensor for hydrogen peroxide monitoring. *Biosensors & Bioelectronics* **22**, 2994-3000.

- Obeso JA, Rodriguez-Oroz MC, Goetz CG, Marin C, Kordower JH, Rodriguez M, Hirsch EC, Farrer M, Schapira AHV & Halliday G. (2010). Missing pieces in the Parkinson's disease puzzle. *Nature Medicine* **16**, 653-661.
- Ramalingam M & Kim S-J. (2012). Reactive oxygen/nitrogen species and their functional correlations in neurodegenerative diseases. *Journal of Neural Transmission* **119**, 891-910.
- Rice ME. (2011). H<sub>2</sub>O<sub>2</sub>: A Dynamic Neuromodulator. *Neuroscientist* **17**, 389-406.
- Rose S, Melnyk S, Pavliv O, Bai S, Nick TG, Frye RE & James SJ. (2012). Evidence of oxidative damage and inflammation associated with low glutathione redox status in the autism brain. *Translational psychiatry* **2**, e134.
- Ryan MR, Lowry JP & Oneill RD. (1997). Biosensor for neurotransmitter L-glutamic acid designed for efficient use of L-glutamate oxidase and effective rejection of interference. *Analyst* **122**, 1419-1424.
- Saulskaya NB & Fofonova NV. (2006). Effects of N-methyl-D-aspartate on extracellular citrulline level in the rat nucleus accumbens. *Neuroscience Letters* **407**, 91-95.
- Shams S, Kavaliers M, Foley KA, Ossenkopp KP & MacFabe DF. (2009). Reduced social interaction, anxiety-like behavior and hypoactivity following systemic administrations of propionic acid in juvenile male rats. *Society for Neuroscience Abstract Viewer and Itinerary Planner* **39**.
- Shimizu K, Matsubara K, Ohtaki K, Fujimaru S, Saito O & Shiono H. (2003). Paraquat induces long-lasting dopamine overflow through the excitotoxic pathway in the striatum of freely moving rats. *Brain Research* **976**, 243-252.
- Sogut S, Zoroglu SS, Ozyurt H, Yilmaz HR, Ozugurlu F, Sivasli E, Yetkin O, Yanik M, Tutkun H, Savas HA, Tarakcioglu M & Akyol O. (2003). Changes in nitric oxide levels and antioxidant enzyme activities may have a role in the pathophysiological mechanisms involved in autism. *Clinica Chimica Acta* **331**, 111-117.
- Sweeten TL, Posey DJ, Shankar S & McDougle CJ. (2004). High nitric oxide production in autistic disorder: A possible role for interferon-gamma. *Biological Psychiatry* **55**, 434-437.
- Valko M, Leibfritz D, Moncol J, Cronin MTD, Mazur M & Telser J. (2007). Free radicals and antioxidants in normal physiological functions and human disease. *International Journal of Biochemistry & Cell Biology* **39**, 44-84.

- Vargas DL, Nascimbene C, Krishnan C, Zimmerman AW & Pardo CA. (2005). Neuroglial activation and neuroinflammation in the brain of patients with autism. *Annals of Neurology* **57**, 67-81.
- Walsh P, Elsabbagh M, Bolton P & Singh I. (2011). In search of biomarkers for autism: scientific, social and ethical challenges. *Nature Reviews Neuroscience* **12**, 603-612.
- Wellstead P & Cloutier M. (2011). An energy systems approach to Parkinson's disease. *Wiley Interdisciplinary Reviews-Systems Biology and Medicine* **3**, 1-6.
- Wink DA & Mitchell JB. (1998). Chemical biology of nitric oxide: Insights into regulatory, cytotoxic, and cytoprotective mechanisms of nitric oxide. *Free Radical Biology and Medicine* **25**, 434-456.
- Wisniewski N, Moussy F & Reichert WM. (2000). Characterization of implantable biosensor membrane biofouling. *Fresenius Journal of Analytical Chemistry* **366**, 611-621.

## Publications & Conferences

### *Publications*

1. Finnerty NJ, O'Riordan SL, Palsson E & Lowry JP. (2012). Brain nitric oxide: Regional characterisation of a real-time microelectrochemical sensor. *Journal of Neuroscience Methods* 209, 13-21.
2. Finnerty NJ, O'Riordan SL, Brown FO, Serra PA, O'Neill RD & Lowry JP. (2012). *In vivo* characterisation of a Nafion<sup>®</sup>-modified Pt electrode for real-time nitric oxide monitoring in brain extracellular fluid. *Analytical Methods* 4, 550-557.
3. Lowry JP, Finnerty NJ, O'Riordan SL, Wellstead P & Cloutier M. *In-vivo* real-time measurements support a mathematical prediction of neuronal pathogenesis of Parkinson's disease as bistability in a neurochemical switch. (*Manuscript in progress*).

### *Conferences*

1. *Real-time detection of oxidative and nitrosative stress markers in anaesthetised and freely-moving animals. Oral presentation* at the 6<sup>th</sup> Annual Meeting of Neuroscience Ireland (2011).
2. *The development of a catalase-based biosensor for in-vivo monitoring of hydrogen peroxide. Poster presentation* at the 6<sup>th</sup> Conference on Analytical sciences Ireland (CASi) (2011).
3. *A catalase based biosensor for in vivo monitoring of hydrogen peroxide. Poster presentation* at the 13<sup>th</sup> International Conference on *In-vivo* Methods (2010).

*“All of Old. Nothing else ever. Ever tried. Ever failed. No matter.  
Try again. Fail again.  
Fail better.”*

Samuel Beckett